Cerium Cyclopentadienyl Chemistry

DISSERTATION

der Mathematisch-Naturwissenschaftlichen Fakultät
der Eberhard Karls Universität Tübingen
zur Erlangung des Grades eines
Doktors der Naturwissenschaften
(Dr. rer. nat.)

vorgelegt von
M. Sc. Lars Hirneise
aus Reutlingen

Tübingen
2021

Gedruckt mit Genehmigung der Mathematisch-Naturwissenschaftlichen Fakultät der Eberhard Karls Universität Tübingen.

Tag der mündlichen Qualifikation:	22.12.2021
Dekan:	Prof. Dr. Thilo Stehle
1. Berichterstatter:	Prof. Dr. Reiner Anwander
2. Berichterstatter:	Prof. Dr. Doris Kunz

Cerium Cyclopentadienyl Chemistry

Lars Hirneise

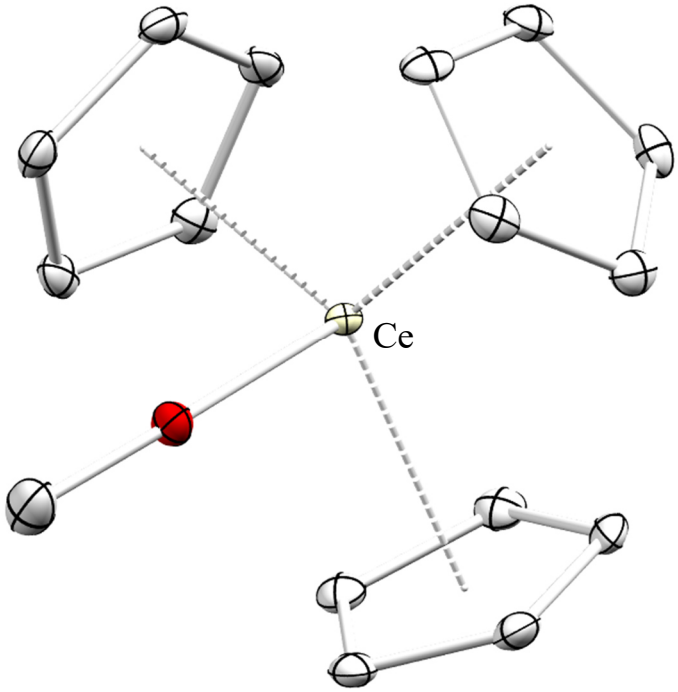

Preface

The following thesis consists of a review on the synthesis and reactivity of cerium cyclopentadienyl complexes, a summary of the main results, and original scientific papers. The work has been carried out at the Institut für Anorganische Chemie of the Eberhard Karls Universität Tübingen, Germany, over the period from November 2018 to March 2021 under the supervision of Prof. Dr. Reiner Anwander. Funding has been gratefully received from the Deutsche Forschungsgemeinschaft (DFG).

Acknowledgements

First of all, I would like to thank my supervisor Prof. Dr. Reiner Anwander for giving me the opportunity to perform my doctoral studies in your laboratory and accepting me into your group. Thank you for providing me with the very interesting research topic on cerium(IV) chemistry and the chance to immerse into cyclic voltammetry as its side kick as well. I am particularly grateful for your helpful and directional advice and the new ideas that you introduced.

A special thanks goes to Dr. Cäcilia Maichle-Mössmer for the crystal measurements and refinements and Elke Niquet for the tedious set up of many pitchblack crystals for measurement.

Special thanks go to the collaboration partners Prof Dr. Bernd Speiser and Georg Zitzer for their helpful discussions and CV measurements and Prof. Dr. Wolfgang Scherer and Jan Langmann for all the SQUID experiments. The friendly joint work was very insightful and broadened my inorganic horizon. Further thanks go to Dr. Nicole Mews for all her help regarding cyclovoltammetric measurements as well as Dr. Jochen Friedrich for the introduction into electrochemistry and Dr. Andreas Berkefeld for the allocation of the potentiostat. I would like to further thank Dr. Klaus Eichele and Kristina Strohmaier for the maintaince of high standard equipment, as well as their help regarding NMR spectroscopy. Additionally, I'd like to thank Wolfgang Bock for performing countless elemental analyses.

I want to thank Tobias Wolf, Elke Niquet and Karl-Heinz Ableitner for maintaining the equipment in the laboratory and their helpful hand whenever there were problems and Sabine Ehrlich for her help as the administrative mastermind. In addition, I would like to thank the staff of the metal, glass and electronics workshops for their work in providing and repairing all sorts of lab equipment.

Additionaly, I would like to thank all my former and current coworkers of the Anwander group, especially Dr. Uwe Bayer for the helpful discussions and advice in the ways of cerium and VIIG1. Thanks go to Damir Barisic, Tassilo Berger, Dr. Verena Birkelbach, Dr. Lorenz Bock, Martin Bonath, Denis Burghardt, Dennis Buschmann, Dr. Dominic Diether, Dr. Jochen Friedrich, Dr. Christoph Hollfelder, Markus Katzenmayer, Felix Kracht, Jakob Lebon, Dr. Yucang Liang, Dr. Leilei Luo, Eric Moinet, Alexandros Mortis, Theresa Rieser, Dr. Dorothea Schädle, Dr. David Schneider, Andrea Sonström, Georgios Spiridopoulos, Dr. Christoph Stuhl, Dr. Renita Thim-Spöring, Simon Trzmiel and Dr. Benjamin Wolf for the good and supportive working environment.

Exceptional thanks to my love and wife Jana Katharina, thank you for brighten me up, for all the discussions, for all the magnificent moments we shared and thank you for all the love and support. You make my life perfect and I am incredibly thankful that I found you!

Insbesondere möchte ich mich bei meinen Eltern (Sabine und Reimund) bedanken, die mich Zeit meines Lebens, während meines Studiums und während der Doktorarbeit in jeglicher Art tatkräftig unterstützt haben. Meinem Bruder Axel möchte ich für all die tollen Gespräche, Diskussionen, Jam-Sessions und Spieleabende danken.

Contents

Abbreviations

Ar	2,6-Di(*iso*)propylphenyl	Cp'''	1,2,4-Tris(trimethylsilyl)-cyclopentadienyl
Bn	Benzyl	CV	Cyclic Voltammetry
bipy	2,2'-Bipyridine	Cp^{tBu}	*Tert*-butylcyclopentadienyl
bq	*p*-Benzoquinone	Cp^{tt}	1,3-Bis(*tert*-butyl)cyclopenta-dienyl
*n*Bu	*n*-Butyl	Cp^{ttt}	1,2,4-Tris(*tert*-butyl) cyclopenta-dienyl
*t*Bu	*tert*-Butyl	DEPT	Distortionless Enhancement by Polarization Transfer
btsa	Bis(trimethylsilyl)amido	DFT	Density-functional Theory
CAN	Ceric Ammonium Nitrate	dipp	2,6-Di(*iso*)propylpentadienyl
$CeCl_3$*	$CeCl_3(thf)_{1.04}$	dme	Dimethoxyethane
COSY	Correlated Spectroscopy	do	Donor
COT	Cyclooctatetraenyl	DRIFT	Diffuse Reflectance Infrared Fourier Transform
Cp	Cyclopentadienyl	E^0	Formal Potential
Cp^{Me}	Methylcyclopentadienyl	ΔE_p	Peak Separation
Cp^{tet}	Tetramethylcyclopentadienyl	EC / ECE	E electron transfer C chemical reaction
Cp*	Pentamethylcyclopentadienyl	EA	Elemental Analysis
Cp'	Trimethylsilyl-cyclopentadienyl	*e.g.*	*exempli gratia*
Cp''	1,3-Bis(trimethylsilyl)-cyclopentadienyl	Et	Ethyl

et al.	*et alii* or *et aliae*	ppm	Parts per Million
Fc	Ferrocene	*n*Pr	*n*-Propyl
Flu	Fluorenyl	*i*Pr	*iso*-Propyl
Flu$^{t\mathrm{Bu}}$	2,7-Di(*tert*-butyl)fluorenyl	py	Pyridine
HMBC	Heteronuclear Multiple Bond Correlation	Pz	Pyrazolyl
HSQC	Heteronuclear Single Quantum Coherence	Red	Reduction
Ind	Indenyl	RT	Ambient Temperature
IR	Infrared	SCE	Saturated Calomel Electrode
Ln	Rare-earth metals (Sc, Y, La – Lu)	SQUID	Superconductiong Quantum Interference Device
Me	Methyl	thf	Tetrahydrofuran
Mes	Mesityl	TIP	Temperature Independent Paramagnetism
NHC	Imidazol-2-ylidene (*N*-heterocyclic carbene)	tmeda	Tetramethylethylenediamine
NMR	Nuclear Magnetic Resonance	tol	Toluene
OTf	Triflato	UV-Vis	Ultraviolet–Visible
Ox	Oxidation	VT	Variable Temperature
Ph	Phenyl	XANES	X-ray Absorption Near Edge Structure

Summary

Cerium has an outstanding importance among the rare-earth metals (Sc, Y, La-Lu) due to its reversible redox chemistry. Although especially cerium(IV) oxide has achieved industrial importance as catalyst and polishing agent, the metalorganic chemistry of tetravalent cerium compounds has attracted greater attention only recently. This is due to difficulties in the stabilization of the +IV oxidation state, which is highly dependent on the ligand sphere. This work approaches the issue by research toward the stability and formation of organocerium(IV) compounds, especially regarding the effects of the ligand sphere.

Initially, new cerium(III) fluorenyl complexes were synthesized, in order to serve as precursors for cerium(IV) chemistry. Accordingly, $FluCeX_2(thf)_3$ (X = Cl, I) gave access to the respective half-sandwich complexes $FluCeR_2(thf)_x$, bearing aryloxy, alkoxy, cyclopentadienyl, siloxy and pyrazolato ligands. Such complexes proved particularly stable at low temperatures, suffering ligand rearrangement processes at ambient temperature to the sandwich complexes $Flu_2CeR(thf)_x$ in the case of alkoxy, siloxy, and pyrazolato ligands. Treatment of the Ce(III) species with halogenating agents led to the formation of 9-halogenidofluorene and 1,1'-bifluorene, a transformation which could be controlled stoichiometrically.

Ate complex $Cp^*_2CeCl_2K(thf)_2$ could be successfully oxidized, affording complexes of the type $Cp^*_2Ce(OR)_2$ with alkoxy and siloxy ligands as well as $Cp^*_2Ce(OR)Cl$ with aryloxy ligands. Again, ligand rearrangement occurred at ambient temperature, but resulted in the formation of the first half-sandwich cerium(IV) complexes $Cp^*Ce(OR)_3$ with R = $SiPh_3$ and *t*Bu. Cyclic voltammetry revealed a better stabilization of the +IV oxidation state in the order aryloxy < siloxy < alkoxy. Additionally, a stronger stabilization and limited Ce(III/IV) reversibility was observed for half-sandwich in comparison to sandwich complexes.

Finally, the stability of organocerium(IV) complexes was further investigated starting from cyclopentadienides $Cp^{H/Me}_3CeX$ with X = Cl, Br, I and using the chlorido complex as a precursor for salt-metathesis reactions. Application of this protocol resulted in a range of thermally stable complexes $Cp^{H/Me}_3Ce(OR)$ with R = Me, Et, *i*Pr, *t*Bu, CH_2*t*Bu, $SiMe_3$, $SiEt_3$, $Si(iPr)_3$ and $SiPh_3$. Magnetic measurements revealed temperature-independent paramagnetism (TIP) instead of diamagnetism and positive magnetic susceptibilities. Cyclic voltammetry revealed chemical and electrochemical Ce(III/IV) reversibility for halogenido and siloxy

ligand and an EC or ECE type behavior for alkoxy complexes. The formal potentials span a wide range, opening the possibility to tune the electrochemical potentials by ligand variations. The stabilization of the cerium(IV) center was shown to increase in the series I < Br < Cl < siloxy < alkoxy and Cp < Cp^{Me} thus increasing with more electron donating ligands.

Zusammenfassung

Aufgrund seiner reversiblen Redox-Chemie besitzt Cer außergewöhnliche Relevanz im Vergleich mit den anderen Seltenerdmetallen (Sc, Y, La-Lu). Exemplarisch hierfür steht die industrielle Verwendung von Cer(IV) oxid als redox-aktivem Katalysator und Poliermittel. Dagegen wurden auf dem Gebiet der Metallorgainschen Chemie von vierwertigem Cer erst in jüngerer Zeit große Fortschritte gemacht. Dies liegt insbesondere an der Schwierigkeit, vierwertiges Cer zu stabilisieren, was in großem Maße von der Ligandensphäre beeinflusst wird. Diese Arbeit nimmt sich diesem Problem an, indem die Bildung und Stabilität von Cer(IV)-Komplexen, insbesondere in Hinblick auf die Effekte unterschiedlicher Liganden, untersucht werden.

Zunächst wurden neuartige Cer(III)-Fluorenyl-Komplexe synthetisiert, die als Vorstufe für die Cer(IV)-Chemie dienen sollten. Entsprechend wurden im Zuge dieser Arbeit die Verbindungen $FluCeX_2(thf)_3$ (X = Cl, I) synthetisiert und in Salz-Metathese-Reaktionen eingesetzt, um die entsprechenden Halbsandwich-Komplexe $FluCeR_2(thf)_x$ mit Alkoholat-, Silanolat- und Pyrazolat-Liganden bei niedrigen Temperaturen herzustellen. Bei Raumtemperatur wurden Liganden-Disproportionierungsreaktionen beobachtet, die im Falle von Alkoholat-, Silanolat- und Pyrazolat-Liganden zu den Sandwich-Komplexen $Flu_2CeR(thf)_x$ führten. Bei Kontakt mit halogenierenden Oxidationsmitteln erfolgte eine Reaktion zu Cer(III)-Spezies und 9-Halogenfluoren sowie 1,1‘-Bifluoren. Diese Umsetzung konnte stöchiometrisch kontrolliert werden.

Bei Verwendung des At-Komplexes $Cp^*_2CeCl_2K(thf)_2$ als Edukt gelang schließlich die Oxidation zu Komplexen des Typs $Cp^*_2Ce(OR)_2$ mit Alkoholat- und Silanolat-Liganden sowie $Cp^*_2Ce(OR)Cl$ mit Phenolat-Liganden. Wieder wurde bei Raumtemperatur eine Umorganisation der Liganden beobachtet, die jedoch in der Bildung der ersten Cer(IV)-Halbsandwich-Komplexe $Cp^*Ce(OR)_3$ mit R = $OSiPh_3$ und *t*Bu resultierte. Cyclovoltammetrische Analysen der Komplexe offenbarten eine zunehmende Stabilisierung der Oxidationsstufe +IV in der Reihenfolge Phenolat < Silanolat < Alkoholat. Weiterhin

zeigten die Halbsandwich-Komplexe verglichen mit den entsprechenden Sandwich-Komplexen ebenfalls eine stärkere Stabilisierung sowie eine eingeschränkte Reversibilität.

Zuletzt wurde die Stabilität von Organocer(IV)-Komplexen ausgehend von den Triscyclopentadienyl-Derivaten $Cp^{H/Me}{}_3CeR$ mit R = Cl, Br, I weitergehend untersucht. Der Chlorid-Komplex wurde als Edukt für Salzmetathese-Reaktionen genutzt, die für die Reste R = OMe, OEt, O*i*Pr, O*t*Bu, OCH_2tBu, $OSiMe_3$, $OSiEt_3$, $OSi(iPr)_3$ and $OSiPh_3$ erfolgreich waren. Magnetische Messungen zeigten temperaturunabhängigen Paramagnetismus (TIP) auf, mit positiven magnetischen Suszeptibilitäten. In cyclovoltammetrischen Experimenten verhielten sich die Halogenid- und Silanolatkomplexe chemisch und elektrochemisch reversibel, während Alkoholat-Komplexe Cyclovoltammogramme des EC- oder ECE-Typs aufwiesen. Die Formalpotentiale überspannen eine große Bandbreite und eröffnen damit die Möglichkeit, das elektrochemische Potential durch die Ligandenwahl zu steuern. Die Stabilisierung von Cer(IV) nahm in der Reihenfolge I < Br < Cl < Silanolat < Alkoholat sowie $Cp < Cp^{Me}$ mit zunehmend Elektronen-donierenden Liganden zu.

Publications

Publications incorporated into this thesis

Paper I Radical Coupling at Cerium Fluorenyl Complexes
Lars Hirneise, Cäcilia Maichle-Mössmer, and Reiner Anwander
Manuscript

Paper II Pentamethylcyclopentadienyl Complexes of Cerium(IV): Synthesis, Reactivity, and Electrochemistry
Lars Hirneise, Cäcilia Maichle Mössmer, and Reiner Anwander
Inorg. Chem., **2021**, (accepted)
Accepted for Publication (23.10.2021)

Paper III Tuning Organocerium Electrochemical Potentials by Extending Tris(cyclopentadienyl) Scaffolds with Terminal Halogenido, Siloxy and Alkoxy Ligands
Lars Hirneise, Jan Langmann, Georg Zitzer, Lukas Ude, Cäcilia Maichle-Mössmer, Wolfgang Scherer, Bernd Speiser, and Reiner Anwander
Organometallics, **2021**, *40*, 11, 1786 − 1800
https://doi.org/10.1021/acs.organomet.1c00276

Personal Contribution

Paper I:

All reactions and analyses presented were planned and conducted by myself. Analyses include ^{1}H NMR spectroscopy and DRIFT spectroscopy. Elemental analyses were performed by Wolfgang Bock and structural analyses by single crystal X-ray diffraction were performed by Dr. Cäcilia Maichle-Mössmer. The publication was written by myself.

Paper II:

All reactions and analyses presented were planned and carried out by myself, including ^{1}H and ^{1}H-^{29}Si HSQC NMR spectroscopy, DRIFT spectroscopy, UV-Vis spectroscopy amd cyclic voltammetry. Elemental analyses were performed by Wolfgang Bock and structural analyses by single crystal X-ray diffraction were performed by Dr. Cäcilia Maichle-Mössmer. The manuscript was written by myself.

Paper III:

All reactions and analyses presented were planned and conducted by myself. Analyses include one-dimensional (^{1}H, ^{13}C{^{1}H}) and two-dimensional (^{1}H-^{13}C HSQC, ^{1}H-^{13}C HMBC, ^{1}H-^{1}H COSY, ^{1}H-^{29}Si HSQC) NMR spectroscopy, DRIFT spectroscopy, and cyclic voltammetry. Manuscript writing was also done by me. Elemental analyses were performed by Wolfgang Bock. The structural analyses by single crystal X-ray diffraction were performed by Dr. Cäcilia Maichle-Mössmer. Magnetic SQUID measrurements were performed by Jan Langmann. Lukas Ude contributed the experimental work for $Cp^{Me}_{3}CeBr$ and Georg Zitzer contributed to electrochemical investigation of $Cp^{Me}_{3}Ce(OSiPh_3)$. Prof. Dr. Bernd Speiser contributed to the interpretation of the electrochemical data and Prof. Dr. Wolfgang Scherer to the interpretation of the magnetic data.

Some reactions and analyses were conducted during my master thesis.

Objective of this Thesis

The main emphasis of this thesis is to investigate the reactivity of trivalent and tetravalent cerium cyclopentadienyl complexes and the influence of the chemical environment on the stabilization of the oxidation state +IV.

Chapter A gives an overview of the synthesis and reactivity of trivalent cerium cyclopentadienyl complexes and the pathways available to access organometallic tetravalent cerium compounds. In each chapter another supporting ligand class is highlighted.

Chapter B contains a summary of the main results of this thesis and is divided into three parts:

- Cerium(III)-Fluorenyl Chemistry and Fluorenyl Coupling
- Cerium(IV)-Sandwich and Half-Sandwich Complexes
- Stabilization of Cerium(IV)-Cyclopentadienyl Complexes

In **Chapter C** unpublished results, which are not part of a publication or manuscript, are presented. Here, *ansa*-cyclopentadienyl and *ansa*-indenyl cerium complexes are described.

Chapter E is a compilation of publications.

A

Cerium

Cyclopentadienyl

Chemistry

Introduction

Since the discovery of ferrocene in 1951 the monoanionic cyclopentadienyl ligand C_5H_5 (Cp) soon became a keystone in metalorganic chemistry, due to its exceptional stabilizing effect.[1-3] With its $pK_a(H_2O)$ value of 15, cyclopentadiene shows unusually high acidity compared to other hydrocarbons, owing to its aromaticity with six π-electrons in the anionic form.[4] Therefore, deprotonation is easily achieved using mostly alkali metals, alkali-metal hydrids or other organolithium or sodium reagents like *n*-butyllithium. The cyclopentadienyl ligand can also be substituted to change its electronic and steric properties, *e.g.* with alkyl substituents or fused aromatic cycles, leading from monomethyl to pentamethyl cyclopentadienyl C_5Me_5 (Cp*) or fluorenyl $C_{13}H_{10}$ (Flu) ligands.[5-6] Coordination to the metal center takes place routinely in a η^5 coordination mode and leads in case of two Cp^R ligands to commonly called sandwich complexes, with the metal center between the two arene "plates". Cyclopentadienyl chemistry gained further impact by its supporting role in homogeneous Ziegler-Natta-catalysis for α-olefin polymerization, after the heterogenous mixed catalysts were awarded with the Nobel Prize in 1963.[7-9] For their contributions to the field of emerging organometallic sandwich and half-sandwich complexes (complexes with one cyclopentadienyl ligand and additional other ligands) and the understanding of its bonding situation the Nobel Prize in 1973 was bestowed upon Fischer and Wilkinson.[10-11] Today, over 80% of organometallic complexes contain cyclopentadienyl ligands, testifying their stabilizing ability and significance.[6]

Among the rare-earth metals (Sc, Y, La – Lu) cerium bears an exceptional significance due to its redox chemistry and natural abundance. In coordination compounds rare-earth metals exist usually in the +3 oxidation state, while for other oxidation states particularly stable electronic configurations are required, which is the case for Eu and Yb (+2) and Ce, Tb or Pr (+4). Molecular complexes of terbium (+4) and praseodymium (+4) are known since 2019.[12-15] The most stable complexes in the +4 oxidation state are formed by cerium ($4f^0$), based on the closed-shell electronic configuration of the noble gas xenon. This can be utilized/exploited in oxidation agents such as ceric ammonium nitrate $(NH_4)_2Ce(NO_3)_6$ (CAN), in catalysis or as redox-active molecular materials or as a role model for Pu(+4) chemistry.[16-17] While cerium materials, and in particular CeO_2 are commonly used in catalyst systems in gasoline engines, as polishing agent, in illuminants and plenty further applications, the molecular chemistry of cerium has been less investigated, especially in the oxidation state +4.[18-19] This overview

aims to elucidate the progress, which has been made in organometallic cerium cyclopentadienyl chemistry in both oxidation states.

Cerium(III) Cyclopentadienyl Chemistry

2.1 Cerium(III) Tris(Cyclopentadienyl) Complexes

The first organometallic cerium complex Cp_3Ce (**1**) was synthesized in 1954 by Wilkinson and Birmingham starting from $CeCl_3$ and NaCp.[20] Compound **1** showed thermal stability up to at least 400 °C, thus making purification via sublimation possible, and featured three η^5-cyclopentadienyl ligands in contrast to d-metal metallocene complexes.[20] What is common to all trivalent cerium complexes, is that they are extremely sensitive to oxygen and water.[20] In the course of the following decades various additional tris(cyclopentadienyl) cerium(III) complexes have been synthesized, differing from each other by substitution at the cyclopentadienyl ligand, which is introduced afore complexation, and/or a variety of different neutral donor ligands, stabilizing the ligand sphere. Scheme A1 displays an overview including the use of Cp **1**[20-26], C_5H_4Me (Cp^{Me}) **2**[27-30], C_5H_4tBu (Cp^{tBu}) **3**[31-37], $C_5H_4SiMe_3$ (Cp') **4**[32-35, 38-39], $C_5H_4(SiMe_2tBu)$ **5**[40], 1,3-di(*tert*butyl)cyclopentadienyl (Cp^{tt}) **6**[41], 1,3-di(trimethylsilyl)cyclo-pentadienyl (Cp'') **7**[28], C_5Me_4H (Cp^{tet}) **8**[42] and indenyl (Ind) **9**[38, 43] as ligand.[44]

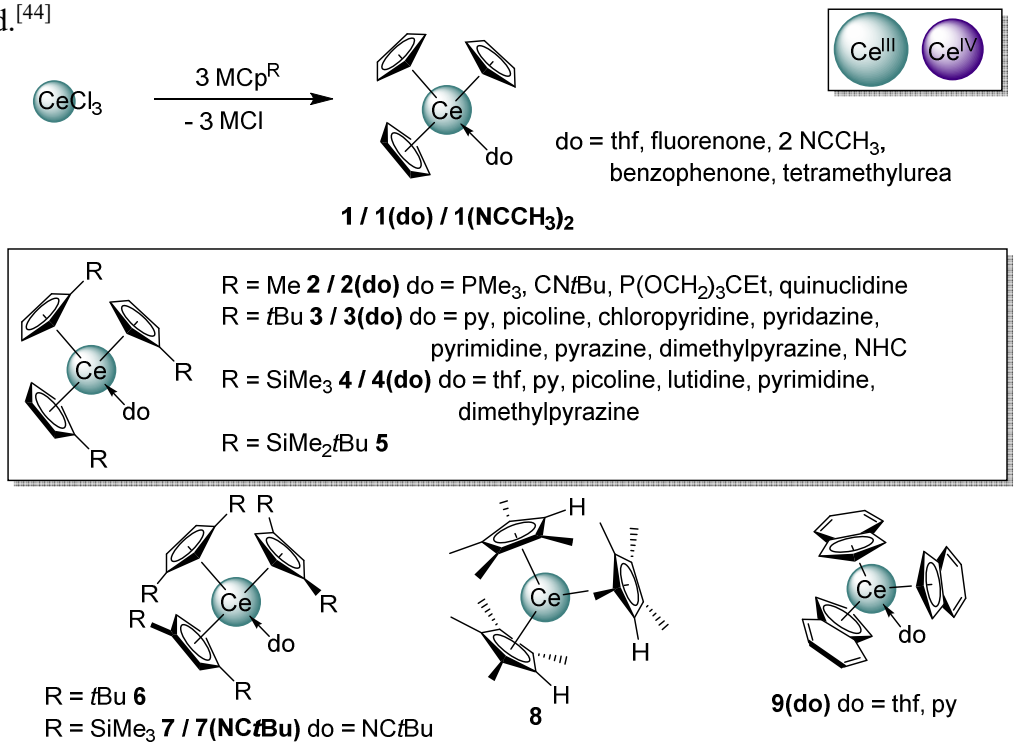

Scheme A1. Synthesis of cerium(III) tris(cyclopentadienyl) (**1**) and overview of possible substitution patterns of cerium(III) tris(cyclopentadienyl) complexes **2** to **8** as well as tris(indenyl) complex **9** in combination with different donor (do) molecules.

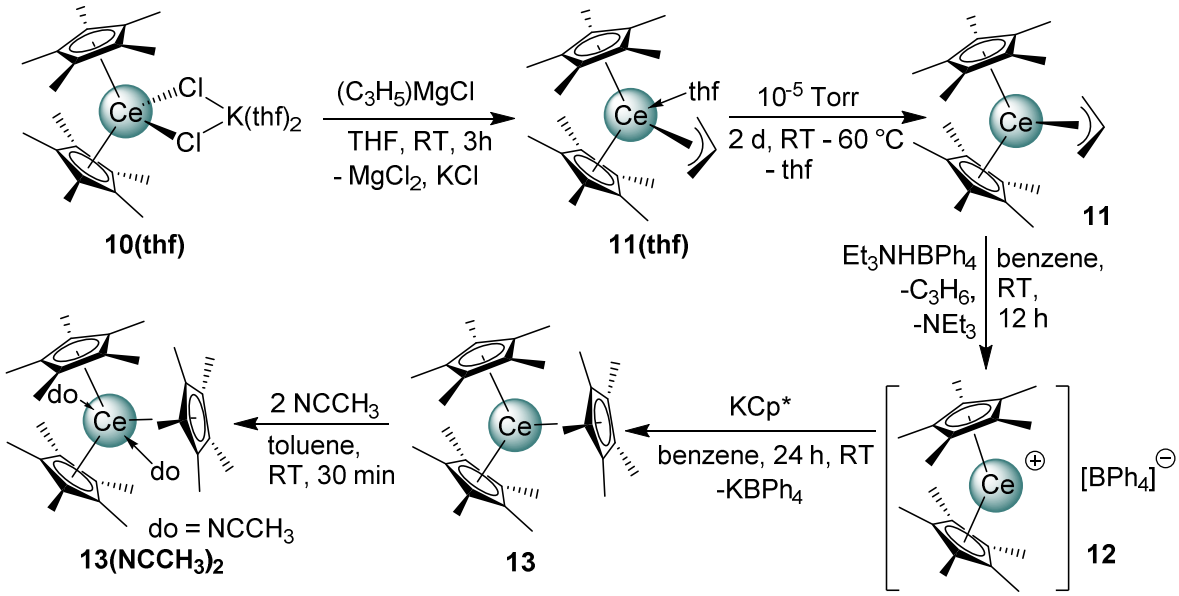

Scheme A2. Synthesis route toward elusive cerium(III) tris(pentamethylcyclopentadienyl) **13** and its donor adduct **13(NCCH$_3$)$_2$** starting from the bis(chlorido) ate complex **10(thf)**.

Instead of starting from cerium(III) halogenides it is also possible to use ceric ammonium nitrate (CAN) as a starting material, although this leads to more side products.[23] The solid-state structures of the Ce(III) complexes show a pseudo tetrahedral coordination mode, when one donor molecule is attached. The donorfree complexes with small substitutents like **1** and **2** lead to a weak η^1 interaction to the closest Cp/Cp^{Me} of the next molecule to saturate the ligand sphere, displaying oligomerization in the case of [Cp$^{Me}{}_3$Ce]$_4$ (**2**).[25, 28] Increasing the steric bulk (**3** to **7** and **9**) leads to a pseudo trigonal coordination of the donor free product, which is the only mode for **5**, **6** and **8**, because of steric encumbrance.[40-42] Another exception is **1(NCCH$_3$)$_2$**, for it provides space for two solvent molecules leading to a pseudo trigonal bipyramidal geometry.[21] Interestingly, when the steric bulk is increased even more in the form of pentamethylcyclopentadienyl (Cp*), the salt metathesis reaction starting from $CeCl_3$ does not lead to the desired complex **13**, but instead to incomplete substitution product Cp*$_2$CeCl$_2$K(thf) (**10(thf)**).[45-46] The route to the elusive Cp*$_3$Ce (**13**), finally found in 2005 by Evans *et al.*, is shown in Scheme A2 and starts with **10(thf)** nevertheless, by reaction to allyl complex **11(thf)** and subsequent sublimation under loss of thf to **11**.[47-48] Treatment with Et_3NHBPh_4 leads to the formation of the solvent separated ion pair **12**, which is then reacted to **13** by the use of KCp*.[47-49] The synthesis required silylated glassware and the absence of any donating solvent, due to the high reactivity of **13**, which readily reacts with CO, ethylene, thf and H_2 alkyl-like and with CO_2 under insertion.[48, 50] The high reactivity can be ascribed

to the high steric demand of the Cp* ligand in contrast to the metal size, which is expressed in long Ce−C bond distances (2.850 – 2.954 Å). Additionally, **13** shows sterically induced reactivity with $Se{=}PPh_3$, $AgBPh_4$, C_8H_8 and phenazine as well as sterically induced reduction to form 1,1'-bis(pentamethylcyclopentadiene).[48, 51]

2.2 Cerocene Halide Complexes

Similarly to the formation of **10(thf)**, cerium-derived metallocene chloride complexes have been discovered in 1986. They can be synthesized directly from $CeCl_3$ with bulky ligands, when the formation of an easily accessible tris(cyclopentadienyl) cerium complex is infeasible, as in the case of $Cp^*_2CeCl_2Li(OEt_2)_2$ (**14**).[45, 52] According to the alkali metal employed in the salt metathesis reaction different ate complexes are possible. Atwood *et al*. obtained $Cp^*_2CeCl_2K(thf)_2$ (**10(thf)**), proceeding from KCp* and showed the possibility of the formation of monomeric $Cp^*_2CeCl(thf)$ (**15**) via sublimation.[46] Other characterized complexes with these structural motifs are $[C_5(i\text{Pr})_4H]_2CeCl_2Na(tmeda)$ exhibiting a zigzag chain polymeric structure, as well as monomeric Cp^{ttt}_2CeCl (Cp^{ttt} = 1,2,4-tri-*tert*-butylcyclopentadienyl) and $Cp^{tt}_2CeCl_2Li(tmeda)$.[53-55] Another common motif for cerium(III) bis(cyclopentadienyl) complexes is oligomerization by ruling out both ate complexation and the presence of donor solvent. This is the case for $[Cp'_2CeCl]_2$ (**16**), which was synthesized starting from $Ce(AlMe_4)_3$ via $Cp'_2Ce(AlMe_4)$ and $AlMe_2Cl$ by our group.[38] Another homologue thereof is **17**, containing Cp^{tt} as a bulky ligand, while in this case the ate complex is evaded by utilization of a sodium salt.[53] Lastly, another binding motif is the formal inclusion of LiCl, which is bridging between two cerium centers in the case of **18**. Compound **18** was synthesized by addition of Li*C*C*t*Bu to **14** in *n*-hexane and obtained as a mixture with $Cp^*_2Ce(CC\textit{t}Bu)_2Li(thf)$.[56]

Only few metallocene complexes possess Ce−F bonds, including complex **19**, which exhibits an interaction with the borato ligand, which is implicating a separated ion pair for other similar lanthanide complexes.[57] Further characterized cerocenes featuring a fluorido ligand are Cp^{ttt}_2CeF (**33**) and $Cp^{ttt}_2Ce(C_6F_5)$ (**34**), which will be discussed in context with the analogous hydrido compounds, as they show H/F exchange.[58-60] Notably, terminal fluorido ligands are possible by the utilization of sterically demanding substitutions at the cyclopentadienyl ligand.[58-59]

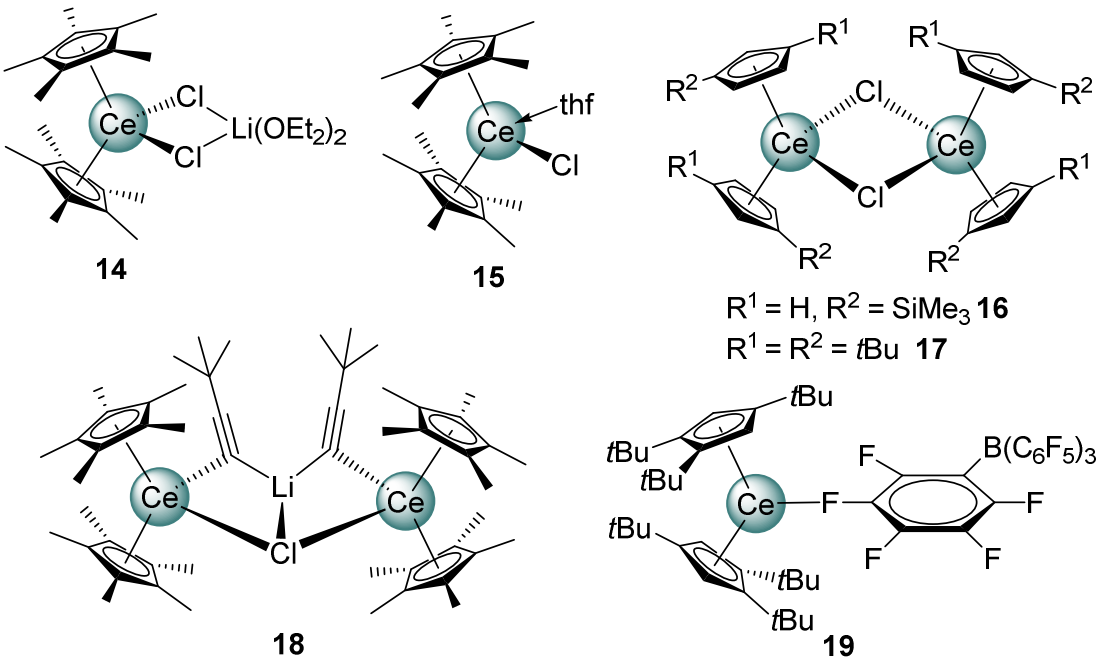

Scheme A3. Summary of other fluorido and chlorido ligated cyclopentadienyl complexes **14** to **19**. Structural motifs range from monomeric ate complexes **14** and donor-stabilized monomers **15** to halogenido-bridged dimeric species **16** and **17**, as well as formal incorporation of LiCl in dimeric species **18**.

Concerning the structural data reported, the most represented cerocene halogenides are the iodido derivatives, which exhibit the same structural motifs as the chlorido complexes do (Scheme A4). Additionally, they feature half-sandwich complexes, like $Cp^*CeI_2(thf)_3$ (**20**). The latter complex was synthesized directly from CeI_3 and KCp* in thf, which is not possible for the chlorido homologue, possibly due to insufficient steric saturation of the ligand sphere of cerium(III).[52, 61-63] An identical motif can be found in complexes $Cp^{tBu}CeI_2(py)_3$ and $Cp''CeI_2(thf)_2$, which share the similarity of sterically bulky cyclopentadienyl ligands.[35, 64] Nevertheless, sandwich complexes are possible too, especially with bigger cyclopentadienyl ligands, *e.g.* $Cp^*_2CeI(NCCH_3)_2$ (**21(NCCH$_3$)$_2$**), which has been synthesized by Folting *et al.* in 1988 and investigated upon its luminescence behavior correlating luminescence energy and lifetime.[62] The same structural motif can be found in $Cp^*_2CeI(NCtBu)_2$, $Cp''_2CeI(thf)$ and $Cp^*_2CeI(do)$, with do = $C_3Me_4N_2$ (NHC) and phenanthroline as well.[35-37, 64] Also, dimeric structures are known, bridged via μ_2-iodido ligands and have been reported for complexes of the type **22** and **23**, starting from CeI_3 via salt-metathesis reaction with sterically bulky cyclopentadienyl ligands.[35, 38, 64] Another complex, containing the iodido ligand, is ethylene bridged permethylindenyl complex **24**, which has been synthesized in 2012 as the first example of an *ansa*-bridged indenyl cerocene.[65] The complex has been characterized by cyclic voltammetry as well, showcasing two irreversible events at +0.49 and +1.19 V vs

SCE.[65] In most cases, the halogenido complexes described above are used as precursors for further salt-metathesis reactions.

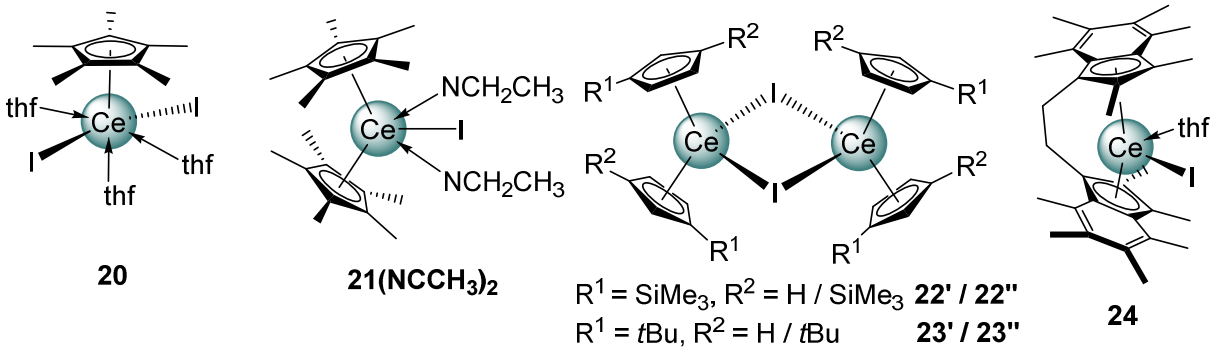

Scheme A4. Summary of cerium(III) metallocene complexes bearing iodido ligands. Structural motifs involve half-sandwich complex **20**, sandwich complex **21(NCCH$_3$)$_2$**, iodido-bridged species **22** and **23** as well as *ansa*-indenyl complex **24**.

2.3 Cerocene Hydride Complexes

The stabilization provided by the metallocene scaffold was displayed in 1991, when the first cerium "hydride" complex was synthesized and structurally characterized by Antipin *et al.* Utilization of tetradentate BH_4^- as a ligand and $[Cp^{tt}_2CeCl]_2$ with Cp^{tt} = 1,3-di-*tert*-butyl resulted in the dimeric structure **25** (Scheme A5), which features four μ_3 hydrogen atoms bridging the two cerium centers and the B atoms and interactions of the remaining hydrogen atoms with one cerium center each.[53] One year later, employing $LiAlH_4$ as a reagent, the hydrido-bridged complex **26** could be obtained, with Ce–H distances of 2.52 and 2.64 Å.[66] Other structural motifs of hydrido ligands are summarized in Scheme A5, such as the monomeric donor-stabilized sandwich complex $Cp^*_2CeH(thf)$ (**27**), which has been obtained by Heeres *et al*. in 1988 via degradation of the fully characterized alkyl complex $Cp^*_2CeCH(SiMe_3)_2$ at ambient temperature via C–H-bond activation. In 2017, it could be crystallized and X-ray crystallographically analyzed.[67-69]

A nonclassical approach was performed by Lappert *et al.* in 2000 by reaction of tris(cyclopentadienyl) cerium complexes with potassium and [18]-crown-6 resulting in the "exotic" complex **28**. Strikingly, one hydrogen atom solely bridges two cerium(III) centers to form an anionic complex with K([18]-crown-6)(tol)$_2$ as the counter ion. The targeted Ce(II) species could not be obtrained.[70-71] A polyhydride complex, exhibiting a tetrameric structure supported by the ligand $C_5Me_4SiMe_3$, was reported in 2011. The cluster formation occurred via hydrogenolysis of $Ce(C_5Me_4SiMe_3)(CH_2SiMe_3)_2(thf)$ with H_2 under loss of tetramethylsilane.[72] Several hydride complexes disguised in the form of borohydrido ligands

have been synthesized as well. For example, the sandwich complex **29** was accessed from the tetrakis-thf adduct of $Ce(BH_4)_3$ in 62% yield.[54] Under similar conditions the formation of the respective half-sandwich complexes could be observed too, such a dimeric $[Cp^RCe(BH_4)_2]_2$.[54]

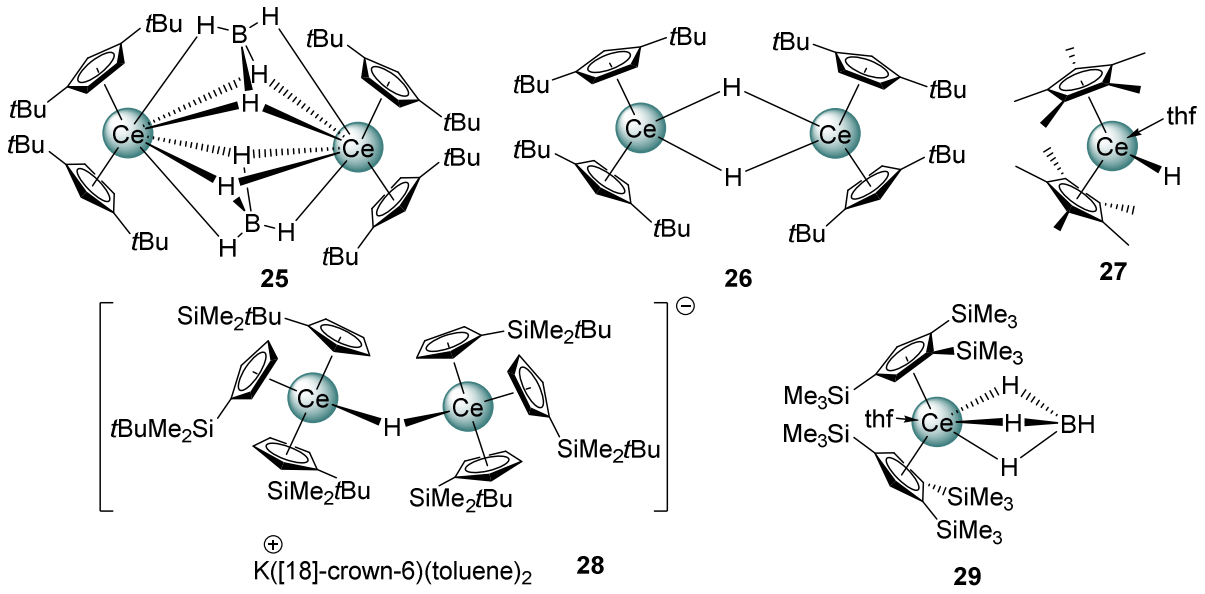

Scheme A5. Overview of realized cerium(III) metallocene hydrido complexes **25** to **29**, stabilized by the use of bulky cyclopentadienyl ligands.

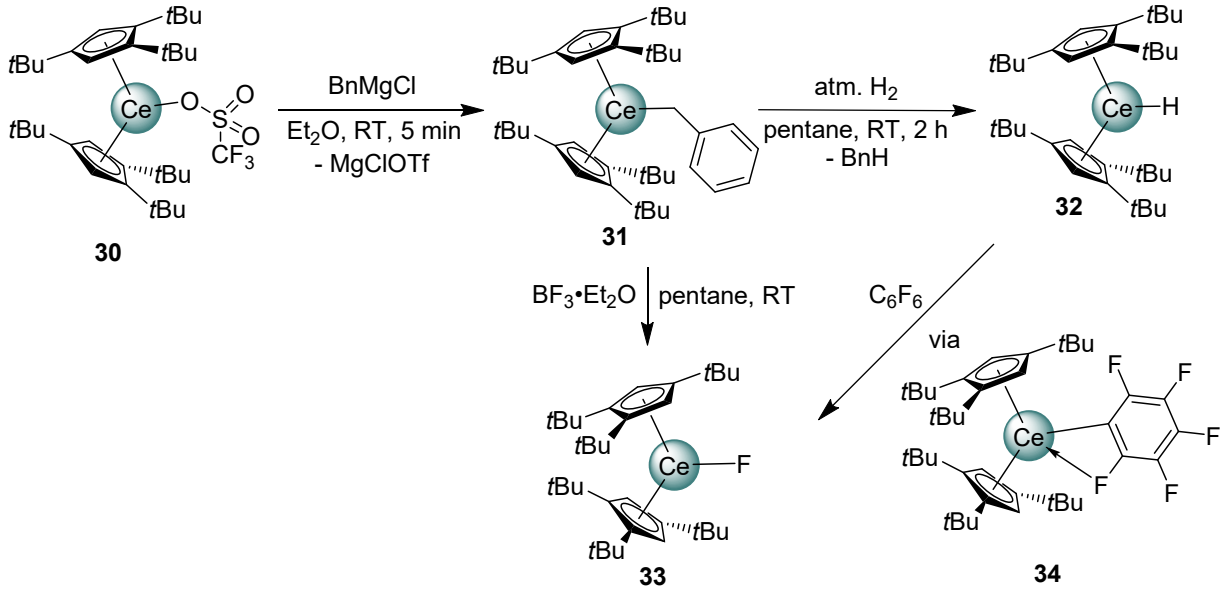

Scheme A6. Direct synthesis of bis(cyclopentadienyl) cerium(III) hydride (**32**) and fluoride (**33**) complexes, proceeding from triflate **30** over benzyl complex **31**. Conversion of **32** to **33** using C_6F_6 via intermediate **34**.

The pathway to the formation of a donor free terminal cerium hydride and fluoride as well is described in Scheme A6 and has been developed by Andersen *et al.* in 2005.[59] Starting from

the homoleptic triflate, the magnesium salt of the cyclopentadienyl ligand was used to form sandwich complex **30**, which was then converted to the benzyl complex **31**.[59] Complex **31** can be used as precursor to give the hydride **32** or fluoride **33** respectively in yields of 85% and 50%.[59] The reactivities of **32** and **33** have been examined extensively by Andersen *et al.* in ten publications since 2005.[58-60, 73-80] Additionally, the conversion of **32** to **33** by reaction with C_6F_6 has been shown, initially forming intermediate **34**, which could be crystallized and decomposed to **33**, H_2 and tetrafluorobenzyne.[59] The hydrogen for fluorine exchange of **32** was shown for $CH_{4-x}F_x$ as well, while the reaction with CO featured insertion and formation of *cis*-enediolate bridged complex **35(*cis*)**, which undergoes isomerization to *trans*-complex **35(*trans*)** at 100 °C over 7 months.[58-60, 73] The reaction of **32** with CO in pentane resulted in oxomethylene bridged complex **36**.[73] Reactions of **32** with CH_3X with X = Cl, Br, I, OMe, OEt, O-*n*Pr, O-*n*Bu and Otf gave complexes of the type Cp^R_2CeX with R = 1,2,4-*t*Bu under release of methane. The triflate complex **37** is depicted in Scheme A7.[74-75, 77, 79] Additionally, complex **32** is active in the hydrogenation of pyridine to piperidine.[80] The reactivities were supported by DFT calculations regarding the respective pathways of H/F exchange or alkane elimination respectively.[58-60, 73-75, 77-80]

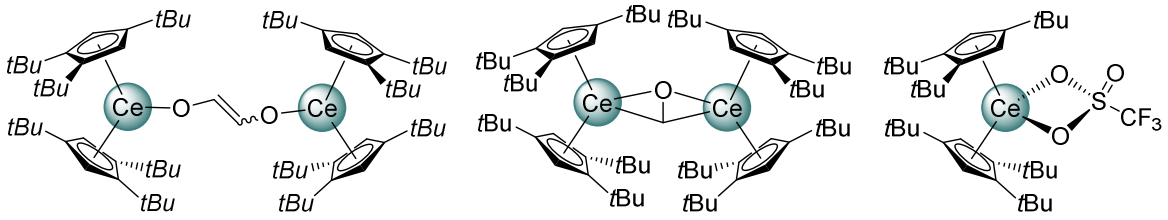

cis/*trans*: **35(*cis*) / 35(*trans*)** **36** **37**

Scheme A7. Reaction products of Cp^{ttt}_2CeH (**32**) with CO, **35** and **36** as well as CH_3OSOCF_3 **37** by means of methane elimination.

2.4 Cerocenes Containing Anionic Oxygen, Sulfur or Selenium Ligands

While the implementation of hydrido ligands triggers further reactivities and the access to a new synthesis route via methane or dihydrogen elimination, anionic oxygen coligands mainly serve the purpose of stabilization of the oxophilic cerium center. Protonolysis reactions are known for homoleptic Ce(O*i*Pr)$_4$, but mainly conversions to different alkoxy or carboxylato ligands have been performed.[81-86] For a wider substitution range usually the employment of cerium amide or silylamide complexes is preferred. In various cases the easily accessible homoleptic triflate Ce(OTf)$_3$ or ceric ammonium nitrate (CAN) could be used as reactants for ligand exchange as well *e.g.* for cyclopentadienyl ligands.[23, 58, 87-88] Similarly, the synthesis of the half-sandwich aryloxy complex **38** proceeded from tris(2,6-di-*tert*-butylphenoxo)cerium by reaction with LiCp*.[89-91] Decrease of the steric bulk by switching to alkoxy ligands, led to

dimeric structures like **39**, which show one terminal and one bridging μ_2-alkoxy ligand for each cerium center.[92] The same structural motif was revealed by the solid-state structures of the respective sandwich complexes of **40** and **41** with bridging *iso*-propoxy or methoxy ligands each, although the synthesis pathways differ largely. While compound **39** was prepared from $Cp^*_2Ce[CH(SiMe_3)_2]$ by reaction with *tert*-butanol, and **40** by reacting Cp^{tBu}_3Ce with HO*i*Pr, complex **41** was obtained by treating the respective tris(cyclopentadienyl) complex Cp^{tt}_3Ce with metallic lithium or potassium and dme.[30, 67, 92-93] The latter route was revisited in 2017 for the formation of $[Cp'_2Ce(\mu_2\text{-}OMe)]_2$, which could not be accessed from crown ether supported cerium complexes formally in the +2 oxidation state.[94] Another comparable complex was synthesized by the reaction of bipyridyl complex **67** (Scheme A12) with benzophenone to yield dimeric **42** with a bridging dialkoxy ligand in a radical pathway.[95]

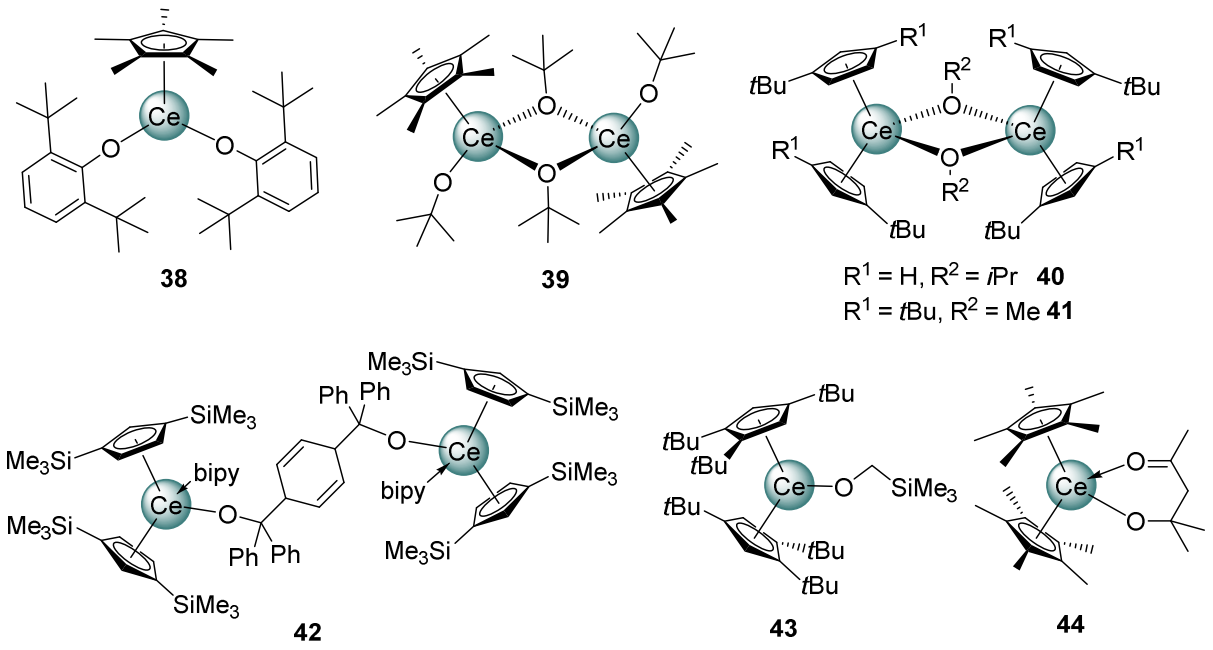

Scheme A8. Cerium(III) metallocene complexes bearing anionic oxygen ligands; mostly alkoxy substituents. Coordination spheres range from monomeric to dimeric sandwich and half sandwich complexes.

Increase of the steric bulk of the cyclopentadienyl moiety also accomplished monomeric complexes, as displayed by **43**, or by **44**, where the donating ability of an intrinsic carbonyl moiety stabilizes the cerium center.[75, 96] Starting from $Cp^{ttt}Ce(CH_2Cp^{tt})$ the reaction with $MeOSiMe_3$ yielded the former complex **43** via a [1,2] silyl-Wittig rearrangement, while treatment of the hydrido species Cp^{ttt}_2CeH with $MeOSiMe_3$ gave the respective methoxy deriviative $Cp^{ttt}_2Ce(OMe)$.[75] Aldolate complex **44** was formed by reaction of alkyl $Cp^*_2Ce[CH(SiMe_3)_2]$ with acetone by hydrogen transfer, whereas more bulky ketones like di-*tert*-butyl ketone did not react.[96] Other structurally characterized oxygen-donating ligands

include triflate complex $Cp^*_2Ce(bipy)(OSO_2CF_3)$, which only exhibits mono-coordination of the triflato ligand in contrast to donor-free complex **37** and alkoxycarbene stabilized complexes, *e.g.* **45** (Scheme A9) reported by Love *et al.*[97-98] Complexes bearing the dianionic oxy ligand were obtained via oxidation − and in most cases as side product −, for example in 1995 by ether activation of a cerium hydride to form **46(thf)** by Evans *et al.* or formation of **47** by Ephritikhine *et al.*[42, 99-100] Again, different structural motifs are realized depending on the sterical bulk of the Cp ligand. Whereas Cp* prefers the formation of dimeric structures (**46**), Cp' seems to favor the trimeric species featuring a six fold ring with alternating cerium and oxygen atoms.[42, 99] The possibility of small molecules brigding between sandwich moieties, can be used to synthesize the respective sulfite or carbonate structures as well in the form of $[Cp^*_2Ce]_2(CO_3)$ or $[Cp^{ttt}_2Ce]_2(SO_3)$.[69, 79] The former could be synthesized via an intermediate oxo-complex by reaction of dimeric $[Cp^*_2CeH]_2$ with CO_2.[69]

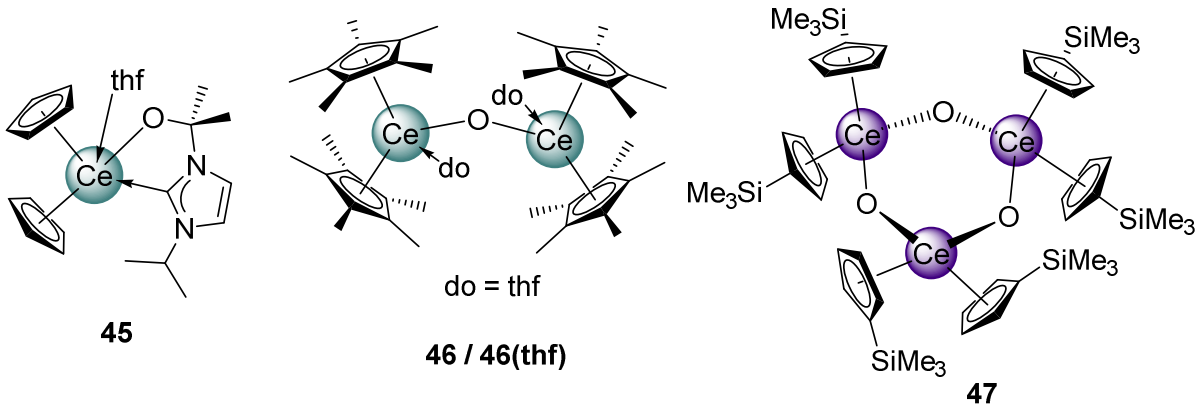

Scheme A9. Cerium(III) metallocene complexes bearing anionic oxygen ligands: alkoxycarbene **45** and oxygen bridged sandwich complexes of Ce(III) (green) **46** and Ce(IV) (purple) **47**.

When employing softer sulfur ligands no simple monomeric half-sandwich complex could be isolated, but instead the formation of dimeric structures as displayed in Scheme A10. The first cerocene complexes containing anionic sulfur ligands, $[Cp^{tBu}_2Ce(\mu_2\text{-}SR)]_2$ with R = *i*Pr (**48**) and Ph, were synthesized in 1990 by Zalkin *et al.* by reaction of Cp^{tBu}_3Ce with the respective thiols analogous to the reaction with alcohols.[30] A similar structural motif can be seen for **49**, which does not show a coordination of the NMe_2 moiety, but instead also forms a dimer via the sulfur atom.[101] Structurally similar, thiophenolato-coordinated complex **50** was synthesized by another protocol applying the sterically bulky Cp^*_3Ce as precursor and reacting it with PhSSPh, which was also feasible for PhSeSePh in the case of lanthanum.[102] Additionally, the incorporation of sulfur or selenium was possible as well to form **51** and **52**

by the reaction of alkyl $Cp^{tt}_2Ce(CH_2Ph\text{-}NMe_2)$ with the elemental chalcogens sulfur and selenium. Similar products were obtained by the oxidation of thiolate **49** or its selenium analogon.[103] As seen in complexes **53** to **55**, any dimeric arrangment can be omitted in the presence of [18]-crown-6 to form separated ion pairs with monomeric anionic cerium moieties and crown ether stabilized alkali metal counter-ions.[104-105] All these complexes have been studied in comparison with their uranium(III) homologues by Ephrikitine *et al.* to gain insight into the differences in bonding between lanthanide(III) and actinide(III) complexes.[35, 37, 104-105] Dithiolene complex **54** revealed that the contraction of the M−S bond, when changing from Ce to U, relates to the larger 5f-orbital mixing in contrast to the cerium 4f-orbitals, resulting in enhanced covalency for the actinide complexes.[104] Utilization of the 2-mercapto benzothiaziolato ligand in **55** led to a half-sandwich complex. [105] The synthesis starts from $Ce(BH_4)_3(thf)_3$ as well as KCp* and 2-mercapto benzothiazolthiolato potassium salt in a ratio of 1:3, resulting in the ate complex, which could be separated using [15]-crown-5.[105]

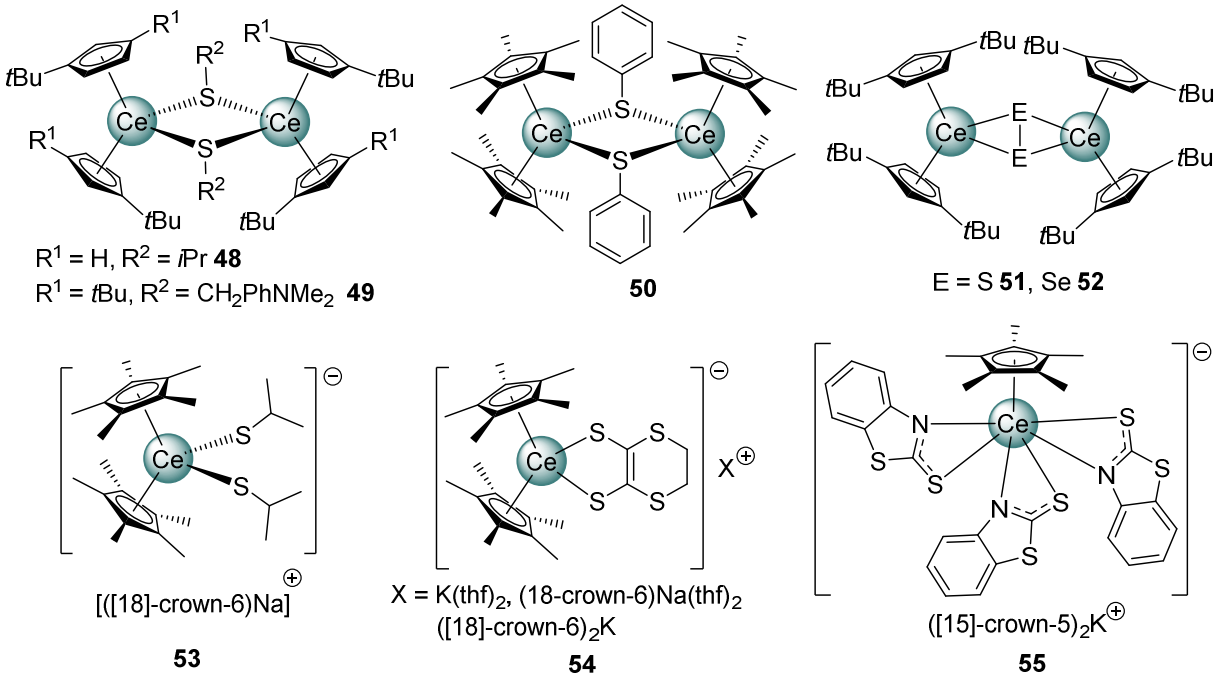

Scheme A10. Cerium(III) metallocene complexes bearing anionic sulfur ligands as thiolates (**48** to **50** and **53**) or bridging di-sulfido or di-selenido (**51** and **52**). Pseudo-tetrahedral coordination in **53**, **54** and **55** is accomplished via abstraction of the respective alkali metal cation by [18]-crown-6.

2.5 Cerocenes Containing Anionic Nitrogen Ligands

In the literature many cerocene amide complexes have been reported. Likely, the half-sandwich complex Cp*Ce(btsa)$_2$ (**56**) (btsa = bistrimethylsilylamide, N(SiMe$_3$)$_2$), obtained in 1989 using the aryloxide complex **38** as a precursor, represents the first example (Scheme A11).[89] The same reaction pathway using a lithium alkyl instead led to the alkyl species **57**. This complex seems to be an active catalyst for ethylene polymerization, but not propylene.[89] Complex **56** shows ligand rearrangement processes in solution resulting in mixtures of homoleptic Ce(btsa)$_3$ and Cp*$_2$Ce(btsa) (**58**). The latter complex could be synthesized by our group in 2017 starting from Cp*$_2$CeCl$_2$K(thf)$_2$ (**10(thf)**) and Kbtsa.[56, 64, 89] Interestingly, the homologous bis(dimethylsilyl)amide complex **59** shows twoY---Si–H β-agostic interactions, while the respective carbon analogon Cp*$_2$Ce(N*i*Pr$_2$) (**60**) does not engage in similar secondary interactions.[56] Scheme A11 shows a synopsis of cerium metallocene complexes containing nitrogen ligands, featuring a multitude of differently substituted sandwich complexes Cp*$_2$Ce(NR$_2$) (**60** and **61**).[56, 106] The majority was synthesized by Anderson *et al.* in order to research the thermal rearrangement of amides to the corresponding enamides **62** under H_2 or CH_4 release. Such reactions occur through β-H or Me elimination upon applying 160-180 °C on solid material for one or two weeks.[106] The relatively high activation barrier is caused by the siginificant geometrical changes during the two-step elimination process.[106] Incorporation of the tetramethylpyrrolato ligand was performed via reaction of Cp*$_2$Ce(BPh$_4$) with the potassium pyrrolate salt to yield **63**, readily available for other rare-earth and actinide metals as Y, Sm and U as well.[107] The compounds were synthesized in order to yield MCp*$_3$ with one Cp* bound in η^1 fashion to get a pseudoalkyl compound. The structure shows additional side arm pseudo η^3 coordination via N, ring and methyl carbon next to the metal.[107] Although benzyl complex **64** is not primarily connected via an amido nitrogen, the NMe$_2$ donor group acts as a stabilizing moiety for one of few structurally characterized cerium alkyl species.[56] In 2019, the reactivity of the Cp^{tt} homologue of **64** was tested resulting in the insertion of benzonitrile (**65**), carbodiimide or isothiocyanates as well as elemental chalcogens (**51**, **52**) showcasing its large reactivity scope.[101, 103]

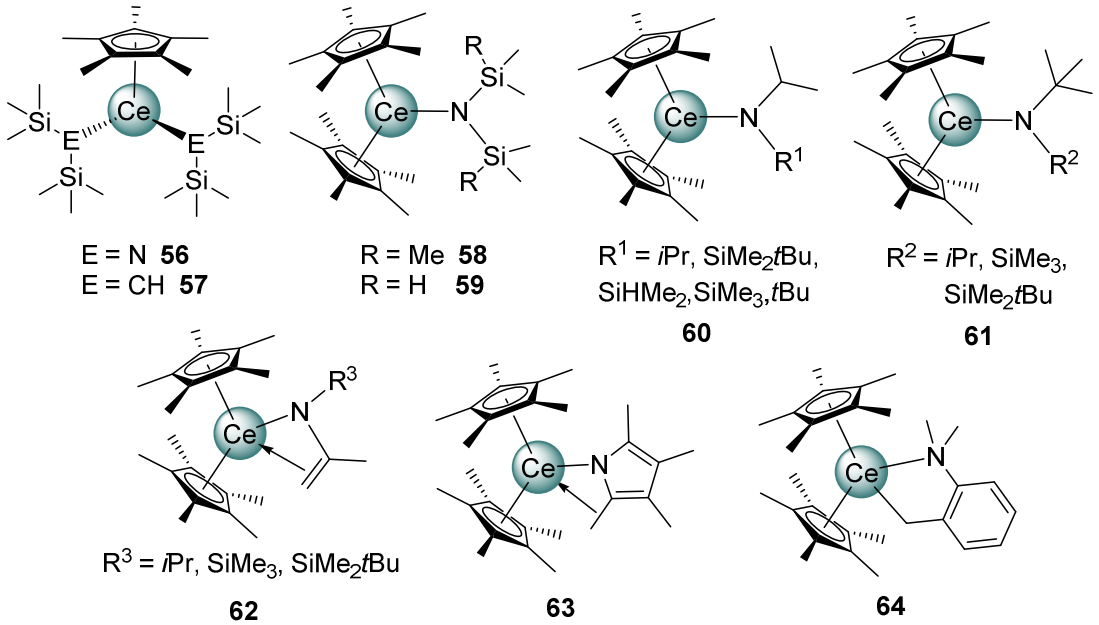

Scheme A11. Synopsis of cerium-metallocene complexes containing anionic amide and silylamide ligands. Complex **64** represents one of the rare examples of a cerium metallocene alkyl complex, in this case stabilized by the donation of the amino moiety.

In 2008, Rheingold *et al.* synthesized a series of metallocene complexes using a terminal bidentate ligand to form **66** (Scheme A12) and its Sm and Y analogues, employing allyl complex **11(thf)**.[108] More recently, in 2017 a series of 2,2'-bipyridyl complexes (**67** and **68**) were synthesized by reaction of metallocene iodido complexes with KC_8 in the presence of 2,2'-bipyridine, to gain insight into lanthanide-radical magnetic interactions [95] The complexes act as selective reducing agents, as revealed by the head-to-tail coupling of benzophenone. Further to this, magnetic measurements, cyclic voltammetry, and quantum mechanical calculations showed that the complexes consist of a Ce(III) ion and a bipyridyl radical anion.[95]

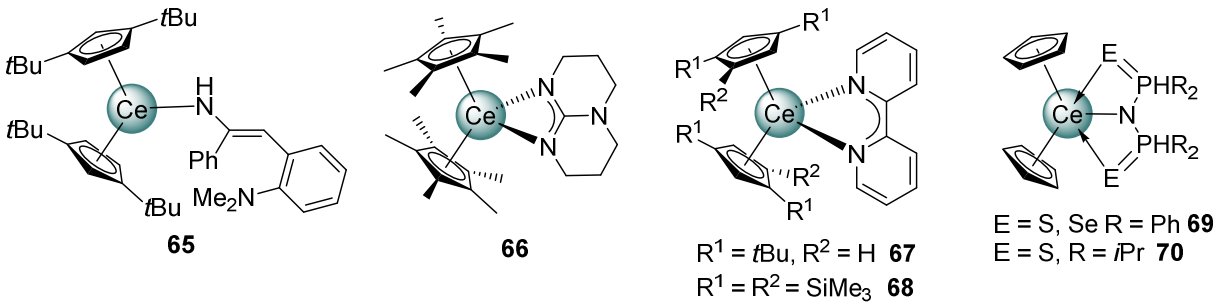

Scheme A12. Selection of further interesting anionic nitrogen based ligands in the form of the respective cerium metallocene complexes **65** to **70**.

Another interesting ligand type has been employed by Ibers *et al.* in case of the functional imido-diphsophino-dichalcogenidos resulting in **69** and **70** via protonolysis reactions. Such complexes show a η^3 coordination involving two chalcogen atoms and one N atom.[109] The ^{31}P signals for all three compounds shifted drastically to lower frequencies in comparison to the diamagnetic Y, La and Yb(II) congeners.[109] Corrole complex **71** was studied with respect to the clustering behavior of anionic cerium(III) corrole complexes, which show a controllable aggregation behavior of oligomers to monomers depending on the capping ligand used.[110] Sodium cyclopentadienide usage led to polymeric structures, while tris(pyrazolyl)borato ligands generated a dimer, but contrarily the depicted complex **71** shows a monomer by encapsulation of the counter ion.[110] Similarly to chalcogen ligands the simple bridging motif **72** is possible, too. The incorporation of cyanido ligands resulted in a trimeric structure, sterically saturated by sandwich metallocene moieties for **72** and **73**.[42, 111] The first characterized dinitrogen complexes of cerium **72** have been synthesized by reaction of Cp^{tet}_3Ce or $Cp^*_2Ce(BPh_4)$ with KC_8 in a dinitrogen atmosphere.[42] By using $^{15}N_2$ in the reaction, the characterization was also possible by ^{15}NMR spectroscopy.[42] Trimeric cyanide complex **73** could be approached by reaction of Cp^*_2CeI with ammonium cyanide in the presence of acetonitrile, which could also be replaced by *t*BuCN.[111]

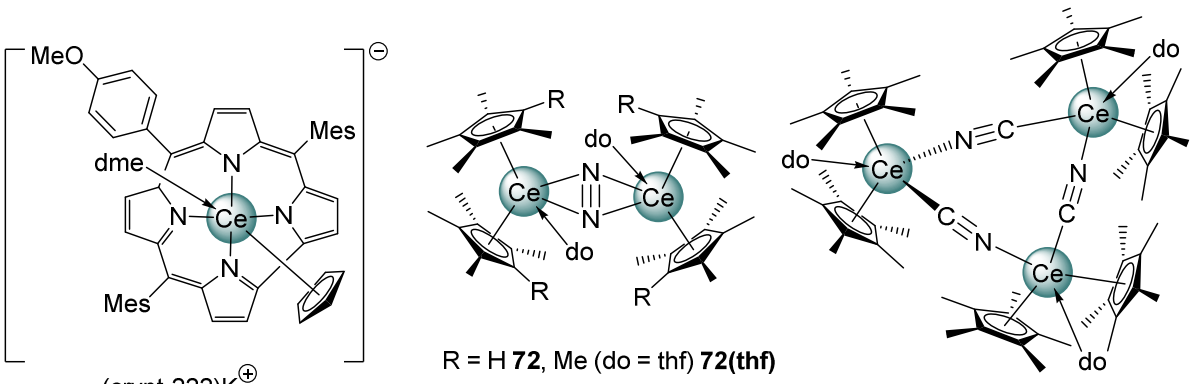

Scheme A13. Depiction of corrole complex **71** and dimeric dinitrogen **72** as well as trimeric cyanide **73** bridged cerium(III) sandwich complexes.

2.6 Other Cerium Cyclopentadienyl Complexes

In 2015 Evans *et al.* discovered a possibility to access the formal +II oxidation state in molecular cerium compounds via reaction with KC_8 in the presence of the [2.2.2]-cryptand in order to separate the potassium cation.[31, 112-114] This procedure proved successful for other rare-earth metals as well and was first conducted with Cp' as a ligand to form intensely colored black/purple complex **74** (Scheme A14). These complexes enable a direct comparison of both +II and +III oxidation states in the same coordination environment.[112-114] The additional electron, switching from +III to +II, was placed in a 5d orbital in the case of cerium in contrast to the rare-earth metals in the traditional +II oxidation state like Eu or Sm, where it can be found in the 4f orbitals. When Cp''_3Ce is reacted with KC_8 and cryptand in benzene, instead a bridiging $[C_6H_6]^{1-}$ moiety was included in between two sandwich metallocene Ce(II) centers.[114] Cerium(II) complexes can be used as reductants, which has been investigated for biphenyl and naphthalene, where the biphenylido and naphthalenido dianions form directly Ce(III) complexes.[112, 114-115] Interestingly, reaction of **74** with cyclooctatetraene led under ligand rearrangement to pseudo-tetrahedrally coordinated complex **75**, among other products

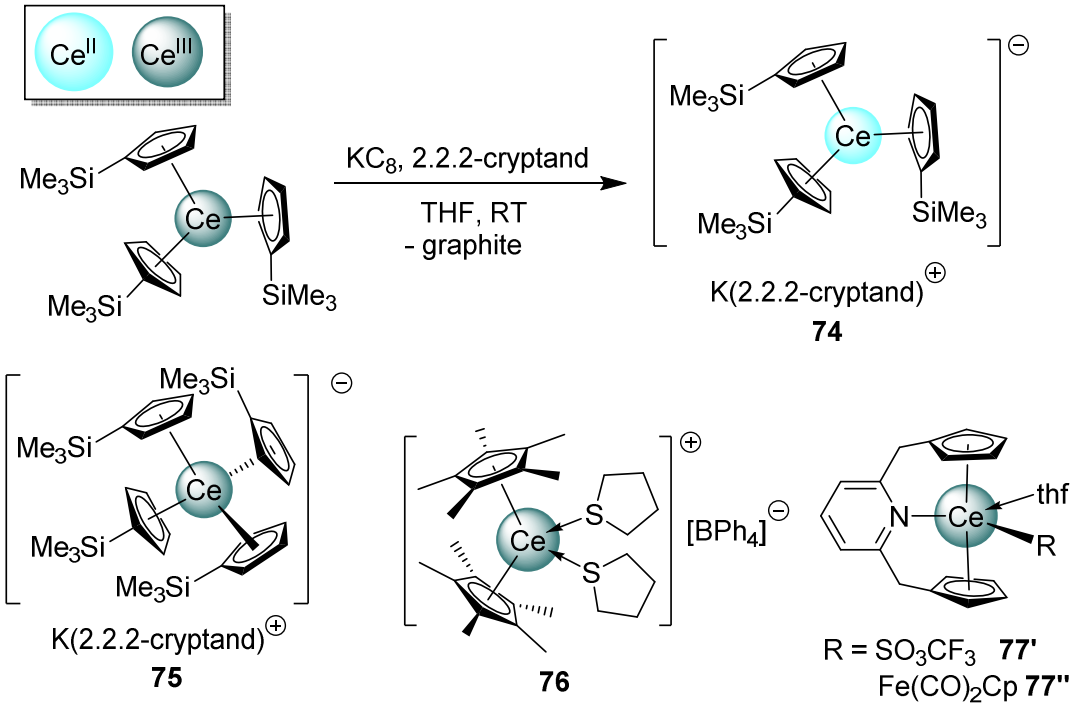

like K(2.2.2-cryptand)Ce(COT)$_2$.[51]

Scheme A14. Summary of interesting and unusual cerium cyclopentadienyl complexes, featuring a Ce(II) derivative, stabilized by the 2.2.2-cryptand (**74**). Additionally, the unique example of a tetra(cyclopentadienyl)-supported cerium complex, although forced with the aid of cryptand still in the trivalent oxidation state (**75**). Complex **76** represents a separated ion pair containing the "naked" $Cp^*_2Ce^+$ moiety. By the means of linking two cyclopentadienyl ligands **77** portrays incorporation of an iron moiety.

Another exceptional finding was the synthesis of the solvent-separated ion pair $[Cp^*_2Ce(do)_2][BPh_4]$ in 1991, which is depicted in Scheme A14 for do = tetrahydrothiophene (**76**), but possible for thf as well, by reaction of $Cp^*_2Ce[CH(SiMe_3)_2]$ with triethylammonium tetraphenylborate.[116] The complex could later be synthesized donor-free, by using the respective allyl derivative, involving the "naked" metallocene moiety $Cp^*_2Ce^+$.[48] Complex **77"** features a rare example of a bimetallic complex, combining d-block and f-block metals by incorporation of a $Fe(CO)_2Cp$ monoanionic moiety.[117] This is realized by a pyridine-bridged tridentate dianionic cyclopentadienyl pincer ligand (L), via the intermediate triflate complex LCeOTf **77'**.[117] The Ce−Fe bond in complex **77"** was analyzed by ^{57}Fe Mössbauer and IR spectroscopy as well as computational analyses, showing highly ionic contributions and a weaker Fe to Ce electron-donation than in the respective Dy complex.[117]

2.7 Cerium(III) Cyclooctatetraenyl Complexes

Dianionic cyclooctatetraenyl $C_8H_8^{2-}$ (COT) represents another cyclic aromatic hydrocarbon ligand, which is used in cerium metallocene chemistry. Although COT is at first sight comparable to the cyclopentadienyl ligand, its chemistry and derived complexes show remarkable differences, most of which are caused by the sterically larger cycle as well as its dianionic charge. Common trivalent cerium COT complexes are depicted in Scheme A15 in combination with ligand substitution patterns and counter ions. For example, $(COT)_2CeNa(thf)_3$ (**79**) shows η^8 coordination of the two COT ligands, which are arranged in a coplanar fashion and a sodium counter ion which is pseudo tetrahedrally coordinated invoving three thf molecules and a COT ligand.[118] Complexes **78** to **81** were synthesized from $CeCl_3$ by salt metathesis reactions with COT alkali-metal salts, and the pathway to **80** includes salt metathesis starting from half-sandwich complex **83**.[118-124] Additionally, the reaction can be started at tetravalent $Ce(IV)(COT)_2$ ("cerocene") by reduction with alkali metals.[125]

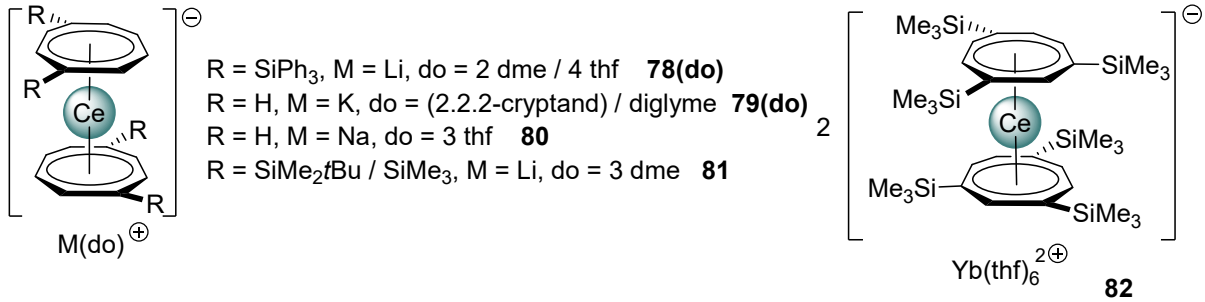

Scheme A15. Summary of substituted trivalent cerocene ate complexes **78** to **82**. Counter ions include mainly alkali metals and in the case of **82** divalent Yb.

In 1999 Edelmann *et al.* reported the synthesis of heterobimetallic complex **82**, which shows a separated ion pair, consisting of two anionic cerocene moieties and one $Yb^{2+}(thf)_6$ cation, which could be synthesized by reacting the $SiMe_3$-substituted cerocene with metallic Yb.[126] In addition to $KCe(COT)_2$ in 1970, Streitwieser *et al.* synthesized the first half-sandwich COT complex in the form of dimeric **83**. The two metal centers in **83** are bridged in a common motif by two μ_2-chlorido ligands, which can be further employed in salt metathesis, and sterically saturated by two thf molecules each.[121, 127-128] When $Ce(OTf)_3$ is used as a precursor the reaction leads to the same structural motif yielding $[(COT)Ce(\mu_2\text{-}OTf)(thf)_2]_2$ which can be used as precursor in a variety of reactions to form heteroallyl, aryloxy, and alkyl complexes.[129-131] The reaction can also be used to form asymmetric COT cyclopentadienyl complexes, which has been shown in 1974 as well by Takats *et al.* to form (COT)CeCp.[130, 132] By reaction of complex **74** with cyclooctatetraene complex **85** was obtained among other ligand scrambling products. **85** shows an asymmetrically substituted cerium(III) anionic entity in combination with a potassium counter ion, in contrast to Th, which results in the tetravalent complex under the same reaction conditions.[51] In 1989, an interesting pathway to monomeric half-sandwich complex **86** was discovered by Takaya *et al.*, via reaction of cerium metal with cyclooctatetraene in the presence of elemental iodine.[133]

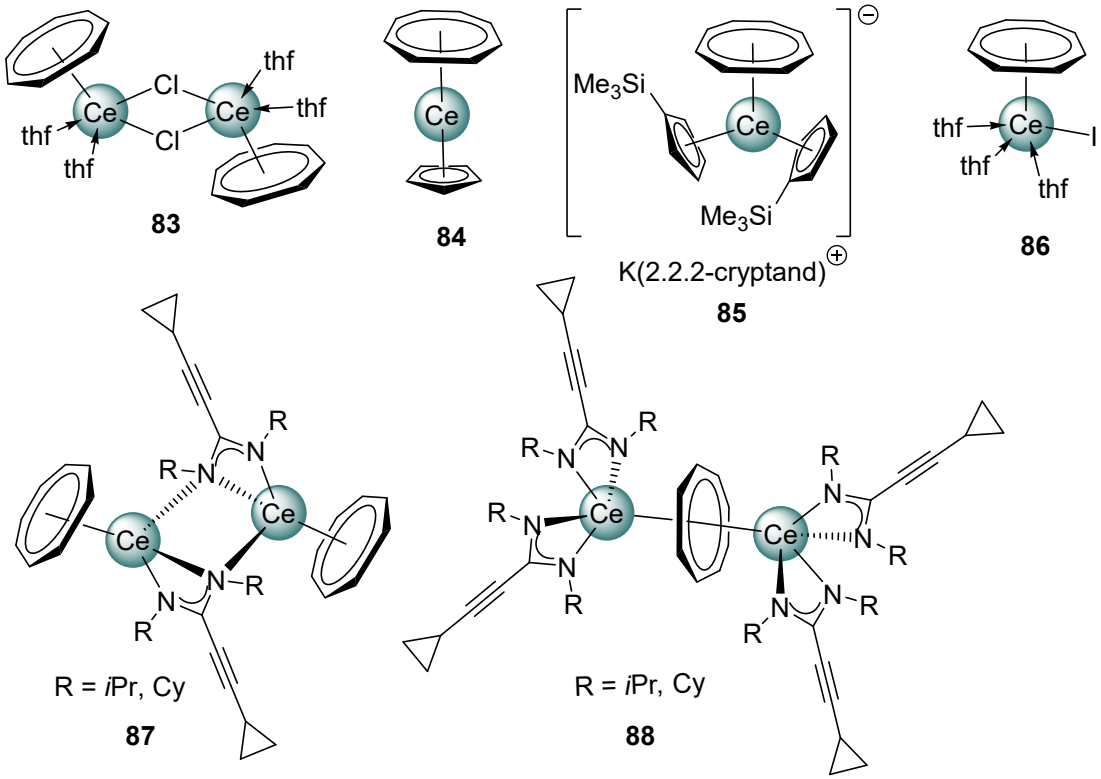

Scheme A16. Synopsis of realized trivalent cyclooctatetraenyl-supported cerium complexes **83** to **88**, including asymmetric cyclooctatetraenyl and cyclopentadienyl bearing complexes **84** and **85**. Interestingly, the cyclooctatetraenyl ligand can trigger the formation of inverse sandwich complexes (**88**).

The comparison between structures **87** and **88** showcases another bonding motif of COT by acting as a bridging two-electron ligand involving two cerium centers with η^8 coordination in an inverse sandwich complex.[134] This can be realized by different reaction conditions: whereas **87** is formed in a one pot reaction of $CeCl_3$ with the respective alkali-metal ligand salts, **88** is synthesized in a controlled manner by starting from an isolated chlorido-bridged alkylethynyl-amidinate complex.[134]

Cerium(IV) Cyclopentadienyl Chemistry

3.1 Early Cerium(IV) Complexes

Due to the access of the noble gas configuration in the +4 oxidation state, cerium forms exceptionally stable tetravalent complexes in contrast to the other rare-earth metals, which remain predominantly in their most stable +3 oxidation state. As hard Lewis acids, rare earth metal cations show a great oxophilicity and due to their frontier orbitals being relatively close to the core the bonding character is drastically different from d-block metals, thus showing mostly ionic bonding and very weak ligand field effects. As a consequence, early cerium(IV) chemistry started with highly electronegative ligands such as oxygen or nitrogen donors and readily available compounds like ceric ammonium nitrate or hexachlorocerates as precursors. The first organometallic cerium(IV) complexes were claimed by Kalsotra *et al*. by reacting $(pyH)_2[CeCl_6]$ with NaCp or NaInd to afford tetrakis(cyclopentadienyl) or indenyl cerium respectively.[135-136] Nevertheless, the products were analyzed solely by elemental analyses and IR spectroscopy and in combination with atypical chemical behavior, like solubility in concentrated nitric acid and stability against alcohols, water, air and dilute acids, which are properties, which no authentic organometallic cerium(IV) complex up-to-date possesses, they arose suspicion.[135-137] The group of Kalsotra *et al.* reported a multitude of other metalorganic complexes, which could not be reproduced and led to the refutation by Deacon *et al.* in 1983, showing that trivalent cerium(III) complexes were formed instead.[135, 137-142]

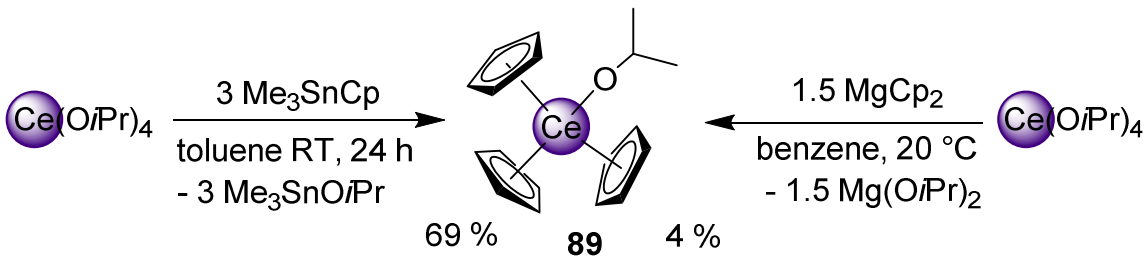

Scheme A17. First synthesis of a tetravalent cerium(IV) cyclopentadienyl complex (**89**) (right) and its improved synthesis (left) changing the cyclopentadienyl transfer reagent.

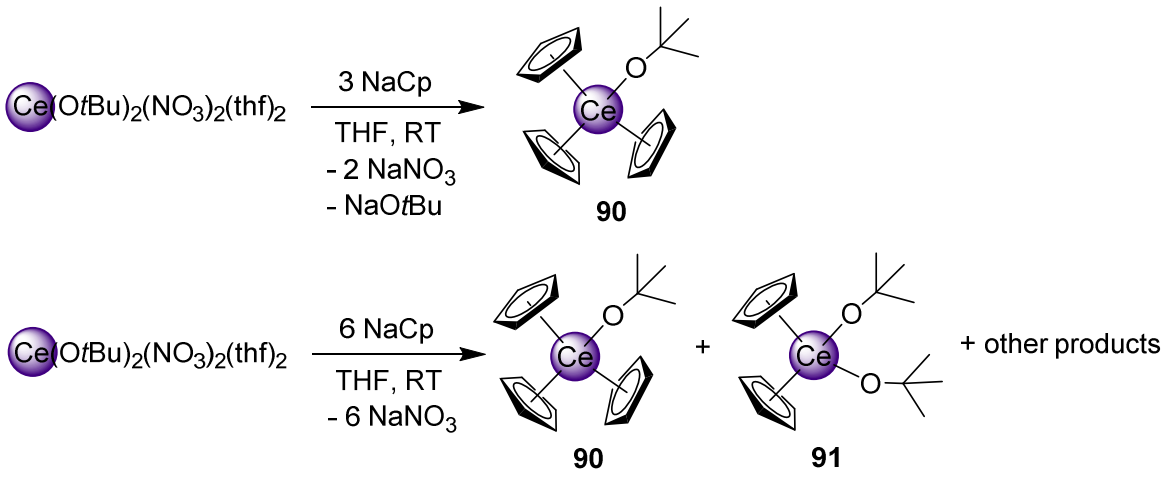

Scheme A18. Synthesis of *tert*-butoxy-substituted cyclopentadienyl cerium(IV) complexes **90** and **91**, starting from CAN, the latter synthesis resulting in a mixture of tris and bis(cyclopentadienyl) cerium(IV) complexes.

The first authentic cerium(IV) cyclopentadienyl complex (**89**) was synthesized by Greco *et al.* in 1976 by the reaction of tetravalent Ce(O*i*Pr)$_4$ with magnesocene to form tris(cyclopentadienyl) cerium alkoxide complex **89** in 4% yield, but showed that sublimation of the thermally remarkably stable product is possible (Scheme A17).[125] By switching the cyclopentadienyl-transfer reagent from magnesocene to non-reducing Me$_3$SnCp the synthesis was later improved by Gulino *et al.*, increasing the yield to 69%.*[143]* Ceric ammonium nitrate (CAN) was later used by Evans *et al.* as a tetravalent precursor to form the homologous *tert*-butoxy complex **90**.[87] Additionally, the same group showed that use of excess of sodium cyclopentadienide did not yield the homoleptic tetrakis(cyclopentadienyl) cerium(IV) complex, but instead a mixture of the tris and bis(cyclopentadienyl) complexes **90** and **91** along with other ligand scrambling products (Scheme A18).[87] For better visibility, in the schemes the respective oxidation state is emphasized by a green sphere for cerium(III) and a violet sphere for cerium(IV) complexes. To this date tetrakis(cyclopentadienyl) cerium(IV) has remained elusive, and the only tetrakis(cyclopentadienyl)-ligated complex known is ion pair separated [Cp'$_4$Ce][K(2.2.2-cryptand)] (**75**). The formation of **75** is forced by usage of the [2.2.2]-cryptand, but it could not be oxidized so far.[51] While sandwich complex **91** could not be isolated or crystallized, the application of the same synthesis route with larger cyclopentadienyl ligands, like mono or bis(trimethylsilyl)-substituted Cp' or Cp'', proved successful more than 25 years later to yield **92**.[144] Starting in the tetravalent oxidation state drastically limits the scope of substitution, as the precursor dictates the alkoxy ligand and few variations are possible. Additionally, the cyclopentadienyl ligand can be altered only marginally before structural changes in the products occur, *e.g.* by ligand redistribution. This can be circumvented by using trivalent cerium precursors in combination with oxidation agents.

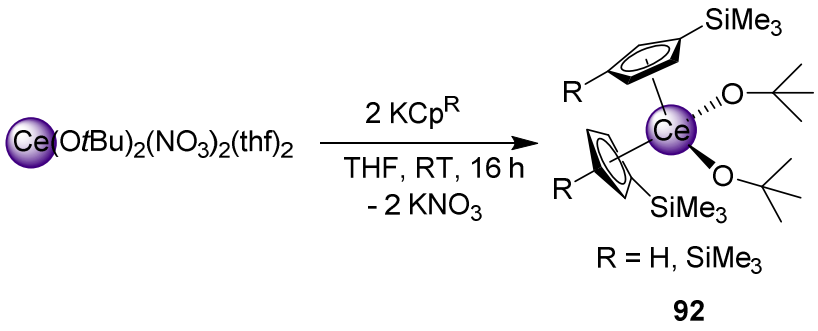

92

Scheme A19. Synthesis of tetravalent sandwich complexes **92**, initially starting with tetravalent CAN.

3.2 Oxidative Approach to Cerium(IV)-Cyclopentadienyl Complexes

The first oxidative approach on tetravalent metallorganic cerium(IV) complexes was performed by our group in 2010, by utilization phenyliodine(III) dichloride $PhICl_2$ as oxidant.[145] The hypervalent organoiodine reagent was employed in combination with $Ce[N(SiMe_3)_2]_3$ and most importantly Cp_3Ce in toluene to yield the respective chlorinated products $Ce[N(SiMe_3)_2]_3Cl$ and tris(cyclopentadienyl) cerium(IV) chloride Cp_3CeCl (**93**) in 57% yield, which is depicted in Scheme A20.[145] The oxidation reaction to **93** was accompanied by an immediate color change from yellow to black and the electronic state could be easily tracked via ^1H NMR, which changed from a broad paramagnetic signal at 2.22 ppm to a sharp diamagnetic signal at 4.74 ppm.[145]

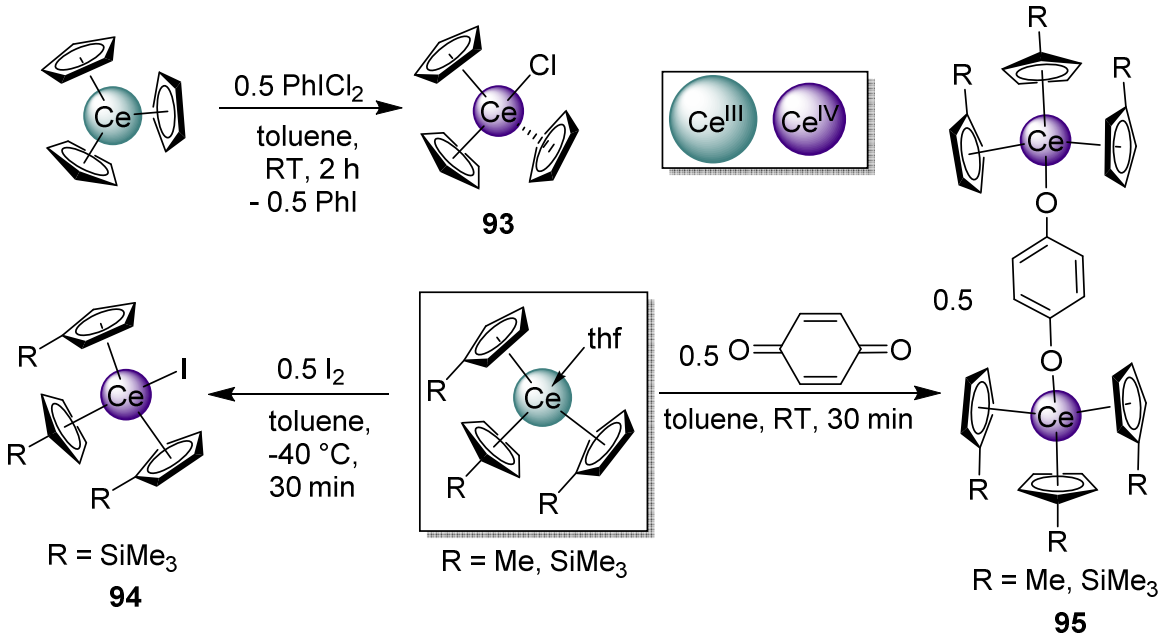

Scheme A20. Synthesis of tetravalent cyclopentadienyl complexes from trivalent derivatives using oxidation agents common in cerium(IV) chemistry like iodobenzene dichloride, elemental iodine, and *para*-benzoquinone; complexes **93** to **95** bear halogenido ligands or a briding quinolate moiety.

The promising oxidative approach was used again in 2017 by our group, but different oxidation agents were used this time, as the work-up procedure to separate PhI might be difficult. As precursors methyl- und $SiMe_3$-substituted cyclopentadienyls Cp^{Me} and Cp' were used to form darkly colored tetravalent cerium(IV) complexes **94** by reaction with elemental iodine, while the dimeric **95** features a dianionic hydroquinolato linker.[38] In contrast to the trivalent complexes the smaller ionic radius of cerium(IV) in combination with an additional anionic ligand leads to monomeric complexes and bifunctional reagents like benzoquinone is essential to form dimeric structures.[38] Complex **94** showed ligand reorganization processes to yield $[Cp'_2CeI]_2$ and other trivalent species as side products, when performing the reaction at ambient temperature instead of −40 °C.[38] Thus, the oxidation with hexachloroethane depicted in Scheme A21, resulting in the respective chloride complexes **96** in 68 to 71% yield, proved superior. In the following, **96** was employed in a salt-metathesis reaction with KO*t*Bu to further elucidate any derivatization chemistry.[38] As only minor side products and no scrambling to trivalent cerium species was observed, this oxidative route was used later in this work as a foundation for investigating into the chemical and electrochemical stability of the tetravalent cerium(IV) center depending on its chemical environment.

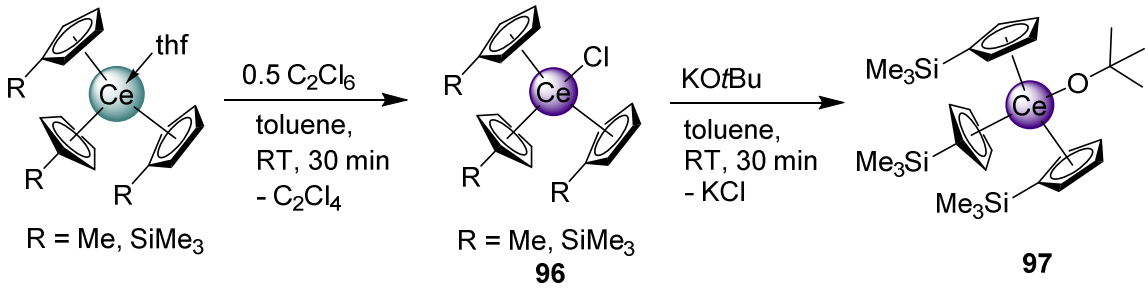

Scheme A21. Utilization of hexachloroethane as an oxidation agent by formation of tris(cyclopentadienyl) cerium(IV) halogenide complex **96**, which can be further employed in salt-metathesis reactions, *e.g.* with potassium *tert*-butoxide to complex **97**.

3.3 Cerocene

In 1976, tetravalent bis(cyclooctatetraenyl) cerium(IV) ("cerocene", **98**) was synthesized by Greco *et al.* by reaction of cerium(IV) isopropoxide with triethylaluminium in the presence of an excess of cyclooctatetraene (as solvent) at 140 °C for two hours. This reaction resulted in black crystals or red-violet powder in 66% yield.[125] Cerocene is pyrophoric when exposed to oxygen, but is relatively stable in purified water, showing only slow decomposition.[125] The solid-state structure of cerocene is isomorphous to the uranium and thorium analogs, showing a symmetrical sandwich coordination. The reaction with metallic potassium is possible and

yields quantitatively [Ce(COT)$_2$][K(do)] with do = dme and diglyme, in the presence of donor solvents.[125]

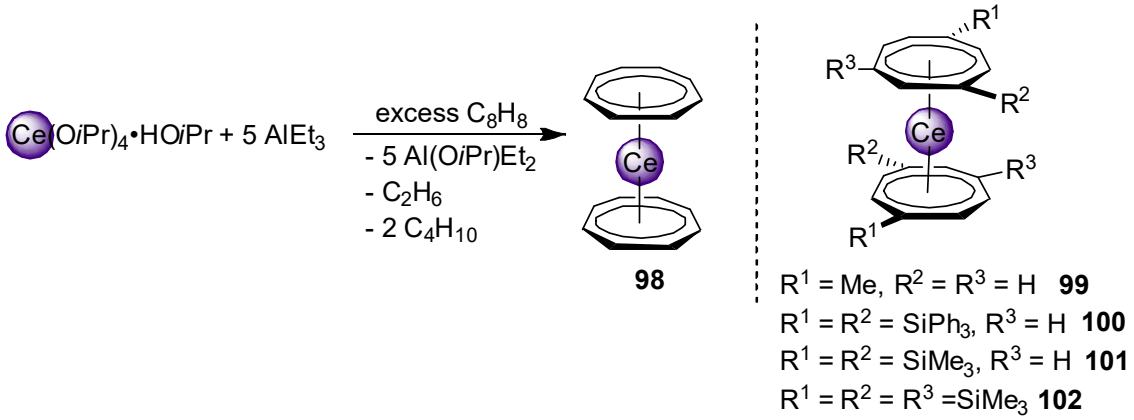

Scheme A22. Synthesis of bis(cyclooctatetraenyl) cerium(IV) ("cerocene") starting from the tetravalent homoleptic *iso*-propoxide complex Ce(O*i*Pr)$_4$. Reduction by using alkali metals is readily possible. Complexes **99** to **102** show differently substituted cerocene complexes.

Scheme A22 (right) depicts successful COT substitution patterns, which have been characterized by X-ray structure analysis. Compounds **99** and **100** were synthesized starting from $CeCl_3$ via salt metathesis, whereas **101** and **102** were synthesized starting from Ce(OTf)$_3$.[119, 122, 124, 146-147] Nevertheless, all compounds were oxidized using AgI to form the substituted cerocene, Ag(0) and KI, which provides also an improved synthesis of **98**.[119, 122, 124, 146-147] Although cerocene is known for almost 50 years, its electronic structure and ambivalence between Ce(III) and Ce(IV) configurations is still under discussion.[18, 148-151] The question arose due to quantum mechanical calculations in 1989, when Fulde *et al.* postulated the presence of temperature independent paramagnetism (TIP) with a magnetic susceptibility $\chi_m > 0$ in contrast to diamagnetism ($\chi_m < 0$), due to the electronic configuration Ce(III)(4f^1)(COT$^{1.5-}$)$_2$, where one electron of the COT ligand is allocated to the cerium center leaving a formal radical anion ligand.[152-155] This orbital singlet configuration was calculated to be lower in energy in contrast to configuration Ce(IV)(4f^0)(COT^{2-})$_2$, which would be diamagnetic, like its respective Th(IV) analogon.[152-154] While the latter is supported by its diamagnetic ^{1}H NMR spectra, cyclic voltammetry, and gas phase photoelectron spectra, further calculations, absorption, luminescence, and XANES measurements for this cerium compound indicate a Ce(III) ground state.[125, 147, 152-153, 156-163] Magnetic measurements revealed a small temperature independent paramagnetism and a slightly positive χ_m value, which was supported by quantum mechanical calculations, which suggested the ground state as admixture of the two wave functions allocated to Ce(III)(4f^1)(COT$^{1.5-}$)$_2$ and Ce(IV)(4f^0)(COT^{2-})$_2$.[153-155, 157-158, 164-165] Thus, the electronic nature of cerium(IV) in

cerocene is today seen as a multiconfigurational ground state with a true valence between +3 and +4.[157-158] Chemically, cerocene and its derivatives can still be considered as tetravalent complexes, as the values of oxidation numbers in Lewis structures is assigned due to closed-shell configurations, which is just an approximation in covalent systems, but on close look show intermediate valencies. Therefore, the discussion of the valency of cerocene can be seen as a reminder to see formal oxidation numbers as a tool to understand chemical behavior and not as a physical description. This is showcased for cerocene complex **101**, as the reaction with cobaltocene results in the chemical reduction to yield complex $[CoCp_2][Ce(COT'')_2]$ (**103**) (COT'' = 1,3,6-$(SiMe_3)_3$COT), similarly to the reduction with alkali metals (Scheme A23).[146] A further reactivity was discovered in 2007, when heating cerocene (**98**) yielded triple decker $Ce_2(COT)_3$, which could be converted by excess of cyclooctatetraen back to cerocene in good yield and purity.[164]

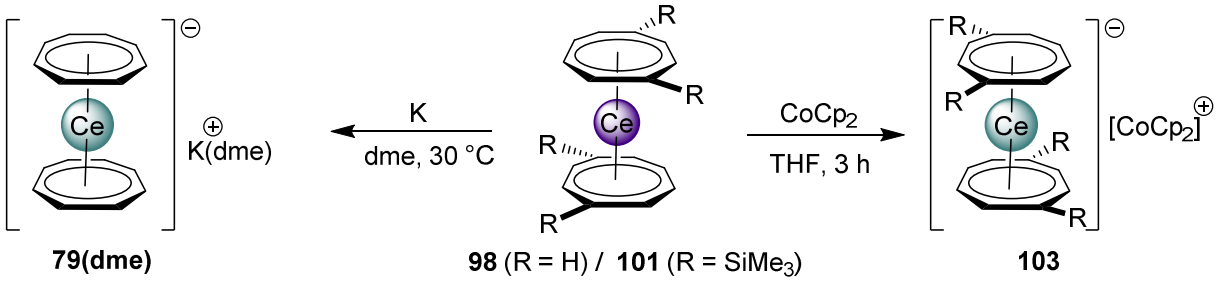

Scheme A23. Chemical reduction of cerocene complexes **98** and **101** with potassium to **79(diglyme)** or cobaltocene to **103**.

3.4 Bispentalene Complexes

Another cyclopentadienyl derived ligand is the rarely used bispentalene ligand, which was used to form cerium(IV) cyclopentadienyl complexes as well and can be distinctly compared to cerocene complexes.[166] In 2007, complex **104** was prepared starting from $CeCl_3$ as a separated ion pair and subsequently oxidized using $Ag[BPh_4]$ to afford tetravalent complex **105**.[167] Similarly to cerocene, magnetic studies, XANES, and DFT calculations indicated that a multiconfigurational ground state is present in **105**, accounting for the observed temperature independent paramagnetism (TIP).[167] The paramagnetic contributions were assigned to a configuration with a hole in the ligand shell, which is antiferromagnetically coupled to an f electron; nevertheless the formal oxidation state stays +IV, according with its chemical behavior.[167] In the same year, bis(permethylpentalene)cerium(IV) (**106**) was synthesized as cerocene analogue as well, using the lithium pentalenide in combination with an excess of 1,2-dichloroethane, and obtained as purple crystals with 61% yield after sublimation.[168] The complex has been shown to exist in a valency close to Ce(III) by XANES measurements and

DFT calculations, providing an example of the self-contained Kondo effect, which is also present in cerocene.[152, 156, 168] The Kondo effect is caused by a local magnetic moment, which spin polarizes local conduction electrons and hereby forms a magnetic singlet.[156, 168] Both results suggest that pentalene and COT ligands show remarkable electronic similarities, although their complexes are structurally distinct, indicating that the TIP behavior of cerium(IV) complexes could be a more general principle, which has been supported by TIP behavior and calculations of a multiconfigurational ground state even in CeO_2.[148, 169]

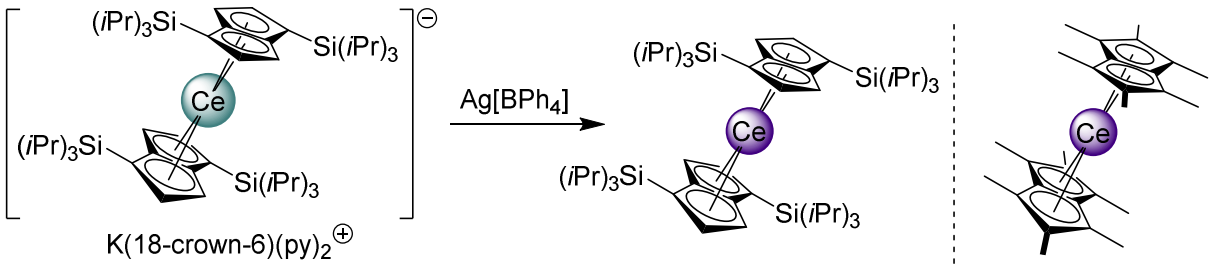

104 **105** **106**

Scheme A24. Oxidation of anionic bispentalene complex **104** with the use of silver tetraphenylborate, resulting in tetravalent cerium(IV) bispentalene complex **105**, allowing direct comparison (left). On the right, the permethylated bispentalene complex **106** is shown.

B

Summary of the Main Results

Cerium(III)-Fluorenyl Complexes and Fluorenyl Coupling

In the literature the stabilizing influence of cyclopentadienyl ligands on cerium in the oxidation state +4 has been demonstrated by several publications, starting with $Cp_3Ce(O\textit{i}Pr)$ and cerocene.[125] While alkyl- and trimethylsilyl-substituted cyclopentadienyl ligands have been used extensively, conjugated ring systems have been rarely used (*e.g.,* $(Ind)_3Ce(thf)$) and not subjected to oxidation reactions.[38, 144] In addition to a likely stabilization, the fluorenyl ligand enables multiple coordination modes ranging from η^1 to η^6 via haptotropic shifts.[170-172] The search for new precursors, in order to form cerium-fluorenyl complexes led to the synthesis of monosubstituted $\mathbf{A^{Cl}}$ and $\mathbf{A^{I}}$ exclusively, independent of the stoichiometry of KFlu used (Scheme B1). In contrast, the use of 2,7-di-*tert*-butyl-substituted fluorenyl ligand $Flu^{t\mathrm{Bu}}$ led to $(Flu^{t\mathrm{Bu}})_3Ce(thf)$ (**B**) instead, despite the steric increase of the ligand, indicating that the increased solubility of $KFlu^{t\mathrm{Bu}}$ plays a key role. While solid-state structures of mono-substituted products $\mathbf{A^{Cl}}$ and $\mathbf{A^{I}}$ feature η^5 coordination, complex **B** exhibits two fluorenyls with η^5 and one fluorenyl ligand with η^1 coordination, providing the possibility for a direct comparison between both coordination modes within the same molecule. ^{1}H NMR experiments of **B** show that all fluorenyl ligands are chemically and magnetically equivalent with the coordination switch being too fast on the NMR timescale.

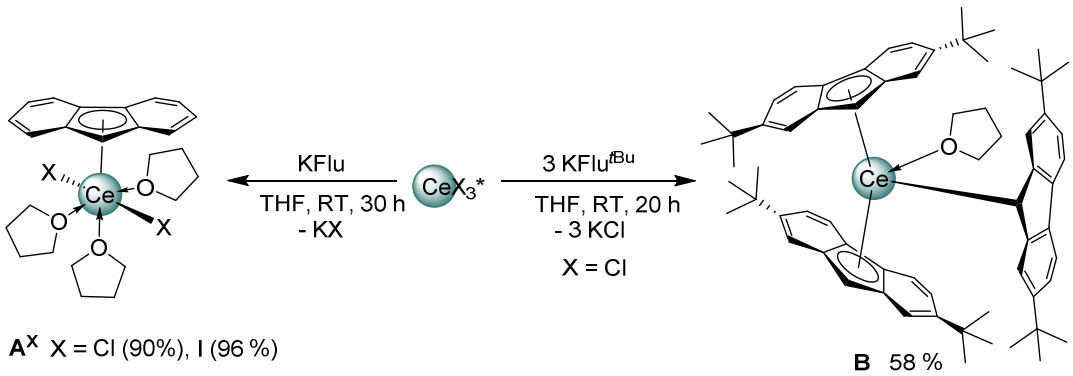

Scheme B1. Synthesis of $FluCeCl_2(thf)_3$ ($\mathbf{A^{Cl}}$), $FluCeI_2(thf)_3$ ($\mathbf{A^{I}}$) (left) and $Flu^{t\mathrm{Bu}}{}_3Ce(thf)$ (**B**) (right).

In order to elucidate the scope of follow-up reactions $\mathbf{A^{Cl}}$ was employed in salt-metathesis reactions with different ligand types. Accordingly, bright orange half-sandwich complexes $(Flu)CeR_2$ with R = siloxy (**C**), aryloxy (**D**), cyclopentadienyl (**E**), alkoxy (**F**), and pyrazolato (**G**) ligands could be accessed successfully in good yields (Scheme B2). Apart from complex **D**, which is stable at ambient temperature, all compounds engage in ligand reorganization processes at ambient temperature, which could be decelerated by reaction and storage at −40 °C.

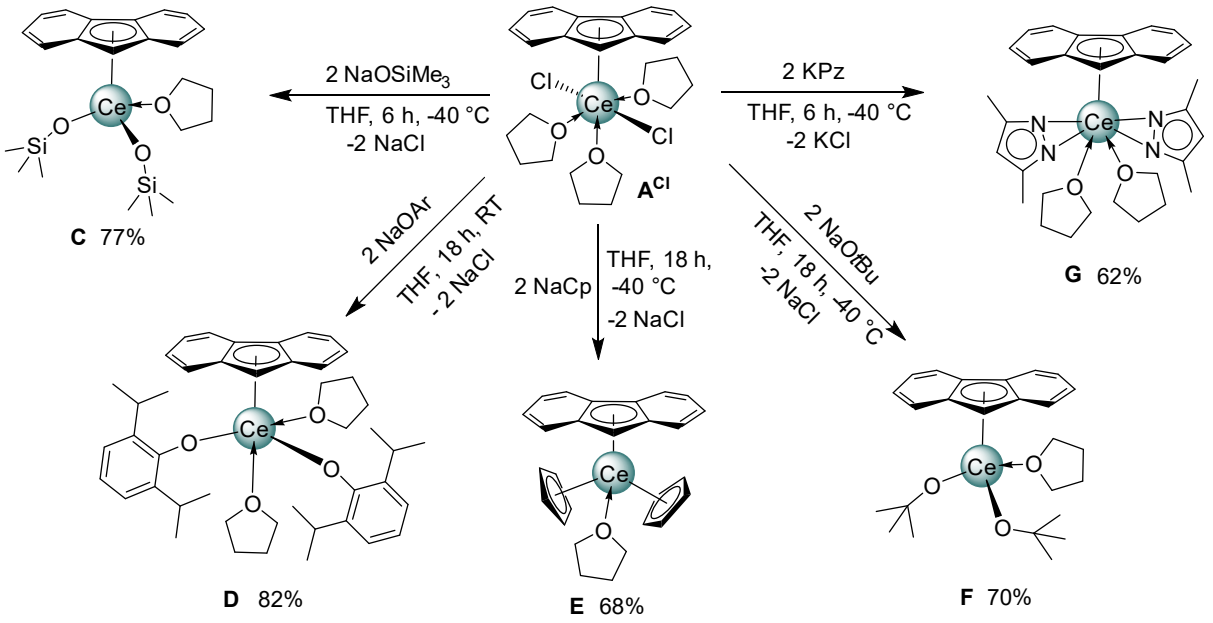

Scheme B2. Synthesis of half-sandwich complexes (Flu)Ce(OSiMe$_3$)$_2$(thf) (**C**), (Flu)Ce(OAr)$_2$(thf) (**D**), (Flu)CeCp$_2$(thf) (**E**), (Flu)Ce(O*t*Bu)$_2$(thf), and (Flu)CePz(thf)$_2$ (**G**).

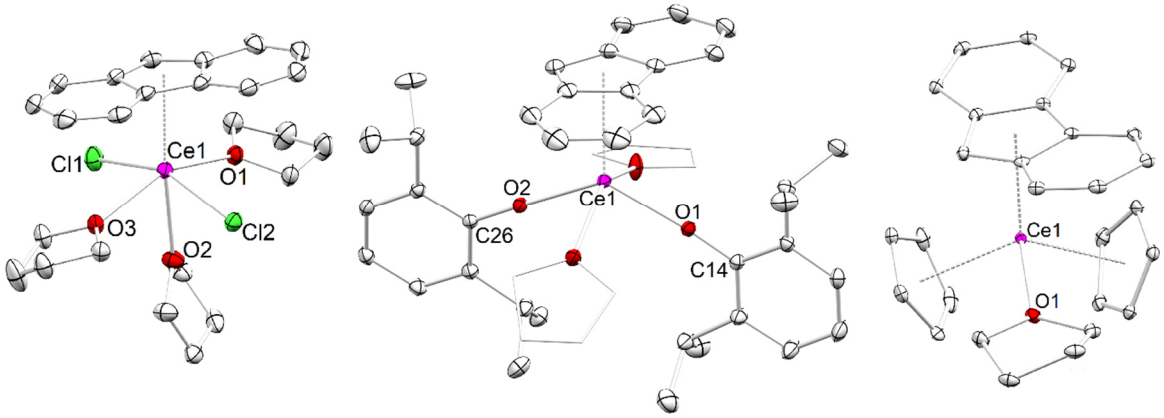

Figure B1. Crystal structures of (Flu)CeCl$_2$(thf)$_3$ (**A**^{Cl}, left), (Flu)CeOAr$_2$(thf)$_2$ s(**D**), and (Flu)CeCp$_2$(thf) (**E**, right).

The ligand rearrangement at ambient temperature is visualized exemplarily for pyrazolato ligands in Scheme B3, which results in the formation of homoleptic cerium pyrazolate and novel sandwich complex **(**Flu**)**$_2$CePz(thf) (**J**). The former could be separated together with other decomposition products by toluene extraction, affording **J** in low yields. Interestingly, a crystal structure of the separated ion pair [CePz$_2$(thf)$_5$]$^+$[Flu]$^-$ (**I**) could be obtained in the reaction mixture, corroborating the fluctuating coordination of the fluorenyl ligand and revealing an intermediate, which facilitates the ligand rearrangement processes. Additionally, the solid-state structures enable a direct comparison of half-sandwich, sandwich and ion pair separated complexes **G**, **I** and **J**, revealing longer average Ce−N distances for half-sandwich complexes (**G**: 2.480 Å, **I**: 2.475 Å), compared to **J** (2.413 Å) despite the increased sterical bulk. The same trend is true for the Ce−centroid distances (2.646 Å for **G** to 2.574 Å for **J**).

The purification of sandwich complexes proved difficult, due to product mixtures, but was successful for **(**Flu**)**$_2$CePz(thf) (**J**) and **(**Flu**)**$_2$Ce(O*t*Bu)(thf), while congeneric **(**Flu**)**$_2$Ce(OSiMe$_3$)(thf) was observed in the form of a solid-state structure as decomposition product of **C**.

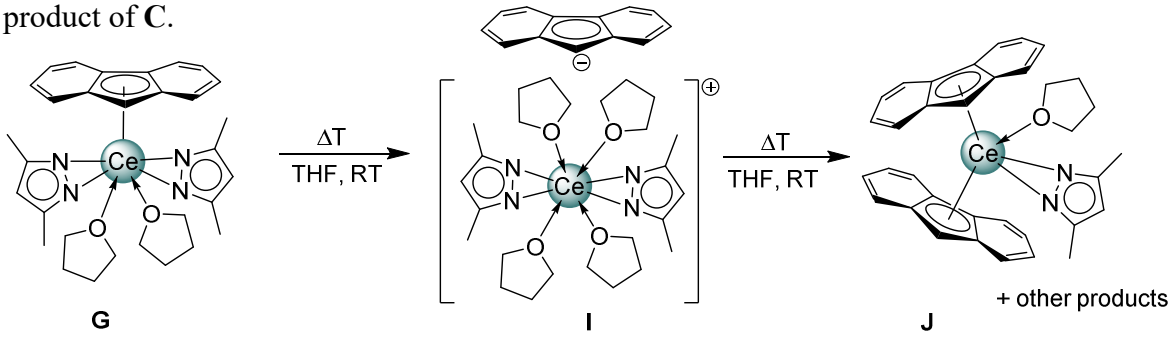

Scheme B3. Ligand rearrangement process of half-sandwich complex (Flu)Ce(Pz)$_2$(thf) (**G**) to (Flu)$_2$Ce(Pz)(thf) (**J**) via [Ce(Pz)$_2$(thf)$_5$]$^+$[Flu]$^-$ (**I**).

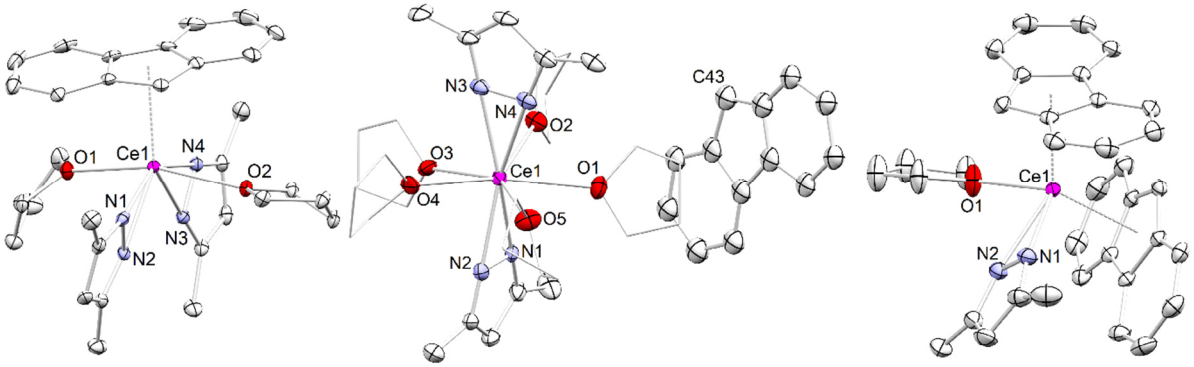

Figure B2. Crystal structures of **(**Flu**)**CePz$_2$(thf) **G**, (Flu)$_2$CePz(thf) **I** and [CePz$_2$(thf)$_5$]$^+$[Flu]$^-$ **J** (left to right).

The reaction of **A**^{Cl} with lithium thiomesitolate resulted in an incomplete reaction accomplishing the trimeric product [**(**Flu**)**Ce(SMes)Cl]$_3$Li(SMes)(thf)$_2$, whereas the use of 2,4-di-*iso*propyl-pentadienyl (dipp) instead of cyclopentadienyl ligands led to the formation of unprecedented Ce(dipp)$_3$ (**K**) (Scheme B4). Similarly, (Flu)CeCp$_2$(thf) (**E**) forms Cp$_3$Ce(thf) by ligand scrambling at ambient temperatures, but this side reaction seems to occur on a much slower timescale; it can be sufficiently slowed down by conducting the reaction at −40 °C. Complex **K** could be obtained directly by the reaction of CeCl$_3$* with K(dipp) (Scheme B4).

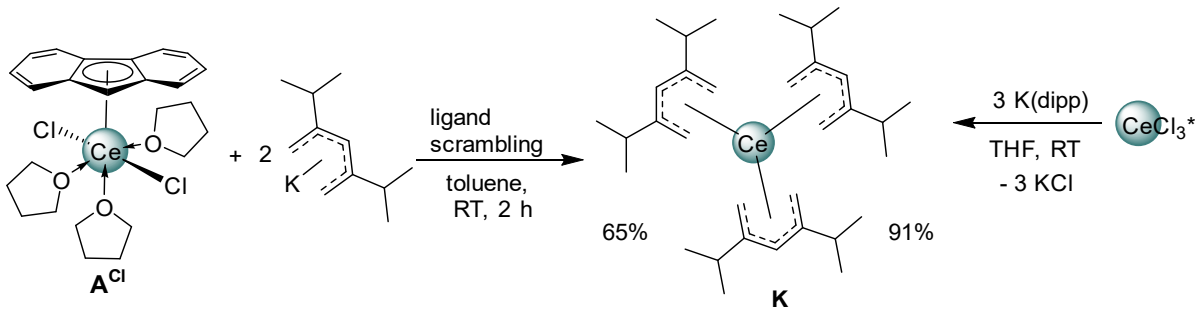

Scheme B4. Synthesis of Ce(dipp)$_3$ **K** starting from (Flu)CeCl$_2$(thf)$_3$ (**A**^{Cl}, left) or CeCl$_3$* (right).

Upon exposure to halogenating oxidants like hexachloroethane C_2Cl_6, $TeBr_4$, and I_2 complexes **A** to **J** produced 9-halogenido fluorene, 1,1'-bifluorene and other products instead of yielding cerium(IV) complexes. This will be elucidated paradigmatically for $(Flu)CeCl_2(thf)_3$ (Scheme B5). The reaction of $\mathbf{A^{Cl}}$ with C_2Cl_6 occured instantly, accompanied by a color change from orange to colorless and the quantitative precipitation of crystalline $CeCl_3(thf)_4$, probably the driving force of the reaction. The reaction is assumed to proceed via "$FluCeCl_3(thf)_x$", which instantly undergoes sterically induced reduction, which has been reported for other cerium(IV) complexes like Cp^*_3Ce as well, producing the respective radical coupling products.[48] In contrast to similar reactions, the product can be controlled via the amount of C_2Cl_6 to form either 9-halogenido fluorene with 1.1 equivalents or 1,1'-bifluorene with 0.45 equivalents selectively (93% and 81% selectivity), with fluorene as major side product. Other oxidation agents showed barely any stoichiometry control, I_2 produced mainly bifluorene and $TeBr_4$ mainly 9-bromofluorene. The reactivity of C_2Cl_6 was tested on $(Ind)_3Ce(thf)$ and $CeBn_3$ as well producing excusively 1-chloroindene and benzyl chloride, respectively.

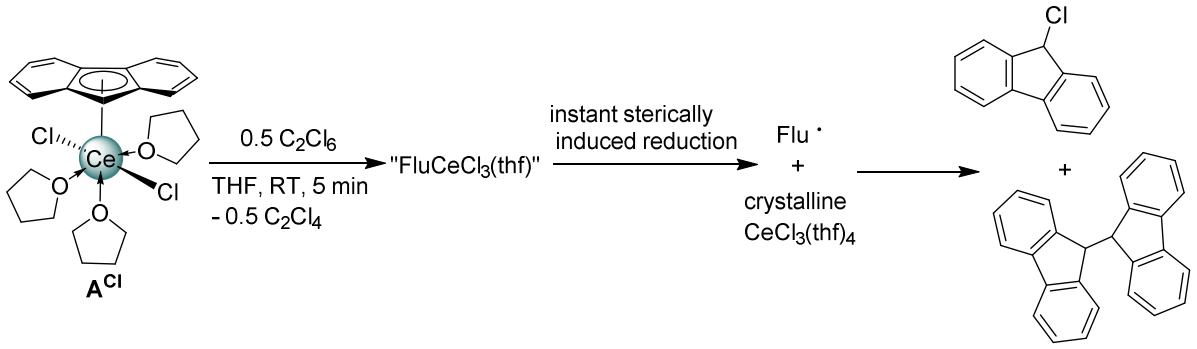

Scheme B5. Formation of 9-chlorofluorene and 1,1'-bifluorene upon reaction of $\mathbf{A^{Cl}}$ with C_2Cl_6.

To conclude, the fluorenyl ligand was found to support ligand rearrangement processes by its ability to readily change coordination modes in the trivalent state. The reactions with halogenating oxidation agents produced the halogenated or radical coupled product. Although the latter could be controlled stoichiometrically, any isolable cerium(IV) metallocenes could not be accomplished, but instead mono, bis and tris(substituted) cerium(III) fluorenyl compounds.

Cerium(IV) Sandwich and Half-Sandwich Complexes

In order to synthesize sandwich complexes of cerium(IV) sterically demanding cyclopentadienyl ligands like $C_5H_3(SiMe_3)_2$ (Cp'') or $C_5H_2(SiMe_3)_3$ (Cp''') need to be used. Otherwise, tris(cyclopentadienyl) complexes are formed, when performing salt-metathesis

reactions.[38, 144] Furthermore, the employed alkali metal can change the course of the reaction, which is displayed in Scheme B6, as the salt-metathesis reaction of potassium tetramethylcyclopentadienide, KC_5HMe_4 (KCp^{tet}), with $CeCl_3$* led to dark green Cp^{tet}_3Ce,[173-174] whereas the reaction with the lithium congener resulted in the formation of bright pink ate complex $[Cp^{tet}_2CeCl_2Li(thf)_2]_2$ (**L**^{tet}). Upon contact of **L**^{tet} with oxidation agents like C_2Cl_6, decomposition and ill-defined mixtures were observed. Complex $Cp^*_2CeCl_2A(thf)_2$ (**L***; A = K, Li) reacted similarly and cyclic voltammetry revealed irreversible oxidation signals at −0.54 V vs Fc/Fc^+ (**L**^{tet}) and −0.57 V vs Fc/Fc^+ (**L***), indicating too much steric hindrance or insufficient stabilization of the +IV oxidation state.

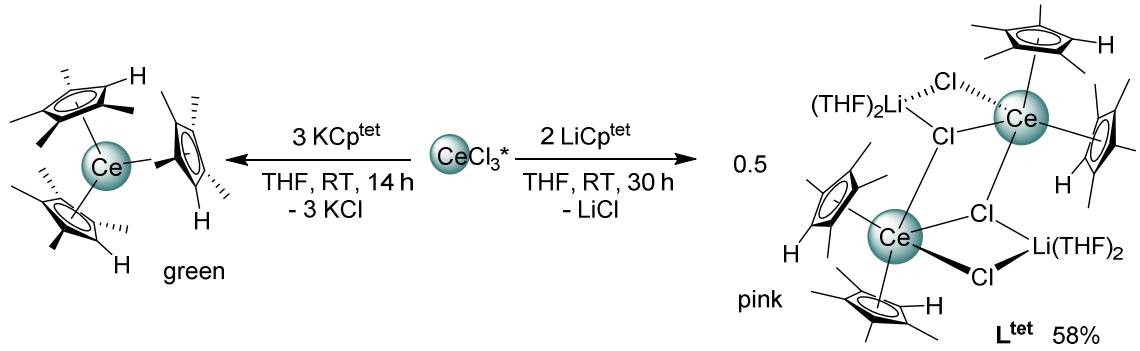

Scheme B6. Alkali metal influence on formation of tris(tetramethylcyclopentadienyl) cerium(III) or dimeric bis(tetramethylcyclopentadienyl) ate complex **L**^{tet} (left).

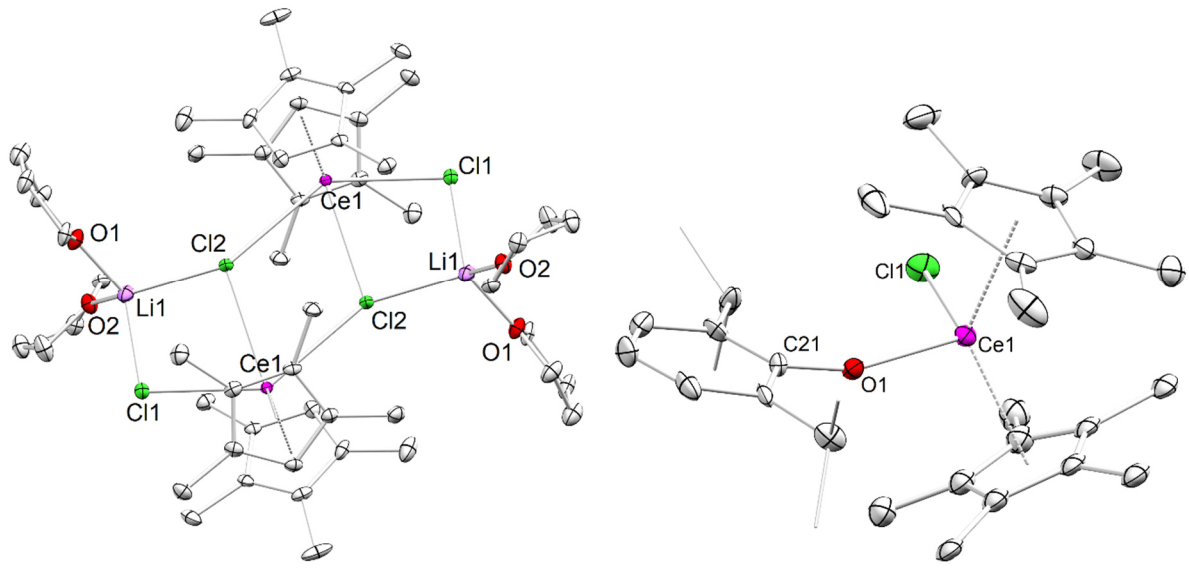

Figure B3. Crystal structures of dimeric $[Cp^{tet}_2CeCl_2Li(thf)_2]_2$ (**L**^{tet}, left) and $Cp^*_2Ce(OAr)Cl$ (**P**, right).

Thus, the reaction was performed in the presence of stabilizing alkoxy and siloxy ligands, resulting in the formation of the desired products $Cp^*_2Ce(OR)_2$ (**M**^{R} with R = Et, *i*Pr, *t*Bu, CH_2tBu) and $Cp^*_2Ce(OSiR_3)_2$ (**N**^{R} with R = Me, Et, Ph) in one pot syntheses (Scheme B7). Reaction with sodium 2,6-di-*iso*propylphenolate (OAr) resulted in incomplete substitution

and yielded complex **P**, probably due to the steric hindrance of the aryloxy and Cp* ligands in combination with the decrease in metal ion size upon oxidation. Employment of $\mathbf{L}^{tet}$ as starting material did not lead to stable cerium(IV) metallocenes, in accordance with the electrochemical data, which suggest that Cp* exhibits a stronger stabilizing influence on cerium(IV) than Cp^{tet}.

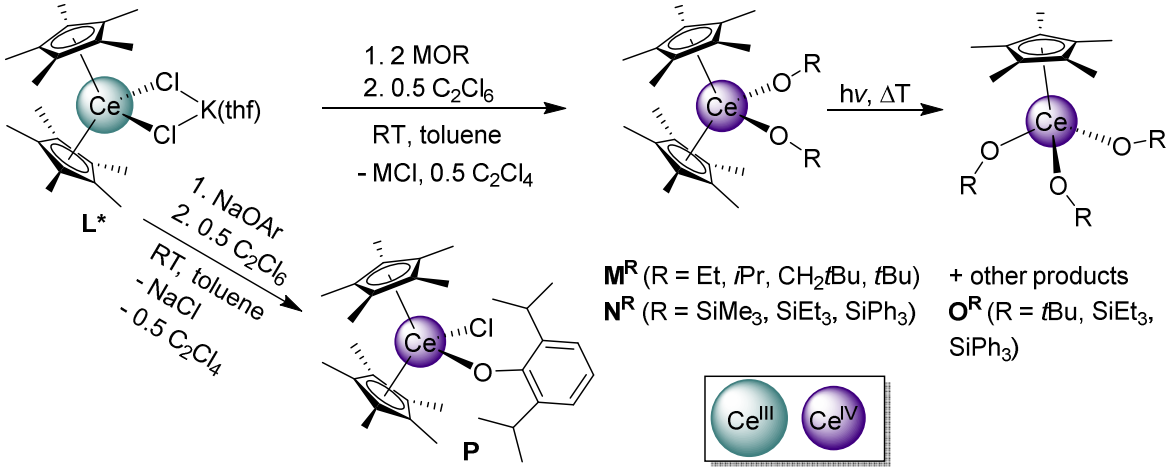

Scheme B7. Synthesis of $Cp^*_2CeCl_2K(thf)_2$ toward sandwich complexes $Cp^*_2Ce(OR)_2$ ($\mathbf{M}^{R}$, R = Et, *i*Pr, CH_2*t*Bu, *t*Bu), $Cp^*_2Ce(OSiR_3)_2$ ($\mathbf{N}^{R}$, R = Me, Et, Ph), and $Cp^*_2Ce(OAr)Cl$ (**P**), as well as half-sandwich complexes Cp^*CeR_3 ($\mathbf{O}^{R}$, R = *t*Bu, $SiEt_3$, $SiPh_3$) via ligand rearrangement.

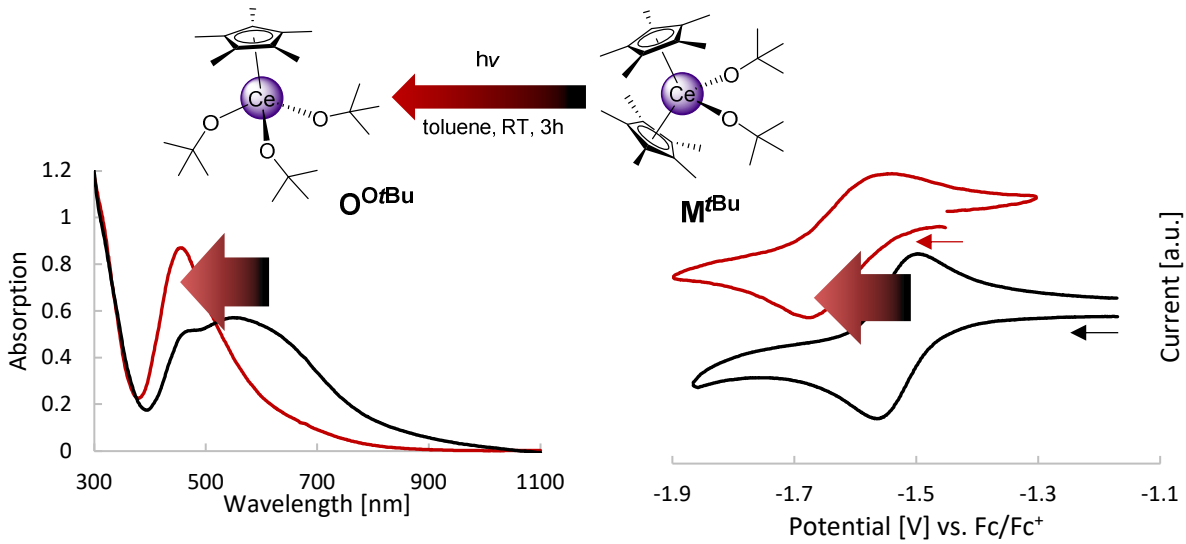

Figure B4. Ligand rearrangement of $Cp^*_2Ce(OtBu)_2$ ($\mathbf{M}^{tBu}$, **black**) toward $Cp^*Ce(OtBu)_3$ ($\mathbf{O}^{OtBu}$, **red**) (top). UV/Vis spectrum featuring the shift from purple to brown (left) and cyclic voltammograms depicting the increase in stabilization (right), when substituting one Cp* by an alkoxy ligand.

The cerium(IV)-sandwich complexes $\mathbf{M}^{tBu}$, $\mathbf{N}^{Et}$ and $\mathbf{N}^{Ph}$ with sterically demanding substituents show follow-up reactivity under light and ambient temperature leading to ligand

rearrangement. Accordingly, the first reported cerium(IV)-half-sandwich complexes $\mathbf{O}^{\mathbf{R}}$ were synthesized and could be isolated for R = O*t*Bu and $OSiPh_3$. The use of R = $OSiEt_3$ resulted in a mixture of sandwich and half-sandwich complex, indicating that the process is sterically induced. The reaction is accompanied by a color change from dark blue (556 nm) to brown (456 nm) ($\mathbf{M}^{t\mathbf{Bu}}$) and dark blue (563 nm) to violet (521 nm) ($\mathbf{N}^{\mathbf{Ph}}$), respectively, which results in blue shifts of the UV/Vis absorbance spectra (Figure B6). The ligand rearrangement does not stop at complexes **O**, instead further decomposition led to mixtures including homoleptic cerium alkoxide or siloxide complexes over several weeks even at −40 °C. All cerium(IV) complexes showed remarkable solublity, even in tetramethylsilane or pentane, due to the high lipophilic surface area, which – in combination with kinetic lability − made crystallization very cumbersome.

Figure B5 depicts the solid-state structure of $Cp^*_2Ce(OEt)_2$ ($\mathbf{M}^{\mathbf{Et}}$), which adopts the pseudo-tetrahedral coordination typical of cerium(IV)-metallocene complexes. Furthermore, the cyclic voltammogram of $\mathbf{M}^{\mathbf{Et}}$, which exhibits one chemically reversible and electrochemically quasi-reversible redox process at −1.56 V vs Fc/Fc^+, emphasizes the excellent stabilization of the cerium(IV) center (a full synopsys of cyclovoltammetric data can be found in Table B1). The changes from sandwich to half-sandwich complex are visualized in Figure B4, indicating that the ligand rearrangement leads to an increase in thermodynamic as well as electrochemical stabilization, but is accompanied by a loss of electrochemical reversibility.

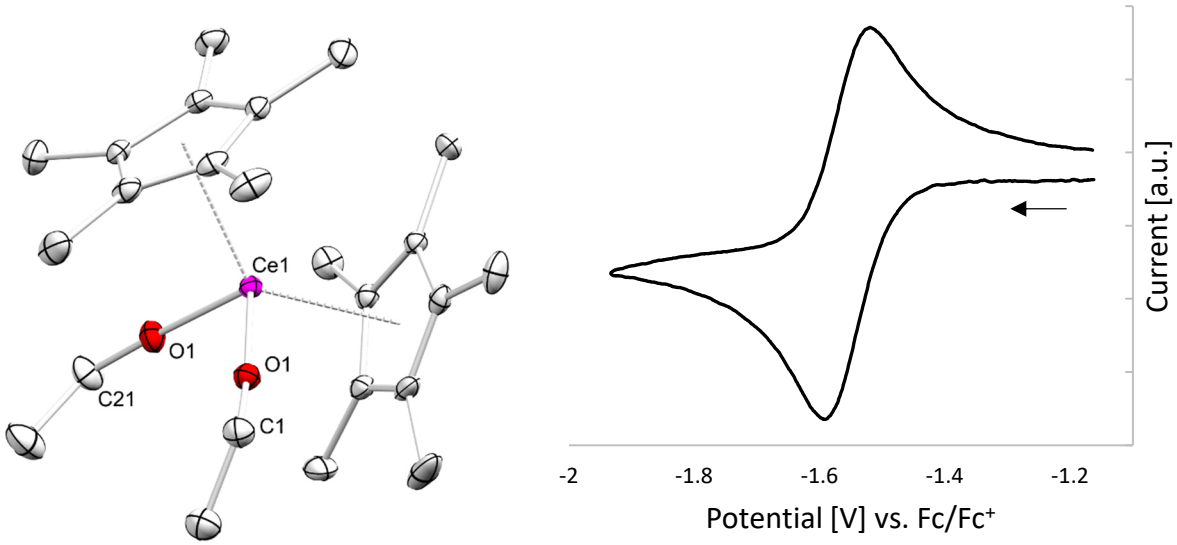

Figure B5. Crystal structure of $Cp^*_2Ce(OEt)_2$ ($\mathbf{N}^{\mathbf{Et}}$, left) and corresponding cyclic voltammogram of the cerium(III/IV) redox couple vs Fc/Fc^+ in THF at 50 mV/s; arrow indicates scan direction (right).

Stabilization of Cerium(IV) Tris(Cyclopentadienyl) Complexes

To further investigate the effects of the chemical environment on the stabilization of the cerium(IV) center with respect to reduction, a series of tris(cyclopentadienyl) cerium(IV) complexes was prepared. The feasibility of the oxidative approach starting from $Cp_3Ce(thf)$ or $Cp^{Me}{}_3Ce(thf)$ was reported by our group in 2010 and 2017 and resulted in complexes Cp_3CeCl (**Q**^{Cl}) and $Cp^{Me}{}_3CeCl$ (**R**^{Cl}).[38, 145] For further comparison the respective bromide and iodide complexes Cp_3CeX (**Q**^{X}) and $Cp^{Me}{}_3CeX$ (**R**^{X}), with X = Br and I, have been synthesized in good yields (Scheme B8) using $TeBr_4$ and I_2 as oxidation agents. The solid-state structure in Figure B6 revealed pseudo-tetrahedral coordination, which is the case for all following structures.

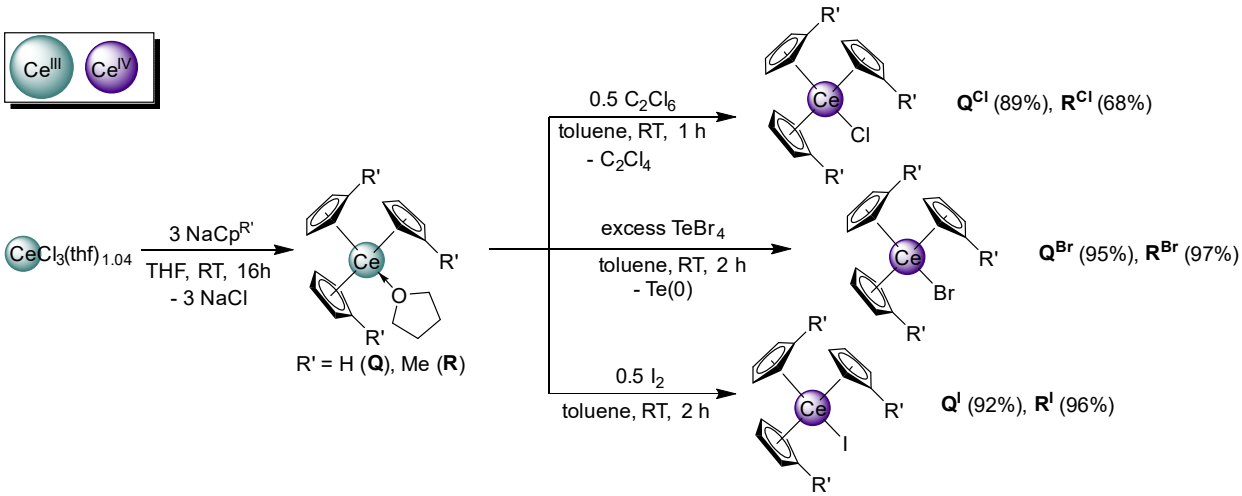

Scheme B8. Synthesis of $Cp^R{}_3Ce(thf)$ (**Q**, R = H; **R**, R = Me) and subsequent oxidation to yield $Cp^R{}_3CeCl$ (**Q**^{Cl} / **R**^{Cl}), $Cp^R{}_3CeBr$ (**Q**^{Br} / **R**^{Br}), and $Cp^R{}_3CeI$ (**Q**^{I} / **R**^{I}).

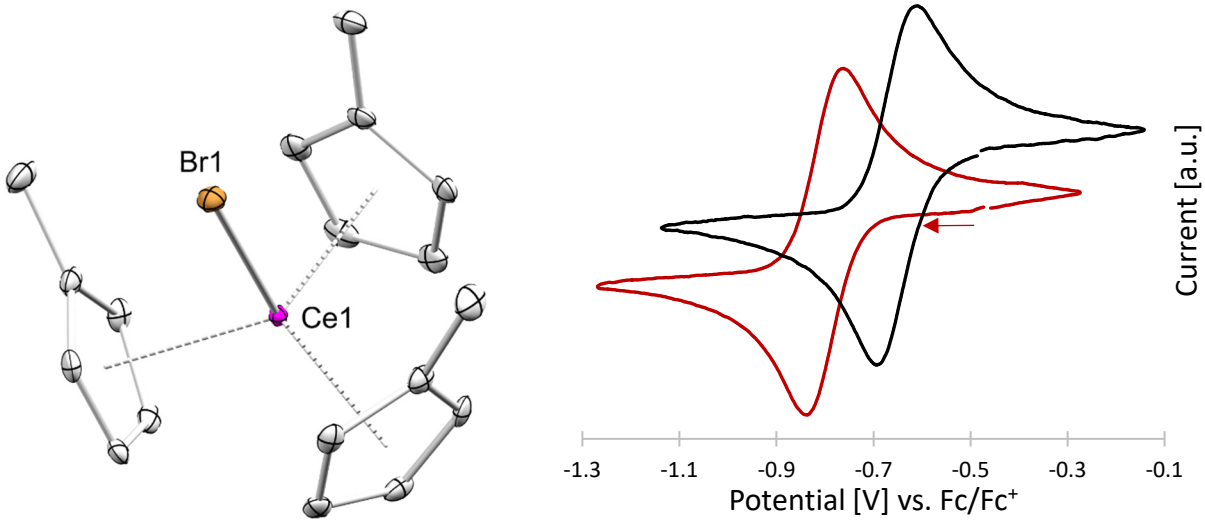

Figure B6. Crystal structure of $Cp^{Me}{}_3CeBr$ (**R**^{Br}, left) and corresponding cyclic voltammograms of the cerium(III/IV) redox couple of $Cp^{Me}{}_3CeCl$ (**R**^{Cl}, red) and Cp_3CeBr (**Q**^{Br}, black) vs Fc/Fc^+ in THF at 50 mV/s; arrows indicate scan direction (right).

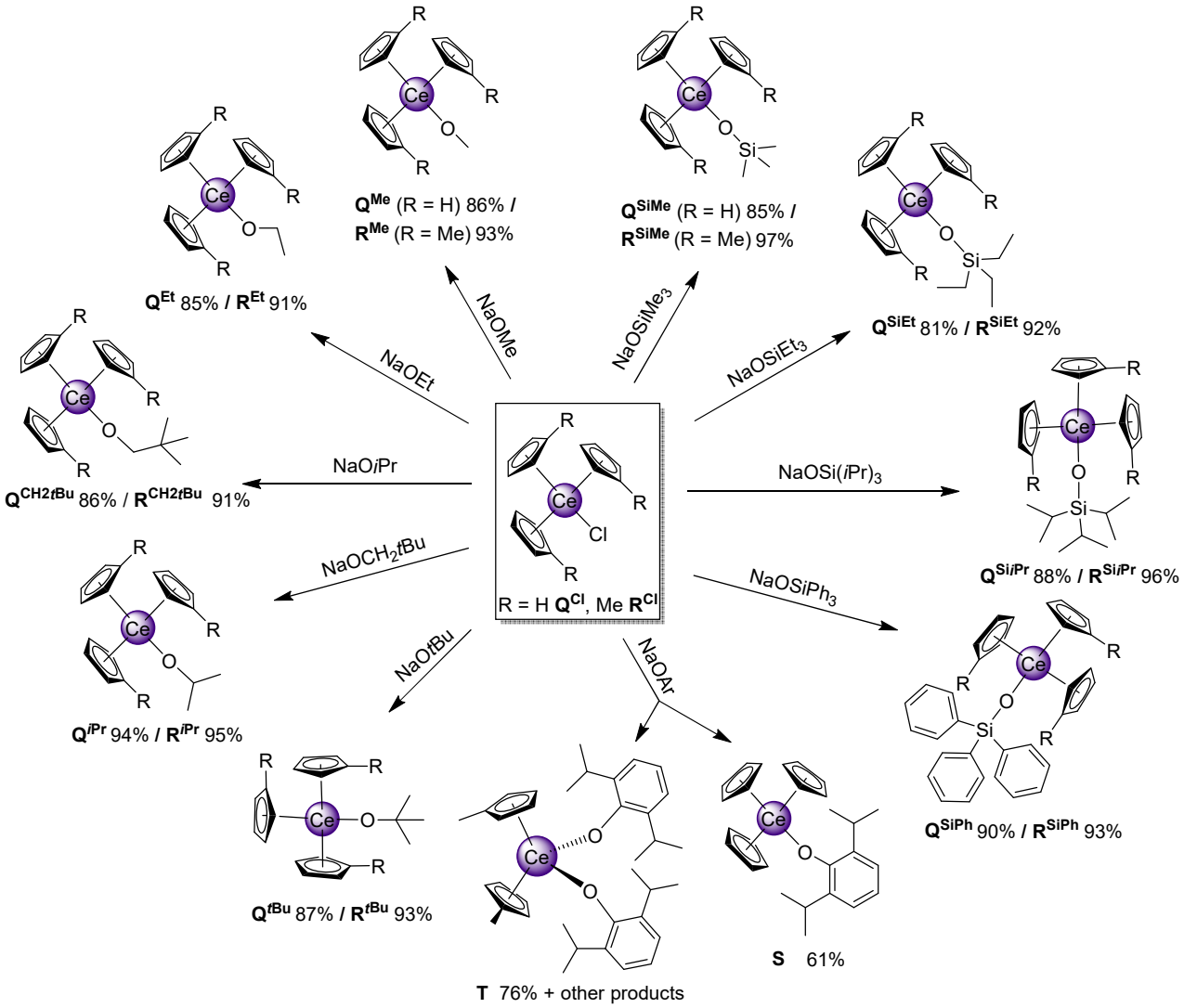

Scheme B9. Synthesis of Cp-supported complexes Cp_3CeX (**Q**) and Cp^{Me}-supported complexes $Cp^{Me}{}_3CeX$ (**R**) with alkoxy (X = OMe, OEt, O*i*Pr, OCH_2tBu, O*t*Bu) and siloxy co-ligands (X = $OSiMe_3$, $OSiEt_3$, $OSi(iPr)_3$, $OSiPh_3$) as well as aryloxide complexes $Cp_3Ce(OAr)$ (**S**) and $Cp^{Me}{}_2Ce(OAr)_2$ (**T**) with OAr = 2,6-di-*iso*propyl-phenoxy, in yields ranging from 61% to 97%.

Chloride complexes $\mathbf{Q^{Cl}}$ and $\mathbf{R^{Cl}}$ were used in salt-metathesis reactions yielding cyclopentadienyl-supported complexes Cp_3CeX (**Q**) and methylcyclopentadienyl-supported complexes $Cp^{Me}{}_3CeX$ (**R**) with alkoxy (X = OMe, OEt, CH_2tBu, O*i*Pr, O*t*Bu) and siloxy (X = $OSiMe_3$, $OSiEt_3$, $OSi(iPr)_3$, $OSiPh_3$) substituents in good yields ranging from 81% to 97%. The aryloxy ligand 2,6-di-*iso*propyl-phenolate (OAr) could be employed as well, but led only to $Cp_3Ce(OAr)$ (**S**) for the unsubstituted cyclopentadienyl ligand. Utilization of the sterically more demanding Cp^{Me} ligand resulted in ligand reorganization and formation of sandwich complex $Cp^{Me}{}_2Ce(OAr)_2$ (**T**); the latter could be synthesized in 76% yield, when using two equivalents of aryloxide salt. The scope of possible products and respective thermal stability (successful sublimation for $\mathbf{Q^{iPr}}$ and $\mathbf{R^{iPr}}$) are remarkable and showcase the stability imparted

by the tris(cyclopentadienyl) scaffold, which supports ligands as sterically different as methoxy and aryloxy (Figure B7).

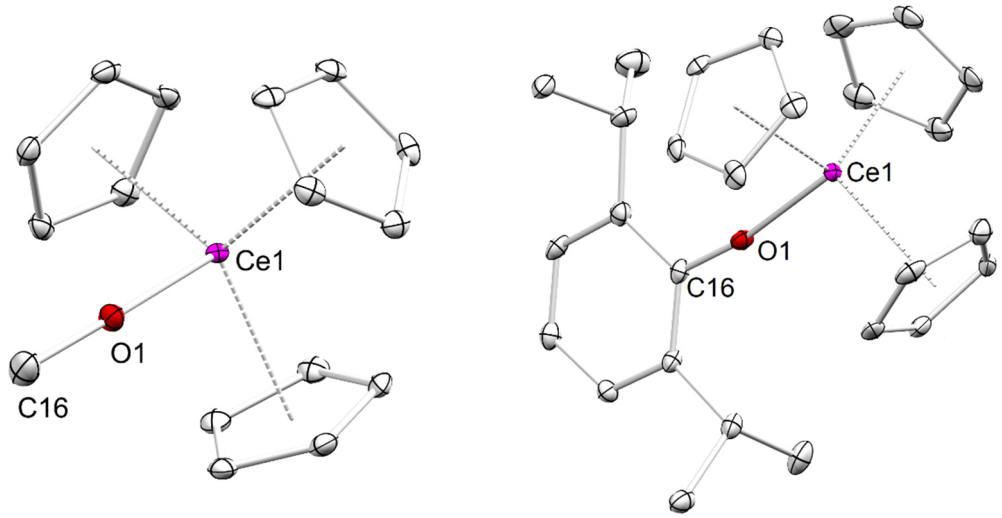

Figure B7. Crystal structures of $Cp_3Ce(OMe)$ (**Q^{Me}**, left) and $Cp_3Ce(OAr)$ (**S**, right).

Interestingly, ^{1}H NMR spectroscopy revealed that the α-H protons of alkoxy ligands (Ce−OC*H*) in all synthesized compounds show characteristic down-field shifts at 5.31 to 6.40 ppm, despite an otherwise diamagnetic spectrum, indicating heavy deshielding and removal of electron density at the respective protons by the proximity to the cerium(IV) center. The precise electronic nature of the cerium(IV) center was further investigated by SQUID magnetic measurements, revealing temperature-independent paramagnetism (TIP) instead of diamagnetism. The slightly positive magnetic susceptibilities between 1.53 and $3.9 \cdot 10^{-4}$ emu/mol indicate the presence of a Van Vleck paramagnetism, caused by a multiconfigurational ground state between Ce(IV, f^0) in combination with an anionic ligand and Ce(III, f^1) with a radical ligand, similarly as reported in cerocene and CeO_2.[148, 164, 169]

The electrochemical stabilization of the cerium(IV) center with respect to reduction was determined via cyclic voltammetry, which revealed two types of behavior: halide (Figure B6) and siloxide complexes exhibit chemically and electrochemically reversible redox processes, whereas alkoxide complexes feature an EC or ECE mechanism, with *in situ* follow-up reactions at slow scan rates and a transition to chemical reversibility at high scan rates. The formal potentials of all one electron processes could be obtained and can be tuned by variation of the chemical environment from −0.583 V (Cp_3CeI, **Q^I**) to −1.259 V vs Fc/Fc^+ ($Cp^{Me}{}_3Ce(OEt)$, **R^{iPr}**). The electrochemical results allow a direct comparison and reveal increasing stabilization of the cerium(IV) oxidation state and more negative formal potentials in the series I < Br < Cl < aryloxy < siloxy < alkoxy and Cp < Cp^{Me} (Figure B9, Table B1).

This is in accordance with the additional data from the sandwich complexes, which showed that Cp* provided increased stabilization in contrast to Cp^{tet}. Even though Cp* complexes show the best stabilization of the observed molecules, their ligand rearrangement behavior stresses the fact that kinetic and electrochemical stabilization do not necessarily correlate. Synoptically, it can be found, that an increase in electron density at the cerium center leads to a better stabilization of the cerium center and accordingly, stronger electron donating groups and ligands lead to an increased stabilization of the cerium(IV) oxidation state.

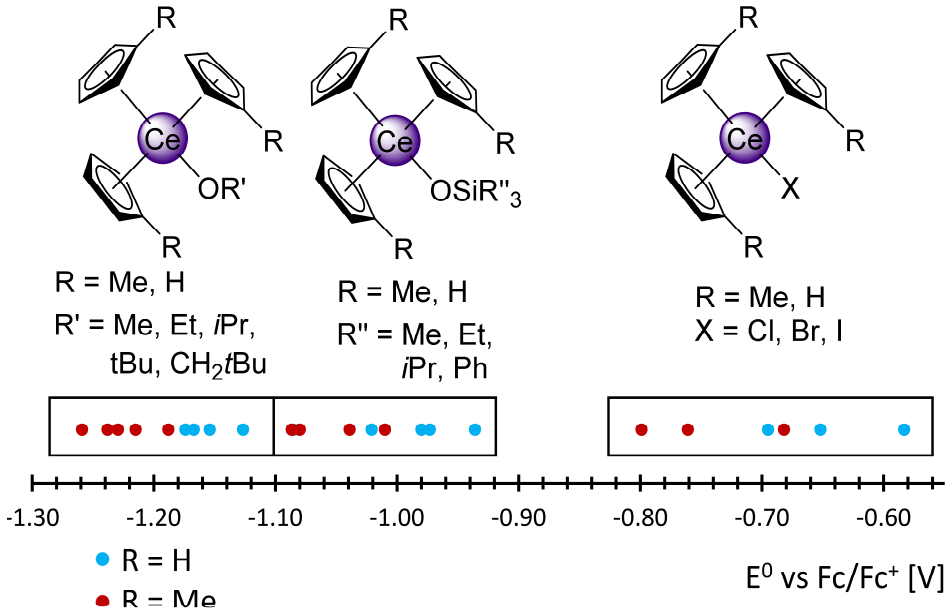

Figure B8. Synopsis of the increase in electrochemical stabilization by halogenido < siloxy < alkoxy ligands; for cyclopentadienyl and methylcyclopentadienyl ligands: Cp < Cp^{Me}.

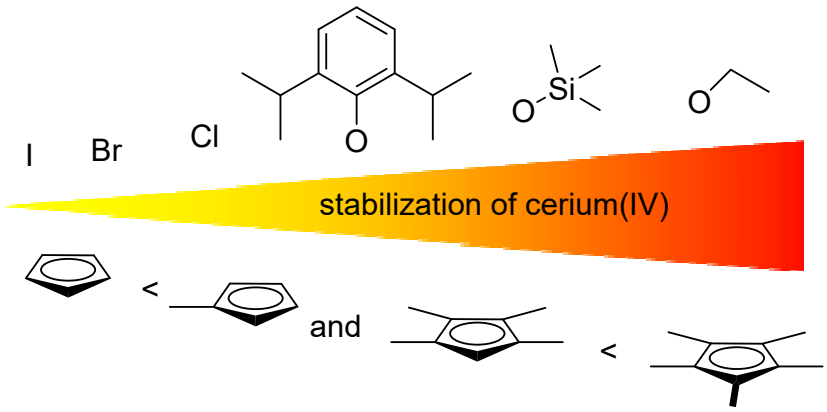

Figure B9. Increasing stabilization of the cerium(IV) oxidation state by monoanionic cyclopentadienyl, halogenido, aryloxy, alkoxy, and siloxy ligands.

Table B1. Electrochemical data for all cerium(III/IV) couples [potentials vs Fc/Fc^+, at a scan rate of 50 mV/s (* = 1V/s)], sorted by increasing stability of the cerium(IV) oxidation state.

Complex	E^0 vs Fc/Fc^+ [V]	E_{Red} vs Fc/Fc^+ [V]	E_{Ox} vs Fc/Fc^+ [V]	ΔE_P [mV]	i_{Ox}/i_{Red}
$Cp_3Ce(thf)$	−0.263	−0.300	−0.227	73	0.85
$Cp^{Me}_3Ce(thf)$	−0.377	−0.408	−0.347	61	0.89
$Cp^{tet}_2CeCl_2Li(thf)$	0.516*	−0.641*	−0.516*	125*	0.42*
$Cp^*_2CeCl_2K(thf)$	(irr.)	–	−0.567	–	–
Cp_3CeI	−0.583	−0.631	−0.535	96	0.97
Cp_3CeBr	−0.652	−0.694	−0.609	85	0.98
Cp^{Me}_3CeI	−0.682	−0.724	−0.640	84	0.99
Cp_3CeCl	−0.695	−0.960	−0.730	70	0.96
Cp^{Me}_3CeBr	−0.764	−0.816	−0.713	103	0.98
Cp^{Me}_3CeCl	−0.801	−0.837	−0.764	73	1.00
$Cp^*_2Ce(OAr)Cl$	−0.831	−0.863	−0.799	64	0.93
$Cp_3Ce(OAr)$	−0.865	−0.898	−0.833	65	0.92
$Cp^{Me}_2Ce(OAr)_2$	−0.876	−0.997	−0.755	242	0.85
$Cp_3Ce(OSiPh_3)$	−0.936	−0.970	−0.903	67	1.00
$Cp_3Ce(OSiEt_3)$	−0.973	−1.003	−0.943	60	0.95
$Cp_3CeOSi(iPr)_3$	−0.980	−1.013	−0.948	65	0.92
$Cp^{Me}_3Ce(OSiPh_3)$	−1.013	−1.044	−0.981	63	0.93
$Cp_3Ce(OSiMe_3)$	−1.021	−1.058	−0.984	74	0.96
$Cp^{Me}_3CeOSi(iPr)_3$	−1.039	−1.070	−1.009	61	0.99
$Cp^{Me}_3Ce(OSiEt_3)$	−1.080	−1.115	−1.045	70	0.99
$Cp^{Me}_3Ce(OSiMe_3)$	−1.089	−1.124	−1.054	70	1.00
$Cp_3Ce(OMe)$	−1.102*	−1.167*	−1.037*	130*	0.75*
$Cp^*_2Ce(OSiPh_3)_2$	−1.137	−1.264	−1.010	254	0.95
$Cp_3Ce(OCH_2tBu)$	−1.151*	−1.209*	−1.093*	116*	0.77*
$Cp_3Ce(OEt)$	−1.155*	−1.245*	−1.096*	143*	0.72*
$Cp_3Ce(OtBu)$	−1.174*	−1.223*	−1.124*	99*	0.87*
$Cp_3Ce(OiPr)$	−1.177*	−1.210*	−1.145*	65*	0.81*
$Cp^{Me}_3Ce(OMe)$	−1.206*	−1.452*	−0.961*	491*	0.99*
$Cp^{Me}_3Ce(OCH_2tBu)$	−1.220*	−1.271*	−1.169*	102*	0.96*
$Cp^*_2Ce(OSiMe_3)_2$	−1.229	−1.260	−1.197	63	0.90
$Cp^{Me}_3Ce(OiPr)$	−1.244*	−1.311*	−1.177*	134*	0.97*
$Cp^{Me}_3Ce(OtBu)$	−1.252*	−1.313*	−1.191*	122*	0.98*
$Cp^{Me}_3Ce(OEt)$	−1.252*	−1.309*	−1.194*	115*	0.92*
$Cp^*Ce(OSiPh_3)_3$	−1.445	−2.186	−0.704	1482	0.82
$Cp^*_2Ce(OCH_2tBu)_2$	−1.514	−1.555	−1.473	82	0.95
$Cp^*_2Ce(OtBu)_2$	−1.531	−1.565	−1.497	68	1.00
$Cp^*_2Ce(OEt)_2$	−1.555	−1.591	−1.519	72	0.92
$Cp^*_2Ce(OiPr)_2$	−1.562	−1.602	−1.522	80	1.00
$Cp^*Ce(OtBu)_3$	−1.608	−1.677	−1.540	137	0.80

C

Unpublished Results

Ansa-Cyclopentadienyl and -Indenyl Cerium(III) Chemistry

Introduction

Although the synthesis route toward oxygen- and nitrogen-ligated cerium(IV) complexes has been investigated on various occasions, cerium(IV) halide complexes are still very rare. In most cases halogenido ligands are introduced in the course of the oxidation with halogenating oxidants like C_2Cl_6 or $TeBr_4$.[18, 38] One reason could be that halogenido ligands provide less stabilization toward the +IV oxidation state (Paper 3). Only cerium(IV) complexes bearing a single halogenido ligand are known. In order to achieve kinetic stabilization and prevent ligand reorganization and to avoid the formation of $CeCl_3$, *ansa*-cyclopentadienyl and *ansa*-indenyl complexes were aiming for the titanocene dichloride analogon of cerium. *Ansa*-type ligands are well-established in polymerization catalysts for other rare-earth metals, but were not used with the target of achieving cerium(IV) complexes.[175-178]

Results and Discussion

The general reaction pathway is depicted in Scheme C1 and features salt metathesis as the primary synthesis route. By using potassium or lithium as counter ions the formation of ate complexes was envisaged, which should subsequently be oxidized resulting in putative bis(chloride) complexes (Scheme C1 top). As intended, the formation of ate complexes was achieved with complex **U**, which can be spotted by the connectivity in Figure C1. However, the charge assignment proved problematic, therefore just qualitative aspects can be discussed. The product establishes a three-dimensional layer structure with polymeric layers of the cerium(III) complex and layers of Li atoms surrounded by multiple thf molecules. The central unit of the polymeric cerium layer features trimeric chloride-bridged clusters, which is depicted in Scheme C2. Each cerium(III) center is symmetrically surrounded by one *ansa*-cyclopentadienyl ligand and three μ_2-chlorido ligands, bridging three cerium centers and building a six-membered ring. One chloride ligand bridges the three Ce centers in a μ_3 fashion. Interestingly, the dimethylsilyl moiety of the *ansa*-cyclopentadienyl backbone shows interactions with lithium atoms of the next trimeric unit. This planar and symmetric environment leads to the layer structure, which can be also observed macroscopically, in the form of slimy consistency. Under reduced pressure the compound does not become a dry powder, but remains sticky, which made crystallization cumbersome. Elemental analyses also showed very low carbon and hydrogen values, due to the incorporated LiCl. Despite the

highly symmetric ligand environment, the ^{1}H NMR spectra were not conclusive, additionally impeded by the paramagnetic cerium(III) core. Notwithstanding an ate complex could be synthesized, but the polymeric structure seemed to hinder oxidation. Common oxidation agents used in cerium chemistry, like C_2Cl_6, I_2, $TeBr_4$ and *para* benzoquinone (bq) did not result in the respective cerium(IV) complexes, but instead showed no reaction (C_2Cl_6, I_2) or instant decomposition ($TeBr_4$, bq) as indicated by ^{1}H NMR spectroscopy.

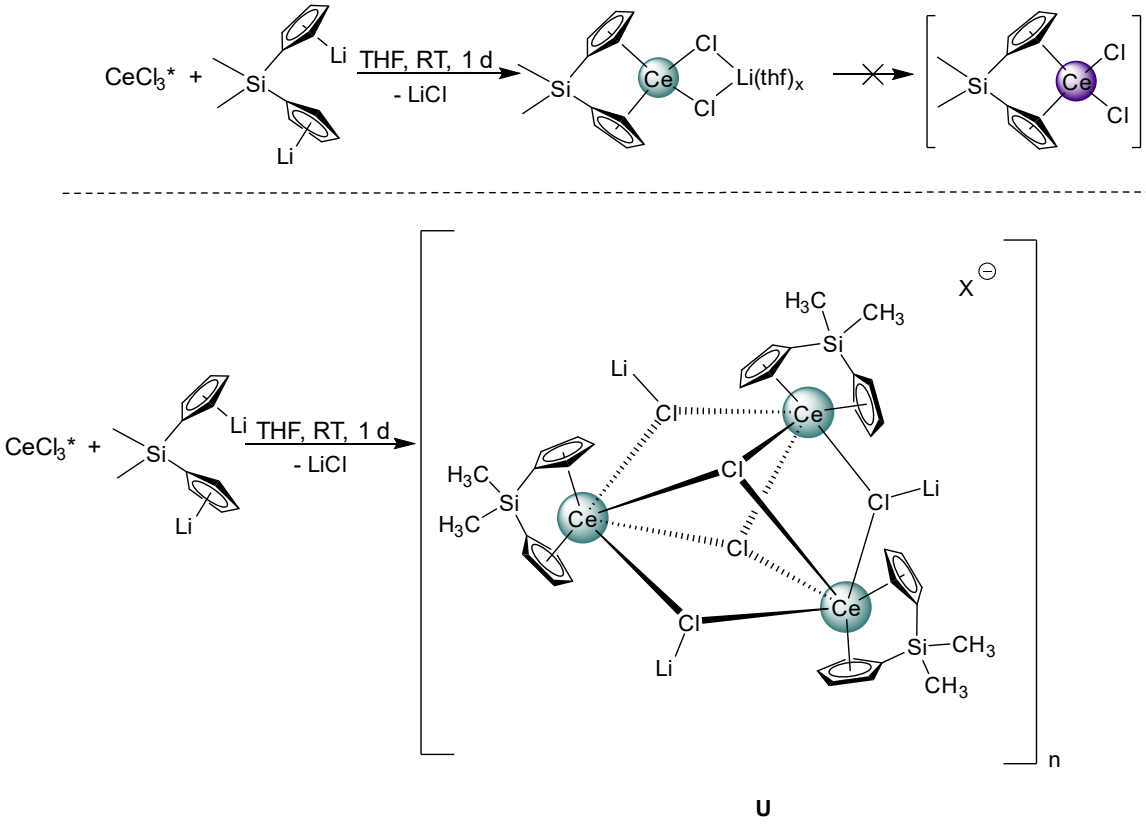

Scheme C1. Synthesis route of cerous **U**.

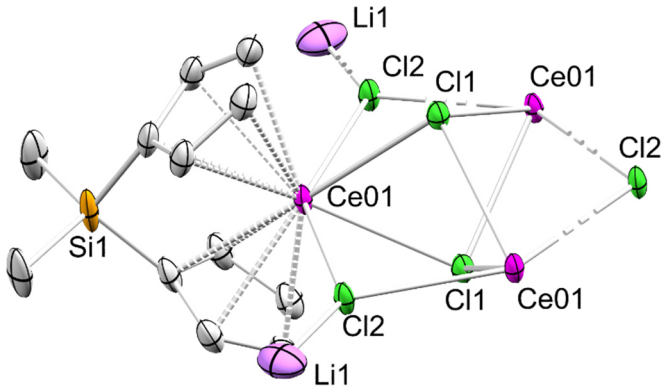

Figure C1. Section of the layer structure of connectivity of $[(Me_2SiCp_2)CeCl]_3(Li_3Cl_2X)$ (**U**).

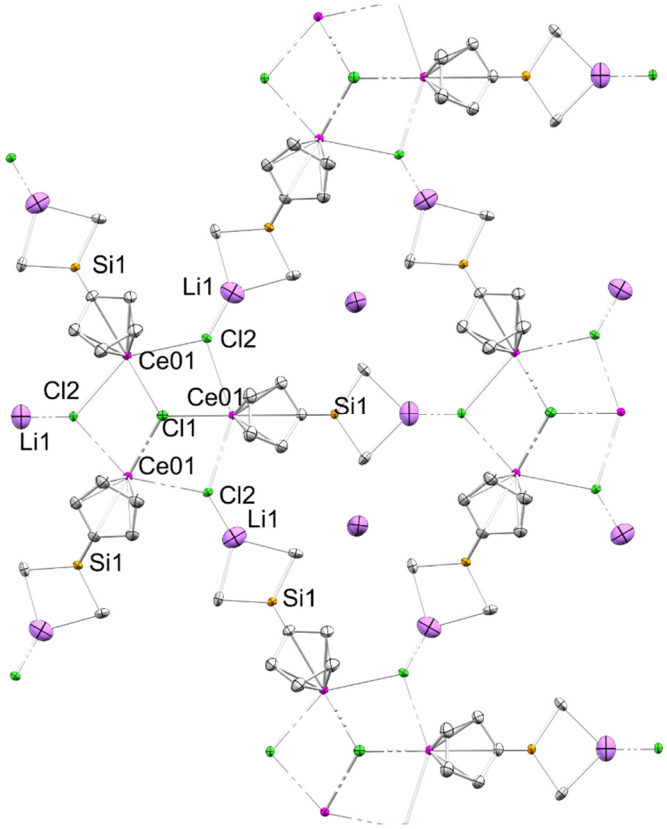

Figure C2. Top-down view on the layer structure of connectivity of $[(Me_2SiCp_2)CeCl]_3(Li_3Cl_2X)$ (**U**).

In order to increase the stability of the resulting *ansa*-complex, the addition of alkoxy coligands was probed, similar to the reaction toward $Cp^*_2Ce(OEt)_2$ ($\mathbf{N^{Et}}$). The reaction of **U** with NaOEt yielded in an intricate product mixture, of which side product **V** could be characterized via X-ray diffraction. Interestingly, the *ansa*-cyclopentadienyl backbone has been attacked, forming a strong Si−O bond in the process, but despite its high oxophilicity no ethoxy ligand was attached to the cerium(III) center. Instead, one unsubstituted cyclopentadienyl ligand is still attached, in addition to the *in situ* formed donor-functionalized cyclopentadienyl ligands $CpSi(Me_2)OEt$, which show an additional coordination of the oxygen to the cerium(III) center. A possible reaction mechanism is depicted in Scheme C2, but the complex could not be obtained by targeted synthesis, as always product mixtures occurred. Nevertheless, the solid-state structure allows an explanation of the instant decomposition, when adding ethoxide salts, because the strained $SiMe_2$ backbone can be attacked nucleophilically.

The solid-state structure revealed a distorted pseudo-trigonal bipyramidal coordination geometry with cyclopentadienyl centroids lying in the plane. The unsubstituted cyclopentadienyl ligand is slightly closer to the cerium center, probably caused by sterics.

Nevertheless, the Cp(SiMe$_2$)OEt ligands show unperturbed η^5 coordination as well. Interestingly, the Ce–O distances are very long, even compared to the distances of donor solvents like thf (*e.g.* in the case of $\mathbf{A}^{\mathbf{Cl}}$). The biting angle of the Cp(SiMe)OEt moiety, Cnt–Ce–O, in complex **V** is on average 83.87°, which is remarkable for a relatively small ligand. The combination of the large bite angle paired with the stabilization provided by the chelating OEt moiety, marks the ligand a potential target for future ligand syntheses.

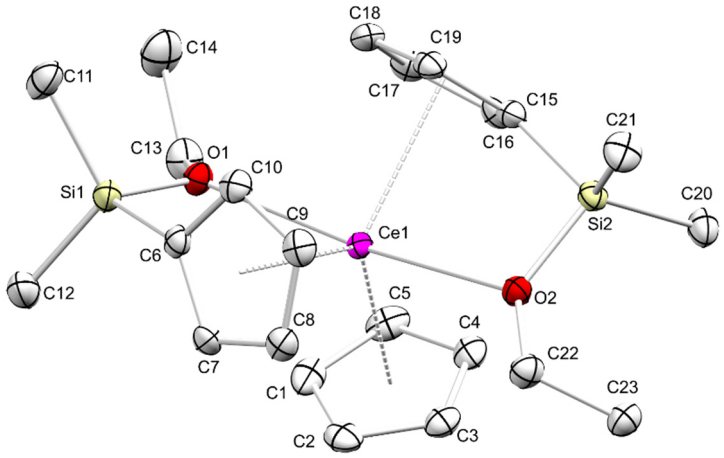

Figure C3. Crystal structure of [CpSi(OEt)Me$_2$]CeCp (**V**). Selected interatomic distances and angles: Ce–Cnt (Cp(SiMe)OEt) avg. 2.586 Å, Ce–C (Cp(SiMe)OEt) avg. 2.849 Å, Ce–Cnt (Cp) 2.575 Å, Ce–C(Cp) avg. 2.840 Å, Ce–O1 2.743(3) Å, Ce–O2 2.667(3) Å, Si–O avg. 1.686 Å, C–Si–O avg. 98.55°, Cnt–Ce–O avg. 83.87°.

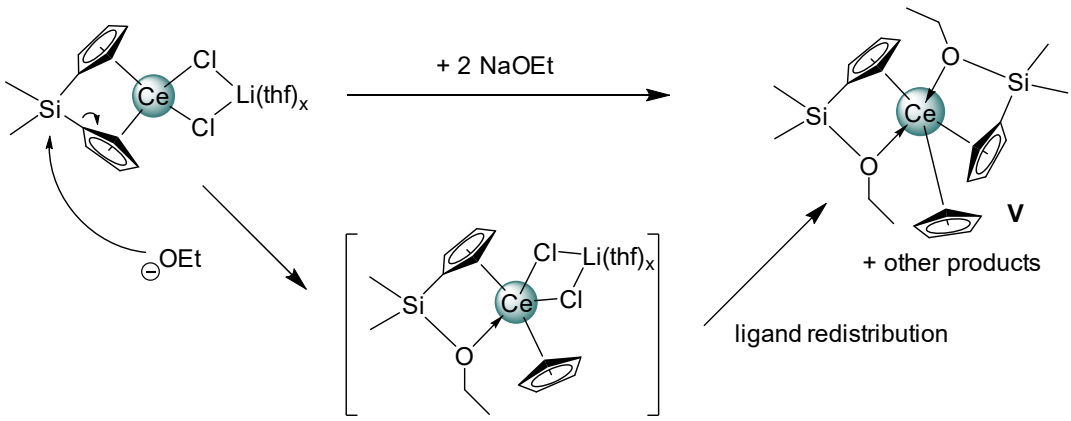

Scheme C2. Possible reaction mechanism toward **V**.

In addition to *ansa*-cyclopentadienyl ligands *ansa*-indenyl ligands were tested as well. The syntheses are shown in Scheme C3. Similarly, the purification proved difficult and elemental analyses with low carbon and hydrogen values suggested the incorporation of KCl as well. Due to poor solubility in solvents other than thf, removal of KCl was not possible. The slimy

consistency of the substances seemed to hinder crystallization, instead a highly viscose slurry was formed, and upon slow evaporation of the solvent, an amorphic powder was obtained.

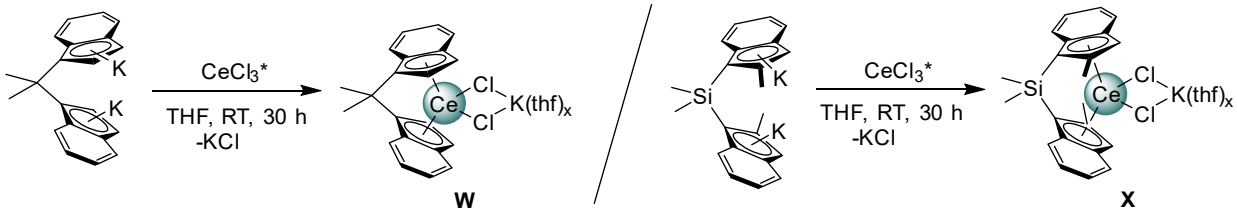

Scheme C3. **Synthesis paths to *ansa*-indenyl complexes.**

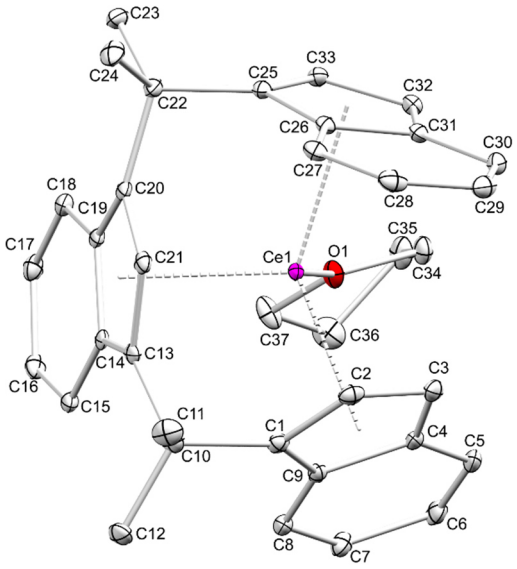

Figure C4. Crystal structure of [Ind(CMe$_2$)Ind(CMe$_2$)Ind]Ce(thf) **Y**. Selected bond lengths and angles: Ce−Cnt avg. 2.542 Å, Ce−C (range) 2.673(2) Å (C21) to 2.876(2) Å (C32), Ce−O 2.4898(16) Å, C1−C10−C13 100.74(13)°, C20−C22−C25 104.65(17)°, Cnt(C1−C9)−Ce−Cnt(C13−C21) 105.25°, Cnt(C13−C21)−Ce−Cnt(C25−C33) 104.78°.

Nonetheless, single-crystalline side product **Y** was achieved upon slow evaporation at ambient temperature over several weeks, demarcating itself from the bulk by its deep blue color and clear-cut edges. The crystal structure showed to be the cerium complex **Y** with a ligand consisting of three indenyl moieties, bridged by two CMe$_2$ groups like a tridentate ligand. This exemplifies that carbon backbones as well as silicon ones are not inert to decomposition. The solid-state structure shows a pseudo-tetrahedral coordination mode, with the peripheral indenyl ligands directed away from each other. Surprisingly, although three indenyl moieties show η^5 coordination via cyclopentadienyl rings the structure is sterically saturated by a thf molecule. This available space indicates that, despite a decrease in ionic radii, when oxidizing cerium(III) to cerium(IV), the ligand sphere is not completely crowded and the difficulties of achieving Ce(IV) complexes may concern the oxidation pathway

(kinetically) or the insufficient stability of the cerium(IV) complex (thermodynamically). It could not be ruled out, whether the ligand was formed by decomposition of the cerium *ansa*-complex by slow-evaporation or if it was present as minor side product in the potassium precursor.

Experimental Section

General Procedures. All operations were performed under rigorous exclusion of oxygen and moisture in an argon atmosphere, using standard Schlenk, high-vacuum, and glovebox techniques (MB Braun MB150B-G-I; <0.1 ppm of O_2, <0.1 ppm of H_2O). Solvents were dried and degassed prior to use and provided by an MBraun SPS800. Benzene-d*6* (99.5%) was received from Deutero GmbH and thf-d*8* from Eurisotop. These deuterated solvents were dried over NaK alloy for a minimum of 48 h and filtered through a filter pipette (Whatman) before use. Anhydrous $CeCl_3$ (99.99%) (Sigma Aldrich) was converted into $CeCl_3(thf)_{1.04}$ via soxhlet extraction. *n*BuLi and KH were purchased from Sigma-Aldrich and used as received. $H_2Cp_2SiMe_2$,[179-181] $H_2Ind_2CMe_2$,[182] and H_2(2-Me-Ind)$_2SiMe_2$[183] were prepared according to literature procedures and reacted with *n*BuLi or KH in standard procedures. NMR spectra were recorded on a Bruker AVII + 400 (^{1}H: 400.13 MHz; ^{13}C: 100.61 MHz), AVI + 300 (^{29}Si: 79.5 MHz) or AVII + 500 (^{1}H: 500.13 MHz; ^{13}C: 125.76 MHz) spectrometer in dried and deuterated solvents. DRIFT spectra were recorded on a ThermoFisher Scientific NICOLET 6700 FTIR spectrometer using dried KBr and KBr windows. The collected data were converted using the Kubelka−Munk refinement. CHN elemental analyses were performed on an Elementar Vario MICRO cube.

[(Me_2SiCp_2)$CeCl_2Li(thf)]_3$ (U). $CeCl_3(thf)_{1.04}$ (240.1 mg, 0.747 mmol) and $Li_2Cp_2SiMe_2$ (149.4 mg, 0.747 mmol) were suspended in thf (18 mL) and stirred for five days at ambient temperature. The mixture was filtered and the filtrate concentrated. Slow evaporation at −40 °C yielded pale yellow crystals of **U** (188.5 mg, 0.344 mmol, 46%). Elemental analysis (%) calcd for $C_{20}H_{30}CeCl_2LiO_2Si$ (548.50 g mol^{-1}): C 43.80, H 5.51; found: C 44.04, H 5.45.

(Me_2CInd_2)$CeCl_2K$ (W). $CeCl_3(thf)_{1.04}$ (88.4 mg, 0.275 mmol) and $K_2Ind_2CMe_2$ (95.9 mg, 0.275 mmol) were suspended in thf (18 mL) and stirred for three days at ambient temperature. The mixture was filtered and the filtrate concentrated. Slow evaporation at −40 °C yielded green powder of **W** (113.8 mg, 0.236 mmol, 86%). Crystallization at ambient temperature via slow evaporation led to dark blue crystals of **Y**, which could be characterized by X-ray diffraction, among the bulk of **W**. Elemental analysis (%) calcd for $C_{21}H_{18}CeCl_2K$ (481.38 g mol^{-1}): C 52.40, H 3.77; found: C 52.83 H 3.67.

[Me_2Si(2-Me-Ind)$_2$]$CeCl_2K$(thf) (X). $CeCl_3(thf)_{1.04}$ (76.5 mg, 0.238 mmol) and K_2(2-Me-Ind)$_2SiMe_2$ (93.5 mg, 0.238 mmol) were suspended in thf (15 mL) and stirred for three days at ambient temperature. The mixture was filtered and the filtrate concentrated. Slow evaporation at −40 °C yielded an orange powder of **X** (93.5 mg, 0,147 mmol, 62%). Elemental analysis calcd for $C_{26}H_{30}CeCl_2KOSi$ (636.72 g mol^{-1}): C 49.05, H 4.75; found: C 50.34, H 4.25.

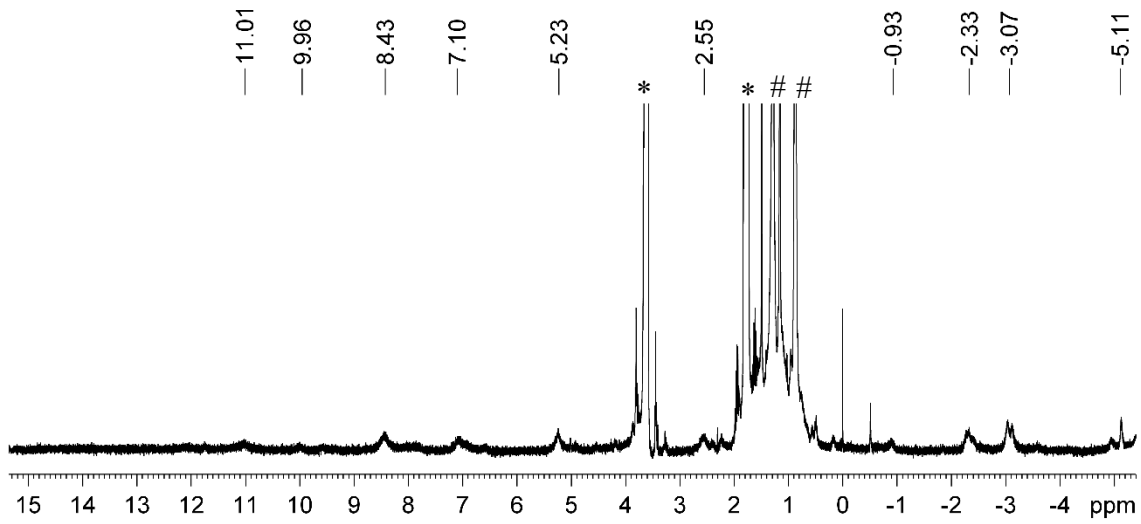

Figure C5. ^{1}H NMR spectrum (400.1 MHz, thf-*d8*, 26 °C) of **U** (* → thf-*d8*, # → *n*-hexane).

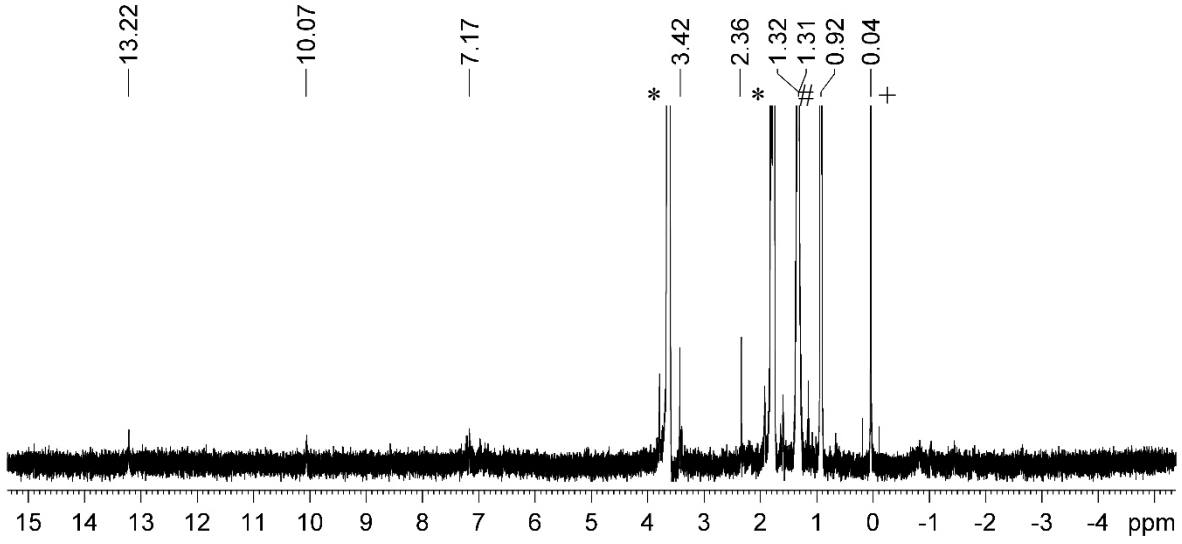

Figure C6. ^{1}H NMR spectrum (400.1 MHz, thf-*d8*, 26 °C) of **V** (* → thf-*d8*, # → *n*-hexane, + → $SiMe_4$).

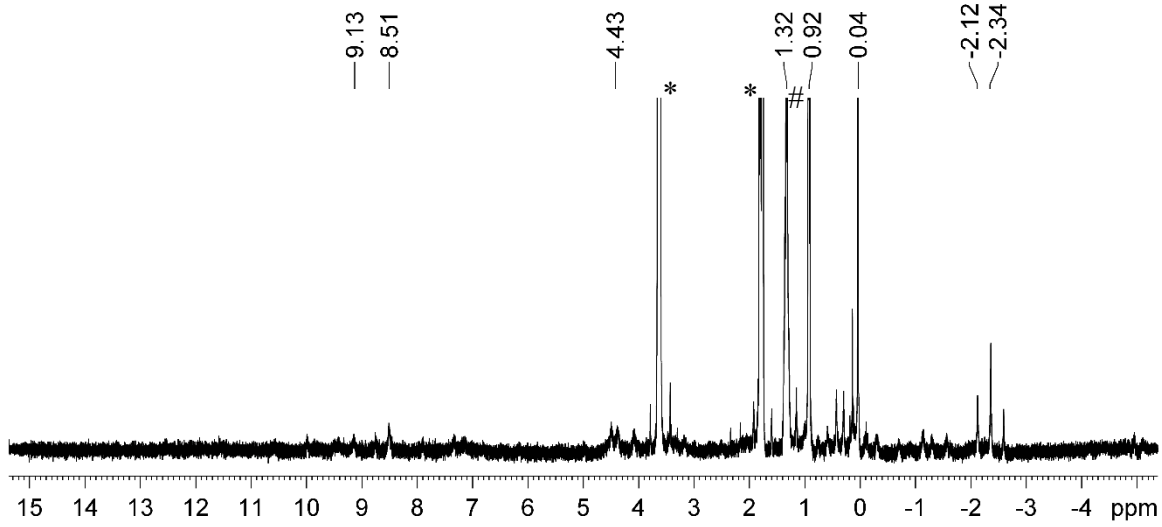

Figure C7. ^{1}H NMR spectrum (400.1 MHz, thf-*d8*, 26 °C) of **W** (* → thf-*d8*, # → *n*-hexane).

Table C1. Crystallographic data for compounds **U**, **V** and **Y**.

	U	**V**	**Y**
project name	LK131	LK136	LH267
formula	$C_{144}H_{168}Ce_{12}Cl_{12}Li_2Si_{12}$	$C_{23}H_{35}CeO_2Si_2$	$C_{37}H_{37}CeO$
M [g · mol^{-1}]	4356.57	539.81	637.78
λ [Å]	0.71073	0.71073	0.71073
cell	hexagonal	monoclinic	monoclinic
space group	$P\bar{6}2m$	$P2_{1/n}$	$P2_{1/c}$
a [Å]	13.807(3)	12.5915(16)	8.9815(2)
b [Å]	13.807(3)	12.8732(16)	19.0078(5)
c [Å]	13.673(3)	15.7249(19)	16.8514(4)
α [°]	90	90	90
β [°]	90	107.524(3)	104.1630(10)
γ [°]	120	90	90
V [Å^3]	2257.4(11)	2430.6(5)	2789.408(12)
Z	1	4	4
F(000)	2106	1100	1300
T [K]	100(2)	100(2)	100(2)
ρ_{calcd} [g · mol^3]	3.205	1.475	1.519
μ [mm^{-1}]	6.504	1.987	1.661
R_1 (I>2σ(I))	0.0251	0.0439	0.0274
ωR_2 (all data)	0.0632	0.1187	0.0674
Goodness of fit	1.052	1.051	1.118

D

Bibliography

[1] T. J. Kealy, P. L. Pauson, *Nature* **1951**, *168*, 1039-1040.

[2] S. A. Miller, J. A. Tebboth, J. F. Tremaine, *J. Chem. Soc.* **1952**, 632-635.

[3] R. B. Woodward, M. Rosenblum, M. C. Whiting, *J. Am. Chem. Soc.* **1952**, *74*, 3458-3459.

[4] F. A. Carey, R. J. Sundberg, H. J. Schafer, D. Hoppe, G. Erker, D. Fischer-Henningsen, S. Freund, S. Graf, *Organische Chemie: ein weiterführendes Lehrbuch*, Wiley-VCH, **1995**.

[5] P. Jutzi, *Chem. Rev.* **1986**, *86*, 983-996.

[6] C. Janiak, H. Schumann, *Adv. Organomet. Chem.* **1991**, *33*, 291-393.

[7] K. Ziegler, E. Holzkamp, H. Breil, H. Martin, *Angew. Chem.* **1955**, *67*, 541-547.

[8] G. Natta, *Angew Chem* **1964**, *76*, 553-566.

[9] G. Natta, *Science* **1965**, *147*, 261-272.

[10] E. O. Fischer, W. Pfab, *Z. Naturforsch. B* **1952**, *7*, 377-379.

[11] G. Wilkinson, M. Rosenblum, M. C. Whiting, R. B. Woodward, *J. Am. Chem. Soc.* **1952**, *74*, 2125-2126.

[12] A. R. Willauer, C. T. Palumbo, R. Scopelliti, I. Zivkovic, I. Douair, L. Maron, M. Mazzanti, *Angew. Chem.* **2020**, *132*, 3577-3581.

[13] A. R. Willauer, C. T. Palumbo, F. Fadaei-Tirani, I. Zivkovic, I. Douair, L. Maron, M. Mazzanti, *J. Am. Chem. Soc.* **2020**, *142*, 5538-5542.

[14] N. T. Rice, I. A. Popov, D. R. Russo, J. Bacsa, E. R. Batista, P. Yang, J. Telser, H. S. La Pierre, *J. Am. Chem. Soc.* **2019**, *141*, 13222-13233.

[15] C. T. Palumbo, I. Zivkovic, R. Scopelliti, M. Mazzanti, *J. Am. Chem. Soc.* **2019**, *141*, 9827-9831.

[16] V. Sridharan, J. C. Menéndez, *Chem. Rev.* **2010**, *110*, 3805-3849.

[17] J. Xu, E. Radkov, M. Ziegler, K. N. Raymond, *Inorg. Chem.* **2000**, *39*, 4156-4164.

[18] R. Anwander, M. Dolg, F. T. Edelmann, *Chem. Soc. Rev.* **2017**, *46*, 6697-6709.

[19] D. Esrafilzadeh, A. Zavabeti, R. Jalili, P. Atkin, J. Choi, B. J. Carey, R. Brkljača, A. P. O'Mullane, M. D. Dickey, D. L. Officer, *Nat. Commun.* **2019**, *10*, 1-8.

[20] J. Birmingham, G. Wilkinson, *J. Am. Chem. Soc.* **1956**, *78*, 42-44.

[21] L. Xing-Fu, S. Eggers, J. Kopf, W. Jahn, R. Dieter Fischer, C. Apostolidis, B. Kanellakopulos, F. Benetollo, A. Polo, G. Bombieri, *Inorg. Chim. Acta* **1985**, *100*, 183-199.

[22] A. R. Crozier, K. W. Törnroos, C. Maichle-Mössmer, R. Anwander, *Eur. J. Inorg. Chem.* **2013**, 409-414.

[23] P. S. Gradeff, K. Yunlu, T. J. Deming, J. M. Olofson, J. W. Ziller, W. J. Evans, *Inorg. Chem.* **1989**, *28*, 2600-2604.

[24] Â. Domingos, N. Marques, A. Pires de Matos, M. G. Silva-Valenzuela, L. B. Zinner, *Polyhedron* **1993**, *12*, 2545-2549.

[25] U. Baisch, S. Pagano, M. Zeuner, J. Schmedt auf der Günne, O. Oeckler, W. Schnick, *Organometallics* **2006**, *25*, 3027-3033.

[26] C. Wenqi, L. Guanyang, X. Jusong, W. Gecheng, Z. Yin, J. Zhongsheng, *J. Organomet. Chem.* **1994**, *467*, 75-78.

[27] J. G. Brennan, S. D. Stults, R. A. Andersen, A. Zalkin, *Organometallics* **1988**, *7*, 1329-1334.

[28] S. D. Stults, R. A. Andersen, A. Zalkin, *Organometallics* **1990**, *9*, 115-122.

[29] S. Stults, A. Zalkin, *Acta Cryst. C* **1987**, *43*, 430-432.

[30] S. D. Stults, R. A. Andersen, A. Zalkin, *Organometallics* **1990**, *9*, 1623-1629.

[31] M. A. Angadol, D. H. Woen, C. J. Windorff, J. W. Ziller, W. J. Evans, *Organometallics* **2019**, *38*, 1151-1158.

[32] M. Thouraya, B. Jean-Claude, T. Pierre, E. Michel, *Eur. J. Inorg. Chem.* **2004**, 1996-2000.

[33] T. Mehdoui, J.-C. Berthet, P. Thuéry, M. Ephritikhine, *Dalton Trans.* **2004**, 579-590.

[34] T. Mehdoui, J.-C. Berthet, P. Thuéry, L. Salmon, E. Rivière, M. Ephritikhine, *Chem. Eur. J.* **2005**, *11*, 6994-7006.

[35] T. Mehdoui, J.-C. Berthet, P. Thuéry, M. Ephritikhine, *Dalton Trans.* **2005**, 1263-1272.

[36] T. Mehdoui, J.-C. Berthet, P. Thuéry, M. Ephritikhine, *Chem. Commun.* **2005**, 2860-2862.

[37] M. Ephritikhine, *Organometallics* **2013**, *32*, 2464-2488.

[38] D. Schneider, N. Harmgarth, F. T. Edelmann, R. Anwander, *Chem. Eur. J.* **2017**, *23*, 12243-12252.

[39] J. L. Krinsky, S. G. Minasian, J. Arnold, *Inorg. Chem.* **2011**, *50*, 345-357.

[40] S. Al-Juaid, Y. K. Gun'ko, P. B. Hitchcock, M. F. Lappert, S. Tian, *J. Organomet. Chem.* **1999**, *582*, 143-152.

[41] C. D. Sofield, R. A. Andersen, *J. Organomet. Chem.* **1995**, *501*, 271-276.

[42] W. J. Evans, D. B. Rego, J. W. Ziller, *Inorg. Chem.* **2006**, *45*, 10790-10798.

[43] A. Zazzetta, A. Greco, *Acta Cryst. B* **1979**, *35*, 457-460.

[44] H. Schumann, *Angew. Chem. Int. Ed.***1984**, *23*, 474-493.

[45] M. D. Rausch, K. J. Moriarty, J. L. Atwood, J. A. Weeks, W. E. Hunter, H. G. Brittain, *Organometallics* **1986**, *5*, 1281-1283.

[46] W. J. Evans, J. M. Olofson, H. Zhang, J. L. Atwood, *Organometallics* **1988**, *7*, 629-633.

[47] W. J. Evans, C. A. Seibel, J. W. Ziller, *J. Am. Chem. Soc.* **1998**, *120*, 6745-6752.

[48] W. J. Evans, J. M. Perotti, S. A. Kozimor, T. M. Champagne, B. L. Davis, G. W. Nyce, C. H. Fujimoto, R. D. Clark, M. A. Johnston, J. W. Ziller, *Organometallics* **2005**, *24*, 3916-3931.

[49] T. J. Mueller, J. W. Ziller, W. J. Evans, *Dalton Trans.* **2010**, *39*, 6767-6773.

[50] E. W. J., M. T. J., Z. J. W., *Chem. Eur. J.* **2010**, *16*, 964-975.

[51] C. T. Palumbo, M. E. Fieser, J. W. Ziller, W. J. Evans, *Organometallics* **2017**, *36*, 3721-3728.

[52] P. N. Hazin, J. W. Bruno, H. G. Brittain, *Organometallics* **1987**, *6*, 913-918.

[53] E. B. Lobkovsky, Y. K. Gun'ko, B. M. Bulychev, V. K. Belsky, G. L. Soloveichik, M. Y. Antipin, *J. Organomet. Chem.* **1991**, *406*, 343-352.

[54] F. Ortu, D. Packer, J. Liu, M. Burton, A. Formanuik, D. P. Mills, *J. Organomet. Chem.* **2018**, *857*, 45-51.

[55] M. D. Walter, D. Bentz, F. Weber, O. Schmitt, G. Wolmershäuser, H. Sitzmann, *New. J. Chem.* **2007**, *31*, 305-318.

[56] D. Schneider, R. Anwander, *Eur. J. Inorg. Chem.* **2017**, 1180-1188.

[57] J. Liu, D. Reta, J. A. Cleghorn, Y. X. Yeoh, F. Ortu, C. A. P. Goodwin, N. F. Chilton, D. P. Mills, *Chem. Eur. J.* **2019**, *25*, 7749-7758.

[58] E. L. Werkema, E. Messines, L. Perrin, L. Maron, O. Eisenstein, R. A. Andersen, *J. Am. Chem. Soc.* **2005**, *127*, 7781-7795.

[59] L. Maron, E. L. Werkema, L. Perrin, O. Eisenstein, R. A. Andersen, *J. Am. Chem. Soc.* **2005**, *127*, 279-292.

[60] E. L. Werkema, R. A. Andersen, *J. Am. Chem. Soc.* **2008**, *130*, 7153-7165.

[61] P. N. Hazin, J. C. Huffman, J. W. Bruno, *Organometallics* **1987**, *6*, 23-27.

[62] P. N. Hazin, C. Lakshminarayan, L. S. Brinen, J. L. Knee, J. W. Bruno, W. E. Streib, K. Folting, *Inorg. Chem.* **1988**, *27*, 1393-1400.

[63] P. N. Hazin, J. W. Bruno, G. K. Schulte, *Organometallics* **1990**, *9*, 416-423.

[64] F. Ortu, J. M. Fowler, M. Burton, A. Formanuik, D. P. Mills, *New. J. Chem.* **2015**, *39*, 7633-7639.

[65] P. Ransom, T. A. Q. Arnold, A. L. Thompson, J.-C. Buffet, D. O'Hare, *Dalton Trans.* **2012**, *41*, 11267-11269.

[66] Y. K. Gun'ko, B. M. Bulychev, G. L. Soloveichik, V. K. Belsky, *J. Organomet. Chem.* **1992**, *424*, 289-300.

[67] H. J. Heeres, J. Renkema, M. Booij, A. Meetsma, J. H. Teuben, *Organometallics* **1988**, *7*, 2495-2502.

[68] O. T. Summerscales, E. R. Batista, B. L. Scott, M. P. Wilkerson, A. D. Sutton, *Eur. J. Inorg. Chem.* **2016**, 4551-4556.

[69] O. T. Summerscales, C. M. Moore, B. L. Scott, M. P. Wilkerson, A. D. Sutton, *Organometallics* **2017**, *36*, 4682-4685.

[70] Y. K. Gun'ko, P. B. Hitchcock, M. F. Lappert, *Organometallics* **2000**, *19*, 2832-2834.

[71] O. Eisenstein, P. B. Hitchcock, A. G. Hulkes, M. F. Lappert, L. Maron, *Chem. Commun.* **2001**, 1560-1561.

[72] M. Nishiura, J. Baldamus, T. Shima, K. Mori, Z. Hou, *Chem. Eur. J.* **2011**, *17*, 5033-5044.

[73] E. L. Werkema, L. Maron, O. Eisenstein, R. A. Andersen, *J. Am. Chem. Soc.* **2007**, *129*, 6662-6662.

[74] E. L. Werkema, R. A. Andersen, A. Yahia, L. Maron, O. Eisenstein, *Organometallics* **2009**, *28*, 3173-3185.

[75] E. L. Werkema, A. Yahia, L. Maron, O. Eisenstein, R. A. Andersen, *Organometallics* **2010**, *29*, 5103-5110.

[76] E. L. Werkema, R. A. Andersen, L. Maron, O. Eisenstein, *Dalton Trans.* **2010**, *39*, 6648-6660.

[77] E. L. Werkema, A. Yahia, L. Maron, O. Eisenstein, R. A. Andersen, *New. J. Chem.* **2010**, *34*, 2189-2196.

[78] E. L. Werkema, L. Castro, L. Maron, O. Eisenstein, R. A. Andersen, *Organometallics* **2012**, *31*, 870-881.

[79] E. L. Werkema, L. Castro, L. Maron, O. Eisenstein, R. A. Andersen, *New. J. Chem.* **2013**, *37*, 132-142.

[80] L. Perrin, E. L. Werkema, O. Eisenstein, R. A. Andersen, *Inorg. Chem.* **2014**, *53*, 6361-6373.

[81] U. Bayer, L. Bock, C. Maichle-Mössmer, R. Anwander, *Eur. J. Inorg. Chem.* **2020**, *2020*, 101-106.

[82] D. Bradley, A. Chatterjee, W. Wardlaw, *J. Chem. Soc* **1956**, 2260-2264.

[83] D. C. Bradley, A. K. Chatterjee, W. Wardlaw, *J. Chem. Soc* **1956**, 3469-3472.

[84] D. C. Bradley, A. K. Chatterjee, W. Wardlaw, *J. Chem. Soc* **1956**, 2260-2264.

[85] D. Bradley, A. Chatterjee, W. Wardlaw, *J. Chem. Soc* **1957**, 2600-2604.

[86] D. Bradley, R. Mehrotra, I. Rothwell, A. Singh, *Alkoxo and aryloxo derivatives of metals*, Elsevier, **2001**.

[87] W. J. Evans, T. J. Deming, J. W. Ziller, *Organometallics* **1989**, *8*, 1581-1583.

[88] W. J. Evans, T. J. Deming, J. M. Olofson, J. W. Ziller, *Inorg. Chem.* **1989**, *28*, 4027-4034.

[89] H. J. Heeres, A. Meetsma, J. H. Teuben, R. D. Rogers, *Organometallics* **1989**, *8*, 2637-2646.

[90] H. J. Heeres, A. Meetsma, J. H. Teuben, *J. Chem. Soc, Chem. Commun.* **1988**, 962-963.

[91] M. Booij, N. H. Kiers, H. J. Heeres, J. H. Teuben, *J. Organomet. Chem.* **1989**, *364*, 79-86.

[92] H. J. Heeres, J. H. Teuben, R. D. Rogers, *J. Organomet. Chem.* **1989**, *364*, 87-96.

[93] Y. K. Gun'ko, P. B. Hitchcock, M. F. Lappert, *J. Organomet. Chem.* **1995**, *499*, 213-219.

[94] C. T. Palumbo, L. E. Darago, C. J. Windorff, J. W. Ziller, W. J. Evans, *Organometallics* **2018**, *37*, 900-905.

[95] F. Ortu, J. Liu, M. Burton, J. M. Fowler, A. Formanuik, M.-E. Boulon, N. F. Chilton, D. P. Mills, *Inorg. Chem.* **2017**, *56*, 2496-2505.

[96] G. Helgesson, S. Jagner, *Organometallics* **1992**, *11*, 350-356.

[97] P. L. Arnold, T. Cadenbach, I. H. Marr, A. A. Fyfe, N. L. Bell, R. Bellabarba, R. P. Tooze, J. B. Love, *Dalton Trans.* **2014**, *43*, 14346-14358.

[98] D. Kazhdan, W. A. Chomitz, W. H. Harman, T. M. Hoette, C.-H. Park, *Acta Cryst. E* **2007**, *63*, 1656.

[99] B.-J. Deelman, M. Booij, A. Meetsma, J. H. Teuben, H. Kooijman, A. L. Spek, *Organometallics* **1995**, *14*, 2306-2317.

[100] J. C. B. T. Mehdoui, P. Thuery, M. Ephritikhine, *CCDC* **2013**.

[101] D. Gu, C. Yi, W. Ren, *Inorg Chem* **2019**, *58*, 9260-9269.

[102] T. J. Mueller, G. W. Nyce, W. J. Evans, *Organometallics* **2011**, *30*, 1231-1235.

[103] D. Gu, C. Yi, W. Ren, *Inorg. Chem.* **2019**, *58*, 9260-9269.

[104] M. Roger, L. Belkhiri, P. Thuéry, T. Arliguie, M. Fourmigué, A. Boucekkine, M. Ephritikhine, *Organometallics* **2005**, *24*, 4940-4952.

[105] M. Roger, L. Belkhiri, T. Arliguie, P. Thuéry, A. Boucekkine, M. Ephritikhine, *Organometallics* **2008**, *27*, 33-42.

[106] S. S. Rozenel, L. Perrin, O. Eisenstein, R. A. Andersen, *Organometallics* **2017**, *36*, 97-108.

[107] C. L. Webster, J. E. Bates, M. Fang, J. W. Ziller, F. Furche, W. J. Evans, *Inorg. Chem.* **2013**, *52*, 3565-3572.

[108] W. J. Evans, E. Montalvo, D. J. Dixon, J. W. Ziller, A. G. DiPasquale, A. L. Rheingold, *Inorg. Chem.* **2008**, *47*, 11376-11381.

[109] P. Sekar, J. A. Ibers, *Inorg. Chim. Acta* **2006**, *359*, 2751-2755.

[110] K. C. Armstrong, S. Hohloch, T. D. Lohrey, R. A. Zarkesh, J. Arnold, M. R. Anstey, *Dalton Trans.* **2016**, *45*, 18653-18660.

[111] J. Maynadié, J.-C. Berthet, P. Thuéry, M. Ephritikhine, *Organometallics* **2007**, *26*, 2623-2629.

[112] C. M. Kotyk, M. R. MacDonald, J. W. Ziller, W. J. Evans, *Organometallics* **2015**, *34*, 2287-2295.

[113] M. E. Fieser, M. R. MacDonald, B. T. Krull, J. E. Bates, J. W. Ziller, F. Furche, W. J. Evans, *J. Am. Chem. Soc.* **2015**, *137*, 369-382.

[114] C. M. Kotyk, M. E. Fieser, C. T. Palumbo, J. W. Ziller, L. E. Darago, J. R. Long, F. Furche, W. J. Evans, *Chem. Sci.* **2015**, *6*, 7267-7273.

[115] W. J. Evans, *Organometallics* **2016**, *35*, 3088-3100.

[116] H. J. Heeres, A. Meetsma, J. H. Teuben, *J. Organomet. Chem.* **1991**, *414*, 351-359.

[117] C. P. Burns, X. Yang, S. Sung, J. D. Wofford, N. S. Bhuvanesh, M. B. Hall, M. Nippe, *Chem. Commun.* **2018**, *54*, 10893-10896.

[118] U. Kilimann, M. Schaefer, R. Herbst-Irmer, F. T. Edelmann, *J. Organomet. Chem.* **1994**, *469*, C15-C18.

[119] A. Edelmann, V. Lorenz, C. G. Hrib, L. Hilfert, S. Blaurock, F. T. Edelmann, *Organometallics* **2013**, *32*, 1435-1444.

[120] J. J. Le Roy, I. Korobkov, J. E. Kim, E. J. Schelter, M. Murugesu, *Dalton Trans.* **2014**, *43*, 2737-2740.

[121] K. O. Hodgson, K. N. Raymond, *Inorg. Chem.* **1972**, *11*, 3030-3035.

[122] T. R. Boussie, D. C. Eisenberg, J. Rigsbee, A. Streitwieser, A. Zalkin, *Organometallics* **1991**, *10*, 1922-1928.

[123] F. Mares, K. Hodgson, A. Streitwieser, *J. Organomet. Chem.* **1970**, *24*, C68-C70.

[124] V. Lorenz, B. M. Schmiege, C. G. Hrib, J. W. Ziller, A. Edelmann, S. Blaurock, W. J. Evans, F. T. Edelmann, *J Am Chem Soc* **2011**, *133*, 1257-1259.

[125] A. Greco, S. Cesca, W. Bertolini, *J. Organomet. Chem.* **1976**, *113*, 321-330.

[126] U. Reissmann, P. Poremba, L. Lameyer, D. Stalke, F. T. Edelmann, *Chem. Commun.* **1999**, 1865-1866.

[127] F. Mares, K. O. Hodgson, A. Streitwieser, *J. Organomet. Chem.* **1971**, *28*, C24-C26.

[128] S. Anfang, G. Seybert, K. Harms, G. Geiseler, W. Massa, K. Dehnicke, *Z. Anorg. Allg. Chem.* **1998**, *624*, 1187-1192.

[129] H.-D. Amberger, F. T. Edelmann, J. Gottfriedsen, R. Herbst-Irmer, S. Jank, U. Kilimann, M. Noltemeyer, H. Reddmann, M. Schäfer, *Inorg. Chem.* **2009**, *48*, 760-772.

[130] U. Reißmann, P. Poremba, M. Noltemeyer, H.-G. Schmidt, F. T. Edelmann, *Inorg. Chim. Acta* **2000**, *303*, 156-162.

[131] U. Kilimann, M. Schäfer, R. Herbst-Irmer, F. T. Edelmann, *J. Organomet. Chem.* **1994**, *469*, C10-C14.

[132] J. D. Jamerson, A. P. Masino, J. Takats, *J. Organomet. Chem.* **1974**, *65*, C33-C36.

[133] K. Mashima, H. Takaya, *Tetrahedron Lett.* **1989**, *30*, 3697-3700.

[134] F. M. Sroor, C. G. Hrib, P. Liebing, L. Hilfert, S. Busse, F. T. Edelmann, *Dalton Trans.* **2016**, *45*, 13332-13346.

[135] B. L. Kalsotra, R. K. Multani, B. D. Jain, *Isr. J. Chem.* **1971**, *9*, 569-572.

[136] B. Kalsotra, S. Anand, R. Multani, B. Jain, *Chem. Inf. Dienst Org. Chem.* **1971**, *2*.

[137] B. L. Kalsotra, R. K. Multani, B. D. Jain, *J. Inorg. Nucl.* **1972**, *34*, 2679-2680.

[138] B. L. Kalsotra, R. K. Multani, B. D. Jain, *Chem. Ind. (London)* **1972**, 339-340.

[139] K. M. Shushma, R. K. Multani, B. L. Kalsotra, *J. Chin. Chem. Soc.* **1973**, *20*, 171-173.

[140] S. Kapur, B. L. Kalsotra, R. K. Multani, *J. Inorg. Nucl.* **1974**, *36*, 932-934.

[141] S. Kapur, R. K. Multani, *J. Organomet. Chem.* **1973**, *63*, 301-303.

[142] G. B. Deacon, T. D. Tuong, D. G. Vince, *Polyhedron* **1983**, *2*, 969-970.

[143] A. Gulino, M. Casarin, V. P. Conticello, J. G. Gaudiello, H. Mauermann, I. Fragala, T. J. Marks, *Organometallics* **1988**, *7*, 2360-2364.

[144] A. Sutton, D. Clark, B. Scott, J. Gordon, *Inorganics* **2015**, *3*, 589.

[145] P. Dröse, A. R. Crozier, S. Lashkari, J. Gottfriedsen, S. Blaurock, C. G. Hrib, C. Maichle-Mössmer, C. Schädle, R. Anwander, F. T. Edelmann, *J. Am. Chem. Soc.* **2010**, *132*, 14046-14047.

[146] U. Kilimann, R. Herbst-Irmer, D. Stalke, F. T. Edelmann, *Angew. Chem. Int. Ed.* **1994**, *33*, 1618-1621.

[147] A. Streitwieser, S. A. Kinsley, C. H. Jenson, J. T. Rigsbee, *Organometallics* **2004**, *23*, 5169-5175.

[148] C. Booth, R. L. Halbach, G. Nocton, L. Maron, R. A. Andersen, *Inorg. Chem*., **2016**, 57, 12, 7290.

[149] D. E. Smiles, R. A. Andersen, E. R. Batista, D. L. Clark, J. M. Keith, S. A. Kozimor, R. L. Martin, D. K. Shuh, S. C. E. Stieber, T. Tyliszczak, S. G. Minasian, *Inorg. Chem*., **2018**, 256.

[150] R. L. Halbach, G. Nocton, C. H. Booth, L. Maron, R. A. Andersen, *Inorg. Chem.* **2018**, *57*, 7290-7298.

[151] W. Lukens, C. H. Booth, M. D. Walter, *Dalton Trans.* **2021**, Ahead of Print.

[152] C. Neumann, P. Fulde, *Z. Phys. B, Condens. Matter* **1989**, *74*, 277-278.

[153] M. Dolg, P. Fulde, W. Kuechle, C. S. Neumann, H. Stoll, *J. Chem. Phys.* **1991**, *94*, 3011-3017.

[154] M. Dolg, P. Fulde, H. Stoll, H. Preuss, A. Chang, R. M. Pitzer, *Chem. Phys.* **1995**, *195*, 71-82.

[155] M. Dolg, P. Fulde, *Chem. Eur. J.* **1998**, *4*, 200-204.

[156] C. H. Booth, M. D. Walter, M. Daniel, W. W. Lukens, R. A. Andersen, *Phys. Rev. Lett.* **2005**, *95*, 267202.

[157] O. Moossen, M. Dolg, *Chem. Phys. Lett.* **2014**, *594*, 47-50.

[158] M. Dolg, John Wiley & Sons Ltd., **2015**, 425-450.

[159] D. E. Smiles, E. R. Batista, C. H. Booth, D. L. Clark, J. M. Keith, S. A. Kozimor, R. L. Martin, S. G. Minasian, D. K. Shuh, S. C. E. Stieber, T. Tyliszczak, *Chem. Sci.* **2020**, Ahead of Print.

[160] N. Roesch, A. Streitwieser, Jr., *J. Am. Chem. Soc.* **1983**, *105*, 7237-7240.

[161] A. Streitwieser, Jr., S. A. Kinsley, J. T. Rigsbee, I. L. Fragala, E. Ciliberto, *J. Am. Chem. Soc.* **1985**, *107*, 7786-7788.

[162] N. M. Edelstein, P. G. Allen, J. J. Bucher, D. K. Shuh, C. D. Sofield, N. Kaltsoyannis, G. H. Maunder, M. R. Russo, A. Sella, *J. Am. Chem. Soc.* **1996**, *118*, 13115-13116.

[163] H.-D. Amberger, H. Reddmann, F. T. Edelmann, *J. Organomet. Chem.* **2005**, *690*, 2238-2242.

[164] M. D. Walter, C. H. Booth, W. W. Lukens, R. A. Andersen, *Organometallics* **2009**, *28*, 698-707.

[165] W. Liu, M. Dolg, P. Fulde, *Inorg. Chem.* **1998**, *37*, 1067-1072.

[166] O. T. Summerscales, F. G. N. Cloke, *Coord. Chem. Rev.* **2006**, *250*, 1122-1140.

[167] G. Balazs, F. G. N. Cloke, J. C. Green, R. M. Harker, A. Harrison, P. B. Hitchcock, C. N. Jardine, R. Walton, *Organometallics* **2007**, *26*, 3111-3119.

[168] A. Ashley, G. Balazs, A. Cowley, J. Green, C. H. Booth, D. O'Hare, *Chem. Commun.* **2007**, 1515-1517.

[169] R. L. Halbach, G. g. Nocton, C. H. Booth, L. Maron, R. A. Andersen, *Inorg. Chem.* **2018**, *57*, 7290-7298.

[170] L. F. Veiros, *J. Organomet. Chem.* **1999**, *587*, 221-232.

[171] L. F. Veiros, *Organometallics* **2000**, *19*, 5549-5558.

[172] T. A. Albright, P. Hofmann, R. Hoffmann, C. P. Lillya, P. A. Dobosh, *J. Am. Chem. Soc.* **1983**, *105*, 3396-3411.

[173] T. F. Jenkins, D. H. Woen, L. N. Mohanam, J. W. Ziller, F. Furche, W. J. Evans, *Organometallics* **2018**, *37*, 3863-3873.

[174] C. A. P. Goodwin, J. Su, T. E. Albrecht-Schmitt, A. V. Blake, E. R. Batista, S. R. Daly, S. Dehnen, W. J. Evans, A. J. Gaunt, S. A. Kozimor, N. Lichtenberger, B. L. Scott, P. Yang, *Angew. Chem. Int. Ed.* **2019**, *58*, 11695-11699.

[175] J. Okuda, *Dalton Trans.* **2003**, 2367-2378.

[176] E. Kirillov, J.-F. Carpentier, *Chem. Rec.* **2021**, *21*, 357-375.

[177] T. K. Panda, C. G. Hrib, P. G. Jones, J. Jenter, P. W. Roesky, M. Tamm, *Eur. J. Inorg. Chem.* **2008**, 4270-4279.

[178] A. L. McKnight, R. M. Waymouth, *Chem. Rev.* **1998**, *98*, 2587-2598.

[179] N. Suzuki, Y. Masubuchi, Y. Yamaguchi, T. Kase, T. K. Miyamoto, A. Horiuchi, T. Mise, *Macromolecules* **2000**, *33*, 754-759.

[180] P. Jutzi, R. Dickbreder, *Chem. Ber.* **1986**, *119*, 1750-1754.

[181] G. Desurmont, M. Tanaka, Y. Li, H. Yasuda, T. Tokimitsu, S. Tone, A. Yanagase, *J. Polym. Sci. A Polym. Chem.* **2000**, *38*, 4095-4109.

[182] A. Winter, J. Rohrmann, V. Dolle, M. Antberg, W. Spaleck, Hoechst A.-G., Germany . **1991**, 10.

[183] A. Winter, M. Antberg, W. Spaleck, J. Rohrmann, V. Dolle, Hoechst A.-G., Germany . **1992**, 21.

E

Publications

Paper I

Radical Coupling at Cerium Fluorenyl Complexes

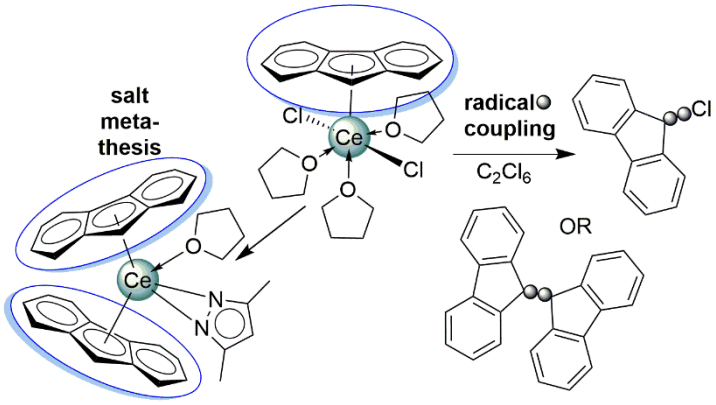

Manuscript

Radical Coupling at Cerium Fluorenyl Complexes

Lars Hirneise, Cäcilia Maichle-Mössmer, and Reiner Anwander*

*Institut für Anorganische Chemie, Eberhard Karls Universität Tübingen, Auf der Morgenstelle 18, 72076 Tübingen, Germany

KEYWORDS cerium; organometallic; fluorenyl; oxidation; carbon-carbon coupling

ABSTRACT: The first structurally characterized fluorenyl (Flu) complexes of cerium are reported, bearing one, two and three fluorenyl ligands. The reaction of $CeX_3(THF)_x$ (X = Cl, I) with KFlu led to the half-sandwich complexes $FluCeX_2(THF)_3$. The chloride derivative was utilized in salt-metathesis reactions, affording complexes $FluCeR_2(THF)_X$ with R = O*t*Bu, $OSiMe_3$, $OC_6H_3iPr_2$-2,6, Me_2Pz, and Cp (x = 1 or 2; Me_2Pz = 3,5-dimethylpyrazolato). The halogenido-exchanged mono(fluorenyl) complexes are prone to ligand redistribution at ambient temperature leading to the respective sandwich complexes $Flu_2CeX(THF)$. Utilization of K(2,10-*t*Bu_2Flu) (KFlu$^{t\text{Bu}}$) gave tris(fluorenyl) complex Flu$^{t\text{Bu}}{}_3$Ce(THF) instead, showcasing two η^5 and one η^1 bound fluorenyl ligands. Treatment of $FluCeCl_2(THF)_3$ with halogenating oxidants like C_2Cl_6, I_2 or $TeBr_4$ did not afford stable cerium(IV) species, but mixtures of 9-halogenidofluorene and 1,1'-bifluorene. Selective fluorenyl coupling reactions could be achieved for C_2Cl_6.

INTRODUCTION

In fact, cerium fluorenyl complexes were first mentioned in a paper of 1971 by Kalsotra *et al.*, claiming the synthesis of "tetra(fluorenyl) cerium(IV)".[1] This organoceric compound was stated to display a light yellow color, thermal stability up to 104° C, as well as solubility in protic solvents like ethanol.[1] The formation of "tetra(fluorenyl) cerium(IV)" $Ce(C_{13}H_9)_4$ (as was that of "tetra(cyclopentadienyl) cerium(IV)" $CeCp_4$) according to the original protocol (employing $(pyH)_2CeCl_6$ as a precursor) was later refuted by Deacon et al.[2] Few rare-earth-metal (Ln) complexes bearing a nonfunctionalized "free-standing" fluorenyl (Flu) ligand were reported before 2000,[3] the most notable being bis(fluorenyl) samarium, obtained from SmI_2.[3] Further research on Ln-Flu chemistry has mainly focused on the design of *ansa*-lanthanocene complexes[4-11] and Flu-tethered/linked constrained geometry complexes[12-16] and their use in polymerization catalysis.[17] The X-ray crystal structures of the first neutral mono(fluorenyl) complexes, $FluLnI_2(pyridine)_3$ (Ln = La, Nd), were reported by Giesbrecht *et al.* in 2005.[18] Our recent studies on fluorenyl-supported tetramethylaluminate complexes also emphasized the particular stability of half-sandwich complexes of the larger rare earth metals.[19] On the other hand sterically demanding fluorenyl ligand also stabilize half-sandwich derivatives of the smaller rare-earth metal a shown e.g., for $(Tbf)Y(CH_2SiMe_3)_2(THF)$ (Tbf = tetrabenzo[a,c,g,i]fluorenyl).[20]

To this day, neither tris(fluorenyl) rare-earth-metal complexes nor any cerium fluorenyl derivatives have been fully characterized. Since cerium provides ready access to the oxidation state +IV, we were tempted to investigate into the redox chemistry of cerium fluorenyl complexes. The redox potential of cerium strongly depends on its ligand environment, but organocerium(IV) compounds like Cp_3CeCl are isolable and have been fully characterized.[21-23] The electron-donating capability of the ligands was ascribed an important role in stabilizing the cerium(IV) oxidation state.[23-25] In the case of asymmetric ruthenium complexes the relative electron-donating power of Cp-type ligands was shown to be increasing in the order pentachlorocyclopentadienyl, acetylcyclopentadienyl, cyclopentadienyl, indenyl, pentamethylcyclopentadienyl and fluorenyl by electrochemical measurements. This is consistent with our findings regarding the redox potentials of cyclopentadienyl and methylcyclopentadienyl complexes of cerium(IV).[24, 26] Thus the fluorenyl ligand should in theory provide a good stabilization of the cerium(IV), in terms of electron-donation capability. However, in contrast to their cyclopentadienyl congeners, fluorenyl ligands engage in distinct coordination chemistry, as revealed by the ease haptotropic coordination switches ranging from η^1 to η^6.[27] Such ring-slippage has been shown to be increasingly involved in the reactivity with an extension of the systems π systems.[28-30] The most common coordination mode observed in rare-earth-metal complexes is the η^5 mode as revealed e.g. in the case of $Flu_2Sm(thf)_2$[3, 31] or $FluLnI_2(pyridine)_3$ (Ln = La, Nd).[18] The switch to η^3-allylic bonding or σ bonds (η^1 coordination) involving C1 is in most cases triggered by steric encumbrance or formation of polymer chain structures as in the case of $[NaFlu(tmeda)]_n$.[28, 32] In particular, alkali-metal fluorenyl salts, supported by different donor ligands provide a good

overview of the possible coordination modes. In the case of the binuclear structure of $(KFlu)_2(DIGLYME)$ the relatively rare η^6 coordination to the benzyl rings was detected, while the analogous lithium compound formed an separated ion pair.[33] Moreover, the polymeric structures of the DIGYLME adducts of sodium and rubidium fluorenide revealed multiple alternating coordination modes between η^1 and η^5.[33] The use of crown ethers afforded complete fluorenyl anion separation for [K(18-crown-6)][Flu].[34] Although the formation of such "metals-in-a-box" are also known for alkaline-earth metal fluorenyl complexes[35] and other cyclopentadienyl derivatives, extensive haptotropic shifts seem exclusive for indenyl and fluorenyl ligands.[34] This additional feature of the fluorenyl ligands might trigger further reactivity and reaction pathways for cerium complexes. Note that while Cerium (IV) alkyl or allyl complexes have not yet been isolated, the Schelter group has recently reported on the isolation and full characterization of a covalant cerium(IV) aryl complex.[36]

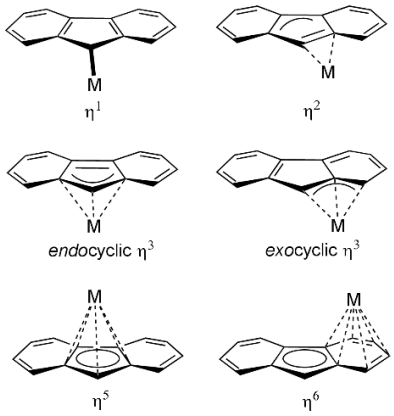

Figure 1. Different coordination modes in fluorenyl ligands, available through haptotropic shifts.[28]

RESULTS AND DISCUSSION

Cerium(III) Dihalogenido Precursors including an Unprecedented Tris(fluorenyl) Complex. Cyclopentadienyl (Cp^R) ligands (CpR = C_5H_5, C_5H_4Me, $C_5H_4SiMe_3$, $C_5H_3(SiMe_3)_2$, C_5Me_5) were shown to be capable of stabilizing the +IV oxidation state of cerium. Since these Cp^R ligands also support chemically and often electrochemically reversible cerium-centered redox properties, it stirred up the question of the feasibility of a similar ceric fluorenyl (Flu) chemistry.[24-25] As aforementioned, in contrast to the strictly η^5 bound cyclopentadienyl ligand, fluorenyl is prone to $\eta^5 \rightarrow \eta^3 \rightarrow \eta^1$ coordination switches, thus tailoring to enhanced reactivity and alternative reaction pathways.[29, 37-38]

When treating cerium(III) chloride with 1-5 equivalents of Li, Na and K fluorenide, we were surprised to learn that only one species could be isolated. Regardless of how much excess of fluorenyl salt was used, crystallization always led to the half-sandwich complex $FluCeCl_2(THF)_3$ (**1^{Cl}**). Performing an equimolar reaction, **1^{Cl}** could be obtained in 90% crystalline yield (**Scheme 1**). Usage of commercially available CeI_3 under the same conditions led to respective iodide complex $FluCeI_2(THF)_3$ (**1^{I}**) both of which could be analyzed via X-ray diffraction (XRD).

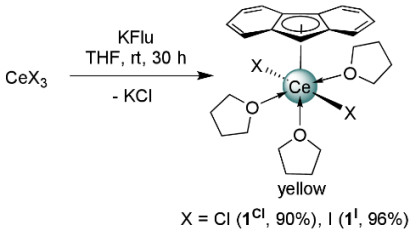

Scheme 1. Synthesis of $FluCeCl_2(THF)_3$ **1^{Cl}** and $FluCeI_2(THF)_3$ **1^{I}**

The solid-state structure of **1^{Cl}** is depicted in **Figure 2**, showing (like **1^{I}**) a pseudo-octahedral coordination geometry. The trans positioned chlorido (iodido) ligands and the three coordinated THF molecules are bent slightly away from the sterically more demanding fluorenyl. The Ce-Cnt (centroid) distance accounts for similar 2.595 Å (**1^{Cl}**) and 2.590 Å (**1^{I}**), which is slightly longer than the distances found in cyclopentadienyl complexes like $Cp_3Ce(thf)$ (2.480 Å) and pentamethylcyclopentadienyl derivatives such as monomeric half-sandwich $Cp^*CeI_2(THF)_3$ (2.523 Å) and metallocene $Cp^*_2CeCl_2K$ (avg. Ce–C(ring) 2.79 Å).[39-40] For reasons of steric oversaturation homoleptic Cp^*_3Ce features an extremely large Ce-Cnt distance of 2.619 Å.[40-42] As expected the Ce-halogen distances elongate from **1^{Cl}** (avg. 2.737 Å) to **1^{I}** (avg. 3.158 Å), whereas the Ce–O(THF) distances barely vary. Compared to $FluLaI_2(pyridine)_3$ with a La–Cnt distance of 2.593 Å and La–I distances of 3.240 and 3.174 Å, the distance to the fluorenyl ligand is almost identical, while the M–I bond is elongated for the lanthanum complex.[18]

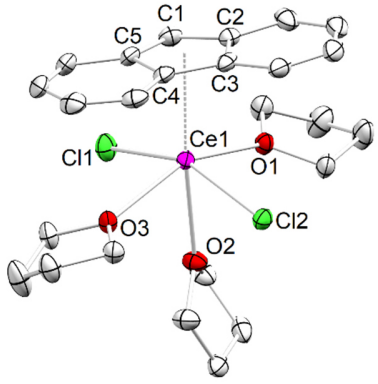

Figure 2. Crystal structure of $FluCeCl_2(THF)_3$ (**1^{Cl}**). Hydrogen atoms are omitted for clarity. Atomic displacement ellipsoids are set at the 30% probability level. Selected interatomic distances and angles are listed in **Table 1**.

When performing the equimolar reaction of $CeCl_3(THF)_{1.04}$ with *tert*-butyl-substituted fluorenyl salt K(2,10-*t*Bu$_2$Flu) (KFlu^{tBu}) fully exchanged Flu$^{tBu}{}_3$Ce(THF) (**2**) formed (**Scheme 2**). Amazingly, despite the higher steric demand (Flu^{tBu} versus Flu), the formation of a half sandwich complex along the lines of **1^{Cl}** was not observed. To our knowledge **2** represents the first tris(fluorenyl) rare-earth-metal complex. In stark contrast, tris(indenyl) derivatives $(Ind)_3Ln$ and $(Ind)_3Ln(Do)$ have been extensively investigated including the crystal structure of $Ind_3Ce(py)$.[43] Moreover, the existence of **3** definitely rules out sterics to be the crucial factor for the formation of **1^{Cl}**. At ambient temperature, the $CeCl_3(THF)_{1.04}$/KFlu^{tBu} reaction required a large excess of the cerium chloride and gave only a crystalline yield of 19%, after a stirring period of 2 d. Applying the same conditions with an equimolar mixture of $CeCl_3(TFH)_{1.04}$ and KFlu^{tBu}, the reaction was incomplete with large amounts of the fluorenyl salt left.

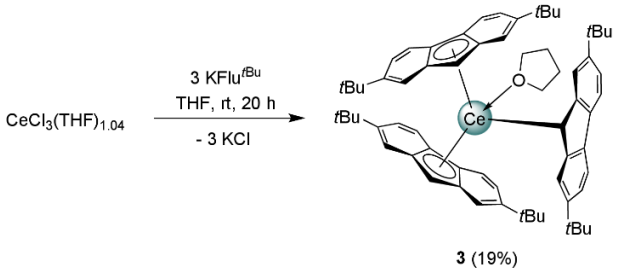

Scheme 2. Synthesis of Flu$^{tBu}{}_3$Ce(THF) (**2**).

The solid-state structure of **2** bears two η^5 and one η^1 coordinated fluorenyl ligands, showcasing distinct coordination modes in the same molecule for direct comparison (**Figure 3**). Whereas the η^5 coordination involves Ce–C(Flu) distances ranging from 2.722(3) to 3.083(3) Å and Ce–Cnt distances of 2.578 and 2.613 Å, the η^1 coordination to C55 is indicated by a shorter Ce–C(Flu) distance of 2.648(3) Å and a wide Ce1–C55–Cnt angle of 105.71°, which is even wider than the respective Li–C1–Cnt angle of LiFlu(THF)$_3$ (Figure S24) and a Ce1–C55–C54 angle of 110.31(18)°. The other Ce–C(Flu) distance are as long as 4.030(3) Å (C49), accounting for Ce–Cnt distance of 3.212 Å. For comparison, the Ce–C(silylalkyl) distance in donor-free (and hence formally lower coordinated complex alkyl complex Cp*$_2$Ce[CH(SiMe$_3$)$_2$] was reported as 2.546(5) Å. Furthermore, the Ce–C(ring) distances in $Ind_3Ce(py)$ range from 2.748(5) Å to 3.009(5) Å.[43]

The distinct fluorenyl coordination modes in **3** are not preserved in solution, as there is no signal splitting of 2:1 for the ligand protons. Thus, all three fluorenyl ligands are chemically equivalent and the coordination switch appears too fast on the NMR timescale. Instead, the corresponding ^{1}H NMR spectrum displays seven signals for the fluorenyl protons and one singulet for all *t*Bu groups. Interestingly, this indicates some magnetic inequality, which has also been detected for substituted indenyl ligands due to prochiral effects, which could be also applying for **2**, particularly considering that the sterical bulk on **2** aggravates rotation of the fluorenyl ligands.[44]

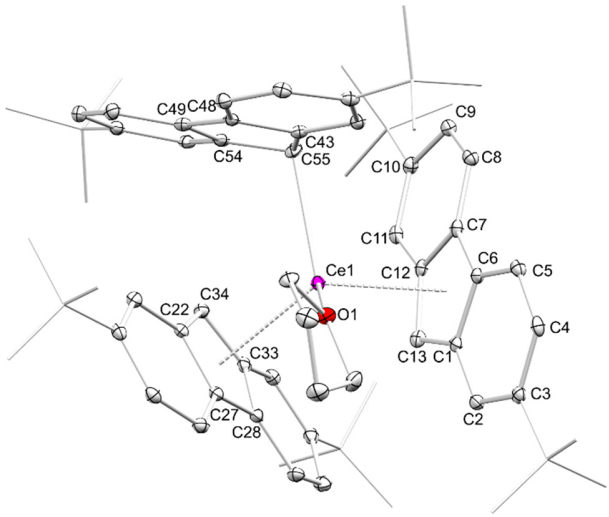

Figure 3. Crystal structure of Flu$^{tBu}{}_3$Ce(THF) (**2**). Hydrogen atoms are omitted for clarity. Atomic displacement ellipsoids are set at the 30% probability level. Selected interatomic distances and angles are listed in **Table 1**.

Salt-metathesis Reactions Promoted by FluCeCl$_2$(THF)$_3$ (1^{Cl}). Given the preferred formation and stability toward ligand redistribution of compound $FluCeCl_2(THF)_3$ (**1^{Cl}**), we next aimed at salt-metathetic ligand exchange. Targeted Cl/R exchange should further improve the thermodynamic and electrochemical stabilization of any envisioned/putative Ce(IV) fluorenyl complexes, particularly in case of R = alkoxy or siloxy.[24-25, 45] Accordingly, the following ligand types could be implemented in complexes **3^{R}**: cyclopentadienyl (using NaCp), aryloxy (NaOC$_5$H$_3$*i*Pr$_2$-2,6 = NaOAr), alkoxy (NaO*t*Bu), siloxy (NaOSiMe$_3$) and pyrazolato (potassium 3,5-dimethylpyrazolate = Me$_2$Pz (see **Scheme 3**). These reactions were carried out at −40°C in THF for 6 to 18 h and subsequently extracted with toluene. At ambient temperatures the toluene extract led to ligand rearrangement processes in all cases with the exception of the aryloxy derivative **3^{OAr}**. Although ligand rearrangement can be sufficiently suppressed at lower temperature (−40°C), it took place as side reaction to produce the sandwich complexes **4^{R}**. The sandwich compound Flu$_2$Ce(Me$_2$Pz)(THF) (**4^{Pz}**) could be synthesized and purified, while single-crystalline material was obtained also for Flu$_2$Ce(O*t*Bu)(THF) (**4^{OtBu}**) and Flu$_2$Ce(OSiMe$_3$)(THF) (**4^{OSiMe3}**) (vide infra).

The crystal structures of the mono(fluorenyl)s FluCe(OC$_5$H$_3$*i*Pr$_2$-2,6)$_2$(THF)$_2$ (**3^{OAr}**), FluCe(Me$_2$Pz)$_2$(THF)$_2$ (**3^{Pz}**), and FluCeCp$_2$(THF) (**3^{Cp}**) are depicted in **Figure 4**. The cerium centers in complexes **3^{OAr}** and **3^{Pz}** both adopt a slightly bent pseudo square pyramidal coordination geometry, clearly dictated by the flat spread of the fluorenyl ligand. The Ce–centroid (Cnt) distances amount to 2.625 Å

($\mathbf{3}^{\mathbf{OAr}}$) and 2.646 Å ($\mathbf{3}^{\mathbf{Pz}}$). It appears that the latter represents the longest distance for a cerium to a cyclopentadienyl-type ligand detected so far and stresses the fact, that such fluorenyl half-sandwich complexes **1** show generally longer Ce–Cnt distances than the respective sandwich complexes **4**. The Ce–O(aryloxy) distances (avg. 2.219 Å) in $\mathbf{3}^{\mathbf{OAr}}$ are slightly longer than the ones reported for 6-coordinate $Ce(OC_5H_3iPr_2\text{-}2,6)_3(THF)_3$ (avg. 2.12 Å). The η^5-fluorenyl ligand is sterically more demanding than the aryloxy ligand giving space to the additional coordination of only two THF molecules.[46] For further comparison, the half-sandwich complex $Cp^*Ce(OC_5H_3tBu_2\text{-}2,6)_2$ synthesized by Heeres *et al*. and bearing a slightly bulkier aryloxy ligand shows even longer Ce–O distances (avg. 2.253 Å) but an average Ce–C distance of 2.76 Å in comparison with 2.886 Å for $\mathbf{3}^{\mathbf{OAr}}$.[47] The pyrazolato derivative $\mathbf{3}^{\mathbf{Pz}}$ is isostructural to $\mathbf{3}^{\mathbf{OAr}}$ with *trans*-positioned η^2-pyrazolato instead of the aryloxies. The Ce–N distances average 2.480 Å matching those of the four terminal ones in adducts $[Ce(Me_2Pz)_3(Do)]_2$ (avg. 2.478 Å (Do = THF), avg. 2.475 Å (Do = HMe_2Pz)).[48]

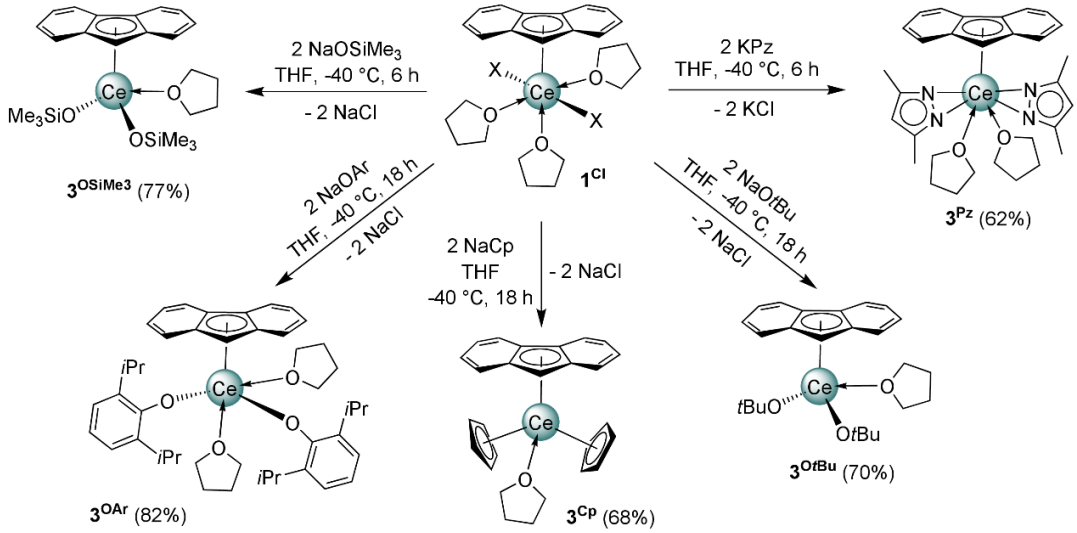

Scheme 3. Overview of salt -metathesis reactions of $\mathbf{1}^{\mathbf{Cl}}$ affording cerous half-sandwich complexes with alkoxy, siloxy, aryloxy, pyrazolato, and cyclopentadienyl ligands.

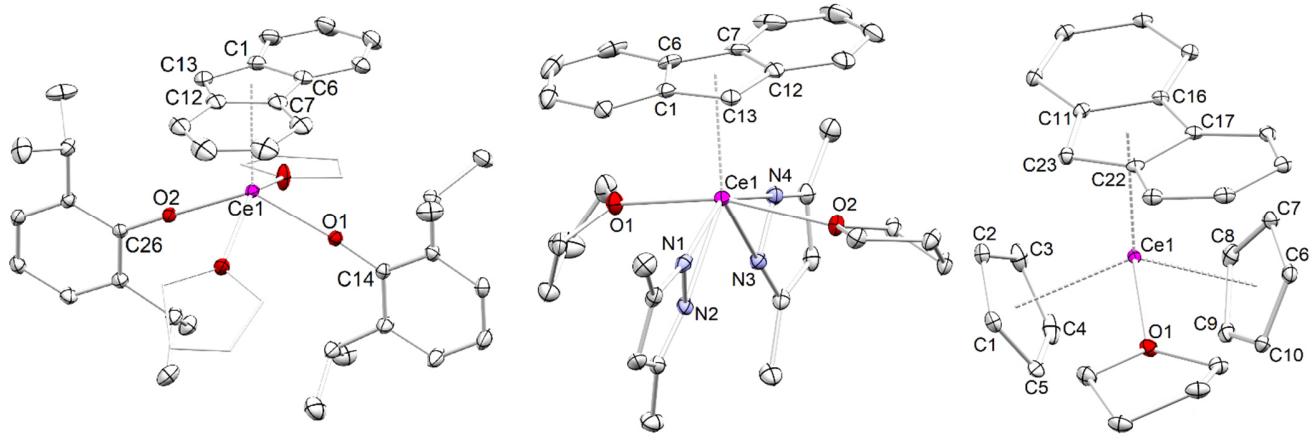

Figure 4. Crystal structures of $FluCe(OC_5H_3iPr_2\text{-}2,6)_2(THF)_2$ ($\mathbf{3}^{\mathbf{OAr}}$, left), $Flu_2Ce(Me_2Pz)(THF)$ ($\mathbf{3}^{\mathbf{Pz}}$, middle), and $FluCeCp_2(THF)$ ($\mathbf{3}^{\mathbf{Cp}}$, right). Hydrogen atoms and lattice toluene ($\mathbf{3}^{\mathbf{OAr}}$) are omitted for clarity. Atomic displacement ellipsoids are set at the 30% probability level. Selected interatomic distances and angles are listed in **Table 1**.

The mono(fluorenyl) compound $FluCeCp_2(THF)$ ($\mathbf{3}^{\mathbf{Cp}}$) represents a rare example of a rare-earth-metal complex bearing different (non-linked) η^5-coordinated cyclopentadienyl-type ligands. Other examples include trivalent Cp^*_2LnCp (Ln = Nd, Sm)[49] or divalent $FluYbCp^*(dme)$.[50] The isolation of such complexes with sterically less demanding ligands is counteracted by ligand rearrangement and formation of the respective homoleptic

complexes. This is also the case for heteroleptic $\mathbf{3^{Cp}}$. Treating $\mathbf{1^{Cl}}$ with NaCp at ambient temperature gave $Cp_3Ce(thf)$ as the major side product, but after toluene extraction of $\mathbf{3^{Cp}}$ to remove $Cp_3Ce(THF)$ and other impurities no further scrambling has been observed at −40 °C.[42, 51] Also for $\mathbf{3^{Cp}}$, the Ce−Cnt(Flu) distance of 2.637 Å is rather long. Even the comparatively shorter Ce−Cnt(Cp) distances of avg. 2.548 Å are considerably longer than those in $Cp_3Ce(THF)$ (avg.2.480 Å),[42] indicating significant steric hindrance. Well-examined unsymmetrical metallocenes relate to the metals Fe, Ru and Os, e.g. FluFeCp or FluRuCp*, where the haptotropic rearrangements of fluorenyl ligands has been studied.[26, 37, 52]

The ligand rearrangement processes involving the pyrazolato ligand have been elucidated in more detail, as not only the half-sandwich complex $\mathbf{3^{Pz}}$ (vide supra) could be isolated (**Scheme 4**). Additionally, the sandwich complex $Flu_2Ce(Me_2Pz)(THF)$ ($\mathbf{4^{Pz}}$) could be obtained in 37% yield upon warming to ambient temperature (**Scheme 5**). Assuming ligand rearrangement to tris(pyrazolyl) $[Ce(Me_2Pz)_3(THF)]_2$ as the dominant reaction path, which could be detected among other unidentified products in the NMR spectrum, a maximum yield of 50% to $\mathbf{4^{Pz}}$ should be possible.[48] Furthermore, crystallization of the chilled reaction mixture (in THF) before toluene extraction did not only yield half-sandwich $\mathbf{3^{Pz}}$ but also crystals of $[Flu]^-[Ce(Me_2Pz)_2(THF)_5]^+$ ($\mathbf{3^{Pz,THF}}$). The latter complex $\mathbf{3^{Pz,THF}}$ features a solvent-separated ion pair, reaffirming easily separable/abstracable fluorenyl anions (**Figure 5**).[19] Indeed, $\mathbf{3^{Pz,THF}}$ is the first rare-earth-metals complex bearing a solvent-only separated fluorenyl anion (Ce−centroid distance = 6.822 Å).

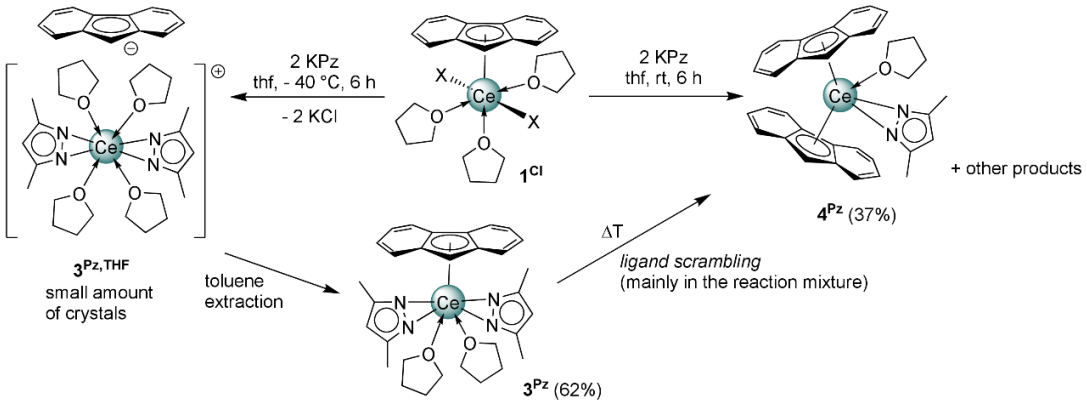

Scheme 4. Solvent- and temperature dependent cerium fluorenyl pyrazolato chemistry

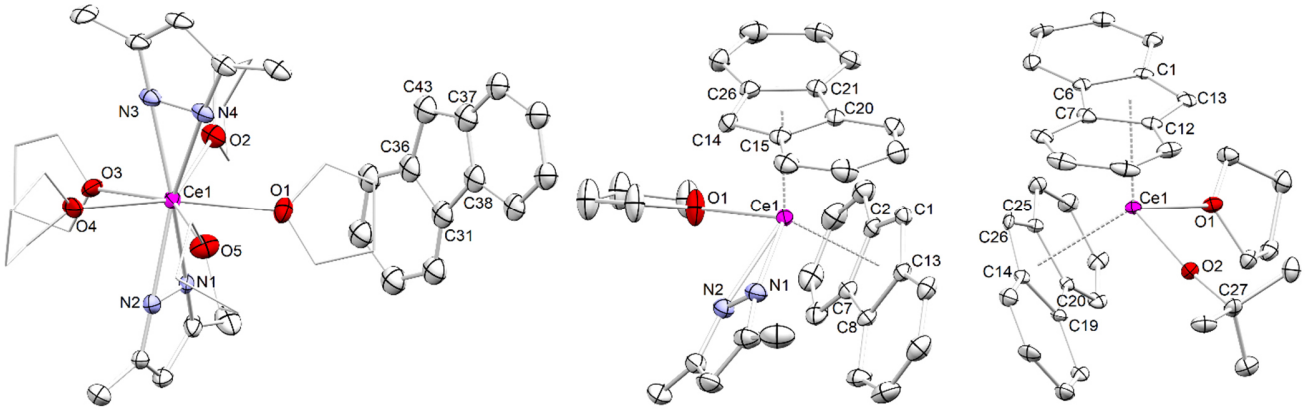

Figure 5. Crystal structures of $FluCe(Me_2Pz)_2(THF)_4$ ($\mathbf{3^{Pz,THF}}$, left), $Flu_2Ce(Me_2Pz)(THF)$ ($\mathbf{2^{Pz}}$, middle), and $Flu_2Ce(O\mathit{t}Bu)(THF)$ ($\mathbf{2^{O\mathit{t}Bu}}$, right). Hydrogen atoms have been omitted for clarity. Atomic displacement ellipsoids are set at the 30% probability level. Selected interatomic distances and angles are listed in **Table 1**.

It has been revealed previously that such solvent-separated fluorenyl anions are favorably observed in the presence of crown ethers or other multidentate O-donors like for $[BaFlu(18\text{-crown-}6)(pyridine)]^+$ $[Flu]^-$ and $[M(diethyleneglycol–dimethylether)_2]^+$ $[Flu]^-$ (M = Li, Na).[33, 53] The Ce−N distances of the 7-coordinate cation of $\mathbf{3^{Pz,THF}}$ (avg. 2.475 Å) are slightly shorter than 7-coordinate charge-balanced $\mathbf{3^{Pz}}$. The cerium center in $\mathbf{3^{Pz,THF}}$ adopts a rare pseudo-pentagonal bipyramidal coordination geometry, with the THF ligands in the equatorial positions. The *trans*-positioned pyrazolato ligands feature a torsion angle of 93.3° (N2N1−N3N4) to minimize steric hindrance of the methyl groups.

Sandwich complex $Flu_2Ce(Me_2Pz)(THF)$ ($\mathbf{4^{Pz}}$) shows a pseudo tetrahedral geometry and a staggered conformation of the fluorenyl ligands, which has been also found for other lanthanide sandwich fluorenyl complexes (e.g., $Flu_2La(AlMe_4)$).[19] The two fluorenyl ligands bear an angle of 125.6° and display Ce–Cnt distances of 2.574 Å, which are way shorter than that in half-sandwich complex $\mathbf{3^{Pz}}$ (2.646 Å). The Ce–N distance amounts to 2.413 Å in average, and is thus also shorter than those in $\mathbf{3^{Pz}}$ and $\mathbf{3^{Pz,THF}}$. In fact, it is to our knowledge the shortest distance known in literature for this particular ligand. For futher comparison, the donor-free complex $[Ce(Me_2Pz)_3]_4$ shows roughly similar average Ce–N distances of 2.436 Å for the terminal η^2 bound pyrazolato ligands.[54]

Similarly to the chloride/pyrazolato ligand exchange, alkoxy and siloxy implementation led to the formation of the sandwich complexes as the major ligand rearrangement products (**Scheme 5**). A shown in **Scheme 3**, the exchange reactions at low temperature of −40 °C led to the half-sandwich complexes $FluCe(OR)_2(THF)$ in yields of 70% ($\mathbf{3^{OtBu}}$, R = O*t*Bu) and 77% ($\mathbf{3^{OSiMe3}}$, R = $OSiMe_3$). The sandwich complexes $Flu_2Ce(OtBu)(THF)$ ($\mathbf{4^{OtBu}}$) and $Flu_2Ce(OSiMe_3)(THF)$ ($\mathbf{4^{OSiMe3}}$) could be isolated and crystallized only as side products from equimolar ambient-temperature reactions. There, the bulk of the product was still $\mathbf{3^{R}}$, but the comparatively lower solubility of the sandwich complexes favored crystallization. Correspondingly, the respective alkoxy, siloxy, aryloxy or pyrazolato ligands impart higher solubility than the fluorenyl ligand.

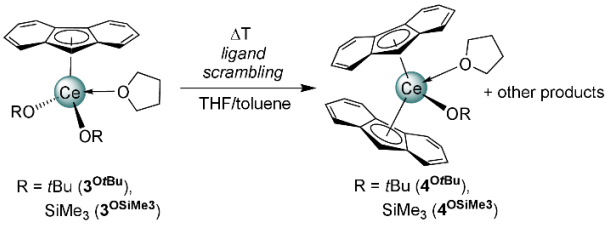

Scheme 5. Ligand scrambling reaction of half-sandwich complexes $\mathbf{3^{OtBu}}$ and $\mathbf{3^{OSiMe3}}$ toward sandwich complexes $\mathbf{4^{OtBu}}$ and $\mathbf{4^{OSiMe3}}$ at ambient temperature or crystallization.

The cerous metallocenes $\mathbf{4^{OtBu}}$ and $\mathbf{4^{OSiMe3}}$ are isostructural to $\mathbf{4^{Pz}}$. Similarly, the Ce–Cnt distances are rather short (avg. 2.854 and 2.583 Å) and the Cnt–Ce–Cnt angles are 125.1° ($\mathbf{4^{OtBu}}$) and 126.3° ($\mathbf{4^{OSiMe3}}$). As expected, the Ce–O distance is slightly shorter for $\mathbf{4^{OtBu}}$ (2.096(4) Å) in comparison to $\mathbf{4^{OSiMe3}}$ (2.113(4) Å). The terminal *tert*-butoxy ligands in homoleptic trivalent complex $[Ce(OtBu)_3]_4$[46] display slightly shortened Ce–O distances of avg. 2.08 Å (5-coordinate cerium) and $[Cp^*Ce(OtBu)_2]_2$ shows slightly elongated terminal Ce–O dostamces of avg. 2.120 Å.[55] For further comparison, the Ce–O(siloxy) distance of $\mathbf{4^{OSiMe3}}$ appears to be short in comparison to those detected in the few known trivalent cerium siloxide complexes, like $[Ce(OSiPh_3)_3(thf)_3](thf)$ (avg. 2.222 Å).

Unlike the chloride/OAr exchange reaction, treatment of $\mathbf{1^{Cl}}$ with lithium thiomesitolate $Li(SC_6H_2Me_3\text{-}2,4,6)$ (= LiSMes) at ambient temperature proved less effective. The complicated mixture did only produce the partly exchanged $\{Ce_3Li\}$-bimetallic cluster $Flu_3Ce_3(SC_6H_2Me_3\text{-}2,4,6)_4Cl_3Li(THF)_2$ (**5**) (**Scheme 6**). The small crystalline yield of 22% could not be improved by starting out with proper stoichiometry, which failed to give the desired product. Due to bad crystal quality, the XRD analysis only provided the connectivity of **5** (Figure S23) ruling out a detailed discussion of the metrical parameters. In complex **5**, the half-sandwich motif retained but both the thiolato and non-exchanged chorido ligands are located in bridging positions. Three μ_2-thiolato ligands and the cerium centers form a distorted 6-membered ring, with μ_3-chloridos above and below this metallacycle. The symmetry of the structure is broken by a "non-reacted" LiSMes(THF) fragment, which connects to two cerium centers via the μ_2-thiolato and a μ_2-chlorido ligand, respectively. Overall, each cerium center is 6-coordinate with distorted pseudo-octahedral coordination geometries, but interestingly each cerium center exhibits a distinct ligand sphere. Applying a protonolysis protocol a structural related non-ate complex $[Cp^*_2Ce(SPh)]_2$ could be accessed by reaction of Cp^*_3Ce with PhSSPh with coupling product Cp*–Cp* as byproduct.[56]

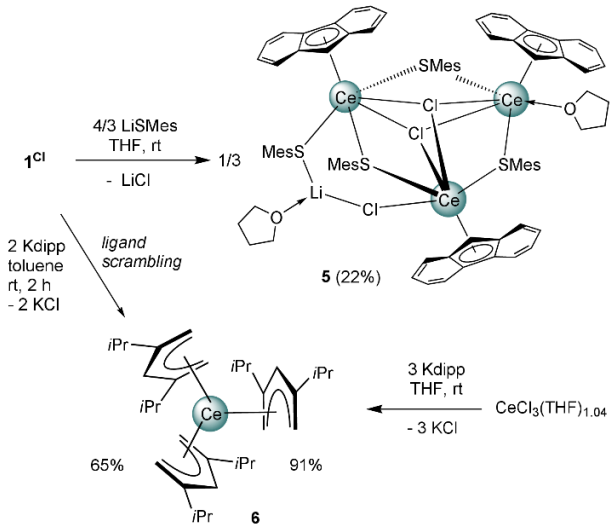

Scheme 6. Salt-metathesis reactions of $\mathbf{1^{Cl}}$ showing incomplete Cl/thiolato exchange forming the $\{Ce_3Li\}$-bimetallic cluster **5**, and rapid ligand rearrangement toward homoleptic $Ce(dipp)_3$ (**6**).

Examination of increasingly basic ligands in exchange reactions according to Scheme 3 did lead to decomposition or follow-up reactivity such as ligand scrambling. This was the case for amides $LiNH_2$, $LiNMe_2$, $LiNiPr_2$ and silylamides $Li(N(SiHMe_2)_2$ and $LiN(SiMe_3)_2$, where complicated product mixtures were observable via NMR spectroscopy. Products identified form these reactions are $LiFlu(THF)_3$ (Figure S24)

and $Ce[N(SiMe_3)_2]_3$. The rapid formation of non-targeted decomposition products was also observed for alkyls MeLi, KBn, $LiCH_2SiMe_3$ and *n*BuLi. In contrast, treatment of $\mathbf{1^{Cl}}$ with potassium 2,4-diisopropylpentadienide (Kdipp) salt Kdipp with $\mathbf{1^{Cl}}$ led to a rather directed ligand rearrangement, affording bright orange donor-free $Ce(dipp)_3$ (**6**) in 65% yield. This corresponds to a nearly complete conversion of Kdipp. The ligand rearrangement to **6** seems similar to that occurring along the cyclopentadienyl derivative $\mathbf{3^{Cp}}$, but more pronounced and faster, possibly due to the haptotropic coordination switches assessable to "open" pentadienyls. The respective half-sandwich complex could not be obtained, even at −40°. The direct synthesis using a 1:3 mixture of $CeCl_3(thf)_{1.04}$ and Kdipp gave **6** in a crystalline yield of 91%.[57] The solid-state structure of complex **6** (**Figure 6**) is isostructural to $Ce(pdl)_3$ (pdl= 2,4-*t*$Bu_2C_5H_5$),[57] showing a typical short-long-short-long pattern across the pentadienyl ligand indicative of ionic bonding. The Ce−Cnt distance averages 2.395 Å, thus being slightly longer than the respective one in $Ce(pdl)_3$ (avg. 2.373 Å).[57]

Table 1. Overview of selected interatomic distances (Å) and angles (deg) of the compounds $\mathbf{1^{Cl}}$, $\mathbf{1^{I}}$, **2**, $\mathbf{3^{Cp}}$, $\mathbf{3^{OAr}}$, $\mathbf{3^{Pz}}$, $\mathbf{3^{Pz,THF}}$, $\mathbf{4^{Pz}}$, $\mathbf{4^{OtBu}}$, $\mathbf{4^{OSiMe3}}$, and **6** (Cnt = Flu/Cp ring centroid)

	Ce–C(Flu)$_{range}$	Ce–C(Flu) avg.	Ce–Cnt (Flu)	Ce–X	X–R	Cnt–Ce–Cnt	Cnt–Ce–X	Ce–X–R
$FluCeCl_2(THF)_3$ ($\mathbf{1^{Cl}}$) (X=Cl)	2.756(3) (C1) – 2.965(3) (C7)	2.860	2.595	2.7360(9) 2.7379(8)	–	–	102.3 100.8	–
$FluCeI_2(THF)_3$ ($\mathbf{1^{I}}$) (X=I)	2.752(3) (C1) – 2.967(3) (C7)	2.856	2.590	3.1323(3) 3.1836(3)	–	–	101.58	–
$Flu^{tBu}{}_3Ce(THF)$ (**2**) (X=C55, R=C)	2.722(3) (C33) – 3.083(3) (C6)	2.870	2.578 2.613 3.212	2.648(3) 4.030(3) (C49)	1.441(4) 1.448(4)	123.1 119.0 104.4	99.2 112.8	110.3(2) 92.5(2)
$FluCeCp_2(THF)$ ($\mathbf{3^{Cp}}$) (X/R=C(Cp)) * X=Cnt(Cp)	2.7967(2) (C23) – 2.984(2) (C17)	2.905	2.637	2.535* 2.560*	1.396(3) – 1.413(3)	118.7 116.6 117.3	–	–
$FluCe(OAr)_2(THF)_2$ ($\mathbf{3^{OAr}}$) (X=O, R=C)	2.806(2) (C12) – 2.961(2) (C1)	2.886	2.625	2.226(1) 2.212(1)	1.342(2) 1.344(2)	–	116.5 112.3	174.5(1) 177.5(1)
$FluCe(Me_2Pz)_2(THF)_2$ ($\mathbf{3^{Pz}}$) (X/R=N)	2.819(4) (C13) – 3.014(4) (C7)	2.914	2.646	2.516(4) 2.476(4) 2.443(4) 2.486(4)	1.387(5) 1.402(5)	–	102.8	72.3(2) 75.2(2)
$FluCe(Me_2Pz)_2(THF)_5$ ($\mathbf{3^{Pz,THF}}$) (X/R=N)	6.498 (C36) – 7.219 (37)	6.910	6.822	2.48(2) 2.47(2)	1.40(3) 1.37(4)	–	75.3 103.3 100.0 81.3	73(1) 75(1)
$Flu_2Ce(Me_2Pz)(THF)$ ($\mathbf{4^{Pz}}$) (X/R=N)	2.714(3) (C1) – 2.946(3) (C7)	2.849	2.574	2.406(3) 2.419(3)	1.397(4)	125.6	105.0 1071 101.8 128.6	72.7(2) 73.7(2)
$Flu_2Ce(OtBu)(THF)$ ($\mathbf{4^{OtBu}}$) (X=O, R=C)	2.765(6) (C26) – 2.927(C6)	2.863	2.588 2.581	2.096(4)	1.424(8)	125.1	113.4 109.0	172.7(4)
$Flu_2Ce(OSiMe_3)(THF)$ ($\mathbf{4^{OSiMe3}}$) (X=O, R=Si)	2.737(5) (C13) – 2.944(5) (C6)	2.845	2.587 2.579	2.133(4)	1.619(4)	126.3	110.1 111.0	173.2(2)
$Ce(dipp)_3$ **6**	2.718(3) (C14) – 2.866(13) (C1)	2.818	2.401 2.392 2.391	–	–	120.4 120.5 119.1	–	–

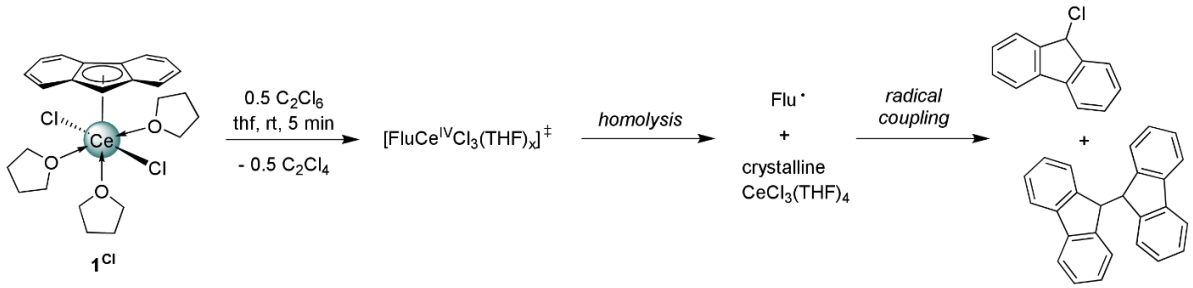

Scheme 7. Proposed reaction pathway of $\mathbf{1^{Cl}}$ with hexachloroethane yielding mixtures of 9-chlorofluorene and bifluorene.

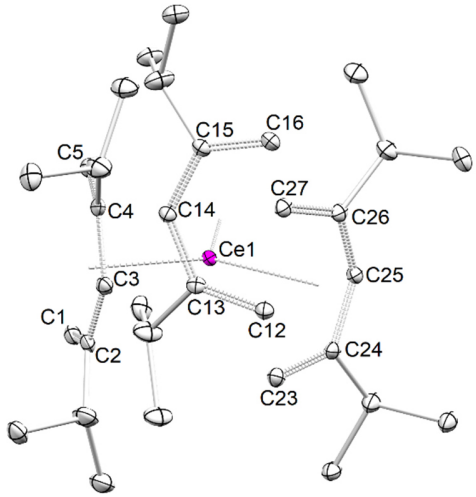

Figure 6. Crystal structure of Ce(dipp)$_3$ (**6**). Hydrogen atoms are omitted for clarity. Atomic displacement ellipsoids are set at the 30% probability level. Selected interatomic distances and angles are listed in **Table 1**.

Reactivity toward Oxidants: Radical Coupling. Aiming at cerium(IV) complexes, the reactivity of the obtained cerium(III) compounds toward common oxidation agent C_2Cl_6 was examined. In addition, the reaction of $\mathbf{1^{Cl}}$ with several oxidation reagents (C_2Cl_6, $TeBr_4$, I_2, 1,4-benzoquinone) was investigated more closely. Addition of one half an equivalent of hexachloroethane to an orange solution of half-sandwich complex $\mathbf{1^{Cl}}$ gave instantly a colorless reaction mixture. Its ^{1}H NMR spectrum revealed the presence of only diamagnetic products, with the proton positioned at the 5-membered ring acting as a useful probe. Instead of a diamagnetic cerium(IV) species, like putative "FluCeCl$_3$(THF)$_x$", the formation of a mixture of 9-chlorofluorene (5.92 ppm in thf-d$_8$) and 1,1'-bifluorene (4.80 ppm in CDCl$_3$) was observed (**Scheme 7**). Apart from 1,1'-bifluorene, CeCl$_3$(THF)$_4$ could be analyzed by XRD. Crystalline CeCl$_3$(THF)$_4$ could be obtained after separation of the organic components by toluene extraction. The formation of 1,1'-bifluorene strongly indicates the presence of transient fluorenyl radicals, possibly emerging from a short-lived cerium(IV) species in solution (**Scheme 7**). This redox behavior is a favored reaction path in organocerium chemistry,[22, 58] and was recently observed along the formation of metallocene Cp*$_2$CeR$_2$ yielding 1,1*-bis(pentamethylcyclopentadiene) as a side product.[25, 41] A radical pathway is also strongly suggested by the formation of 9-chlorofluorene. Interestingly, the 1,1'-bifluorene/9-chlorofluorene product ratio can be controlled to some extent via the amount of C_2Cl_6. When treating $\mathbf{1^{Cl}}$ with a large excess of C_2Cl_6 only the formation of 9-chlorofluorene was observed. Addition of 1.1 equivalents of C_2Cl_6 resulted in 93% selectivity for 9-chlorofluorene, beside 5% 9-*H*-fluorene (HFlu) and 2% bifluorene. Employing 0.45 equivalents of C_2Cl_6 instead, 81% bifluorene was generated, with HFlu (17%) and 9-chlorofluorene (2%) as byproducts. The reaction of $\mathbf{1^{Cl}}$ with other halogenating agents like I_2 or $TeBr_4$ gave bifluorene as well (72% and 22%, respectively), along with the respective 9-halogenidofluorenes as side product. Additionally, the formation of minor amounts of HFlu (3.49 ppm in thf-d$_8$, 3.89 ppm in C_6D_6) was observed. C_2Cl_6 was tested on the other fluorenyl complexes as well resulting similarly in mixtures of fluorenyl species with no isolable cerium(IV) species. In contrast, Ce(dipp)$_3$ (**6**) behaved inert toward the halogenating agents under study.

Clearly, the reactivity of cerium(III) fluorenyl complexes toward halogenating oxidants follows a reaction path different from that of cyclopentadienyl derivatives. For example, the transformation of cerous Cp$^{Me}_3$Ce(THF) to ceric Cp$^{Me}_3$CeX (X=Cl, Br, I) proceeds smoothly. The feasibility of $\eta^5 \rightarrow \eta^3 \rightarrow \eta^1$ coordination switches, even of charge-separated fluorenyl anion in donor solvents such as THF, trigger decomposition pathways, characteristic of cerium(IV) complexes.[21, 24, 59] η^3 and η^1 coordination would involve highly elusive Ce(IV) allyl and alkyl species, respectively. On the other, the radical pathways observed in this study might be exploited for carbon carbon bond formation reactions otherwise difficult to achieve. The coupling of fluorene to 1,1'-bifluorene by radical pathways is common in d-block metal chemistry, as revealed for, e.g., iron(III)-isoporphyrin complexes or, even in a catalytic manner, for Ru$_3$(CO)$_{12}$ or CoCl$_2$.[60-62]

In order to expand the scope of potential cerium redox chemistry, 1,4-benzoquinone was probed as non-halogenating oxidant.[45] Correspondingly, treatment of a solution of $\mathbf{1^{Cl}}$ with 1,4-benzoquinone led to an immediate color change to dark blue and subsequently the formation of a suspension. The suspension consisted of a colorless solution, with fluorene and bifluorene as the major diamagnetic components, as well as of a deep blue solid, insoluble in any organic solvents. Although we did not attempt to identify the intensely colored residues, it can be

hypothesized that the redox chemistry will involve the formation of cerous semiquinolate derivatives.[45] The possibility of C–C coupling using C_2Cl_6 as reagent was tested on Bz_3Ce (Bz = benzyl), too, resulting quantitatively in the formation of benzylchloride and $Ind_3Ce(thf)$, which produced 1-chloroindene and $CeCl_3$ as side product.

CONCLUSIONS

The synthesis and derivatization of $FluCeX_2(THF)_3$ (X=Cl, I) showcases the feasibility of fluorenyl-based cerium half-sandwich complexes. Respective salt metathesis reactions give easy access to momomeric alkoxy, siloxy, aryloxy, pyrazolato and cyclopentadienyl derivatives $FluCeR_2(THF)_x$. With the exception of the aryloxy complex $FluCe(OC_5H_3iPr_2\text{-}2,6)_2(THF)$, all compounds readily engage in ligand rearrangement processes to form sandwich complexes $Flu_2CeR(THF)$. The routine sandwich-type structural motif with staggered η^5-coordinated fluorenyl ligands has been elucidated for R = O*t*Bu, $OSiMe_3$, and Me_2Pz. The potential $\eta^5 \rightarrow \eta^3 \rightarrow \eta^1$ coordination switch has been detected in the solid-state structure of tris(fluorenyl) $Flu^{tBu}{}_3Ce(THF)$, which features two fluorenyl rings in η^5 and one in η^1 coordination mode. This coordinative flexibility most likely bears on the cerium(III/IV) redox chemistry, so far counteracting the isolation of a cerium(IV) fluorenyl compound. However, the reaction of complex $FluCeCl_2(THF)_3$ with halogenating oxidants like C_2Cl_6 can be tuned to selectively form 1,1'-bifluorene or 9-chlorofluorene, according to radical pathways.

EXPERIMENTAL SECTION

All operations were performed under rigorous exclusion of oxygen and moisture in an argon atmosphere, using standard Schlenk, high-vacuum, and glovebox techniques (MB Braun MB150B-G-I; <0.1 ppm of O_2, <0.1 ppm of H_2O). Solvents were dried and degassed prior to use and provided by an MBraun SPS800. Benzene-d_6 (99.5%) was received from Deutero GmbH and THF-d_8 from Eurisotop. The deuterated solvents were dried over NaK alloy for a minimum of 48 h and filtered through a filter pipette (Whatman) before use. Anhydrous $CeCl_3$ (99.99%) (Sigma Aldriche) was converted into $CeCl_3(THF)_{1.04}$ via Soxhlet extraction. Hexachloroethane, NaO*t*Bu, $NaOSiMe_3$, and CeI_3 were purchased from Sigma-Aldrich and used as received. NaCp[63] and NaOAr[64], KFlu[65], LiSMes[66], KMe_2Pz[67], Kdipp[68], $Ce(CH_2Ph)_3$,[69] and $Ind_3Ce(THF)$[59] were prepared according to literature procedures. NMR spectra were recorded on a Bruker AVII + 400 (^{1}H: 400.13 MHz; ^{13}C: 100.61 MHz), AVI + 300 (^{29}Si: 79.5 MHz) or AVII + 500 (^{1}H: 500.13 MHz; ^{13}C: 125.76 MHz) spectrometer in dried and deuterated solvents. DRIFT spectra were recorded on a ThermoFisher Scientific NICOLET 6700 FTIR spectrometer using dried KBr and KBr windows. The collected data were converted using the Kubelka–Munk refinement. CHN elemental analyses were performed on an Elementar Vario MICRO cube.

$FluCeCl_2(THF)_3$ ($\mathbf{1^{Cl}}$). $CeCl_3(thf)_{1.04}$ (824.5 mg, 2.564 mmol) and KFlu (524.0 mg, 2.564 mmol) were suspended in THF (18 mL) and stirred for 7 d at ambient temperature. The mixture was filtered and the filtrate concentrated multiple times to yield crystals of $\mathbf{1^{Cl}}$ (1.369 g, 2.310 mmol, 90%) at −40 °C suitable for XRD. ^{1}H NMR (400.1 MHz, THF-d_8, 26°C): δ = 8.56 (s, 2H, Flu), 3.80 (s, 3H, Flu), 3.62 (m, 12H, THF), 3.13 (s, 2H, Flu), 2.15 (s, 2H, Flu), 1.78 (m, 12H, THF) ppm. DRIFT: $\tilde{\nu}$ = 3041 (w), 2981 (m), 2883 (m), 1594 (w), 1475 (m), 1444 (m), 1328 (s), 1223 (m), 1198 (w), 1118 (vw), 1019 (s), 986 (vw), 915 (w), 863 (s), 753 (vs), 726 (s), 436 (m), 423 (w) cm^{-1}. Elemental analysis (%) calcd for $C_{25}H_{33}CeCl_2O_3$ (592.55 g mol^{-1}): C 50.67, H 5.31; found: C 49.84, H 5.37.

$FluCeI_2(THF)_3$ ($\mathbf{1^I}$). CeI_3 (200.4 mg, 0.3848 mmol) and KFlu (78.6 mg, 0.3848 mmol) were suspended in THF (15 mL) and stirred for 3 d at ambient temperature. The mixture was filtered and the filtrate concentrated to yield yellow crystals of $\mathbf{1^I}$ (259.0 mg, 0.3682 mmol, 96%) at −40°C. ^{1}H NMR (400.1 MHz, THF-d_8, 26°C): δ = 11.41 (s, 2H, Flu), 5.00 (s, 2H, Flu), 3.66 (s, 12H, THF), 2.51 (s, 2H, Flu), 2.34 (s, 2H, Flu), 1.81 (s, 12H, THF) ppm. DRIFT: $\tilde{\nu}$ = 3028 (w), 2980 (s), 2885 (m), 1594 (w), 1475 (m), 1444 (m), 1346 (vw), 1326 (m), 1221 (w), 1198 (w), 1037 (vw), 1013 (vs), 924 (w), 880 (vs), 851 (vs), 830 (s), 757 (vs), 745 (s), 727 (s), 709 (w), 668 (w), 439 (w) cm^{-1}. Elemental analysis (%) calcd for $C_{21}H_{25}CeI_2O_2$ (703.35 g mol^{-1}): C 35.86, H 3.58; found: C 36.33, H 4.29.

$(Flu^{tBu})_3Ce(THF)$ (2). $CeCl_3(thf)_{1.04}$ (103.7 mg, 0.3276 mmol) and $KFlu^{tBu}$ (105.3 mg, 0.3276 mmol) were suspended in THF (18 mL) and stirred for 2 d at ambient temperature. The mixture was filtered and the filtrate concentrated to yield yellow crystals of **2** (64.9 mg, 0.0621 mmol, 19%) at −40 °C suitable for X ray diffraction. ^{1}H NMR (400.1 MHz, THF-d_8, 26°C): δ = 10.47 (s, 3H, Flu), 8.68 (s, 3H, Flu), 8.32 (s, 3H, Flu), 7.37 (s, 3H, Flu), 5.28 (s, 3H, Flu), 3.65 (m, 4H, THF), 2.82 (s, 3H, Flu), 1.81 (m, 4H, THF), 1.67 (s, 3H, Flu), 1.05 (s, 54H, *t*Bu) ppm. DRIFT: $\tilde{\nu}$ = 2960 (vs), 2902 (m), 2866 (m), 1590 (s), 1479 (w), 1460 (w), 1392 (vw), 1361 (m), 1338 (m), 1305 (vw), 1260 (s), 1207 (w), 1086 (w), 908 (w), 864 (w), 802 (s), 745 (m), 729 (vs), 694 (vw), 671 (s), 653 (w) cm^{-1}. Elemental analysis (%) calcd for $C_{67}H_{83}CeO$ (1044.52 g mol^{-1}): C 77.04, H 8.01; found: C 76.82, H 7.79.

$FluCe(OC_6H_3iPr_2\text{-}2,6)_2(THF)_2$ ($\mathbf{3^{OAr}}$). Compound $\mathbf{1^{Cl}}$ (53.7 mg, 0.0906 mmol) was dissolved in THF (10 mL) and $Na(OC_6H_3iPr_2\text{-}2,6)$ (36.3 mg, 0.181 mmol) was added at ambient temperature. The mixture was stirred for 18 h at ambient temperature. Then the mixture was filtrated, the solution evaporated to dryness and the residue extracted with toluene (10 mL). Upon concentration and storage at −40 °C $\mathbf{3^{OAr}}$ was obtained as bright red crystals (59.5 mg, 0.0740 mmol, 82%). ^{1}H NMR (400.1 MHz, THF-d_8, 26°C): δ = 27.45 (s, 1H, FluH), 15.71 (s, 3H), 12.97 (d, J_{HH} = 5.9 Hz; 4H, *m*-Ar), 11.01 (s, 2H), 6.67 (s, 2H), 3.84 (s, 2H), 3.65 (m, 8H, THF), 3.48 (s,

12H, CH(CH_3)$_2$), 2.03 (s, 2H), 1.81 (m, 8H, THF), 0.74 (s, 2H), −0.07 (s, 2H) ppm. DRIFT: $\tilde{\nu}$ = 2957 (s), 2863 (w), 1589 (w), 1460 (m), 1431 (vs), 1357 (w), 1324 (s), 1261 (vs), 1222 (w), 1203 (s), 1103 (vw), 1025 (m), 884 (m), 866 (m), 850 (s), 762 (m), 750 (s), 733 (w), 722 (w), 703 (vw), 691 (w), 565 (m) cm^{-1}. Elemental analysis (%) calcd for $C_{45}H_{59}CeO_4$ (804.08 g mol^{-1}): C 67.22, H 7.40; found: C 66.77, H 6.89.

FluCeCp$_2$(THF) (3^{Cp}). Compound **1^{Cl}** (70.7 mg, 0.119 mmol) was dissolved in THF (12 mL) and NaCp (21.0 mg, 0.239 mmol) was added at −40 °C. The mixture was stirred for 18 h at −40 °C. The mixture was then filtrated at −40 °C, the solution evaporated to dryness and the residue extracted with toluene (10 mL). Upon concentration and storage at −40 °C, **3^{Cp}** was obtained as orange crystals (41.3 mg, 0.0814 mmol, 68%) suitable for XRD. ^{1}H NMR (400.1 MHz, THF-d$_8$, 26°C): δ = 26.41 (s, 1H, FluH), 10.05 (s, 10H, CpH), 8.35 (s, 2H, Flu), 4.27 (s, 2H, Flu), 3.85 (s, 2H, Flu), 2.94 (s, 2H, Flu), −3.77 (s, 4H, THF), −7.82 (s, 4H, THF) ppm. DRIFT: $\tilde{\nu}$ = 3039 (m), 2956 (m), 1590 (w), 1558 (vw), 1471 (w), 1444 (w), 1328 (m), 1224 (w), 1199 (w), 1016 (m), 985 (vw), 560 (w), 783 (s), 765 (s), 754 (vs), 728 (m), 567 (vw), 496 (vw), 443 (m), 421 (w) cm^{-1}. Elemental analysis (%) calcd for $C_{27}H_{27}CeO$ (507.63 g mol^{-1}): C 63.88, H 5.36; found: C 63.49, H 5.21.

FluCe(OSiMe$_3$)$_2$(THF) (3^{OSiMe3}). Compound **1^{Cl}** (63.5 mg, 0.107 mmol) was dissolved in THF (10 mL) and NaOSiMe$_3$ (24.0 mg, 0.214 mmol) was added at ambient temperature. The mixture was stirred for 6 h while turning pale orange, evaporated to dryness and subsequently the residue extracted with toluene (10 mL). Concentration and storage at −40 °C gave orange crystals of **3^{OSiMe3}** (46.0 mg, 0.0828, 77%). The crystals proved not suitable for XRD (amorphous or intergrown), but dark orange crystals of **4^{OtBu}** could be hand-picked among the bulk of **3^{OtBu}**. ^{1}H NMR (400.1 MHz, THF-d$_8$, 26°C): δ = 10.90 (s, 18H, SiMe$_3$), 6.05 (s, 3H, Flu), 4.77 (s, 6H, Flu), −0.87 (s, 4H, THF), −4.63 (s, 4H, THF) ppm. DRIFT: $\tilde{\nu}$ = 3060 (w), 3038 (w), 2950 (s), 1590 (vw), 1473 (vw), 1446 (m), 1402 (w), 1325 (w), 1298 (vw), 1245 (s), 1019 (w), 1000 (w), 942 (vs), 889 (s), 836 (s), 737 (vs), 697 (vs), 673 (vs), 423 (m) cm^{-1}. Elemental analysis (%) calcd for $C_{23}H_{35}CeO_3Si_2$ (555.82 g mol^{-1}): C 49.70, H 6.35; found: C 50.53, H 6.38.

FluCe(O*t*Bu)$_2$(THF) (3^{OtBu}). Compound **1^{Cl}** (90.5 mg, 0.153 mmol) was dissolved in THF (12 mL) and NaO*t*Bu (29.4 mg, 0.306 mmol) was added at −40 °C. The mixture was stirred for 18 h at −40 °C while the solution turned from orange to yellow. The mixture was then filtrated −40 °C, the solution evaporated to dryness and the residue extracted with toluene (10 mL). Upon concentration and storage at −40 °C **3^{OtBu}** was obtained as yellow crystals (55.8 mg, 0,107 mmol, 70%). The crystals proved not suitable for XRD (amorphous), but orange crystals of **4^{OtBu}** could be hand-picked among the bulk of **3^{OtBu}**. ^{1}H NMR (400.1 MHz, THF-d$_8$, 26°C): δ = 20.34 (s, 4H), 14.13 (s, 3H), 9.47 (s, 2H), 7.15 (s, 6H), 5.79 (s, 3H), 4.98 (s, 7H), −3.61 (s, 8H), −12.09 (s, 2H) ppm. DRIFT: $\tilde{\nu}$ = 3039 (vw), 2962 (vs), 1589 (vs), 1469 (w), 1445 (w), 1355 (m), 1325 (m), 1222 (s), 1194 (vs), 1021 (vw), 980 (vs), 932 (s), 893 (w), 752 (s), 740 (m), 725 (m), 516 (m), 478 (m), 434 (w) cm^{-1}. Elemental analysis (%) calcd for $C_{25}H_{35}CeO_3$ (523.67 g mol^{-1}): C 57.34, H 6.74; found: C 56.27, H 7.59.

FluCe(Me$_2$Pz)$_2$(THF)$_2$ (3^{Pz}). Compound **1^{Cl}** (82.4 mg, 0.139 mmol) was dissolved inTHF (10 mL) and KMe$_2$Pz (37.3 mg, 0.278 mmol) was added at −40 °C. The mixture was stirred for 6 h at −40 °C. The mixture was then filtrated −40 °C, toluene (15 mL) was added, and the solution concentrated. Storage at −40 °C yielded **3^{Pz}** as orange crystals (54.8 mg, 0,0857 mmol, 62%). ^{1}H NMR (400.1 MHz, THF-d$_8$, 26°C): δ = 12.54 (s, 2H), 11.77 (s, 1H), 7.86 (s, 2H), 6.21 (s, 4H), 5.83 (s, 12H, Pz(CH_3)$_2$), 3.65 (m, 12H, THF), 1.81 (m, 12H, THF) ppm. DRIFT: $\tilde{\nu}$ = 3036 (m), 2980 (m), 2917 (m), 1591 (w), 1515 (vs), 1473 (m), 1429 (s), 1366 (vw), 1325 (s), 1222 (m), 1198 (w), 1029 (s), 1007 (s), 986 (w), 959 (w), 920 (vw), 874 (s), 770 (m), 752 (vs), 731 (s), 724 (s), 693 (m), 433 (m) cm^{-1}. Elemental analysis (%) calcd for $C_{31}H_{39}CeN_4O_2$ (639.80 g mol^{-1}): C 58.20, H 6.14, N 8.76; found: C 55.52, H 6.09, N 8.50 (no better elemental analysis could be obtained).

Flu$_2$Ce(Me$_2$Pz)(THF) (4^{Pz}). Compound **1^{Cl}** (109.3 mg, 0.1845 mmol) was dissolved in THF (12 mL) and KMe$_2$Pz (49.5 mg, 0.3689 mmol) was added at ambient temperature. The mixture was stirred for 6 h, filtrated, and the filtrate evaporated to dryness. Upon extraction with toluene (12 mL), concentration and storage at −40 °C **2^{Pz}** was obtained as orange crystals (43.5 mg, 0.0682 mmol, 37%). ^{1}H NMR (400.1 MHz, THF-d$_8$, 26°C): δ = 12.60 (s, 1H, PzH), 7.82 (s, 4H, Flu), 7.32 (s, 6H, Flu), 5.85 (s, 6H, Flu), 5.37 (s, 2H, Flu), 3.91 (s, 6H, Pz(CH_3)$_2$), 3.65 (m, 4H, THF), 1.81 (m, 4H, THF) ppm. DRIFT: $\tilde{\nu}$ = 3030 (m), 2919 (w), 1591 (m), 1516 (m), 1473 (m), 1443 (m), 1431 (s), 1326 (s), 1222 (m), 1199 (m), 1023 (w), 1003 (w), 986 (vw), 871 (w), 773 (w), 750 (vs), 729 (s), 692 (w), 432 (m), 422 (m) cm^{-1}. Elemental analysis (%) calcd for $C_{35}H_{33}CeN_2O$ (637.78 g mol^{-1}): C 65.91, H 5.22, N 4.39; found: C 65.26, H 5.72, N 5.00.

Flu$_3$Ce$_3$(SC$_6$H$_2$Me$_3$-2,4,6)$_4$Cl$_3$Li(THF)$_2$ (5). Compound **1^{Cl}** (47.5 mg, 0.0802 mmol) was dissolved in THF (12 mL) and Li(SC$_6$H$_2$Me$_3$-2,4,6) (30.2 mg, 0.159 mmol) was added at ambient temperature. The mixture was stirred for 6 h, filtrated, and the filtrate evaporated to dryness. Upon extraction with toluene (12 mL), concentration and storage at −40 °C **5** was obtained as yellow crystals (10.6 mg, 0.00596 mmol, 22%). Elemental analysis (%) calcd for $C_{83}H_{87}Ce_3Cl_3LiO_2S_4$ (1778.53 g mol^{-1}): C 56.05, H 4.93, S 7.21; found: C 55.85, H 5.27, S 6.73.

Ce(dipp)$_3$ (6). $CeCl_3(THF)_{1.04}$ (81.4 mg, 0.253 mmol) and Kdipp (144.7 mg, 0.761 mmol) were suspended in THF (15 mL) and stirred for 20 h at ambient temperature. The red mixture was filtrated, evaporated to dryness and the residue extracted with toluene (15 mL). Upon concentration and storage at −40 °C bright orange crystals of **6** (137.1 mg, 0.2308 mmol, 91%) suitable for XRD had formed. ^{1}H NMR (400.1 MHz, THF-d$_8$, 26°C): δ = 17.94 (s, 6H, C*H*(CH$_3$)$_2$), 15.39 (s, 3H, C*H*-3), 3.17 (s, 18H, CH(C*H*$_3$)$_2$), 2.81 (s, 6H, CH$_{terminal}$), −6.79 (s, 18H, CH(C*H*$_3$)$_2$), −7.39 (s, 6H, CH$_{terminal}$) ppm. DRIFT: $\tilde{\nu} = 3088$ (w), 2962 (vs), 2924 (m), 2866 (m), 1556 (w), 1528 (w), 1453 (s), 1375 (m), 1358 (s), 1326 (w), 1228 (vw), 1163 (w), 1148 (w), 1087 (m), 906 (vw), 798 (s), 769 (s), 652 (w), 596 (w) cm^{-1}. Elemental analysis (%) calcd for $C_{33}H_{57}Ce$ (593.94 g mol^{-1}): C 66.74, H 9.67; found: C 66.29, H 9.57. Alternative route to **6**: compound **1^{Cl}** (47.0 mg, 0.0793 mmol) was dissolved in THF (12 mL) and Kdipp (30.2 mg, 0.159 mmol) was added at ambient temperature. The mixture was stirred for 6 h, filtrated, and the filtrate evaporated to dryness. Upon extraction of the residue with toluene (12 mL), concentration and storage at −40 °C **6** was obtained as bright orange crystals (30.5 mg, 0.0514 mmol, 65%).

Reactivity toward oxidation agents.

Compound **1^{Cl}** (81.2 mg, 0.137 mmol) was dissolved in THF (5 mL) and a solution of C_2Cl_6 (15.6 mg, 0.0659 mmol) in THF (2 mL) was added at ambient temperature. The reaction turned pale yellow instantly and upon toluene extraction 21.2 mg of colorless solid were obtained (94% when relating to bifluorene) The ^{1}H NMR spectrum showed a mixture of 1,1'-bifluorene (81%), fluorene (17%) and 9-chlorfluorenyl (2%). Upon crystallization 1,1'-bifluorene was revealed.

Compound **1^{Cl}** (50.8 mg, 0.0857 mmol) was dissolved in THF (5 mL) and a solution of C_2Cl_6 (24.6 mg, 0.104 mmol) in THF (2 mL) was added at ambient temperature. The reaction turned pale rose and upon toluene extraction 20.4 mg of a colorless solid were obtained. The ^{1}H NMR spectrum showed a mixture of 9-chlorofluorene (93%), fluorene (5%) and 1,1'-bifluorene (2%).

Compound **1^{Cl}** (17.4 mg, 0.0294 mmol) was dissolved in THF (2 mL) and a solution of benzylchloride (3.7 mg, 0.0294 mmol) in THF (1 mL) was added at ambient temperature. The reaction turned pale yellow instantly. The solvent was removed under reduced pressure and the ^{1}H NMR spectrum revealed 1-benzyl-fluorene as only product in quantitative yield after toluene extraction.

Compound **1^{Cl}** (34.8 mg, 0.0587 mmol) was dissolved in THF (3 mL) and a solution of I_2 (7.5 mg, 0.0294 mmol) in THF (1 mL) was added at ambient temperature. The reaction turned pale yellow instantly and a colorless precipitation occurred ($CeCl_3(THF)_x$). Upon solvent removal and toluene extraction a pale yellow solid was obtained in quantitative yield, which was analyzed as 1,1'-bifluorene.

Compound **1^{Cl}** (29.9 mg, 0.0505 mmol) was dissolved in THF (3 mL) and a solution of $TeBr_4$ (5.6 mg, 0.0126 mmol) in THF (2 mL) was added at ambient temperature. The reaction turned yellow instantly and a black precipitation (Te(0)) occurred. The ^{1}H NMR spectrum revealed a mixture of 1,1'-bifluorene, 9-bromofluorene and fluorene. The obtained crystals were analyzed by XRE as $CeBr_3(THF)_3$.

ASSOCIATED CONTENT

X-ray structural data in CIF format, for of **1^{Cl}**, **1^{I}**, **1^{Cp}**, **1^{OAr}**, **1^{Pz}(thf)$_2$**, **1^{Pz}(thf)$_5$**, **2^{Pz}**, **2^{OtBu}**, **3**, **4**, LiFlu(thf)$_3$ and **5**. ^{1}H-NMR spectra of **1**-**4** and reactivity studies and IR spectra. This material is available free of charge via the Internet at http://pubs.acs.org.

AUTHOR INFORMATION

Corresponding Author

* Institut für Anorganische Chemie, Eberhard Karls Universität Tübingen, Auf der Morgenstelle 18, 72076 Tübingen, Germany; E-Mail: reiner.anwander@uni-tuebingen.de; http://uni-tuebingen.de/syncat-anwander

ORCID
Cäcilia Maichle-Mössmer: 0000-0001-7638-1610
Reiner Anwander: 0000-0002-1543-3787
Lars Hirneise: 0000-0003-2715-9882

Notes

The authors declare no conflict of interest.

REFERENCES

1. Kalsotra, B. L.; Multani, R. K.; Jain, B. D., Studies on tetrafluorenyl cerium(IV). J. Inorg. Nucl. Chem. 1972, 34 (8), 2679-2680.
2. Deacon, G. B.; Tuong, T. D.; Vince, D. G., Refutation of the synthesis of tetrakis(cyclopentadienyl)cerium(IV). Polyhedron 1983, 2 (9), 969-970.
3. Evans, W. J.; Gummersheimer, T. S.; Boyle, T. J.; Ziller, J. W., Synthesis and Structure of New Soluble Organosamarium(II) Reagents: (Indenyl)$_2$Sm(THF) and (Fluorenyl)$_2$Sm(THF)$_2$. Organometallics 1994, 13 (4), 1281-1284.
4. Eppinger, J.; Spiegler, M.; Hieringer, W.; Herrmann, W. A.; Anwander, R., C_2-Symmetric *ansa*-Lanthanidocene Complexes. Synthesis via Silylamine Elimination and β-SiH Agostic Rigidity. J. Am. Chem. Soc. 2000, 122 (13), 3080-3096.
5. Qian, C.; Nie, W.; Sun, J., C_s-Symmetric *ansa*-Lanthanocenes Designed for Stereospecific Polymerization of Methyl Methacrylate. Synthesis and Structural Characterization of Silylene-Bridged Fluorenyl Cyclopentadienyl Lanthanide Halides, Amides, and Hydrocarbyls. Organometallics 2000, 19 (20), 4134-4140.
6. Qian, C.; Nie, W.; Chen, Y.; Sun, J., Synthesis and crystal structure of one carbon-atom bridged lutetium complex

[$Ph_2C(Flu)(Cp)$]LuN(TMS)$_2$ and catalytic activity for polymerization of polar monomers. J. Organomet. Chem. 2002, 645 (1), 82-86.

7. Dash, A. K.; Razavi, A.; Mortreux, A.; Lehmann, C. W.; Carpentier, J.-F., Amine Elimination Reactions between Homoleptic Silylamide Lanthanide Complexes and an Isopropylidene-Bridged Cyclopentadiene−Fluorene System. Organometallics 2002, 21 (15), 3238-3249.

8. Wang, C.; Xiang, L.; Leng, X.; Chen, Y., Rare-earth metal hydrides supported by silicon-bridged boratabenzene fluorenyl ligands: synthesis, structure and reactivity. Dalton. Trans. 2017, 46 (4), 1218-1227.

9. Cortial, G.; Le Goff, X.-F.; Bousquié, M.; Boisson, C.; Le Floch, P.; Nief, F.; Thuilliez, J., Neutral *ansa*-bis(fluorenyl)silane neodymium borohydrides: synthesis, structural study and behaviour as catalysts in butadiene–ethylene copolymerisation. New J. Chem. 2010, 34 (10), 2290-2297.

10. Laur, E.; Louyriac, E.; Dorcet, V.; Welle, A.; Vantomme, A.; Miserque, O.; Brusson, J.-M.; Maron, L.; Carpentier, J.-F.; Kirillov, E., Substitution Effects in Highly Syndioselective Styrene Polymerization Catalysts Based on Single-Component Allyl *ansa*-Lanthanidocenes: An Experimental and Theoretical Study. Macromolecules 2017, 50 (17), 6539-6551.

11. Rodrigues, A.-S.; Kirillov, E.; Lehmann, C. W.; Roisnel, T.; Vuillemin, B.; Razavi, A.; Carpentier, J.-F., Allyl *ansa*-Lanthanidocenes: Single-Component, Single-Site Catalysts for Controlled Syndiospecific Styrene and Styrene–Ethylene (Co)Polymerization. Chem. Eur. J. 2007, 13 (19), 5548-5565.

12. Deng, M.; Chi, S.; Luo, Y., Rare-earth metal bis(alkyl) complexes bearing pyrrolidinyl-functionalized cyclopentadienyl, indenyl and fluorenyl ligands: synthesis, characterization and the ligand effect on isoprene polymerization. New. J. Chem. 2015, 39 (10), 7575-7581.

13. Jian, Z.; Petrov, A. R.; Hangaly, N. K.; Li, S.; Rong, W.; Mou, Z.; Rufanov, K. A.; Harms, K.; Sundermeyer, J.; Cui, D., Phosphazene-Functionalized Cyclopentadienyl and Its Derivatives Ligated Rare-Earth Metal Alkyl Complexes: Synthesis, Structures, and Catalysis on Ethylene Polymerization. Organometallics 2012, 31 (11), 4267-4282.

14. Trifonov, A. A.; Fedorova, E. A.; Fukin, G. K.; Druzhkov, N. O.; Bochkarev, M. N., C⁻C Coupling and C⁻H Bond Activation—Unexpected Pathways in the Reactions of [Yb(η^5-$C_{13}H_9$)$_2$(thf)$_2$] with Diazadienes. Angew. Chem. Int. Ed. 2004, 43 (38), 5045-5048.

15. Kirillov, E.; Toupet, L.; Lehmann, C. W.; Razavi, A.; Carpentier, J.-F., "Constrained Geometry" Group 3 Metal Complexes of the Fluorenyl-Based Ligands [(3,6-*t*Bu$_2$Flu)SiR$_2$NtBu]: Synthesis, Structural Characterization, and Polymerization Activity. Organometallics 2003, 22 (22), 4467-4479.

16. Jian, Z.; Cui, D.; Hou, Z., Rare-Earth-Metal–Hydrocarbyl Complexes Bearing Linked Cyclopentadienyl or Fluorenyl Ligands: Synthesis, Catalyzed Styrene Polymerization, and Structure–Reactivity Relationship. Chem. Eur. J. 2012, 18 (9), 2674-2684.

17. Wang, B.; Tang, T.; Li, Y.; Cui, D., Copolymerization of ethylene with norbornene catalyzed by cationic rare earth metal fluorenyl functionalized N-heterocyclic carbene complexes. Dalton. Trans. 2009, (41), 8963-8969.

18. Giesbrecht, G. R.; Gordon, J. C.; Clark, D. L.; Scott, B. L., Crystallographic report: (η^5-Fluorenyl)-tris-pyridine-di-iodo-lanthanum(III) and -neodymium(III). Appl. Organomet. Chem. 2005, 19 (1), 98-99.

19. Diether, D.; Tyulyunov, K.; Maichle-Mössmer, C.; Anwander, R., Fluorenyl Half-Sandwich Bis(tetramethylaluminate) Complexes of the Rare-Earth Metals: Synthesis, Structure, and Isoprene Polymerization. Organometallics 2017, 36 (23), 4649-4659.

20. Sun, J.; Berg, D. J.; Twamley, B., Supersize Cp! Tetrabenzo[a,c,g,i]fluorenyl complexes of yttrium. Can. J. Chem. 2017, 95 (4), 363-370.

21. Dröse, P.; Crozier, A. R.; Lashkari, S.; Gottfriedsen, J.; Blaurock, S.; Hrib, C. G.; Maichle-Mössmer, C.; Schädle, C.; Anwander, R.; Edelmann, F. T., Facile Access to Tetravalent Cerium Compounds: One-Electron Oxidation Using Iodine(III) Reagents. J. Am. Chem. Soc. 2010, 132 (40), 14046-14047.

22. Anwander, R.; Dolg, M.; Edelmann, F. T., The difficult search for organocerium(IV) compounds. Chem. Soc. Rev. 2017, 46 (22), 6697-6709.

23. Piro, N. A.; Robinson, J. R.; Walsh, P. J.; Schelter, E. J., The electrochemical behavior of cerium(III/IV) complexes: Thermodynamics, kinetics and applications in synthesis. Coord. Chem. Rev. 2014, 260, 21-36.

24. Hirneise, L.; Langmann, J.; Zitzer, G.; Ude, L.; Maichle-Mössmer, C.; Scherer, W.; Speiser, B.; Anwander, R., Tuning Organocerium Electrochemical Potentials by Extending Tris(cyclopentadienyl) Scaffolds with Terminal Halogenido, Siloxy, and Alkoxy Ligands. Organometallics 2021, 40, 11, 1786-1800.

25. Hirneise, L.; Maichle-Mössmer, C.; Anwander, R., Pentamethylcyclopentadienyl Complexes of Cerium(IV): Synthesis, Reactivity, and Electrochemistry. Inorg. Chem. 2021, X, X, X-X.

26. Gassman, P. G.; Winter, C. H., Preparation, electrochemical oxidation, and XPS studies of unsymmetrical ruthenocenes bearing the pentamethylcyclopentadienyl ligand. J. Am. Chem. Soc. 1988, 110 (18), 6130-6135.

27. Nakamura, H.; Nakayama, Y.; Yasuda, H.; Maruo, T.; Kanehisa, N.; Kai, Y., Alternative η^5- and η^6-Bonding Modes for Bis(fluorenyl)lanthanide Complexes by Reactions with AlR_3 and Succesive Addition of THF. Organometallics 2000, 19 (25), 5392-5399.

28. Veiros, L. F., Haptotropic shifts in organometallic complexes with η^5-coordinated π ligands. J. Organomet. Chem. 1999, 587 (2), 221-232.

29. Veiros, L. F., Haptotropic Shifts in Cyclopentadienyl Organometallic Complexes: Ring Folding vs Ring Slippage. Organometallics 2000, 19 (26), 5549-5558.

30. Albright, T. A.; Hofmann, P.; Hoffmann, R.; Lillya, C. P.; Dobosh, P. A., Haptotropic rearrangements of polyene-MLn complexes. 2. Bicyclic polyene-MCp, M (CO) 3 systems. J. Am. Chem. Soc. 1983, 105 (11), 3396-3411.

31. Razavi, A.; Bellia, V.; De Brauwer, Y.; Hortmann, K.; Lambrecht, M.; Miserque, O.; Peters, L.; Van Belle, S. In Syndiotactic and Isotactic Specific Metailocene Catalysts with Hapto-flexible Cyclopentadienyl-Fluorenyl Ligand, Metalorganic Catalysts for Synthesis and Polymerization, Berlin, Heidelberg, 1999, Springer, 236-247.

32. Corbelin, S.; Kopf, J.; Weiss, E., Über Metallalkyl- und -arylverbindungen, 48 Monomeres, tetrameres und polymeres Natriumfluorenid S [S = $Me_2N(CH_2)_2N(Me)(CH_2)_2NMe_2$, $Me_2N(CH_2)_nNMe_2$ (n = 2, 3)]. Chem. Ber. 1991, 124 (11), 2417-2422.

33. Neander, S.; Körnich, J.; Olbrich, F., Novel fluorenyl alkali metal DIGLYME complexes: synthesis and solid state structures. J. Organomet. Chem. 2002, 656 (1), 89-96.

34. Neander, S.; Tio, F. E.; Buschmann, R.; Behrens, U.; Olbrich, F., Cyclopentadienyl, indenyl, fluorenyl, and pentamethylcyclopentadienyl complexes of potassium with 18-crown-6. J. Organomet. Chem. 1999, 582 (1), 58-65.

35. Harder, S.; Feil, F.; Repo, T., "Alkaline-Earth Metals in a Box": Structures of Solvent-Separated Ion Pairs. Chem. Eur. J. 2002, 8 (9), 1991-1999.

36. Panetti, G. B.; Sergentu, D.-C.; Gau, M. R.; Carroll, P. J.; Autschbach, J.; Walsh, P. J.; Schelter, E. J., Isolation and characterization of a covalent CeIV-Aryl complex with an anomalous ^{13}C chemical shift. Nat. Commun. 2021, 12 (1), 1713.

37. Kirillov, E.; Kahlal, S.; Roisnel, T.; Georgelin, T.; Saillard, J.-Y.; Carpentier, J.-F., Haptotropic Rearrangements in Sandwich (Fluorenyl)(Cyclopentadienyl) Iron and Ruthenium Complexes. Organometallics 2008, 27 (3), 387-393.

38. Brydges, S.; Reginato, N.; Cuffe, L. P.; Seward, C. M.; McGlinchey, M. J., High and low barriers to haptotropic shifts across polycyclic surfaces: the relevance of aromatic character during the migration process. C. R. Chim. 2005, 8 (9), 1497-1505.
39. Hazin, P. N.; Huffman, J. C.; Bruno, J. W., Synthetic and structural studies of pentamethylcyclopentadienyl complexes of lanthanum and cerium. Organometallics 1987, 6 (1), 23-27.
40. Evans, W. J.; Olofson, J. M.; Zhang, H.; Atwood, J. L., Synthesis and X-ray crystal structure of an unusual oligomeric bis(pentamethylcyclopentadienyl) halide complex of cerium: $[(C_5Me_5)_2CeCl_2K(THF)]_n$. Organometallics 1988, 7 (3), 629-633.
41. Evans, W. J.; Perotti, J. M.; Kozimor, S. A.; Champagne, T. M.; Davis, B. L.; Nyce, G. W.; Fujimoto, C. H.; Clark, R. D.; Johnston, M. A.; Ziller, J. W., Synthesis and Comparative η^1-Alkyl and Sterically Induced Reduction Reactivity of $(C_5Me_5)_3Ln$ Complexes of La, Ce, Pr, Nd, and Sm. Organometallics 2005, 24 (16), 3916-3931.
42. Wenqi, C.; Guanyang, L.; Jusong, X.; Gecheng, W.; Yin, Z.; Zhongsheng, J., Syntheses and crystal structures of $(\eta 5\text{-}C_5H_5)_3Ln(THF)$ (Ln = Ce, Er). J. Organomet. Chem. 1994, 467 (1), 75-78.
43. Zazzetta, A.; Greco, A., The structure of triindenylcerium pyridinate. Acta Crystallographica Section B 1979, 35 (2), 457-460.
44. Diether, D.; Maichle-Mössmer, C.; Anwander, R., Implications of Indenyl Substitution for the Structural Chemistry of Rare-Earth Metal (Half-)Sandwich Complexes and Performance in Living Isoprene Polymerization. Organometallics 2019, 38 (15), 3007-3017.
45. Bayer, U.; Werner, D.; Berkefeld, A.; Maichle-Mössmer, C.; Anwander, R., Cerium–quinone redox couples put under scrutiny. Chem. Sci. 2021.
46. Boyle, T. J.; Tribby, L. J.; Bunge, S. D., Synthesis and Structural Characterization of a Series of Carboxylic Acid Modified Cerium(III) Alkoxides. Eur. J. Inorg. Chem. 2006, 2006 (22), 4553-4563.
47. Heeres, H. J.; Meetsma, A.; Teuben, J. H.; Rogers, R. D., Mono(pentamethylcyclopentadienyl) complexes of cerium(III). Synthesis, molecular structure, thermal stability, and reactivity of $(C_5Me_5)CeX_2$ (X = 2,6-di-*tert*-butylphenoxo, $CH(SiMe_3)_2$, and $N(SiMe_3)_2$) complexes. Organometallics 1989, 8 (11), 2637-2646.
48. Deacon, G. B.; Harika, R.; Junk, P. C.; Skelton, B. W.; Werner, D.; White, A. H., The Synthesis, Structures and Polymorphism of the Dimeric Trivalent Rare-Earth 3,5-Dimethylpyrazolate Complexes $[Ln(Me_2pz)_3(thf)]_2$. Eur. J. Inorg. Chem. 2014, 2014 (14), 2412-2419.
49. Evans, W. J.; Ulibarri, T. A., Reactivity of $(C_5Me_5)_2Sm$ with cyclopentadiene and cyclopentadienide: isolation of the mixed-valence complex $(C_5Me_5)_2Sm(III)(.mu.\text{-}C_5H_5)Sm(II)(C_5Me_5)_2$. J. Am. Chem. Soc. 1987, 109 (14), 4292-4297.
50. Trifonov, Alexander A.; Kirillov, Evgenii N.; Dechert, S.; Schumann, H.; Bochkarev, Mikhail N., Fluorenyl and *ansa*-Dimethylsilylbis(fluorenyl) Derivatives of Divalent Ytterbium and Samarium − Synthesis and Structure of the First Mixed-Ligand LnII Classic Sandwich Complex $(C_{13}H_9)(C_5Me_5)Yb(DME)$. Eur. J. Inorg. Chem. 2001, 2001 (10), 2509-2514.
51. Gradeff, P. S.; Yunlu, K.; Deming, T. J.; Olofson, J. M.; Ziller, J. W.; Evans, W. J., Reactivity of ceric ammonium nitrate with sodium cyclopentadienide. The x-ray crystal structure of bis (dimethoxyethane) trinitratocerium. Inorg. Chem. 1989, 28 (13), 2600-2604.
52. Arachchige, S. M.; Heeg, M. J.; Winter, C. H., Synthesis and structural characterization of unsymmetrical osmocenes containing the pentamethylcyclopentadienyl ligand. J. Organomet. Chem. 2005, 690 (19), 4356-4365.
53. Fichtel, K.; Höxter, S.; Behrens, U., Strukturen von polaren Bariumorganylen: Synthese und Struktur von Ether-, Pyridin- und Kronenether-Addukten des Bis(fluorenyl)bariums. Z. Anorg. Allg. Chem. 2006, 632 (12-13), 2003-2009.
54. Werner, D.; Bayer, U.; Rad, N. E.; Junk, P. C.; Deacon, G. B.; Anwander, R., Unique and contrasting structures of homoleptic lanthanum(III) and cerium(III) 3,5-dimethylpyrazolates. Dalton. Trans. 2018, 47 (17), 5952-5955.
55. Heeres, H. J.; Teuben, J. H.; Rogers, R. D., Novel monopentamethylcyclopentadienyl alkoxides of La and Ce; X-ray crystal structure of $(C_5Me_5Ce(OCMe_3)_2)_2$. J. Organomet. Chem. 1989, 364 (1), 87-96.
56. Mueller, T. J.; Ziller, J. W.; Evans, W. J., Sigma bond metathesis with pentamethylcyclopentadienyl ligands in sterically crowded $(C_5Me_5)_3M$ complexes. Dalton. Trans. 2010, 39 (29), 6767-6773.
57. Raeder, J.; Reiners, M.; Baumgarten, R.; Münster, K.; Baabe, D.; Freytag, M.; Jones, P. G.; Walter, M. D., Synthesis and molecular structure of pentadienyl complexes of the rare-earth metals. Dalton. Trans. 2018, 47 (41), 14468-14482.
58. Yin, H.; Carroll, P. J.; Manor, B. C.; Anna, J. M.; Schelter, E. J., Cerium Photosensitizers: Structure–Function Relationships and Applications in Photocatalytic Aryl Coupling Reactions. J. Am. Chem. Soc. 2016, 138 (18), 5984-5993.
59. Schneider, D.; Harmgarth, N.; Edelmann, F. T.; Anwander, R., Ceric Cyclopentadienides Bearing Alkoxy, Aryloxy, Chlorido, or Iodido Co-Ligands. Chem. Eur. J. 2017, 23 (50), 12243-12252.
60. Gericke, R.; Doyle, L. M.; Farquhar, E. R.; McDonald, A. R., Oxo-Free Hydrocarbon Oxidation by an Iron(III)-Isoporphyrin Complex. Inorg. Chem. 2020, 59 (19), 13952-13961.
61. Sridevi, V. S.; Leong, W. K.; Zhu, Y., Catalytic Reductive Coupling of 9-Bromofluorene. Organometallics 2006, 25 (1), 283-288.
62. Al-Afyouni, M. H.; Huang, T. A.; Hung-Low, F.; Bradley, C. A., Synthesis of bifluorenes via cobalt halide radical coupling. Tetrahedron Lett. 2011, 52 (26), 3261-3265.
63. Panda, T. K.; Gamer, M. T.; Roesky, P. W., An Improved Synthesis of Sodium and Potassium Cyclopentadienide. Organometallics 2003, 22 (4), 877-878.
64. See, X. Y.; Beaumier, E. P.; Davis-Gilbert, Z. W.; Dunn, P. L.; Larsen, J. A.; Pearce, A. J.; Wheeler, T. A.; Tonks, I. A., Generation of TiII Alkyne Trimerization Catalysts in the Absence of Strong Metal Reductants. Organometallics 2017, 36 (7), 1383-1390.
65. Gawley, R. E.; Zhang, X.; Wang, Q. In Potassium hydride, John Wiley & Sons, Ltd.: 2007; pp 1-5.
66. Leis, C.; Zybill, C.; Lachmann, J.; Müller, G., Silylene complexes stabilized by sulphur substituents; a structure and reactivity study. Polyhedron 1991, 10 (11), 1163-1171.
67. Kozimor, S. A.; Bartlett, B. M.; Rinehart, J. D.; Long, J. R., Magnetic Exchange Coupling in Chloride-Bridged 5f−3d Heterometallic Complexes Generated via Insertion into a Uranium(IV) Dimethylpyrazolate Dimer. J. Am. Chem. Soc. 2007, 129 (35), 10672-10674.
68. Barisic, D.; Buschmann, D. A.; Schneider, D.; Maichle-Mössmer, C.; Anwander, R., Rare-Earth-Metal Pentadienyl Half-Sandwich and Sandwich Tetramethylaluminates–Synthesis, Structure, Reactivity, and Performance in Isoprene Polymerization. Chem. Eur. J. 2019, 25 (18), 4821-4832.
69. Wooles, A. J.; Mills, D. P.; Lewis, W.; Blake, A. J.; Liddle, S. T., Lanthanide tri-benzyl complexes: structural variations and useful precursors to phosphorus-stabilised lanthanide carbenes. Dalton. Trans. 2010, 39 (2), 500-510.

Supporting Information

Radical Coupling at Cerium Fluorenyl Complexes

Lars Hirneise, Cäcilia Maichle-Mössmer, and Reiner Anwander*

*Institut für Anorganische Chemie, Eberhard Karls Universität Tübingen, Auf der Morgenstelle 18, 72076 Tübingen, Germany

KEYWORDS cerium; organometallic; fluorenyl; oxidation; carbon-carbon coupling

Table of Contents

NMR spectra

* → solvent, # → small impurities

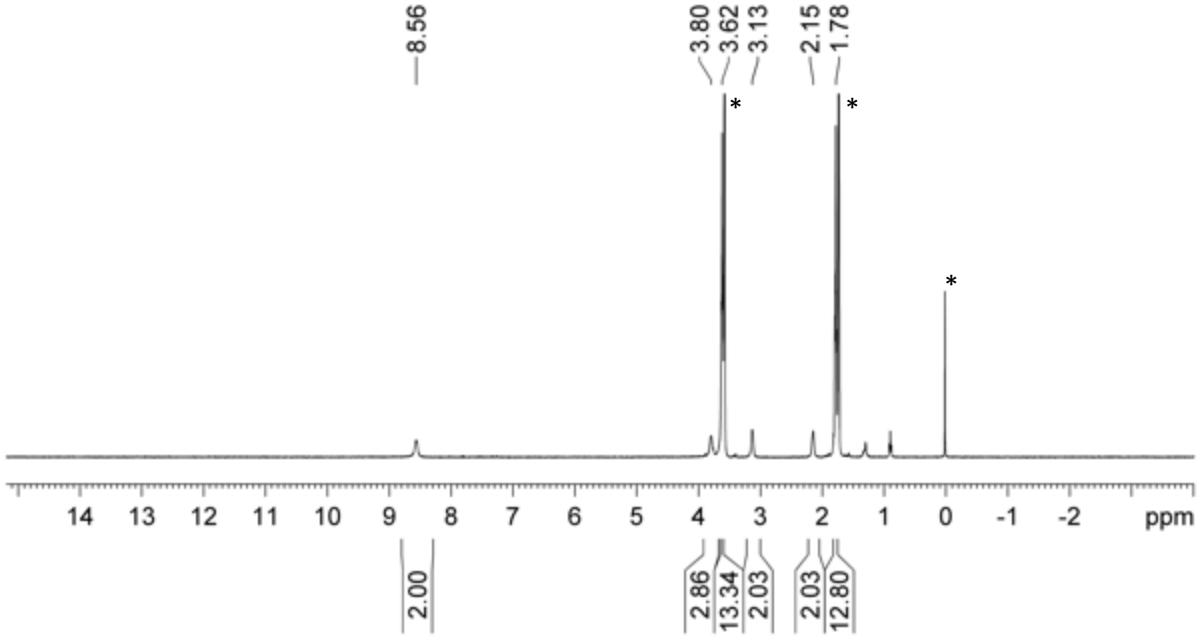

Figure S1. ^{1}H NMR spectrum (400.1 MHz, THF-d_8, 26 °C) of $FluCeCl_2(THF)_3$ (**1^{Cl}**) (* $SiMe_4$).

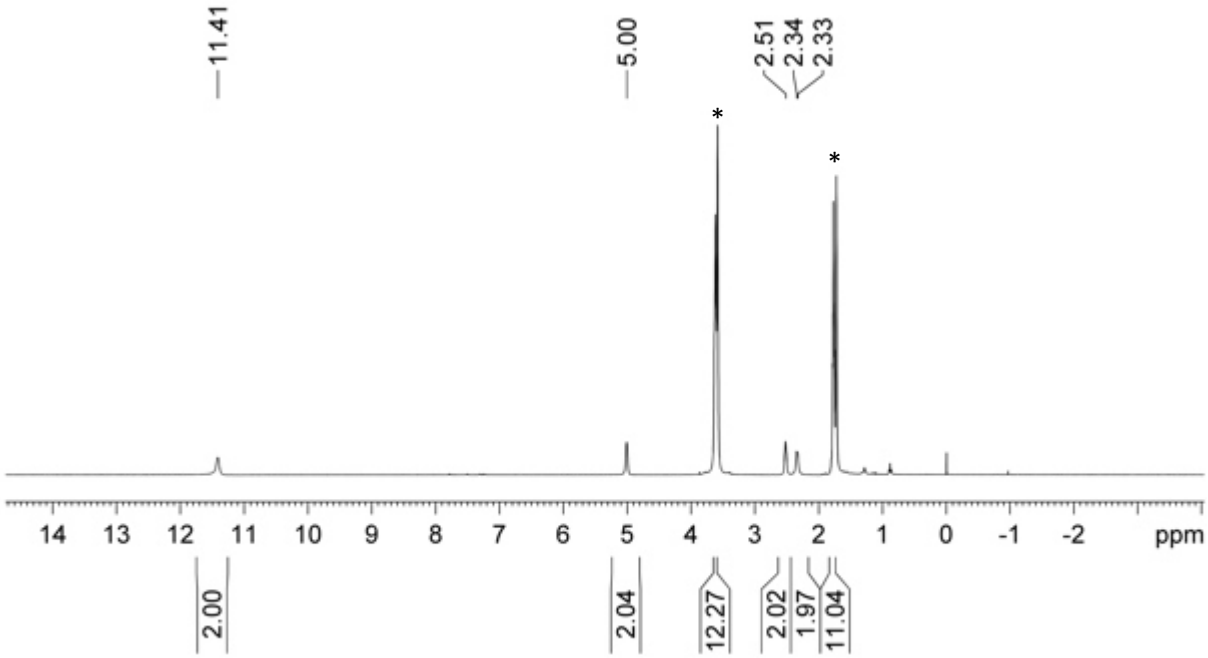

Figure S2. ^{1}H NMR spectrum (400.1 MHz, THF-d_8, 26 °C) of $FluCeI_2(THF)_3$ (**1^{I}**).

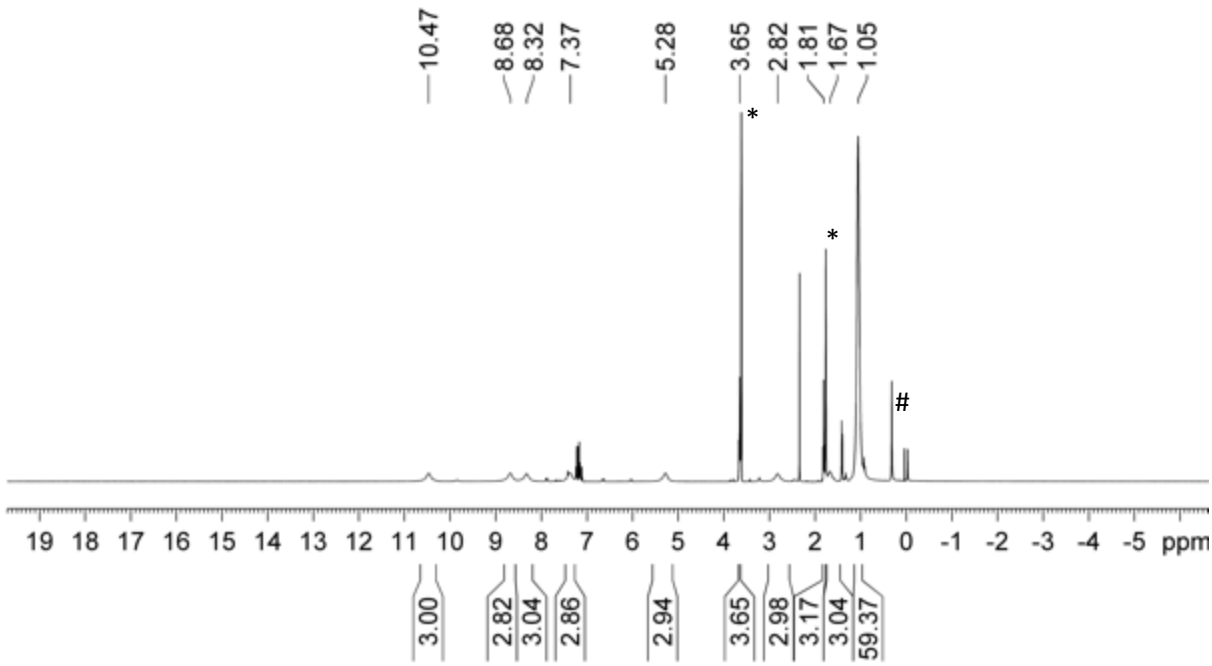

Figure S3. ^{1}H NMR spectrum (400.1 MHz, THF-d_8, 26 °C) of Flu$^{t\mathrm{Bu}}{}_3$Ce(THF) (**2**).

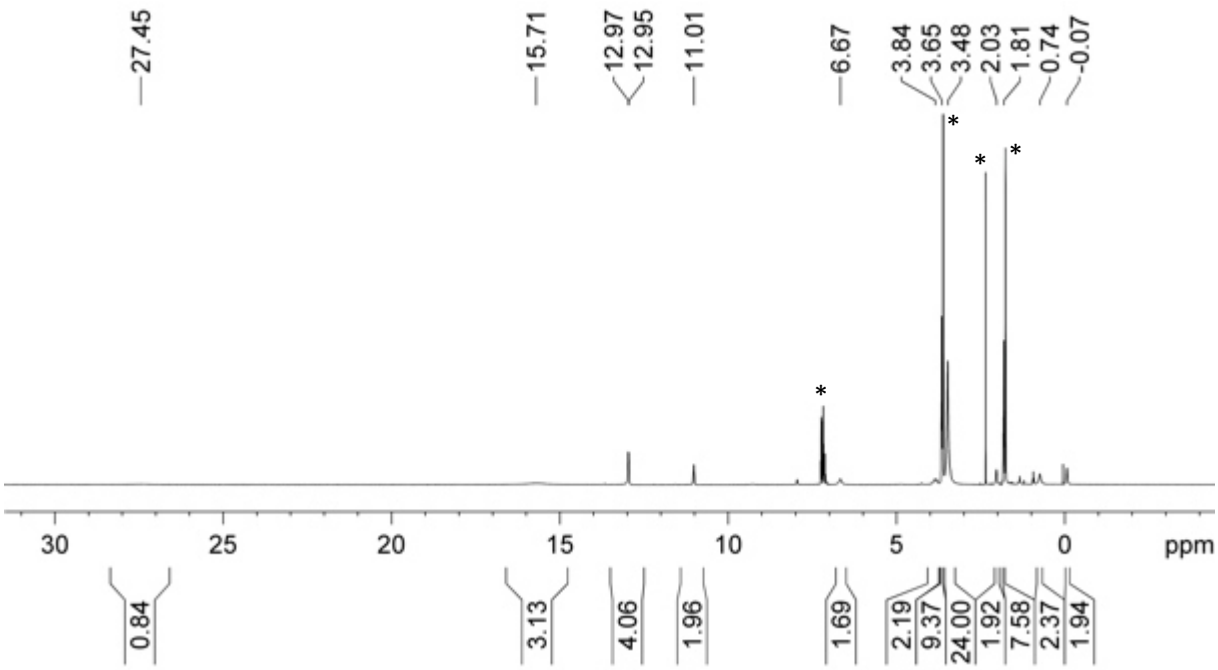

Figure S4. ^{1}H NMR spectrum (400.1 MHz, THF-d_8, 26 °C) of FluCe(OC$_6$H$_3$*i*Pr$_2$-2,6)$_2$(THF)$_2$ (**3$^{\mathrm{OAr}}$**).

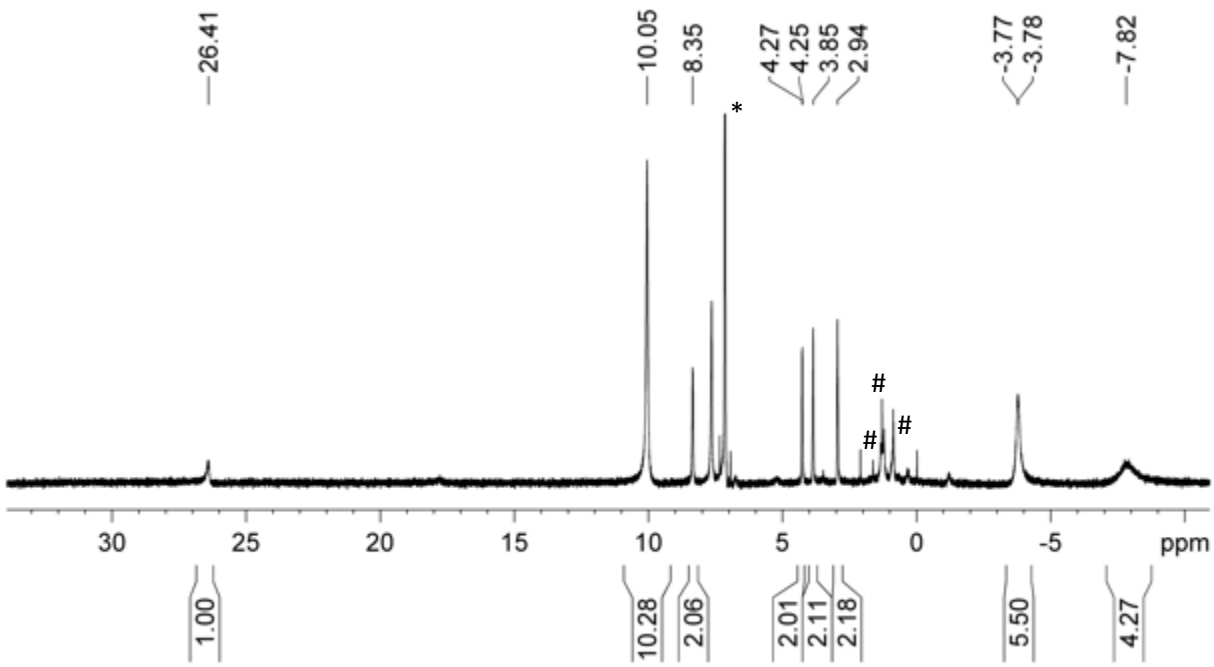

Figure S5. ^{1}H NMR spectrum (400.1 MHz,THF-d_8, 26 °C) of FluCeCp$_2$(THF) (**3^{Cp}**).

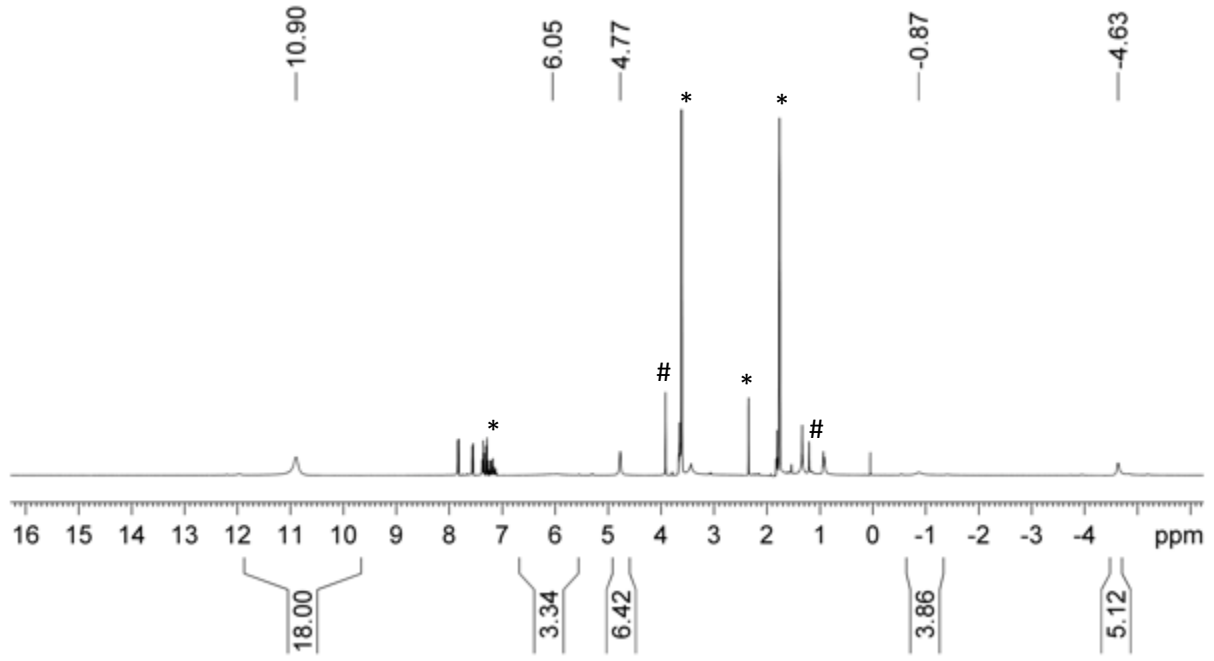

Figure S6. ^{1}H NMR spectrum (400.1 MHz, THF-d_8, 26 °C) of FluCe(OSiMe$_3$)$_2$(THF) (**3^{OSiMe3}**).

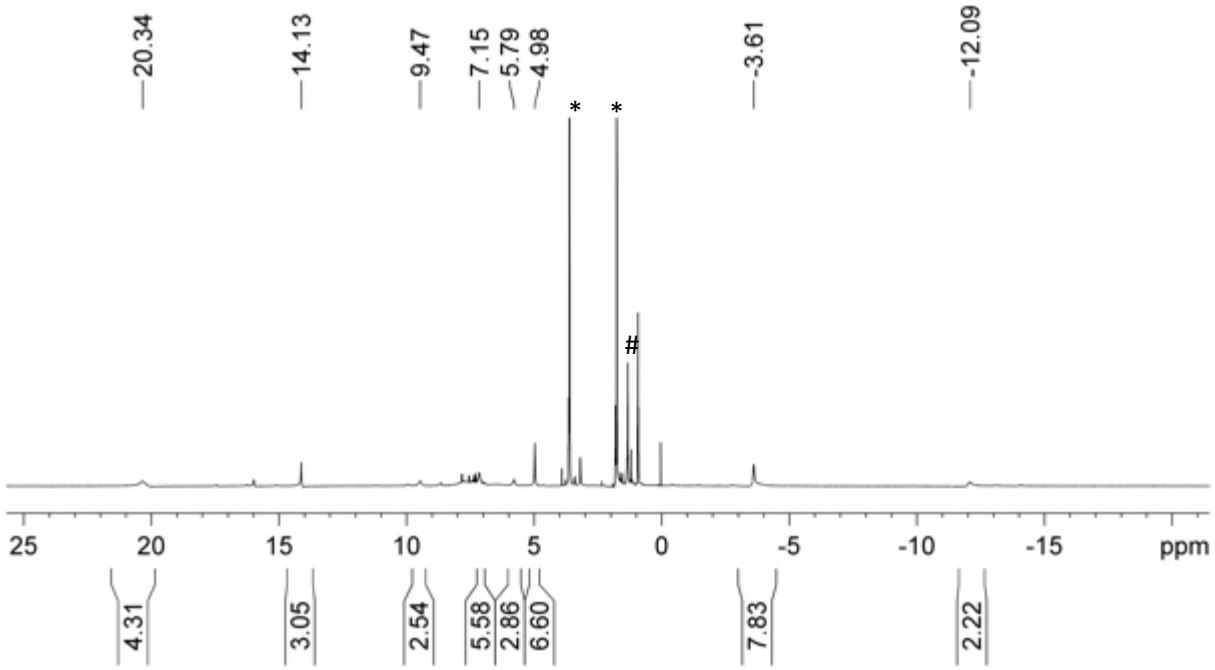

Figure S7. ^{1}H NMR spectrum (400.1 MHz, THF-d_8, 26 °C) of FluCe(O*t*Bu)$_2$(THF) (**3^{OtBu}**).

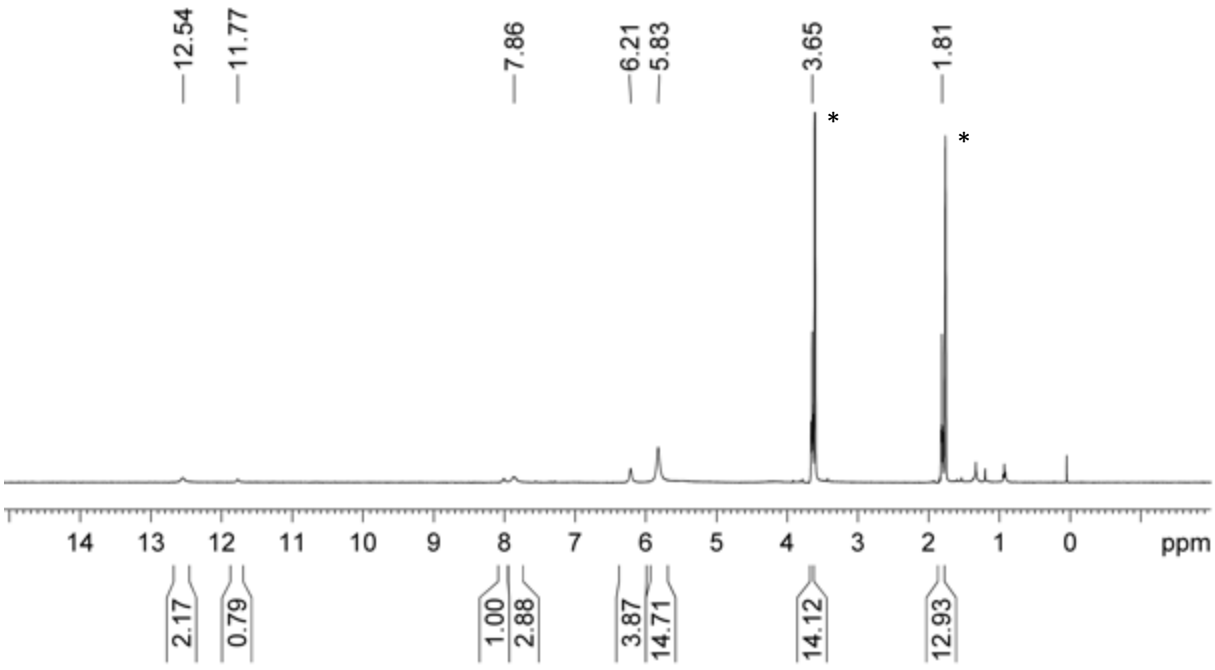

Figure S8. ^{1}H NMR spectrum (400.1 MHz, THF-d_8, 26 °C) of FluCe(Pz)$_2$(THF)$_2$ (**3^{Pz}**).

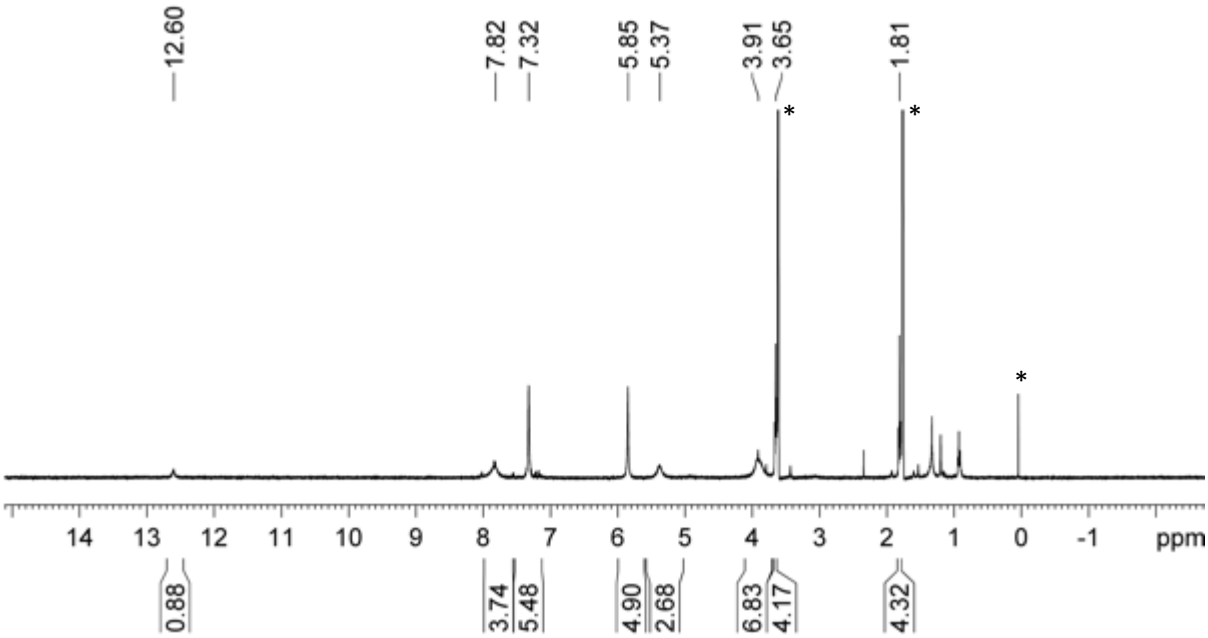

Figure S9. ^{1}H NMR spectrum (400.1 MHz, THF-d_8, 26 °C) of $Flu_2Ce(Pz)(THF)$ (**4^{Pz}**).

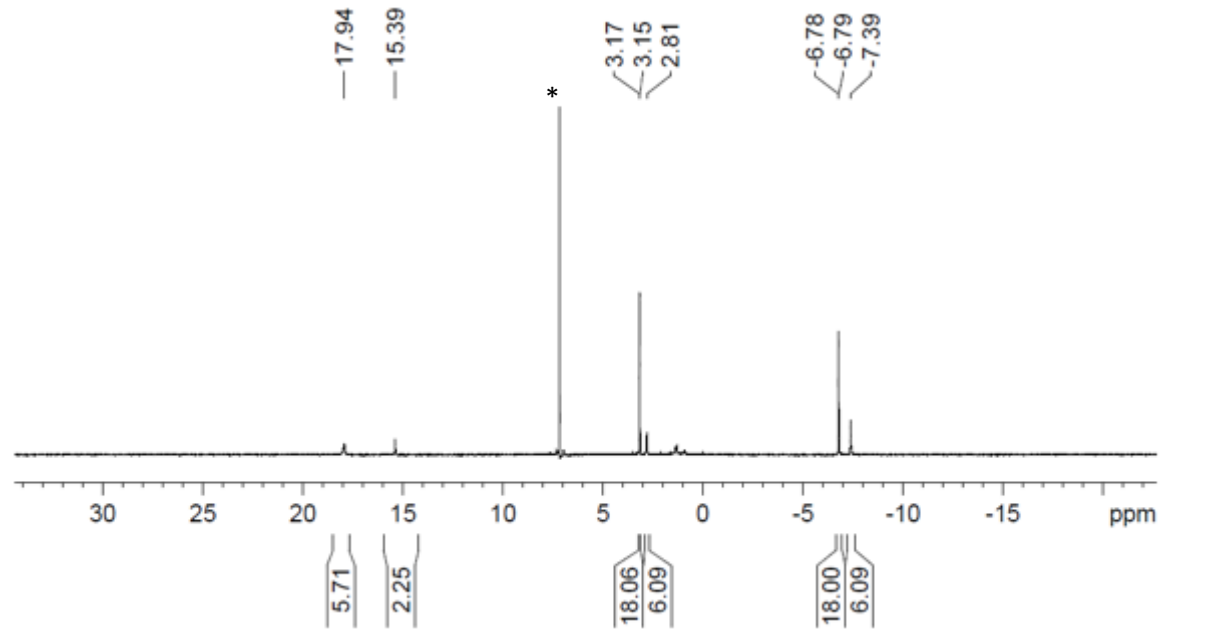

Figure S10. ^{1}H NMR spectrum (400.1 MHz, C_6D_6, 26 °C) of $Ce(dipp)_3$ (**6**).

NMR Spectra of Reactions with Oxidants

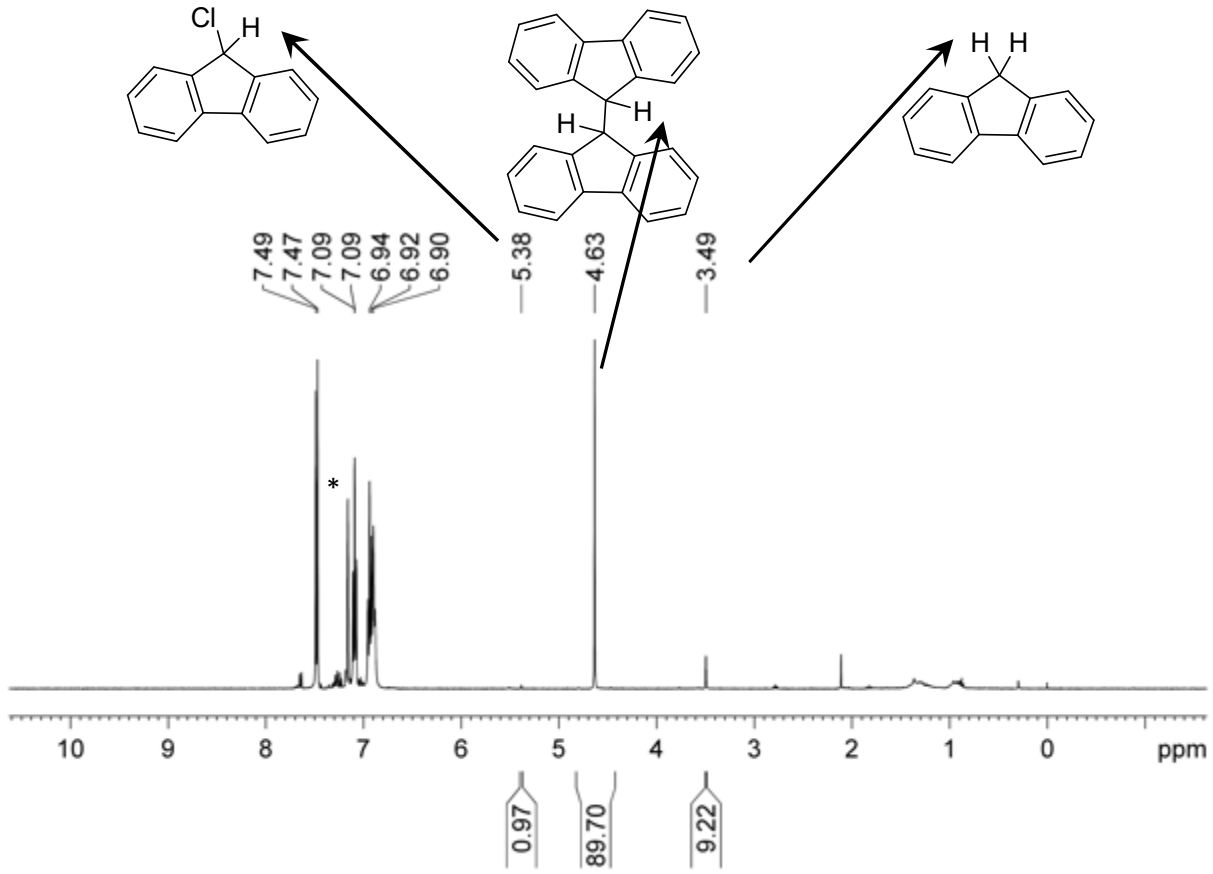

Figure S11. ^{1}H NMR spectrum (400.1 MHz, C_6D_6, 26 °C) of the reaction of $FluCeCl_2(THF)_3$ (**1^{Cl}**) with <0.5 equiv. C_2Cl_6 affording 1,1'-bifluorene.

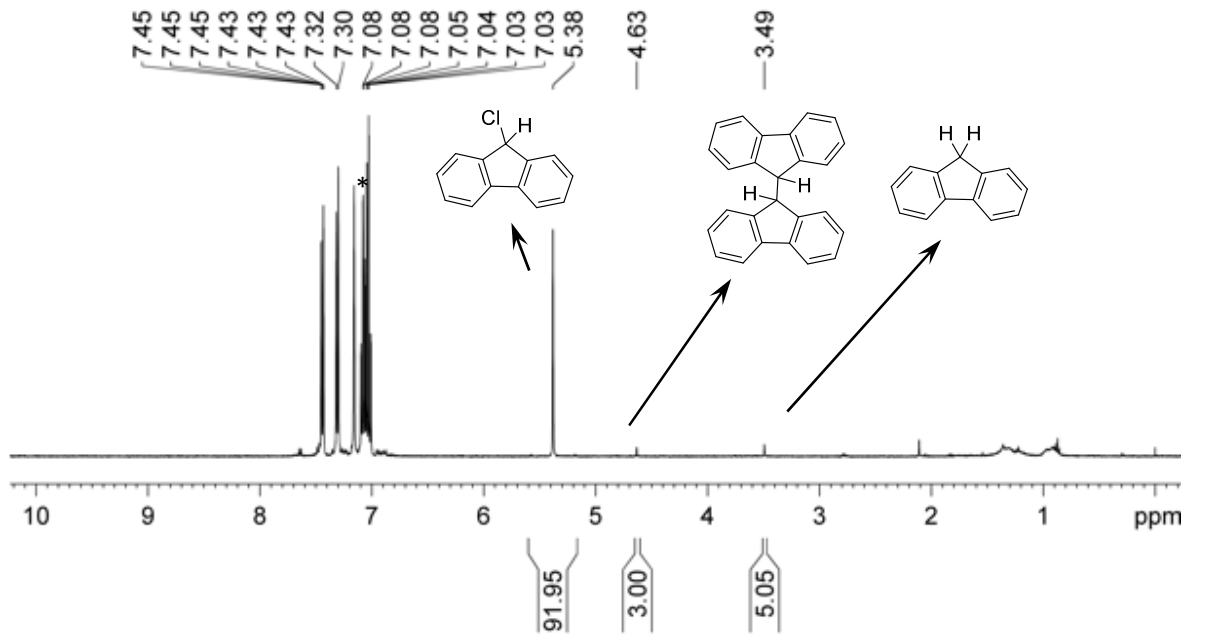

Figure S12. ^{1}H NMR spectrum (400.1 MHz,C_6D_6, 26 °C) of the reaction of $FluCeCl_2(THF)_3$ (**1^{Cl}**) with >1 equiv. C_2Cl_6 affording 9-chlorofluorene.

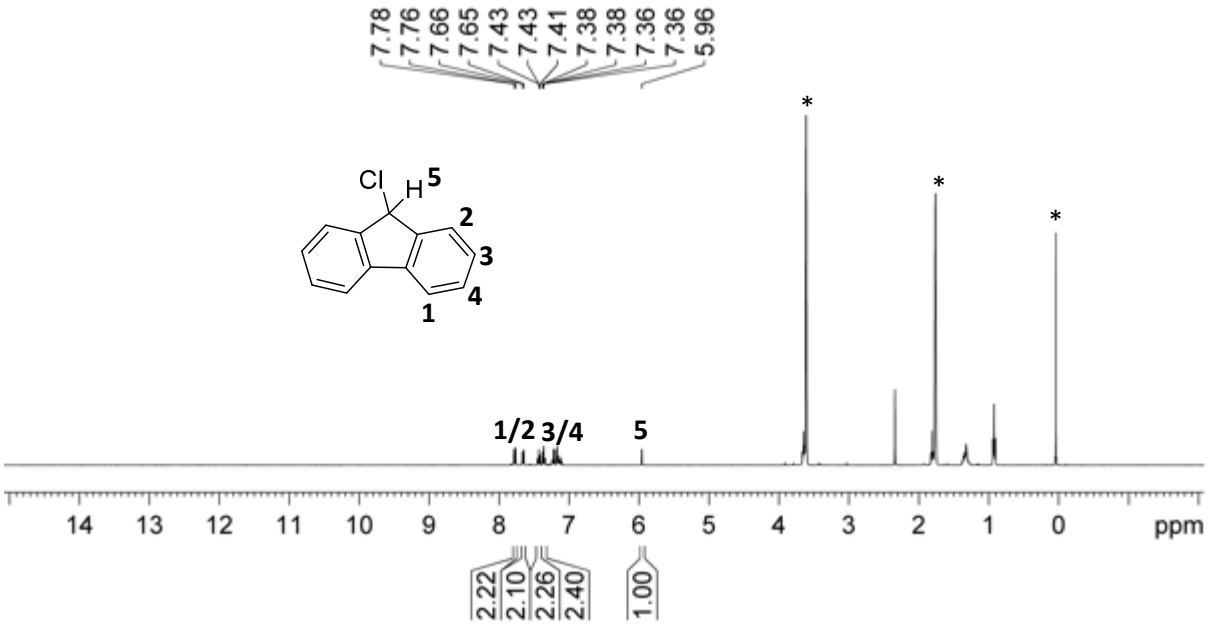

Figure S13. ^{1}H NMR spectrum (400.1 MHz, THF-d_8, 26 °C) of the reaction of $FluCeCl_2(THF)_3$ (**1^{Cl}**) with excess C_2Cl_6 affording 9-chlorfluorene.

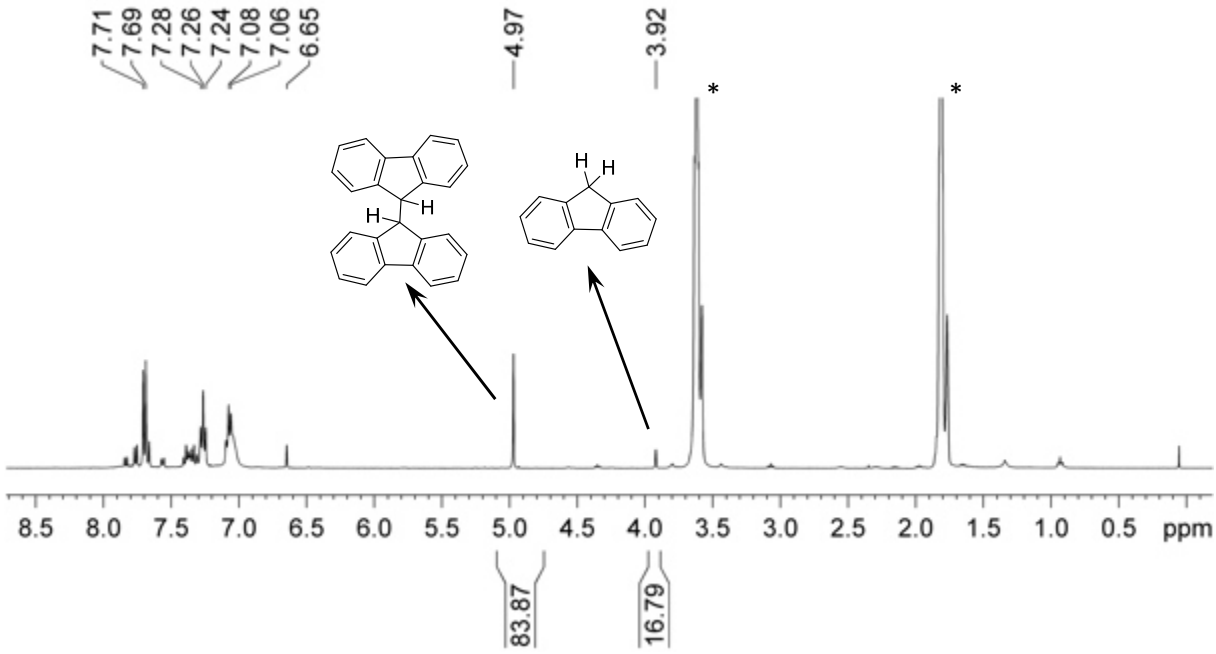

Figure S14. ^{1}H NMR spectrum (400.1 MHz, THF-d_8, 26 °C) of the reaction of $FluCeCl_2(THF)_3$ (**1^{Cl}**) with 0.5 equiv. I_2 affording mainly 1,1'-bifluorene and fluorene.

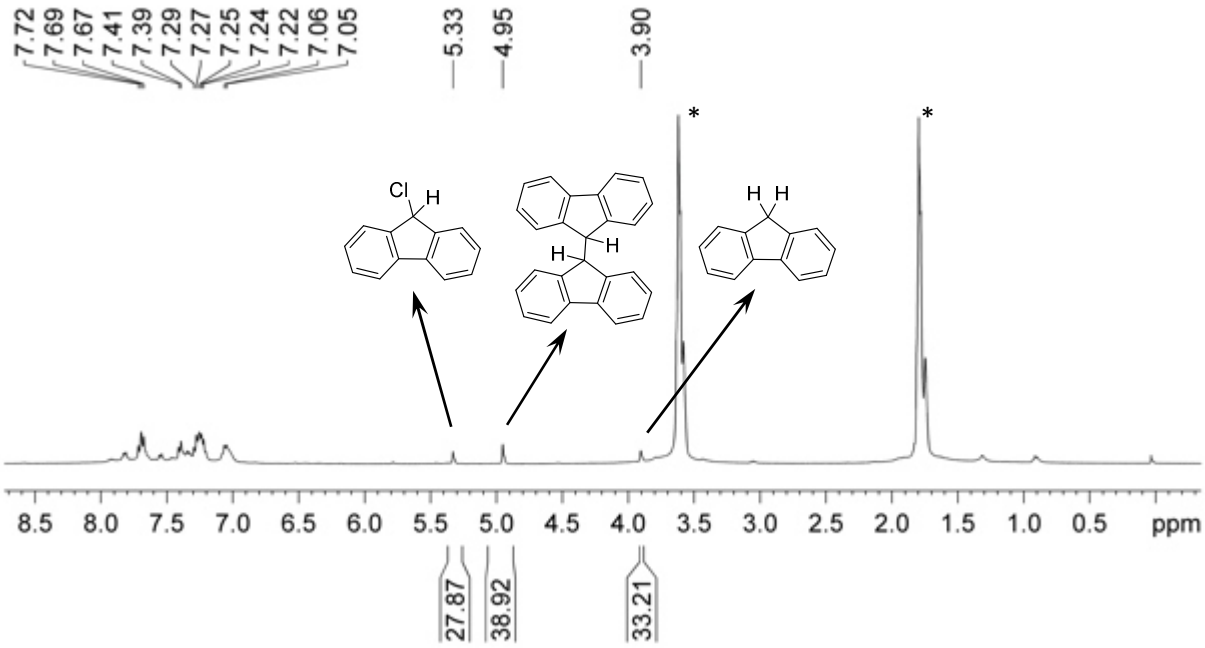

Figure S15. ^{1}H NMR spectrum (400.1 MHz, THF-d_8, 26 °C) of the reaction of $FluCeCl_2(THF)_3$ (**1^{Cl}**) with 0.25 equiv. $TeBr_4$ affording mainly 1,1'-bifluorene and fluorene.

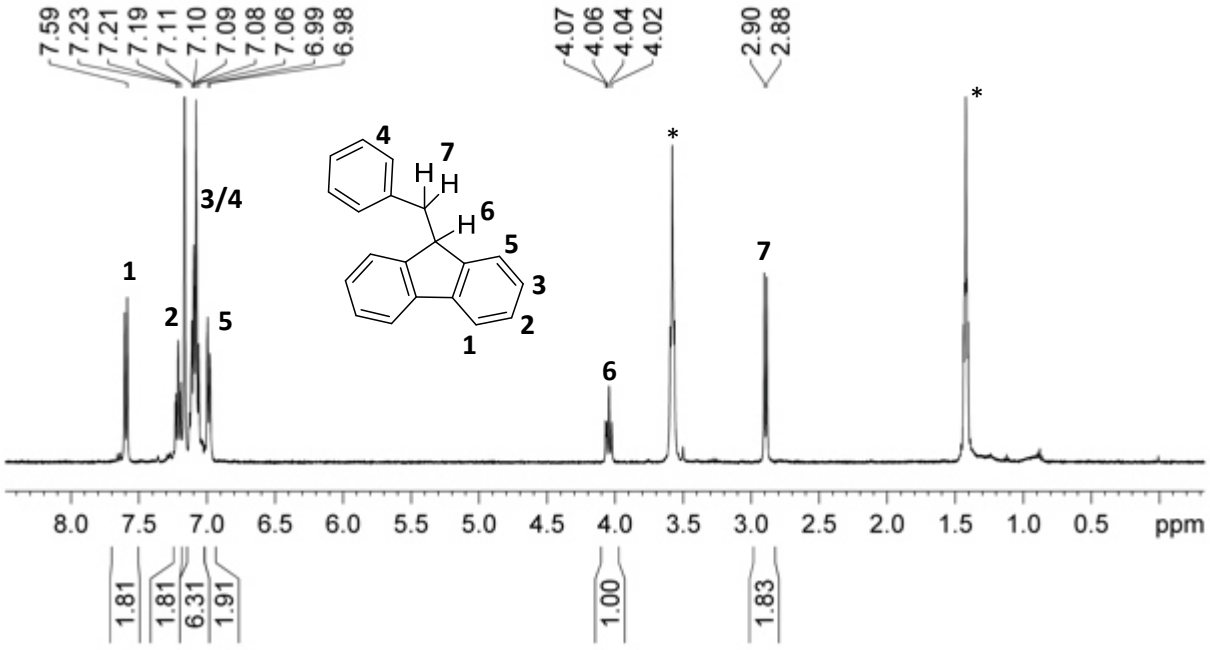

Figure S16. ^{1}H NMR spectrum (400.1 MHz, THF-d_8, 26 °C) of the reaction of $FluCeCl_2(THF)_3$ (**1^{Cl}**) with 1 equiv. benzylchloride affording mainly 9-benzylfluorene.

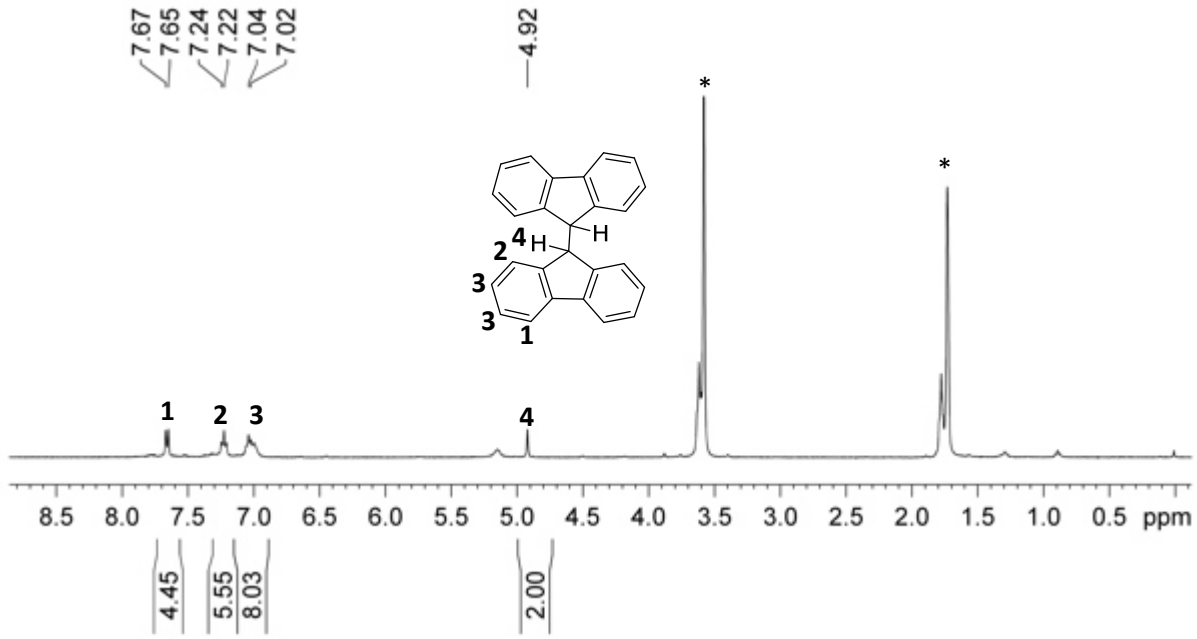

Figure S17. ^{1}H NMR spectrum (400.1 MHz, THFd_8, 26 °C) of the reaction of FluCeCl_2(THF)$_3$ (**1^{Cl}**) with 1 equiv. 1,4-benzoquinone affording mainly 1,1'-bifluorene.

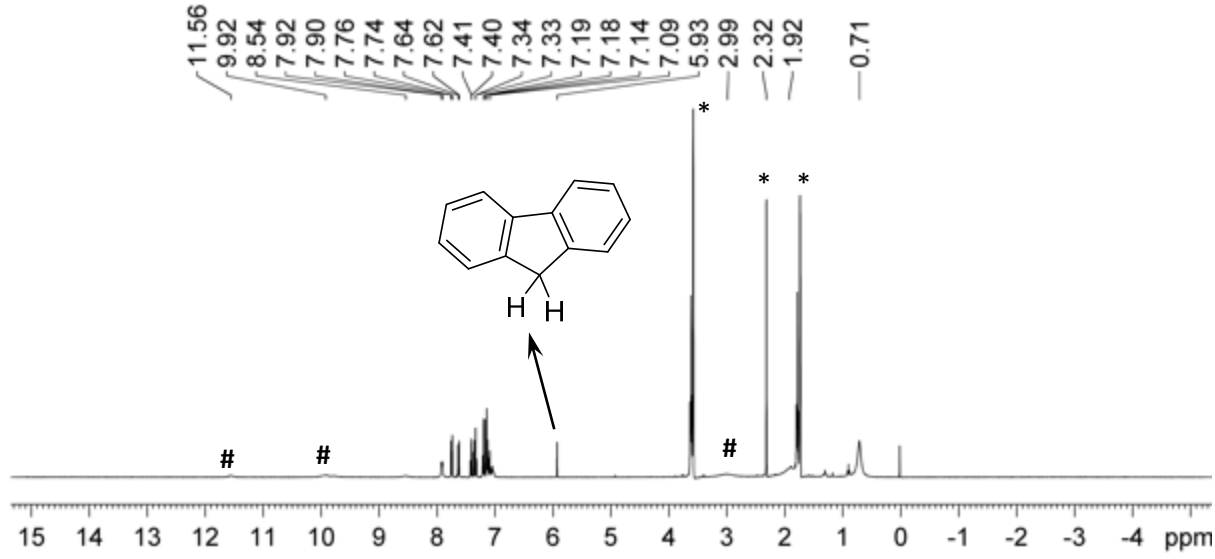

Figure S18. ^{1}H NMR spectrum (400.1 MHz, thf-d_8, 26 °C) of the reaction of FluCe(OAr)$_2$(THF)$_2$ (**3^{OAr}**) with C_2Cl_6 affording fluorene (+) and small paramagnetic signals (#).

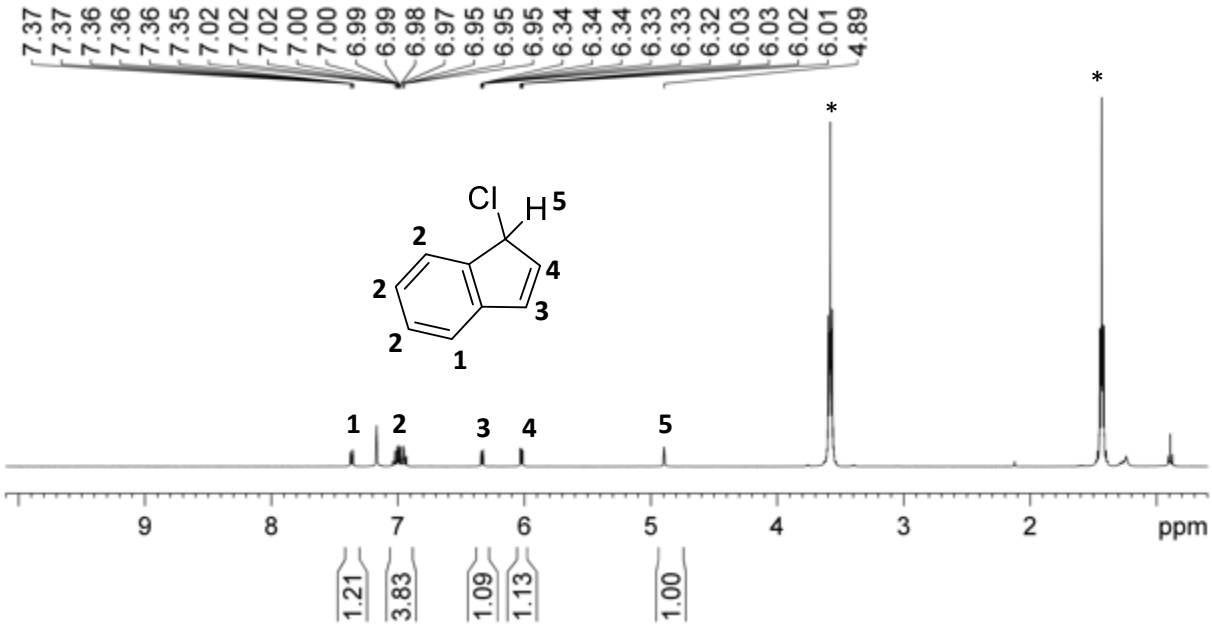

Figure S19. ^{1}H NMR spectrum (400.1 MHz, thf-d_8, 26 °C) of the reaction of $Ind_3Ce(THF)$ with 1.5 equiv. C_2Cl_6 affording 1-chloroindene.

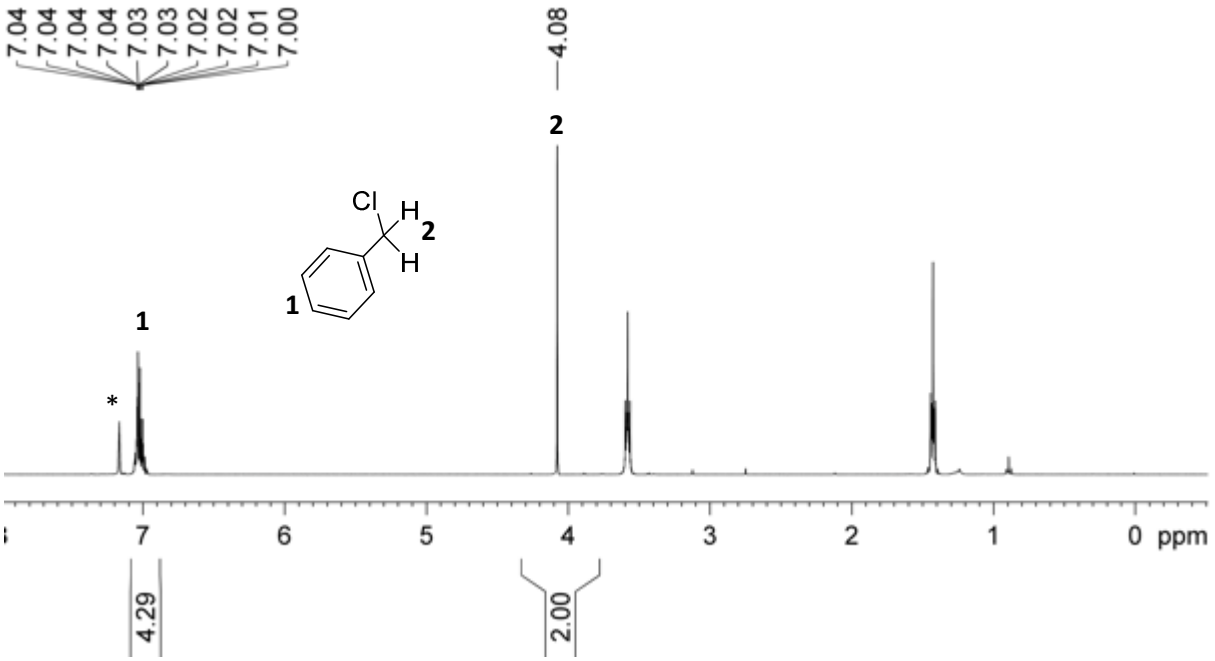

Figure S20. ^{1}H NMR spectrum (400.1 MHz, C_6D_6, 26 °C) of the reaction of $Ce(CH_2Ph)_3$ with 1.5 equiv. C_2Cl_6 affording benzylchloride.

Solid-State Structures

Crystals for X-Ray crystallography were grown using saturated solutions of toluene (**1**^{Cp}, **1**^{OAr}, **2**^{OfBu}, **2**^{OSiMe3}, **2**^{Pz}, **4** and **5**) or thf (**1**^{Cl}, **1**^{I}, **1**^{Pz}**(thf)**$_2$, **1**^{Pz}**(thf)**$_4$, **3**). Suitable crystals for X-Ray analysis were handpicked in a glovebox, coated with Parabar 10312 and stored on microscope slides. Data collection were done on a *Bruker* APEX II Duo diffractometer by using QUAZAR optics and Mo K_α (λ = 0.71073 Å). The data collection strategy was determined using COSMO[4] employing ω scans. Raw data were processed by APEX[5] and SAINT,[6] corrections for absorption effects were applied using SADABS.[7] The structures were solved by direct methods and refined against all data by full-matrix least-squares methods on F^2 using SHELXTL[8] and SHELXLE.[9] Plots were generated by using CCDC Mercury 3.19.1.[10] Further details regarding the refinement and crystallographic data are listed in Table S3 and in the CIF files.

[1] COSMO, v. 1.61; Bruker AXS Inc., Madison, WI, 2012.

[2] APEX 3, v. 2016.5-0; Bruker AXS Inc., Madison, WI, 2012.

[3] SAINT, v. 8.34A; Bruker AXS Inc., Madison, WI, 2010.

[4] L. Krause, R. Herbst-Irmer, G. M. Sheldrick, D. Stalke, J. Appl. Cryst. 2015, 48, 3-10.

[5] G. M. Sheldrick, Acta Crystallogr., Sect. A 2015, 71, 3-8.

[6] C. B. Hübschle, G. M. Sheldrick, B. J. Dittrich, J. Appl. Cryst. 2011, 44, 1281-1284.

[7] C. F. Macrae, I. J. Bruno, J. A. Chisholm, P. R. Edgington, P. McCabe, E. Pidcock, L. Rodriguez-Monge, R.Taylor, J. van de Streek, P. A. Wood, J. Appl. Cryst. 2008, 41, 466-470.

Table S1. Collection of crystallographic data of $\mathbf{1^{Cl}}$, $\mathbf{1^{I}}$, **2**, $\mathbf{3^{Cp}}$, $\mathbf{3^{Pz}}$, $\mathbf{3^{Pz,THF}}$, $\mathbf{3^{OAr}}$, $\mathbf{4^{OtBu}}$, $\mathbf{4^{OSiMe3}}$, $\mathbf{4^{Pz}}$, **5**, LiFlu(THF)$_3$, and **6**

	$\mathbf{1^{Cl}}$	$\mathbf{1^{I}}$	**2**	$\mathbf{3^{Cp}}$	$\mathbf{3^{Pz}}$
formula	$C_{25}H_{33}CeCl_2O_3$	$C_{25}H_{33}CeI_2O_3$	$C_{74}H_{91}CeO$	$C_{27}H_{27}CeO$	$C_{31}H_{39}CeN_4O_2$
M [g · mol^{-1}]	592.53	775.43	1136.58	507.60	639.78
λ [Å]	0.71073	0.71073	0.71073	0.71073	0.71073
cell	monoclinic	monoclinic	monoclinic	monoclinic	monoclinic
space group	$P2_1/c$	$P2_1/c$	$P2_1/c$	$P2_1/c$	$P2_1/c$
a [Å]	15.7295(9)	17.7588(12)	13.3994(7)	12.3611(14)	24.742(3)
b [Å]	19.0754(11)	18.7839(13)	18.7291(10)	9.2882(11)	9.5613(12)
c [Å]	16.9069(10)	15.9243(11)	24.6500(13)	18.301(2)	25.071(3)
α [°]	90	90	90	90	90
β [°]	93.2310(10)	93.7160(10)	100.894(2)	94.103(2)	99.538(3)
γ [°]	90	90	90	90	90
V [Å^3]	5064.8(5)	5300.9(6)	6074.6(6)	2095.8(4)	5849.0(13)
Z	8	8	4	4	8
F(000)	2392	2968	2404	1020	2616
T [K]	100(2)	100(2)	100(2)	100(2)	100(2)
ρ_{calcd} [g · mol^3]	1.554	1.943	1.243	1.609	1.453
μ [mm^{-1}]	2.032	4.070	0.793	2.187	1.590
R_1 ($I>2\sigma(I)$)	0.0378	0.0288	0.0439	0.0226	0.0399
ωR_2 (all data)	0.0850	0.0710	0.0997	0.0558	0.0945
Goodness of fit	1.064	1.062	1.017	1.077	1.027

Table S2. Collection of crystallographic data of $\mathbf{1}^{Cl}$, $\mathbf{1}^{I}$, **2**, $\mathbf{3}^{Cp}$, $\mathbf{3}^{Pz}$, $\mathbf{3}^{Pz,THF}$, $\mathbf{3}^{OAr}$, $\mathbf{4}^{OtBu}$, $\mathbf{4}^{OSiMe3}$, $\mathbf{4}^{Pz}$, **5**, LiFlu(THF)$_3$, and **6** (continued)

	$\mathbf{3}^{Pz,THF}$	$\mathbf{3}^{OAr}$	$\mathbf{4}^{OtBu}$	$\mathbf{4}^{OSiMe3}$	$\mathbf{4}^{Pz}$
formula	$C_{43}H_{63}CeN_4O_5$	$C_{59}H_{75}CeO_4$	$C_{34}H_{35}CeO_2$	$C_{33}H_{35}CeO_2Si$	$C_{35}H_{33}CeN_2O$
M [g · mol^{-1}]	856.09	988.31	615.74	631.84	637.75
λ [Å]	0.71073	0.71073	0.71073	0.71073	0.71073
cell	monoclinic	monoclinic	monoclinic	monoclinic	monoclinic
space group	Cc	$P2_1/c$	$P2_1/c$	$P2_1/c$	$P2_1/c$
a [Å]	19.380(17)	18.1532(12)	12.089(2)	16.683(2)	15.8625(18)
b [Å]	15.573(14)	13.3312(9)	14.929(3)	9.4666(13)	9.7332(12)
c [Å]	14.649(14)	21.5653(15)	15.165(2)	19.889(3)	19.971(3)
α [°]	90	90	90	90	90
β [°]	107.50(3)	97.5890(10)	95.445(4)	92.109(2)	112.598(2)
γ [°]	90	90	90	90	90
V [Å^3]	4217(7)	5173.2(6)	2724.7(8)	33138.9(7)	2846.6(6)
Z	4	4	4	4	4
F(000)	1788	2076	1252	1384	1292
T [K]	100(2)	100(2)	100(2)	100(2)	173(2)
ρ_{calcd} [g · mol^3]	1.349	1.269	1.501	1.434	1.488
μ [mm^{-1}]	1.126	0.924	1.700	1.519	1.629
R_1 ($I>2\sigma(I)$)	0.0575	0.0301	0.0498	0.0416	0.0373
ωR_2 (all data)	0.1341	0.0731	0.1083	0.1023	0.0954
Goodness of fit	1.013	1.027	0.980	1.013	1.035

Table S3. Collection of crystallographic data of $\mathbf{1^{Cl}}$, $\mathbf{1^{I}}$, **2**, $\mathbf{3^{Cp}}$, $\mathbf{3^{Pz}}$, $\mathbf{3^{Pz,THF}}$, $\mathbf{3^{OAr}}$, $\mathbf{4^{OtBu}}$, $\mathbf{4^{OSiMe3}}$, $\mathbf{4^{Pz}}$, **5**, LiFlu(THF)$_3$, and **6** (continued)

	5*	FluLi (THF)$_3$	**6**
formula	$C_{97}H_{103}Ce_3Cl_3LiO_2S_4$	$C_{25}H_{33}LiO_3$	$C_{33}H_{57}Ce$
M [g · mol^{-1}]	1962.68	388.45	593.90
λ [Å]	0.71073	0.71073	0.71073
cell	monoclinic	monoclinic	monoclinic
space group	$P2_1/n$	$P2_1/c$	$P2_1/c$
a [Å]	19.990(2)	7.3630(5)	11.1289(8)
b [Å]	31.191(3)	14.4664(9)	11.9637(8)
c [Å]	31.945(3)	20.6822(13)	23.7661(16)
α [°]	90	90	90
β [°]	96.918(3)	92.7720(10)	93.3260(10)
γ [°]	90	90	90
V [Å^3]	19772(3)	2200.4(2)	3159.0(4)
Z	8	4	4
F(000)	–	840	1252
T [K]	100(2)	100(2)	100(2)
ρ_{calcd} [g · mol^3]	–	1.173	1.249
μ [mm^{-1}]	–	0.074	1.458
R_1 (I>2σ(I))	–	0.0421	0.0368
ωR_2 (all data)	–	0.1156	0.0899
Goodness of fit	–	1.041	1.022

*connectivity

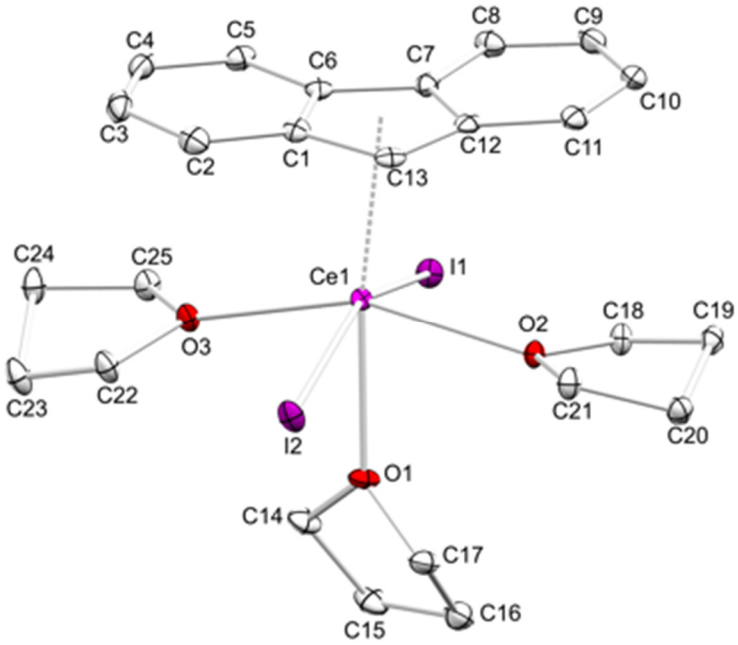

Figure S21. Crystal structure of **1**^{I}. Hydrogen atoms are omitted for clarity. Atomic displacement ellipsoids are set at the 30% probability level. Selected interatomic distances and angles are listed in Table 1.

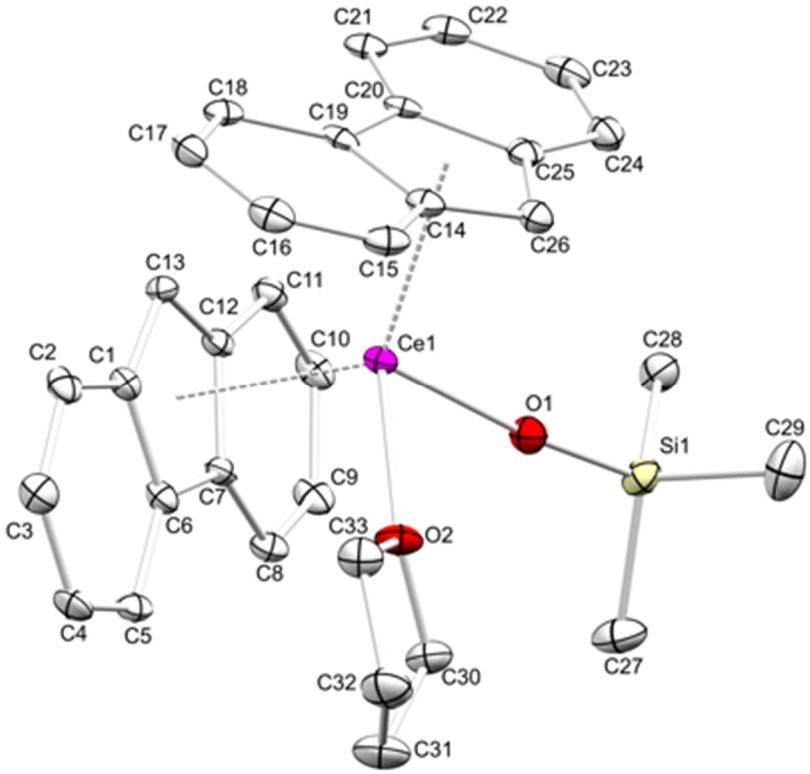

Figure S22. Crystal structure of **4**^{OSiMe3}. Hydrogen atoms and lattice toluene are omitted for clarity. Atomic displacement ellipsoids are set at the 30% probability level. Selected interatomic distances and angles are listed in Table 1.

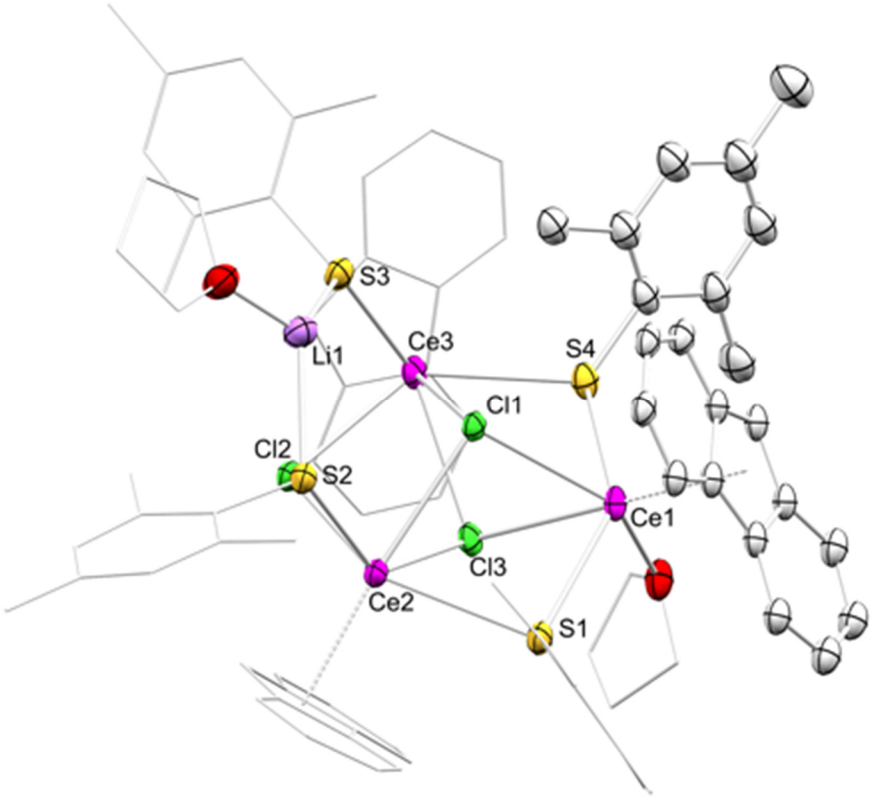

Figure S23. Connectivity structure of **5**. Hydrogen atoms are omitted for clarity. Atomic displacement ellipsoids are set at the 30% probability level.

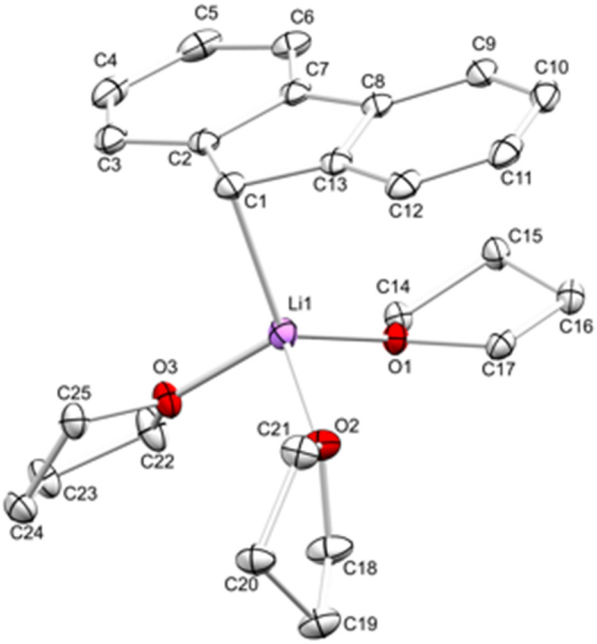

Figure S24. Crystal structure of LiFlu(THF)$_3$. Hydrogen atoms have been omitted for clarity. Atomic displacement ellipsoids are set at the 30% probability level. Selected distances and angles: Li-C1 2.294(2) Å, Li1-C2/C13 2.673(2) Å, Li1-O 1.879(2) (O1) – 1.973(2) (O2), Li1-C1-C2 88.71(8)°, Li1-C1-Cnt(Flu) 87.50°.

IR Spectra

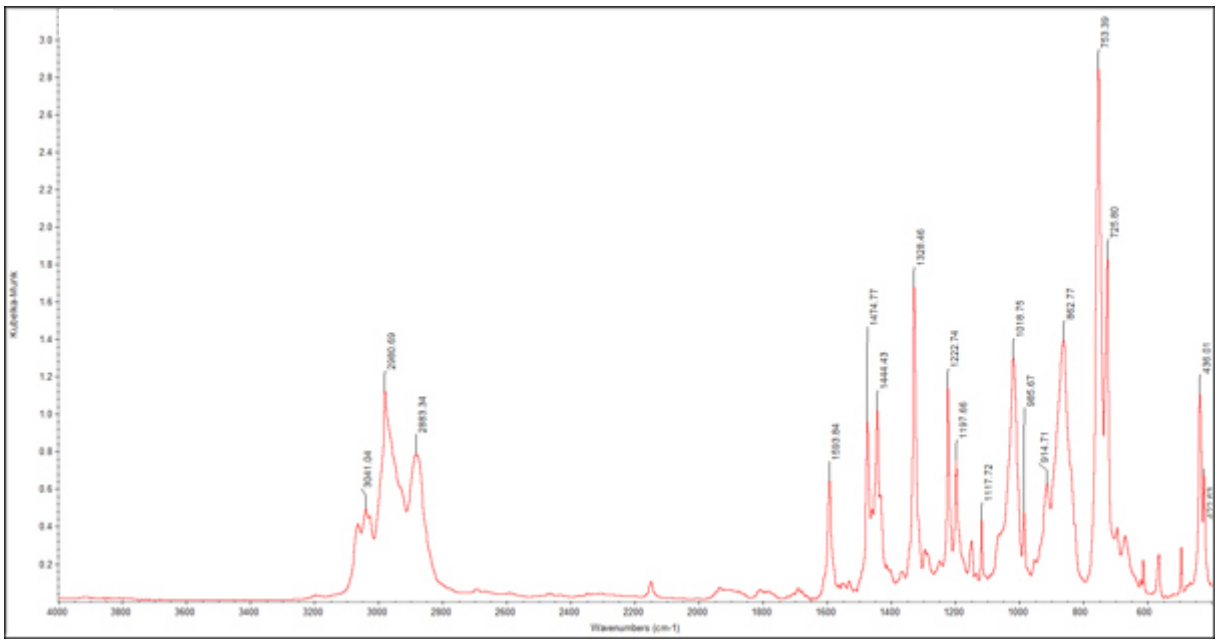

Figure S25. DRIFT spectrum of $FluCeCl_2(THF)_3$ ($\mathbf{1^{Cl}}$).

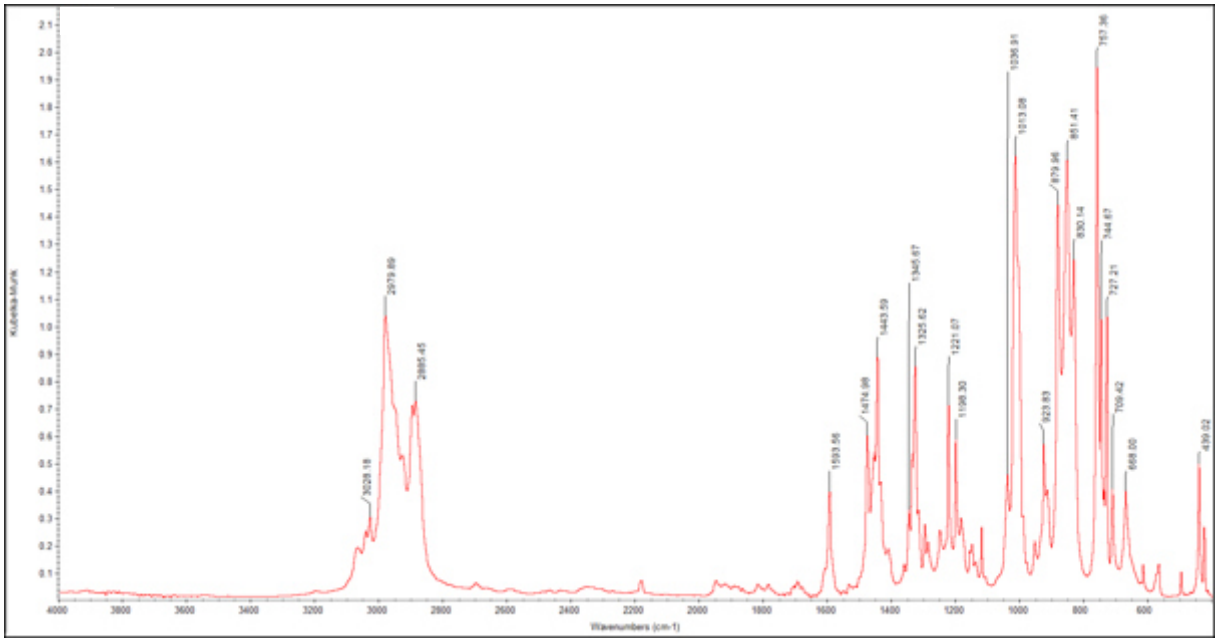

Figure S26. DRIFT spectrum of $FluCeI_2(THF)_3$ ($\mathbf{1^{I}}$).

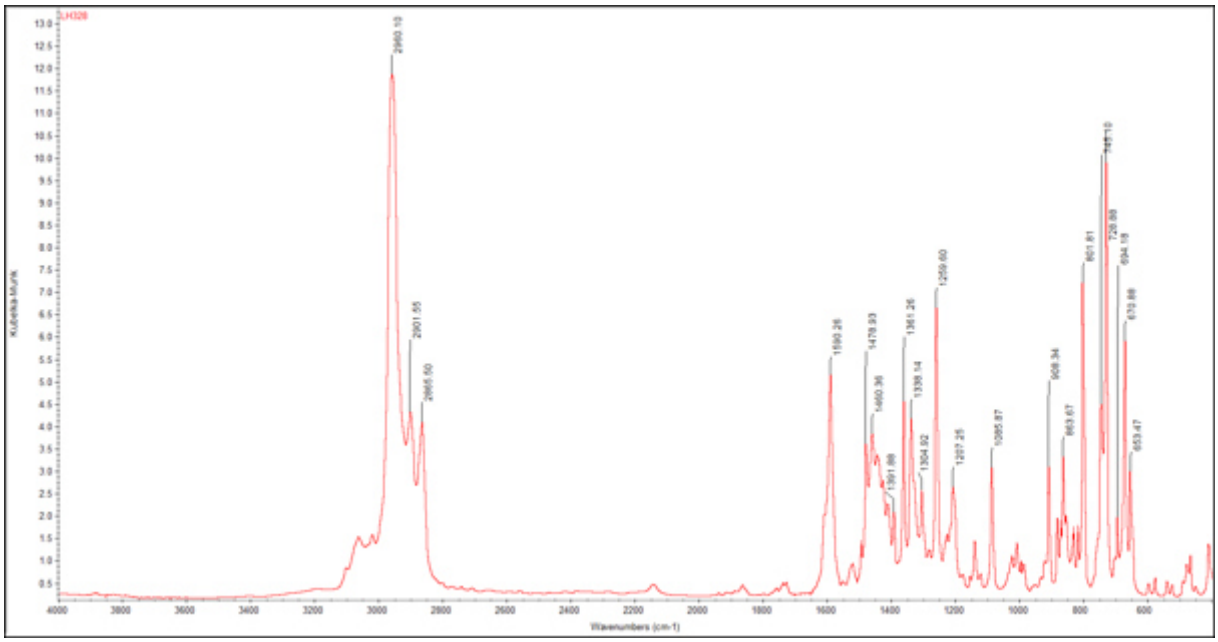

Figure S27. DRIFT spectrum of Flu$^{t\mathrm{Bu}}{}_3$Ce(THF) (**2**).

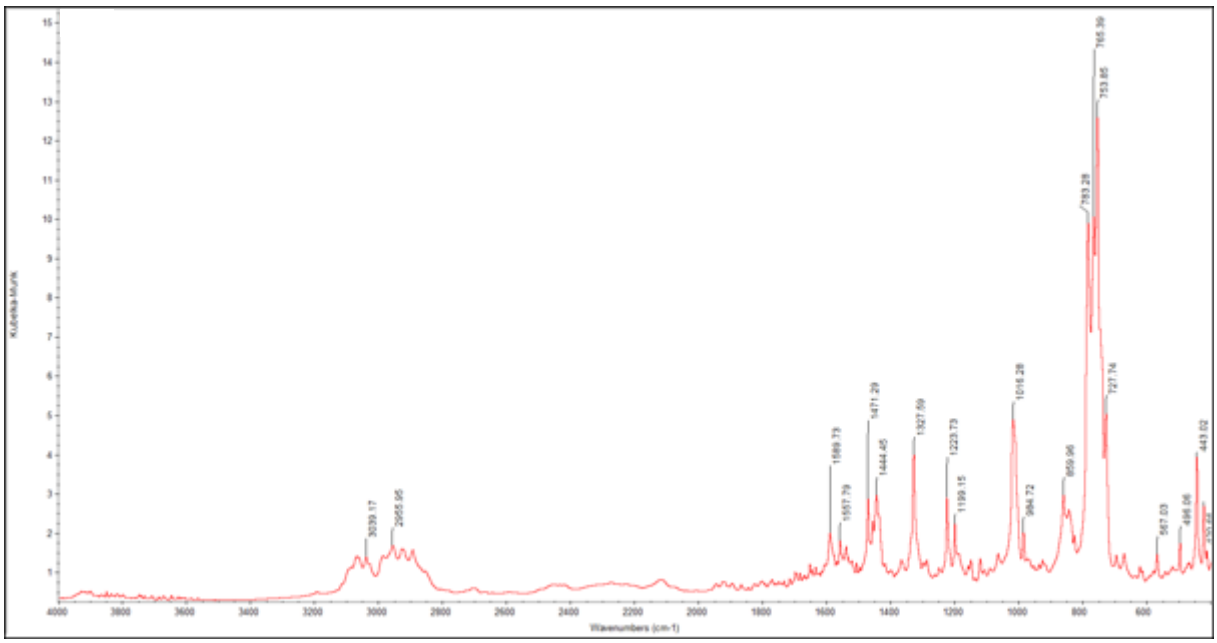

Figure S28. DRIFT spectrum of FluCeCp$_2$(THF) (**3$^{\mathrm{Cp}}$**).

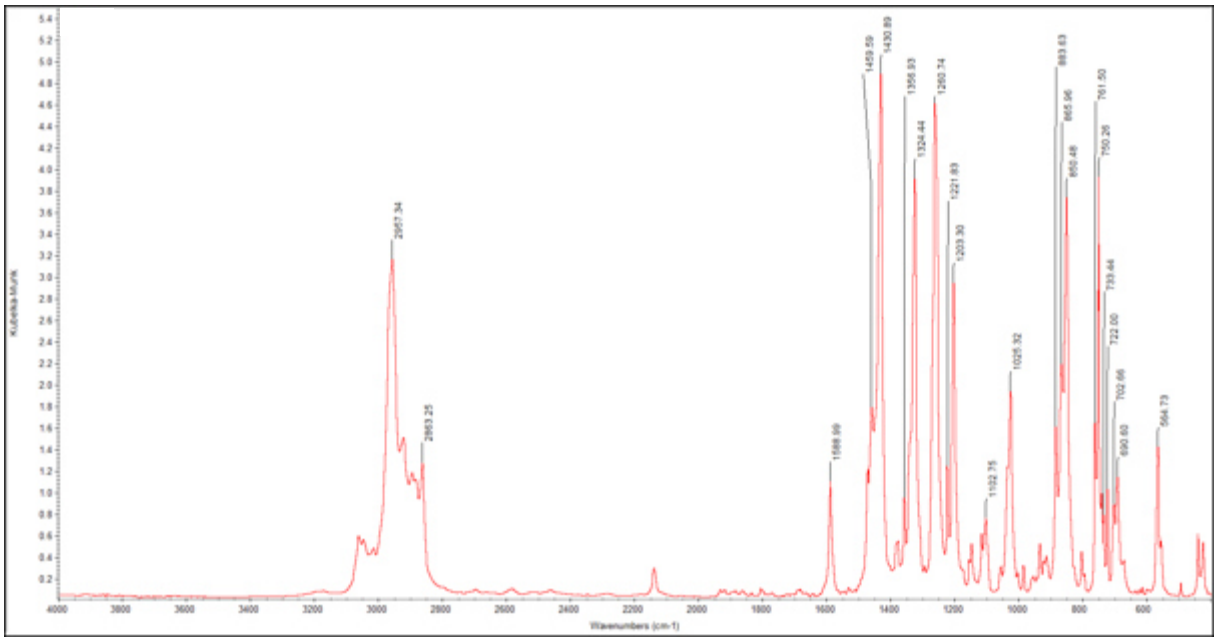

Figure S29. DRIFT spectrum of FluCe(OAr)$_2$(THF)$_2$ (**3^{OAr}**).

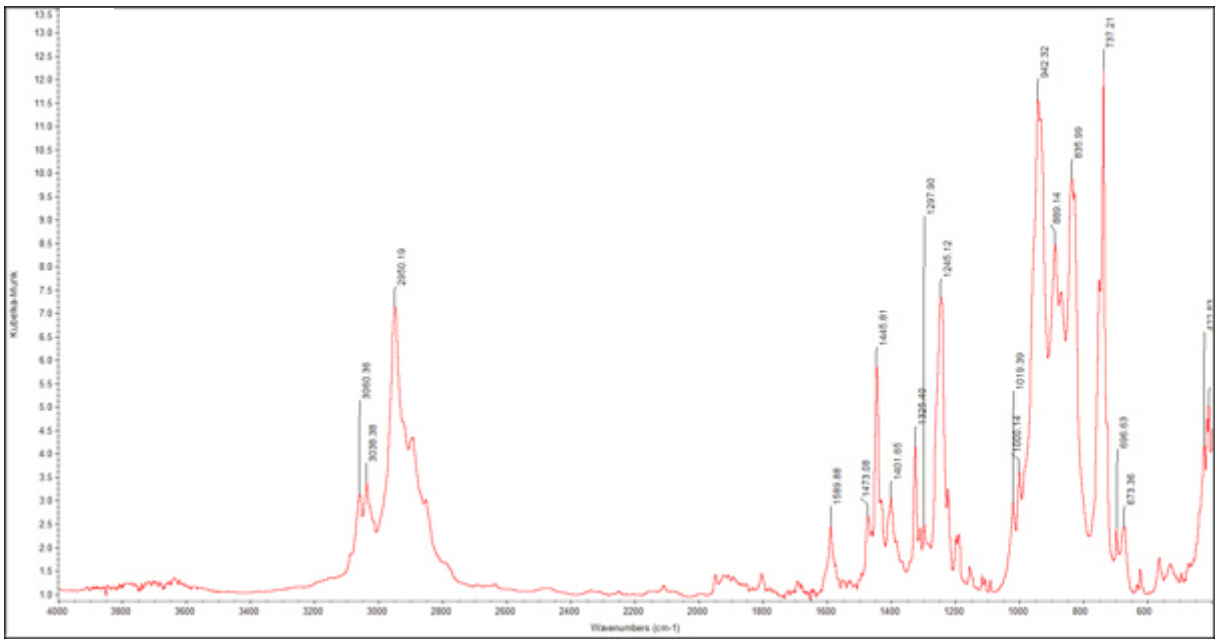

Figure S30. DRIFT spectrum of FluCe(OSiMe$_3$)$_2$(THF) (**3^{OSiMe3}**).

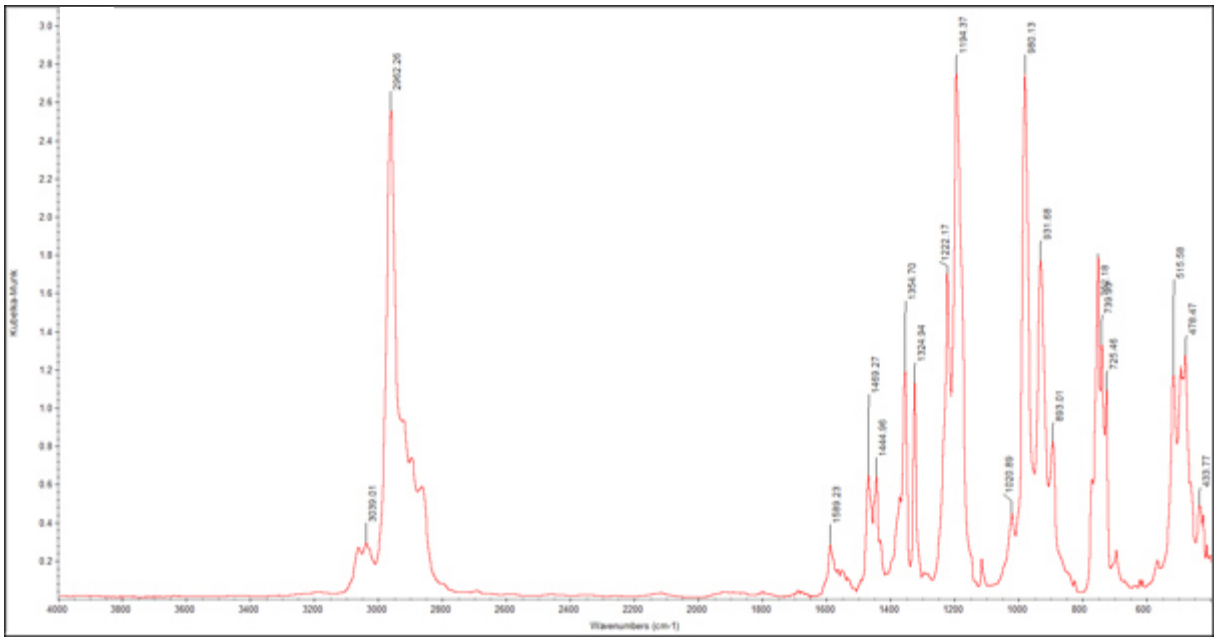

Figure S31. DRIFT spectrum of FluCe(O*t*Bu)$_2$(THF) (**3$^{O\mathit{t}Bu}$**).

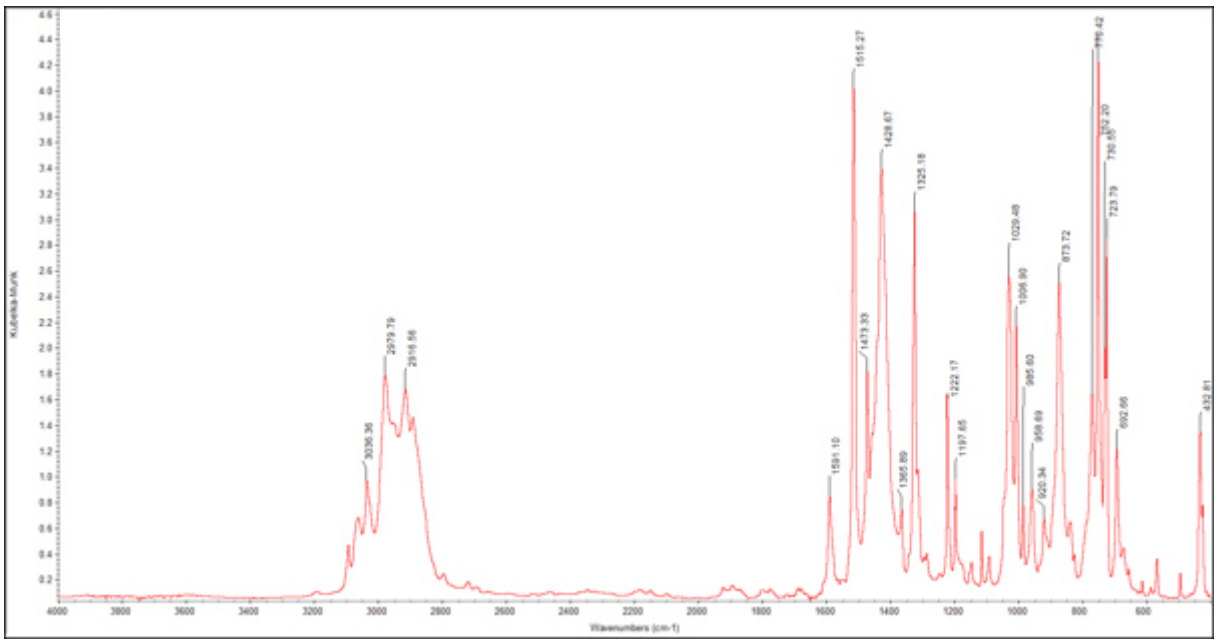

Figure S32. DRIFT spectrum of FluCe(Pz)$_2$(THF)$_2$ (**3^{Pz}**).

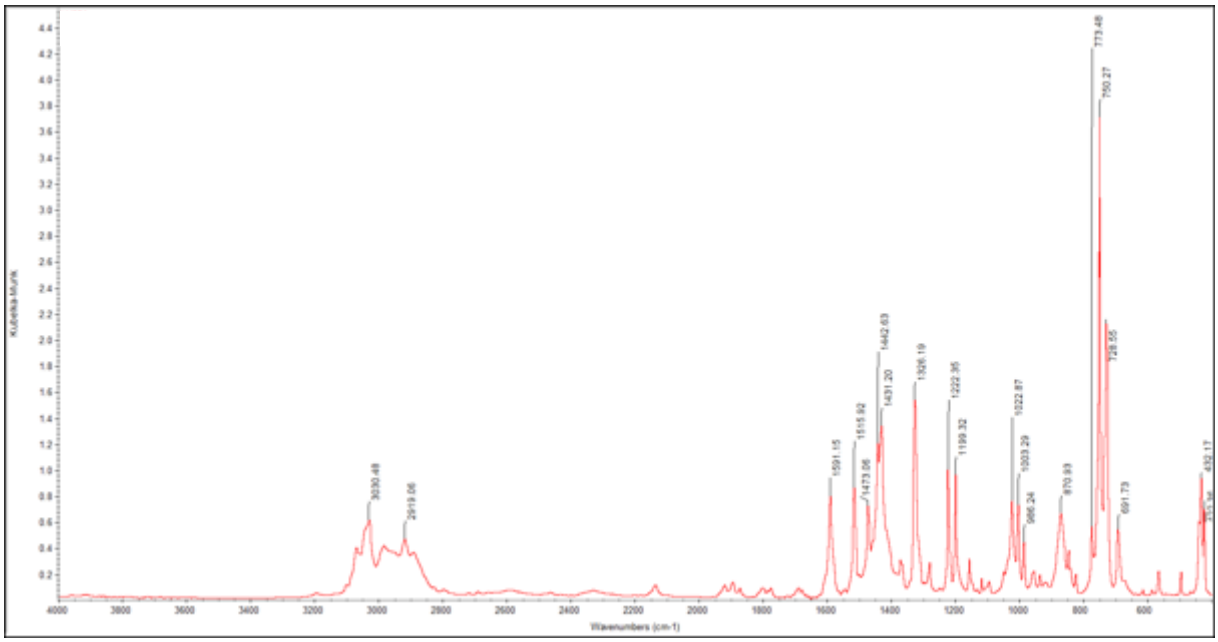

Figure S33. DRIFT spectrum of $Flu_2Ce(Pz)(THF)$ (**4^{Pz}**).

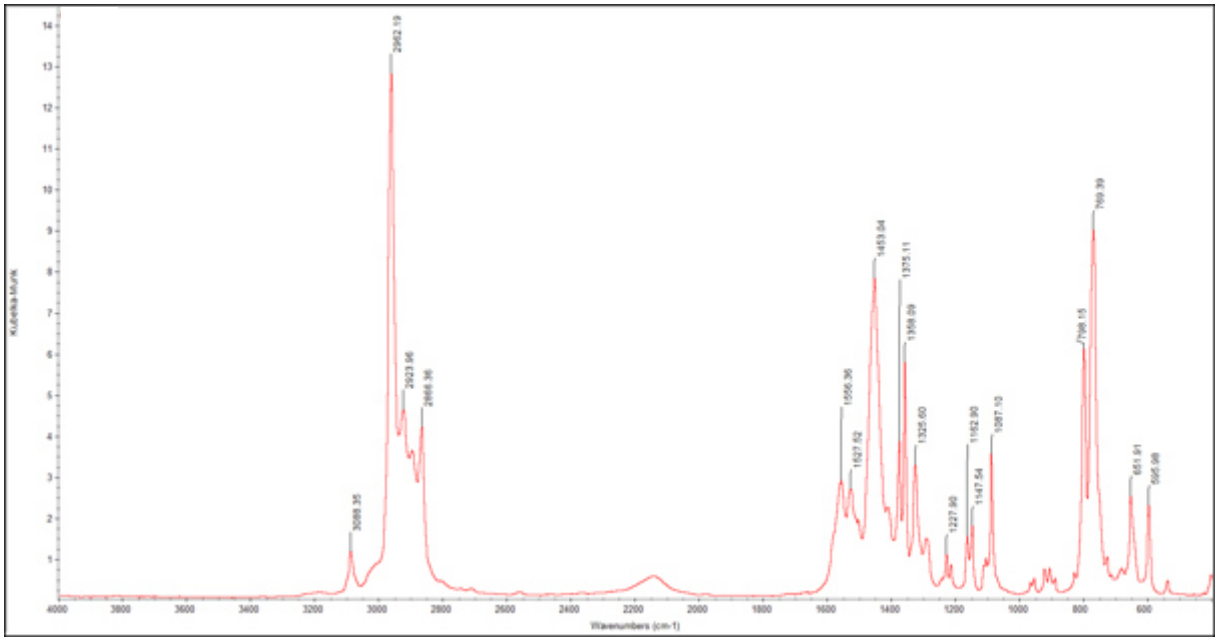

Figure S34. DRIFT spectrum of $Ce(dipp)_3$ (**6**).

Paper II

Pentamethylcyclopentadienyl Complexes of Cerium(IV) – Synthesis, Reactivity, and Electrochemistry

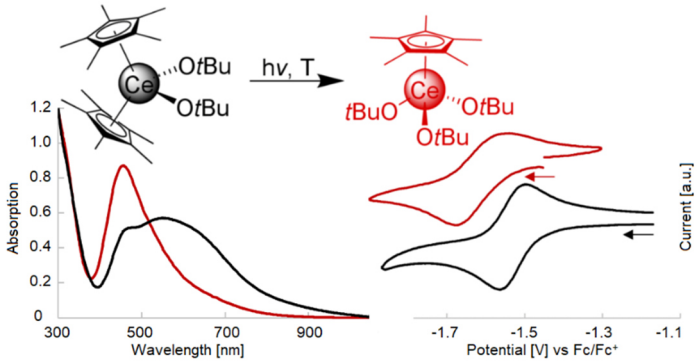

Accepted for publication
reprinted with permission from Inorganic Chemistry, **2021**

PENTAMETHYLCYCLOPENTADIENYL COMPLEXES of CERIUM(IV): SYNTHESIS, REACTIVITY, and ELECTROCHEMISTRY

Lars Hirneise, Cäcilia Maichle-Mössmer, and Reiner Anwander*

*Institut für Anorganische Chemie, Eberhard Karls Universität Tübingen, Auf der Morgenstelle 18, 72076 Tübingen, Germany

KEYWORDS cerium(IV); alkoxy; siloxy; pentamethylcyclopentadienyl; cyclic voltammetry

ABSTRACT: Treatment of $Cp^*_2CeCl_2K(THF)$ with alkali-metal alkoxides and siloxides in the presence of hexachloroethane generates the monomeric bis(pentamethylcyclopentadienyl) (Cp*) cerium(IV) complexes $Cp^*_2Ce(OR)_2$ ($Cp^* = C_5Me_5$; R = Et, *i*Pr, CH_2tBu, *t*Bu, $SiMe_3$, $SiPh_3$). Large substituents R trigger ligand scrambling to half-sandwich complexes $Cp^*Ce(OR)_3$, which could be isolated for R = *t*Bu and $SiPh_3$. Similar reactions with sodium aryloxide NaOAr (OAr = OC_6H_3iPr$_2$-2,6) lead to $Cp^*_2Ce(OAr)Cl$. Treatment of tris(cyclopentadienyl) complexes Cp^R_3CeCl (Cp^H = Cp = C_5H_5, $Cp^{Me} = C_5H_4Me$) with NaOAr afford $Cp^{Me}_2Ce(OAr)_2$ and $Cp_3Ce(OAr)$, respectively. The cerium(IV) complexes display a pseudo-tetrahedral geometry in the solid state. Cyclic voltammetry revealed mostly chemical reversible as well as electrochemically quasi-reversible redox processes with potentials ranging from −0.84 to −1.61 V vs Fc/Fc^+. Switching from sandwich to half-sandwich complexes decreased the electrochemical potentials drastically, showing better stabilization of the cerium(IV) center in the case of $Cp^*Ce(OR)_3$ in contrast to $Cp^*_2Ce(OR)_2$. Enhanced stabilization of the cerium +IV oxidation state could be further demonstrated in the series alkoxy > siloxy > aryloxy as well as $C_5Me_5 > C_5HMe_4$.

INTRODUCTION

Cyclopentadienyl ligands have played a key role in the development of organorare-earth chemistry, including that of the most abundant and redox-active element cerium.[1-3] The first cerium cyclopentadienyl compounds were described in 1956 presenting the synthesis of ornage-yellow tris(cyclopentadienyl) complex Cp_3Ce (Cp = C_5H_5).[4] Utilization of the pentamethylcylopentadienyl (Cp*) ligand was reported 19 years later leading to the isolation of mixed Cp*/halogenido cerium(III) ate complexes $Cp^*_2CeCl_2K(THF)_2$ and $[Cp^*_2CeI_2][K(THF)_2]$ and monomeric half-sandwich compounds like $Cp^*CeI_2(THF)_3$.[5-9] In contrast to the smaller parent Cp ligand, the homoleptic complex $[Cp^*_3Ce]$ could not be accessed in such salt-metathesis reactions, which instead resulted in mixed ligand species. However, the latter could be utilized in consecutive salt-metathesis reactions to afford, e.g., the alkyl complex $Cp^*_2Ce[CH(SiMe_3)_2]$.[10,11] In particular, $Cp^*_2Ce[CH(SiMe_3)_2]$ has later been shown to engage in C–H-bond activation, cyclodimerization and oligomerization of alkynes as well the formation of propargyl/allenyl complexes.[12-16] Application of a salt-metathesis sequence with cerium aryloxide instead of halides led to the half-sandwich complex $Cp^*Ce(OC_6H_3t$Bu$_2$-2,6$)_2$.[17] Another mixed alkoxy/Cp* complex was obtained in 1989 by protonolysis of $Cp^*_2Ce[CH(SiMe_3)_2]$ with *t*BuOH, accomplishing dimeric $[Cp^*Ce(Ot$Bu$)_2]_2$ via loss of a Cp* ligand.[18] Teuben et al. reported also on the first cationic cerocene(III) species, $[Cp^*_2Ce(Do)_2][BPh_4]$ (Do = THF, tetrahydrothiophene).[19] Later on, Evans *et al*. employed such ion pairs for the synthesis of long sought after Cp^*_3Ce. Homoleptic Cp^*_3Ce was shown to be highly reactive toward small molecules including H_2, CO, ethylene and THF,[20-21] but also allowed for additional nitrile and isocyanide donor (Do) coordination in $Cp^*_3Ce(Do)_2$.[22] The reaction of $[Cp^*_2Ce][BPh_4]$ with KC_8 and N_2 inTHF led to the first dinitrogen complexes of cerium, $[Cp^*_2Ce(THF)]_2(\mu\text{-}\eta^2\text{:}\eta^2\text{-}N_2)$, along with oxidized side-product $(Cp^*_2Ce)_2(\mu\text{-}O)$.[23] More recently, the thermally induced conversion of a series of amide complexes $Cp^*_2Ce(NR'R''_2)$ (e.g., R' = $SiMe_3$, R'' = $CHMe_2$) into enamides was reported.[24] Our group elaborated on the synthesis of amide and acetylide complexes from $Cp^*_2CeCl_2K(THF)_2$ via salt metathesis,[25] affording complexes $Cp^*_2Ce[N(SiHMe_2)_2]$ and $Cp^*_2Ce(C{\equiv}Ct$Bu$)_2$Li(THF). The latter ate complex did not form a stable cerium(IV) oxidation product.[25] In 2017, carbonato derivative $[Cp^*_2Ce]_2(\mu\text{-}CO_3)$ was obtained by treatment of both $[Cp^*_2Ce(\mu\text{-}H)]_2$ and $[Cp^*_2Ce]_2(\mu\text{-}O)$ with CO_2, reiterating the stability of the "Cp^*_2Ce" fragment.[26] Mixed cerous cyclopentadienyl/alkoxy complexes of the type $Cp^R_2Ce(OR')_2$ include $[(C_5H_3t$Bu$_2)_2Ce(OMe)]_2$ as well $[(C_5H_4t$Bu$)_2Ce(Oi$Pr$)]_2$.[27,28] Related bis(cyclopentadienyl) cerium(IV) complexes comprise trimeric oxy derivative $[(C_5H_4SiMe_3)_2Ce(O)]_3$,[29] as well as *tert*-butoxides $[C_5H_3(SiMe_3)_2]_2Ce(OtBu)_2$,[30] $[C_5H_4(SiMe_3)]_2Ce(Ot$Bu$)_2$,[30] and $Cp_2Ce(Ot$Bu$)_2$,[31] resulting from reactions with ceric ammonium nitrate as the key precursor.[32-35]

As shown above, many cerium(III) complexes bearing Cp* ligands are known in literature. However, it is striking that there are no reports on ceric complexes bearing the

Cp* ligand, although other substituted cyclopentadienyl ligands form stable Ce(IV) complexes. In fact, the increasingly electron-donating character of the Cp* ligand should theoretically better stabilize the cerium(IV) center with respect to reduction.[36] Such alleged stabilization is most likely counteracted by sterics or not yet achieved due to unfavored reaction protocols. Herein we report the first cerium(IV)-Cp* complexes, exploiting the oxidation of ate complex $Cp^*_2CeCl_2K(THF)$ in the presence of the chlorinating agent C_2Cl_6 and the stabilizing effect of alkoxy ligands. The oxidation has so far proven difficult with established oxidation agents in cerium(IV) chemistry.[25]

RESULTS AND DISCUSSION

Cerium(III) Precursor Selection. Given previous successful cerium(III) ate complex redox transformations,[35,37] the easily obtainable cerous derivative $Cp^*_2CeCl_2K(THF)$ (**1***) was considered a potential redox precursor.[5,9] We also targeted the respective cerium(III) complex derived for the slightly less bulky cyclopentadienyl ligand Cp^{tet} (C_5Me_4H). Accordingly, the bright pink $[Cp^{tet}_2CeCl_2Li(THF)_2]_2$ (**1**^{tet}) could be obtained by salt-metathesis reaction in 58% crystalline yield (Scheme 1). Using the potassium or sodium salt of HCp^{tet} instead of $LiCp^{tet}$ led to $Cp^{tet}_3Ce(THF)$ exclusively, which was closer investigated by Schumann et al. and Evans *et al.*[23,38] Initial oxidation attempts of **1**^{tet} and **1*** aiming at putative tetravalent complexes $[Cp^{tet}_2CeCl_2]$ or $[Cp^*_2CeCl_2]$, respectively, using common oxidants like C_2Cl_6 and $TeBr_4$ failed,[35] only leading to ligand scrambling and decomposition. This may be either due to steric mismatch, insufficient stabilization of the +IV state by the weakly stabilizing chlorido ligand or availability of a favored redox-induced decomposition pathway.

As reported previously for sterically crowded pentamethylcyclopentadienyl complexes of samarium and uranium the oxidative dimerization of Cp* to form decamethyl-1,1'-dihydrofulvalene was observed as a side product, concomitantly with the cerium center undergoing a sterically induced reduction.[20,39-41]

Scheme 1. Synthesis of $[Cp^{tet}_2CeCl_2Li(THF)_2]_2$ (1^{tet})[a]

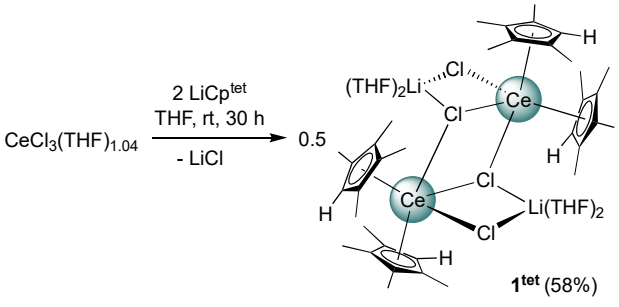

[a] $Cp^{tet} = C_5HMe_4$

Figure 1 shows the molecular representation of the dimeric solid-state structure of **1**^{tet}, with the two $Cp^{tet}_2CeCl_2Li(THF)_2$ subunits being isostructural to **1*** and $Cp^*_2CeCl_2Li(OEt_2)_2$. Bridging halogenido ligands as well as the formation of dimeric structures and ate complexes to accomplish steric saturation are not unusual in cerium(III) chemistry, although the combination of all three factors is rare.[12,25] Overall, the average Ce–Cp distances are barely longer (0.03 Å) for the Cp* derivative, but the Cl–Ce–Cl angle is much wider accounting to 81.67(1)° compared to 72.88(3)° for **1**^{tet} (Table 6).[5] This is accompanied by slightly longer Ce–Cl distances for **1**^{tet}.

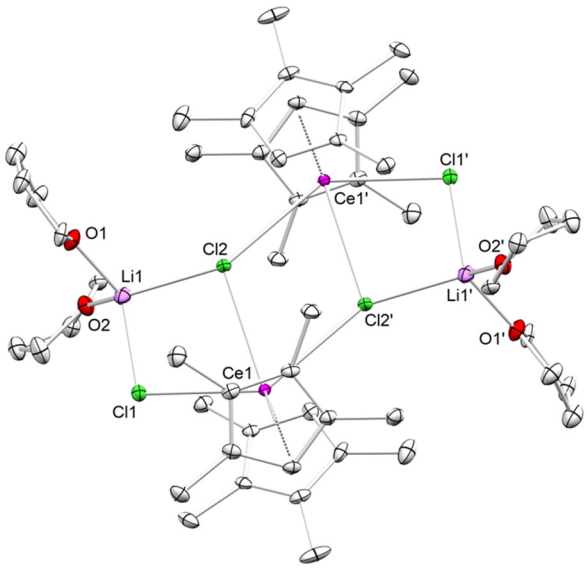

Figure 1. Crystal structure of $[Cp^{tet}_2CeCl_2Li(THF)_2]_2$ (**1**^{tet}), with atomic displacement ellipsoids set at the 30% probability level. Hydrogen atoms are omitted for clarity. Selected interatomic distances and angles are listed in Table 6.

The redox behavior of the cerocene ate complexes in hand was further investigated using cyclic voltammetry. Both **1*** and **1**^{tet} show irreversible cyclic voltammograms, bearing four oxidation signals for **1*** and two for **1**^{tet}, but little to none reduction signals (Figures S23 and S26, Supporting Information). The respective first oxidation steps are shown in Figure 2, revealing close potentials of –0.54 V vs Fc/Fc^+ for **1**^{tet} and –0.57 V vs Fc/Fc^+ at 50 mV/s for **1***. The oxidation potentials of both compounds shift for varying scan rates, but this behavior is more pronounced for **1***. The electrochemical data of **1**^{tet} (Table 1) show a slight shift of the oxidation peak as well as the presence of a small reduction signal for faster scan rates. At 2.5 V/s the peak current ratio i_{pa}/i_{pc} of 0.51 indicates that few of the oxidized compound gets electrochemically reduced as well.

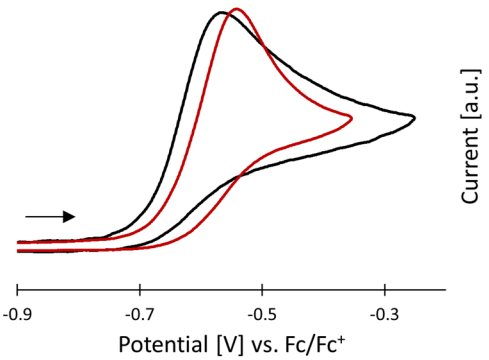

Figure 2. Cyclic voltammograms of the cerium(III/IV) redox couples of $Cp^*_2CeCl_2K(THF)$ (**1***, black) and $[Cp^{tet}_2CeCl_2Li(THF)_2]_2$ (**1**^{tet}, red) vs Fc/Fc^+ in THF at GC obtained at a scan rate of 50 mV/s; arrow indicates scan direction; c(analyte) 1 mM, c(electrolyte) 0.1 M $[nPr_4N][B(C_6H_3(CF_3)_2\text{-}3,5)_4]$.

Table 1. Electrochemical Data for the Cerium(III/IV) Couple of 1^{tet} vs Fc/Fc^+ in THF

ν (mV/s)	E_{pa} (V)	E_{pc} (V)	E^0 (V)	ΔE_p (V)	i_{pc}/i_{pa}
50	−0.542	−*	−*	−*	−*
100	−0.534	−*	−*	−*	−*
250	−0.531	−*	−*	−*	−*
500	−0.521	−*	−*	−*	−*
1000	−0.516	−0.641	−0.516	0.125	0.42
2000	−0.509	−0.612	−0.509	0.103	0.49
2500	−0.511	−0.601	−0.511	0.090	0.51

*could not be determined

The irreversibility of the redox step as well as the presence of several other oxidation steps indicate further reactivity upon oxidation, which was also observed for the chemical oxidation. Although both oxidation signals lie in the same range, it appears that for small scan rates the Cp* ligand adds more stability to the cerium(IV) oxidation state than Cp^{tet}, possibly linked to its stronger electron donating capability. A more stable cerium(IV) species is generated *in situ*. Compared to the oxidation potentials of $Cp_3Ce(THF)$ at −0.27 V vs Fc/Fc^+ and $Cp^{Me}{}_3Ce(THF)$ at −0.38 V vs Fc/Fc^+ both potentials are more negative, thus revealing an easier oxidizability of **1*** and $\mathbf{1}^{tet}$.[36] The stability of the formed cerium(IV) complex is reversed as **1*** and $\mathbf{1}^{tet}$ feature electrochemical irreversibility and follow-up reactivity, whereas $Cp^{H/Me}{}_3Ce(THF)$ show chemical reversibility concluding that a more stable cerium(IV) species is generated *in situ*.

Cerium(IV) Alkoxide and Siloxide Complexes. Because of the irreversibility of the direct oxidation of dichlorido ate complexes **1*** and $\mathbf{1}^{tet}$, initial "ate" modification and subsequent oxidation was pursued as an alternative approach to access stable cerium(IV) compounds. As shown previously the salt-metathetical exchange of the chlorido ligands by amido and other nitrogen-based monoanionic ligands led to the formation of alkali metal-free complexes of the type $Cp^*{}_2CeR$.[11,24-25] Since oxidation attempts of these latter complexes failed so far, we envisaged oxygen-based entities like alkoxy, siloxy and aryloxy ligands to be more suitable offering the advantages of less steric bulk and enhanced Ce(IV) stabilization through the Ce–O bonds. However, when removing the metathesis salt after the reaction of **1*** with MOR or when using purified starting materials like $Cp^*{}_2Ce(C_3H_5)(THF)$[20,42] the subsequent oxidation failed. Much to our delight, treatment of dichlorido ate complexes **1*** with both reagents (MOR and oxidant) *in situ* brought about the long sought after result of cerium(IV) Cp* complexes.

The general reaction pattern involves the initial treatment of **1*** with two equivalents of a sodium or potassium salt of the oxygen-based ligand for 10 minutes. Then, the reaction mixture is oxidized using half of an equivalent of hexachloroethane until **1*** is fully depleted, as indicated by color. This one-pot reaction works for a variety of alkoxy and siloxy ligands, resulting in the respective complexes $Cp^*{}_2Ce(OR)_2$ ($\mathbf{2}^{R}$) and $Cp^*{}_2Ce(OSiR_3)_2$ ($\mathbf{4}^{R}$) (Scheme 2). The heteroleptic cerium(IV) complexes show dark blue to violet colors as well as display very good solubility even in *n*-pentane and tetramethylsilane. The extreme solubility in combination with the formation of a slurry upon solvent removal made purification challenging. Such behavior has also been known for similar compounds like $[Cp^*Ce(O\mathit{t}Bu)_2]_2$, which was reportedly cumbersome to crystallize with low yields due to good solubility in hydrocarbon solvents.[18]

Scheme 2. Reaction Pathway to Ceric Sandwich Complexes 2 and 4 Employing Cerous 1*, and Decomposition to Ceric Half-sandwich Complexes 3 and 5

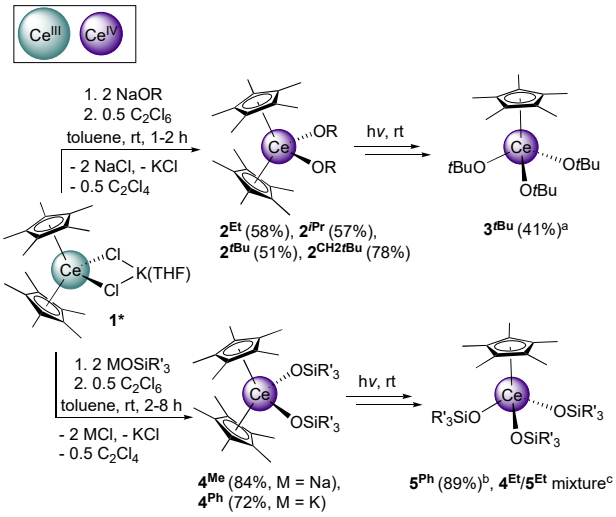

[a] Yield for direct formation from **1*** without pre-isolation of $\mathbf{2}^{tBu}$.

[b] Yield for direct formation from **1*** and 3 equivalents of $KOSiPh_3$, without pre-isolation of $\mathbf{4}^{Ph}$.

[c] Reaction time of 2 h: 32% $\mathbf{4}^{Et}$ and 68% $\mathbf{5}^{Et}$ (yield by ^1H NMR).

Some of the reported compounds (vide infra) are very sensitive toward light and heat (even at ambient temperature) showing decomposition in hours to days. Such decomposition yields the first ceric half-sandwich complexes of the type $Cp^*Ce(OR)_3$, as observed for $Cp^*Ce(OEt)_3$ ($\mathbf{3}^{Et}$) via NMR spectroscopy and isolable for $Cp^*Ce(O\mathit{t}Bu)_3$ ($\mathbf{3}^{tBu}$) and $Cp^*Ce(OSiPh_3)_3$ ($\mathbf{5}^{Ph}$). Accordingly, sterically demanding ligands favor rapid decomposition and the formation of comparatively stable half-sandwich complexes. It is proposed that the respective ate complexes bearing the oxygen-based ligands are formed *in situ*, and then get directly oxidized by C_2Cl_6, driven by concomitant alkali-metal chloride elimination. Using excess of alkali-metal salts NaOR or MOSiR'$_3$ (M = Na, K) diminishes the yields of $\mathbf{2}^{R}$ and $\mathbf{3}^{R}$, as more of the side products are formed, including homoleptic $Ce(OR)_3$ /$Ce(OSiR'_3)_3$ or dinuclear $[Cp^*Ce(OR)_2]_2$ /$[Cp^*Ce(OSiR'_3)_2]_2$. Such reaction pathways also apply in the case of ligand scrambling and/or decomposition.

More precisely , the reactions described in Scheme 2 lead to the alkoxy complexes $Cp^*{}_2Ce(OEt)_2$ ($\mathbf{2}^{Et}$), $Cp^*{}_2Ce(O\mathit{i}Pr)_2$ ($\mathbf{2}^{iPr}$), $Cp^*{}_2Ce(OCH_2\mathit{t}Bu)_2$ ($\mathbf{2}^{CH2tBu}$), and $Cp^*{}_2Ce(O\mathit{t}Bu)_2$ ($\mathbf{2}^{tBu}$), as well as $Cp^*{}_2Ce(OSiMe_3)_2$ ($\mathbf{4}^{Me}$) and $Cp^*{}_2Ce(OSiPh_3)_2$ ($\mathbf{4}^{Ph}$) when applying siloxy ligands. The reaction of **1*** with alkali-metal (Li, Na) methoxide occurred by color, but any substantial amount of identifiable product could not be obtained. The smaller sized ligands OEt, O*i*Pr, and $OSiMe_3$ ligands afford complexes that are stable at ambient temperature and under visible light, whereas more sterically demanding ligands like O*t*Bu, $OSiEt_3$ and $OSiPh_3$ lead to fast ligand scrambling toward $Cp^*Ce(O\mathit{t}Bu)_3$ ($\mathbf{3}^{tBu}$), $Cp^*Ce(OSiEt_3)_3$ ($\mathbf{5}^{Et}$), and $Cp^*Ce(OSiPh_3)_3$ ($\mathbf{5}^{Ph}$). The choice of alkali metal influences the reactivity as NaO*t*Bu gave $\mathbf{3}^{tBu}$ directly

whereas with KO*t*Bu the intermediate **2**$^{t\mathrm{Bu}}$ lasts longer and can be isolated more easily. ^{1}H NMR spectroscopy is a useful tool to assign alkoxy ligands in close proximity to a cerium(IV) center.[36] Accordingly, diamagnetically sharp signals and downfield shifted protons in α position of the alkoxy ligands (Ce–O–C*H*) to 5.31 (**2**$^{\mathrm{Et}}$), 5.48 (**2**$^{\mathrm{CH2}t\mathrm{Bu}}$), and 5.73 (**2**$^{i\mathrm{Pr}}$) ppm are in accordance with literature data.[36]

The transformation of **2**$^{t\mathrm{Bu}}$ to **3**$^{t\mathrm{Bu}}$ took place in the reaction mixture parallel to the intended reaction making purification problematic. The ligand $OSiEt_3$ led to a product mixture of $Cp^*_2Ce(OSiEt_3)_2$ (**4**$^{\mathrm{Et}}$) and $Cp^*Ce(OSiEt_3)_3$ (**5**$^{\mathrm{Et}}$) in variable ratios, depending on the reaction conditions applied (longer reaction times at ambient temperature increased the ratio of **5**$^{\mathrm{Et}}$: **4**$^{\mathrm{Et}}$). The triethylsiloxy derivatives could not be isolated, but monitored via NMR (Figure S10 et seq.). Equally, longer reaction times at ambient temperature and storage above −40 °C can lead to a mixture of **4**$^{\mathrm{Ph}}$ and **5**$^{\mathrm{Ph}}$ (Figure S16). While the sandwich complex **4**$^{\mathrm{Ph}}$ could be isolated, this was burdensome in the case of **5**$^{\mathrm{Ph}}$, which was barely separable from **4**$^{\mathrm{Ph}}$ and other decomposition products. After purification and crystallization, decomposition at ambient temperature took place much slower (over one week for **4**$^{\mathrm{Ph}}$) and did no longer shift the sandwich/half-sandwich ratios, thus making full characterization of **2**$^{t\mathrm{Bu}}$ and **4**$^{\mathrm{Ph}}$ possible. Interestingly, the yield of **5**$^{\mathrm{Ph}}$ could be significantly increased to 89% when applying a mixture of **1*** and $KOSiPh_3$ in a 1:3 ratio.

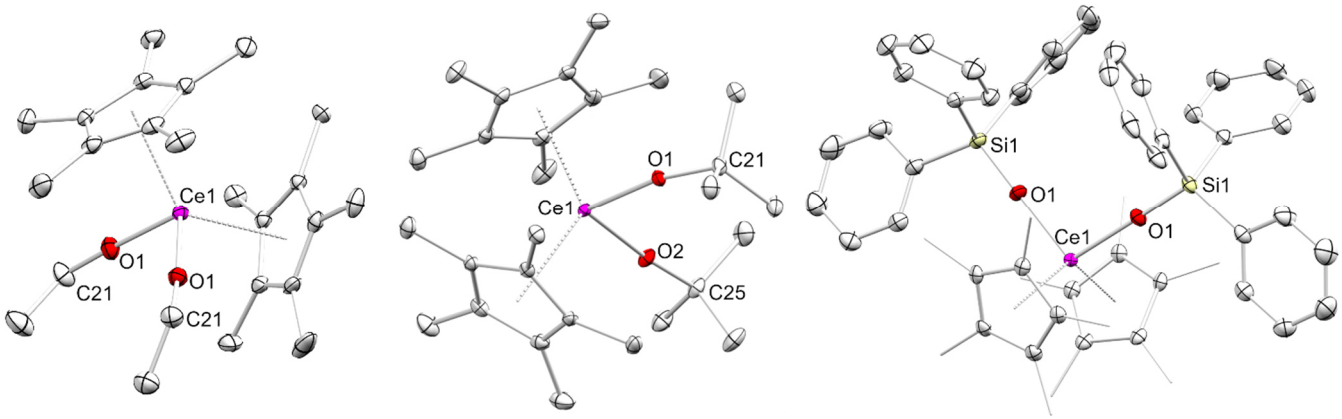

Figure 3. Crystal structures of $Cp^*_2Ce(OEt)_2$ (**2**$^{\mathrm{Et}}$, left), $Cp^*_2Ce(O\mathit{t}Bu)_2$ (**2**$^{t\mathrm{Bu}}$, middle), and $Cp^*_2Ce(OSiPh_3)_2$ (**4**$^{\mathrm{Ph}}$, right), with atomic displacement ellipsoids set at the 30% probability level. Hydrogen atoms are omitted for clarity. Selected interatomic distances and angles are listed in Table 6.

Trivalent compound $[Cp^*Ce(OtBu)_2]_2$ could be detected as decomposition product in the case of **2**$^{t\mathrm{Bu}}$ and **3**$^{t\mathrm{Bu}}$, and also analyzed by X-ray diffraction (XRD), corroborating the presence of redox-decomposition pathways.[18] The dimeric cerium(III) complex has first been synthesized via reaction of $Cp^*_2Ce[CH(SiMe_3)_2]$ with *t*BuOH, providing another example of the loss of a Cp* ligand in exchange for an alkoxy ligand.[18] As this follow-up reaction occurred in the reaction mixture before extraction with $SiMe_4$ and crystallization, the presence of other reactants seems to trigger the formation of trivalent $[Cp^*Ce(O\mathit{t}Bu)_2]_2$.

The solid-state structures of **2**$^{\mathrm{Et}}$, **2**$^{t\mathrm{Bu}}$, and **4**$^{\mathrm{Ph}}$ are depicted in Figure 3, showing similar pseudo tetrahedral structural motifs with two Cp* ligands in a bent sandwich arrangement and two adjacent alkoxy/siloxy ligands. The higher steric demand of the *t*Bu substituents in **2**$^{t\mathrm{Bu}}$ involve slightly larger Ce–O and Ce–Cp* distances than in **2**$^{\mathrm{Et}}$ (Table 6). Unsurprisingly, the Ce–O bond in **4**$^{\mathrm{Ph}}$ is elongated compared to those in **2**$^{\mathrm{Et}}$ and **2**$^{t\mathrm{Bu}}$, while the Ce–Cp* distances are in the same range as are the Cp*–Ce–Cp* angles. The overall structural motif of these first cerium(IV)–Cp* derivatives is similar to the ones of **1*** and **1**$^{\mathrm{tet}}$ discussed above and of the cerium(III) ate complexes $[Na(18\text{-crown-}6)(thf)_2]^+[Cp^*_2Ce(S(\mathit{i}Pr))_2]^-$ as well as the dimeric cerous $[Cp^*_2CeH]_2$, $[Cp^*Ce(O\mathit{t}Bu)_2]_2$, and $[Cp^*_2Ce(SPh)]_2$.[18,26,43] Most relevant, isostructural complexes were also found in the presence of other bulky cyclopentadienyls such as in complexes $[C_5H_3(SiMe_3)_2]_2Ce(O\mathit{t}Bu)_2$ and $[C_5H_4(SiMe_3)]_2Ce(O\mathit{t}Bu)_2$ derived from ceric ammonium nitrate (CAN) as the precursor.[30] The terminal Ce–O distance of $[Cp^*Ce(O\mathit{t}Bu)_2]_2$ is slightly elongated (2.116(6) Å) compared to **2**$^{t\mathrm{Bu}}$ (2.1024(14) and 2.0868(14) Å) as it is expected for the contraction of the metal ion with increasing nuclear charge. Compared to $[C_5H_3(SiMe_3)_2]_2Ce(O\mathit{t}Bu)_2$, **2**$^{t\mathrm{Bu}}$ shows slightly elongated distances to the Cp and O*t*Bu ligands as well as a more acute O–Ce–O angle, reflecting the changed steric and electronic properties of the cyclopentadienyl ligands.[30] The prevalence of the bent sandwich structural motif in both oxidation states point to its stability, while the follow-up reactivity of the ceric derivatives, in particular for the larger alkoxy ligands, documents enhanced steric pressure at the smaller cerium(IV).

Electrochemical experiments were performed on all isolated compounds to assess the stabilization of the cerium(IV) oxidation state. All potentials are referenced vs the Fc/Fc^+ redox couple. The cyclic voltammograms and key data of **2**$^{\mathrm{Et}}$ and **4**$^{\mathrm{Me}}$ (Figure 4, Table 2) show chemically reversible redox processes featuring a (quasi-)reversible one-electron transfer step. The peak separation of 72/63 mV is close to the ideal limit of 58 mV for electrochemically reversible one-electron redox steps at slow scan rates, and increasing for fast scan rates. This indicates quasi-reversibility at higher *v* or insufficient compensation of the *iR* drop. The peak current ratio i_{pa}/i_{pc} is close to one, demonstrating chemical reversibility as almost all substrate gets re-oxidized at the reverse sweep. The analysis of the peak current as function of the square root of the scan rate leads to a fit of $R^2 > 0.998$ (**2**$^{\mathrm{Et}}$) and $R^2 > 0.999$ (**4**$^{\mathrm{Me}}$), indicative of a diffusion controlled redox-step. Thus, the formal potential E^0 can be derived as the mid-point potential in the respective cyclic voltammograms and is evidently independent of the scan rate. Similarly, this is the case for **2**$^{\mathrm{Et}}$, **2**$^{i\mathrm{Pr}}$, **2**$^{\mathrm{CH2}t\mathrm{Bu}}$, **2**$^{t\mathrm{Bu}}$, and **4**$^{\mathrm{Me}}$. The respective formal potentials range from −1.52 (**2**$^{\mathrm{CH2}t\mathrm{Bu}}$) to −1.56 (**2**$^{\mathrm{Et}}$) V vs Fc/Fc^+ for the alkoxy complexes, thus differing only marginally.

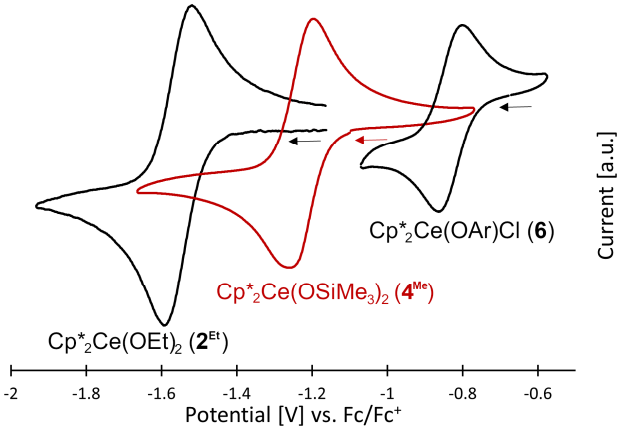

Figure 4. Cyclic voltammograms of the cerium(III/IV) redox couples of $Cp^*_2Ce(OEt)_2$ (**2**^{Et}), $Cp^*_2Ce(OSiMe_3)_2$ (**4**^{Me}), and $Cp^*_2Ce(OAr)_2$ (**6**) vs Fc/Fc^+ in THF at GC obtained at a scan rate of 50 mV/s (**2**^{Et}, **4**^{Me}) and 250 mV/s (**6**); arrow indicates scan direction; c(analyte) 1 mM, c(electrolyte) 0.1 M $[n\mathrm{Pr}_4\mathrm{N}][\mathrm{B}(\mathrm{C}_6\mathrm{H}_3(\mathrm{CF}_3)_2\text{-}3,5)_4]$.

Table 2. Electrochemical Data for the Cerium(III/IV) Couples of 2^{Et} and 4^{Me} vs Fc/Fc$^+$ in THF

ν [mV/s]	E_{pa} (V)	E_{pc} (V)	E^0 (V)	ΔE_p (V)	i_{pa}/i_{pc}
2^{Et}					
50	−1.519	−1.591	−1.555	0.072	0.92
100	−1.517	−1.600	−1.559	0.083	0.94
250	−1.507	−1.605	−1.556	0.098	0.96
500	−1.499	−1.615	−1.557	0.116	0.97
1000	−1.487	−1.621	−1.554	0.134	0.98
2000	−1.475	−1.637	−1.556	0.162	1.00
4^{Me}					
50	−1.197	−1.260	−1.229	0.063	0.90
100	−1.193	−1.258	−1.226	0.065	0.98
250	−1.186	−1.261	−1.224	0.075	0.98
500	−1.181	−1.263	−1.222	0.082	0.98
1000	−1.177	−1.268	−1.223	0.091	0.97
2000	−1.169	−1.277	−1.223	0.108	0.97

With the exception of **2**^{CH2tBu} the potentials tend to be more negative for smaller substituents and higher pK_a values of the corresponding alcohols. The siloxy complex **4**^{Me} shows a less negative potential of −1.23 V vs Fc/Fc^+, hence showcasing the lower stabilization of the cerium(IV) center by siloxy in contrast to alkoxy ligands. The potential of **4**^{Me} is comparable to Cp^{Me}_3CeOR (R = *i*Pr / CH_2tBu) with values of −1.24 / −1.22 V vs Fc/Fc^+.[36]

The ligand scrambling of **2**^{tBu} to **3**^{tBu} (Scheme 2) was also examined by electrochemical methods revealing a shift in the cyclic voltammograms to more negative potentials for the half-sandwich complex (Figure 5). The change of the potential is accompanied by a change of the electrochemical data (Table 3). While **2**^{tBu} shows chemical as well as electrochemical reversibility, the **3**^{tBu} behaves differently. Most importantly, the peak current ratios are far below one, indicating chemical irreversibility, caused by follow-up reactivity of EC type. For faster scan rates the ratios i_{pa}/i_{pc} increase, typical for chemical quasi-reversibility. The peak separation is also above the range of an electrochemical reversible one-electron process. Overall, the data suggest a follow-up reaction of the EC type for slow scan rates and a pseudo reversibility chemically as well as electrochemically for fast scan rates above 500 mV/s. Consequently, the formal potentials are determined as mid-point potentials at a rate of 2 V/s, when the follow-up reactions become insignificant. Nevertheless, the mid-point potentials show no scan-rate dependence whatsoever.

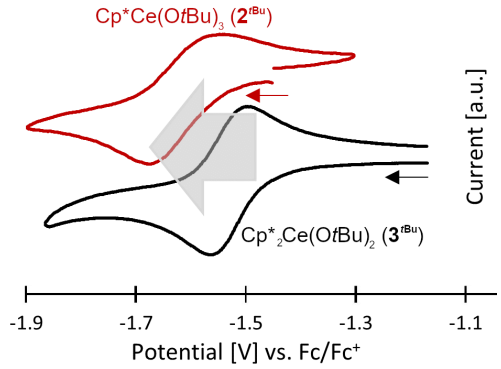

Figure 5. Cyclic voltammograms of the cerium(III/IV) redox couples $Cp^*_2Ce(Ot\mathrm{Bu})_2$ (**2**^{tBu}, black) and $Cp^*Ce(Ot\mathrm{Bu})_3$ (**3**^{tBu}, red) vs Fc/Fc+ in THF at GC obtained at a scan rate of 50 mV/s; arrow indicates scan direction; c(analyte) 1 mM, c(electrolyte) 0.1 M $[n\mathrm{Pr}_4\mathrm{N}][\mathrm{B}(\mathrm{C}_6\mathrm{H}_3(\mathrm{CF}_3)_2\text{-}3,5)_4]$.

Table 3. Electrochemical Data for the Cerium(III/IV) Couple of 3^{tBu} vs Fc/Fc$^+$ in THF

ν [mV/s]	E_{pa} (V)	E_{pc} (V)	E^0 (V)	ΔE_p (V)	i_{pa}/i_{pc}
50	−1.540	−1.677	−1.608	0.137	0.80
100	−1.524	−1.669	−1.596	0.145	0.84
250	−1.507	−1.700	−1.603	0.193	0.88
500	−1.480	−1.697	−1.588	0.217	0.90
1000	−1.458	−1.729	−1.593	0.271	0.92
2000	−1.452	−1.742	−1.597	0.290	0.95

Upon Cp*/O*t*Bu exchange the potential changed from −1.53 to −1.61 V vs Fc/Fc^+. Thus, substitution of one Cp* ligand via another O*t*Bu group leads to a better stabilization of the cerium(IV) oxidation state. Besides the stronger bond formed, the conversion also results in less steric encumbrance, which seems to be the deciding factor, as no such behavior was observed for smaller alkoxy ligands. Consequently, **3**^{tBu} is kinetically as well as thermodynamically more stable than **2**^{tBu}.

The trend toward separated redox signals is even more pronounced for the two coupled compounds **4**^{Ph} and **5**^{Ph} (Figure 6). Cp*/$OSiPh_3$ ligand exchange upon decomposition led to a wide separation of the reduction and oxidation events as well as a more negative reduction signal. This behavior was not totally unexpected as homoleptic siloxide complexes are known to feature widely separated signals.[44] In particular, $Ce[OSi(Ot\mathrm{Bu})_3]_4$ revealed redox-modulated molecular rearrangement processes, supposedly reflected in its large peak separation of 1.15 V and potentials of E_{pc} = −1.46 and E_{pa} = −0.31 V vs Fc/Fc^+ (Table 4).[44] Other measurements of $Ce[OSi(Ot\mathrm{Bu})_3]_4$ even showed separations of 1.53 V (E_{pc} = −1.72 / E_{pa} = −0.19 V vs Fc/Fc^+) with a comparable mid-point potential.[45] Ligand reorganization processes also could be involved in case of **5**^{Ph} even without side arm coordination.[45] The related tetravalent homoleptic complexes of $[Ce(OSiEt_3)_4]$ and $[Ce\{OSi(i\mathrm{Pr})_3\}_4]$ exhibit large peak separations of > 300 mV as well, with mid-point potentials of −1.19 / −1.30 V vs Fc/Fc^+.[46] Moreover,

the redox potentials of cerium(III) ate complex $KCe(OSiPh_3)_4(THF)_3$ (E_{pc} = −1.61 / E_{pa} = −0.58 V vs Fc/Fc^+) also show a large separation of 1.03 V at 50 mV/s.[47] Although wide peak separations make direct comparisons difficult, complex **5^{Ph}** seems to show better stabilization of the cerium(IV) state than the homoleptic siloxide complexes reported above.

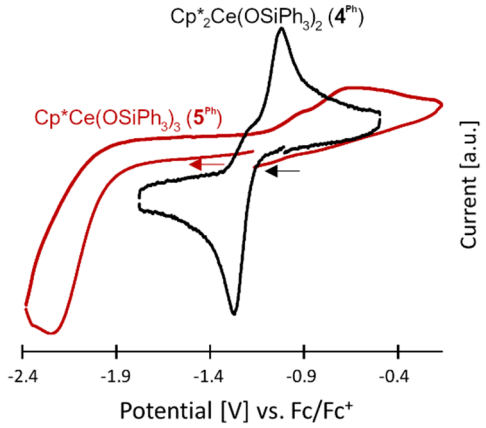

Figure 6. Cyclic voltammograms of the cerium(III/IV) redox couples of $Cp^*_2Ce(OSiPh_3)_2$ (**4^{Ph}**, black) and $Cp^*Ce(OSiPh_3)_3$ (**5^{Ph}**, red) vs Fc/Fc+ in THF at GC obtained at a scan rate of 50 mV/s; arrow indicates scan direction; c(analyte) 1 mM, c(electrolyte) 0.1 M $[nPr_4N][B(C_6H_3(CF_3)_2\text{-}3,5)_4]$.

Table 4. Electrochemical Data for the Cerium(III/IV) couple of 4^{Ph} and 5^{Ph} vs Fc/Fc^+ in THF

ν [mV/s]	E_{pa} (V)	E_{pc} (V)	E^0 (V)	ΔE_p (V)	i_{pa}/i_{pc}
4^{Ph}					
50	−1.010	−1.264	−1.137	0.254	0.95
100	−0.998	−1.266	−1.132	0.268	1.00
250	−0.993	−1.280	−1.136	0.287	0.98
500	−0.983	−1.288	−1.135	0.305	0.99
1000	−0.986	−1.298	−1.142	0.312	0.93
2000	−0.976	−1.309	−1.142	0.333	0.96
5^{Ph}					
50	−0.704	−2.186	−1.445	1.482	0.82
100	−0.668	−2.212	−1.440	1.544	0.81
250	−0.635	−2.245	−1.440	1.610	0.83
500	−0.603	−2.276	−1.439	1.673	0.83
1000	−0.559	−2.306	−1.432	1.747	0.84
2000	−0.587	−2.334	−1.460	1.747	0.86

The electrochemical data of **4^{Ph}** also revealed a relatively large peak separation of >254 mV (Table 4), indicating a electrochemical quasi-reversibility or irreversibility, but the peak current ratios are close to 1, signaling chemical reversibility. Diffusion control applies and the mid-point potentials display scan rate independence, suggesting chemical reversibility and electrochemical quasi-reversibility. The formal potentials are therefore derived as mid-point potentials. This is not easily possible for compound **5^{Ph}** which exhibits chemical irreversibility (i_{pa}/i_{pc} <0.9 even for high scan rates, Table 4) and widely separated signals around 1.5 V as well as scan rate dependent redox signals. The mid-point potentials between −1.43 and −1.46 V vs Fc/Fc^+ appear relatively stable, but are strongly shifted toward more negative potentials upon $Cp^*/OSiPh_3$ ligand exchange. This is in accordance with the similar results obtained for the conversion of **2^{tBu}** into **3^{tBu}**, but likewise to an even greater extent when considering the reduction signals (−1.26 (**4^{Ph}**) vs −2.19 (**5^{Ph}**)). Consequently, half-sandwich complexes of the type $Cp^*Ce(OR)_3$ seem to stabilize the cerium(IV) center better than their respective sandwich counter parts of the type $Cp^*_2Ce(OR)_2$, but show a wider separation of the oxidation and reduction signals.

The ligand scrambling observed for **2^{tBu}** and **4^{Ph}** ("sandwich/half-sandwich switch") goes with a strong change in color. The dark and ink blue **2^{tBu}** (556 nm (5472 ± 118 L mol^{-1} cm^{-1})) gets converted into the dark brown **3^{tBu}** (456 nm (4941 ± 110 L mol^{-1} cm^{-1})), as seen from the blueshift in the respective UV/Vis absorption spectra (Figure 7). Minor impurities of **3^{tBu}** lead to the respective shoulder in the spectrum of **2^{tBu}** and decomposition accompanied by a color change could be noticed within minutes when conducting the experiment. Likewise, the transformation of **4^{Ph}** to **5^{Ph}** resulted in a color change from dark blue (563 nm (714 ± 73 L mol^{-1} cm^{-1})) to violet (**5^{Ph}**: 521 nm (2597 ± 123 L mol^{-1} cm^{-1})) (Figure 8). Overall, the structural similarity of these complexes can be seen qualitatively in the UV/Vis spectra, with the exchange of Cp* for alkoxy/siloxy implying a blueshift in both cases. The substitution of O*t*Bu for $OSiPh_3$ results in redshifts of 7 nm (**2^{tBu}** versus **4^{Ph}**) and 65 nm (**3^{tBu}** versus **5^{Ph}**).

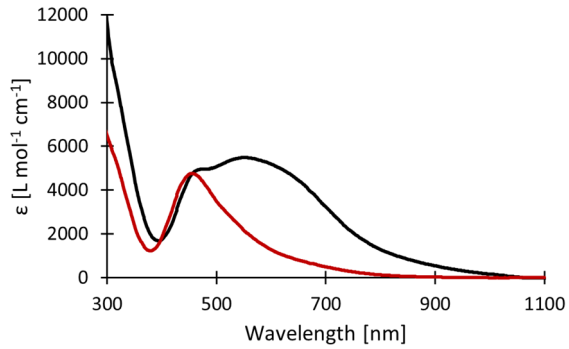

Figure 7. UV-Vis spectra of $Cp^*_2Ce(OtBu)_2$ (**2^{tBu}**, black) and $Cp^*Ce(OtBu)_3$ (**3^{tBu}**, red) in toluene.

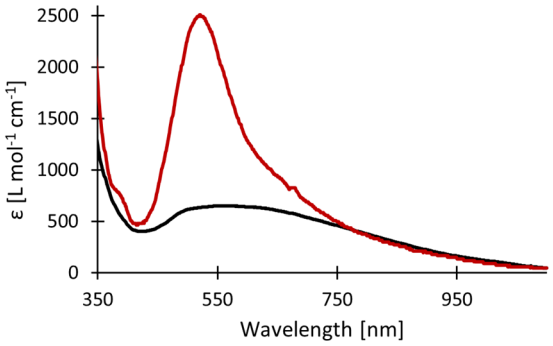

Figure 8. UV-Vis spectra of $Cp^*_2Ce(OSiPh_3)_2$ (**4^{Ph}**, black) and $Cp^*Ce(OSiPh_3)_3$ (**5^{Ph}**, red) in toluene.

Cerium(IV) Aryloxide Complexes. Application of the synthesis protocol as depicted in Scheme 2, however, using one equivalent of the aryloxide salt $NaOC_6H_3iPr_2$-2,6 (NaOAr) gave ceric $Cp^*_2Ce(OAr)Cl$ (**6**) instead of putative $Cp^*_2Ce(OAr)_2$ (Scheme 3). The latter could not be obtained even with larger quantities of sodium aryloxide,

rather leading to the formation of a mixture of **6** and presumably Cp*Ce(OAr)$_2$Cl (identified by ^{1}H-NMR spectroscopy). This can be rationalized on the basis of increased steric demand of the aryloxy ligand compared to the alkoxy and siloxy ligands. This is also evident from previously described related cerium(III) aryloxy complex Cp*Ce(OC$_6$H$_3$*t*Bu$_2$-2,6)$_2$, which is monomeric as well, in contrast to dimeric [Cp*Ce(O*t*Bu)$_2$]$_2$ and dimeric thiolate derivatives.[18,25,39,48] The same goes for amide complexes like monomeric Cp*Ce[N(SiMe$_3$)$_2$]$_2$, which seldom form ate complexes or dimers and are also not applicable to the synthesis protocol used herein.[11,24,48]

Scheme 3. Synthesis of Mono(aryloxy) Complex Cp*$_2$Ce(OC$_6$H$_3$*i*Pr$_2$-2,6)Cl (6)[a]

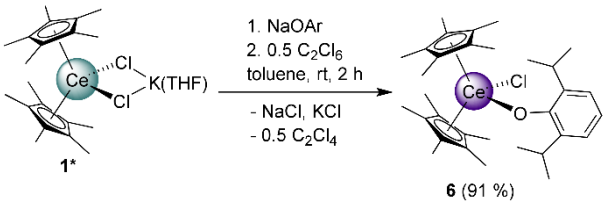

[a] OAr = OC$_6$H$_3$*i*Pr$_2$-2,6

The solid-state structure of **6** is depicted in Figure 9 being isostructural to the other Cp*$_2$CeR$_2$-type complexes, except for its asymmetry due to the presence of three different ligands. The Ce–Cp* distances are barely different from **2^{Et}** and the Ce–O distance accounts to 2.150(10) Å which matches those of the large triphenylsiloxy ligand in **4^{Ph}** (av. 2.1548 Å) and Cp$_3$Ce(OSiPh$_3$) (2.1331(19) Å) (Table 6).[36]

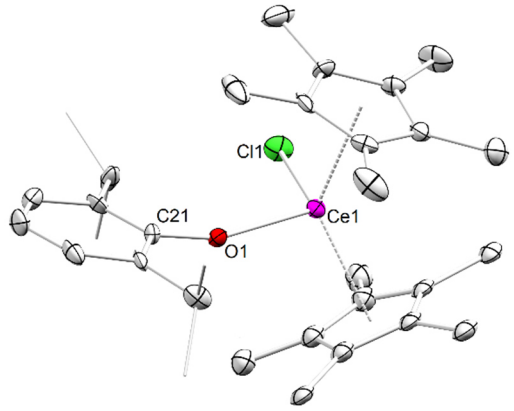

Figure 9. Crystal structure of Cp*$_2$Ce(OAr)Cl (**6**), with atomic displacement ellipsoids set at the 30% probability level. Hydrogen atoms are omitted for clarity. Selected interatomic distances and angles are listed in Table 6.

Structurally authenticated Ce(IV) complexes bearing monovalent aryloxy ligands are rare featuring homoleptic complex Ce(OC$_6$H$_3$Ph$_2$-2,6)$_4$ (Ce–O, 2.101(3)-2.125(3) Å)[49] and heteroleptic Ce(OAr^P)$_3$(OSiMe$_3$) (OAr^P = OC$_6$H$_2$PPh$_2$-6-Me-4-*t*Bu-6-κ^2*O,P*; Ce–O(Ar), 2.162(2)-2.190(2) Å).[50] The Ce(IV)Cl(OC$_6$H$_3$*i*Pr$_2$-2,6) moiety was recently reported in the dinuclear anionic complex [NEt$_4$]$_2$[(TP)Ce$_2$Cl$_4$(OAr)$_2$(THF)$_2$] supported by the TP tetraphenolato ligand.[51] The Ce–Cl distance of 2.638(5) Å in compound **6** appears slightly shorter compared to the those in tris(cyclopentadienyl) complexes like Cp$_3$CeCl (2.6666(7) Å) or Cp$^{Me}_3$CeCl (2.658(1) Å).[52,53] The remaining chlorido ligand may be useful for further salt metathesis attempts, which will be investigated in future work.

In order to enforce the formation of Cp^{R}Ce(OAr)$_2$-type sandwich complexes, we examined less bulky cyclopentadienyl ligands and switched to a synthesis protocol, applying the known tris(cyclopentadienyl) complexes Cp$_3$CeCl[52] and Cp$^{Me}_3$CeCl[53] as ceric precursors (Scheme 4).

Scheme 4. Synthesis of Cp$^{Me}_2$Ce(OC$_6$H$_3$*i*Pr$_2$-2,6)$_2$ (7) and Cp$_3$Ce(OC$_6$H$_3$*i*Pr$_2$-2,6) (8)[a]

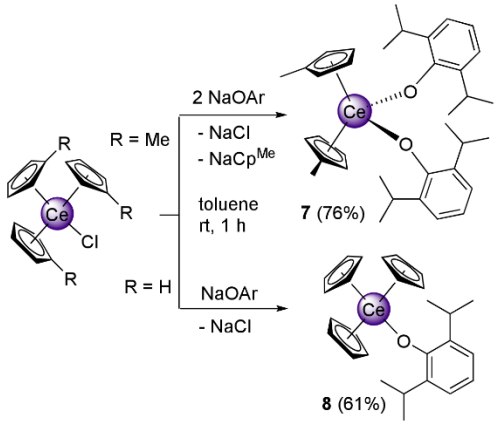

[a] OAr = OC$_6$H$_3$*i*Pr$_2$-2,6

Surprisingly, in the case of Cp$^{Me}_3$CeCl, treatment with two equivalents of NaOC$_6$H$_3$*i*Pr$_2$-2,6 or equimolar reactions led to Cp$^{Me}_2$Ce(OAr)$_2$ (**7**) instead of Cp$^{Me}_3$Ce(OAr). This is in contrast to alkoxy, siloxy, and halogenido derivatives investigated so far, which all form Cp$^{Me}_3$CeX-type compounds.[36] The respective complex Cp$^{Me}_3$Ce(OAr) could be observed in traces in the ^{1}H NMR spectrum (Figure S20), but could not be isolated. Instead, fast ligand scrambling led to **7** and ceric byproducts, which could not be identified. When using the sterically least crowded Cp$_3$CeCl as the precursor the targeted complex Cp$_3$Ce(OAr) (**8**) was formed and any conversion to a bis(cyclopentadienyl) compound was not observed.

The solid-state structure of Cp$_3$Ce(OC$_6$H$_3$*i*Pr$_2$-2,6) (**8**) bears a pseudo tetrahedral geometry (Figure 10) with a Ce–O distance of 2.151(4) Å, matching the 2.150(10) Å of Cp*$_2$Ce(OC$_6$H$_3$*i*Pr$_2$-2,6)Cl (**6**) (Table 6). The Ce–C distances lie in the expected range.[36]

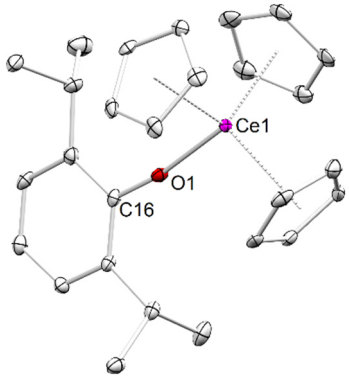

Figure 10. Crystal structure of Cp$_3$Ce(OC$_6$H$_3$*i*Pr$_2$-2,6) (**8**), with atomic displacement ellipsoids set at the 30% probability level. Hydrogen atoms are omitted for clarity. Selected bond lengths and angles are listed in Table 6.

The cyclic voltammograms of the aryloxide complexes revealed two types of behavior. Compounds **6** and **8** both exhibit chemical reversible and electrochemically (quasi-)reversible cyclic voltammograms, by all characteristics discussed above (Figures 4 and S49). However, compound $Cp^{Me}_2Ce(OC_6H_3iPr_2\text{-}2,6)_2$ (**7**, Figure 11) shows a more complex cyclic voltammogram including multiple oxidation and reduction signals. The electrochemical data of **7** exhibit a large peak separation of >242 mV, which increases with growing scan rate. Additionally, the peak current ratios lie between 0.85 and 0.96, indicating that a majority of substrate reduced gets re-oxidized.

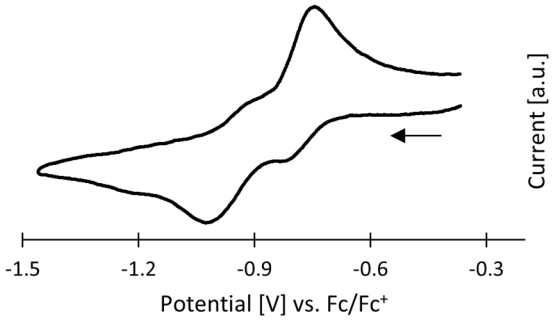

Figure 11. Cyclic voltammogram of the cerium(III/IV) redox couple of $Cp^{Me}_2Ce(OAr)_2$ (**7**) vs Fc/Fc^+ in THF at GC obtained at a scan rate of 250 mV/s; arrow indicates scan direction; c(analyte) 1 mM, c(electrolyte) 0.1 M $[n Pr_4N][B(C_6H_3(CF_3)_2\text{-}3,5)_4]$.

In total the data suggest an ECE mechanism and reactivity *in situ* in combination with a peak separation, thus combining chemical reversibility and electrochemical irreversibility. The mid-point potentials display a slight shift with increasing scan rate and both redox processes are diffusion controlled. The mid-point potential of −0.88 V vs Fc/Fc^+ at 50 mV/s is close to those of **6** (−0.84 V vs Fc/Fc^+) and **8** (−0.87 V vs Fc/Fc^+).

The less negative potentials compared to the respective siloxy and alkoxy compounds, account for a lower stabilization to the cerium(IV) center. This is in accordance with the data obtained for $Ce(OC_6H_3Ph_2\text{-}2,6)_4$ (E_{pa} = −0.46 V, E_{pc} = −0.54 V).[49] As observed for compounds of the type Cp_3CeX or Cp^{Me}_3CeX, the halogenido ligand seems to lead to a lesser stabilization, whereas substitution at the cyclopentadienyl ligand with electron donating groups leads to a better stabilization. The potentials of compounds **6** to **8** are located in between the potentials halide complex Cp^{Me}_3CeCl (−0.80 V vs Fc/Fc^+) and siloxide complex $Cp_3Ce(OSiPh_3)$ (−0.94 V vs Fc/Fc^+), in accordance with intermediate stabilization of the cerium +IV oxidation state.

The reduction potentials of all compounds under study are listed in Table 5, sorted by increasing stability of the cerium(IV) oxidation state. It is evident that the cerium(IV) center is better stabilized by alkoxy than siloxy than aryloxy ligands. The change from bis to mono Cp* complexes also results in a stronger stabilization of the +IV oxidation state. The change from $Cp^{H/Me}$ to Cp* is accompanied by a major increase in stabilization of the cerium(IV) as the respective $Cp^{H/Me}_3CeR$ complexes show potentials ranging from −0.94 to −1.09 V vs Fc/Fc^+ for R = siloxy and −1.10 to −1.25 V vs Fc/Fc^+ for R = alkoxy.[36]

Table 5. Potentials vs Fc/Fc^+ of 1 to 8 at a Scan Rate of 50 mV/s Sorted by Increasing Stability of the Cerium(IV) Oxidation State

Compound		E^0 (V)
$Cp^*_2CeCl_2K(THF)$	**1***	E_{Ox} = −0.57 (irr.)
$[Cp^{tet}_2CeCl_2Li(THF)_2]_2$	$\mathbf{1^{tet}}$	E_{Ox} = −0.54 (irr.)
$Cp^*_2Ce(OAr)Cl$	**6**	−0.84
$Cp_3Ce(OAr)$	**8**	−0.87
$Cp^{Me}_2Ce(OAr)_2$	**7**	−0.88 ($E^{1/2}$) E_{red} = −1.00; E_{Ox} = −0.76
$Cp^*_2Ce(OSiPh_3)_2$	$\mathbf{4^{Ph}}$	−1.15 ($E^{1/2}$) E_{red} = −1.26; E_{Ox} = −1.01
$Cp^*_2Ce(OSiMe_3)_2$	$\mathbf{4^{Me}}$	−1.23
$Cp^*Ce(OSiPh_3)_3$	$\mathbf{5^{Ph}}$	−1.44 ($E^{1/2}$) E_{red} = −2.19; E_{Ox} = −0.70
$Cp^*_2Ce(OCH_2tBu)_2$	$\mathbf{2^{CH2tBu}}$	−1.52
$Cp^*_2Ce(OtBu)_2$	$\mathbf{2^{tBu}}$	−1.53
$Cp^*_2Ce(OiPr)_2$	$\mathbf{2^{iPr}}$	−1.55
$Cp^*_2Ce(OEt)_2$	$\mathbf{2^{Et}}$	−1.56
$Cp^*Ce(OtBu)_3$	$\mathbf{3^{tBu}}$	−1.60 (−1.61 at 2 V/s)

OAr = $OC_6H_3iPr_2$-2,6.

Further comparison with literature known complexes reveals that the heteroleptic alkoxide complexes $\mathbf{2^R}$ show even better stabilization than cerocene $Ce(C_8H_8)_2$ (−1.4 V vs Fc/Fc+)[54] and recently reported alkali-metal capped cerium(IV) imido complexes using the TriNOx ligand (ranging from −1.39 to −1.41 V vs Fc/Fc^+).[55] Compound $Cp^*Ce(OtBu)_3$ ($\mathbf{3^{tBu}}$) exhibits the highest negative potential of −1.60 V vs Fc/Fc^+, exerting a remarkable stabilizing effect. This is comparable with the best stabilizing, but yet chemically reversible complexes known for molecular cerium(IV) chemistry, as reported for $Ce(omtaa)_2$ bearing a potential of −1.7 V vs Fc/Fc^+.[56] The aryloxy and siloxy ligands achieve potentials in the range of multidentate anionic oxygen ligands, showcasing Cp* as a ligand with a great potential of stabilizing the cerium(IV) center, assuming also kinetic stability.[35] It should be also mentioned that alkoxy ligands tend to disfavor chemical and electrochemical reversibility in cyclic voltammetry.

Finally, to further verify the cerium +IV oxidation state, magnetic measurements (Evans' method) of $\mathbf{2^{Et}}$, $\mathbf{3^{tBu}}$, and **7** have been conducted. The effective magnetic moments in the range between 0.58 (**7**) and 1.58 μ_B ($\mathbf{2^{CH2tBu}}$) are in agreement with the presence of the +IV oxidation state and temperature-independent paramagnetism. The latter behavior has been observed in similar complexes.[36,57,58]

CONCLUSIONS

Like pentamethylcyclopentadienyl (Cp*), the marginally smaller tetramethylcyclopentadienyl ligand (Cp^{tet}) triggers the formation of redox-active cerous ate complexes ($[Cp^{tet}_2CeCl_2Li(THF)_2]_2$ versus $Cp^*_2CeCl_2K(THF)$). While their direct oxidation was unsuccessful, one-pot tandem reactions conducted with $Cp^*_2CeCl_2K(THF)$ and alkali-metal alkoxides and siloxides as well as hexachloroethane as an oxidant gave broad excess to the ceric derivatives $Cp^*_2Ce(OR)_2$ (R = Et, *i*Pr, *t*Bu, CH_2tBu, $SiMe_3$ and $SiPh_3$). For the ligands O*t*Bu, $OSiEt_3$ and $OSiPh_3$, half-sandwich complexes $Cp^*Ce(OR)_3$ are formed as major kinetic secondary products, which is

easily followed by a blueshifts in the UV/Vis absorption spectra. Use of the sterically demanding aryloxy ligand $OC_6H_3iPr_2$-2,6 selectively gave the mono(aryloxy) derivative $Cp^*_2Ce(OAr)Cl$, while the alternative synthesis protocol [$(C_5H_4Me)_3CeCl$/NaOAr] favored the bis(aryloxy) complex $(C_5H_4Me)_2Ce(OAr)_2$. Cyclic voltammetry revealed mostly chemical reversible and electrochemical quasi-reversible redox processes and a better stabilization of the cerium(IV) center in the orders Cp^* > Cp^{tet} as well as alkoxy > siloxy > aryloxy and alkoxy/siloxy > Cp^*. The "sandwich/half-sandwich switch" ($Cp^*_2Ce(OR)_2$ versus $Cp^*Ce(OR)_3$) also led to a substantial stabilization of the +IV oxidation state with respect to reduction ($Cp^*Ce(OtBu)_3$: –1.60 V vs Fc/Fc^+) but at the expense of losing chemical and electrochemical reversibility. Although the stabilization of cerium(IV) is markedly affected by different ligand types, with more electron-donation leading to a better stabilization, sterics/kinetics often overrule such redox scenarios.

Table 6. Overview of Selected Interatomic Distances and Angles of Compounds $\mathbf{1^{tet}}$, $\mathbf{2^{Et}}$, $\mathbf{2^{tBu}}$, $\mathbf{4^{Ph}}$, 6, and 8 along with Relevant Compounds from Literature

	Ce–C(Cp^R) range [Å]	Ce–C (Cp^R) avg. [Å]	Ce–Cnt[a] avg. [Å]	Ce–X [Å]	AM–R [Å]	Cnt–Ce–Cnt [°]/ X–Ce–X [°]	Cnt–Ce–X [°]	Ce–X–R [°]
$[Cp^{tet}_2CeCl_2Li(THF)_2]_2$	2.756(3)	2.800	2.526	2.8321(9)	2.334(6)	125.65 /	116.59	98.58(15) (R=Li)
(**1^{tet}**)	–			2.9736(9)	2.385(6)	72.88	97.77	93.20(15) (R=Li)
X = Cl, AM = Li	2.841(3)			2.9924(9)		140.46(3)	117.73	112.41(3) (R=Ce)
							97.75	
							96.18	
							98.84	
$Cp^*_2CeCl_2Li(OEt_2)_2$	2.80(3)	2.83	-	2.812(1)	2.39(4)	- /	-	89(1)
(ref 5)	–					81.67(1)		
X = Cl, AM = Li	2.89 (4)							
$Cp^*_2CeCl_2K(THF)_2$	2.77(1)	2.793	-	2.778(3)	3.081(3)	- /	-	98.3(1)
(**1***) (ref 9)	–			2.776(2)	3.077(3)	86.52(8)		156.3(3)
X = Cl, AM = K	2.83(1)				3.157(3)			98.3(1)
					3.152(3)			141.5(1)
$Cp^*_2Ce(OEt)_2$	2.740(4)	2.757	2.488	2.075(3)	1.400(5)	133.3/	103.1	178.0(3)
(**2^{Et}**)	–			2.093(5)	1.399(7)	105.1(2)	104.2	175.3(5)
X = O, R = Et	2.775(4)						104.6	
							103.9	
$Cp^*_2Ce(OtBu)_2$	2.733(2)	2.805	2.540	2.0868(14)	1.429(2)	126.09 /	107.04	166.14(13)
(**2^{tBu}**)	–			2.1024(14)	1.432(2)	97.72(5)	107.90	172.40(14)
X = O, R = *t*Bu	2.887(2)						106.64	
							107.86	
$Cp^*_2Ce(OSiPh_3)_2$	2.740(3)	2.771	2.504	2.1549(19)	1.627(2)	129.3 /	105.4	177.30(13)
(**4^{Ph}**)	–					103.9	105.2	
X = O, R = Si	2.798(3)							
$Cp^*_2Ce(OAr)Cl$	2.713(15)	2.746	2.490	2.150(10)	1.358(16)	134.1 /	X = Cl:	162.1(9)
(**6**)	–			(X = O)	(X = O)	104.5(3)	101.65	(X = O)
X = O/Cl, R = Ar	2.787(14)			2.638(5)			99.92	
				(X = Cl)			X = O:	
							107.05	
							106.02	
$Cp_3Ce(OAr)$	2.731(6)	2.771	2.500	2.151(4)	1.360(7)	115.20	105.82	171.6(4)
(**8**)	–					112.44	102.08	
X = O, R = Ar	2.811(6)					116.61	102.67	
$(C_5H_3(SiMe_3)_2)_2Ce(OtBu)_2$	2.733(9)	2.784	2.511	2.077(5)	1.417(10)	121.7/	108.7	175.9(5)
(ref 30)	–			2.097(6)	1.432(12)	103.9	105.8	174.4(6)
X = O, R = *t*Bu	2.812(9)						105.6	
							109.9	
$[Cp^*Ce(OtBu)_2]_2$	2.78(1)	2.817	2.55	bridging:	1.47(1)	- /	122.1	bridging:
(ref 18)	–			2.380(6)	1.46(1)	74.4(2)	120.1	122.6(6)
X = O, R = *t*Bu	2.84(2)			–	1.44(1)	–	114.8	–
				2.431(6)	1.45(1)	111.8(2)	122.9	127.0(6)
				terminal:			123.3	terminal:
				2.116(6)			113.8	176.9(7)
				2.124(6)				176.6(7)

[a] Cnt = Cp ring centroid.

EXPERIMENTAL SECTION

General considerations and methods. All operations were performed under rigorous exclusion of oxygen and moisture in an argon atmosphere, using standard Schlenk, high-vacuum, and glovebox techniques (MB Braun MB150B-G-I; <0.1 ppm of O_2, <0.1 ppm of H_2O). Solvents were dried and degassed prior to use and provided by an MBraun SPS800. Benzene-d_6 (99.5%) was received from Deutero GmbH and thf-d_8 from Eurisotop. The deuterated solvents were dried over NaK alloy for a minimum of 48 h and filtered through a filter pipette (Whatman) before use. Anhydrous $CeCl_3$ (99.99%) (Sigma Aldrich) was converted into $CeCl_3(thf)_{1.04}$ via Soxhlet extraction. Hexachloroethane, NaO*t*Bu, KO*t*Bu, and $NaOSiMe_3$ were purchased from Sigma-Aldrich and used as received. NaOEt,[59] NaO*i*Pr,[60] sodium *neo*pentoxide,[61] $NaOSiEt_3$,[62] $NaOSiPh_3$,[63] [*n*Pr$_4$N][B{Ar(3,5-CF_3)}$_4$],[64] KCp*,[65] LiCp^{tet} (analogous to LiCp*),[66] $KOSiPh_3$,[67] $NaOC_6H_3iPr_2$-2,6,[68] Cp_3CeCl,[52] $Cp^{Me}{}_3CeCl$,[53] and $Cp^*{}_2CeCl_2K(THF)$ (**1***)[9] were prepared according to literature procedures. NMR spectra were recorded on a Bruker AVII + 400 (^{1}H: 400.13 MHz; ^{13}C: 100.61 MHz) or AVI + 300 (^{29}Si: 79.5 MHz) spectrometer in dried and deuterated solvents. DRIFT spectra were recorded on a ThermoFisher Scientific NICOLET 6700 FTIR spectrometer using dried KBr and KBr windows. The collected data were converted using the Kubelka–Munk refinement. UV/Vis measurements have been carried out in toluene on a PG Instruments T60 UV-Vis spectrophotometer. CHN elemental analyses were performed on an Elementar Vario MICRO cube. The effective magnetic moments (μ_{eff}) and susceptibilities were determined in C_6D_6 by Evans' method on a Bruker AVII + 400 instrument at 299 K using hexamethyldisiloxane as an internal standard.

Cyclic voltammetry (CV) experiments were performed with a Nordic Electrochemistry ECi-200 workstation applying the IR-compensation mode. The data were recorded using Nordic Electrochemistry EC4 DAQ software (version 4.1.90.1) and processed with EC-4 VIEW software (version 1.2.36.1). The CV experiments were performed in a glovebox under argon atmosphere at ambient temperature. The setup comprised a 4 mL vial, equipped with a CHI 104 glassy carbon disc working electrode (CH Instruments, Inc.), a platinum wire counter electrode and a Ag/AgCl quasi reference electrode. The surface of the working electrode was polished prior to the measurement. Solutions containing ~1 mM of analyte and 0.1 M [*n*Pr$_4$N][B{Ar(3,5-CF_3)}$_4$] supporting electrolyte were used for the electrochemical analysis. The scan rate dependent background of the electrolyte was recorded for each measurement and subtracted from the analyte data. The potentials are reported in [V] vs. the Fc/Fc^+ couple, which was used as internal standard for cell calibration and determined at the end of each measurement.

[Cp$^{tet}{}_2$CeCl$_2$Li(THF)$_2$]$_2$ (1^{tet}): $CeCl_3(THF)_{1.04}$ (57.1 mg, 0.355 mmol) and LiC_5Me_4H (45.5 mg, 0.178 mmol) were suspended in THF (15 mL) and stirred for 30 h at ambient temperature while turning yellow. Afterwards, the reaction mixture was evaporated under vacuum, the residual solid extracted with toluene to give a pink colored solution, which was separated and concentrated under reduced pressure. The concentrated solution was stored at −40°C to afford **1^{tet}** (54.5 mg, 58%) as bright pink crystals. ^{1}H NMR (400.1 MHz, thf-d_8, 26 °C): δ = 10.19 (s, 12H, CpMe_4H), 3.62 (m, 4H, thf), 1.78 (m, 4H, thf), −0.02 (s, 2H, CpMe$_4$*H*), −2.10 (s, 18H, CpMe_4H) ppm. ^{7}Li-{^{1}H} NMR (116.6 MHz, thf-*d*8, 26 °C): δ = −6.32 ppm. DRIFT: $\tilde{\nu}$ = 2964 (s), 2934 (s), 2892 (vs), 2854 (s), 2720 (w), 1456 (w), 1381 (w), 1329 (w), 1177 (w), 1043 (vs), 893 (m), 785 (m), 773 (s), 614 (w) cm^{-1}. UV/Vis: 422 nm (375 ± 81 L mol^{-1} cm^{-1}). Elemental analysis (%) calcd for $C_{26}H_{42}CeCl_2LiO_2$ (604.58 g mol^{-1}): C 51.65, H 7.00; found: C 51.45, H 7.28.

General synthesis of ceric alkoxides 2^R: compound **1*** and two equivalents of the alkali-metal alkoxide were suspended in toluene and stirred for 10 min, then C_2Cl_6 was added. The mixture was stirred for 1 or 2 h until compound **1*** had completely reacted (full consumption of bright yellow solid), and was subsequently filtered and the separated solution evaporated to dryness under vacuum. The resulting dark violet/purple solid was treated with *n*-hexane to form a colorless precipitate. The suspension was filtered and the separated solution dried under vacuum. The dark violet/purple product **2^R** was extracted with $SiMe_4$ and crystallized from a saturated $SiMe_4$ solution at −40 °C. All synthesis steps were performed under exclusion of light and the product always stored at −40 °C (to minimize ligand scrambling).

Cp*$_2$Ce(OEt)$_2$ (2^{Et}): compound **1*** (202.7 mg, 0.342 mmol), NaOEt (46.5 mg, 0.684 mmol), toluene (15 mL), C_2Cl_6 (40.5 mg, 0.171 mmol), 2 h. Product **2^{Et}** was obtained as dark violet crystals (98.6 mg, 58%). ^{1}H NMR (400.1 MHz, C_6D_6, 26 °C): δ = 5.31(q, 4H, J_{HH} = 7.0 Hz; C*H*$_2$CH$_3$), 2.75 (s, 30H, Cp*), 1.39 (t, 6H, J_{HH} = 7.0 Hz; CH$_2$C*H*$_3$) ppm. ^{13}C{^{1}H} NMR (100.6 MHz, C_6D_6, 26 °C): δ = 130.0 (*C*$_5$Me$_5$), 69.4 (*C*H$_2$CH$_3$), 22.2 (CH$_2$*C*H$_3$), 10.7 (C$_5$*Me*$_5$) ppm. DRIFT: $\tilde{\nu}$ = 2963 (s), 2912 (s), 2855 (s), 2719 (w), 1438 (m), 1376 (m), 1349 (w), 1114 (s), 1103 (s), 1061 (s), 904 (m), 884 (w), 781 (w), 484 (m) cm^{-1}. UV/Vis: 559 nm (2251 ± 91 L mol^{-1} cm^{-1}). Elemental analysis (%) calcd for $C_{24}H_{40}CeO_2$ (500.70 g mol^{-1}): C 57.57, H 8.05; found: C 56.87, H 7.18.

Cp*$_2$Ce(O*i*Pr)$_2$ (2^{iPr}): compound **1*** (178.5 mg, 0.301 mmol), NaO*i*Pr (49.4 mg, 0.602 mmol), toluene (10 mL) and stirred for 10 min, C_2Cl_6 (35.7 mg, 0.151 mmol). 2 h. Product **2^{iPr}** was obtained as dark purple crystals (91.0 mg, 57%). ^{1}H NMR (400.1 MHz, C_6D_6, 26 °C): δ = 5.73 (sep, 2H, J_{HH} = 6.1 Hz; C*H*(CH$_3$)$_2$), 2.82 (s, 30H, Cp*), 1.44 (d, 12H, J_{HH} = 6.1 Hz; CH(C*H*$_3$)$_2$) ppm. DRIFT: $\tilde{\nu}$ = 2960 (s), 2921 (s), 2854 (s), 2611 (w), 1449 (m), 1376 (m), 1355 (m), 1327 (m), 1157 (m), 1125 (s), 981 (s), 971 (s), 835 (m), 530 (m), 482 (w), 441 (m), 420 (m) cm^{-1}. UV/Vis: 560 nm (2494 ± 102 L mol^{-1} cm^{-1}). Elemental analysis (%) calcd for $C_{26}H_{44}CeO_2$ (528.75 g mol^{-1}): C 59.06, H 8.39; found: C 58.77, H 8.00.

Cp*$_2$Ce(OCH$_2$*t*Bu)$_2$ (2^{CH2tBu}): compound **1*** (117.3 mg, 0.198 mmol), NaOCH$_2$*t*Bu (43.6 mg, 0.396 mmol), toluene (12 mL), C_2Cl_6 (23.4 mg, 0.099 mmol), 2 h. Product **2^{CH2tBu}** was obtained as dark purple crystals (90.0 mg, 78%). ^{1}H NMR (400.1 MHz, C_6D_6, 26 °C): δ = 5.48 (s, 4H, C*H*$_2$*t*Bu), 2.88 (s, 30H, Cp*), 1.14 (s, 18H, CH$_2$C(C*H*$_3$)$_3$) ppm. DRIFT: $\tilde{\nu}$ = 2950 (s), 2861 (m), 2685 (w), 1478 (w), 1458 (w), 1390 (w), 1377 (w), 1359 (w), 1103 (m), 1086 (s), 1070 (vs), 1020 (m), 596 (s), 435 (m) cm^{-1}. UV/Vis: 556 nm (4293 ± 194 L mol^{-1} cm^{-1}). Elemental analysis (%) calcd for $C_{30}H_{52}CeO_2$ (584.86 g mol^{-1}): C 61.61, H 8.96; found: C 62.94, H 8.58. Although these results are outside the range viewed as establishing analytical purity, they are provided to

illustrate the best values obtained to date (major issue: progressing decomposition/rearrangement reactions).

Cp*$_2$Ce(O*t*Bu)$_2$ (2^{tBu}): compound **1*** (47.5 mg, 0.080 mmol), KO*t*Bu (18.0 mg, 0.160 mmol), toluene (12 mL), C_2Cl_6 (9.5 mg, 0.040 mmol), 1 h. Product **2^{tBu}** was obtained as dark violet crystals (22.7 mg, 51%). ^{1}H NMR (400.1 MHz, C_6D_6, 26 °C): δ = 3.01 (s, 30H, Cp*), 1.59 (s, 18H, C(CH_3)$_3$) ppm. DRIFT: $\tilde{\nu}$ = 2966 (vs), 2921 (s), 2858 (m), 1653 (m), 1558 (m), 1506 (w), 1456 (m), 1437 (w), 1354 (m), 1180 (s), 957 (vs), 940 (vs), 772 (w), 498 (m), 478 (m) cm^{-1}. UV/Vis: 556 nm (5472 ± 118 L mol^{-1} cm^{-1}). Elemental analysis (%) calcd for $C_{28}H_{48}CeO_2$ (556.81 g mol^{-1}): C 60.40, H 8.69; found: C 57.92, H 7.33. Although these results are outside the range viewed as establishing analytical purity, they are provided to illustrate the best values obtained to date (major issue: rapid decomposition/rearrangement reactions).

Cp*Ce(O*t*Bu)$_3$ (3^{tBu}): compound **1*** (139.0 mg, 0.235 mmol) and NaO*t*Bu (45.1 mg, 0.469 mmol) were suspended in toluene (10 mL) and stirred for 10 min, then C_2Cl_6 (27.8 mg, 0.118 mmol) was added. The mixture was stirred for 6 h until compound **1*** had completely reacted, turning first violet then brown. Subsequent filtration and evaporation of the obtained solution to dryness under vacuum left a dark brown solid. Addition of *n*-hexane resulted in a colorless precipitate. The solution was filtered and dried under vacuum. The dark brown product **3^{tBu}** was extracted with $SiMe_4$ and crystallized from a saturated $SiMe_4$ solution at −40°C (48.0 mg, 41%). ^{1}H NMR (400.1 MHz, C_6D_6, 26 °C): δ = 2.87 (s, 15H, Cp*), 1.32 (s, 27H, *t*Bu) ppm. DRIFT: $\tilde{\nu}$ = 2964 (s), 2921 (m), 2859 (w), 1454 (w), 1378 (w), 1355 (m), 1225 (w), 1181 (s), 987 (m), 957 (vs), 774 (m), 501 (m), 480 (w) cm^{-1}. UV/Vis: 456 nm (4941 ± 110 L mol^{-1} cm^{-1}). Elemental analysis (%) calcd for $C_{22}H_{42}CeO_3$ (494.69 g mol^{-1}): C 53.42, H 8.56; found: C 53.66, H 8.26.

Cp*$_2$Ce(OSiMe$_3$)$_2$ (4^{Me}): compound **1*** (135.4 mg, 0.229 mmol) and $NaOSiMe_3$ (51.3 mg, 0.457 mmol) were suspended in toluene (10 mL) and stirred for 10 min, then C_2Cl_6 (27.1 mg, 0.115 mmol) was added. The mixture was stirred for 2 h until compound **1*** had completely reacted. Subsequent filtration and evaporation of the obtained solution to dryness under vacuum left a dark blue solid. Addition of *n*-hexane resulted in a colorless precipitate. The solution was filtered and dried under vacuum. The dark blue product **4^{Me}** was extracted with $SiMe_4$ and crystallized from a saturated $SiMe_4$ solution at −40°C (113.9 mg, 84%). ^{1}H NMR (400.1 MHz, C_6D_6, 26 °C): δ = 3.13 (s, 30H, Cp*), 0.50 (s, 18H, $SiMe_3$) ppm. ^{13}C{^{1}H} NMR (100.6 MHz, C_6D_6, 26 °C): δ = 133.6 (C_5Me_5), 11.0 (C_5Me_5), 5.3 ($SiMe_3$) ppm. ^{29}Si(HSQC) NMR (79.5 MHz, C_6D_6, 26 °C): δ = +0.4 ($SiMe_3$) ppm. DRIFT: $\tilde{\nu}$ = 2951 (s), 2909 (s), 1440 (w), 1378 (w), 1245 (s), 949 (s), 914 (vs), 879 (vs), 833 (vs), 749 (s), 676 (w), 449 (m) cm^{-1}. UV/Vis: 582 nm (1899 ± 81 L mol^{-1} cm^{-1}). Elemental analysis (%) calcd for $C_{26}H_{48}CeO_2Si_2$ (588.95 g mol^{-1}): C 53.02, H 8.22; found: C 52.42, H 7.47.

Cp*$_2$Ce(OSiEt$_3$)$_2$ (4^{Et})/Cp*Ce(OSiEt$_3$)$_3$ (5^{Et}): compound **1*** (134.7 mg, 0.227 mmol) and $NaOSiEt_3$ (70.1 mg, 0.4545 mmol) were suspended in toluene (12 mL) and stirred for 10 min, then C_2Cl_6 (27.0 mg, 0.114 mmol) was added. The mixture was stirred for 2 h until compound **1*** had completely reacted. Subsequent filtration and evaporation of the obtained solution to dryness under vacuum left a dark violet solid. Addition of *n*-hexane gave a colorless precipitate. The solution was filtered and dried under vacuum. The crude dark violet product mixture of **4^{Et}** (32%) and **5^{Et}** (68%) (combined: 139.5 mg) was washed with a chilled $SiMe_4$ solution (139.5 mg, 92%). ^{1}H NMR (400.1 MHz, C_6D_6, 26 °C): δ = **4^{Et}**: 3.29 (s, 30H, Cp*), 1.35 (t, 18H, J_{HH} = 7.9 Hz; CH_2CH_3), 1.15 (q, 12H, J_{HH} = 7.9 Hz; CH_2CH_3); **5^{Et}**: 3.19 (s, 15H, Cp*), 1.16 (t, 27H, J_{HH} = 7.9 Hz; CH_2CH_3), 0.68 (q, 18H, J_{HH} = 7.9 Hz; CH_2CH_3) ppm. ^{29}Si(HSQC) NMR (79.5 MHz, C_6D_6, 26 °C): δ = **4^{Et}** : +6.5 ($SiEt_3$); **5^{Et}** : +9.1 ($SiEt_3$) ppm.

Cp*$_2$Ce(OSiPh$_3$)$_2$ (4^{Ph}): compound **1*** (171.6 mg, 0.290 mmol) and $KOSiPh_3$ (182.1 mg, 0.580 mmol) were suspended in toluene (10 mL) and stirred for 10 min, then C_2Cl_6 (34.3 mg, 0.145 mmol) was added. The mixture was stirred for 2 h until compound **1*** had completely reacted. Subsequent filtration and evaporation of the obtained solution to dryness under vacuum left a dark blue solid. (turned violet if reacted too long). Addition of *n*-hexane resulted in a colorless precipitate. The solution was filtered and dried under vacuum. The dark blue product **4^{Ph}** was extracted with $SiMe_4$ and crystallized from a saturated $SiMe_4$ solution at −40 °C (200.3 mg, 72%). All synthesis steps were performed under exclusion of light and the product always stored at −40 °C (ligand scrambling to **5^{Ph}** still takes place over several weeks). ^{1}H NMR (400.1 MHz, C_6D_6, 26 °C): δ = 8.31 (d, 12H, J_{HH} = 7.3 Hz; *o*CH), 7.35 (m, 18H, *p*CH + *m*CH), 3.72 (s, 30H, Cp*) ppm. ^{29}Si(HSQC) NMR (79.5 MHz, C_6D_6, 26 °C): δ = -23.6 ($SiPh_3$) ppm. DRIFT: $\tilde{\nu}$ = 3065 (m), 2957 (m), 2914 (m), 2855 (m), 1456 (w), 1427 (m), 1378 (w), 1110 (s), 1064 (w), 1029 (w), 990 (w), 941 (s), 912 (s), 880 (s), 742 (m), 704 (vs), 517 (vs), 431 (w) cm^{-1}. UV/Vis: 563 nm (714 ± 73 L mol^{-1} cm^{-1}). Elemental analysis (%) calcd for $C_{56}H_{60}CeO_2Si_2$ (961.38 g mol^{-1}): C 69.96, H 6.29; found: C 69.81, H 6.70.

Cp*Ce(OSiPh$_3$)$_3$ (5^{Ph}): compound **1*** (37.6 mg, 0.0634 mmol) and $KOSiPh_3$ (59.9 mg, 0.190 mmol) were suspended in toluene (15 mL) and stirred for 5 min, then $TeBr_4$ (28.4 mg, 0.0634 mmol) was added. The mixture was stirred for 8 h and was subsequently filtered and the separated solution evaporated to dryness under vacuum. To the obtained violet solid, a *n*-hexane/toluene mixture (9:1) was added resulting in a light purple precipitate. The solution was filtered and dried under vacuum giving dark purple **5^{Ph}** (62.1 mg, 89%), which was washed with $SiMe_4$ multiple times, but could not be obtained very pure. ^{1}H NMR (400.1 MHz, C_6D_6, 26 °C): δ = 7.81 – 7.84 (m, 18H, *o*CH), 7.18 – 7.22 (m, 9H, *p*CH), 7.11 – 7.14 (m, 18H, *m*CH) 3.47 (s, 15H, Cp*) ppm. ^{29}Si(HSQC) NMR (79.5 MHz, C_6D_6, 26 °C): δ = −21.0 ppm. DRIFT: $\tilde{\nu}$ = 3064 (m), 2996 (w), 2914 (m), 1483 (w), 1427(m), 1113 (s), 1028 (w), 997 (w), 949 (s), 884 (vs), 741 (m), 709 (s), 700 (s), 517 (vs), 418 (w) cm^{-1}. UV/Vis: 521 nm (2597 ± 123 L mol^{-1} cm^{-1}). Elemental analysis (%) calcd for $C_{64}H_{60}CeO_3Si_3$ (1101.55 g mol^{-1}): C 69.78, H 5.49; found: C 70.89, H 6.88. Although these results are outside the range viewed as establishing analytical purity, they are provided to illustrate the best values obtained to date (major issue: purification of product formed in a one-pot reaction).

Cp*$_2$Ce(OC$_6$H$_3$*i*Pr$_2$-2,6)Cl (6): compound **1*** (62.5 mg, 0.105 mmol) and $NaOC_6H_3iPr_2$-2,6 (21.1 mg, 0.105 mmol) were suspended in toluene (10 mL) and stirred for 10 min, then C_2Cl_6 (12.5 mg, 0.053 mmol) was added. The mixture was stirred for 2 h until compound **1*** has completely reacted, and was subsequently filtered and the obtained solution evaporated to dryness under

vacuum. To the dark blue solid (turned violet if reacted too long), *n*-hexane was added resulting in a colorless precipitate. The solution was filtered and dried under vacuum. The dark blue product **6** was extracted with $SiMe_4$ and crystallized from a saturated $SiMe_4$ solution at −40 °C (59.6 mg, 91%). ^{1}H NMR (400.1 MHz, C_6D_6, 26 °C): δ = 7.34 – 7.40 (m, 2H, *m*-ArCH), 6.45 (t, 1H, J_{HH} = 7.6 Hz; *p*-ArCH), 4.95 (dsep, 2H, J_{HH} = 6.6 Hz; C*H*$(CH_3)_2$), 3.93 (s, 30H, Cp*), 1.68 (dd, 12H, J_{HH} = 6.6 Hz; CH(C*H*$_3)_2$) ppm. DRIFT: $\tilde{\nu}$ = 3052 (w), 2960 (vs), 2917 (s), 2864 (s), 1456 (m), 1428 (vs), 1370 (m), 1360 (w), 1322 (m), 1248 (s), 1195 (vs), 1106 (w), 1093 (w), 1041 (w), 886 (m), 855 (vs), 792 (w), 781 (w), 749 (s), 693 (m), 573 (m) cm^{-1}. UV/Vis: 603 nm (3689 ± 314 L mol^{-1} cm^{-1}). Elemental analysis (%) calcd for $C_{44}H_{64}CeO_2$ (623.29 g mol^{-1}): C 61.66, H 7.60; found: C 61.87, H 7.31.

$Cp^{Me}_2Ce(OC_6H_3iPr_2$-2,6)$_2$ (**7**): Cp^{Me}_3CeCl (115.6 mg, 0.280 mmol) and $NaOC_6H_3iPr_2$-2,6 (112.2 mg, 0.560 mmol) were suspended in toluene (10 mL) and stirred for 1 h. Afterwards, the mixture was filtered and the obtained solution evaporated to dryness under vacuum. To the dark violet solid, *n*-hexane was added resulting in a colorless precipitate. The solution was filtered and dried under vacuum. The dark violet product **7** was extracted with $SiMe_4$ and crystallized from a saturated $SiMe_4$ solution at −40 °C (138.1 mg, 76%). ^{1}H NMR (400.1 MHz, C_6D_6, 26 °C): δ = 7.25 (d, 4H, J_{HH} = 7.6 Hz; *m*-C*H*), 6.67 (t, 2H, J_{HH} = 7.6 Hz; *p*-C*H*), 5.59 (t, 4H, J_{HH} = 2.6 Hz; $CpH_{3/4}$), 5.75 (t, 4H, J_{HH} = 2.6 Hz; $CpH_{2/5}$), 4.20 (sep, 4H, J_{HH} = 6.8 Hz; C*H*$(CH_3)_2$), 1.39 (d, 24H, J_{HH} = 6.8 Hz; CH(C*H*$_3)_2$) ppm. DRIFT: $\tilde{\nu}$ = 3057 (w), 2955 (s), 2924 (m), 2865 (m), 1493 (w), 1456 (m), 1428 (s), 1380 (w), 1358 (w), 1321 (s), 1426 (s), 1199 (s), 1112 (w), 1095 (w), 1042 (w), 933 (w), 886 (m), 856 (s), 779 (s), 755 (s), 693 (m), 570 (m)cm^{-1}. UV/Vis: 529 nm (8721 ± 320 L mol^{-1} cm^{-1}). Elemental analysis (%) calcd for $C_{36}H_{48}CeO_2$ (652.89 g mol^{-1}): C 66.23, H 7.41; found: C 65.98, H 6.94.

$Cp_3Ce(OC_6H_3iPr_2$-2,6) (**8**): Cp_3CeCl (104.0 mg, 0.280 mmol) and $NaOC_6H_3iPr_2$-2,6 (56.2 mg, 0.280 mmol) were suspended in toluene (10 mL) and stirred for 1 h. Afterwards, the mixture was filtered and the separated solution evaporated to dryness under vacuum. To the dark brown solid, *n*-hexane was added resulting in a colorless precipitate. The solution was filtered and dried under vacuum. The dark brown product **8** was crystallized from a saturated toluene solution at −40 °C (87.3 mg, 61%). ^{1}H NMR (400.1 MHz, C_6D_6, 26 °C): δ = 7.56 (d, 2H, J_{HH} = 7.8 Hz; ArCH), 5.23 (s, 15H, CpH), 4.20 (sep, 2H, J_{HH} = 6.9 Hz; C*H*$(CH_3)_2$), 2.91 (s, 30H, Cp*), 1.39 (d, 24H, J_{HH} = 6.9 Hz; CH(C*H*$_3)_2$) ppm. DRIFT: $\tilde{\nu}$ = 3050 (w), 2959 (m), 2863 (w), 1456 (w), 1445 (w), 1429 (m), 1379 (w), 1358 (w), 1323 (m), 1251 (m), 1198 (s), 1110 (w), 1096 (w), 1060 (w), 1012 (m), 937 (w), 885 (w), 850 (m), 780 (s), 768 (vs), 754 (m), 692 (w), 567 (m), 425 (w) cm^{-1}. UV/Vis: 411 nm (4869 ± 248 L mol^{-1} cm^{-1}), 455 nm (4744 ± 236 L mol^{-1} cm^{-1}), 669 nm (2449 ± 112 L mol^{-1} cm^{-1}). Elemental analysis (%) calcd for $C_{27}H_{32}CeO$ (512.67 g mol^{-1}): C 63.26, H 6.29; found: C 63.94, H 6.17.

ASSOCIATED CONTENT

Supporting Information

The Supporting Information is available free of charge at http://pubs.acs.org/doi/xxxx.

Supporting figures, detailed crystallographic data, spectroscopic data (NMR), and analytical details (PDF).

Accession Codes

CCDC 2108589–2108594 contain the supplementary crystallographic data for this paper. These data can be obtained free of charge via www.ccdc.cam.ac.uk/data_request/cif, or by emailing data_request@ccdc.cam.ac.uk, or by contacting The Cambridge Crystallographic Data Centre, 12 Union Road, Cambridge CB2 1EZ, UK; fax: +44 1223 336033.

AUTHOR INFORMATION

Corresponding Author

* reiner.anwander@uni-tuebingen.de

ORCID

Cäcilia Maichle-Mössmer: 0000-0001-7638-1610
Reiner Anwander: 0000-0002-1543-3787
Lars Hirneise: 0000-0003-2715-9882

Notes

The authors declare no competing financial interest.

REFERENCES

1. Schumann, H., Organolanthanoid Compounds. *Angew. Chem. Int. Ed.* **1984**, *23*, 474-493.
2. Evans, W. J., Organometallic Lanthanide Chemistry. *Adv. Organomet. Chem.* **1985**, *24*, 131-177.
3. Schumann, H.; Meese-Marktscheffel, J. A.; Esser, L., Synthesis, Structure, and Reactivity of Organometallic .pi.-Complexes of the Rare Earths in the Oxidation State Ln3+ with Aromatic Ligands. *Chem. Rev.* **1995**, *95*, 865-986.
4. Birmingham, J.; Wilkinson, G., The cyclopentadienides of scandium, yttrium and some rare earth elements. *J. Am. Chem. Soc.* **1956**, *78*, 42-44.
5. Rausch, M. D.; Moriarty, K. J.; Atwood, J. L.; Weeks, J. A.; Hunter, W. E.; Brittain, H. G., Synthetic, x-ray structural and photoluminescence studies on pentamethylcyclopentadienyl derivatives of lanthanum, cerium and praseodymium. *Organometallics* **1986**, *5*, 1281-1283.
6. Schumann, H.; Albrecht, I.; Loebel, J.; Hahn, E.; Hossain, M. B.; Van der Helm, D., Organometallic compounds of the lanthanides. 36. Bis (pentamethylcyclopentadienyl) halide and alkyl derivatives of the lanthanides. *Organometallics* **1986**, *5*, 1296-1304.
7. Hazin, P. N.; Bruno, J. W.; Brittain, H. G., Luminescence spectra of a series of cerium (III) halides and organometallics. Probes of bonding properties using 4f-5d excited states. *Organometallics* **1987**, *6*, 913-918.
8. Hazin, P. N.; Huffman, J. C.; Bruno, J. W., Synthetic and structural studies of pentamethylcyclopentadienyl complexes of lanthanum and cerium. *Organometallics* **1987,** *6* (1), 23-27.
9. Evans, W. J.; Olofson, J. M.; Zhang, H.; Atwood, J. L., Synthesis and X-ray crystal structure of an unusual oligomeric bis(pentamethylcyclopentadienyl) halide complex of cerium: $[(C_5Me_5)_2CeCl_2K(THF)]_n$. *Organometallics* **1988**, *7*, 629-633.
10. Jeske, G.; Lauke, H.; Mauermann, H.; Swepston, P. N.; Schumann, H.; Marks, T. J., Highly reactive organolanthanides. Systematic routes to and olefin chemistry of early and late bis(pentamethylcyclopentadienyl) 4f hydrocarbyl and hydride complexes. *J. Am. Chem. Soc.***1985**, *107*, 8091-8103.
11. Heeres, H. J.; Renkema, J.; Booij, M.; Meetsma, A.; Teuben, J. H., Bis(pentamethylcyclopentadienyl) complexes of cerium(III). Crystal structure of $(C_5Me_5)_2CeCH(SiMe_3)_2$. *Organometallics* **1988**, *7*, 2495-2502.
12. Heeres, H. J.; Meetsma, A.; Teuben, J. H., CH Activation of Acetonitrile By Alkyl vomounds of the Early Lanthanoids:

Alkylverbindungen der frühen Lanthanoide: Dimeric Cyanmethyl-Lanthanoid Complexes with CH_2CN Bridges. *Angew. Chem. Int. Ed.* **1990**, *129*, 420-422.
13. Heeres, H.; Heeres, A.; Teuben, J., Organolanthanide-catalyzed cyclodimerizations of disubstituted alkynes. *Organometallics* **1990**, *9*, 1508-1510.
14. Booij, M.; Kiers, N. H.; Heeres, H. J.; Teuben, J. H., On the synthesis of monopentamethylcyclopentadienyl derivatives of yttrium, lanthanum, and cerium. *J. Organomet. Chem.* **1989**, *364*, 79-86.
15. Heeres, H.; Teuben, J., Catalytic oligomerization of terminal alkynes by lanthanide carbyls $(\eta^5\text{-}C_5Me_5)_2$ LnCH $(SiMe_3)_2$ (Ln= Y, La, Ce). *Organometallics* **1991**, *10*, 1980-1986.
16. Quiroga Norambuena, V. F.; Heeres, A.; Heeres, H. J.; Meetsma, A.; Teuben, J. H.; Hessen, B., Synthesis, Structure, and Reactivity of Rare-Earth Metallocene η^3-Propargyl/Allenyl Complexes. *Organometallics* **2008**, *27*, 5672-5683.
17. Heeres, H. J.; Meetsma, A.; Teuben, J. H., Cerium aryloxides as precursors for monopentamethylcyclpenta-dienyl organocerium(III) compounds; X-ray crystal structure of (η^5-pentamethylcyclopentadienyl)bis(2,6-di-*t*-butyl-phenoxo)cerium. *J. Chem. Soc., Chem. Commun.* **1988**, 962-963.
18. Heeres, H. J.; Teuben, J. H.; Rogers, R. D., Novel monopentamethylcyclopentadienyl alkoxides of La and Ce; X-ray crystal structure of $(C_5Me_5Ce(OCMe_3)_2)_2$. *J. Organomet. Chem.* **1989**, *364*, 87-96.
19. Heeres, H. J.; Meetsma, A.; Teuben, J. H., Synthesis of cationic cerium compounds $[Cp^*_2Ce(L)_2][BPh_4]$ (L = tetrahydrofuran or tetrahydrothiophene) and the crystal structure of the tetrahydrothiophene derivative. *J. Organomet. Chem.* **1991**, *414*, 351-359.
20. Evans, W. J.; Perotti, J. M.; Kozimor, S. A.; Champagne, T. M.; Davis, B. L.; Nyce, G. W.; Fujimoto, C. H.; Clark, R. D.; Johnston, M. A.; Ziller, J. W., Synthesis and Comparative η^1-Alkyl and Sterically Induced Reduction Reactivity of $(C_5Me_5)_3Ln$ Complexes of La, Ce, Pr, Nd, and Sm. *Organometallics* **2005**, *24*, 3916-3931.
21. Amberger, H.-D.; Reddmann, H.; Mueller, T. J.; Evans, W. J., Electronic structures of organometallic complexes of f elements LXXIII: Parametric analysis of the crystal field splitting pattern of tris(η^5-pentamethylcyclopentadienyl) cerium(III). *J. Organomet. Chem.* **2010**, *695*, 1293-1299.
22. Evans, W. J.; Mueller, T. J.; Ziller, J. W., Lanthanide versus Actinide Reactivity in the Formation of Sterically Crowded $[(C_5Me_5)_3MLn]$ Nitrile and Isocyanide Complexes. *Chem. Eur. J.* **2010**, *16*, 964-975.
23. Evans, W. J.; Rego, D. B.; Ziller, J. W., Synthesis, Structure, and ^{15}N NMR Studies of Paramagnetic Lanthanide Complexes Obtained by Reduction of Dinitrogen. *Inorg. Chem.* **2006**, *45*, 10790-10798.
24. Rozenel, S. S.; Perrin, L.; Eisenstein, O.; Andersen, R. A., Experimental and DFT Computational Study of β-Me and β-H Elimination Coupled with Proton Transfer: From Amides to Enamides in Cp^*_2MX (M = La, Ce). *Organometallics* **2017**, *36*, 97-108.
25. Schneider, D.; Anwander, R., Pentamethylcyclopentadienyl-Supported Cerocene(III) Complexes. *Eur. J. Inorg.* **2017**, 1180-1188.
26. Summerscales, O. T.; Moore, C. M.; Scott, B. L.; Wilkerson, M. P.; Sutton, A. D., Cerium(III) Carbonate Formation from $\{CeCp^*_2H\}_2$ and Carbon Dioxide: Structure and Mechanistic Insights. *Organometallics* **2017**, *36*, 4682-4685.
27. Gun'ko, Y. K.; Hitchcock, P. B.; Lappert, M. F., Activation of a C=O bond by reaction of a tris(cyclopentadienyl)lanthanide complex with an alkali metal in dimethoxyethane (DME); crystal structures of [Ndη-$C_5H_3(SiMe_3)_2$-1,3(μ-OMe)$_2$Li(DME)] and [{Ce(η-C_5H_3tBu$_2$-1,3)$_2$(μ-OMe)$_2$]. *J. Organomet. Chem.* **1995**, *499*, 213-219.
28. Stults, S. D.; Andersen, R. A.; Zalkin, A., Chemistry of trivalent cerium and uranium metallocenes: reactions with alcohols and thiols. *Organometallics* **1990**, *9*, 1623-1629.
29. Roger, M. A., Therese; Thuéry, Pierre; Ephritikhine, Michel, Experimental Crystal Structure Determination. *CCDC* **2019**.
30. Sutton, A.; Clark, D.; Scott, B.; Gordon, J., Synthesis and Characterization of Cerium(IV) Metallocenes. *Inorganics* **2015**, *3*, 589.
31. Evans, W. J.; Deming, T. J.; Ziller, J. W., The utility of ceric ammonium nitrate-derived alkoxide complexes in the synthesis of organometallic cerium(IV) complexes. Synthesis and first x-ray crystallographic determination of a tetravalent cerium cyclopentadienide complex, $(C_5H_5)_3Ce(OCMe_3)$. *Organometallics* **1989**, *8*, 1581-1583.
32. Sroor, F. M. E., F., *Cerium: Molecular Structure, Technological Applications and Health Effects*. Nova Science Publishers: Hauppage N. Y., 2012.
33. Piro, N. A.; Robinson, J. R.; Walsh, P. J.; Schelter, E. J., The electrochemical behavior of cerium(III/IV) complexes: Thermodynamics, kinetics and applications in synthesis. *Coord. Chem. Rev.* **2014**, *260*, 21-36.
34. So, Y.-M.; Leung, W.-H., Recent advances in the coordination chemistry of cerium(IV) complexes. *Coord. Chem. Rev.* **2017**, *340*, 172-197.
35. Anwander, R.; Dolg, M.; Edelmann, F. T., The difficult search for organocerium(iv) compounds. *Chem. Soc. Rev.* **2017**, *46*, 6697-6709.
36. Hirneise, L.; Langmann, J.; Zitzer, G.; Ude, L.; Maichle-Mössmer, C.; Scherer, W.; Speiser, B.; Anwander, R., Tuning Organocerium Electrochemical Potentials by Extending Tris(cyclopentadienyl) Scaffolds with Terminal Halogenido, Siloxy, and Alkoxy Ligands. *Organometallics* **2021**, *40*, 1786-1800.
37. Bayer, U.; Bock, L.; Maichle-Mössmer, C.; Anwander, R., A Facile Route toward Ceric Silylamide $[Ce\{N(SiHMe_2)_2\}_4]$. *Eur. J. Inorg. Chem.* **2020**, 101-106.
38. Schumann, H.; Glanz, M.; Hemling, H., Metallorganische verbindungen der Lanthanoide: LXXIV. Tris(tetramethylcyclopentadienyl)komplexe der Lanthanoide. *J. Organomet. Chem.* **1993**, *445*, C1-C3.
39. Mueller, T. J.; Ziller, J. W.; Evans, W. J., Sigma bond metathesis with pentamethylcyclopentadienyl ligands in sterically crowded $(C_5Me_5)_3M$ complexes. *Dalton Transactions* **2010**, *39*, 6767-6773.
40. Macomber, D. W.; Rausch, M. D., (η^5-Cyclopentadienyl)-and (η^5-pentamethylcyclopentadienyl) copper compounds containing phosphine, carbonyl, and η^2-acetylenic ligands. *J. Am. Chem. Soc.* **1983**, *105*, 5325-5329.
41. Jutzi, P.; Hielscher, B., Preparation of tin and germanium metallocenes from tetravalent precursors. *Organometallics* **1986**, *5*, 1201-1204.
42. Evans, W. J.; Seibel, C. A.; Ziller, J. W., Unsolvated Lanthanide Metallocene Cations $[(C_5Me_5)_2Ln][BPh_4]$: Multiple Syntheses, Structural Characterization, and Reactivity Including the Formation of $(C_5Me_5)_3Nd$. *J. Am. Chem. Soc.* **1998**, *120*, 6745-6752.
43. Mehdoui, T.; Berthet, J.-C.; Thuéry, P.; Salmon, L.; Rivière, E.; Ephritikhine, M., Lanthanide(III)/Actinide(III) Differentiation in the Cerium and Uranium Complexes $[M(C_5Me_5)_2(L)]^{0,+}$ (L=2,2′-Bipyridine, 2,2′:6′,2″-Terpyridine): Structural, Magnetic, and Reactivity Studies. *Chem. Eur. J.* **2005**, *11*, 6994-7006.
44. Friedrich, J.; Qiao, Y.; Maichle-Mössmer, C.; Schelter, E. J.; Anwander, R., Redox-enhanced hemilability of a tris(tert-butoxy)siloxy ligand at cerium. *Dalton Trans.* **2018**, *47*, 10113-10123.
45. Willauer, A. R.; Palumbo, C. T.; Fadaei-Tirani, F.; Zivkovic, I.; Douair, I.; Maron, L.; Mazzanti, M., Accessing the+ IV Oxidation State in Molecular Complexes of Praseodymium. *J. Am. Chem. Soc.* **2020**, *142*, 5538-5542.
46. Friedrich, J.; Maichle-Mössmer, C.; Schrenk, C.; Schnepf, A.; Anwander, R., Ceric Ammonium Nitrate and Ceric Ammonium Chloride as Precursors for Ceric Siloxides: Ammonia and Ammonium Inclusion. *Eur. J. Inorg. Chem.* **2019**, 79-90.
47. Willauer, A. R.; Palumbo, C. T.; Scopelliti, R.; Zivkovic, I.; Douair, I.; Maron, L.; Mazzanti, M., Stabilization of the Oxidation State +IV in Siloxide-Supported Terbium Compounds. *Angew. Chem. Int. Ed.* **2020**, *59*, 3549-3553.
48. Heeres, H. J.; Meetsma, A.; Teuben, J. H.; Rogers, R. D., Mono(pentamethylcyclopentadienyl) complexes of cerium(III). Synthesis, molecular structure, thermal stability, and reactivity of $(C_5Me_5)CeX_2$ (X = 2,6-di-*tert*-butylphenoxo, $CH(SiMe_3)_2$, and $N(SiMe_3)_2$) complexes. *Organometallics* **1989**, *8*, 2637-2646.

49. Williams, U. J.; Schneider, D.; Dorfner, W. L.; Maichle-Mossmer, C.; Carroll, P. J.; Anwander, R.; Schelter, E. J., Variation of electronic transitions and reduction potentials of cerium(IV) complexes. *Dalton Trans.* **2014**, *43*, 16197-16206.
50. Sinclair, F.; Hlina, J. A.; Wells, J. A. L.; Shaver, M. P.; Arnold, P. L., Ring opening polymerisation of lactide with uranium(IV) and cerium(IV) phosphinoaryloxide complexes. *Dalton Trans.* **2017**, *46*, 10786-10790.
51. Gray, S. J.; Brown, K.; Lam, F. Y. T.; Garden, J. A.; Arnold, P. L., Dinuclear Ce(IV) Aryloxides: Highly Active Catalysts for Anhydride/Epoxide Ring-Opening Copolymerization. *Organometallics* **2021**, *40*, 948-958.
52. Dröse, P.; Crozier, A. R.; Lashkari, S.; Gottfriedsen, J.; Blaurock, S.; Hrib, C. G.; Maichle-Mössmer, C.; Schädle, C.; Anwander, R.; Edelmann, F. T., Facile Access to Tetravalent Cerium Compounds: One-Electron Oxidation Using Iodine(III) Reagents. *J. Am. Chem. Soc.* **2010**, *132*, 14046-14047.
53. Schneider, D.; Harmgarth, N.; Edelmann, F. T.; Anwander, R., Ceric Cyclopentadienides Bearing Alkoxy, Aryloxy, Chlorido, or Iodido Co-Ligands. *Chem. Eur. J.* **2017**, *23*, 12243-12252.
54. Streitwieser, A.; Kinsley, S. A.; Jenson, C. H.; Rigsbee, J. T., Synthesis and Properties of Di-π-[8]annulenecerium(IV), Cerocene. *Organometallics* **2004**, *23*, 5169-5175.
55. Solola, L. A.; Zabula, A. V.; Dorfner, W. L.; Manor, B. C.; Carroll, P. J.; Schelter, E. J., Cerium(IV) Imido Complexes: Structural, Computational, and Reactivity Studies. *J. Am. Chem. Soc.* **2017**, *139*, 2435-2442.
56. Williams, U. J.; Mahoney, B. D.; Lewis, A. J.; DeGregorio, P. T.; Carroll, P. J.; Schelter, E. J., Single Crystal to Single Crystal Transformation and Hydrogen-Atom Transfer upon Oxidation of a Cerium Coordination Compound. *Inorg. Chem.* **2013**, *52*, 4142-4144.
57. Halbach, R. L.; Nocton, G.; Booth, C. H.; Maron, L.; Andersen, R. A., Cerium Tetrakis(tropolonate) and Cerium Tetrakis(acetylacetonate) Are Not Diamagnetic but Temperature-Independent Paramagnets. *Inorg. Chem.* **2018**, *57*, 7290-7298.
58. Booth, C. H.; Walter, M. D.; Daniel, M.; Lukens, W. W.; Andersen, R. A., Self-Contained Kondo Effect in Single Molecules. *Phys. Rev. Lett.* **2005**, *95*, 267202.
59. M., S., Über die Einwirkung von Alkali auf Äthylalkohol und die "Stickoxyd-Reaktion" von Wilhelm Traube. *Ber. Dtsch. Chem. Ges.* **1924**, *57*, 1611-1615.
60. Lochmann, L.; Coupek, J.; Lim, D., Preparation of some alkoxides of alkali metals. *Collect. Czech. Chem. Commun.* **1970**, *35*, 733-736.
61. Boyle, T. J.; Alam, T. M.; Tafoya, C. J.; Mechenbier, E. R.; Ziller, J. W., Syntheses, Characterizations, and X-ray Structures of Alkali Metal Derivatives of Titanium(IV) Neopentoxides. *Inorg. Chem.* **1999**, *38*, 2422-2428.
62. D'Alfonso, G.; Dragonetti, C.; Galli, S.; Lucenti, E.; Macchi, P.; Roberto, D.; Ugo, R., Surface organometallic chemistry — Carbonyl complexes of Re(I) with silanolates as models of silica anchored rhenium carbonyl species. *Can. J. Chem.* **2005**, *83*, 1017-1024.
63. Hyde, J. F.; Johannson, O. K.; Daudt, W. H.; Fleming, R. F.; Laudenslager, H. B.; Roche, M. P., Sodium and Potassium Salts of Triorganosilanols. *J. Am. Chem. Soc.* **1953**, *75*, 5615-5618.
64. Thomson, R. K.; Scott, B. L.; Morris, D. E.; Kiplinger, J. L., Synthesis, structure, spectroscopy and redox energetics of a series of uranium(IV) mixed-ligand metallocene complexes. *C. R. Chim.* **2010,** *13*, 790-802.
65. Min, E. Y. J.; Bercaw, J. E.; Chen, S.; Xue, Z.-L., Bis(η^5-pentamethylcyclopentadienyl) complexes of niobium and tantalum. *Inorg. Synth.* **2014**, *36*, 52-57.
66. Robbins, J. L.; Edelstein, N. M.; Cooper, S. R.; Smart, J. C., Syntheses and electronic structures of decamethylmanganocenes. *J. Am. Chem. Soc.* **1979**, *101*, 3853-3857.
67. Coan, P. S.; Streib, W. E.; Caulton, K. G., A triangular heterometallic siloxide containing barium. *Inorg. Chem.* **1991,** *30*, 5019-5023.
68. See, X. Y.; Beaumier, E. P.; Davis-Gilbert, Z. W.; Dunn, P. L.; Larsen, J. A.; Pearce, A. J.; Wheeler, T. A.; Tonks, I. A., Generation of TiII Alkyne Trimerization Catalysts in the Absence of Strong Metal Reductants. *Organometallics* **2017**, *36*, 1383-1390.

Supporting Information

PENTAMETHYLCYCLOPENTADIENYL COMPLEXES of CERIUM(IV): SYNTHESIS, REACTIVITY, and ELECTROCHEMISTRY

Lars Hirneise, Cäcilia Maichle-Mössmer, and Reiner Anwander*

Institut für Anorganische Chemie, Eberhard Karls Universität Tübingen, Auf der Morgenstelle 18, 72076 Tübingen, Germany

* to whom correspondence should be addressed: E-Mail reiner.anwander@uni-tuebingen.de

Table of Contents

Magnetic Measurements (Evan's method)

Table S1. Data from Magnetic Measurements of Compounds 2^{Et}, 3^{tBu}, and 7 (Evans' method)

Compound	X_{mass} [10^{-7} cm^3 kg^{-1}]	X_{mol} [10^{-4} cm^3 mol^{-1}]	X_{para} [10^{-4} cm^3 mol^{-1}]	μ_{eff} [μ_B]
2^{CH2tBu}	18.7	10.9	10.4	1.58
3^{tBu}	7.87	3.89	3.34	0.90
7	3.81	1.95	1.40	0.58

NMR spectra

* → solvent, # → small impurities

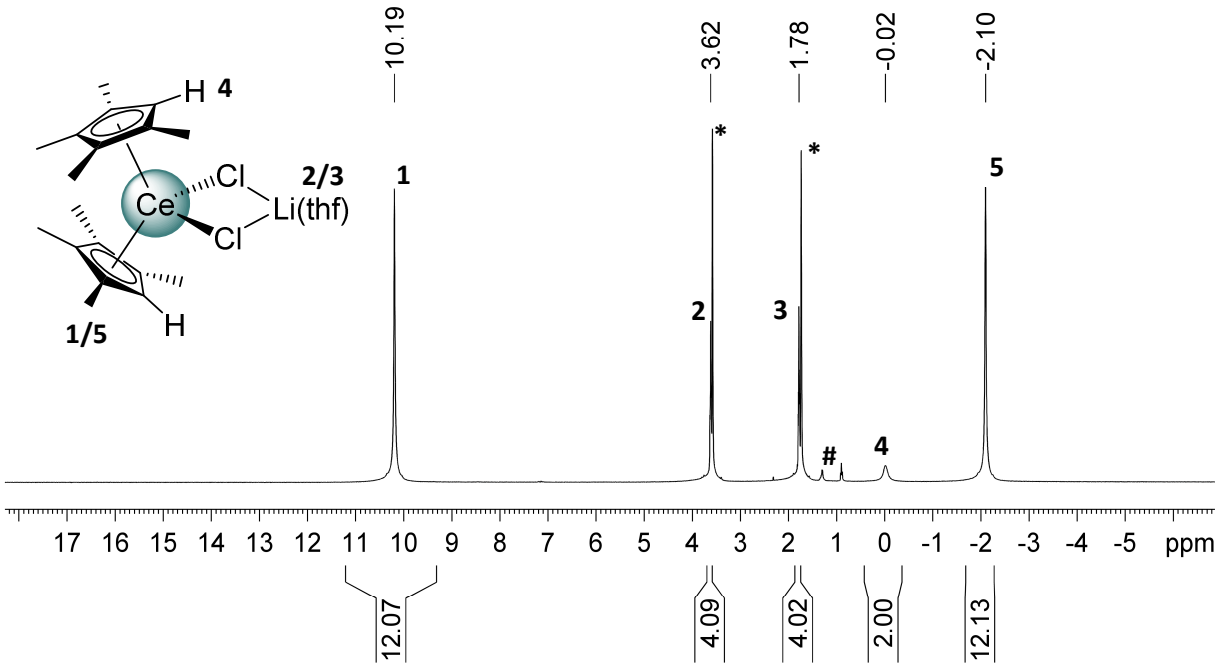

Figure S1. ^1H NMR spectrum (400.1 MHz, thf-*d*8, 26 °C) of **1^{tet}**.

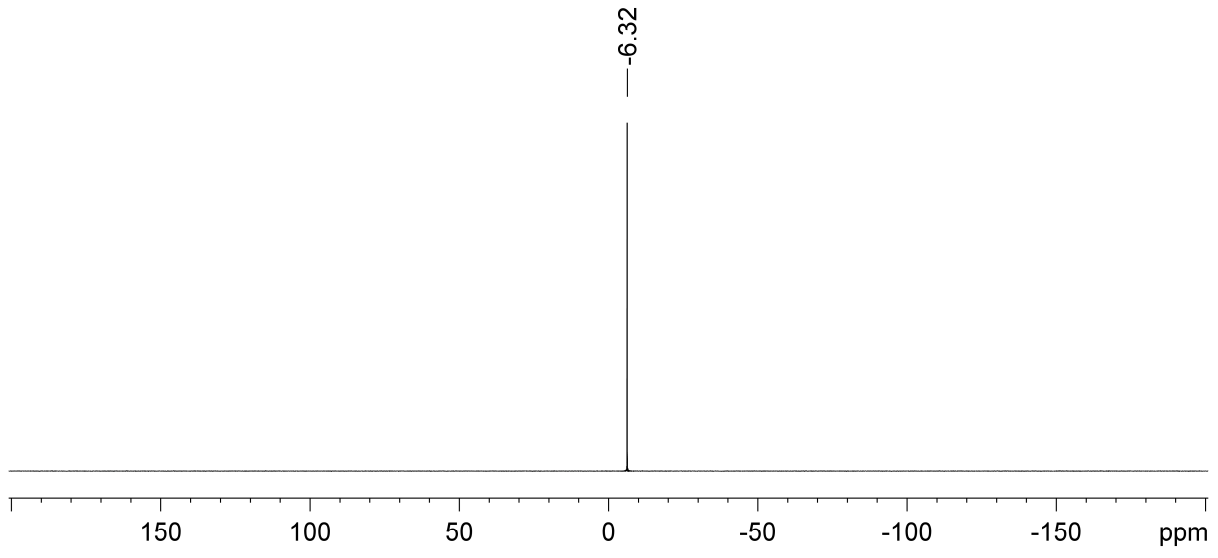

Figure S2. ^7Li-{^1H} NMR spectrum (116.6 MHz, thf-*d*8, 26 °C) of **1^{tet}**.

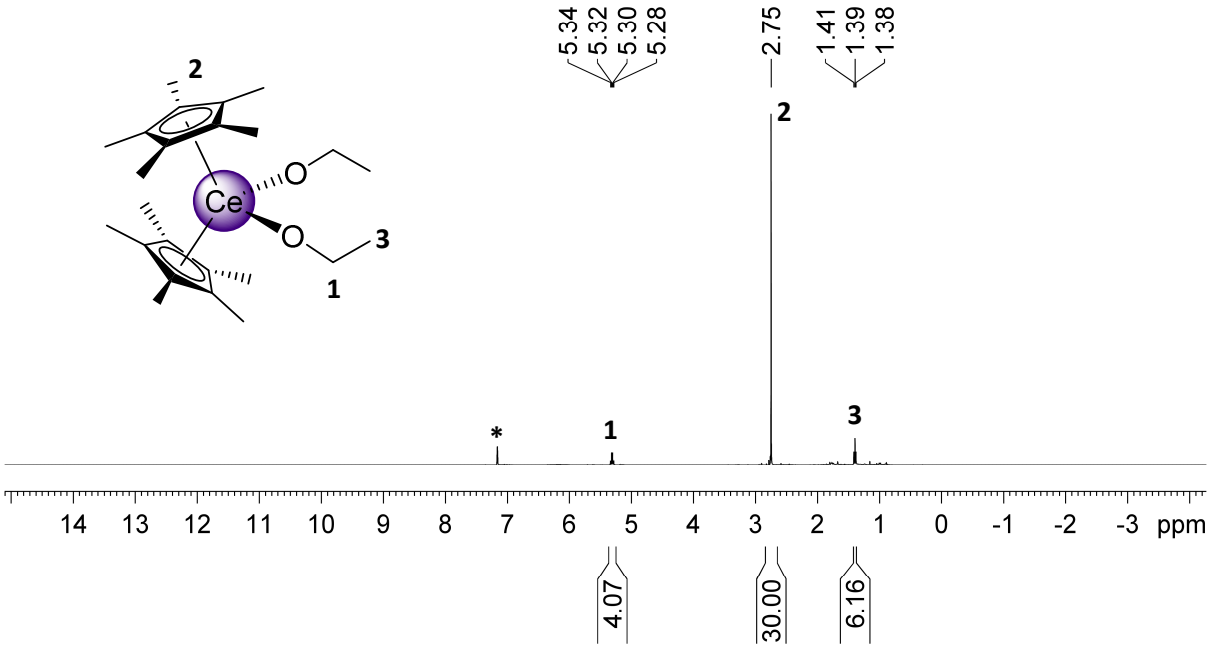

Figure S3. ^{1}H NMR spectrum (400.1 MHz, C_6D_6, 26 °C) of **2^{Et}**.

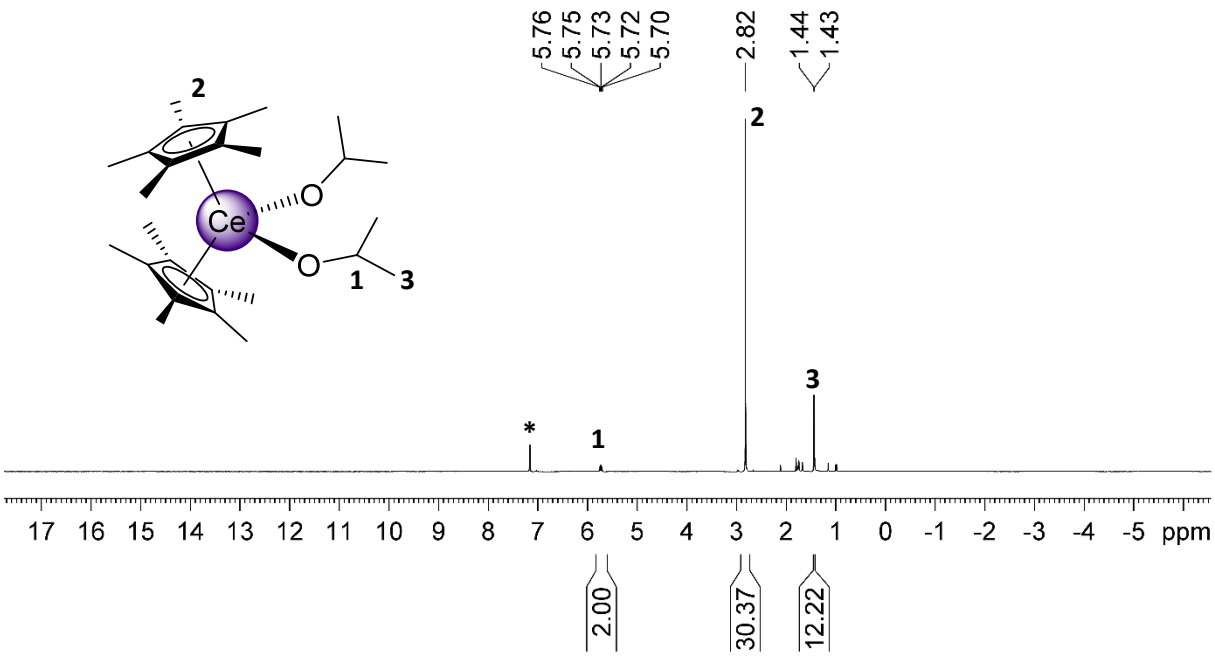

Figure S4. ^{1}H NMR spectrum (400.1 MHz, C_6D_6, 26 °C) of **2^{iPr}**.

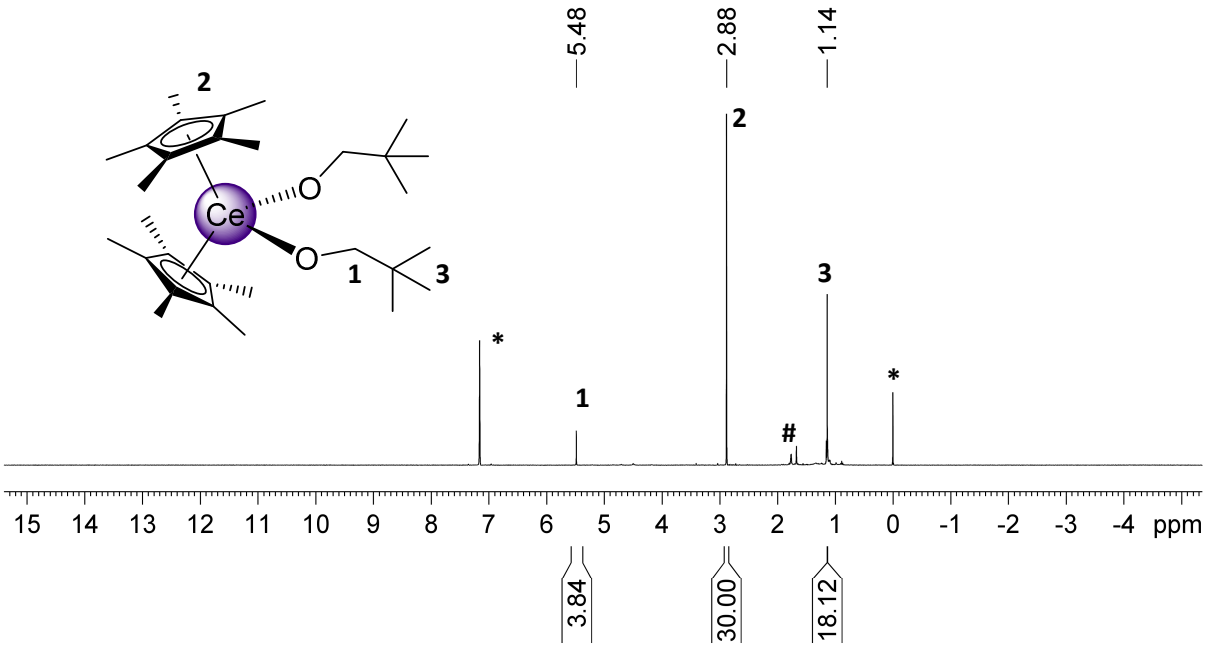

Figure S5. ^{1}H NMR spectrum (400.1 MHz, C_6D_6, 26 °C) of $\mathbf{2}^{\mathbf{CH2}t\mathbf{Bu}}$.

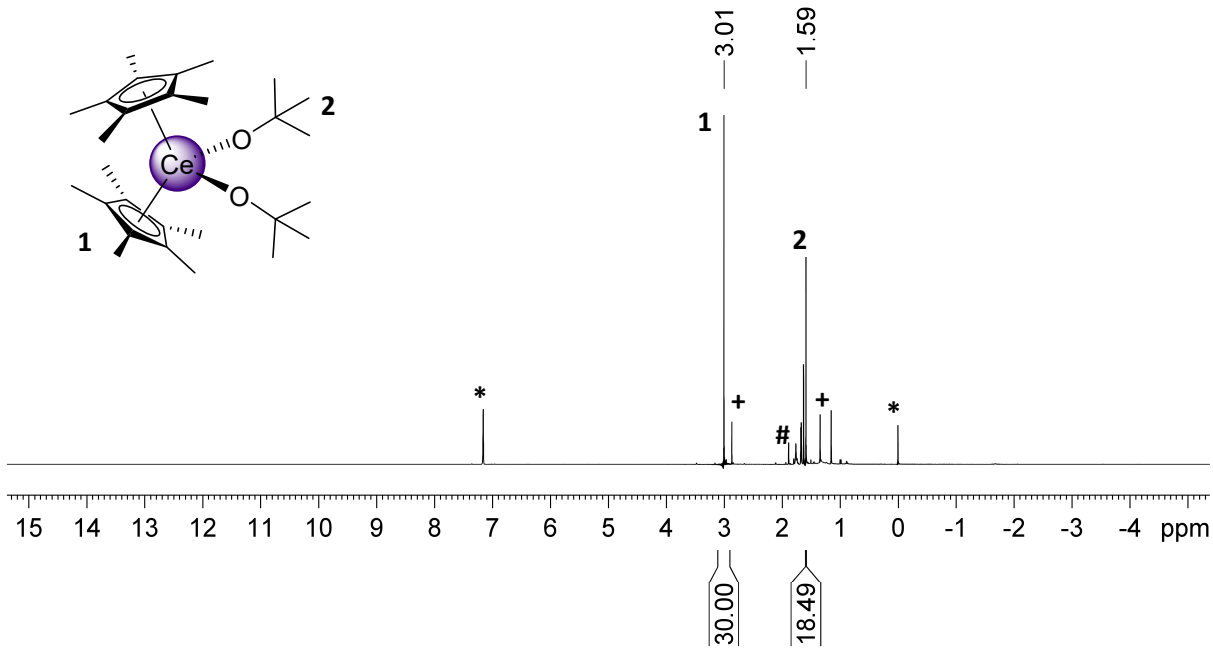

Figure S6. ^{1}H NMR spectrum (400.1 MHz, C_6D_6, 26 °C) of $\mathbf{2}^{t\mathbf{Bu}}$, impurities of $\mathbf{3}^{t\mathbf{Bu}}$ (+) and $SiMe_4$ visible.

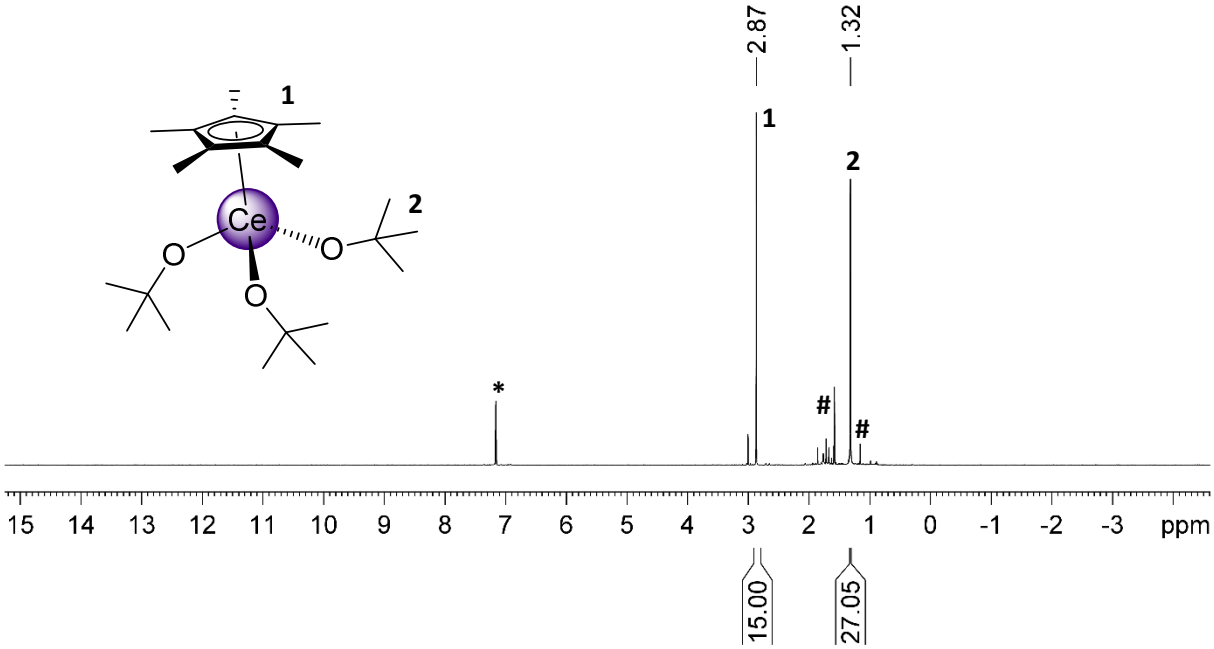

Figure S7. ^{1}H NMR spectrum (400.1 MHz, C_6D_6, 26 °C) of **3**$^{t\mathrm{Bu}}$.

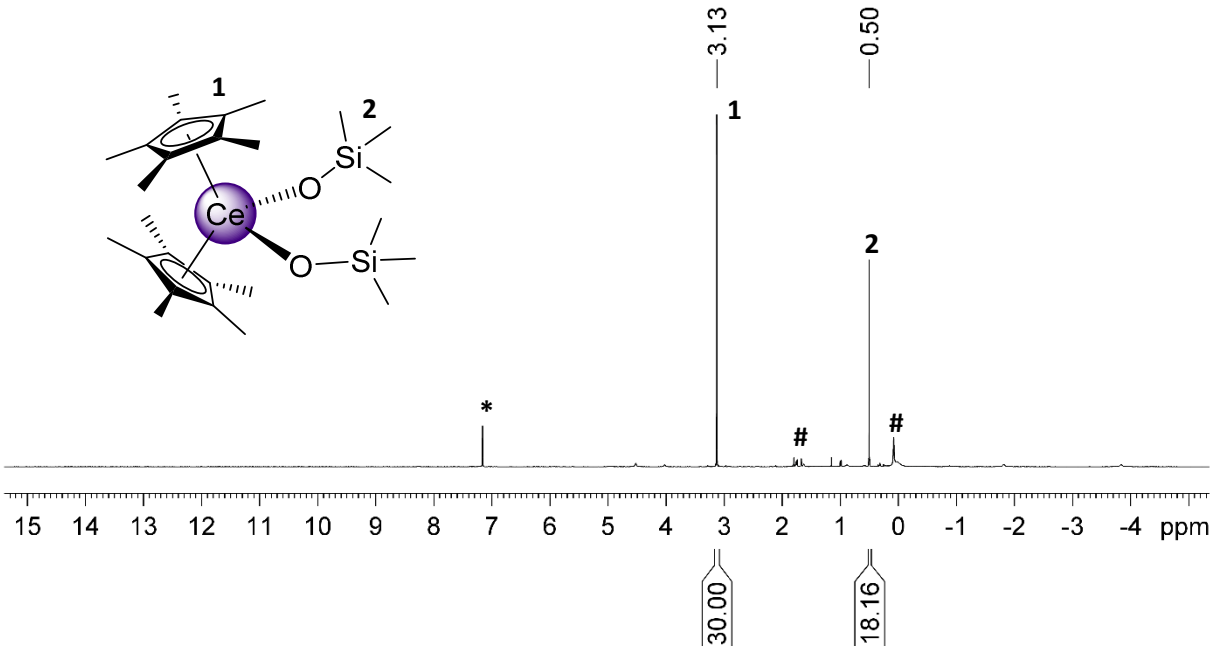

Figure S8. ^{1}H NMR spectrum (400.1 MHz, C_6D_6, 26 °C) of **4**$^{\mathrm{Me}}$.

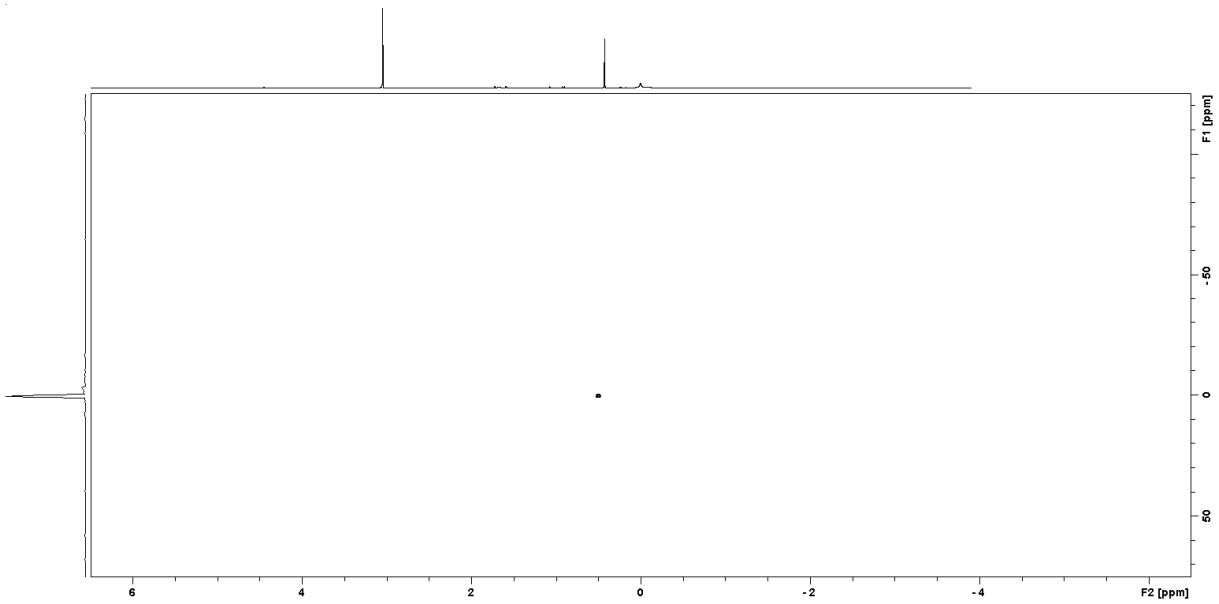

Figure S9. ^{1}H-^{29}Si HSQC NMR spectrum (79.5 MHz, C_6D_6, 26 °C) of $\mathbf{4^{Me}}$.

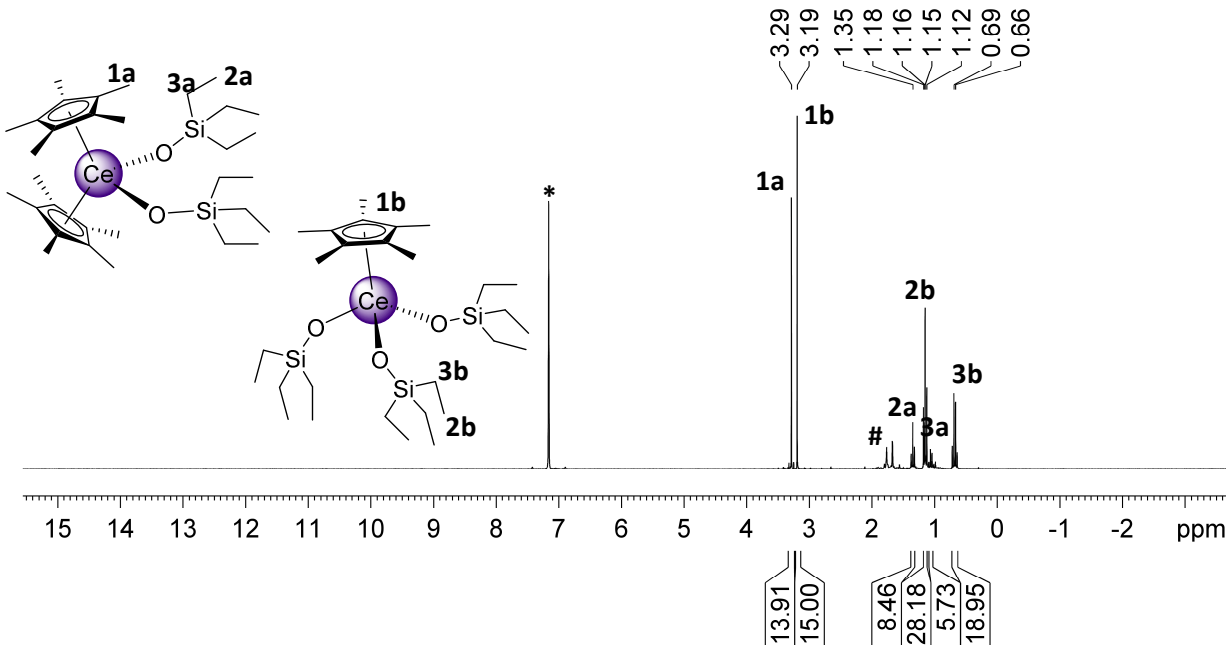

Figure S10. ^{1}H NMR spectrum (400.1 MHz, C_6D_6, 26 °C) of a mixture of $\mathbf{4^{Et}}$ and $\mathbf{5^{Et}}$.

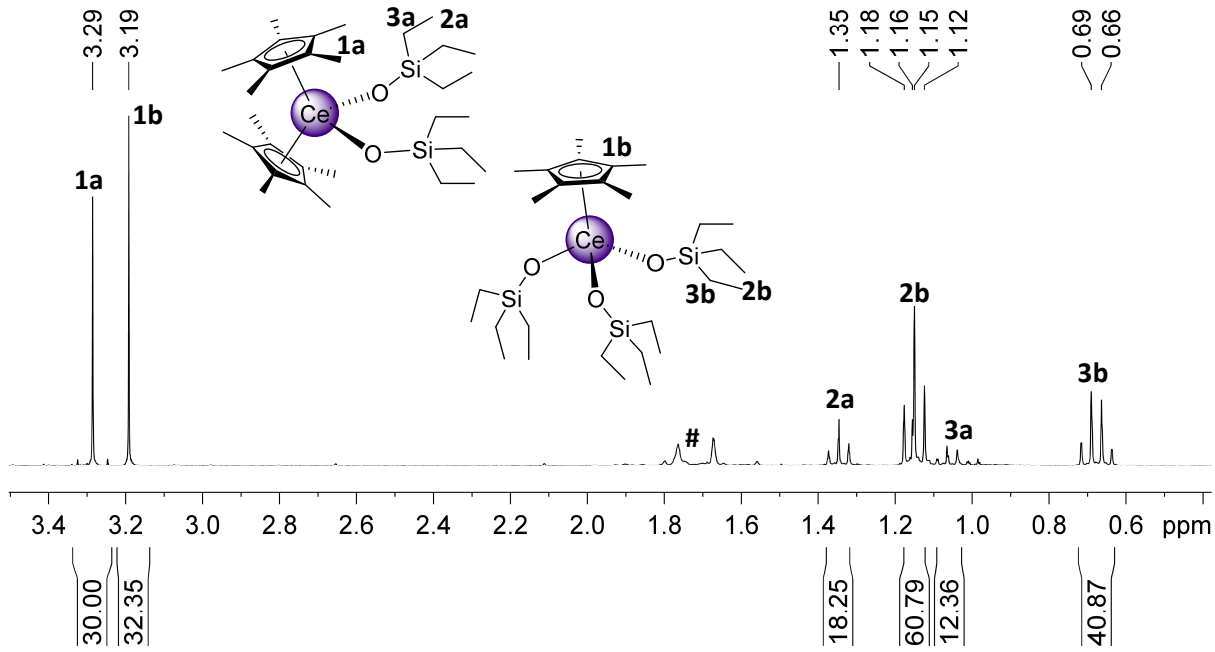

Figure S11. Section of ^{1}H NMR spectrum (400.1 MHz, C_6D_6, 26 °C) of a mixture of **4^{Et}** and **5^{Et}**.

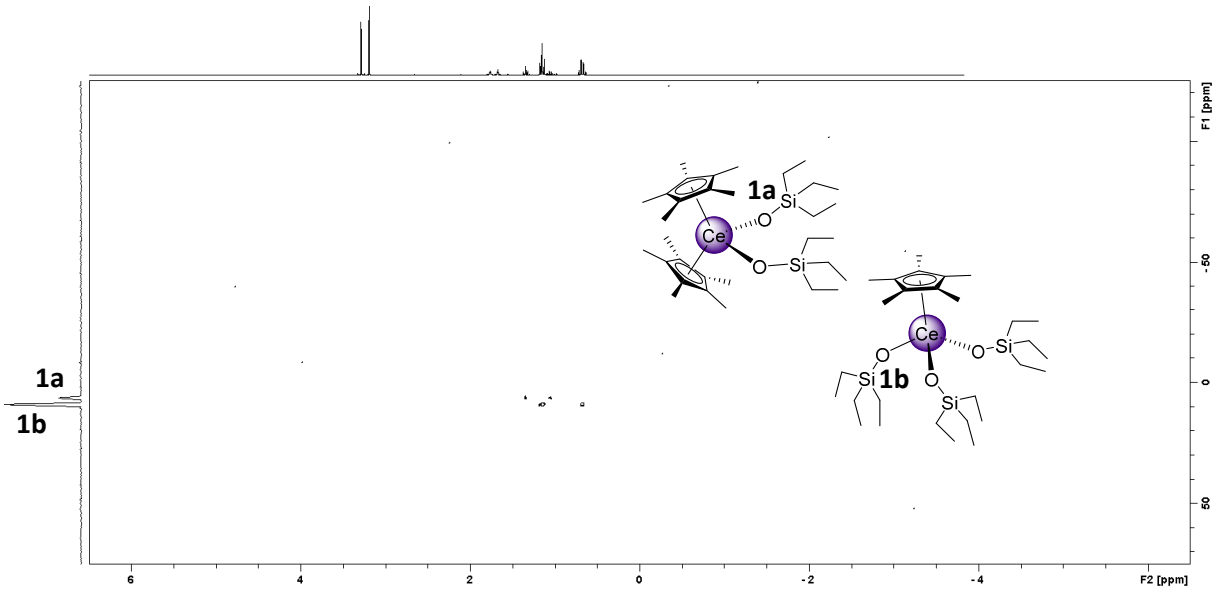

Figure S12. ^{1}H-^{29}Si HSQC NMR spectrum (79.5 MHz, C_6D_6, 26 °C) of a mixture of **4^{Et}** and **5^{Et}**.

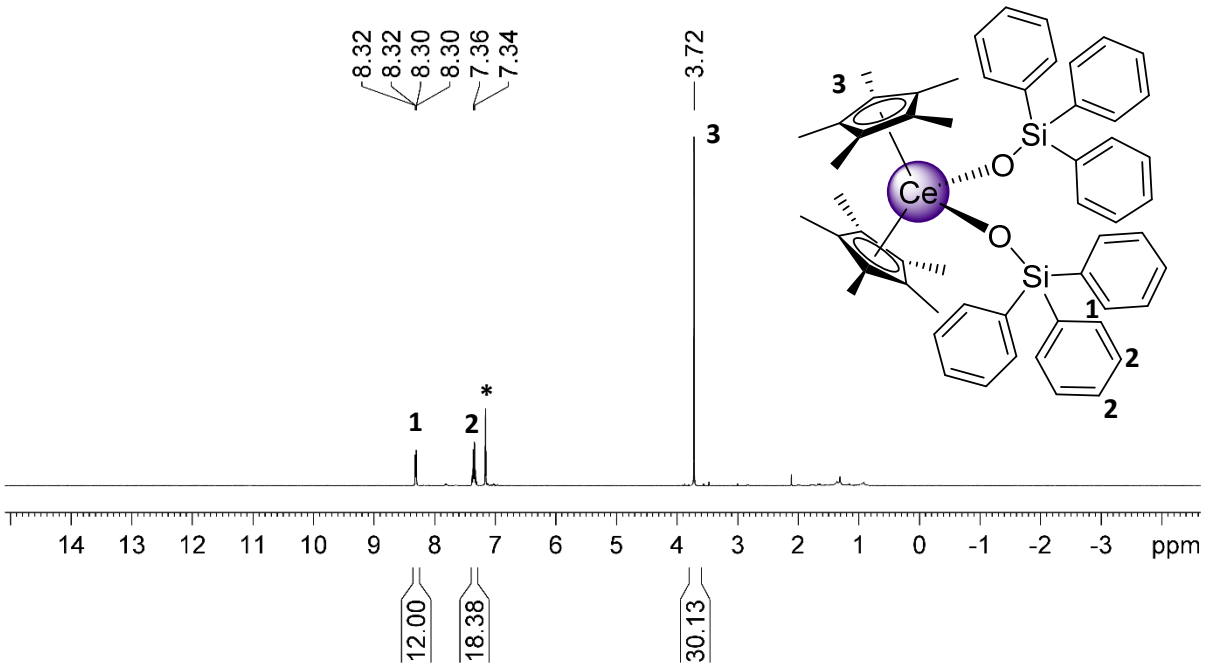

Figure S13. ^{1}H NMR spectrum (400.1 MHz, C_6D_6, 26 °C) of **4^{Ph}**.

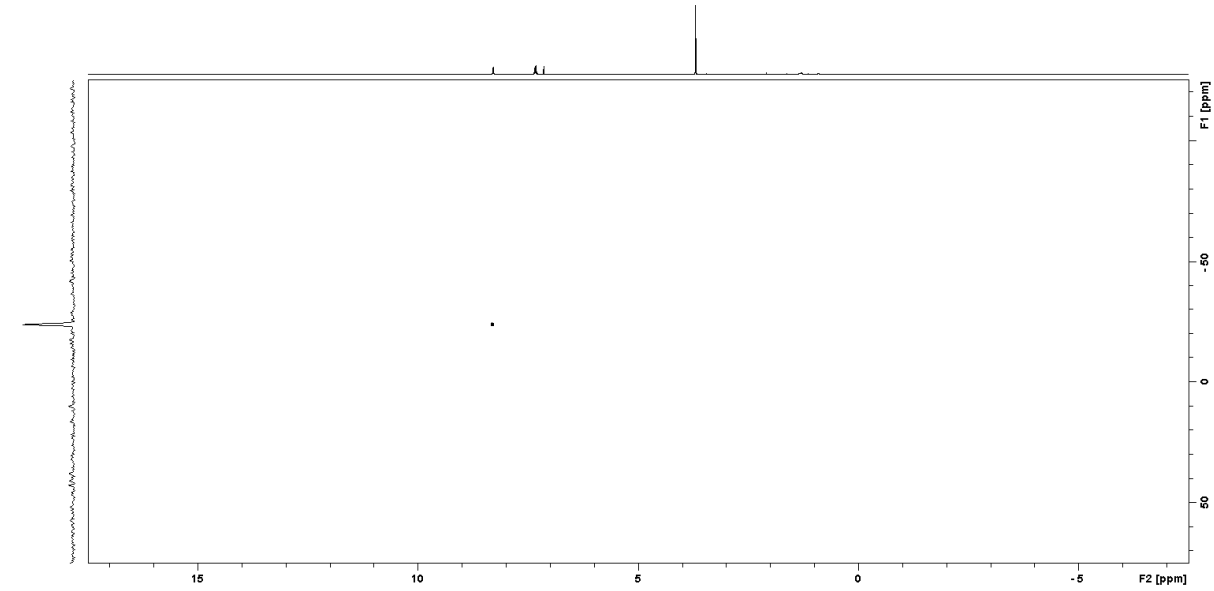

Figure S14. ^{1}H-^{29}Si HSQC NMR spectrum (79.5 MHz, C_6D_6, 26 °C) of **4^{Ph}**.

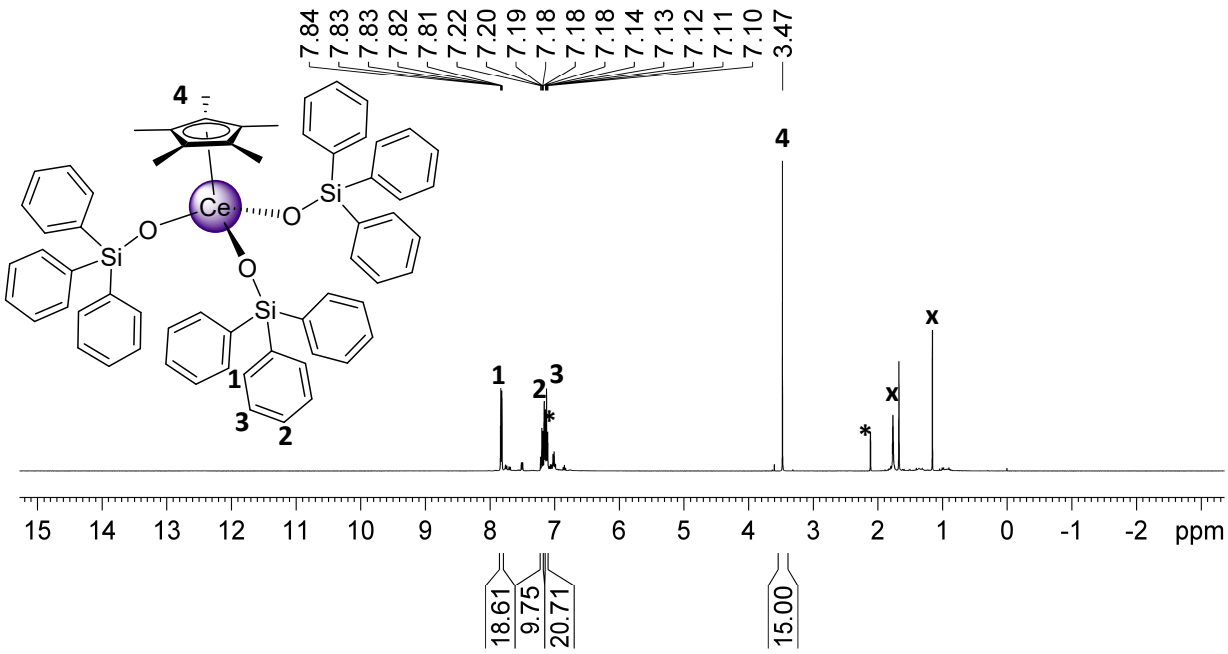

Figure S15. ^{1}H NMR spectrum (400.1 MHz, C_6D_6, 26 °C) of a mixture of **5^{Ph}**, with impurities of Cp*−Cp* (^{x}).

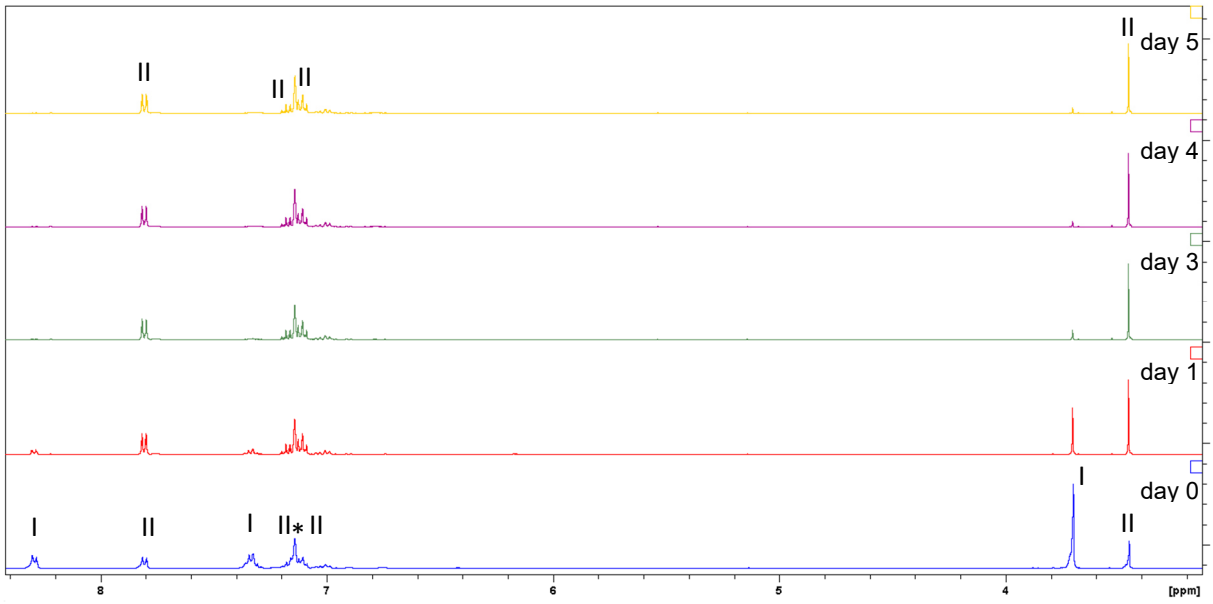

Figure S16. ^{1}H NMR spectra (400.1 MHz, C_6D_6, 26 °C) at 1 – 5 days of a reaction mixture of **4^{Ph}** (I) and **5^{Ph}** (II) at ambient light and temperature.

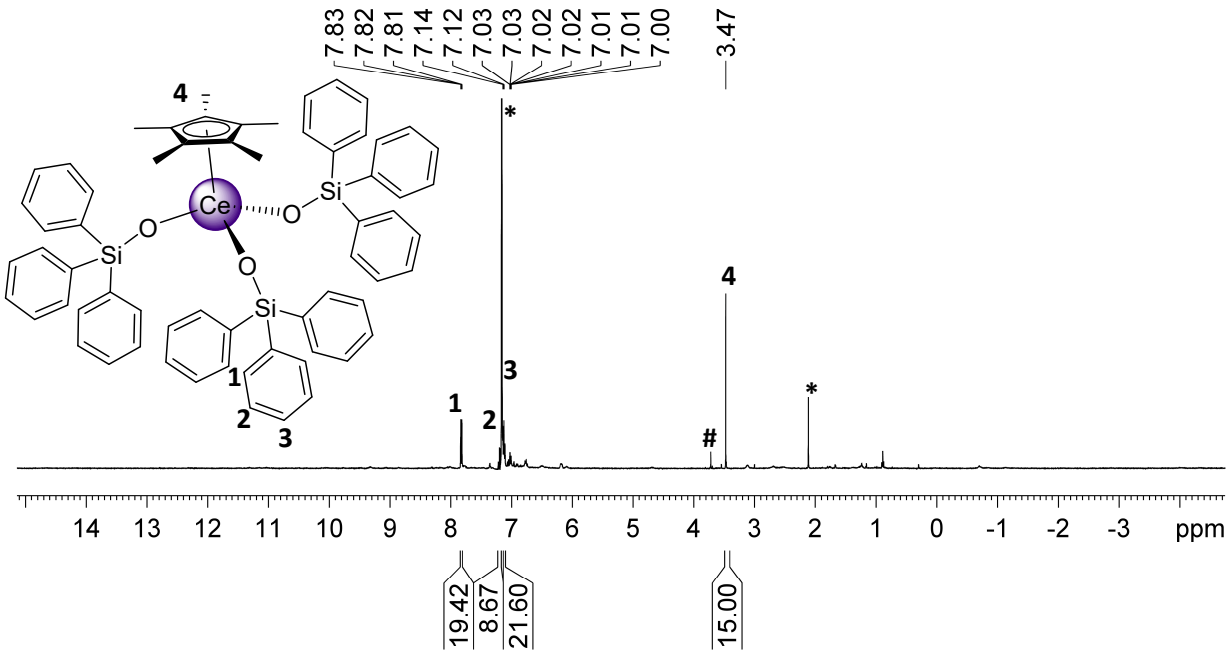

Figure S17. ^{1}H NMR spectrum (400.1 MHz, C_6D_6, 26 °C) of **5^{Ph}**, with minor **4^{Ph}** (#) impurities.

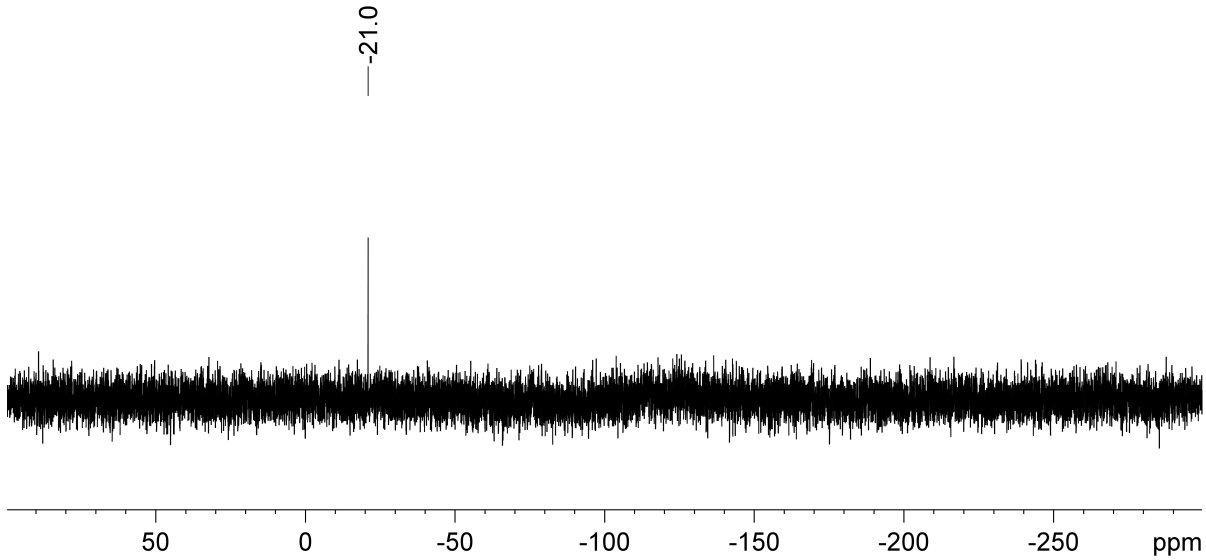

Figure S18. ^{29}Si{^{1}H} NMR spectrum (79.5 MHz, C_6D_6, 26 °C) of **5^{Ph}**.

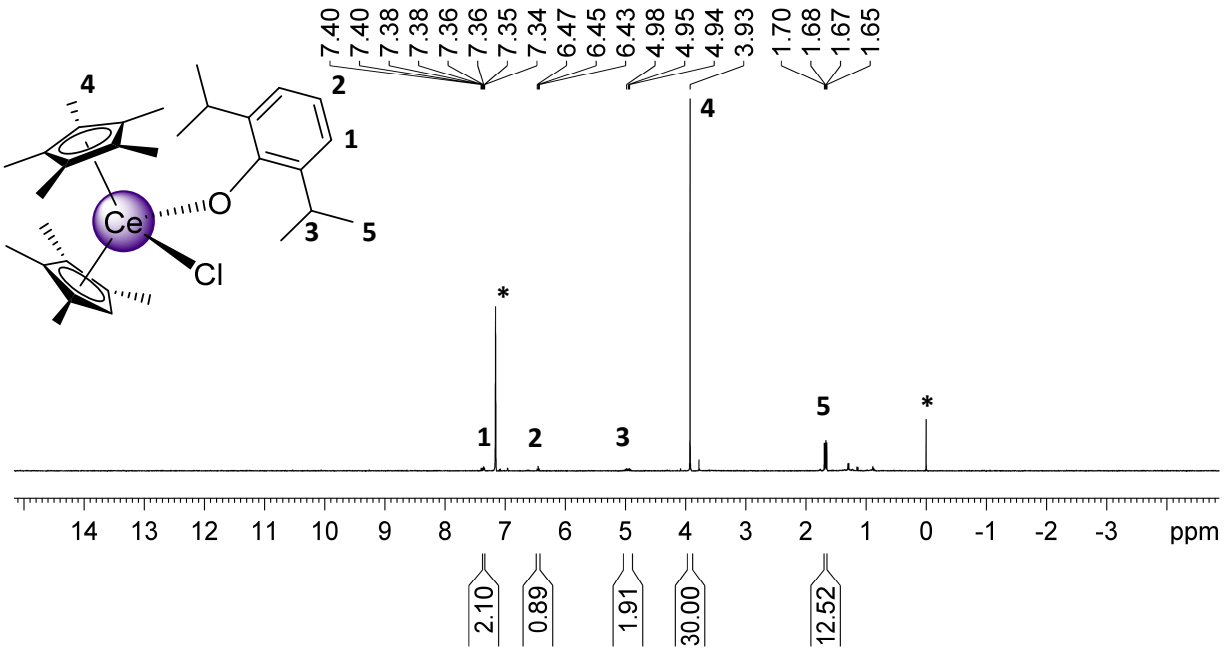

Figure S19. ^{1}H NMR spectrum (400.1 MHz, C_6D_6, 26 °C) of **6**.

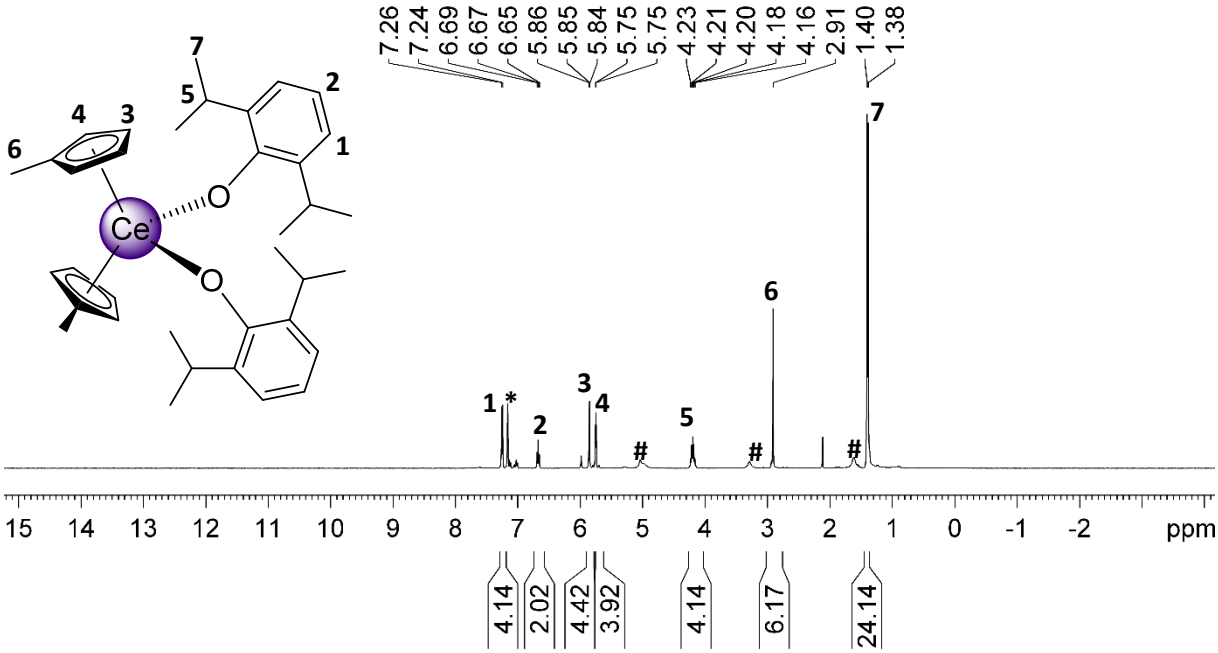

Figure S20. ^{1}H NMR spectrum (400.1 MHz, C_6D_6, 26 °C) of **7**, with minor cerium(III) impurities (#).

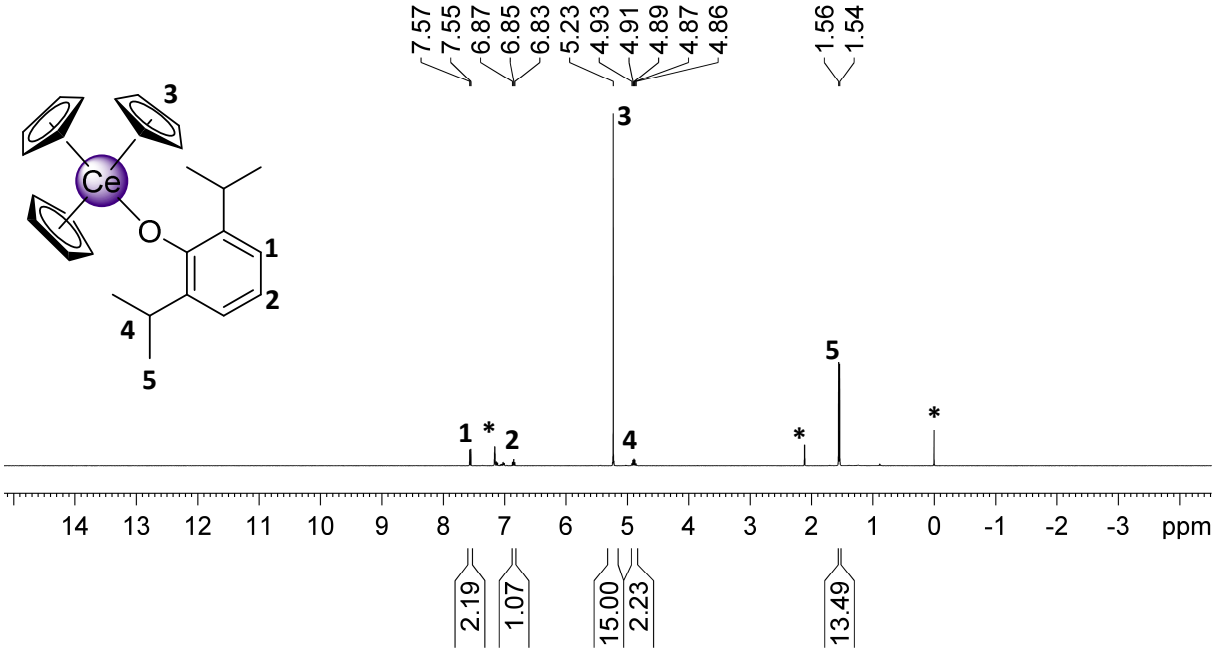

Figure S21. ^{1}H NMR spectrum (400.1 MHz, C_6D_6, 26 °C) of **8**.

Solid-State Structures

Crystals for X-ray crystallography were grown using saturated solutions of tetramethylsilane (**2**^{Et}, **2**^{tBu}, **4**^{Ph}**, 6**), THF (**1**^{tet}), and toluene (**8**). Suitable crystals for X-Ray analysis were handpicked in a glovebox, coated with Parabar 10312 and stored on microscope slides. Data collection was done on a *Bruker* APEX II Duo diffractometer by using QUAZAR optics and Mo K_α (λ = 0.71073 Å). The data collection strategy was determined using COSMO[1] employing ω scans. Raw data were processed by APEX[2] and SAINT,[3] corrections for absorption effects were applied using SADABS.[4] The structures were solved by direct methods and refined against all data by full-matrix least-squares methods on F^2 using SHELXTL[5] and SHELXLE.[6] Disorder models for **1**^{tet}, **2**^{tBu} and **6** are calculated using DSR,[7] a program included in ShelXle, for refining disorder. Plots were generated by using CCDC Mercury 3.19.1.[8] Further details regarding the refinement and crystallographic data are listed in Table S2 and in the CIF files. The crystal quality of compound **8** was of minor quality. Restraints (SIMU/RIGU) were necessary to refine the structure.

[1] COSMO, v. 1.61; Bruker AXS Inc., Madison, WI, 2012.

[2] APEX 3 V. 2017.3-0, Bruker AXS Inc., Madison, WI, 2017.

[3] *SAINT v. 8.38A,* Bruker AXS Inc., Madison, WI, 2017.

[4] L Krause, L.; Herbst-Irmer, R.; Sheldrick, G. M.; Stalke, D. Comparison of silver and molybdenum microfocus X-ray sources for single-crystal structure determination. *J. Appl. Cryst.* **2015**, *48*, 3-10.

[5] G Sheldrick, G. M. SHELXTL – Integrated space-group and crystal-structure determination. *Acta Cryst.* **2015**, *A71*, 3–8.

[6] Hübschle, C. B.; Sheldrick, G. M.; Dittrich, B. ShelXle: a Qt graphical user interface for SHELXL. *J. Appl. Cryst.* **2011**, *44*, 1281-1284.

[7] Kratzert, D.; Holstein, J. J.; Krossing, I. DSR: enhanced modelling and refinement of disordered structures with SHELXL. *J. Appl. Cryst.* **2015,** *48,* 933-938.

[8] C. F. Macrae, I. J. Bruno, J. A. Chisholm, P. R. Edgington, P. McCabe, E. Pidcock, L. Rodriguez-Monge, R.Taylor, J. van de Streek, P. A. Wood, J. Appl. Cryst. 2008, 41, 466-470.

Table S2. Collection of Crystallographic Data of 1^{tet}, 2^{Et}, 2^{tBu}, 4^{Ph}, 6, and 8

	$\mathbf{1^{tet}}$	$\mathbf{2^{Et}}$	$\mathbf{2^{tBu}}$	$\mathbf{4^{Ph}}$	**6**	**8**
CCDC	2108590	2108592	2108593	2108594	2108591	2108589
formula	$C_{52}H_{84}Ce_2Cl_4Li_2O_4$	$C_{24}H_{40}CeO_2$	$C_{28}H_{48}CeO_2$	$C_{56}H_{60}CeO_2Si_2$	$C_{32}H_{47}CeOCl$	$C_{27}H_{32}CeO$ •0.6 (C_7H_8)
M [$\mathbf{g \cdot mol^{-1}}$]	1209.11	500.68	556.78	961.34	623.26	574.07
$\boldsymbol{\lambda}$ [Å]	0.71073	0.71073	0.71073	0.71073	0.71073	0.71073
cell	monoclinic	monoclinic	monoclinic	orthorhombic	orthorhombic	monoclinic
space group	$P2_1/c$	$P2_1/c$	$P2_1/c$	Pbcn	$Pca2_1$	Pn
a [Å]	13.1468(19)	10.638(2)	19.315(3)	17.266(4)	19.799(4)	14.6171(9)
b [Å]	15.448(2)	16.025(4)	18.033(3)	16.545(4)	16.256(3)	11.4440(7)
c [Å]	15.030(2)	14.169(3)	17.845(3)	16.941(4)	18.719(3)	24.1214(14)
α [°]	90	90	90	90	90	90
β [°]	113.981(2)	92.579(4)	117.51	90	90	91.001(1)
γ [°]	90	90	90	90	90	90
V [$Å^3$]	2788.9(7)	2413.1(9)	5512.4(13)	4840(2)	6024.5(19)	4034.4(4)
Z	2	4	8	4	8	6
F(000)	1236	1032	2320	1992	2576	1760
T [K]	173(2)	100(2)	100(2)	100(2)	100(2)	100(2)
ρ_{calcd} [$\mathbf{g \cdot mol^3}$]	1.440	1.378	1.342	1.319	1.374	1.418
μ [mm^{-1}]	1.843	1.901	1.671	1.030	1.621	1.713
R_1[a] ($I>2\sigma(I)$)	0.0356	0.0383	0.0284	0.0306	0.0615	0.0409
ωR_2 (all data) [a]	0.0819	0.0934	0.0686	0.0763	0.1385	0.0793
Goodness of fit	1.020	1.019	1.067	1.112	1.009	0.996

[a] $R1 = \Sigma(||F_0|-|F_c||)/\Sigma|F_0|, F_0 > 4\sigma(F_0)$. $wR2 = \{\Sigma[w(F_0^2-F_c^2)^2/\Sigma[w(F_0^2)^2]\}^{1/2}$.

Electrochemical Studies /Cyclovoltammetric Data

[BARF] = [$B(C_6H_3(CF_3)_2$-3,5)$_4$]

Table S3. Electrochemical data for the redox couple of complex **1*** vs Fc/Fc^+ in THF

Scan speed	E_{pa} vs Fc/Fc^+ [V]	E_{pc} vs Fc/Fc^+ [V]	E^0 vs Fc/Fc^+ [V]	ΔE [V]	i_{pc}/i_{pa}
50 mV/s	-0.567	-	-	-	-
100 mV/s	-0.556	-	-	-	-
250 mV/s	-0.536	-	-	-	-
500 mV/s	-0.508	-	-	-	-
1000 mV/s	-0.473	-	-	-	-
2000 mV/s	-0.432	-	-	-	-

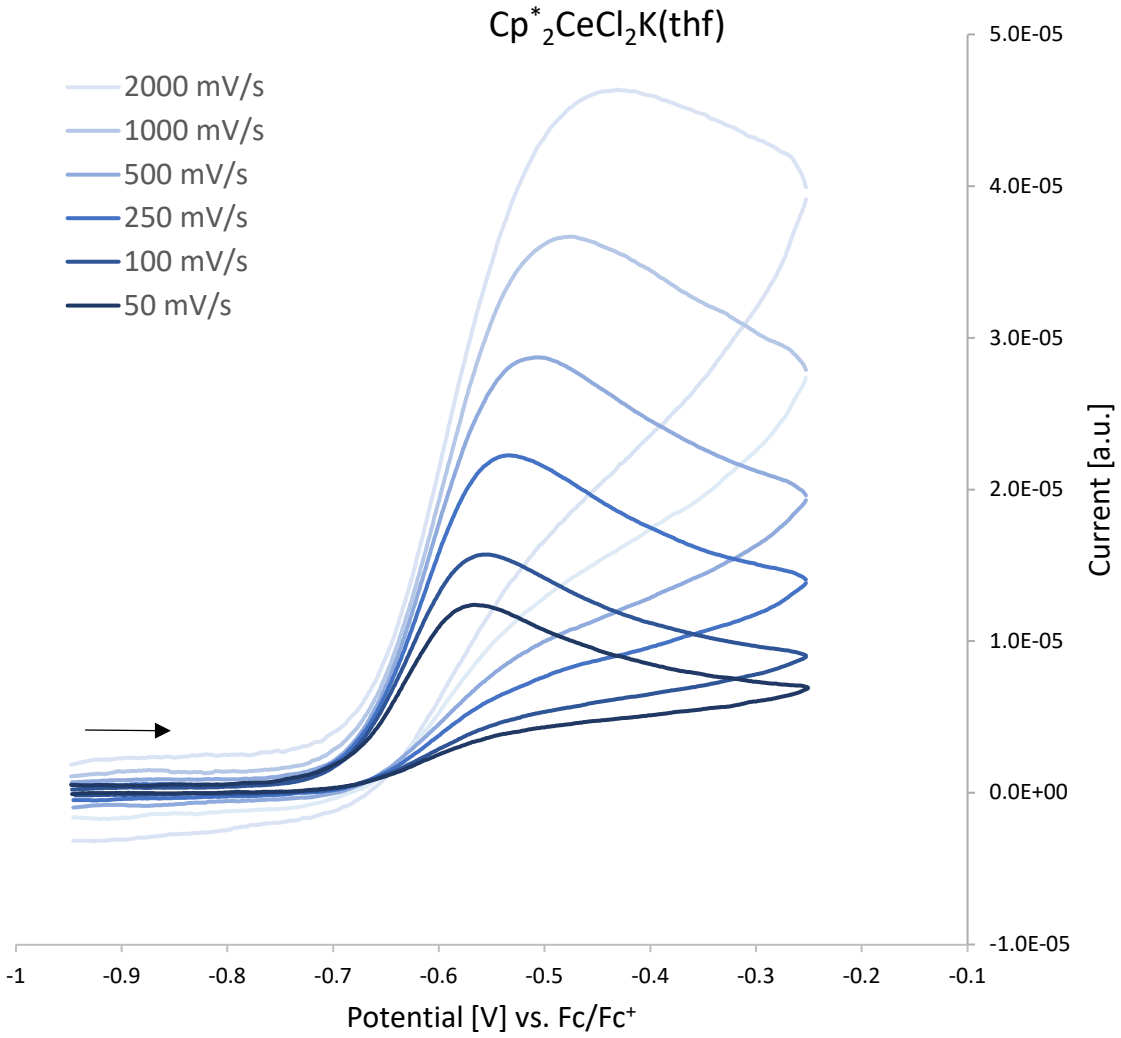

Figure S22. Isolated cerium(III/IV) redox couple of **1*** vs Fc/Fc^+ in THF obtained at different scan rates; arrow indicates the scan direction; *c*(analyte) 1 mM, *c*(electrolyte) 0.1 M [*n*Pr_4N][BARF].

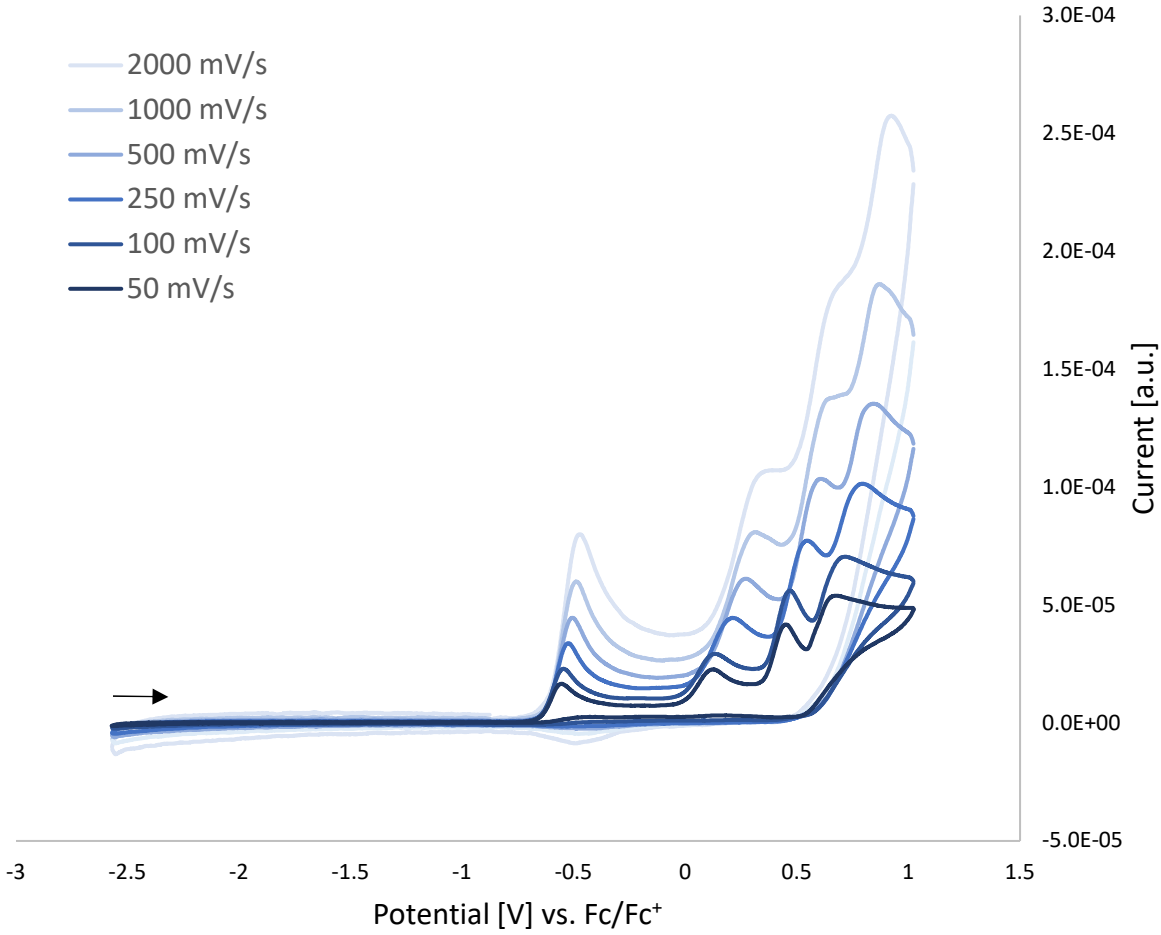

Figure S23. Cyclic voltammogram of **1*** vs Fc/Fc^+ in THF obtained at different scan rates; arrow indicates the scan direction; *c*(analyte) 1 mM, *c*(electrolyte) 0.1 M [*n*Pr_4N][BARF].

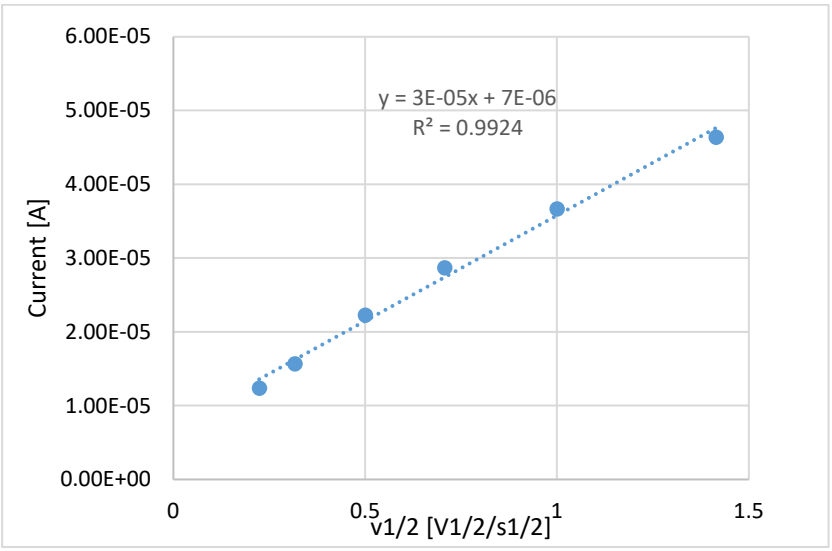

Figure S24. I_p versus $v^{1/2}$ plot of the anodic (blue) redox features of **1***.

Table S4. Electrochemical data for the redox couple of complex **1**^{tet} vs Fc/Fc^+ in THF

Scan speed	E_{pa} vs Fc/Fc^+ [V]	E_{pc} vs Fc/Fc^+ [V]	E^0 vs Fc/Fc^+ [V]	ΔE [V]	i_{pc}/i_{pa}
50 mV/s	-0.542	-	-	-	-
100 mV/s	-0.534	-	-	-	-
250 mV/s	-0.531	-	-	-	-
500 mV/s	-0.521	-	-	-	-
1000 mV/s	-0.516	-0.641	-0.516	0.125	0.42
2000 mV/s	-0.509	-0.612	-0.509	0.103	0.49
2500 mV/s	-0.511	-0.601	-0.511	0.090	0.51

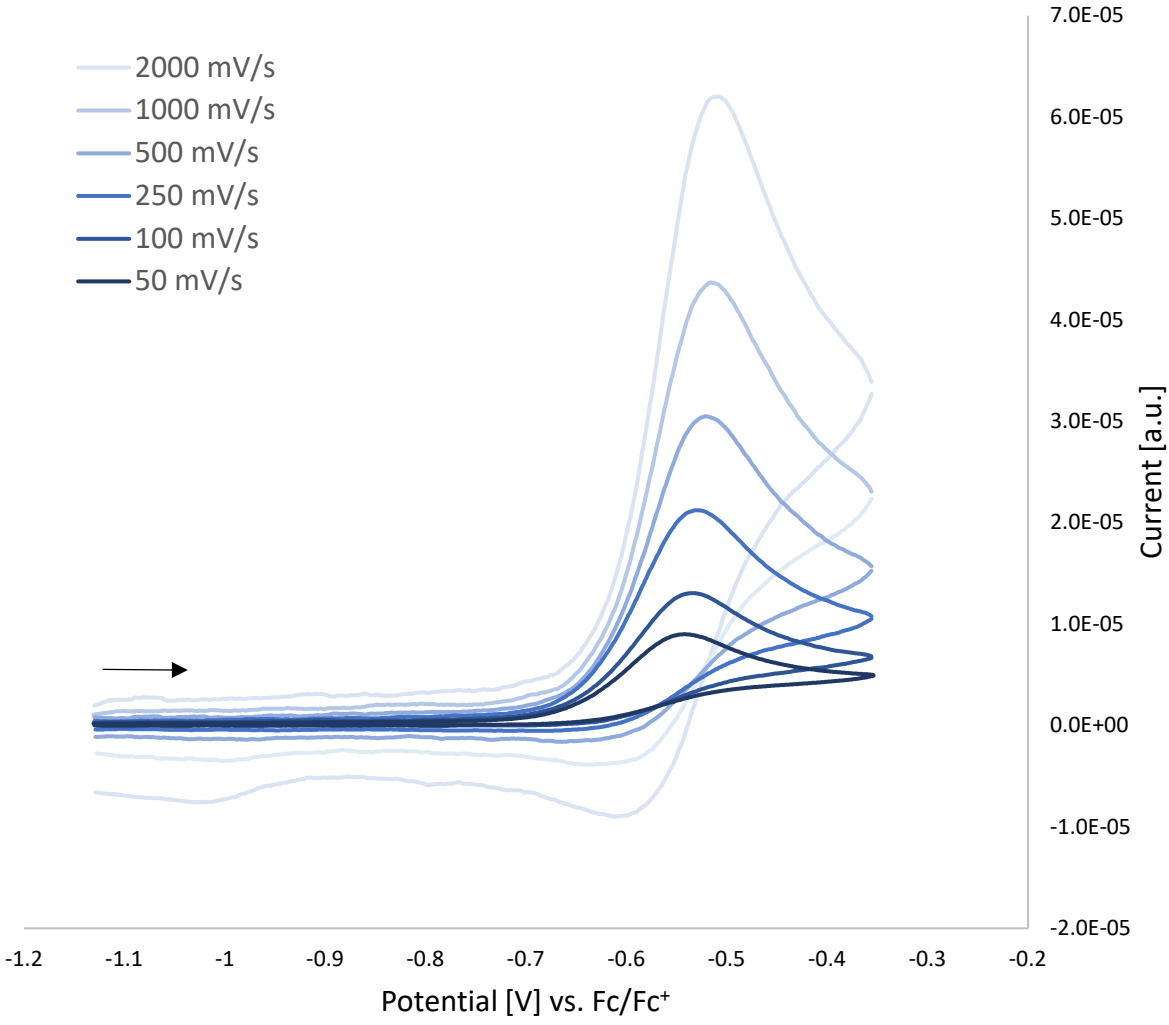

Figure S25. Isolated cerium(III/IV) redox couple of **1**^{tet} vs Fc/Fc^+ in THF obtained at different scan rates; arrow indicates the scan direction; *c*(analyte) 1 mM, *c*(electrolyte) 0.1 M [*n*Pr$_4$N][BARF].

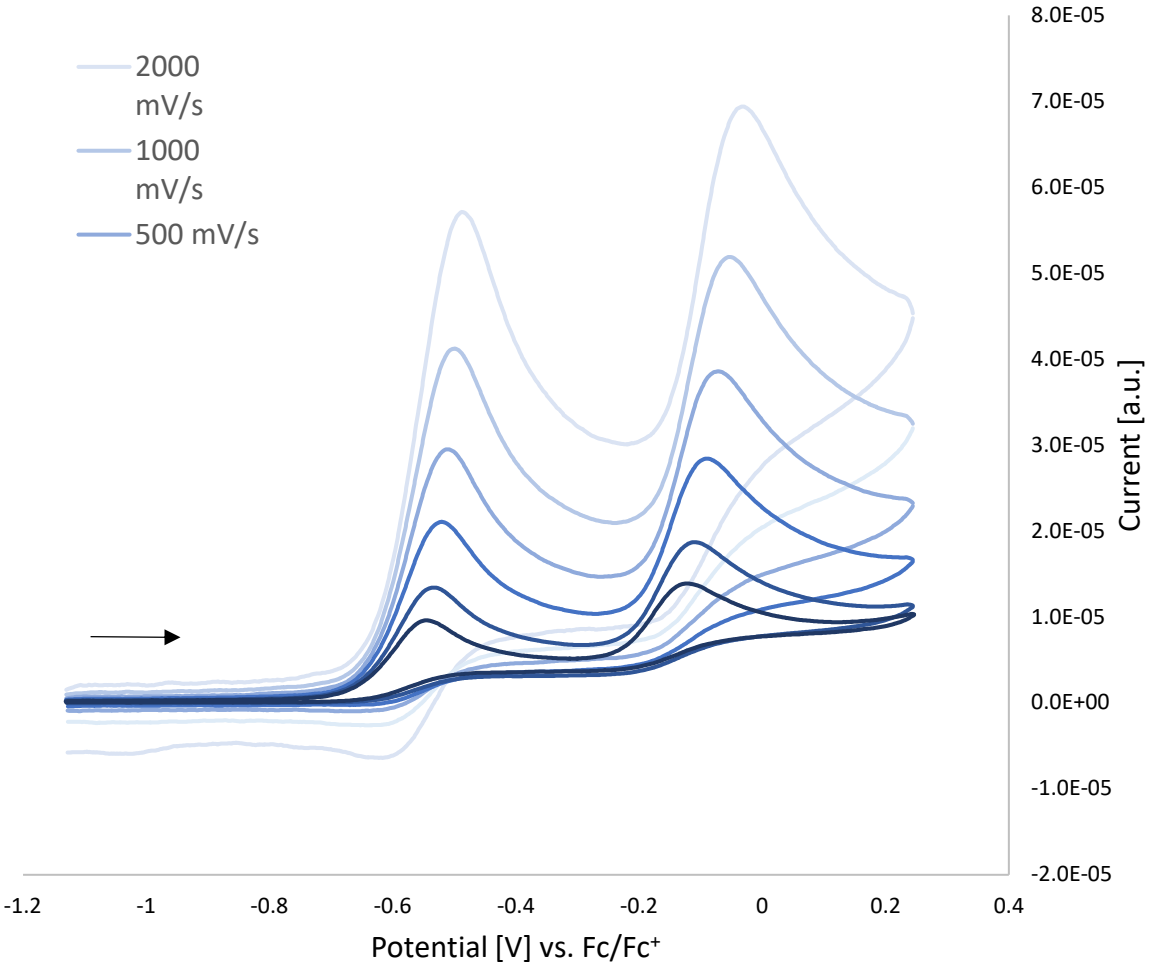

Figure S26. Cyclic Voltammogram of **1**^{tet} vs Fc/Fc$^+$ in THF obtained at different scan rates; arrow indicates the scan direction; *c*(analyte) 1 mM, *c*(electrolyte) 0.1 M [*n*Pr$_4$N][BARF].

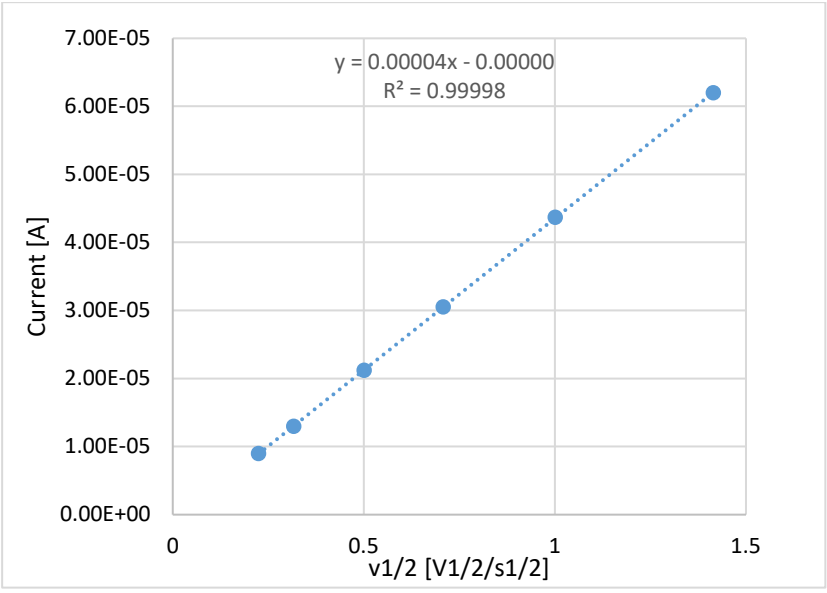

Figure S27. I_p versus $v^{1/2}$ plot of the anodic (blue) redox features of **1**^{tet}.

Table S5. Electrochemical data for the redox couple of complex $\mathbf{2^{Et}}$ vs Fc/Fc^+ in THF

Scan speed	E_{pa} vs Fc/Fc^+ [V]	E_{pc} vs Fc/Fc^+ [V]	E^0 vs Fc/Fc^+ [V]	ΔE [V]	i_{pc}/i_{pa}
50 mV/s	-1.519	-1.591	-1.555	0.072	0.92
100 mV/s	-1.517	-1.600	-1.559	0.083	0.94
250 mV/s	-1.507	-1.605	-1.556	0.098	0.96
500 mV/s	-1.499	-1.615	-1.557	0.116	0.97
1000 mV/s	-1.487	-1.621	-1.554	0.134	0.98
2000 mV/s	-1.475	-1.637	-1.556	0.162	1.00

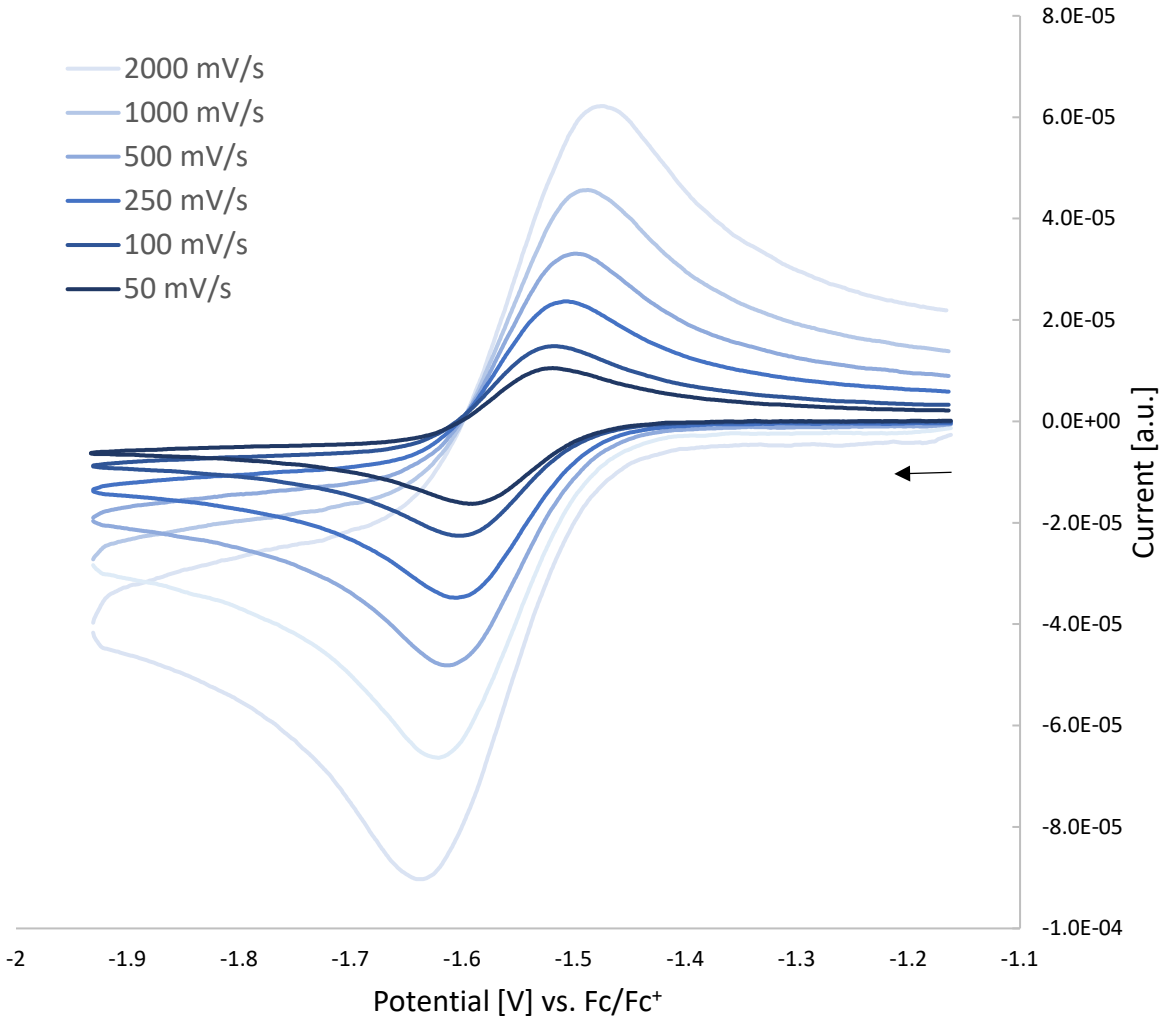

Figure S28. Cerium(III/IV) redox couple of $\mathbf{2^{Et}}$ vs Fc/Fc^+ in THF obtained at different scan rates; arrow indicates the scan direction; *c*(analyte) 1 mM, *c*(electrolyte) 0.1 M [*n*Pr$_4$N][BARF].

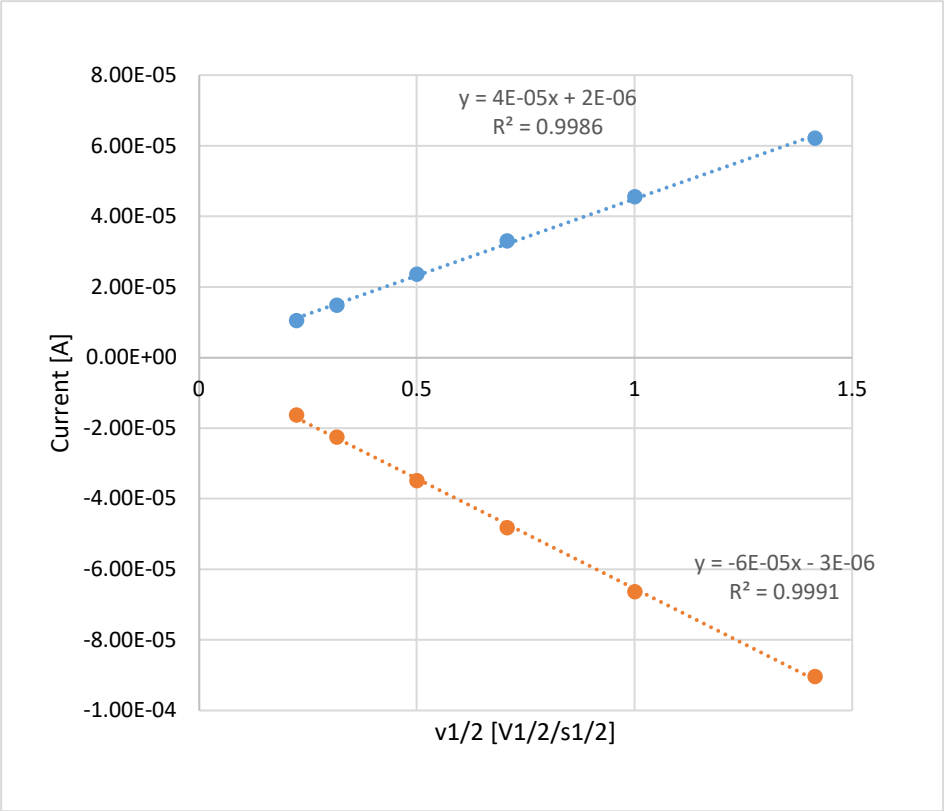

Figure S29. I_p versus $v^{1/2}$ plot of the anodic (blue) and cathodic (orange) redox features of **2^{Et}**.

Table S6. Electrochemical data for the redox couple of complex **2^{iPr}** vs Fc/Fc^+ in THF

Scan speed	E_{pa} vs Fc/Fc^+ [V]	E_{pc} vs Fc/Fc^+ [V]	E^0 vs Fc/Fc^+ [V]	ΔE [V]	i_{pc}/i_{pa}
50 mV/s	-1.522	-1.602	-1.562	0.080	1.00
100 mV/s	-1.510	-1.595	-1.553	0.085	0.99
250 mV/s	-1.496	-1.598	-1.547	0.102	0.98
500 mV/s	-1.482	-1.600	-1.541	0.118	0.97
1000 mV/s	-1.468	-1.611	-1.540	0.143	0.97
2000 mV/s	-1.456	-1.624	-1.540	0.168	0.96

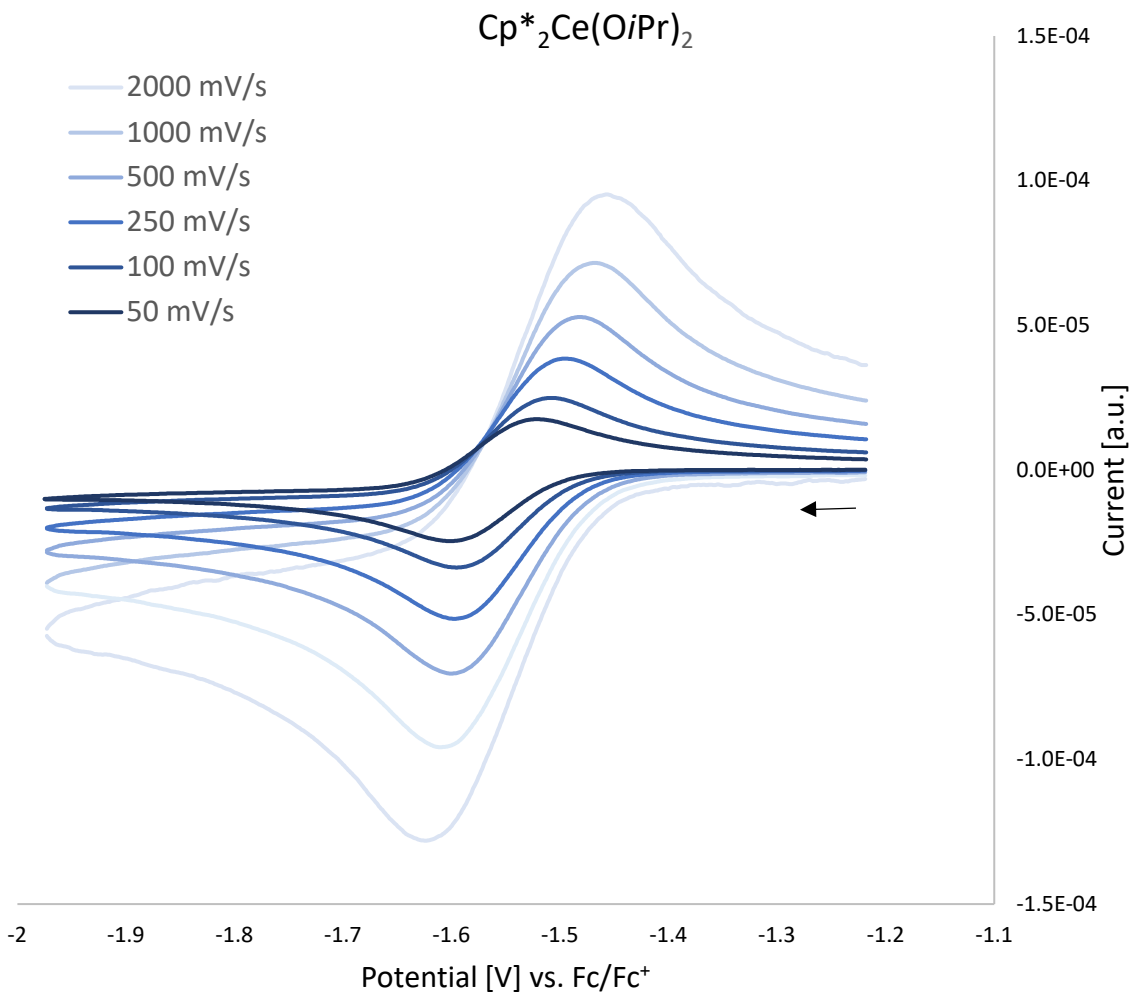

Figure S30. Cerium(III/IV) redox couple of **2**^{iPr} vs Fc/Fc^{+} in THF obtained at different scan rates; arrow indicates the scan direction; *c*(analyte) 1mM, *c*(electrolyte) 0.1 M [*n*Pr_4N][BARF].

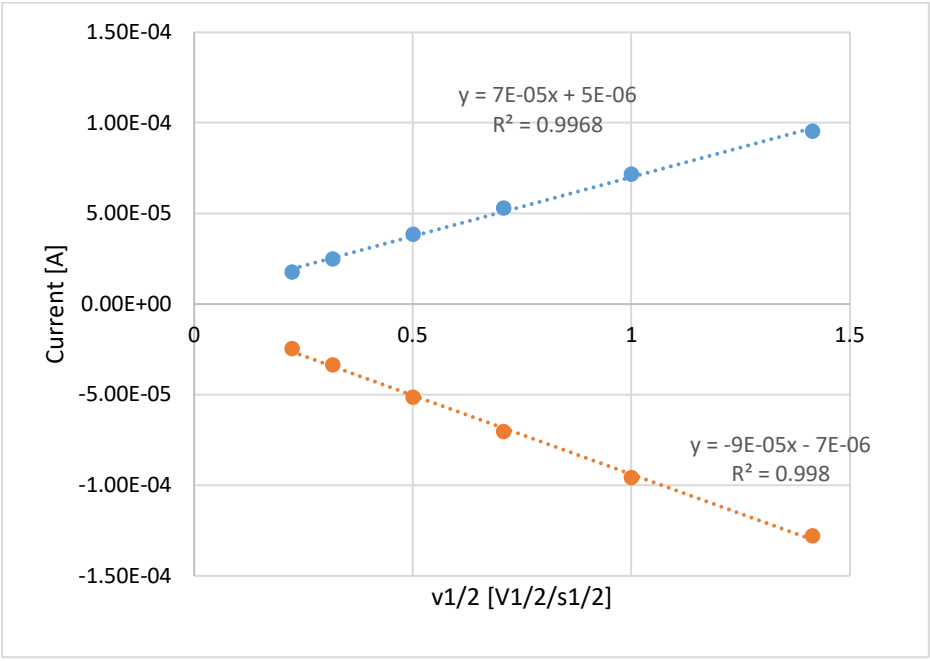

Figure S31. I_p versus $v^{1/2}$ plot of the anodic (blue) and cathodic (orange) redox features of **2**^{iPr}.

Table S7. Electrochemical data for the redox couple of complex $\mathbf{2}^{\mathbf{CH2}t\mathbf{Bu}}$ vs Fc/Fc^+ in THF

Scan speed	E_{pa} vs Fc/Fc^+ [V]	E_{pc} vs Fc/Fc^+ [V]	E^0 vs Fc/Fc^+ [V]	ΔE [V]	i_{pc}/i_{pa}
50 mV/s	-1.473	-1.555	-1.514	0.082	0.95
100 mV/s	-1.466	-1.557	-1.512	0.091	0.95
250 mV/s	-1.453	-1.562	-1.508	0.109	0.95
500 mV/s	-1.444	-1.570	-1.507	0.126	0.95
1000 mV/s	-1.432	-1.578	-1.505	0.146	0.95
2000 mV/s	-1.413	-1.598	-1.506	0.185	0.95

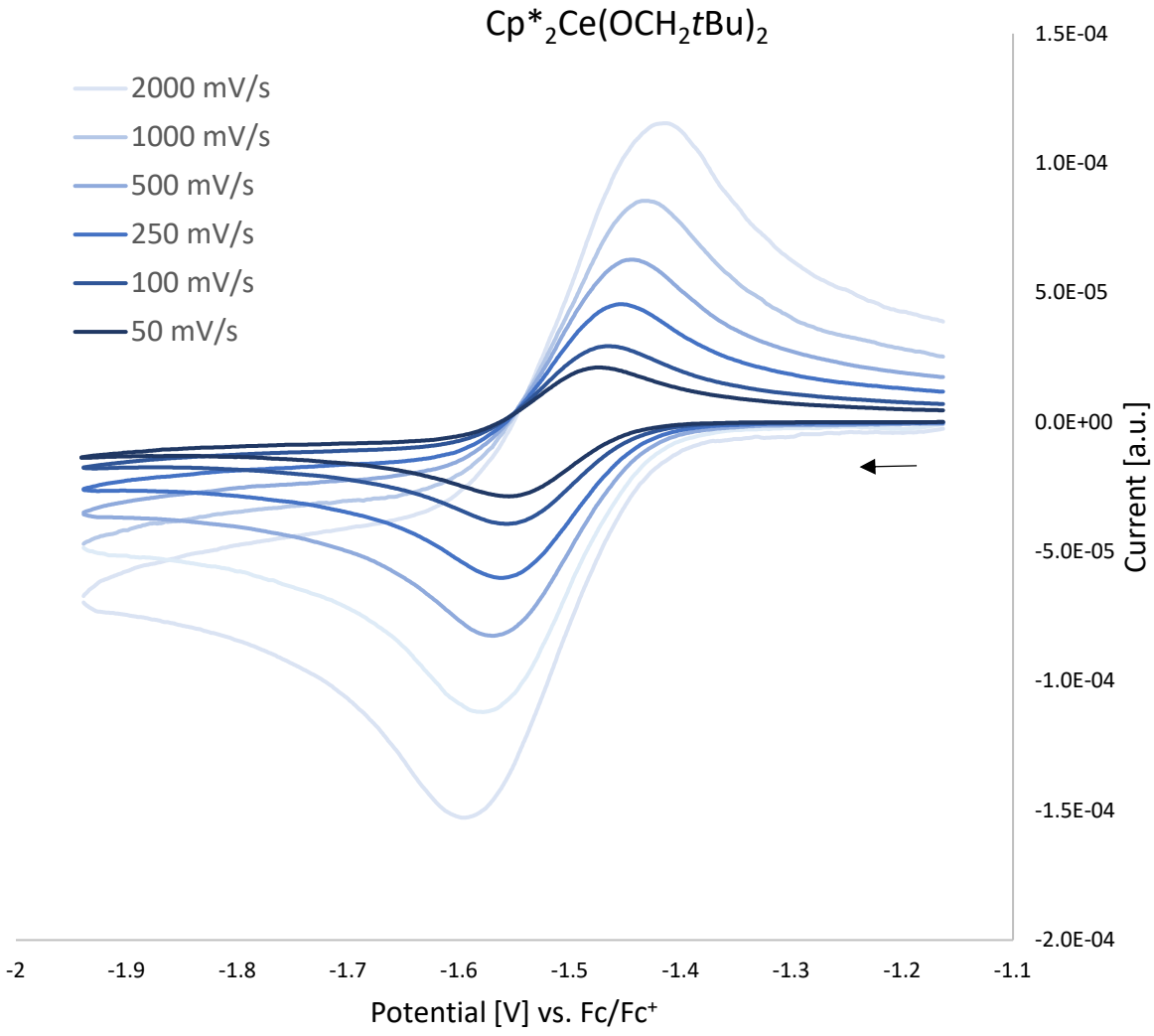

Figure S32. Cerium(III/IV) redox couple of $\mathbf{2}^{\mathbf{CH2}t\mathbf{Bu}}$ vs Fc/Fc^+ in THF obtained at different scan rates; arrow indicates the scan direction; *c*(analyte) 1 mM, *c*(electrolyte) 0.1 M [*n*Pr$_4$N][BARF].

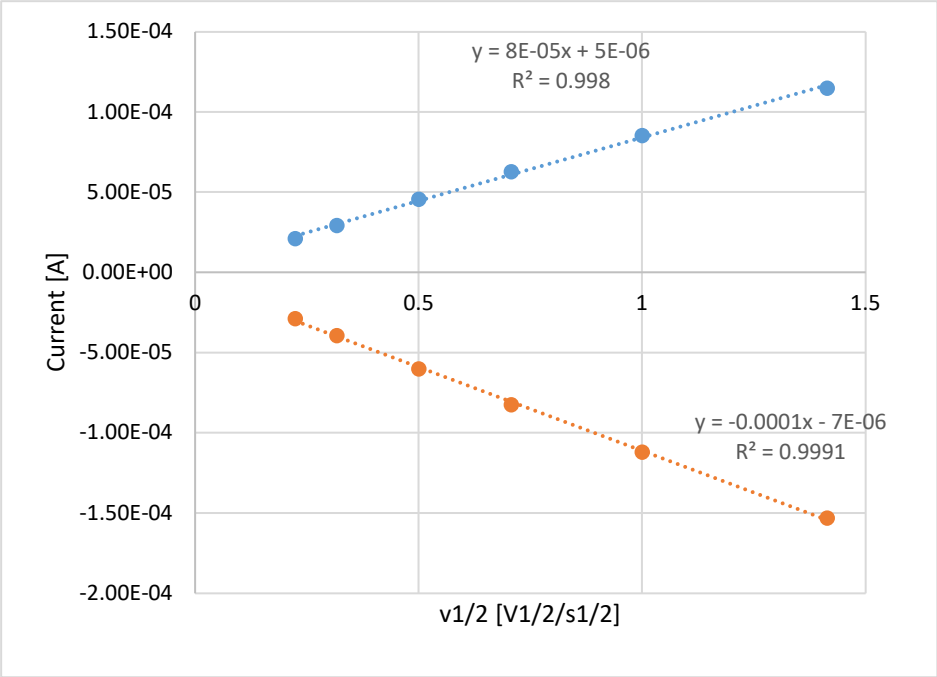

Figure S33. I_p versus $v^{1/2}$ plot of the anodic (blue) and cathodic (orange) redox features of **2**^{CH2tBu}.

Table S8. Electrochemical data for the redox couple of complex **2**^{tBu} vs Fc/Fc^+ in THF

Scan speed	E_{pa} vs Fc/Fc^+ [V]	E_{pc} vs Fc/Fc^+ [V]	E^0 vs Fc/Fc^+ [V]	ΔE [V]	i_{pc}/i_{pa}
50 mV/s	-1.497	-1.565	-1.531	0.068	1.00
100 mV/s	-1.497	-1.570	-1.534	0.073	1.00
250 mV/s	-1.493	-1.567	-1.530	0.074	0.98
500 mV/s	-1.485	-1.569	-1.527	0.084	0.95
1000 mV/s	-1.481	-1.568	-1.525	0.087	0.95
2000 mV/s	-1.481	-1.577	-1.529	0.096	0.94

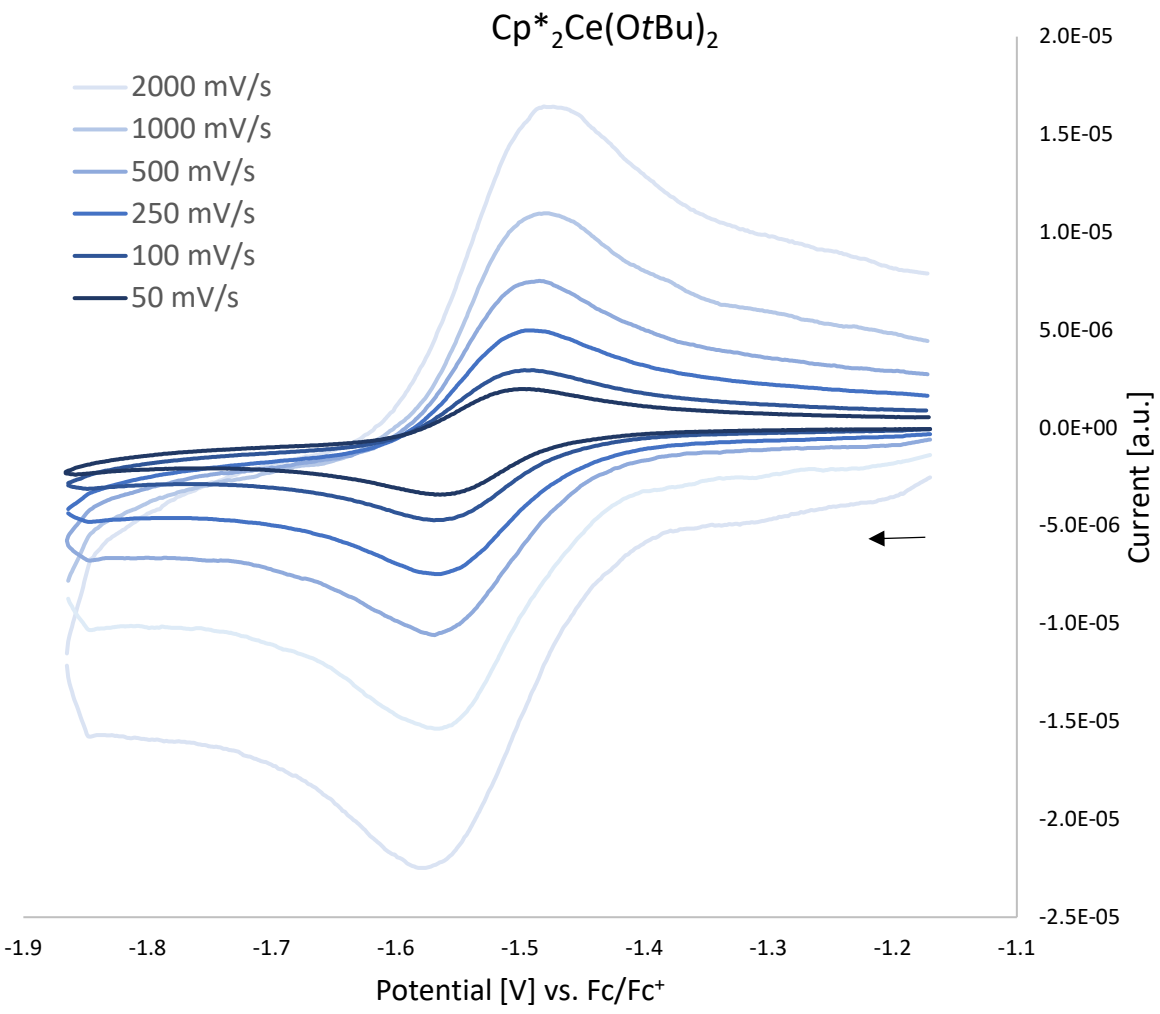

Figure S34. Cerium(III/IV) redox couple of **2**$^{t\mathrm{Bu}}$ vs Fc/Fc^{+} in THF obtained at different scan rates; arrow indicates the scan direction; c(analyte) 1 mM, *c*(electrolyte) 0.1 M [*n*Pr$_4$N][BARF].

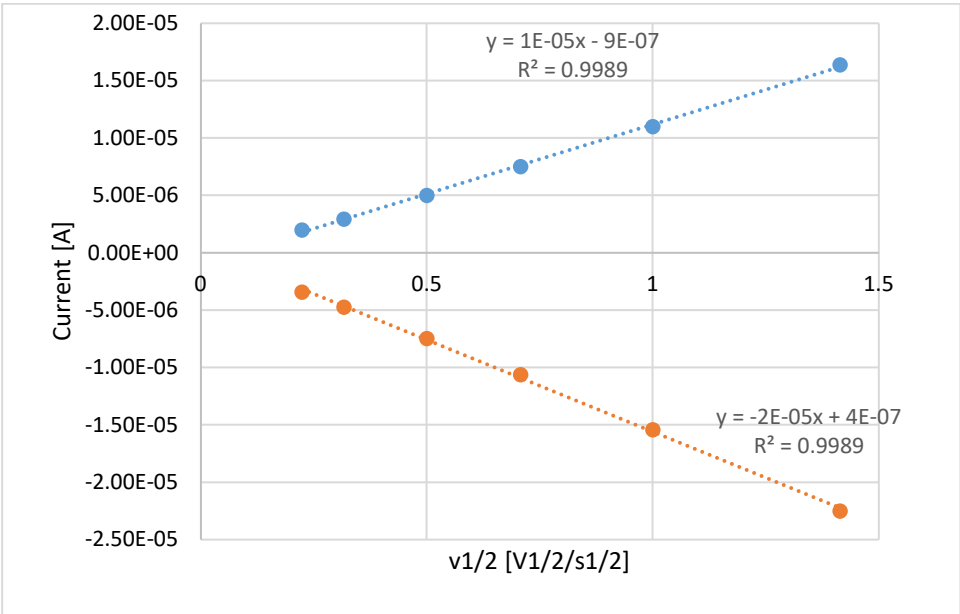

Figure S35. I_p versus $v^{1/2}$ plot of the anodic (blue) and cathodic (orange) redox features of **2**$^{t\mathrm{Bu}}$.

Table S9. Electrochemical data for the redox couple of complex $\mathbf{3}^{t\mathbf{Bu}}$ vs Fc/Fc^+ in THF

Scan speed	E_{pa} vs Fc/Fc^+ [V]	E_{pc} vs Fc/Fc^+ [V]	E^0 vs Fc/Fc^+ [V]	ΔE [V]	i_{pc}/i_{pa}
50 mV/s	-1.540	-1.677	-1.608	0.137	0.80
100 mV/s	-1.524	-1.669	-1.596	0.145	0.84
250 mV/s	-1.507	-1.700	-1.603	0.193	0.88
500 mV/s	-1.480	-1.697	-1.588	0.217	0.90
1000 mV/s	-1.458	-1.729	-1.593	0.271	0.92
2000 mV/s	-1.452	-1.742	-1.597	0.290	0.95

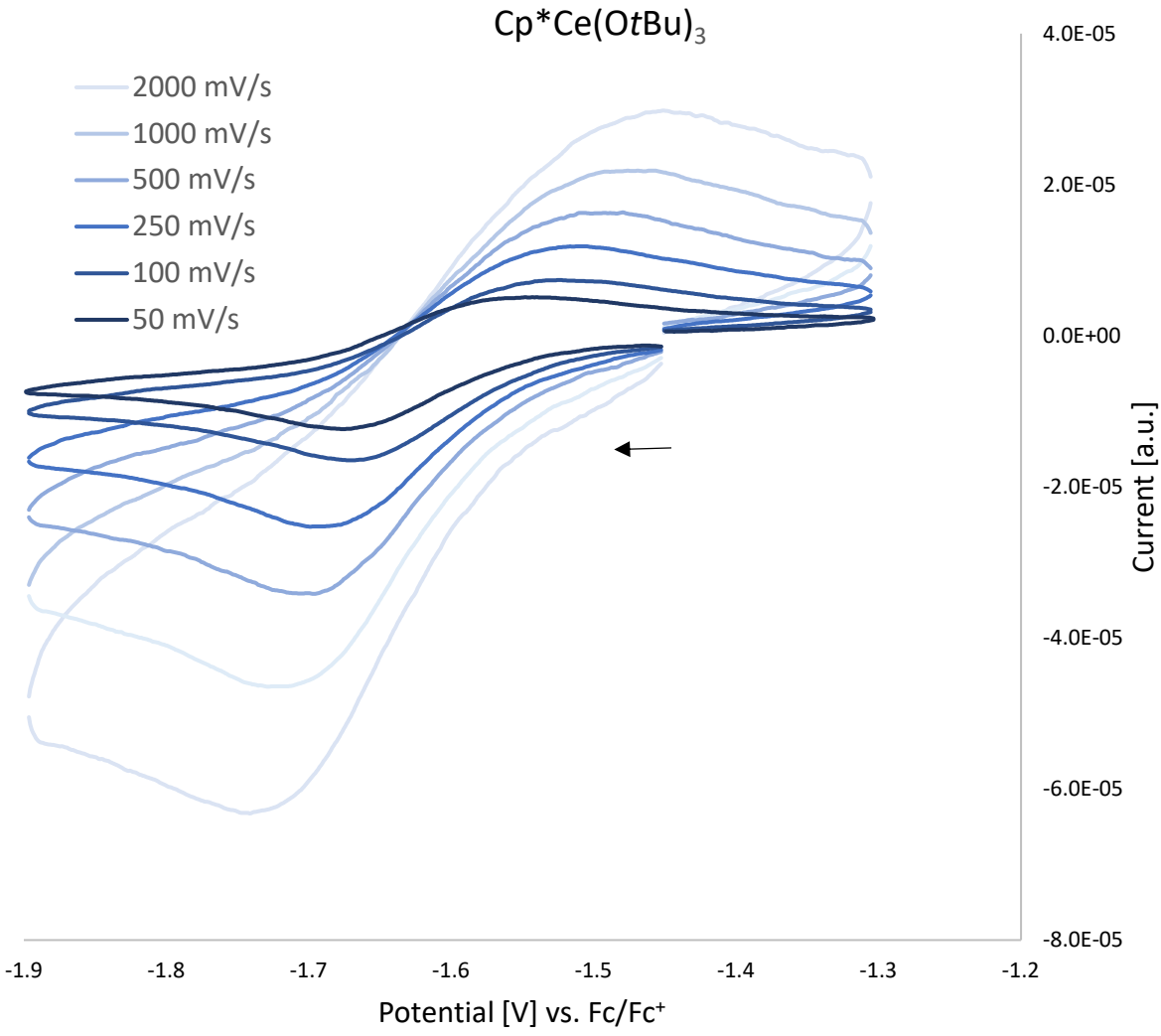

Figure S36. Cerium(III/IV) redox couple of $\mathbf{3}^{t\mathbf{Bu}}$ vs Fc/Fc^+ in THF obtained at different scan rates; arrow indicates the scan direction; *c*(analyte) 1 mM, *c*(electrolyte) 0.1 M [nPr$_4$N][BARF].

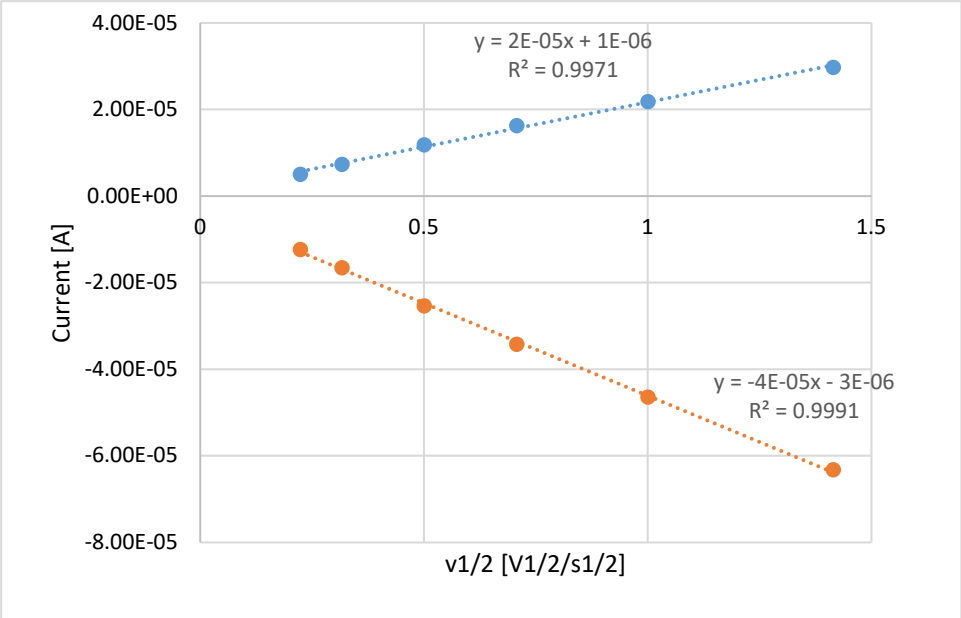

Figure S37. I_p versus $v^{1/2}$ plot of the anodic (blue) and cathodic (orange) redox features of **3**^{tBu}.

Table S10. Electrochemical data for the redox couple of complex **4**^{Me} vs Fc/Fc^+ in THF

Scan speed	E_{pa} vs Fc/Fc^+ [V]	E_{pc} vs Fc/Fc^+ [V]	E^0 vs Fc/Fc^+ [V]	ΔE [V]	i_{pc}/i_{pa}
50 mV/s	-1.197	-1.260	-1.229	0.063	0.90
100 mV/s	-1.193	-1.258	-1.226	0.065	0.98
250 mV/s	-1.186	-1.261	-1.224	0.075	0.98
500 mV/s	-1.181	-1.263	-1.222	0.082	0.98
1000 mV/s	-1.177	-1.268	-1.223	0.091	0.97
2000 mV/s	-1.169	-1.277	-1.223	0.108	0.97

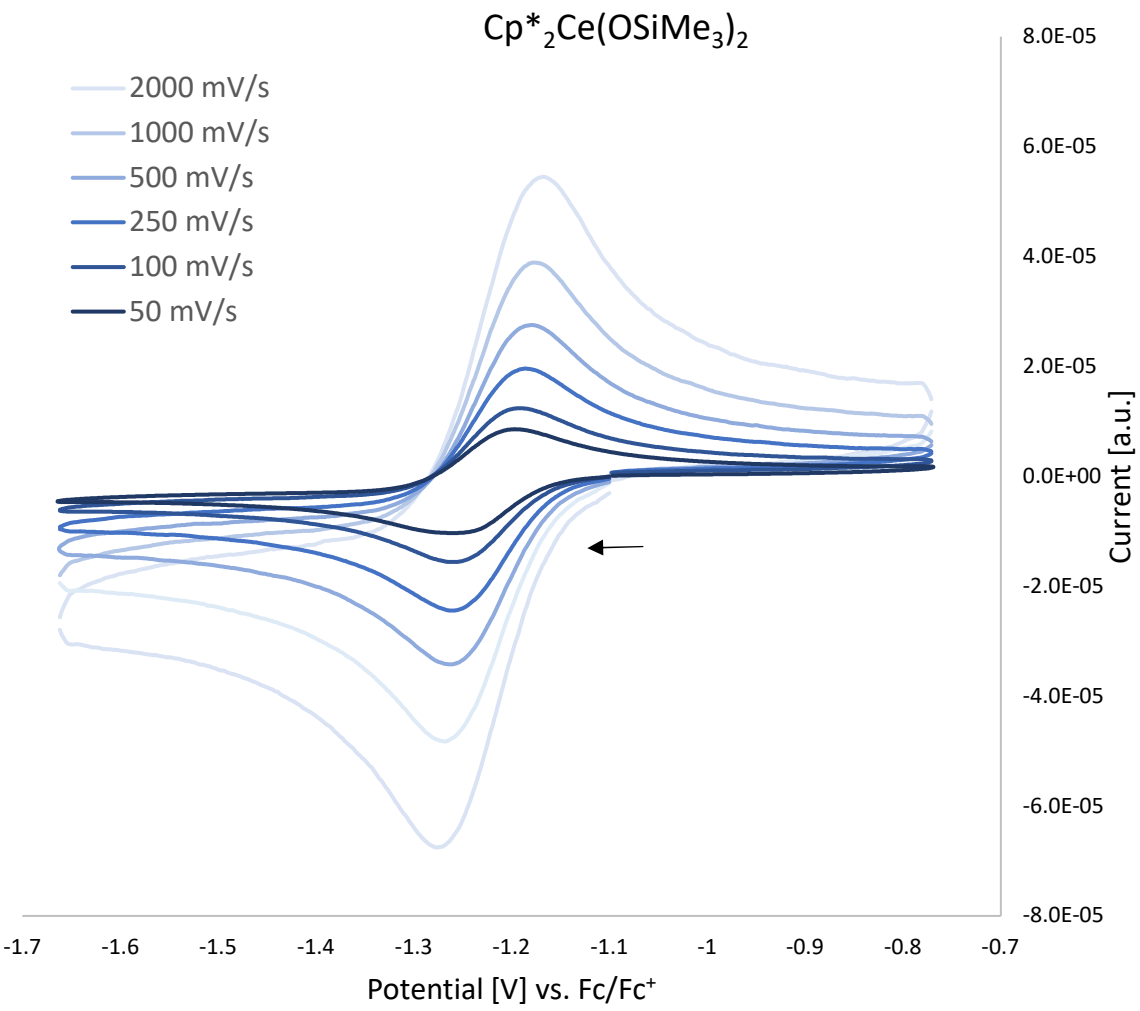

Figure S38. Cerium(III/IV) redox couple of **4^{Me}** vs Fc/Fc^+ in THF obtained at different scan rates; arrow indicates the scan direction; *c*(analyte) 1 mM, *c*(electrolyte) 0.1 M [*n*Pr$_4$N][BARF].

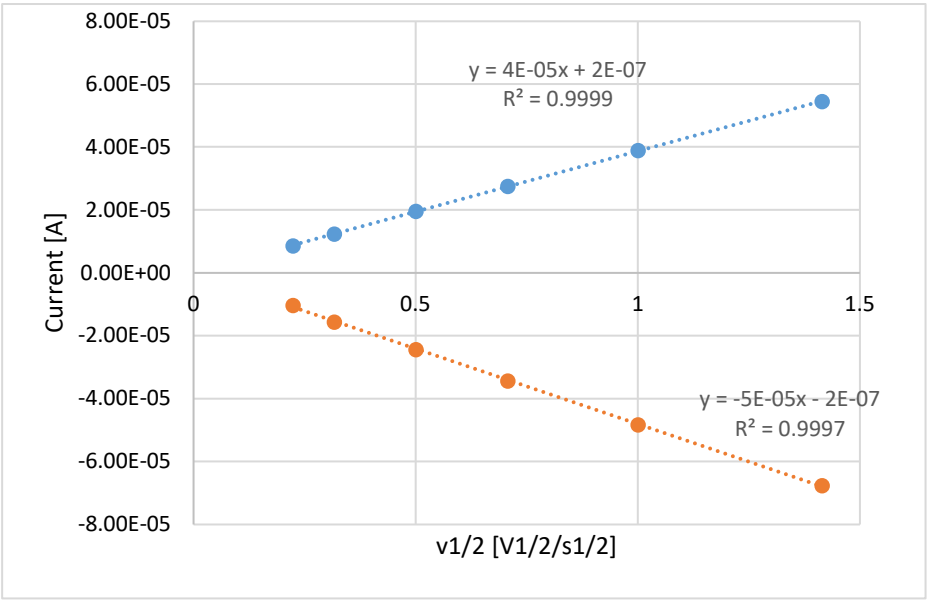

Figure S39. I_p versus $v^{1/2}$ plot of the anodic (blue) and cathodic (orange) redox features of **4^{Me}**.

Table S11. Electrochemical data for the redox couple of complex $\mathbf{4^{Ph}}$ vs Fc/Fc^+ in THF

Scan speed	E_{pa} vs Fc/Fc^+ [V]	E_{pc} vs Fc/Fc^+ [V]	E^0 vs Fc/Fc^+ [V]	ΔE [V]	i_{pc}/i_{pa}
50 mV/s	-1.010	-1.264	-1.137	0.254	0.95
100 mV/s	-0.998	-1.266	-1.132	0.268	1.00
250 mV/s	-0.993	-1.280	-1.136	0.287	0.98
500 mV/s	-0.983	-1.288	-1.135	0.305	0.99
1000 mV/s	-0.986	-1.298	-1.142	0.312	0.93
2000 mV/s	-0.976	-1.309	-1.142	0.333	0.96

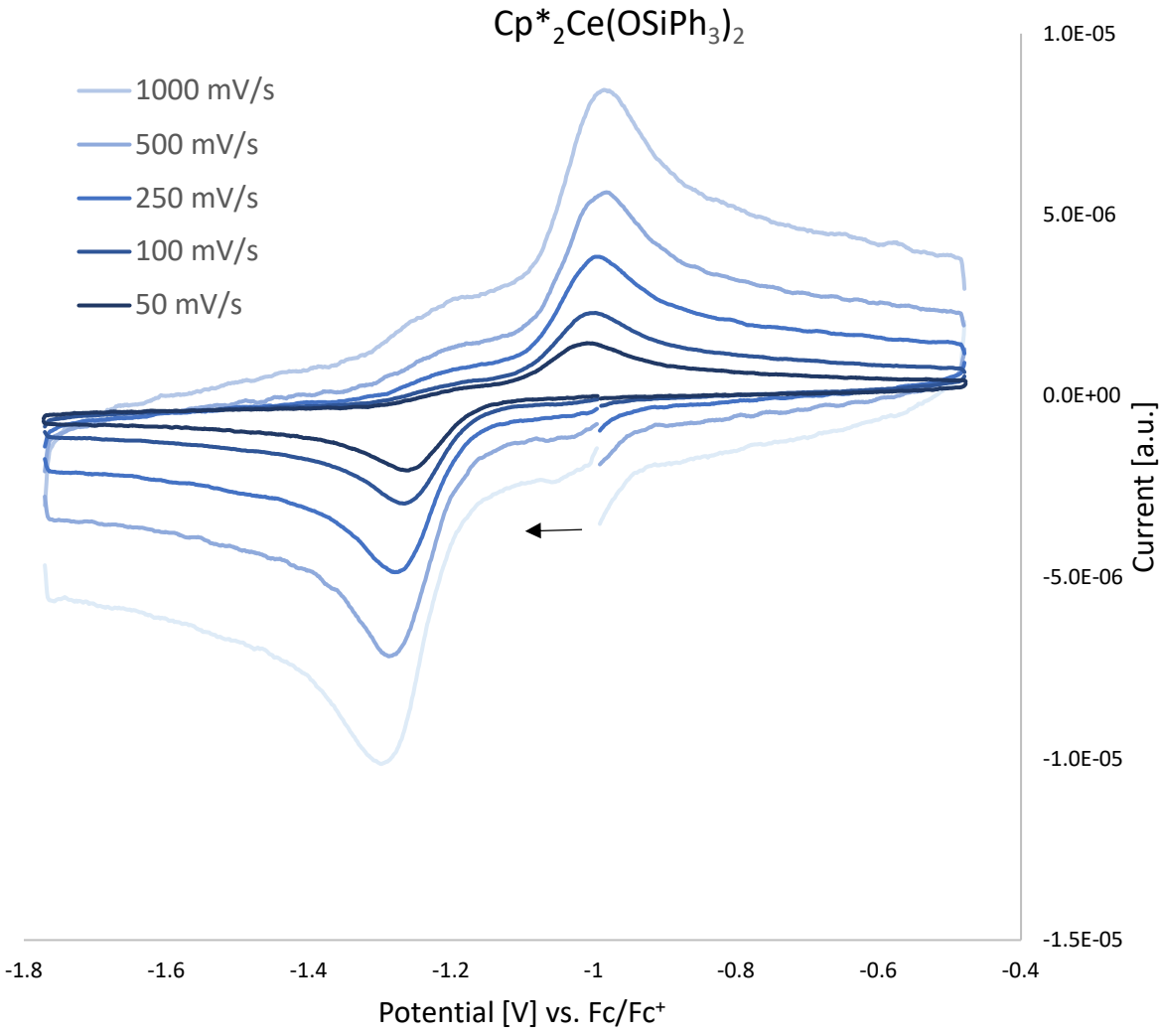

Figure S40. Cerium(III/IV) redox couple of $\mathbf{4^{Ph}}$ vs Fc/Fc^+ in THF obtained at different scan rates; arrow indicates the scan direction; *c*(analyte) 1 mM, *c*(electrolyte) 0.1 M [*n*Pr$_4$N][BARF].

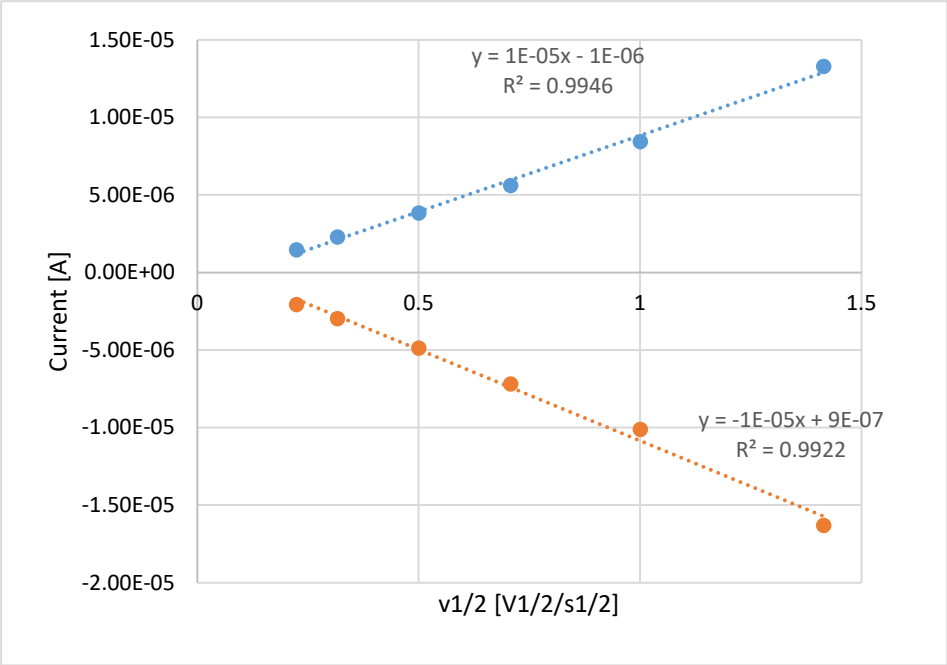

Figure S41. I_p versus $v^{1/2}$ plot of the anodic (blue) and cathodic (orange) redox features of **4^{Ph}**.

Table S1. Electrochemical data for the redox couple of complex **5^{Ph}** vs Fc/Fc^+ in THF

Scan speed	E_{pa} vs Fc/Fc^+ [V]	E_{pc} vs Fc/Fc^+ [V]	E^0 vs Fc/Fc^+ [V]	ΔE [V]	i_{pc}/i_{pa}
50 mV/s	-0.704	-2.186	-1.445	1.482	0.82
100 mV/s	-0.668	-2.212	-1.440	1.544	0.81
250 mV/s	-0.635	-2.245	-1.440	1.610	0.83
500 mV/s	-0.603	-2.276	-1.439	1.673	0.83
1000 mV/s	-0.559	-2.306	-1.432	1.747	0.84
2000 mV/s	-0.587	-2.334	-1.460	1.747	0.86

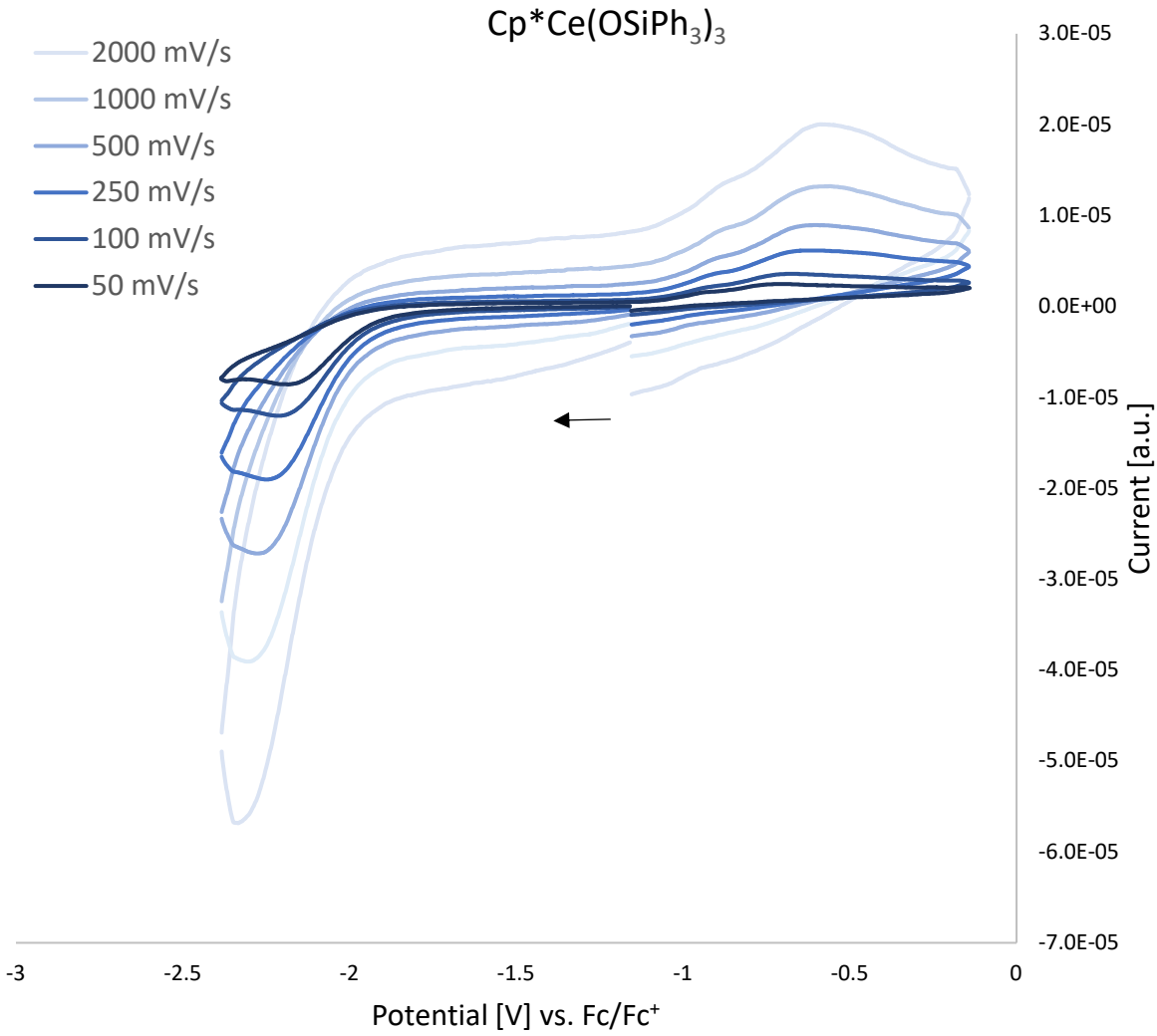

Figure S42. Cerium(III/IV) redox couple of **5^{Ph}** vs Fc/Fc^{+} in THF obtained at different scan rates; arrow indicates the scan direction; *c*(analyte) 1 mM, *c*(electrolyte) 0.1 M [*n*Pr$_4$N][BARF].

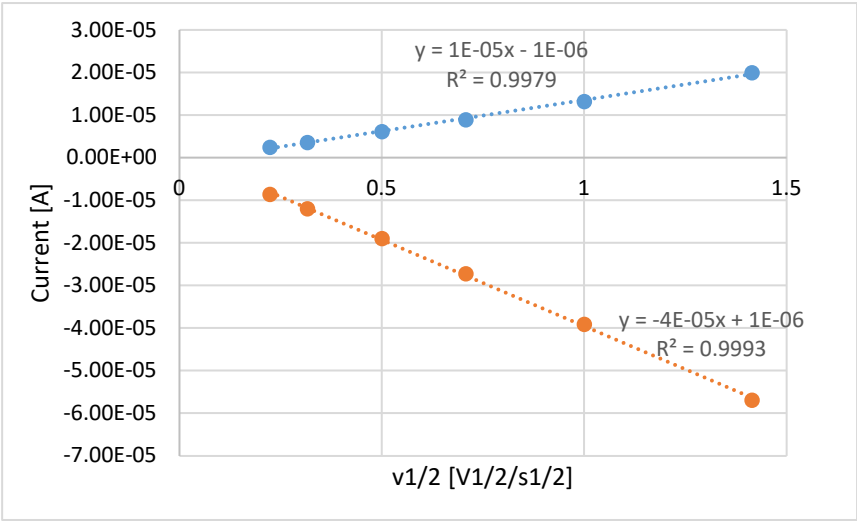

Figure S43. I_p versus $v^{1/2}$ plot of the anodic (blue) and cathodic (orange) redox features of **5^{Ph}**.

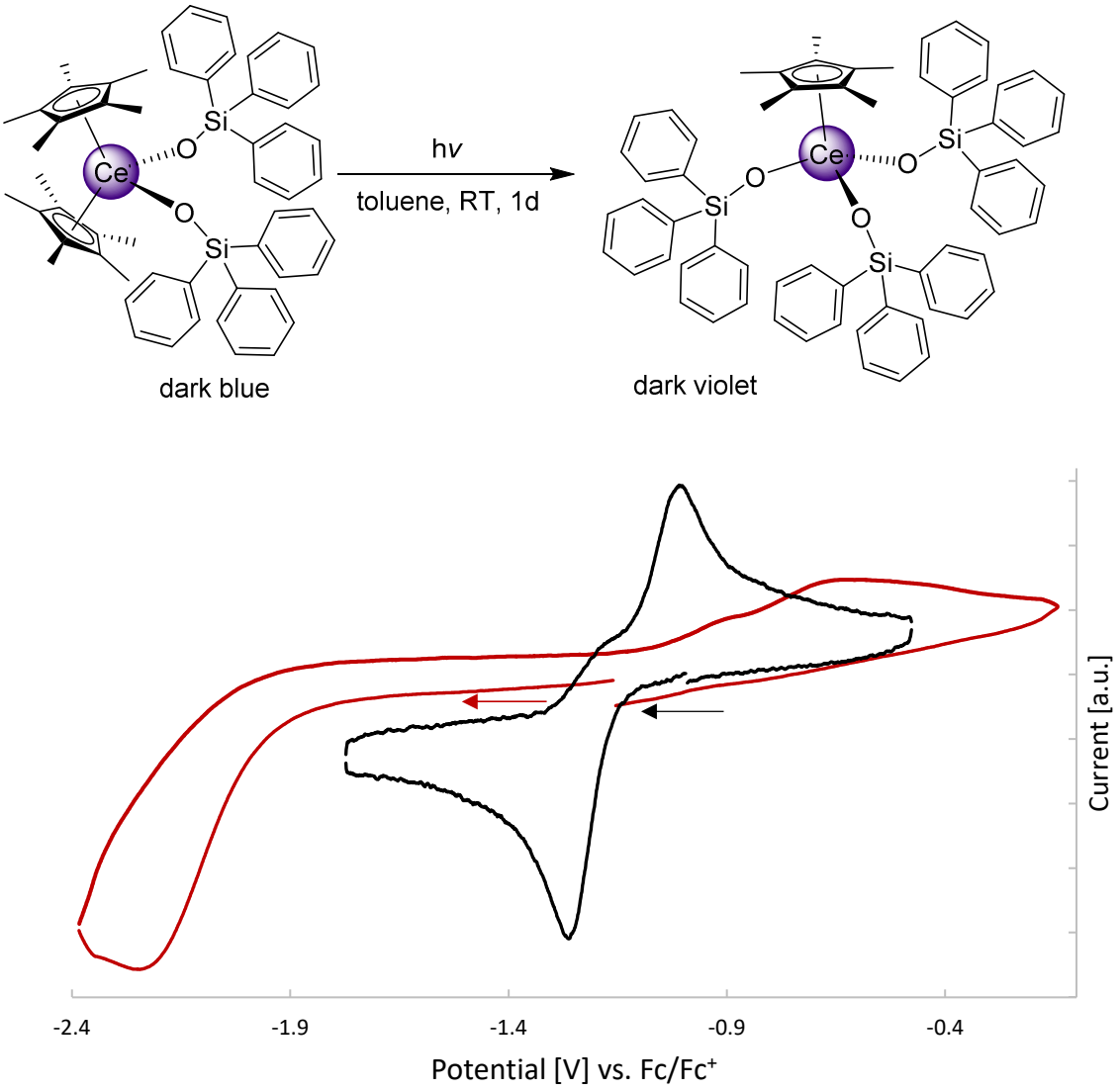

Figure S44. Cyclic voltammograms of the cerium(III/IV) redox couple of $Cp^*_2Ce(OSiPh_3)_2$ **4^{Ph}** (black) and $Cp^*Ce(OSiPh_3)_3$ **5^{Ph}** (red) vs Fc/Fc^+ in THF at GC obtained at a scan rate of 50 mV/s; arrow indicates scan direction; *c*(analyte) 1 mM, *c*(electrolyte) 0.1 M [*n*Pr$_4$N][BARF].

Table S13. Electrochemical data for the redox couple of complex **6** vs Fc/Fc^+ in THF

Scan speed	E_{pa} vs Fc/Fc^+ [V]	E_{pc} vs Fc/Fc^+ [V]	E^0 vs Fc/Fc^+ [V]	ΔE [V]	i_{pc}/i_{pa}
50 mV/s	-0.799	-0.863	-0.831	0.064	0.93
100 mV/s	-0.795	-0.862	-0.829	0.067	0.96
250 mV/s	-0.790	-0.862	-0.826	0.072	1.00
500 mV/s	-0.790	-0.862	-0.826	0.072	1.00
1000 mV/s	-0.785	-0.860	-0.823	0.075	0.98
2000 mV/s	-0.784	-0.868	-0.826	0.084	1.00

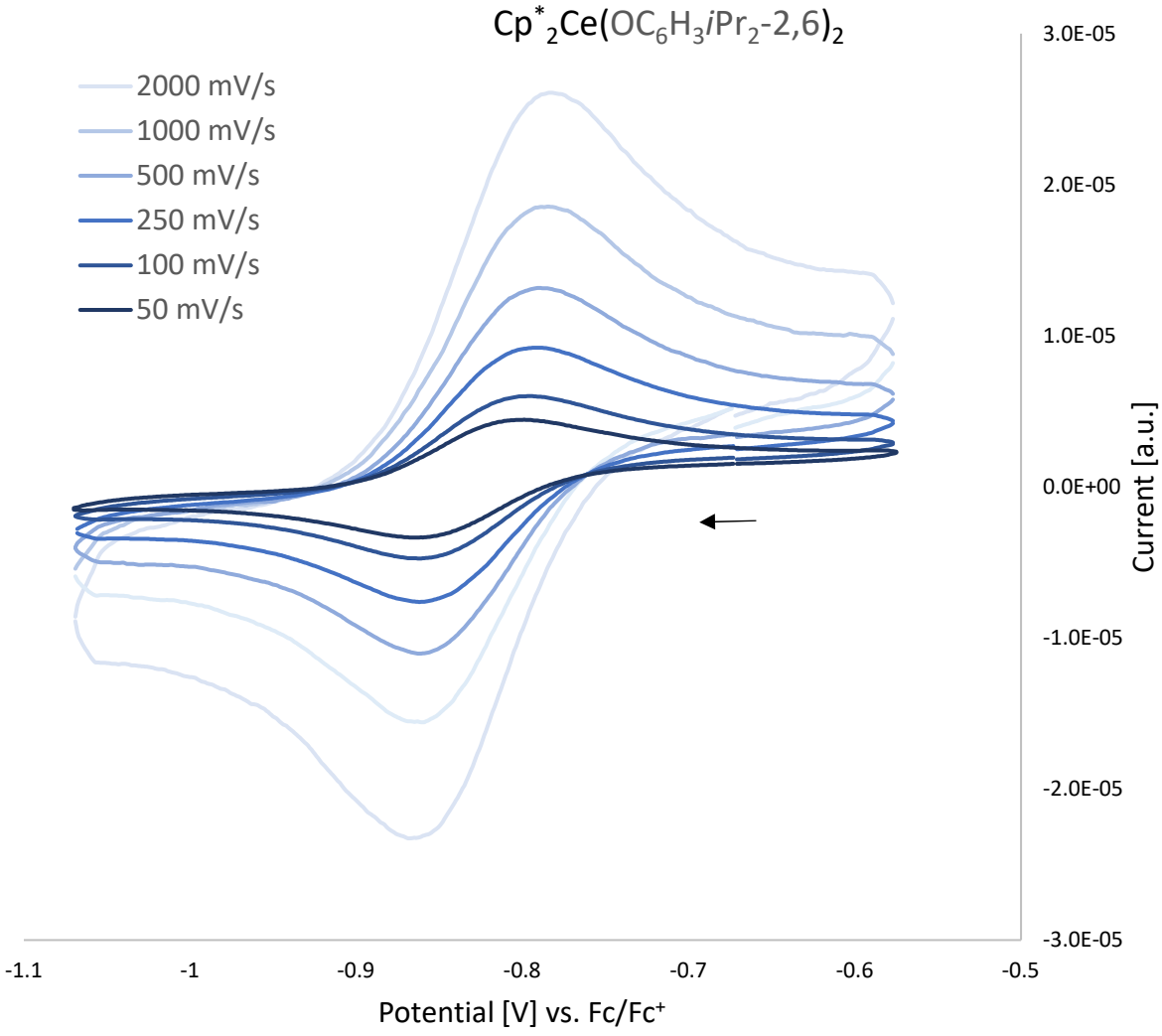

Figure S45. Cerium(III/IV) redox couple of **6** vs Fc/Fc^+ in THF obtained at different scan rates; arrow indicates the scan direction; *c*(analyte) 1 mM, *c*(electrolyte) 0.1 M [*n*Pr$_4$N][BARF].

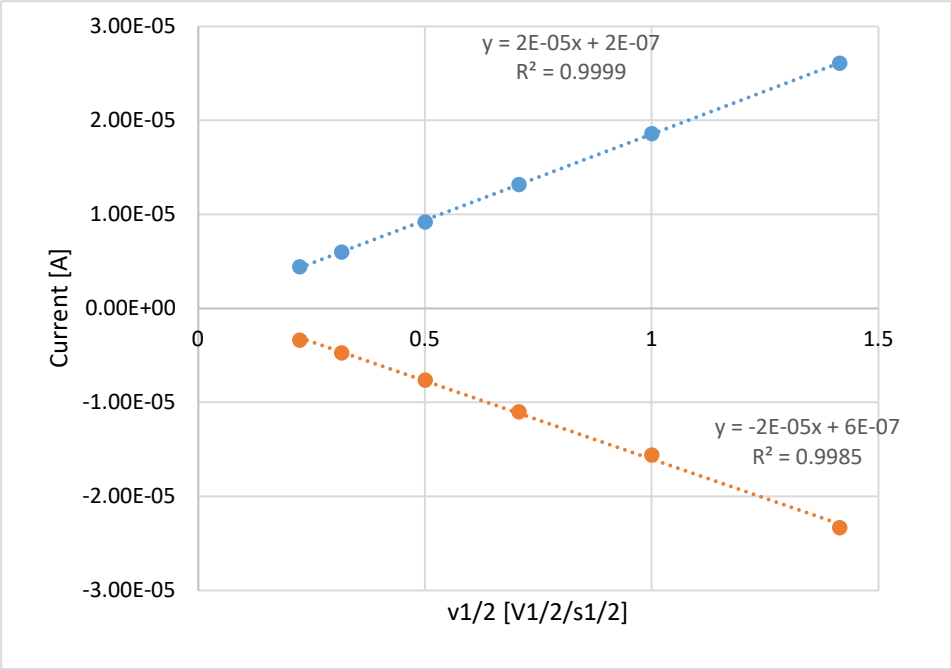

Figure S46. I_p versus $v^{1/2}$ plot of the anodic (blue) and cathodic (orange) redox features of **6**.

Table S14. Electrochemical data for the redox couple of complex **7** vs Fc/Fc^+ in THF

Scan speed	E_{pa} vs Fc/Fc^+ [V]	E_{pc} vs Fc/Fc^+ [V]	E^0 vs Fc/Fc^+ [V]	ΔE [V]	i_{pc}/i_{pa}
50 mV/s	-0.755	-0.997	-0.876	0.242	0.85
100 mV/s	-0.751	-1.004	-0.878	0.253	0.94
250 mV/s	-0.745	-1.027	-0.886	0.282	0.96
500 mV/s	-0.740	-1.045	-0.893	0.305	0.94
1000 mV/s	-0.738	-1.054	-0.896	0.316	0.92
2000 mV/s	-0.734	-1.065	-0.900	0.334	0.88

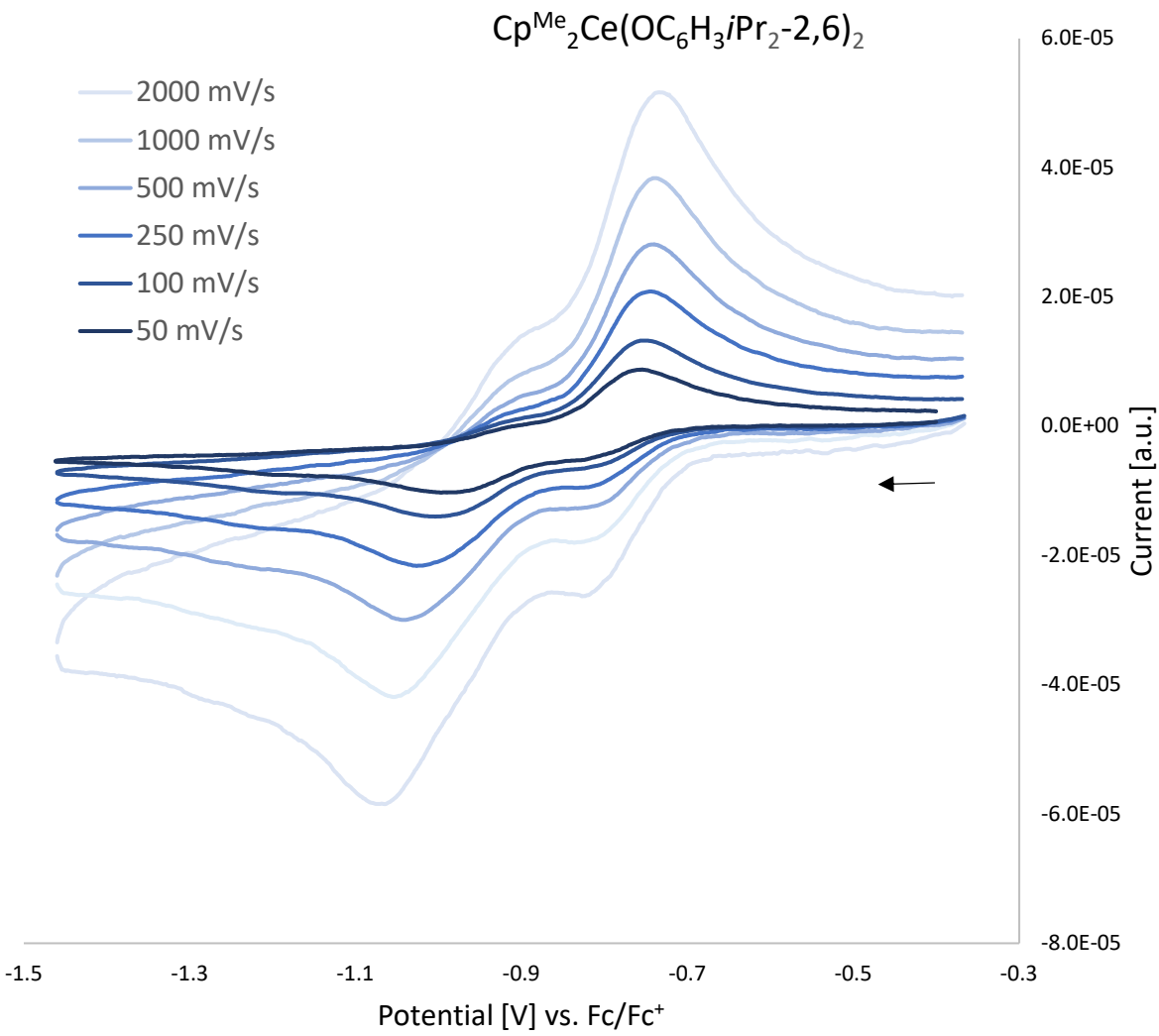

Figure S47. Cerium(III/IV) redox couple of **7** vs Fc/Fc^+ in THF obtained at different scan rates; arrow indicates the scan direction; *c*(analyte) 1 mM, *c*(electrolyte) 0.1 M [*n*Pr$_4$N][BARF].

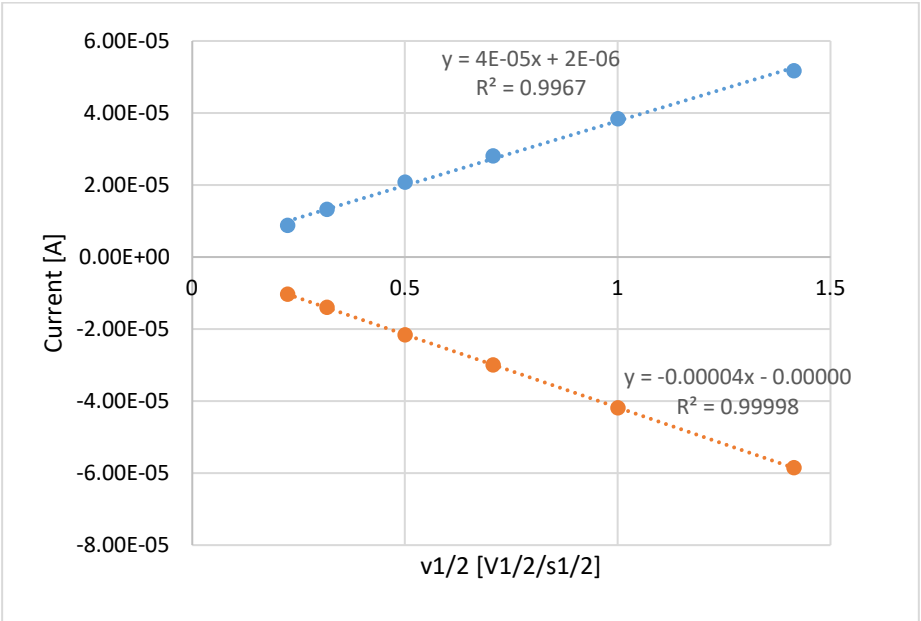

Figure S48. I_p versus $v^{1/2}$ plot of the anodic (blue) and cathodic (orange) redox features of **7**.

Table S15. Electrochemical data for the redox couple of complex **8** vs Fc/Fc^+ in THF

Scan speed	E_{pa} vs Fc/Fc^+ [V]	E_{pc} vs Fc/Fc^+ [V]	E^0 vs Fc/Fc^+ [V]	ΔE [V]	i_{pc}/i_{pa}
50 mV/s	-0.833	-0.898	-0.865	0.065	0.92
100 mV/s	-0.829	-0.899	-0.864	0.070	0.99
250 mV/s	-0.827	-0.902	-0.864	0.075	0.98
500 mV/s	-0.825	-0.905	-0.865	0.080	0.97
1000 mV/s	-0.818	-0.910	-0.864	0.092	0.96
2000 mV/s	-0.817	-0.914	-0.865	0.097	0.95

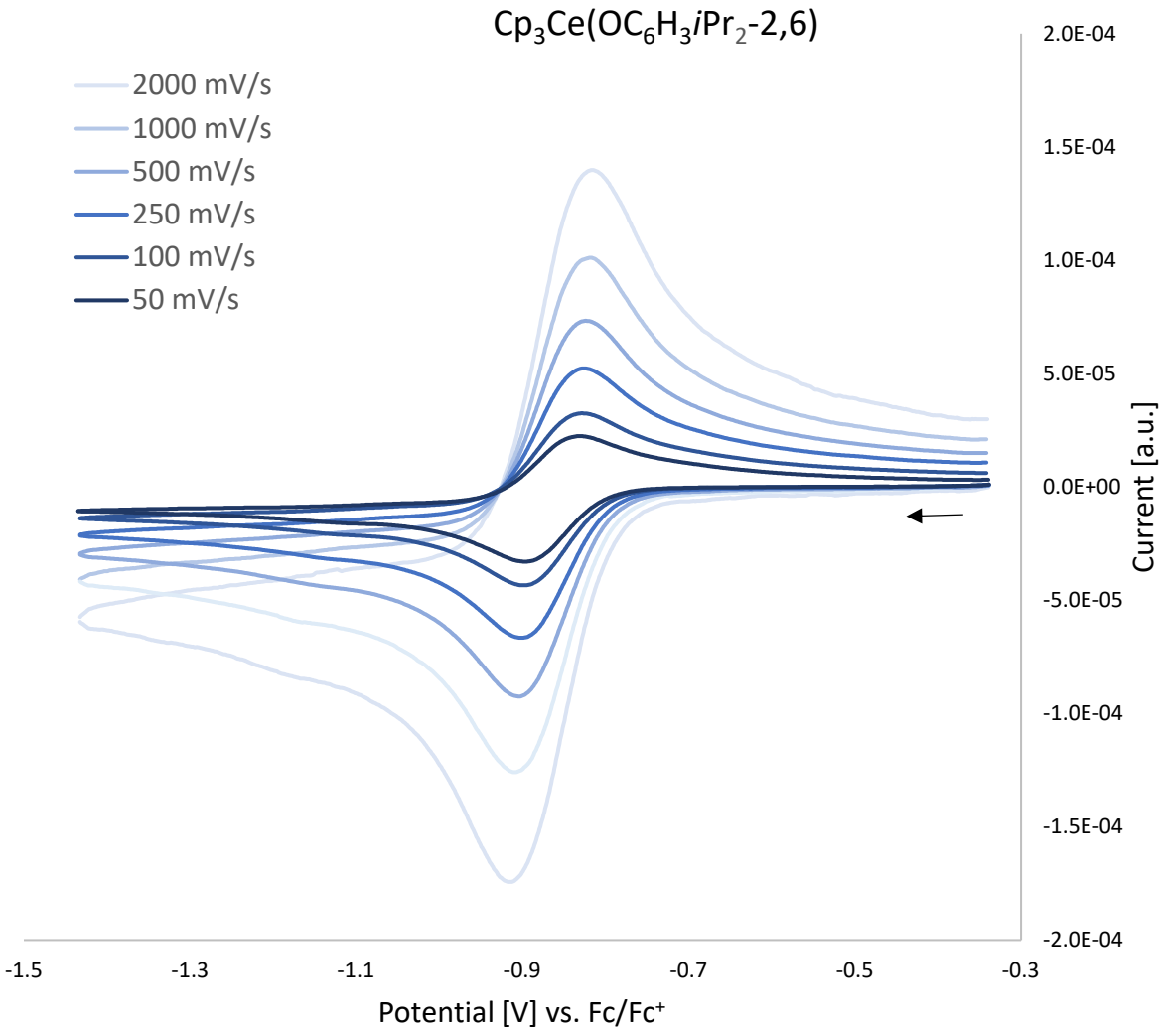

Figure S49. Cerium(III/IV) redox couple of **8** vs Fc/Fc^+ in THF obtained at different scan rates; arrow indicates the scan direction; *c*(analyte) 1 mM, *c*(electrolyte) 0.1 M [nPr$_4$N][BARF].

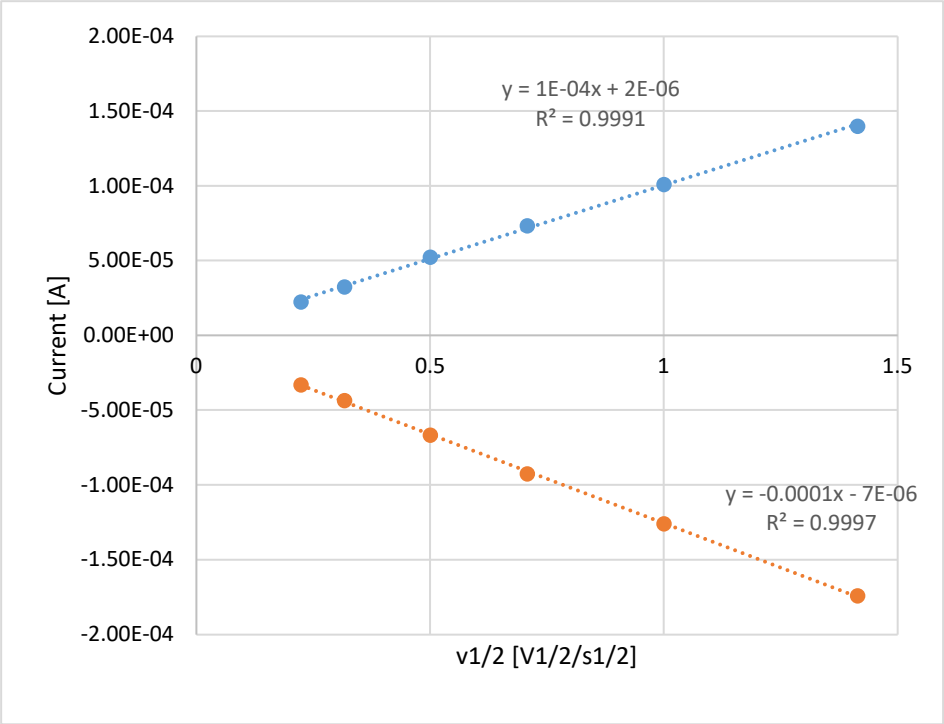

Figure S50. I_p versus $v^{1/2}$ plot of the anodic (blue) and cathodic (orange) redox features of **8**.

UV/Vis Spectra

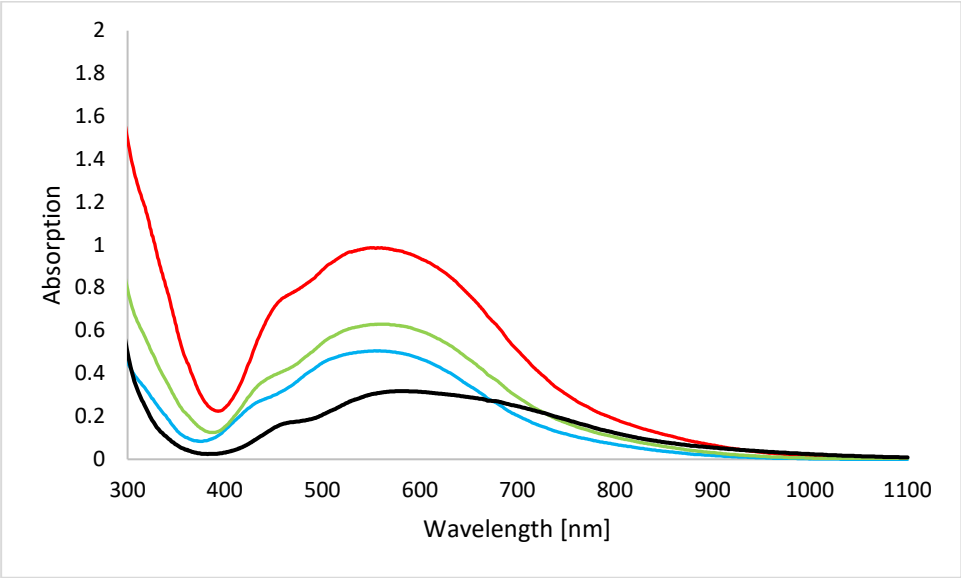

Figure S51. UV/Vis spectra of compounds $\mathbf{2}^{Et}$ (blue), $\mathbf{2}^{iPr}$ (green), $\mathbf{2}^{CH2tBu}$ (red) and $\mathbf{4}^{Me}$ (black).

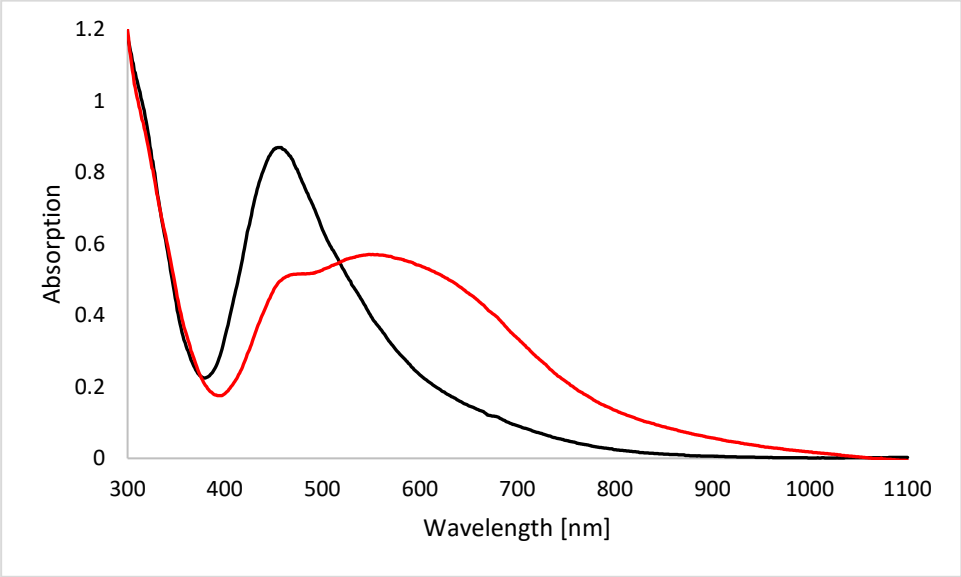

Figure S52. UV/Vis spectra of compounds $\mathbf{2}^{tBu}$ (red) and $\mathbf{3}^{tBu}$ (black).

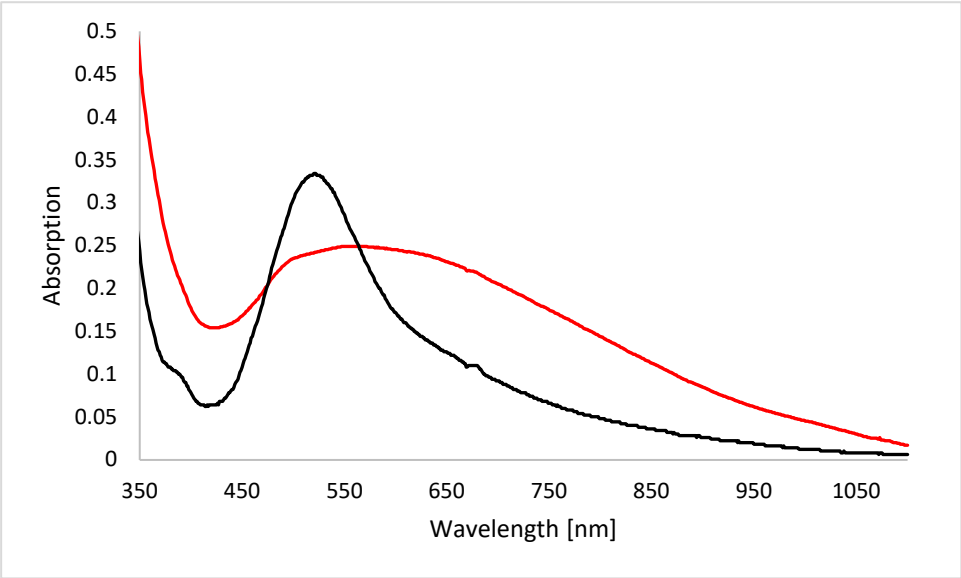

Figure S53. UV/Vis spectra of compounds **4**^{Ph} (red) and **5**^{Ph} (black).

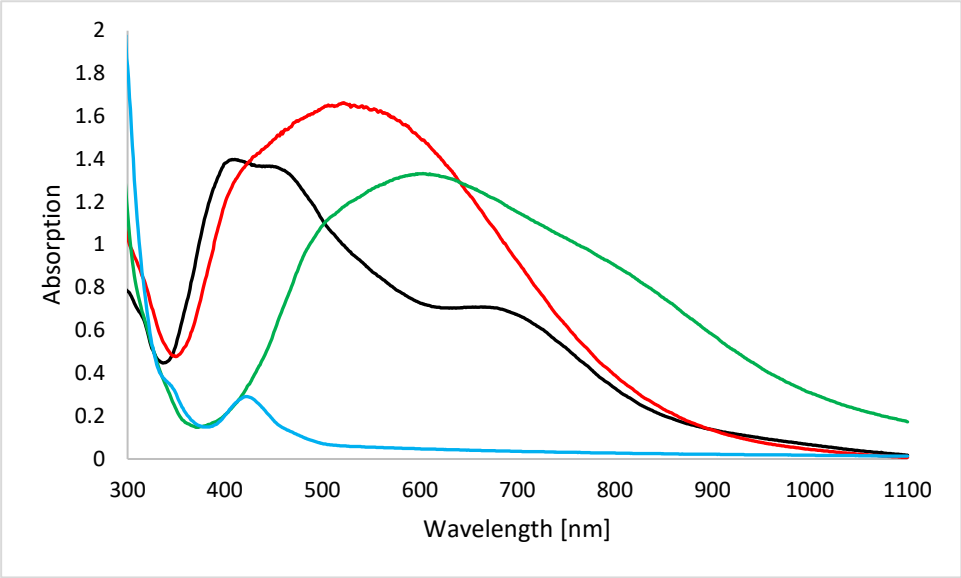

Figure S54. UV/Vis spectra of compounds **1**^{tet} (blue), **6** (green), **7** (red) and **8** (black).

Paper III

Tuning Organocerium Electrochemical Potentials by Extending Tris(cyclopentadienyl) Scaffolds with Terminal Halogenido, Siloxy, and Alkoxy Ligands

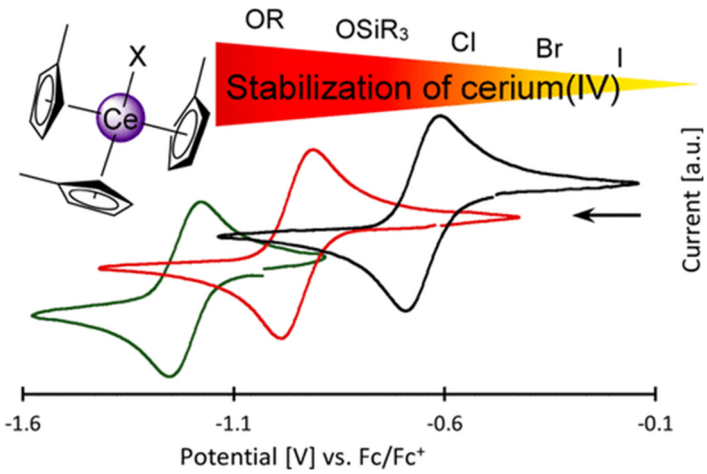

https://doi.org/10.1021/acs.organomet.1c00276
reprinted with permission from
Organometallics, **2021**, 40, 11, 1786 − 1800

ORGANOMETALLICS

pubs.acs.org/Organometallics Article

Tuning Organocerium Electrochemical Potentials by Extending Tris(cyclopentadienyl) Scaffolds with Terminal Halogenido, Siloxy, and Alkoxy Ligands

Lars Hirneise, Jan Langmann, Georg Zitzer, Lukas Ude, Cäcilia Maichle-Mössmer, Wolfgang Scherer,* Bernd Speiser,* and Reiner Anwander*

Cite This: *Organometallics* 2021, 40, 1786–1800 Read Online

ACCESS | Metrics & More | Article Recommendations | Supporting Information

ABSTRACT: Treatment of cerous $Cp^R_3Ce(thf)$ ($Cp^R = C_5H_4R$; R = H, Me) with the halogenating reagents C_2Cl_6, $TeBr_4$, and I_2 afforded the ceric halides Cp^R_3CeX (X = Cl, Br, I) in high yield. Subsequent salt metathesis with sodium alkoxides and siloxides led to a series of alkoxy and siloxy derivatives. Compounds Cp^R_3CeOR' with R′ = Me, Et, CH_2tBu, *i*Pr, *t*Bu, $SiMe_3$, $SiEt_3$, $Si(iPr)_3$ $SiPh_3$ (and $Si(OtBu)_3$) have been isolated and characterized by ^{1}H, ^{13}C, and ^{29}Si NMR and DRIFT spectroscopy, magnetic measurements, X-ray structure analyses, cyclic voltammetry, and elemental analyses. The ceric complexes Cp^R_3CeX and Cp^R_3CeOR' are isostructural, featuring terminal ligands X and OR′. The magnetic measurements revealed temperature-independent paramagnetism (TIP), with positive magnetic susceptibilities in the range χ_0 (1.53–3.9) × 10^{-4} emu/mol. Cyclic voltammetry indicated two types of redox processes: (a) chemical and electrochemical reversibility for halide and siloxide complexes and (b) EC- or ECE-type mechanisms for the alkoxides (chemical reversibility at high scan rates). In all cases formal potentials could be determined ranging from −0.583 V vs Fc/Fc^+ for Cp_3CeI to −1.259 V vs Fc/Fc^+ for $Cp^{Me}_3Ce(OEt)$. The electrochemical data revealed an increase in stabilization with respect to reduction of the cerium(IV) center in the series I < Br < Cl < siloxy < alkoxy ligand and a better stabilization with Cp^{Me} in comparison to Cp ligands by approximately 0.05–0.1 V. As a result, an improved stabilization of Ce(IV) was observed for more strongly electron donating ligands.

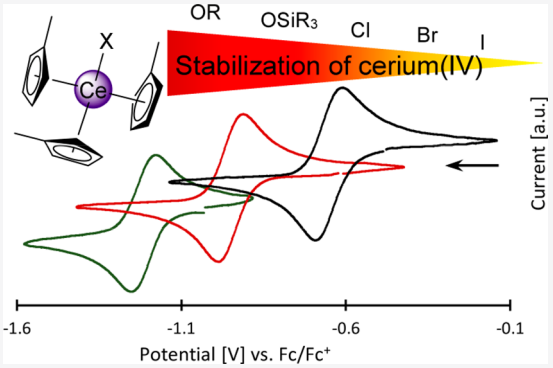

INTRODUCTION

Cerium assumes a unique position within the series of 17 rare-earth metals due to its reversible Ce(III/IV) single-electron-redox chemistry.[1−5] Depending on the coordination sphere and solvent, cerium(IV) potentials are known to span a nominal range of ∼3.5 V, covering strong oxidants but also thermally stable compounds.[2] Ceric ammonium nitrate (CAN) is commonly used in organic synthesis as a one-electron oxidizing agent (E° = 1.61 V vs NHE) and can be handled in an aqueous environment.[6−11] CAN was previously established as a precursor for cerium(IV) alkoxides by Gradeff et al., which paved the way for organocerium(IV) chemistry.[12,13]

Organometallic cerium ("organocerium") chemistry was initially established in 1956 by Birmingham and Wilkinson with the synthesis of tris(cyclopentadienyl) cerium(III), $CeCp_3$ ($Cp = C_5H_5$).[14] It was more than 50 years later that $CeCp_3$ was successfully oxidized with the hypervalent organoiodine(III) compound $PhICl_2$ to afford Cp_3CeCl.[15] While many early reports on putative organocerium(IV) species were later refuted,[16] the first authentic derivatives were synthesized by Greco et al. with "cerocene" $Ce(COT)_2$ (bis(cyclooctatetraenyl) cerium(IV)) and $Cp_3Ce(OiPr)$.[17] The low-yield synthesis of the latter (minute amounts of less than 5%), obtained from $Ce^{IV}(OiPr)_4$, was later improved by Gulino et al. (69% isolated yield) using the nonreducing cyclopentadienyl transfer reagent Me_3SnCp instead of $MgCp_2$.[18] It is worth noting that the isopropoxy derivative $Cp_3Ce(OiPr)$ was the first organocerium(IV) complex to be analyzed by cyclic voltammetry.[18]

The organocerium(IV) compounds $Cp_2Ce(OtBu)_2$ and $Cp_3Ce(OtBu)$ were synthesized by Evans et al. in 1989 starting from CAN, again with cerium already in the oxidation state +4.[19] The *tert*-butoxy derivative $Cp_3Ce(OtBu)$ remained the only ceric cyclopentadienyl derivative characterized by X-ray diffraction (XRD) analysis for over 20 years. More recently, the same CAN-based reaction sequence, via

Received: May 5, 2021
Published: May 24, 2021

$Ce^{IV}(OtBu)_2(NO_3)_2(thf)_2$, gave access to the single-crystalline cerocene(IV) bis(alkoxy) complex $[C_5H_3(SiMe_3)_2\text{-}1,3]_2Ce(OtBu)_2$.[20] Crucially, as initially shown for the synthesis of Cp_3CeCl,[15] the oxidative approach employing cerous tris(cyclopentadienyl) complexes Cp^R_3Ce seemed less prone to ligand redistribution due to the unfavorable formation of Cp^R_4Ce.[15] We could substantiate this hypothesis by clean oxidations of Cp^R_3Ce with trityl chloride, 1,4-benzoquinone, and iodine to give the respective chloride, hydroquinolate and iodide complexes, respectively (Cp^R = Cp^{Me}, C_5H_4Me; Cp′, $C_5H_4SiMe_3$).[21] Moreover, the initial successful salt-metathetical exchange between chlorido species Cp'_3CeCl and KO*t*Bu disclosed a new approach toward ceric alkoxy derivatives.[21] Alkoxy and siloxy ligands are known to strongly stabilize the cerium(IV) center, as evidenced by a broad variety of homoleptic ceric alkoxides and siloxides.[22−30] The robust redox-insensitive siloxy ligands $OSi(OtBu)_3$ and $OSiPh_3$ even allowed for the isolation of molecular terbium(IV) and praseodymium(IV) complexes.[31−33]

The cerium(III/IV) redox behavior can be reasonably assessed by cyclic voltammetry. An overview of the general electrochemical behavior of a broad series of cerium(III/IV) couples in aqueous as well as organic solvents has been given by Schelter et al.[2] However, the electrochemistry of homoleptic cerium alkoxides is likely to be complicated by molecular rearrangement reactions, as revealed by wide peak separations in the cyclic voltammograms of tris(*tert*-butoxy)-siloxy-ligated complexes.[34] We reasoned that a tris(cyclopentadienyl) scaffold would counteract such molecular rearrangements and facilitate a fundamental study of the behavior of the monoanionic ligand X in the ceric complexes Cp^R_3CeX. The present work provides a coherent assessment of the electronic effect of a diverse set of alkoxy, siloxy, and halogenido ligands on cerium(IV) centers, offering a broad tuning range of the electrochemical potential.

RESULTS AND DISCUSSION

Synthesis and Structural Characterization of Ceric Cp^R_3CeX. The readily accessible cerous tris(cyclopentadienyl) complexes $Cp_3Ce(thf)$ (**1a**; Cp = C_5H_5)[14] and $Cp^{Me}_3Ce(thf)$ (**1b**; Cp^{Me} = C_5H_4Me)[35] were selected as starting compounds, mainly for reasons of enhanced steric flexibility.[36] Note that the complex $(C_5Me_4)_3Ce$ refused to undergo oxidation under the applied conditions. The ceric monohalogenido derivatives Cp^R_3CeCl (**2**) and Cp^R_3CeI (**4**) were obtained in high yield according to previously established procedures, employing hexachloroethane (C_2Cl_6) and elemental iodine as oxidants (Scheme 1).[15,21]

The new bromide complexes Cp^R_3CeBr (**3**) could be accessed via reaction with $TeBr_4$, which was initially employed by Lappert et al. for a low-yield synthesis of $Ce[N(SiMe_3)_2]_3Br$ from $Ce[N(SiMe_3)_2]_3$.[37] In contrast to the silylamido ligands, the cyclopentadienyl scaffold seems to favor the formation of the tetravalent complexes **3**. Even using an excess of $TeBr_4$ resulted in a clean reaction and formation of compound **3** in yields >95%. The halogenation reactions were accompanied by an instant color change from bright yellow (cerous **1**) to deep black (ceric **2**−**4**). The ^1H NMR spectra of the halogenated complexes, as representatively shown for the bromido derivative **3b**, revealed signal shifts as expected for diamagnetic compounds (Figure 1; cf. paramagnetic cerous precursor **1b**).

The cerium(IV) chloride complexes **2a** and **2b** were subjected to salt-metathesis reactions with alkali-metal

Scheme 1. Oxidation of $Cp^R_3Ce(thf)$ (1),[14,32] to Form Cerium(IV) Halogenides 2-4

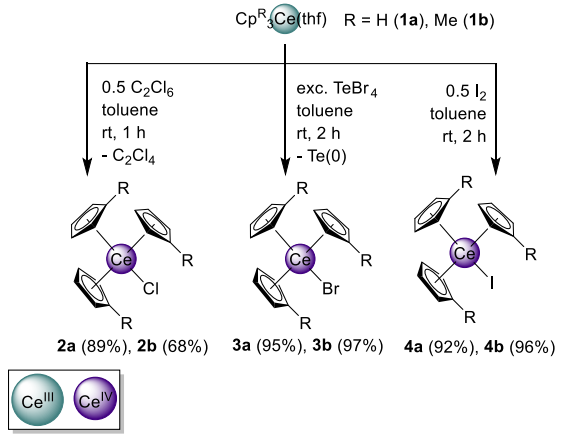

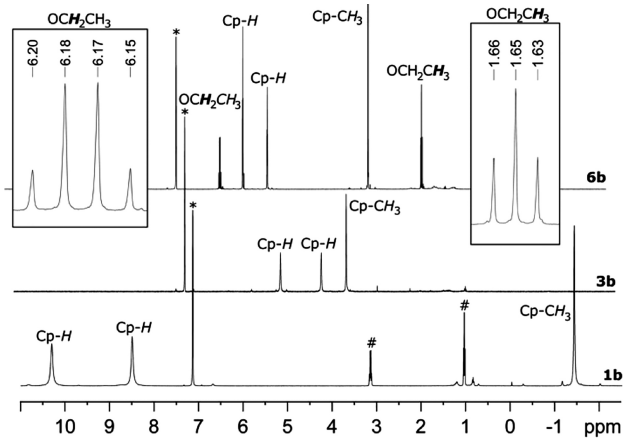

Figure 1. ^1H NMR spectra (400.1 MHz) of compounds $Cp^{Me}_3Ce(thf)$ (**1b**; *c* = 2.7 mg/mL), Cp^{Me}_3CeBr (**3b**), and $Cp^{Me}_3Ce(OEt)$ (**6b**) (C_6D_6, 26 °C) with corresponding Cp-*H*, Cp-C*H*$_3$, and O−C*H*$_2$C*H*$_3$ proton signals. THF signals of **1b** are located at −4.73 and −10.88 ppm, residual Et_2O is marked with #, and C_6D_6 is marked with *.

alkoxides, as shown previously by our group for the synthesis of $Cp'_3Ce(OtBu)$ from Cp'_3CeCl and KO*t*Bu.[21] Accordingly, by employing distinct sodium alkoxides and siloxides a series of monomeric complexes $Cp^R_3Ce(OR)$ (**5**−**13**) could be obtained, in yields ranging from 81% to 97% (Scheme 2). Such tris(cyclopentadienyl) cerium(IV) alkoxides and siloxides are dark brown, which seems to be characteristic of the cyclopentadienyl scaffold bearing cerium(IV). As shown by Rheingold et al. for homoleptic alkoxides, di-*tert*-butyl peroxide can be used as an alternative oxidant.[38] This reagent can be employed for direct conversion of **1a** to $Cp_3Ce(OtBu)$ (**9a**) in 37% yield.

The cerium(IV) alkoxides **5** (OR = OMe), **6** (OR = OEt), **7** (OR = OCH_2tBu), and **8** (OR = $OCHMe_2$) revealed characteristic NMR chemical shifts for the protons in the *α*-position of the alkoxy ligands (Ce−O−C−*H*), as they appear heavily shifted downfield (Table 1). Such a deshielding effect was also observed for the homoleptic cerium(IV) alkoxides $[Ce(OCHMe_2)_4]_3$ and $[Ce(OCH_2tBu)_4]_2(thf)$, albeit to a minor extent.[22,39] The latter complexes show the relevant proton signals at 5.25 and 4.53 ppm, respectively, significantly shifted to lower field in comparison to 4.01 and 3.28 ppm in

https://doi.org/10.1021/acs.organomet.1c00276
Organometallics 2021, 40, 1786−1800

Scheme 2. Scope of Compounds 5−13 Obtained by Salt-Metathesis Reactions of Cp^R_3CeCl (2) with Sodium Alkoxides and Siloxides

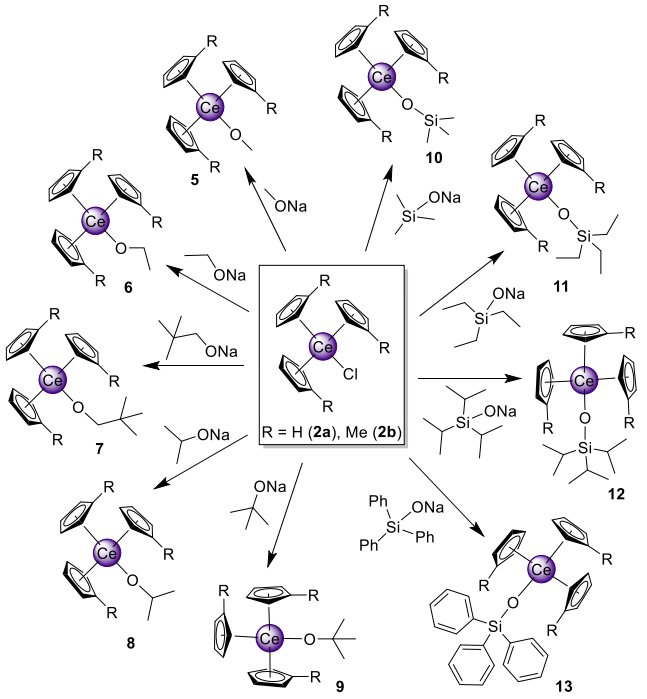

Table 1. NMR Chemical Shifts of the Protons in α-Positions of the Alkoxy Ligands (Ce−O−C−*H*; ppm)

	R = H (**a**)	R = Me (**b**)
$Cp^R_3Ce(OCH_3)$ (**5**)	5.84	5.93
$Cp^R_3Ce(OCH_2tBu)$ (**7**)	5.87	6.09
$Cp^R_3Ce(OCH_2CH_3)$ (**6**)	6.02	6.17
$Cp^R_3Ce[OCH(CH_3)_2]$ (**8**)	6.21	6.40

the free alcohol in $CDCl_3$.[22,39,40] However, the ^{1}H NMR signals of the CH_2 moieties in neopentoxy derivatives $Cp'_3Ce(OCH_2tBu)$ (**7a** and **7b**) are detected at 5.87 and 6.09 ppm, respectively. This indicates a decrease in electron density at the respective protons close to the cerium(IV) center, possibly caused by the +M effect of the alkoxy ligand. The protons are in all cases shifted downfield below the cyclopentadienyl signals. Importantly, the NMR spectra show the signal sets expected for discrete ceric molecules devoid of paramagnetic broadening and shifting. The ^{1}H NMR spectrum of the ethoxy derivative **6b** is representatively shown in Figure 1, the sharp signals/coupling pattern being in accordance with a diamagnetic compound. Similarly, the siloxides **10**−**13** gave NMR spectra indicative of diamagnetic compounds (see the Supporting Information).

The ceric tris(cyclopentadienyl) complexes under study could be obtained as needlelike microcrystals via crystallization from *n*-hexane. Switching to toluene/*n*-hexane mixtures resulted in crystals of suitable size for X-ray diffraction (XRD) analyses. A compilation of selected metrical parameters of complexes **2a**,[15] **2b**,[21] **3b**, **4b**, **5a**, **6a**, **8a**, **8b**, **9a**,[19] **9b**, **10b**, **11a**, **11b**, **13a**, and **13b** is given in Table 2.

Figure 2 depicts the solid-state structure of Cp^{Me}_3CeBr (**3b**), displaying a slightly distorted pseudotetrahedral coordination sphere. Bromide complex **3b** is isostructural with the chloride congener Cp^{Me}_3CeCl (**2b**),[21] showing a Cp ligand alignment where all three methyl substituents point toward the halogenido ligand. In contrast, the Cp ligands of the iodide complex **4b** seem to align differently with two methyl

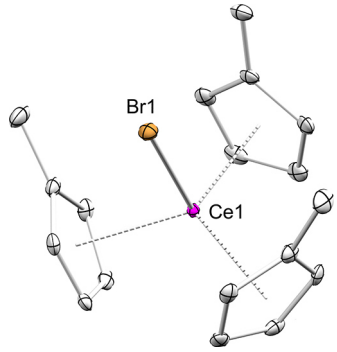

Figure 2. Crystal structure of Cp^{Me}_3CeBr (**3b**). Hydrogen atoms are omitted for clarity. Atomic displacement ellipsoids are set at the 30% probability level. Selected interatomic distances and angles are given in Table 2.

Table 2. Overview of Selected Interatomic Distances and Angles of Compounds 2a,[15] 2b,[19] 3b, 4b, 5a, 6a, 8a, 8b, 9a,[21] 9b, 10b, 11a, 11b, 13a, and 13b

compound	Ce−C(Cp^R) range (Å)	Ce−C(Cp^R) avg. (Å)	Ce−Cnt[a] avg. (Å)	Ce−X (Å)	O−C/Si (Å)	Cnt−Ce−Cnt (deg)	Cnt−Ce−X (deg)	Ce−O−R (deg)
Cp_3CeCl[15] (**2a**)	2.700(2)−2.760(3)	2.733	2.460	2.6666(7)		116.08−117.03	100.08−102.10	
Cp^{Me}_3CeCl[21] (**2b**)	2.716(3)−2.771(3)	2.742	2.482	2.658(1)		116.87−119.90	98.36−103.20	
Cp^{Me}_3CeBr (**3b**)	2.716(2)−2.839(3)	2.758	2.567	2.8283(5)		115.38−119.61	89.39−104.67	
$Cp_3Ce(OMe)$ (**5a**)	2.750(3)−2.784(3)	2.765	2.503	2.0648(19)	1.402(3)	115.71−116.10	100.52−104.33	164.5(2)
$Cp_3Ce(OEt)$ (**6a**)	2.741(8)−2.807(8)	2.774	2.501	2.067(6)	1.412(9)	114.93−116.36	99.45−105.18	166.1(5)
$Cp_3Ce(OiPr)$ (**8a**)	2.752(3)−2.783(3)	2.772	2.501	2.067(2)	1.413(4)	115.17−116.38	99.50−103.82	162.7(2)
$Cp^{Me}_3Ce(OiPr)$ (**8b**)	2.768(2)−2.825(2)	2.785	2.513	2.0814(17)	1.480(17)	115.10−116.54	102.02−102.59	176.59(16)
$Cp_3Ce(OtBu)$[19] (**9a**)	2.741(10)−2.790(9)	2.762	2.512	2.045(6)	1.441(13)	116.9−111.8	103.5−101.7	176.3(6)
$Cp^{Me}_3Ce(OtBu)$ (**9b**)	2.740(9)−2.826(12)	2.781	2.512	2.113(19)	1.41(2)	113.89−117.69	99.87−102.95	168(2)
$Cp^{Me}_3Ce(OSiMe_3)$ (**10b**)	2.733(4)−2.812(4)	2.770	2.487	2.118(2)	1.633(3)	112.57−117.50	100.73−103.33	158.54(16)
$Cp_3Ce(OSiEt_3)$ (**11a**)	2.73(3)−2.794(13)	2.763	2.493	2.108(6)	1.665(9)	115.15−117.72	101.14−101.33	172.8(5)
$Cp^{Me}_3Ce(OSiEt_3)$ (**11b**)	2.704(17)−2.795(8)	2.751	2.500	2.114(6)	1.617(7)	119.59−116.97	101.83−86.89	175.4(5)
$Cp_3Ce(OSiPh_3)$ (**13a**)	2.731(10)−2.813(14)	2.765	2.491	2.1331(19)	1.620(2)	115.09−117.17	99.87−103.39	174.65(12)
$Cp^{Me}_3Ce(OSiPh_3)$ (**13b**)	2.705(7)−2.866(6)	2.775	2.503	2.168(3)	1.616(3)	115.23−116.12	101.43−102.92	154.37(17)

[a]Cnt = Cp^R ring centroid.

https://doi.org/10.1021/acs.organomet.1c00276
Organometallics 2021, 40, 1786−1800

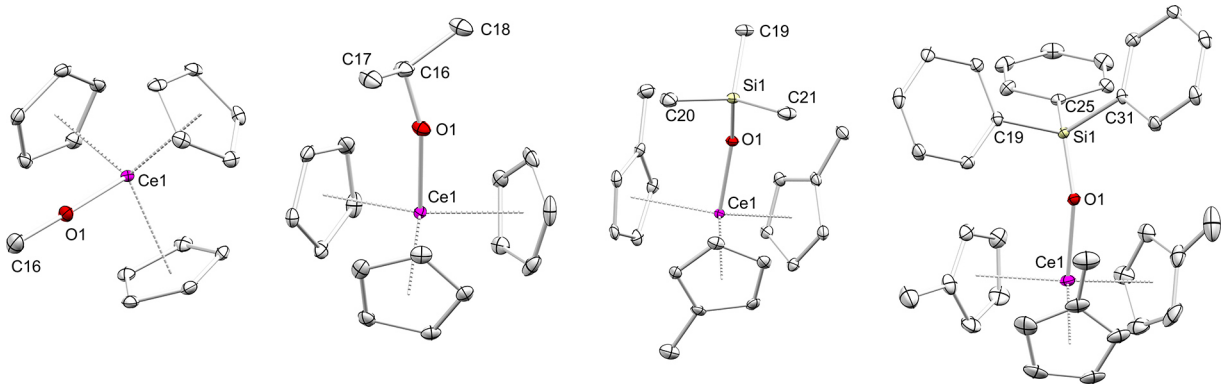

Figure 3. Crystal structures of the alkoxides $Cp_3Ce(OMe)$ (**5a**) and $Cp_3Ce(OiPr)$ (**8a**) as well as of the siloxides $Cp^{Me}{}_3Ce(OSiMe_3)$ (**10b**) and $Cp^{Me}{}_3Ce(OSiPh_3)$ (**13b**), with atomic displacement ellipsoids set at 30% probability. Hydrogen atoms and disorders (**8a**) are omitted for clarity. Selected interatomic distances and angles are given in Table 1.

substituents pointing away from the larger halogenido ligand. The crystal structure of **4b** is heavily disordered (Figure S59), excluding a detailed discussion of the metrical parameters. Unsurprisingly, the Ce−X(halogenido) distances increase with the size of the halogen atom (**2b**, 2.658(1) Å;[21] **3b**, 2.8283(5) Å). The average Ce−Cnt (centroid) distances are the shortest in the case of a more electronegative halogen (**2b**, 2.482 Å; **3b**, 2.567 Å).[21] For further comparison, the Ce−X distances of the four-coordinate mixed silylamido/halogenido complexes $Ce[N(SiMe_3)_2]_3X$ were detected at 2.597(2) Å (X = Cl), 2.766(2) Å (X = Br), and 2.9980(2) Å (X = I), respectively.[41] These are significantly shorter (Cl, Br) than in the Cp derivatives, while the variation of the halogenido ligand barely changes the distance toward the silylamido nitrogen atom (2.217(3), 2.219(7), and 2.2153(9) Å).[42]

The solid-state structures of the alkoxides $Cp_3Ce(OMe)$ (**5a**) and $Cp_3Ce(OiPr)$ (**8a**) as well as of the siloxides $Cp^{Me}{}_3Ce(OSiMe_3)$ (**10b**) and $Cp^{Me}{}_3Ce(OSiPh_3)$ (**13b**) are shown in Figure 3. It is clear that the complexes keep the structural motif of a pseudotetrahedral coordination sphere, as do the other solid-state structures in this study. Even the complex $Cp^{Me}{}_3Ce[OSi(OtBu)_3]_3$ (**14**, S59), bearing a potentially chelating siloxy ligand, exhibits a terminal *κO* coordination mode. Complex **14** was characterized via X-ray diffraction and NMR spectroscopy but was not obtained in pure form and was therefore excluded from further studies. The new alkoxy derivatives display Ce−O distances in the range of 2.0648(19) (**5a**) to 2.113(19) Å (**9b**), matching the 2.045(6) and 2.071(1) Å of the previously reported *tert*-butoxy derivatives **9a**[19] and $Cp'_3Ce(OtBu)$, respectively.[21] The Ce−O distances of the Cp^{Me}-supported complexes are slightly longer, as seen for the isopropoxy derivative **8a** (2.067(2) Å) versus **8b** (2.0814(17) Å).

For further comparison, the terminal Ce−O distances in homoleptic $[Ce(OtBu)_4]_2$[43] and $[Ce(OCH_2tBu)_4]_3$[22] range from 2.058(3) to 2.065(3) Å and from 2.029(1) to 2.030(2) Å, respectively, while the terminal Ce−O(methoxy) distance in $Ce[OSi(OtBu)_3]_3(OCH_3)(thf)_2$ is 2.094(1) Å.[29] Generally, the Ce−O distances span a wide range depending on the coordination number and terminal/μ_x-bridging mode: e.g., as detected for ceric $Ce_3(\mu_3\text{-}OiPr)_2(\mu_s\text{-}OiPr)_3(OiPr)_7$ (2.061(4)−2.721(3) Å).[39] The Ce−O−C angles appear affected by both the sterics of the alkoxy and Cp ligands and the Cp alignment (minimum, OMe/Cp (**5a**) 164.5(2)°; maximum, OiPr/Cp (**8b**) 176.6(2)°). The average Ce−Cnt distances of the alkoxy complexes are very similar (2.503−2.513 Å) but are longer than in the chlorido derivatives (2.460 and 2.482 Å)[15,21] and shorter than in the bromide complex **3b** (2.567 Å).

The Ce−O distances of the siloxide complexes are elongated by approximately 0.05 Å in comparison to the alkoxides, with distances ranging from 2.108(6) Å for **11a** to 2.168(3) Å for **13b**. These are quite comparable to the terminal Ce−O distances of four-coordinate cerous $[Ce(OSiPh_3)_2(\mu\text{-}OSiPh_3)]_2$ (2.185(6) and 2.151(7) Å) and six-coordinate $Ce(OSiPh_3)_4(DME)$ (2.10(1) and 2.13(1) Å).[44,45] The terminal Ce−O distances of $Ce[OSi(OtBu)_3]_4$ range from 2.089(2) to 2.103(2) Å, hence being slightly shorter.[34] On the other hand, the average Ce−Cnt distances, 2.487 Å for **10b** and 2.503 Å for **13b**, are shorter than those of the alkoxy congeners. Also, the Cp^{Me} derivatives exhibit on average longer Ce−Cnt distances in comparison to the Cp analogues, reflecting the increased steric demand (2.493 Å (**11a**) vs 2.500 Å (**11b**); 2.491 Å (**13a**) vs 2.503 Å (**13b**)). Similarly, the Ce−O−Si angles ranging from 154.37(17)° (**13b**) to 178.4(5)° (**11b**) seem to result from steric congestion and/or crystal-packing effects.

Overall, the cyclopentadienyl ligands seem to stabilize cerium(IV), as various ligands can be introduced ranging from methoxy to triphenylsiloxy by exploiting the high oxophilicity of cerium and hence the strong Ce−O bond. No ligand displacement or scrambling was observed for any of the compounds.

Electrochemical Properties. Complexes **1**−**13** were examined by cyclic voltammetry under exclusion of oxygen and moisture in a glovebox (argon atmosphere) at ambient temperature with a glassy-carbon (GC) working electrode. Potentials are referenced to the Fc/Fc^+ redox couple used as an internal standard. An interaction between the cerium compounds and ferrocene was excluded in all cases, which makes the use of the internal standard a viable option. The cerium compounds under study show two typical types of behavior evident from the qualitative shapes of the cyclic voltammograms: a chemically reversible redox process with a quasi-reversible electron transfer step and a mechanism involving a follow-up reaction of the ECE type. Both will be discussed in detail, including some quantitative analysis of the peak data.

Compounds $Cp^R{}_3CeX$ with R = H, Me and X = Cl, Br, I all show qualitatively similar cyclic voltammograms, which will be

https://doi.org/10.1021/acs.organomet.1c00276
Organometallics 2021, 40, 1786−1800

outlined in the following for Cp^{Me}_3CeCl (**2b**). Details on the other complexes can be found in the Supporting Information. The peak separation for **2b** accounts to 73 mV at 50 mV/s, which is close to the ideal value of 58 mV for an electrochemically reversible one-electron-redox step. The value increases with the scan rate v, indicating that the process becomes quasi-reversible at higher v. When the peak current i_p is analyzed as a function of the square root of the scan rate, a straight line of best fit with $R^2 > 0.999$ resulted, indicative of a diffusion-controlled redox step. According to the peak current ratio i_{pa}/i_{pc}, which is close to 1, almost all of the analyte, which is reduced, gets reoxidized.[46] This excludes significant follow-up reactions and is evidence of chemical reversibility. Consequently, the halide complexes show a chemically reversible as well as electrochemically (quasi-)reversible one-electron-redox process. The formal potentials E°—determined as the midpoint potentials $(E_{pa} + E_{pc})/2$—are independent of the scan rate v and are compiled for **2b** in Table 3.

Table 3. Electrochemical Data for the Cerium(III/IV) Peak Couple of Cp^{Me}_3CeCl (2b) vs Fc/Fc^+ in THF[a]

v (mV/s)	E_{pa} (V)	E_{pc} (V)	E° (V)	ΔE_p (V)	i_{pa}/i_{pc}
50	−0.764	−0.837	−0.801	0.073	0.995
100	−0.760	−0.841	−0.801	0.081	0.998
250	−0.754	−0.847	−0.801	0.093	0.995
500	−0.750	−0.852	−0.801	0.102	0.997
1000	−0.746	−0.857	−0.802	0.111	0.994
2000	−0.742	−0.860	−0.801	0.118	0.997

[a]At a glassy-carbon electrode: c(analyte) 1 mM, c(electrolyte) 0.1 M [nPr$_4$N][BARF].

The formal potentials of all halide complexes **2**–**4** range between −0.583 V for **4a** and −0.801 V for **2b** (*vide infra*, Table 6). The cyclic voltammograms of Cp^{Me}_3CeCl (**2b**) and Cp_3CeBr (**3a**, E° = −0.652 V) are displayed in Figure 4. A

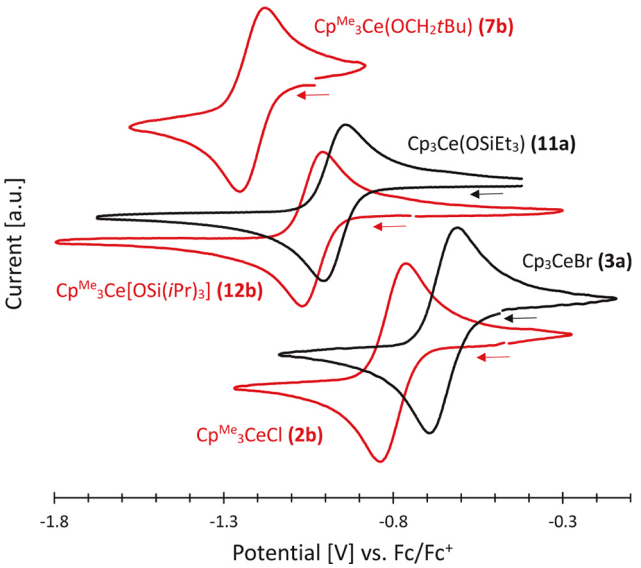

Figure 4. Cyclic voltammograms of the cerium(III/IV) redox couples of Cp^{Me}_3CeCl (**2b**, red), Cp_3CeBr (**3a**, black), $Cp_3Ce(OSiEt_3)$ (**11a**, black), $Cp^{Me}_3Ce[OSi(iPr)_3]$ (**12b**, red), and $Cp^{Me}_3Ce(OCH_2tBu)$ (**7b**, red) vs Fc/Fc^+ in THF at a glassy-carbon electrode obtained at a scan rate of 50 mV/s. Arrows indicate the initial scan direction: c(analyte) 1 mM, c(electrolyte) 0.1 M [nPr$_4$N][BARF].

direct comparison of Cp- and Cp^{Me}-supported complexes (**a** versus **b**) results in more negative potentials for the methyl-substituted derivatives, indicating a better stabilization of the cerium(IV) center by about 0.1 V with respect to reduction. The choice of the halogen atom affects the potential much more strongly, and stabilization of the +IV oxidation state decreases in the order Cl > Br > I.

The electrochemical data of the siloxide complexes feature similar results concerning the redox mechanism. For example, the peak potentials of $Cp^{Me}_3Ce(OSiPh_3)$ (**13b**) exhibit a peak separation of 63 mV at 50 mV/s (Table 4, Figure S112), which

Table 4. Electrochemical Data for the Cerium(III/IV) Peak Couple of $Cp^{Me}_3Ce(OSiPh_3)$ (13b) vs Fc/Fc^+ in THF[a]

v (mV/s)	E_{pa} (V)	E_{pc} (V)	E° (V)	ΔE_p (V)	i_{pa}/i_{pc}
50	−0.981	−1.044	−1.013	0.063	0.93
100	−0.974	−1.047	−1.011	0.073	0.96
250	−0.968	−1.052	−1.010	0.084	1.00
500	−0.965	−1.062	−1.014	0.097	1.00
1000	−0.960	−1.074	−1.017	0.114	1.00
2000	−0.948	−1.082	−1.015	0.134	0.97

[a]At a glassy-carbon electrode: c(analyte) 1 mM, c(electrolyte) 0.1 M [nPr$_4$N][BARF].

increases with v. In combination with $R^2 > 0.999$ for the i_p vs the square root of v plot, this indicates diffusion control and an electrochemically quasi-reversible one-electron-redox mechanism. The peak current ratio i_{pa}/i_{pc} stays close to 1, suggesting chemical reversibility. Moreover, the resulting E° values do not significantly depend on the scan rate.

Compound **13b** was also investigated at a Pt electrode with a THF electrolyte based on 0.1 M NBu_4PF_6 (see the Supporting Information), in scan-rate- and concentration-dependent experiments. The absence of an iR drop is proven by the fact that the peak potentials are independent of the concentration of **13b**. Under these conditions, while chemical reversibility is again apparent, the electron-transfer kinetics are somewhat faster than at the GC electrode and an electrochemically reversible process is found. Given the different electrode material, this appears to be a reasonable behavior. Moreover, the formal potential is shifted from −1.013 to −0.930 V vs Fc/Fc^+, probably caused by the change of the supporting electrolyte anion. The diffusion coefficient of $Cp^{Me}_3Ce(OSiPh_3)$ (**13b**) in the PF_6^--based electrolyte was determined from peak current data as $D = 2.75 \times 10^{-6}$ cm^2/s, and the electron-transfer rate at the Pt electrode was estimated from simulations as $k_s = 0.03$ cm/s. This is more than 1 order of magnitude faster than the result for BINOL-ligated cerium(III) complexes calculated by Schelter et al.,[47] i.e., the electron transfer appears to be more reversible in our cases. Overall, there have been few studies on the kinetics of cerium compounds in organic solvents, as the main focus has been on the investigation of cerium(IV) in aqueous acidic media due to its multiple applications, including batteries (especially V/Ce and Zn/Ce) and fuel cells.[48−50]

The cyclic voltammograms of the siloxide complexes $Cp_3Ce(OSiEt_3)$ (**11a**) and $Cp^{Me}_3Ce[OSi(iPr)_3]$ (**12b**) (Figure 4) show one-electron-redox processes similar to those of the halogenido derivatives, with even smaller peak separations of 60 mV (**11a**) and 61 mV (**12b**). Importantly, the E° values of −0.973 V (**11a**) and −1.039 V (**12b**) are more negative in comparison to the halogenido congeners, indicating a higher

https://doi.org/10.1021/acs.organomet.1c00276
Organometallics 2021, 40, 1786−1800

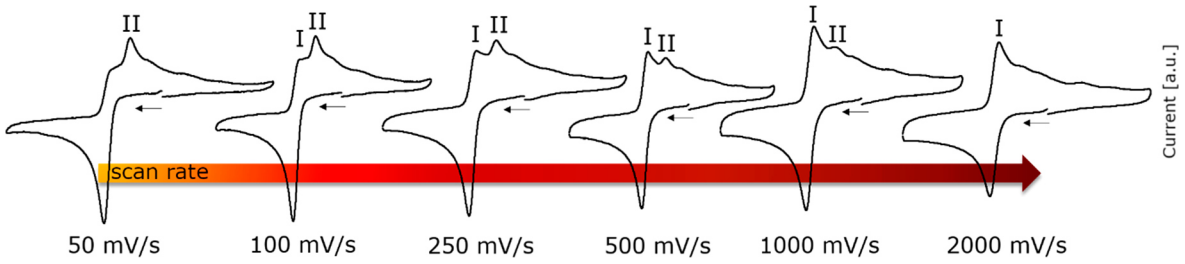

Figure 5. Cyclic voltammograms of the cerium(III/IV) redox couple of $Cp_3Ce(OtBu)$ (**9a**) vs Fc/Fc^+ in THF at a glassy-carbon electrode at different scan rates. Black arrows indicate the initial scan directions: *c*(analyte) 1 mM, *c*(electrolyte) 0.1 M $[nPr_4N][BARF]$.

stabilization toward reduction of cerium(IV) (Table 6). The range of potentials reaches from −0.936 V (**13a**) to −1.087 V (**10b**) (Table 6). Again, Cp^{Me} causes a stronger stabilization of the +IV oxidation state in comparison to Cp. Among the siloxy ligands the triphenylsiloxy ligand exhibits weaker stabilization in comparison to trialkylsiloxy ligands.

In contrast to the cyclic voltammograms of the halide and siloxide complexes, most of the alkoxy derivatives exhibit a different electrochemical behavior. The only electrochemically and chemically reversible case was observed for the neopentoxide complex $Cp^{Me}{}_3Ce(OCH_2tBu)$ (**7b**) (Figure 4). The cyclic voltammograms of the alkoxy/Cp compounds **5a**−**9a** are more complex and display multiple reoxidation signals. The behavior of $Cp_3Ce(OtBu)$ (**9a**) with increasing scan rates (indicated by the red arrow) is exemplarily shown in Figure 5 and numerically summarized in Table 5.

Table 5. Electrochemical Data for the Cerium(III/IV) Couple of $Cp_3Ce(OtBu)$ (9a) vs Fc/Fc^+ in THF[a]

ν (mV/s)	E_{pa} (V)	E_{pc} (V)	E° (V)	ΔE_p (V)	i_{pa}/i_{pc}
50	*b*	−1.200	*b*	*b*	*b*
100	−1.130	−1.204	−1.167	0.073	0.67
250	−1.126	−1.209	−1.168	0.083	0.64
500	−1.131	−1.215	−1.173	0.084	0.75
1000	−1.124	−1.223	−1.174	0.099	0.87
2000	−1.125	−1.231	−1.178	0.106	0.96

[a]At a glassy-carbon electrode: *c*(analyte) 1 mM, *c*(electrolyte) 0.1 M $[nPr_4N][BARF]$. [b]Could not be determined.

For high scan rates the reoxidation peak **I** is prominent (i_{pa}/i_{pc} ratio = 0.96 at 2 V/s), corresponding directly to the reduction peak, as indicated by a ΔE_p value of approximately 106 mV (quasi-reversibility). Only minor additional oxidation signals are found at less negative potentials. With smaller scan rates ν, the relative intensity of oxidation peak **I** decreases (i_{pa}/i_{pc} ratio <0.7), while signal **II** becomes dominant. This scan rate dependence indicates the presence of a kinetic process in the form of a follow-up reaction. For smaller ν, the kinetic process leads to the favorable formation of an intermediate species that can further be oxidized in peak **II**.

Overall, the voltammetric features are consistent with an ECE process. The minor signals remain present at slower ν and may indicate the formation of oxidizable side products. Accordingly, the midpoint potential can only be properly used at scan rates above 0.1 V/s as an approximation for E°. The exact mechanism and product(s) of the follow-up reaction could not be identified, but the formation of $Cp_2Ce(OtBu)_2$ and $[Ce(OtBu)_3]$ in the course of the follow-up reaction could be ruled out by a comparison of the respective cyclic voltammograms and potentials. As the signals are specific for each alkoxy rest, the *in situ* generated species must include at least one alkoxy ligand, ruling out its dissociation. Probably some intermediate of the form "$Cp_2Ce(OR)$" is generated in the chemical step of the ECE process and reoxidized in the reversed scan. Such a species could, however, not be accessed via synthesis.

Interestingly, switching from alkoxy/Cp to alkoxy/Cp^{Me} (**5b** to **9b**) leads to an EC process (for voltammograms, see the Supporting Information), with peak current ratios below 1 for slow scan rates. In contrast to the ECE process, peak **II** is absent, and consequently, the follow-up product does not seem to be oxidizable in the investigated potential range. All alkoxy compounds except for **7b** therefore show redox mechanisms with an irreversible follow-up reaction. Such consecutive reactions are prevalent at slow scan rates and simplify to a quasi-reversible one-electron process for faster time scales, when the "C" step becomes almost insignificant. Table 6 includes only the formal potentials of the alkoxy complexes determined at a scan rate of 1 V/s, to avoid the introduction of potential shifts due to the coupled chemical reaction.

The electrochemical behavior of $Cp_3Ce(OiPr)$ (**8a**) as found in the present work is no exception, being characterized by an ECE mechanism at slow scan rates, which converges into a reversible cyclic voltammogram at high ν. The electrochemical behavior of **8a** was first examined by Gulino et al. in 1988, and a potential of +0.01 V vs Fc/Fc^+ (+0.32 V vs SSCE) in THF using $TBABF_4$ as an electrolyte was stated.[18] No further signals were reported, and the cyclic voltammogram was interpreted as being associated with a fully reversible process. This is in stark contrast to the data obtained in our study. The cyclic voltammograms of **8a** in THF in electrolytes based on $[nPr_4N][BARF]$ and $TBABF_4$ show reduction peak potentials of −1.177/−1.153 V vs Fc/Fc^+ (Figure 6). Both the shape and the potential range deviate clearly from the curve reported previously. For both electrolytes, the ECE-type mechanism is clearly supported by the voltammetric shapes (see scan-rate-dependent voltammograms; Figure 6, bottom graphic).

For an assessment of the organocerium compounds **1**−**13**, the formal redox potentials are graphically summarized in Figure 7. The values of E° reflect the relative thermodynamic stability of the Ce(IV) and Ce(III) redox states. A more negative potential indicates that Ce(IV) is more difficult to reduce. The plot thus highlights the relative stability increase of the +IV oxidation state in complexes $Cp^R{}_3CeX$, when the ligand scaffold is changed from Cp (=C_5H_5, blue) to Cp^{Me} (=C_5H_4Me, red) as well as the presence of distinct coligands X. In addition, a numerical compilation is given in Table 6 by increasingly negative values of E°, i.e., an increasing stability of

https://doi.org/10.1021/acs.organomet.1c00276
Organometallics 2021, 40, 1786−1800

Table 6. Formal Potentials vs Fc/Fc^+ of 1−13 Sorted by Increasing Stability of the Cerium(IV) Oxidation State

compound	E° (V)[a]
$Cp_3Ce(thf)$ (**1a**)	−0.265
$Cp^{Me}{}_3Ce(thf)$ (**1b**)	−0.377
Cp_3CeI (**4a**)	−0.583
Cp_3CeBr (**3a**)	−0.652
$Cp^{Me}{}_3CeI$ (**4b**)	−0.682
Cp_3CeCl (**2a**)	−0.695
$Cp^{Me}{}_3CeBr$ (**3b**)	−0.761
$Cp^{Me}{}_3CeCl$ (**2b**)	−0.801
$Cp_3Ce(OSiPh_3)$ (**13a**)	−0.936
$Cp_3Ce(OSiEt_3)$ (**11a**)	−0.973
$Cp_3Ce[OSi(iPr)_3]$ (**12a**)	−0.980
$Cp^{Me}{}_3Ce(OSiPh_3)$ (**13b**)	−1.013
$Cp_3Ce(OSiMe_3)$ (**10a**)	−1.021
$Cp^{Me}{}_3Ce[OSi(iPr)_3]$ (**12b**)	−1.039
$Cp^{Me}{}_3Ce(OSiEt_3)$ (**11b**)	−1.080
$Cp^{Me}{}_3Ce(OSiMe_3)$ (**10b**)	−1.087
$Cp_3Ce(OMe)$ (**5a**)	−1.102*
$Cp_3Ce(OCH_2tBu)$ (**7a**)	−1.151*
$Cp_3Ce(OEt)$ (**6a**)	−1.155*
$Cp_3Ce(OtBu)$ (**9a**)	−1.174*
$Cp_3Ce(OiPr)$ (**8a**)	−1.177*
$Cp^{Me}{}_3Ce(OMe)$ (**5b**)	−1.206*
$Cp^{Me}{}_3Ce(OCH_2tBu)$ (**7b**)	−1.220*
$Cp^{Me}{}_3Ce(OiPr)$ (**8b**)	−1.244*
$Cp^{Me}{}_3Ce(OtBu)$ (**9b**)	−1.252*
$Cp^{Me}{}_3Ce(OEt)$ (**6b**)	−1.252*
$Ce(C_8H_8)_2$	−1.4 V[b,52]
$Ce(C_8Me_6)_2$	−0.830 V[c,53]
$Ce[C(Ph_2PNSiMe_3)_2]_2$	−1.63 V[54]

[a]At 50 mV/s (* = at 1 V/s) in THF at a glassy-carbon electrode: electrolyte $[nPr_4N][BARF]$. [b]Other data (conditions in parentheses): −1.52 V (SSCE),[18] −1.28 V (NHE, THF, $TBABF_4$),[51] −0.8 V (SCE, THF)[52] or −0.6 V (NHE, THF, $TBAPF_6$).[52] [c]Solvent not stated.

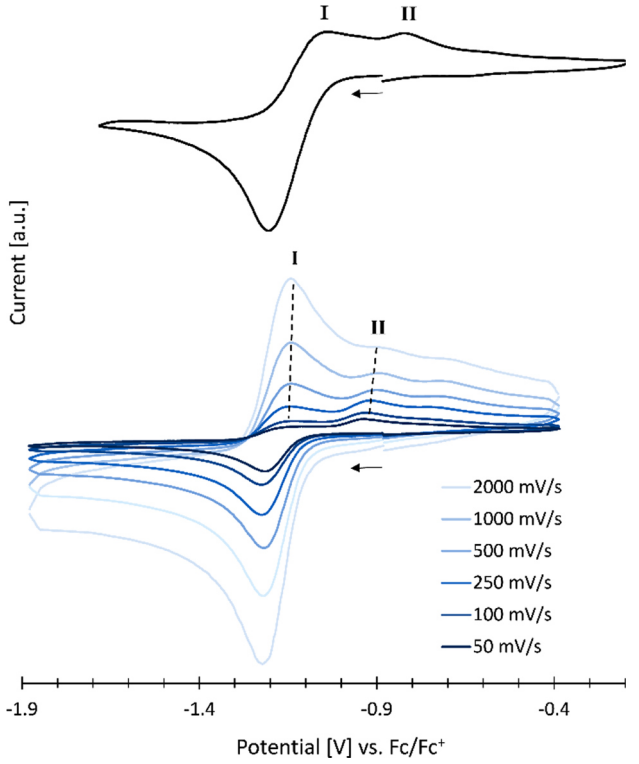

Figure 6. Cyclic voltammograms of the cerium(III/IV) redox couple of $Cp_3Ce(OiPr)$ (**8a**) vs Fc/Fc^+ in THF at a glassy-carbon electrode and different electrolytes obtained at different scan rates (bottom) and a scan rate of 50 mV/s (top). Arrows indicate the initial scan direction: *c*(analyte) 1 mM, *c*(electrolyte) 0.1 M $[nPr_4N][BARF]$ (bottom) and $TBABF_4$ (top).

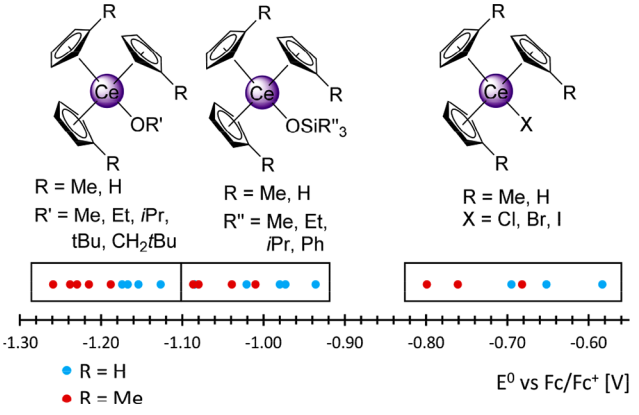

Figure 7. Distinct stabilization of cerium(IV) by alkoxy, siloxy, and halogenido ligands.

the ceric complex toward reduction. This can be correlated with a higher electron density at the Ce(IV) center.

Alkoxy ligands do exert the highest stabilizing effect on the cerium(IV) oxidation state, as revealed by E° values in the range −1.102 V (**5a**) to −1.252 V (**6b** and **9b**). Lower stabilization is achieved in the presence of siloxy, and even less through halogenido ligands. The reason for this order is presumably the ability to donate electron density to the cerium(IV) center, as all ligands have a −I effect, but the +M effect is increasing from halogenido to siloxy and alkoxy ligand. The E° values indicate that halogenido ligands stabilize the cerium(IV) center in the order Cl > Br > I. Again, the −I effect due to the lower electronegativity is superimposed by the +M effect and possibly also by the enhanced steric demand of the higher homologues. Siloxy ligands, especially for X = $OSiMe_3$, stabilize cerium(IV) distinctively better in comparison to the halogenido ligands. Within this series, the steric effect is again demonstrated: for X = $OSiEt_3$ and $OSi(iPr)_3$, and in particular $OSiPh_3$, decreasing stabilization (in comparison to X = $OSiMe_3$) of the +IV oxidation state is found. As observed for the halides and siloxides, the alkoxides achieve maximum stabilization of the Ce(IV) oxidation state for the tris(Cp^{Me}) scaffold. There is also a clear trend that the most acidic proligands HX (lowest pK_a value) form the least stable (most easily reduced) ceric complexes. This fully complies with the above reasoning, since their anions are those with the least ability to donate electron density.

Strikingly, there are only a few organocerium complexes that have been analyzed by electrochemical methods (see also Table 6).[51−54] The potential of cerocene $Ce(\eta^8\text{-}C_8H_8)_2$ is even more negative at −1.4 V vs Fc/Fc^+.[52] The potential of permethylpentalene $Ce(\eta^8\text{-}C_8Me_6)_2$[53] was detected to be very close at −0.83 V vs Fc/Fc^+, matching that of $Cp^{Me}{}_3CeCl$ (**2b**). Overall, the tris(cyclopentadienyl) scaffold implies a higher stabilization of the cerium(IV) center, although it must be

https://doi.org/10.1021/acs.organomet.1c00276
Organometallics 2021, 40, 1786−1800

Table 7. Overview of Magnetic Properties of Compounds 2b, 8b, 11b, and 13b

compound	C_J (emu K/mol)	Θ_{CW} (K)	χ_0 (10^{-4} emu/mol)	μ_{eff}(Curie) (μ_B)	Ce^{3+} impurity (atom %)
$Cp^{Me}{}_3CeCl$ (**2b**)	0.0668(7)	−2.13(5)	3.9(2)	0.731(4)	8.31(9)
$Cp^{Me}{}_3Ce(OiPr)$ (**8b**)	0.0155(2)	−1.69(5)	1.98(6)	0.352(2)	1.92(2)
$Cp^{Me}{}_3Ce(OSiEt_3)$ (**11b**)	0.00629(9)	−2.39(8)	2.36(2)	0.224(2)	0.78(1)
$Cp^{Me}{}_3Ce(OSiPh_3)$ (**13b**)	0.00607(8)	−2.40(7)	1.53(2)	0.220(2)	0.75(1)

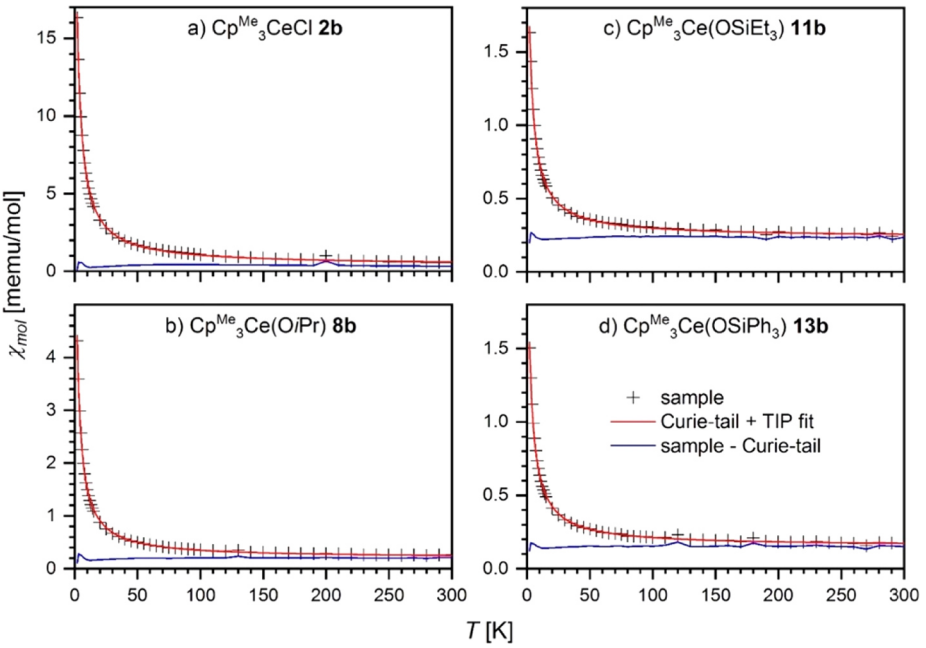

Figure 8. Temperature-dependent molar magnetic susceptibility $\chi_{mol}(T)$ for the complexes $Cp^{Me}{}_3CeCl$ (**2b**, a), $Cp^{Me}{}_3Ce(OiPr)$ (**8b**, b), $Cp^{Me}{}_3Ce(OSiEt_3)$ (**11b**, c), and $Cp^{Me}{}_3Ce(OSiPh_3)$ (**13b**, d) corrected for diamagnetic contributions of the ligand sphere using Pascal's constants (black crosses). The red line represents a modified Curie−Weiss fit including a temperature-dependent (Curie-tail) and a temperature-independent (TIP) part. Subtraction of the Curie-tail from the measured data yields the temperature-independent magnetic contributions, signified by a blue line.

noted that the exact experimental conditions were not specified for $Ce(C_8Me_6)_2$.[53]

Particularly useful in elucidating the stabilization of the Ce(IV) center in the tris(cyclopentadienyl)-supported halides is the comparison to other "complete" halide series such as $[(Me_3Si)_2N]_3CeX$[41] and $(TriNO_x)CeX$ (H_3TriNO_x = N-$[CH_2C_6H_4(2\text{-}t\text{BuNOH})]_3$).[55,56] The silylamide complexes display potentials of −0.56 V vs Fc/Fc^+ (X = F), −0.30 V vs Fc/Fc^+ (X = Cl), and −0.31 V (X = Br) vs Fc/Fc^+, while the iodide derivative $[(Me_3Si)_2N]_3CeI$ was unstable under the experimental conditions.[41] Therefore, the cyclopentadienyl ligands confer better stabilization to cerium(IV) (**2a**, −0.695 V; **2b**, −0.799 V). This is also reflected in the electrochemical behavior of the cerous precursors $Ce[N(SiMe_3)_2]_3$, Cp_3Ce-(thf) (**1a**), and $Cp^{Me}{}_3Ce$(thf) (**1b**). The potential of the homoleptic silylamide was previously determined as +0.35 V ($E_{1/2}$ vs Fc/Fc^+).[41] For complexes **1a** and **1b**, both chemical and electrochemical (quasi-)reversibility was found at potentials of −0.265 and −0.377 V, respectively, in particular for higher scan rates (Table 6). This again confirms the improved stabilization of Ce(IV) in the presence of Cp^{Me} over Cp ligands (by approximately 0.11 V), as **1b** gets oxidized more easily. Moreover, this markedly distinct electrochemical behavior was also revealed by chemical redox reactions. The oxidation of $Ce[N(SiMe_3)_2]_3$ has been attempted with many oxidants, which mostly afforded low yields and product mixtures,[41,57] whereas the oxidation of complexes $Cp^R{}_3Ce$(thf) is quantitative for several agents, including elemental iodine and $TeBr_4$.[15,21,58] On the other hand, the $TriNO_x$ scaffold provides improved stabilization, as evidenced for E_{pc} potentials of −1.40 V (X = F), − 1.26 V (X = Cl), −1.16 V (X = Br), and −1.00 (X = I, I^- completely dissociated) vs Fc/Fc^+, in dichloromethane.[55] For further comparison, the heterobimetallic complexes $[Li_3(dmeda)_3][BINOLate]_3CeX$ display $E_{1/2}$ values of −0.915 V (X = Cl), −0.900 V (X = Br), and −0.950 (X = I) vs Fc/Fc^+, in THF.[59]

Glancing at several homoleptic ceric complexes CeL_4, the stabilization of the cerium(IV) center is very efficient for L = O*t*Bu (E_{pc} = −1.99 V vs Fc/Fc^+)[60] and L = $OSi(OtBu)_3$ (E_{pc} = −1.46 V vs Fc/Fc^+).[34] Interestingly, the aryloxy ligand (L = $OC_6H_3(C_6H_5)_2$-2,6; E_{pc} = −0.54 V vs Fc/Fc^+) is far less stabilizing than the bis(dimethylsilyl)amido fragment (L = $N(SiHMe_2)_2$; E_{pc} = −1.14 V vs Fc/Fc^+).[57] This is in agreement with our findings of alkoxides as efficient stabilizing ligands for the cerium(IV) center, notably much better than Cp ligands, on comparison of homoleptic with heteroleptic alkoxide complexes. However, most homoleptic alkoxides and siloxides show strongly separated peaks in the cyclic voltammograms, probably due to ligand rearrangement processes.[34,47,60] Apparently, this effect can be drastically reduced in discrete heteroleptic complexes supported by cyclopentadienyl ligands.

The most negative potential for the Cp-supported compounds is achieved in $Cp_3Ce(OiPr)$ (**8a**, −1.174 V vs Fc/Fc^+) and is further increased for the Cp^{Me} ancillary ligand

https://doi.org/10.1021/acs.organomet.1c00276
Organometallics 2021, 40, 1786−1800

in $Cp^{Me}_3Ce(OtBu)$ (**9b**) and $Cp^{Me}_3Ce(OEt)$ (**6b**) with −1.252 V vs Fc/Fc^+. The improved stabilization of the cerium(IV) oxidation state in the case of the sterically more demanding Cp^{Me} ligand seems to result from the +I effect exerted by the methyl substituent. In conclusion, the exchange of the ligands X and substitution at the cyclopentadienyl scaffold of Cp^R_3CeX leads to a variation of potentials, with clearly visible trends even for small structural changes. Thus, a gradual fine-tuning of the electrochemical potentials over the range of 650 mV from −0.583 V vs Fc/Fc^+ for **4a** to −1.252 V vs Fc/Fc^+ for **6b** and **9b** is feasible.

Magnetic Properties. The actual oxidation state of cerocene $Ce(\eta^8\text{-}C_8H_8)_2$ as one of the few putative Ce(IV) organometallics has been discussed and examined in detail over many years.[52,61−66] It has been revealed that it chemically reacts as a Ce(IV) compound, e.g. with cobaltocene, but shows temperature-independent paramagnetism (TIP) at temperatures below 150 K and an oxidation state close to Ce(III) with some Ce(IV) character.[4,61] Notwithstanding, the highly negative potential supports a stabilization of the compound in the +IV state.[2] In order to assess the electronic structure of our ceric tris(cyclopentadienyl) complexes, crystalline samples of **2b**, **8b**, **11b**, and **13b** were studied by variable-temperature SQUID magnetometry (Table 7 and Figure 8). Temperature-dependent molar differential susceptibilities $\chi(T) = (M(H_2) - M(H_1))/(H_2 - H_1)$ have been determined from measurements of the magnetic moment M in two different applied magnetic fields H_1 and H_2. By this procedure the parasitic magnetic contribution of small ferromagnetic impurities—if present—in the sample container could be eliminated. The amount of such impurities could be estimated to be smaller than 2.3×10^{-3} atom % for **2b** (assuming the presence of traces of bulk iron with a magnetic moment of 2.2 μ_B).[67] The presence of spurious iron impurities is further supported by a minute hysteresis in additional field-dependent measurements taken at a temperature of 2 K. Diamagnetic susceptibility contributions from the ligand sphere were calculated from Pascal's constants[68] and subtracted from the $\chi(T)$ data to extract the bare cerium contribution. The thus obtained data were fitted to the modified Curie−Weiss law $\chi(T) = \frac{C_J}{T - \Theta_{CW}} + \chi_0$ with Curie constant C_J, Curie−Weiss temperature Θ_{CW}, and a temperature-independent contribution χ_0.

The observation of Curie paramagnetism in the samples, as quantified by C_J and the effective magnetic moment μ_{eff} calculated therefrom, may be attributed to the presence of paramagnetic Ce^{3+} impurities. With the assumption of a total angular momentum quantum number of $J = 5/2$ (corresponding to the Hund ground state $^2F_{5/2}$ of Ce^{3+}), the Ce^{3+} amounts can be estimated as low as 0.75(1) atom % for $Cp^{Me}_3Ce(OSiPh_3)$ (**13b**) and as high as 8.31(9) atom % for Cp^{Me}_3CeCl (**2b**). The comparatively high Ce(III) content for **2b** could be attributed to the occurrence of sample decomposition during the transport and preparation time needed for the SQUID measurements. For **13b** ligand redistribution was observed to a very small extent over several weeks by means of ^1H NMR spectroscopy, revealing the formation of $Cp^{Me}_2Ce(OSiPh_3)_2$ in addition to various Ce(III) species, which could not be isolated, however. All salient precautions have been taken (cooling chain, inert gas atmosphere (Ar) and light protection) to minimize the effects of sample decomposition. Subtraction of the Curie-tail $\chi(T) = \frac{C_J}{T - \Theta_{CW}}$ invariably leaves a positive and temperature-independent residual susceptibility χ_0 for **2b**, **8b**, **11b**, and **13b**, as shown in Figure 7. However, the respective χ_0 values of the temperature-independent paramagnetism (TIP) are small and fall into a narrow range between $[1.53(2)] \times 10^{-4}$ emu/mol for **13b** and $[3.9(2)] \times 10^{-4}$ emu/mol for **2b**. Similar small TIP values were determined by Halbach et al. for $Ce(trop)_4$ ($[1.2(3)] \times 10^{-4}$ emu/mol), $Ce(acac)_4$ ($[2.1(2)] \times 10^{-4}$ emu/mol) and $Ce(tmtaa)_2$ ($[2.33(6)] \times 10^{-4}$ emu/mol) as well as by Booth et al. for cerocene ($[1.4(2)] \times 10^{-4}$ emu/mol).[61,69] The TIP displayed by the reference molecules was explained in terms of van Vleck paramagnetism due to a multiconfigurational ground state featuring intermediate-valent cerium between Ce(III) and Ce(IV).[69−72]

Supporting Information on the magnetic properties in the dissolved state was obtained from NMR spectroscopic measurements at ambient temperature utilizing the Evans method.[73−75] Effective magnetic moments derived in this way are in good agreement with the effective magnetic moments from Curie−Weiss fits of the SQUID data (**2b**, 0.86 μ_B (Evans method[21]) vs 0.73 μ_B (SQUID); **13b**, 0.24 μ_B (Evans method) vs 0.22 μ_B (SQUID)). This points out similar magnetic properties of the investigated compounds in dissolved and crystalline forms.

CONCLUSIONS

Organocerium(IV) halides Cp^R_3CeX ($Cp^R = C_5H_4R$; R = H, Me; X = Cl, Br, I) can be straightforwardly accessed from cerous $Cp^R_3Ce(thf)$ via halogenation with C_2Cl_6, $TeBr_4$, and I_2. The chloride complexes readily engage in salt-metathesis reactions with sodium alkoxides and siloxides. Due to the robust and rigid tris(cyclopentadienyl) scaffold, the discrete complexes Cp^R_3CeX and $Cp^R_3Ce(OR)$ (OR = alkoxy, siloxy) feature the same structural motif with the Ce(IV) center adopting a pseudotetrahedral coordination geometry. The terminal non-Cp ligands provide a unique setting for investigating their bonding toward the cerium center. Note that rare-earth-metal halide and alkoxide/siloxide complexes naturally display distinct agglomeration behavior depending on the steric bulk of the ligand and the oxidation state of the metal center. Cyclic voltammetry revealed that the formal redox potentials of complexes Cp^R_3CeX and $Cp^R_3Ce(OR)$ vary as much as 670 mV. Clearly, better stabilization of the cerium(IV) center is achieved in the presence of more strongly electron donating groups/ligands: alkoxy > siloxy > Cl > Br > I as well as Cp^{Me} > Cp. This is reflected by the boundary values of −0.583 and −1.259 V vs Fc/Fc^+ for complexes Cp_3CeI and $Cp^{Me}_3Ce(OtBu)$, respectively. The magnetic measurements of complexes Cp^{Me}_3CeCl, $Cp^{Me}_3Ce(OiPr)$, $Cp^{Me}_3Ce(OSiEt_3)$, and $Cp^{Me}_3Ce(OSiPh_3)$ revealed temperature-independent paramagnetism, with positive magnetic susceptibilities in the range χ_0 (10^{-4} emu/mol) = 1.53−3.9. Similar magnetic properties of the investigated compounds in dissolved and crystalline forms are supported by matching effective magnetic moments from SQUID data and the Evans method.

EXPERIMENTAL SECTION

All operations were performed under rigorous exclusion of oxygen and moisture under an argon atmosphere, using standard Schlenk, high-vacuum, and glovebox techniques (MB Braun MB150B-G-I; <0.1 ppm of O_2, <0.1 ppm of H_2O). Solvents were dried and degassed prior to use and provided by an MBraun SPS800 solvent purification system. Benzene-d_6 (99.5%) was received from Deutero GmbH. C_6D_6

https://doi.org/10.1021/acs.organomet.1c00276
Organometallics 2021, 40, 1786−1800

was dried over NaK alloy for a minimum of 48 h and filtered through a filter pipet (Whatman) before use. Anhydrous $CeCl_3$ (99.99%) (Sigma-Aldrich) was converted into $CeCl_3(THF)_{1.04}$ via Soxhlet extraction. Hexachloroethane, Na(O*t*Bu), and Na($OSiMe_3$) were purchased from Sigma-Aldrich and used as received. NaOMe was synthesized by reacting sodium with an excess of dry and degassed methanol.[76] NaOEt,[77] NaO*i*Pr,[78] sodium neopentoxide,[79] NaO-$SiEt_3$,[80] $NaOSiPh_3$,[81] $NaOSi(iPr)_3$,[82] $[nPr_4N][B\{Ar(3,5\text{-}CF_3)\}_4]$,[83] NaCp,[84] and $NaCp^{Me}$ [85] were prepared according to literature procedures. $Cp_3Ce(THF)$ (**1a**) was synthesized according to Birmingham et al.,[14] $Cp^{Me}{}_3Ce(THF)$ (**1b**) was synthesized according to Brennan et al.,[35] and $Cp^{Me}{}_3CeCl$ (**2b**) was synthesized according to Schneider et al.[21] NMR spectra were recorded on a Bruker AVII+400 (^1H, 400.13 MHz; ^{13}C, 100.61 MHz), AVI+300 (^{29}Si, 79.5 MHz) or AVII+500 (^1H, 500.13 MHz; ^{13}C, 125.76 MHz) spectrometer in dried and deuterated solvents. DRIFT spectra were recorded on a ThermoFisher Scientific 6700 Nicolet FTIR spectrometer using dried KBr and KBr windows. The collected data were converted using the Kubelka−Munk refinement. CHN elemental analyses were performed on an Elementar Vario MICRO cube. The effective magnetic moments (μ_{eff}) and susceptibilities were determined in C_6D_6 by the Evans method on a Bruker AVII+400 instrument at 299 K, using hexamethyldisiloxane as an internal standard.

Cyclic voltammetry (CV) experiments were performed with a Nordic Electrochemistry ECi-200 workstation applying the *iR*-compensation mode. The data were recorded using Nordic Electrochemistry EC4 DAQ software (version 4.1.90.1) and processed with EC-4 VIEW software (version 1.2.36.1). The CV experiments were performed in a glovebox under an argon atmosphere. The setup comprised a 4 mL vial, equipped with a CHI 104 glassy-carbon-disk working electrode (CH Instruments, Inc.), a platinum-wire counter electrode and a Ag/AgCl quasi reference electrode. The surface of the working electrode was polished prior to the measurement. Solutions containing ∼1 mM of analyte and 0.1 M $[nPr_4N][B\{Ar(3,5\text{-}CF_3)\}_4]$ supporting electrolyte were used for the electrochemical analyses. The scan-rate-dependent background of the electrolyte was recorded for each measurement and subtracted from the analyte data. The potentials are reported in V vs the Fc/Fc^+ couple, which was used as an internal standard for cell calibration, and were determined at the end of each measurement. Especially for the halide complexes the internal use of the standard is important to compensate potential shifts as a result of varying halide concentrations at the Ag/AgCl quasi reference electrode. Separation of the reference electrode through a membrane from the main electrolyte volume was not feasible in the cell configuration used. Compound **13b** was also investigated with a separate three-electrode arrangement versus a $Ag/AgClO_4$ reference electrode with an external ferrocene standard under variation of the concentration and scan rate (for more information on this experiment and the determination of the diffusion coefficient and the standard electron transfer rate constant, see Table S31f).

Measurements of the DC magnetic moments of compounds **2b**, **8b**, **11b**, and **13b** were performed using a Quantum Design MPMS-7 SQUID magnetometer. The temperature dependence of the magnetic moment was determined between 2 and 300 K in applied magnetic fields of 10 and 30 kOe. Additional field-dependent data were collected between −60 and +60 kOe at a temperature of 2 K. The samples were supplied in powdered crystalline form and held by gelatin capsules packed into surrounding plastic straws. An average background obtained from measurements on the blank sample containers prior to filling was subtracted. All sample containers showed a minor magnetic moment in the range of 10^{-5} emu in the temperature range between 2 and 300 K at an applied field of 10 kOe. Continuous inert conditions were ensured by sample preparation in a glovebox under an argon atmosphere and subsequent transfer to the magnetometer in an airtight transport vessel.

Crystals for X-ray crystallography were grown using saturated solutions of toluene (**3b**, **5a**, **6a**, **8a**, **8b**, and **9b**) or mixtures of *n*-hexane and toluene (**10b**, **11a**, **11b**, **13a**, and **13b**). Suitable crystals for X-ray analysis were handpicked in a glovebox, coated with Parabar 10312, and stored on microscope slides. Data collection was done on a Bruker APEX II Duo diffractometer by using QUAZAR optics and Mo Kα radiation (λ = 0.71073 Å). The data collection strategy was determined using COSMO[86] employing ω scans. Raw data were processed by APEX[87] and SAINT,[88] and corrections for absorption effects were applied using SADABS.[89] The structures were solved by direct methods and refined against all data by full-matrix least-squares methods on F^2 using SHELXTL[90] and SHELXLE.[91] Plots were generated by using CCDC Mercury 3.19.1.[92] The disorder was modeled using DSR, a program for refinement of disordered structures with SHELXL.[93] Further details regarding the refinement and crystallographic data are given in Table S3 and in the CIF files.

Cp_3CeCl (2a). Compound **1a** (1.21 g, 2.96 mmol) was suspended in toluene (150 mL) and a solution of C_2Cl_6 (351 mg, 1.48 mmol) in toluene (20 mL) was added, resulting in a fast color change from yellow to black. After 2 h the mixture was evaporated to dryness and extracted with *n*-hexane. Reducing the volume of the solution and storing it at −40 °C afforded crystals of **2a** (978 mg, 89%). ^1H NMR (400.1 MHz, C_6D_6, 26 °C): δ 4.86 (s, 15H, Cp*H*) ppm. $^{13}C\{^1H\}$ NMR (100.6 MHz, C_6D_6, 26 °C): δ 175.5 (Cp) ppm. Analytical data are in accord with those in the literature.[15]

Cp_3CeBr (3a). Compound **1a** (96.2 mg, 0.236 mmol) was suspended in toluene (10 mL), and $TeBr_4$ (50.0 mg, 0.112 mmol) was added, resulting in a color change from yellow to dark brown. After 16 h the mixture was evaporated to dryness and extracted with *n*-hexane. Reducing the volume of the solution and storing it at −40 °C afforded crystals of **3a** (92.8 mg, 95%). ^1H NMR (400.1 MHz, C_6D_6, 26 °C): δ 4.73 (s, 15H, Cp*H*) ppm. $^{13}C\{^1H\}$ NMR (100.6 MHz, C_6D_6, 26 °C): δ 125.8 (Cp) ppm. DRIFT: $\tilde{\nu}$ 3097 (w), 1716 (w), 1699 (w), 1683 (w), 1653 (w), 1558 (w), 1540 (m), 1506 (w), 1456 (w), 1436 (m), 1010 (m), 816 (m), 784 (vs) cm^{-1}. Anal. Calcd for $C_{15}H_{15}CeBr$ (415.31 g mol^{-1}): C, 43.38; H, 3.64. Found: C, 43.80; H, 4.38.

$Cp^{Me}{}_3CeBr$ (3b). Compound **1b** (46.7 mg, 0.104 mmol) was suspended in toluene (15 mL), and $TeBr_4$ (16.8 mg, 0.0376 mmol) was added, resulting in a color change from yellow to black. After 2 h the mixture was filtered and the filtrate evaporated to dryness. Storing a solution of the filtrate in toluene at −40 °C gave crystals of **3b** (46.0 mg, 97%) suitable for XRD analysis. ^1H NMR (400.1 MHz, C_6D_6, 26 °C): δ 5.01 (s, 6H, $CpH_{3/4}$), 4.10 (s, 6H, $CpH_{2/5}$), 3.54 (s, 9H, $CpCH_3$) ppm. $^{13}C\{^1H\}$ NMR (100.6 MHz, C_6D_6, 26 °C): δ 125.2 ($CpC_{2/5}$), 120.4 ($CpC_{3/4}$), 14.6 ($CpCH_3$) (C_{quart} beneath solvent signal) ppm. DRIFT: $\tilde{\nu}$ 3095 (w), 2914 (m), 1491 (m), 1456 (w), 1337 (w), 1027 (m), 861 (m), 840 (m), 788 (vs) cm^{-1}. Anal. Calcd for $C_{18}H_{21}CeBr$ (457.39 g mol^{-1}): C, 47.27; H, 4.63. Found: C, 46.84; H, 4.81.

Cp_3CeI (4a). Compound **1a** (50.5 mg, 0.124 mmol) was suspended in toluene (5 mL), and elemental I_2 (15.7 mg, 0.0620 mmol) was added, resulting in a color change from yellow to dark brown. After 2 h the mixture was evaporated to dryness and extracted with *n*-hexane. Reducing the volume of the solution and storing it at −40 °C afforded crystals of **4a** (52.6 mg, 92%). ^1H NMR (400.1 MHz, C_6D_6, 26 °C): δ 4.76 (s, 15H, Cp*H*) ppm. $^{13}C\{^1H\}$ NMR (100.6 MHz, C_6D_6, 26 °C): δ 126.4 (Cp) ppm. DRIFT: $\tilde{\nu}$ 3072 (m), 1699 (w), 1652 (w), 1558 (w), 1436 (m), 1059 (w), 1010 (m), 784 (vs) cm^{-1}. Anal. Calcd for $C_{15}H_{15}CeI$ (462.31 g mol^{-1}): C, 38.97; H, 3.27. Found: C, 39.17; H, 3.59.

$Cp^{Me}{}_3CeI$ (4b). Compound **1b** (38.4 mg, 0.0854 mmol) was suspended in toluene (5 mL), and elemental I_2 (10.8 mg, 0.0427 mmol) was added, resulting in a color change from yellow to black. After 2 h the mixture was filtered and the filtrate evaporated to dryness. Storing a solution of the filtrate in toluene at −40 °C gave crystals of **3b** (41.6 mg, 96%). ^1H NMR (400.1 MHz, C_6D_6, 26 °C): δ 4.68 (s, 6H, $CpH_{3/4}$), 4.44 (s, 6H, $CpH_{2/5}$), 3.73 (s, 9H, $CpCH_3$) ppm. $^{13}C\{^1H\}$ NMR (100.6 MHz, C_6D_6, 26 °C): δ 136.6 (CpC_{quart}), 126.9 ($CpC_{2/5}$), 125.5 ($CpC_{3/4}$), 14.5 ($CpCH_3$) ppm. DRIFT: $\tilde{\nu}$ 3093(m), 2916 (m), 1488 (m), 1456 (m), 1367 (w), 1337 (w), 1238 (w), 1036 (m), 875 (m), 787 (vs), 606 (w) cm^{-1}. Anal. Calcd for $C_{18}H_{21}CeI$ (504.39 g mol^{-1}): C, 42.86; H, 4.20. Found: C, 42.27; H, 4.74.

https://doi.org/10.1021/acs.organomet.1c00276
Organometallics 2021, 40, 1786−1800

General Procedure for the Transformation of Ceric Chlorides Cp^R_3CeCl (2a/b) into Alkoxides (5−9) and Siloxides (10−14). Compounds **2a**/**2b** were dissolved in toluene (5 mL). A suspension/solution of an equimolar amount of sodium alkoxide/siloxide was added and the mixture stirred at ambient temperature for 8 h, while it turned from black to dark brown-red. Subsequently, the reaction mixture was filtered and the filtrate evaporated to dryness. Storing a solution of the filtrate in toluene or *n*-hexane at −40 °C gave crystals of the ceric alkoxide/siloxide complexes.

*$Cp_3Ce(OMe)$ (**5a**).* Compounds **2a** (57.2 mg, 0.154 mmol) and NaOMe (5.86 mg, 0.154 mmol) gave crystals of **5a** (48.5 mg, 86%, from toluene) suitable for XRD analysis. ^{1}H NMR (400.1 MHz, C_6D_6, 26 °C): δ 5.84 (s, 3H, CH_3), 5.55 (s, 15H, Cp*H*) ppm. $^{13}C\{^1H\}$ NMR (100.6 MHz, C_6D_6, 26 °C): δ 122.7 (Cp), 69.3 (CH_3) ppm. DRIFT: $\tilde{\nu}$ 3090 (w), 2953 (m), 2922 (m), 2867 (m), 2793 (m), 1683 (w), 1653 (w), 1558 (w), 1540 (w), 1456 (w), 1436 (w), 1376 (w), 1350 (w), 1125 (w), 1092 (s), 1011 (m), 893 (w), 771 (s), 418 (m) cm^{-1}. Anal. Calcd for $C_{16}H_{18}CeO$ (366.44 g mol^{-1}): C, 52.44; H, 4.95. Found: C, 52.21; H, 5.67.

*$Cp^{Me}_3Ce(OMe)$ (**5b**).* Compounds **2b** (73.1 mg, 0.177 mmol) and NaOMe (9.56 mg, 0.177 mmol) gave crystals of **5b** (67.5 mg, 93%, from *n*-hexane). ^{1}H NMR (400.1 MHz, C_6D_6, 26 °C): δ 5.93 (s, 3H; OCH_3), 5.74 (t, 6H, J_{HH} = 2.67 Hz; $CpH_{3/4}$), 4.94 (t, 6H, J_{HH} = 2.67 Hz; $CpH_{2/5}$), 2.81 (s, 9H, $CpCH_3$) ppm. $^{13}C\{^1H\}$ NMR (100.6 MHz, C_6D_6, 26 °C): δ 133.0 (CpC_{quart}), 124.1 ($CpC_{2/5}$), 122.0 ($CpC_{3/4}$), 66.1 (OCH_3), 14.6 ($CpCH_3$) ppm. DRIFT: $\tilde{\nu}$ 3074 (w), 2918 (m), 2898 (m), 2871 (m), 2790 (m), 1558 (w), 1506 (w), 1496 (m), 1456 (m), 1372 (w), 1093 (s), 1030 (w), 828 (m), 763 (s) cm^{-1}. Anal. Calcd for $C_{19}H_{24}CeO$ (408.52 g mol^{-1}): C, 55.86; H, 5.92. Found: C, 55.58; H, 6.05.

*$Cp_3Ce(OEt)$ (**6a**).* Compounds **2a** (59.3 mg, 0.160 mmol) and NaOEt (10.9 mg, 0.160 mmol) in toluene (3 mL) gave crystals of **6a** (51.7 mg, 85%, from toluene) suitable for XRD analysis. ^{1}H NMR (400.1 MHz, C_6D_6, 26 °C): δ 6.02 (q, 2H, J_{HH} = 2.67 Hz; CH_2H), 5.58 (s, 15H, Cp*H*), 1.55 (t, 3H, J_{HH} = 2.67 Hz; CH_3) ppm. $^{13}C\{^1H\}$ NMR (100.6 MHz, C_6D_6, 26 °C): δ 122.5 (Cp), 76.6 (CH_2), 22.1 (CH_3) ppm. DRIFT: $\tilde{\nu}$ 3077 (w), 2960 (w), 2922 (w), 2841 (w), 1441 (w), 1369 (w), 1350 (w), 1103 (s), 1061 (s), 1009 (m), 906 (m), 792 (m), 771 (s), 488 (w) cm^{-1}. Anal. Calcd for $C_{17}H_{20}CeO$ (380.46 g mol^{-1}): C, 53.67; H, 5.30. Found: C, 53.74; H, 5.75.

*$Cp^{Me}_3Ce(OEt)$ (**6b**).* Compounds **2b** (72.6 mg, 0.176 mmol) and NaOEt (12.0 mg, 0.176 mmol) gave crystalline **6b** (67.9 mg, 91%, from *n*-hexane, after 5 h). ^{1}H NMR (400.1 MHz, C_6D_6, 26 °C): δ 6.18 (q, 2H, J_{HH} = 6.96 Hz; OCH_2), 5.66 (t, 6H, J_{HH} = 2.69 Hz; $CpH_{3/4}$), 5.11 (dt, 6H, J_{HH} = 2.69 Hz, J_{HH} = 0.46 Hz; $CpH_{2/5}$), 2.85 (s, 9H, $CpCH_3$), 1.64 (t, 3H, J_{HH} = 6.96 Hz; OCH_2CH_3) ppm. $^{13}C\{^1H\}$ NMR (100.6 MHz, C_6D_6, 26 °C): δ 132.4 (CpC_{quart}), 124.1 ($CpC_{2/5}$), 122.0 ($CpC_{3/4}$), 74.3 (CH_2), 22.5 (CH_2CH_3), 14.8 ($CpCH_3$) ppm. DRIFT: $\tilde{\nu}$ 3075 (w), 2963 (m), 2920 (m), 2856 (m), 1558 (w), 1540 (w), 1506 (w), 1495 (m), 1456 (m), 1367 (m), 1348 (w), 1108 (s), 1060 (s), 905 (m), 843 (m), 762 (s), 610 (w), 491 (m) cm^{-1}. Anal. Calcd for $C_{20}H_{26}CeO$ (422.54 g mol^{-1}): C, 56.85; H, 6.20. Found: C, 56.79; H, 6.01.

*$Cp_3Ce(OCH_2tBu)$ (**7a**).* Compounds **2a** (70.3 mg, 0.170 mmol) and $NaOCH_2tBu$ (18.7 mg, 0.170 mmol) gave crystals of **7a** (62.0 mg, 86%, from toluene). ^{1}H NMR (400.1 MHz, C_6D_6, 26 °C): δ 5.87 (s, 2H, CH_2), 5.57 (s, 15H, Cp*H*), 1.28 (s, 9H, *t*Bu) ppm. $^{13}C\{^1H\}$ NMR (100.6 MHz, C_6D_6, 26 °C): δ 122.7 (Cp), 92.6 (CH_2), 36.2 ($C(CH_3)_3$), 26.9 ($C(CH_3)$) ppm. DRIFT: $\tilde{\nu}$ 3077 (w), 2947 (s), 2924 (s), 2860 (m), 2807 (w), 1558 (w), 1457 (w), 1437 (w), 1388 (w), 1358 (w), 1088 (s), 1059 (w), 1021 (m), 770 (s), 601 (m), 435 (w) cm^{-1}. Anal. Calcd for $C_{21}H_{28}CeO$ (422.54 g mol^{-1}): C, 56.85; H, 6.20. Found: C, 56.65; H, 6.30.

*$Cp^{Me}_3Ce(OCH_2tBu)$ (**7b**).* Compounds **2b** (69.6 mg, 0.170 mmol) and $NaOCH_2tBu$ (18.7 mg, 0.170 mmol) gave crystals of **7b** (71.9 mg, 91%, from toluene). ^{1}H NMR (400.1 MHz, C_6D_6, 26 °C): δ 6.09 (s, 2H, CH_2), 5.43 (t, 6H, J_{HH} = 2.59 Hz; $CpH_{3/4}$), 5.37 (t, 6H, J_{HH} = 2.59 Hz; $CpH_{2/5}$), 2.96 (s, 9H, $CpCH_3$), 1.36 (s, 9H, *t*Bu) ppm. $^{13}C\{^1H\}$ NMR (100.6 MHz, C_6D_6, 26 °C): δ 131.7 (CpC_{quart}), 124.4 ($CpC_{2/5}$), 122.4 ($CpC_{3/4}$), 91.2 (CH_2), 36.4 ($C(CH_3)_3$), 27.2 ($C(CH_3)_3$), 14.6 ($CpCH_3$) ppm. DRIFT: $\tilde{\nu}$ 3068 (w), 2949 (s), 2860 (m), 2821 (m), 1494 (w), 1475 (w), 1456 (w), 1388 (w), 1378 (w), 1354 (w), 1075 (s), 1033 (m), 1019 (m), 834 (m), 825 (w), 762 (s), 596 (m), 434 (w) cm^{-1}. Anal. Calcd for $C_{23}H_{32}CeO$ (464.62 g mol^{-1}): C, 59.46; H, 6.94. Found: C, 59.73; H, 6.54.

*$Cp_3Ce(OiPr)$ (**8a**).* Compounds **2a** (75.2 mg, 0.203 mmol) and NaO*i*Pr (16.6 mg, 0.203 mmol) gave crystals of **8a** (75.0 mg, 94%, from toluene) suitable for XRD analysis. ^{1}H NMR (400.1 MHz, C_6D_6, 26 °C): δ 6.21 (sept, 1H, J_{HH} = 6.11 Hz; $CH(CH_3)_2$), 5.59 (s, 15H), 1.53 (d, 6H, J_{HH} = 6.11 Hz; $CH(CH_{3)2}$) ppm. $^{13}C\{^1H\}$ NMR (100.6 MHz, C_6D_6, 26 °C): δ 122.4 (Cp), 82.0 ($CH(CH_3)_2$), 28.6 ($CH(CH_3)_2$) ppm. DRIFT: $\tilde{\nu}$ 3078 (w), 2959 (m), 2924 (w), 2824 (w), 1558 (w), 1437 (w), 1358 (w), 1321 (w), 1157 (w), 1131 (m), 1124 (m), 1059 (w), 1008 (w), 983 (s), 840 (w), 772 (s), 537 (w), 448 (w), 445 (w) cm^{-1}. Anal. Calcd for $C_{18}H_{22}CeO$ (394.49 g mol^{-1}): C, 54.80; H, 5.62. Found: C, 55.42; H, 5.76. Analytics according to literature.[18]

*$Cp^{Me}_3Ce(OiPr)$ (**8b**).* Compounds **2b** (67.5 mg, 0.164 mmol) NaO*i*Pr (13.4 mg, 0.164 mmol) gave crystals of **8b** (68.0 mg, 95%, from toluene) suitable for XRD analysis. ^{1}H NMR (400.1 MHz, C_6D_6, 26 °C): δ 6.40 (sep, 1H, J_{HH} = 6.09 Hz; $CH(CH_3)_2$), 5.52 (t, 6H, J_{HH} = 2.60 Hz; $CpH_{3/4}$), 5.33 (t, 6H, J_{HH} = 2.60 Hz; $CpH_{2/5}$), 2.91 (s, 9H, $CpCH_3$), 1.65 (d, 6H, J_{HH} = 6.09 Hz; $CH(CH_3)_2$) ppm. $^{13}C\{^1H\}$ NMR (100.6 MHz, C_6D_6, 26 °C): δ 131.7 (CpC_{quart}), 124.0 ($CpC_{2/5}$), 122.0 ($CpC_{3/4}$), 80.6 ($CH(CH_3)_2$), 29.1 ($CH(CH_3)_2$), 14.8 ($CpCH_3$) ppm. DRIFT: $\tilde{\nu}$ 3101 (w), 2962 (m), 2921 (m), 2856 (m), 1456 (m), 1198 (s), 1124 (s), 1038 (m), 974 (s), 899 (m), 841 (m), 823 (m), 781 (m), 765 (s), 611 (m), 537 (m) cm^{-1}. Elemental analysis (%) calcd for $C_{21}H_{28}CeO$ (436.57 g mol^{-1}): C, 57.78; H, 6.46. Found: C, 57.39; H, 6.18.

*$Cp_3Ce(OtBu)$ (**9a**).* Compounds **2a** (69.8 mg, 0.188 mmol) and NaO*t*Bu (18.1 mg, 0.188 mmol) gave crystals of **9a** (66.7 mg, 87%, from toluene). ^{1}H NMR (400.1 MHz, C_6D_6, 26 °C): δ 5.61 (s, 15H, Cp*H*), 1.59 (s, 9H, *t*Bu) ppm. $^{13}C\{^1H\}$ NMR (100.6 MHz, C_6D_6, 26 °C): δ 122.3 (Cp), 85.4 ($C(CH_3)_3$), 34.2 ($C(CH_3)$) ppm. Analytical data are in accord with those in the literature.[19] In a alternative route, compound **1a** (36.7 mg, 0.109 mmol) was suspended in toluene (5 mL). A solution of *t*BuOO*t*Bu (8.00 mg, 0.0547 mmol) in toluene (2 mL) was slowly added and the mixture stirred for 16 h at ambient temperature. The resulting brown solution was filtered and the filtrate evaporated to dryness, yielding a brown powder of **9a** (15.8 mg, 35%). Analytical data are in accord with those in the literature.[19]

*$Cp^{Me}_3Ce(OtBu)$ (**9b**).* Compounds **2b** (70.4 mg, 0.171 mmol) and NaO*t*Bu (16.4 mg, 0.171 mmol) gave crystals of **9b** (71.8 mg, 93%, from toluene) suitable for XRD analysis. ^{1}H NMR (400.1 MHz, C_6D_6, 26 °C): δ 5.53 (t, 6H, J_{HH} = 2.68 Hz; $CpH_{3/4}$), 5.38 (t, 6H, J_{HH} = 2.68 Hz; $CpH_{2/5}$), 2.98 (s, 9H, $CpCH_3$), 1.73 (s, 9H, *t*Bu) ppm. $^{13}C\{^1H\}$ NMR (100.6 MHz, C_6D_6, 26 °C): δ 131.1 (CpC_{quart}), 124.1 ($CpC_{2/5}$), 121.9 ($CpC_{3/4}$), 85.0 ($C(CH_3)_3$), 34.8 ($C(CH_3)_3$), 14.9 ($CpCH_3$) ppm. DRIFT: $\tilde{\nu}$ 3088 (w), 2996 (s), 2920 (m), 2858 (w), 1490 (w), 1456 (w), 1378 (w), 1354 (m), 1222 (w), 1181 (s), 1047 (w), 1040 (w), 966 (s), 845 (w), 798 (m), 762 (s), 608 (w), 499 (w), 481 (w) cm^{-1}. Anal. Calcd for $C_{22}H_{30}CeO$ (450.60 g mol^{-1}): C, 58.64; H, 6.71. Found: C, 58.64; H, 6.38.

*$Cp_3Ce(OSiMe_3)$ (**10a**).* Compounds **2a** (55.1 mg, 0.149 mmol) and $NaOSiMe_3$ (16.7 mg, 0.149 mmol) gave crystals of **10a** (57.6 mg, 85%, from toluene). ^{1}H NMR (400.1 MHz, C_6D_6, 26 °C): δ 5.36 (s, 15H, Cp*H*), 0.69 (s, 9H, $SiMe_3$) ppm. $^{13}C\{^1H\}$ NMR (100.6 MHz, C_6D_6, 26 °C): δ 123.2 (Cp), 3.9 ($SiMe_3$) ppm. ^{29}Si(HSQC) NMR (79.5 MHz, C_6D_6, 26 °C): δ 6.0 ($OSiMe_3$) ppm. DRIFT: $\tilde{\nu}$ 3079 (w), 2949 (m), 1683 (w), 1558 (w), 1437 (w), 1240 (m), 1009 (w), 926 (s), 911 (s), 836 (m), 800 (m), 776 (s), 746 (m) cm^{-1}. Anal. Calcd for $C_{18}H_{24}CeOSi$ (424.59 g mol^{-1}): C, 50.92; H, 5.70. Found: C, 50.69; H, 5.55.

*$Cp^{Me}_3Ce(OSiMe_3)$ (**10b**).* Compounds **2b** (64.5 mg, 0.156 mmol) and $NaOSiMe_3$ (17.5 mg, 0.156 mmol) gave crystals of **10b** (70.6 mg, 97%, from toluene) suitable for XRD analysis. ^{1}H NMR (400.1 MHz, C_6D_6, 26 °C): δ 5.41 (t, 6H, J_{HH} = 2.64 Hz; $CpH_{3/4}$), 4.87 (t, 6H, J_{HH} = 2.64 Hz; $CpH_{2/5}$), 3.01 (s, 9H, $CpCH_3$), 0.79 ($SiMe_3$) ppm. $^{13}C\{^1H\}$ NMR (100.6 MHz, C_6D_6, 26 °C): δ 132.6 (CpC_{quart}), 124.9

https://doi.org/10.1021/acs.organomet.1c00276
Organometallics 2021, 40, 1786−1800

($CpC_{2/5}$), 122.7 ($CpC_{3/4}$), 14.9 ($CpCH_3$), 4.7 ($SiMe_3$) ppm. ^{29}Si-(HSQC) NMR (79.5 MHz, C_6D_6, 26 °C): δ 4.1 ($OSiMe_3$) ppm. DRIFT: $\tilde{\nu}$ 3085 (w), 2951 (m), 2920 (m), 1652 (w), 1558 (w), 1496 (w), 1456 (w), 1242 (s), 1046 (w), 1031 (m), 901 (s), 832 (m), 784 (m), 772 (s), 750 (m), 679 (w), 612 (w) cm^{-1}. Anal. Calcd for $C_{21}H_{30}CeOSi$ (466.67 g mol^{-1}): C, 54.05; H, 6.48. Found: C, 53.99; H, 6.41.

*$Cp_3Ce(OSiEt_3)$ (**11a**).* Compounds **2a** (59.5 mg, 0.160 mmol) and $NaOSiEt_3$ (24.7 mg, 0.160 mmol) gave crystals of **11a** (60.6 mg, 81%, from toluene) suitable for XRD analysis. ^{1}H NMR (400.1 MHz, C_6D_6, 26 °C): δ 5.39 (s, 15H, CpH), 1.44 (t, 9H, J_{HH} = 7.73 Hz; CH_3), 1.13 (q, 6H, J_{HH} = 7.73 Hz; CH_2) ppm. ^{13}C{^{1}H} NMR (100.6 MHz, C_6D_6, 26 °C): δ 123.3 (Cp), 8.7 (CH_2), 8.0 (CH_3) ppm. ^{29}Si(HSQC) NMR (79.5 MHz, C_6D_6, 26 °C): δ 10.4 (OSi) ppm. DRIFT: $\tilde{\nu}$ 3099 (w), 2951 (m), 2904 (m), 2867 (m), 1456 (w), 1436 (w), 1411 (w), 1234 (w), 1012 (m), 972 (w), 906 (s), 797 (m), 775 (s), 733 (m), 718 (m) cm^{-1}. Anal. Calcd for $C_{21}H_{30}CeOSi$ (466.67 g mol^{-1}): C, 54.05; H, 6.48. Found: C, 54.11; H, 6.90.

*$Cp^{Me}_3Ce(OSiEt_3)$ (**11b**).* Compounds **2b** (74.5 mg, 0.180 mmol) and $NaOSiEt_3$ (27.8 mg, 0.180 mmol) gave crystals of **11b** (84.7 mg, 92%, from toluene) suitable for XRD analysis. ^{1}H NMR (400.1 MHz, C_6D_6, 26 °C): δ 5.25 (t, 6H, J_{HH} = 2.64 Hz; $CpH_{3/4}$), 5.03 (t, 6H, J_{HH} = 2.64 Hz; $CpH_{2/5}$), 3.12 (s, 9H; $CpCH_3$), 1.49 (t, 9H, J_{HH} = 7.50 Hz; CH_2CH_3), 1.28 (q, 6H, J_{HH} = 7.50 Hz; CH_2CH_3) ppm. ^{13}C{^{1}H} NMR (100.6 MHz, C_6D_6, 26 °C): δ 132.3 (CpC_{quart}), 125.0 ($CpC_{2/5}$), 123.1($CpC_{3/4}$), 14.9 ($CpCH_3$), 9.4 (CH_2CH_3), 8.4 (CH_2CH_3) ppm. ^{29}Si(HSQC) NMR (79.5 MHz, C_6D_6, 26 °C): δ 9.3 ($OSiEt_3$) ppm. DRIFT: $\tilde{\nu}$ 3080 (w), 2949 (m), 2907 (m), 2870 (m), 1456 (w), 1237 (w), 1015 (w), 971 (w), 902 (s), 768 (s), 733 (m), 717 (m) cm^{-1}. Anal. Calcd for $C_{24}H_{36}CeOSi$ (508.75 g mol^{-1}): C, 56.66; H, 7.13. Found: C, 56.73; H, 6.82.

*$Cp_3Ce[OSi(iPr)_3]$ (**12a**).* Compounds **2a** (57.2 mg, 0.154 mmol) and $NaOSi(iPr)_3$ (30.3 mg, 0.154 mmol) gave crystals of **12a** (69.2 mg, 88%, from toluene). ^{1}H NMR (400.1 MHz, C_6D_6, 26 °C): δ 5.37 (s, 15H, CpH), 1.61 (sep, 3H, J_{HH} = 6.37 Hz; $CH(CH_3)_2$), 1.54 (d, 18H, J_{HH} = 6.37 Hz; $CH(CH_3)_2$) ppm. ^{13}C{^{1}H} NMR (100.6 MHz, C_6D_6, 26 °C): δ 123.5 (Cp), 19.1 ($CH(CH_3)_2$), 15.3 ($CH(CH_3)_2$) ppm. ^{29}Si(HSQC) NMR (79.5 MHz, C_6D_6, 26 °C): δ 8.5 (OSi) ppm. DRIFT: $\tilde{\nu}$ 3092 (w), 2959 (m), 2938 (m), 2889 (m), 2862 (m), 1462 (w), 1436 (w), 1011 (w), 992 (w), 893 (s), 882 (s), 840 (w), 806 (m), 773 (s), 668 (m), 652 (w) cm^{-1}. Anal. Calcd for $C_{24}H_{36}CeOSi$ (508.75 g mol^{-1}): C, 56.66; H, 7.13. Found: C, 56.67; H, 7.08.

*$Cp^{Me}_3Ce[OSi(iPr)_3]$ (**12b**).* Compounds **2b** (59.8 mg, 0.145 mmol) and $NaOSi(iPr)_3$ (28.4 mg, 0.145 mmol) gave crystals of **12b** (77.0 mg, 96%, from toluene). ^{1}H NMR (400.1 MHz, C_6D_6, 26 °C): δ 5.22 (t, 6H, J_{HH} = 2.45 Hz; $CpH_{3/4}$), 4.95 (s, 6H, J_{HH} = 2.45 Hz; $CpH_{2/5}$), 3.33 (s, 9H; $CpCH_3$), 1.75 (sep, 3H, J_{HH} = 7.02 Hz; $CH(CH_3)_2$), 1.61 (d, 18H, J_{HH} = 6.51 Hz; $CH(CH_3)_2$) ppm. ^{13}C{^{1}H} NMR (100.6 MHz, C_6D_6, 26 °C): δ 132.1 (CpC_{quart}), 125.3 ($CpC_{2/5}$), 123.8 ($CpC_{3/4}$), 19.4 ($CH(CH_3)_2$), 15.9 ($CH(CH_3)_2$), 15.0 ($CpCH_3$) ppm. ^{29}Si(HSQC) NMR (79.5 MHz, C_6D_6, 26 °C): δ 7.6 (OSi) ppm. DRIFT: $\tilde{\nu}$ 3080 (w), 2938 (m), 2861 (m), 1494 (w), 1457 (w), 1378 (w), 1328 (w), 1034 (w), 991 (w), 951 (w), 896 (s), 883 (s), 845 (m), 766 (s), 667 (m) cm^{-1}. Anal. Calcd for $C_{27}H_{42}CeOSi$ (550.83 g mol^{-1}): C, 58.87; H, 7.69. Found: C, 58.51; H, 7.41.

*$Cp_3Ce(OSiPh_3)$ (**13a**).* Compounds **2a** (58.4 mg, 0.158 mmol) and $NaOSiPh_3$ (47.0 mg, 0.158 mmol) gave crystals of **13a** (86.6 mg, 90%, from toluene) suitable for XRD analysis. ^{1}H NMR (400.1 MHz, C_6D_6, 26 °C): δ 8.32 (d, 6H, J_{HH} = 6.57 Hz; oCH), 7.41 (dd, 6H, J_{HH} = 6.57/7.21 Hz; mCH), 7.34 (t, 3H, J_{HH} = 7.21 Hz; pCH), 5.22 (s, 15H, CpH) ppm. ^{13}C{^{1}H} NMR (100.6 MHz, C_6D_6, 26 °C): δ 140.3 (C_{quart}), 136.1 (o-CH), 129.9 (m-CH), 128 (p-CH (overlapping with solvent signal)), 123.9 (Cp) ppm. ^{29}Si(HSQC) NMR (79.5 MHz, C_6D_6, 26 °C): δ −20.3 ($OSiPh_3$) ppm. DRIFT: $\tilde{\nu}$ 3060 (w), 3038 (w), 2997 (w), 1427 (m), 1110 (m), 1011 (w), 920 (s), 803 (s), 778 (s), 748 (m), 739 (m), 708 (s), 512 (s), 441 (w) cm^{-1}. Anal. Calcd for $C_{33}H_{30}CeOSi$ (610.80 g mol^{-1}): C, 64.89; H, 4.95. Found: C, 64.61; H, 4.79.

*$Cp^{Me}_3Ce(OSiPh_3)$ (**13b**).* Compounds **2b** (85.3 mg, 0.207 mmol) and $NaOSiPh_3$ (61.6 mg, 0.207 mmol) gave crystals of **13b** (126.0 mg, 93%, from toluene) suitable for XRD analysis. ^{1}H NMR (400.1 MHz, C_6D_6, 26 °C): δ 8.40 (d, 6H, J_{HH} = 7.3 Hz; oCH), 7.41 (dd, 6H, J_{HH} = 7.3 Hz, J_{HH} = 7.3 Hz; mCH), 7.34 (t, 3H, J_{HH} = 7.3 Hz; pCH), 5.13 (t, 6H, J_{HH} = 2.58 Hz; $CpH_{3/4}$), 4.78 (t, 6H, J_{HH} = 2.58 Hz; $CpH_{2/5}$), 3.16 (s, 9H; $CpCH_3$) ppm. ^{13}C{^{1}H} NMR (100.6 MHz, C_6D_6, 26 °C): δ 140.8 (C_{quart}), 136.4 (oCH), 135.7 (m-CH), 133.4 (CpC_{quart}), 129.8 (pCH), 125.6 ($CpC_{2/5}$), 124.1 ($CpC_{3/4}$), 14.9 ($CpCH_3$) ppm. ^{29}Si(HSQC) NMR (79.5 MHz, C_6D_6, 26 °C): δ −21.1 (OSi) ppm. DRIFT: $\tilde{\nu}$ 3064 (w), 2923 (w), 1490 (w), 1456 (w), 1426 (m), 1109 (m), 1029 (w), 917 (s), 845 (w), 778 (s), 745 (m), 705 (s), 514 (s) cm^{-1}. Anal. Calcd for $C_{36}H_{36}CeOSi$ (652.88 g mol^{-1}): C, 66.23; H, 5.56. Found: C, 66.07; H, 5.69.

*$Cp^{Me}_3Ce[OSi(OtBu)_3]$ (**14**).* Compounds **2b** (65.2 mg, 0.158 mmol) and $NaOSi(OtBu)_3$ (45.2 mg, 0.158 mmol) gave crystals of **14** suitable for XRD analysis. ^{1}H NMR (400.1 MHz, C_6D_6, 26 °C): δ 5.17 (t, 6H, J_{HH} = 2.69 Hz; $CpH_{3/4}$), 5.13 (t, 6H, J_{HH} = 2.69 Hz; $CpH_{2/5}$), 3.43 (s, 9H, $CpCH_3$), 1.79 (s, 27H, $Si(OtBu)_3$) ppm.

■ ASSOCIATED CONTENT

Supporting Information

The Supporting Information is available free of charge at https://pubs.acs.org/doi/10.1021/acs.organomet.1c00276.

Supporting figures as detailed in the text, detailed crystallographic data, spectroscopic data (NMR and IR), cyclic voltammograms, and data from electrochemical measurements, and data from magnetic measurements (SQUID and Evans measurements) (PDF)

Accession Codes

CCDC 2075865−2075877 contain the supplementary crystallographic data for this paper. These data can be obtained free of charge via www.ccdc.cam.ac.uk/data_request/cif, or by emailing data_request@ccdc.cam.ac.uk, or by contacting The Cambridge Crystallographic Data Centre, 12 Union Road, Cambridge CB2 1EZ, UK; fax: +44 1223 336033.

■ AUTHOR INFORMATION

Corresponding Authors

Wolfgang Scherer − *Institut für Physik, Universität Augsburg, 86159 Augsburg, Germany;* orcid.org/0000-0002-9307-082X; Email: wolfgang.scherer@physik.uni-augsburg.de

Bernd Speiser − *Institut für Organische Chemie, Eberhard Karls Universität Tübingen, 72076 Tübingen, Germany;* orcid.org/0000-0001-5111-8314; Email: bernd.speiser@uni-tuebingen.de

Reiner Anwander − *Institut für Anorganische Chemie, Eberhard Karls Universität Tübingen, 72076 Tübingen, Germany;* orcid.org/0000-0002-1543-3787; Email: reiner.anwander@uni-tuebingen.de

Authors

Lars Hirneise − *Institut für Anorganische Chemie, Eberhard Karls Universität Tübingen, 72076 Tübingen, Germany*

Jan Langmann − *Institut für Physik, Universität Augsburg, 86159 Augsburg, Germany*

Georg Zitzer − *Institut für Organische Chemie, Eberhard Karls Universität Tübingen, 72076 Tübingen, Germany*

Lukas Ude − *Institut für Anorganische Chemie, Eberhard Karls Universität Tübingen, 72076 Tübingen, Germany*

Cäcilia Maichle-Mössmer − *Institut für Anorganische Chemie, Eberhard Karls Universität Tübingen, 72076 Tübingen, Germany;* orcid.org/0000-0001-7638-1610

Complete contact information is available at: https://pubs.acs.org/10.1021/acs.organomet.1c00276

Notes

The authors declare no competing financial interest.

REFERENCES

(1) Sroor, F.; Edelmann, F. in *Cerium: Molecular Structure, Technological Applications and Health Effects*; Nova Science: Hauppage, NY, 2012; pp 73−106.

(2) Piro, N. A.; Robinson, J. R.; Walsh, P. J.; Schelter, E. J. The Electrochemical Behavior of Cerium(III/IV) complexes: Thermodynamics, Kinetics and Applications in Synthesis. *Coord. Chem. Rev.* **2014**, *260*, 21−36.

(3) So, Y.-M.; Leung, W.-H. Recent advances in the coordination chemistry of cerium(IV) complexes. *Coord. Chem. Rev.* **2017**, *340*, 172−197.

(4) Anwander, R.; Dolg, M.; Edelmann, F. T. The Difficult Search for Organocerium(IV) Compounds. *Chem. Soc. Rev.* **2017**, *46*, 6697−6709.

(5) Qiao, Y.; Schelter, E. J. Lanthanide Photocatalysis. *Acc. Chem. Res.* **2018**, *51*, 2926−2936.

(6) Ho, T.-L. Ceric Ion Oxidation in Organic Chemistry. *Synthesis* **1973**, *1973*, 347−354.

(7) Nair, V.; Mathew, J.; Prabhakaran, J. Carbon−Carbon Bond Forming Reactions mediated by Cerium(IV) Reagents. *Chem. Soc. Rev.* **1997**, *26*, 127−132.

(8) Das, A. K. Kinetic and Mechanistic Aspects of Metal Ion Catalysis in Cerium(IV) Oxidation. *Coord. Chem. Rev.* **2001**, *213*, 307−325.

(9) Nair, V.; Balagopal, L.; Rajan, R.; Mathew, J. Recent Advances in Synthetic Transformations Mediated by Cerium(IV) Ammonium Nitrate. *Acc. Chem. Res.* **2004**, *37*, 21−30.

(10) Nair, V.; Deepthi, A. Recent Advances in CAN mediated Reactions in organic Synthesis. *Tetrahedron* **2009**, *65*, 10745−10755.

(11) Sridharan, V.; Menéndez, J. C. Cerium(IV) Ammonium Nitrate as a Catalyst in Organic Synthesis. *Chem. Rev.* **2010**, *110*, 3805−3849.

(12) Gradeff, P. S.; Schreiber, F. G.; Brooks, K. C.; Sievers, R. E. A Simplified Method for the Synthesis of Ceric Alkoxides from Ceric Ammonium Nitrate. *Inorg. Chem.* **1985**, *24*, 1110−1111.

(13) Gradeff, P. S.; Schreiber, F. G.; Mauermann, H. Preparation of Ceric Alkoxides in Glycol Ethers. *J. Less-Common Met.* **1986**, *126*, 335−338.

(14) Birmingham, J.; Wilkinson, G. The Cyclopentadienides of Scandium, Yttrium and Some Rare Earth Elements. *J. Am. Chem. Soc.* **1956**, *78*, 42−44.

(15) Dröse, P.; Crozier, A. R.; Lashkari, S.; Gottfriedsen, J.; Blaurock, S.; Hrib, C. G.; Maichle-Mössmer, C.; Schädle, C.; Anwander, R.; Edelmann, F. T. Facile Access to Tetravalent Cerium Compounds: One-Electron Oxidation Using Iodine(III) Reagents. *J. Am. Chem. Soc.* **2010**, *132*, 14046−14047.

(16) Deacon, G. B.; Tuong, T. D.; Vince, D. G. Refutation of the Synthesis of Tetrakis(cyclopentadienyl)cerium(IV). *Polyhedron* **1983**, *2*, 969−970.

(17) Greco, A.; Cesca, S.; Bertolini, W. New π-Cyclooctatetraenyl and π-Cyclopentadienyl Complexes of Cerium. *J. Organomet. Chem.* **1976**, *113*, 321−330.

(18) Gulino, A.; Casarin, M.; Conticello, V. P.; Gaudiello, J. G.; Mauermann, H.; Fragala, I.; Marks, T. J. Efficient Synthesis, Redox Characteristics, and Electronic Structure of a Tetravalent Tris(cyclopentadienyl)cerium Alkoxide Complex. *Organometallics* **1988**, *7*, 2360−2364.

(19) Evans, W. J.; Deming, T. J.; Ziller, J. W. The Utility of Ceric Ammonium Nitrate-derived Alkoxide Complexes in the Synthesis of Organometallic Cerium(IV) Complexes. Synthesis and First X-ray Crystallographic Determination of a Tetravalent Cerium Cyclopentadienide Complex, $(C_5H_5)_3Ce(OCMe_3)$. *Organometallics* **1989**, *8*, 1581−1583.

(20) Sutton, A.; Clark, D.; Scott, B.; Gordon, J. Synthesis and Characterization of Cerium(IV) Metallocenes. *Inorganics* **2015**, *3*, 589.

(21) Schneider, D.; Harmgarth, N.; Edelmann, F. T.; Anwander, R. Ceric Cyclopentadienides Bearing Alkoxy, Aryloxy, Chlorido, or Iodido Co-Ligands. *Chem. - Eur. J.* **2017**, *23*, 12243−12252.

(22) Friedrich, J.; Schneider, D.; Bock, L.; Maichle-Mössmer, C.; Anwander, R. Cerium(IV) Neopentoxide Complexes. *Inorg. Chem.* **2017**, *56*, 8114−8127.

(23) Bradley, D.; Chatterjee, A.; Wardlaw, W. 439. Structural Chemistry of the Alkoxides. Part VI. Primary Alkoxides of Quadrivalent Cerium and Thorium. *J. Chem. Soc.* **1956**, 2260−2264.

(24) Bradley, D.; Chatterjee, A.; Wardlaw, W. 506. Structural Chemistry of the Alkoxides. Part IX. Tert.-Alkoxides of Quadrivalent Cerium. *J. Chem. Soc.* **1957**, 2600−2604.

(25) Bradley, D. C.; Chatterjee, A. K.; Wardlaw, W. 671. Structural Chemistry of the Alkoxides. Part VII. Secondary Alkoxides of Quadrivalent Cerium and Thorium. *J. Chem. Soc.* **1956**, 3469−3472.

(26) Casely, I. J.; Liddle, S. T.; Blake, A. J.; Wilson, C.; Arnold, P. L. Tetravalent cerium carbene complexes. *Chem. Commun.* **2007**, 5037−5039.

(27) Suh, S.; Guan, J.; Mîinea, L. A.; Lehn, J.-S. M.; Hoffman, D. M. Chemical Vapor Deposition of Cerium Oxide Films from a Cerium Alkoxide Precursor. *Chem. Mater.* **2004**, *16*, 1667−1673.

(28) Aspinall, H. C.; Bacsa, J.; Jones, A. C.; Wrench, J. S.; Black, K.; Chalker, P. R.; King, P. J.; Marshall, P.; Werner, M.; Davies, H. O.; Odedra, R. Ce(IV) Complexes with Donor-Functionalized Alkoxide Ligands: Improved Precursors for Chemical Vapor Deposition of CeO_2. *Inorg. Chem.* **2011**, *50*, 11644−11652.

(29) Friedrich, J.; Maichle-Mössmer, C.; Anwander, R. Synthesis and Derivatisation of Ceric Tris(*tert*-butoxy)siloxides. *Chem. Commun.* **2017**, *53*, 12044−12047.

(30) Friedrich, J.; Maichle-Mössmer, C.; Schrenk, C.; Schnepf, A.; Anwander, R. Ceric Ammonium Nitrate and Ceric Ammonium Chloride as Precursors for Ceric Siloxides: Ammonia and Ammonium Inclusion. *Eur. J. Inorg. Chem.* **2019**, *2019*, 79−90.

(31) Palumbo, C. T.; Zivkovic, I.; Scopelliti, R.; Mazzanti, M. Molecular Complex of Tb in the +4 Oxidation State. *J. Am. Chem. Soc.* **2019**, *141*, 9827−9831.

(32) Willauer, A. R.; Palumbo, C. T.; Scopelliti, R.; Zivkovic, I.; Douair, I.; Maron, L.; Mazzanti, M. Stabilization of the Oxidation State +IV in Siloxide-Supported Terbium Compounds. *Angew. Chem.* **2020**, *132*, 3577−3581.

(33) Willauer, A. R.; Palumbo, C. T.; Fadaei-Tirani, F.; Zivkovic, I.; Douair, I.; Maron, L.; Mazzanti, M. Accessing the +IV Oxidation State in Molecular Complexes of Praseodymium. *J. Am. Chem. Soc.* **2020**, *142*, 5538−5542.

(34) Friedrich, J.; Qiao, Y.; Maichle-Mössmer, C.; Schelter, E. J.; Anwander, R. Redox-enhanced Hemilability of the Tris(*tert*-butoxy)-siloxy Ligand at Cerium. *Dalton Trans.* **2018**, *47*, 10113−10123.

(35) Brennan, J. G.; Stults, S. D.; Andersen, R. A.; Zalkin, A. Crystal structures of $(MeC_5H_4)_3ML$ [M = Uranium or Cerium; L = Quinuclidine or $P(OCH_2)_3CEt$]. Evidence for Uranium to Phosphorus π-Backbonding. *Organometallics* **1988**, *7*, 1329−34.

(36) Schneider, D.; Anwander, R. Pentamethylcyclopentadienyl-Supported Cerocene(III) Complexes. *Eur. J. Inorg. Chem.* **2017**, *2017*, 1180−1188.

(37) Hitchcock, P. B.; Hulkes, A. G.; Lappert, M. F. Oxidation in Nonclassical Organolanthanide Chemistry: Synthesis, Characterization, and X-ray Crystal Structures of Cerium(III) and -(IV) Amides. *Inorg. Chem.* **2004**, *43*, 1031−1038.

(38) Sen, A.; Stecher, H. A.; Rheingold, A. L. Synthesis, Structure, and Reactivity of Homoleptic Cerium(IV) and Cerium(III) Alkoxides. *Inorg. Chem.* **1992**, *31*, 473−479.

(39) Bock, L.; Tran, X.; Liang, Y.; Kramer, M.; Maichle-Mössmer, C.; Anwander, R. SOMC@Periodic Mesoporous Silica Nanoparticles: Meerwein−Ponndorf−Verley Reduction Promoted by Immobilized Rare-Earth-Metal Alkoxides. *Organometallics* **2020**, *39*, 1046−1058.

(40) Vaartstra, B. A.; Huffman, J. C.; Gradeff, P. S.; Hubert-Pfalzgraf, L. G.; Daran, J. C.; Parraud, S.; Yunlu, K.; Caulton, K. G. Alcohol Adducts of Alkoxides: Intramolecular Hydrogen Bonding as a General Structural Feature. *Inorg. Chem.* **1990**, *29*, 3126−3131.

https://doi.org/10.1021/acs.organomet.1c00276
Organometallics 2021, 40, 1786−1800

(41) Williams, U. J.; Carroll, P. J.; Schelter, E. J. Synthesis and Analysis of a Family of Cerium(IV) Halide and Pseudohalide Compounds. *Inorg. Chem.* **2014**, *53*, 6338−6345.
(42) Hitchcock, P. B.; Hulkes, A. G.; Lappert, M. F. Oxidation in Nonclassical Organolanthanide Chemistry: Synthesis, Characterization, and X-ray Crystal Structures of Cerium(III) and -(IV) Amides. *Inorg. Chem.* **2004**, *43*, 1031−1038.
(43) Schläfer, J.; Tyrra, W.; Mathur, S. Octakis(*tert*-butoxo)-dicerium(IV) [$Ce_2(OtBu)_8$]: Synthesis, Characterization, Decomposition, and Reactivity. *Inorg. Chem.* **2014**, *53*, 2751−2753.
(44) Evans, W. J.; Golden, R. E.; Ziller, J. W. A comparative Synthetic and Structural Study of Triphenylmethoxide and Triphenylsiloxide Complexes of the Early Lanthanides, including X-ray Crystal Structures of $La_2(OCPh_3)_6$ and $Ce_2(OSiPh_3)_6$. *Inorg. Chem.* **1991**, *30*, 4963−4968.
(45) Gradeff, P. S.; Yunlu, K.; Gleizes, A.; Galy, J. Synthesis and X-ray Crystal Structure of a Novel Cerium(IV) Arylsiloxide. *Polyhedron* **1989**, *8*, 1001−1005.
(46) Nicholson, R. S. Semiempirical Procedure for Measuring with Stationary Electrode Polarography Rates of Chemical Reactions Involving the Product of Electron Transfer. *Anal. Chem.* **1966**, *38*, 1406−1406.
(47) Robinson, J. R.; Carroll, P. J.; Walsh, P. J.; Schelter, E. J. The Impact of Ligand Reorganization on Cerium(III) Oxidation Chemistry. *Angew. Chem., Int. Ed.* **2012**, *51*, 10159−10163.
(48) Chakrabarti, M. H.; Hajimolana, S. A.; Mjalli, F. S.; Saleem, M.; Mustafa, I. Redox Flow Battery for Energy Storage. *Arab. J. Sci. Eng.* **2013**, *38*, 723−739.
(49) Leung, P.; Li, X.; Ponce de León, C.; Berlouis, L.; Low, C. T. J.; Walsh, F. C. Progress in Redox Flow Batteries, Remaining Challenges and Their Applications in Energy Storage. *RSC Adv.* **2012**, *2*, 10125−10156.
(50) Liu, Y.; Xia, X.; Liu, H. Studies on Cerium (Ce^{4+}/Ce^{3+})−Vanadium(V^{2+}/V^{3+}) Redox Flow Cell—Cyclic Voltammogram response of Ce^{4+}/Ce^{3+} Redox Couple in H_2SO_4 Solution. *J. Power Sources* **2004**, *130*, 299−305.
(51) Streitwieser, A., Jr.; Kinsley, S. A.; Rigsbee, J. T.; Fragala, I. L.; Ciliberto, E. Photoelectron spectra and Bonding in Cerocene, Bis(π-[8]annulene)cerium(IV). *J. Am. Chem. Soc.* **1985**, *107*, 7786−8.
(52) Streitwieser, A.; Kinsley, S. A.; Jenson, C. H.; Rigsbee, J. T. Synthesis and Properties of Di-π-[8]annulenecerium(IV), Cerocene. *Organometallics* **2004**, *23*, 5169−5175.
(53) Ashley, A.; Balazs, G.; Cowley, A.; Green, J.; Booth, C. H.; O'Hare, D. Bis(permethylpentalene)cerium − Another Ambiguity in Lanthanide Oxidation State. *Chem. Commun.* **2007**, *15*, 1515−1517.
(54) Gregson, M.; Lu, E.; Mills, D. P.; Tuna, F.; McInnes, E. J. L.; Hennig, C.; Scheinost, A. C.; McMaster, J.; Lewis, W.; Blake, A. J.; Kerridge, A.; Liddle, S. T. The Inverse-trans-influence in Tetravalent Lanthanide and Actinide Bis(carbene) Complexes. *Nat. Commun.* **2017**, *8*, 14137.
(55) Bogart, J. A.; Lippincott, C. A.; Carroll, P. J.; Booth, C. H.; Schelter, E. J. Controlled Redox Chemistry at Cerium within a Tripodal Nitroxide Ligand Framework. *Chem. - Eur. J.* **2015**, *21*, 17850−17859.
(56) Levin, J. R.; Dorfner, W. L.; Dai, A. X.; Carroll, P. J.; Schelter, E. J. Density Functional Theory as a Predictive Tool for Cerium Redox Properties in Nonaqueous Solvents. *Inorg. Chem.* **2016**, *55*, 12651−12659.
(57) Eisenstein, O.; Hitchcock, P. B.; Hulkes, A. G.; Lappert, M. F.; Maron, L. Cerium masquerading as a Group 4 element: Synthesis, Structure and computational Characterisation of [CeCl-{N-($SiMe_3$)$_2$}$_3$]. *Chem. Commun.* **2001**, *17*, 1560−1561.
(58) Arnold, P. L.; Turner, Z. R.; Kaltsoyannis, N.; Pelekanaki, P.; Bellabarba, R. M.; Tooze, R. P. Covalency in Ce^{IV} and U^{IV} Halide and N-Heterocyclic Carbene Bonds. *Chem. - Eur. J.* **2010**, *16*, 9623−9629.
(59) Robinson, J. R.; Gordon, Z.; Booth, C. H.; Carroll, P. J.; Walsh, P. J.; Schelter, E. J. Tuning Reactivity and Electronic Properties through Ligand Reorganization within a Cerium Heterobimetallic Framework. *J. Am. Chem. Soc.* **2013**, *135*, 19016−19024.
(60) Williams, U. J.; Schneider, D.; Dorfner, W. L.; Maichle-Mössmer, C.; Carroll, P. J.; Anwander, R.; Schelter, E. J. Variation of Electronic Transitions and Reduction Potentials of Cerium(IV) Complexes. *Dalton Trans.* **2014**, *43*, 16197−16206.
(61) Booth, C. H.; Walter, M. D.; Daniel, M.; Lukens, W. W.; Andersen, R. A. Self-Contained Kondo Effect in Single Molecules. *Phys. Rev. Lett.* **2005**, *95*, 267202.
(62) Walter, M. D.; Booth, C. H.; Lukens, W. W.; Andersen, R. A. Cerocene Revisited: The Electronic Structure of and Interconversion Between $Ce_2(C_8H_8)_3$ and $Ce(C_8H_8)_2$. *Organometallics* **2009**, *28*, 698−707.
(63) Kerridge, A.; Coates, R.; Kaltsoyannis, N. Is Cerocene Really a Ce(III) Compound? All-Electron Spin-Orbit Coupled CASPT2 Calculations on Ce(η^8-C_8H_8)$_2$ (M = Th, Pa, Ce). *J. Phys. Chem. A* **2009**, *113*, 2896−2905.
(64) Kerridge, A. Oxidation state and covalency in f-element metallocenes (M = Ce, Th, Pu): a combined CASSCF and topological study. *Dalton Trans.* **2013**, *42*, 16428−16436.
(65) Tricoire, M.; Mahieu, N.; Simler, T.; Nocton, G. Intermediate Valence States in Lanthanide Compounds. *Chem. - Eur. J.* **2021**, *27*, 6860−6879.
(66) Sergentu, D.-C.; Booth, C. H.; Autschbach, J. Probing Multiconfigurational States by Spectroscopy: The Cerium XAS L3-edge Puzzle. *Chem. - Eur. J.* **2021**, *27*, 7239−7251.
(67) Lueken, H. *Magnetochemie: Eine Einführung in Theorie und Anwendung*; Teubner: 1999.
(68) Bain, G. A.; Berry, J. F. Diamagnetic Corrections and Pascal's Constants. *J. Chem. Educ.* **2008**, *85*, 532.
(69) Halbach, R. L.; Nocton, G.; Booth, C. H.; Maron, L.; Andersen, R. A. Cerium Tetrakis(tropolonate) and Cerium Tetrakis-(acetylacetonate) Are Not Diamagnetic but Temperature-Independent Paramagnets. *Inorg. Chem.* **2018**, *57*, 7290−7298.
(70) Van Vleck, J. H. The Theory of Electric and Magnetic Susceptibilities. *Nature* **1932**, *130*, 490−491.
(71) Orchard, A. *Magnetochemistry*; Oxford University Press: Oxford, 2003.
(72) Coreno, M.; de Simone, M.; Green, J. C.; Kaltsoyannis, N.; Coates, R.; Hunston, C.; Narband, N.; Sella, A. Variable Photon Energy Photoelectron Spectroscopy of Tris-cyclopentadienyl Lanthanides. *Dalton Trans.* **2014**, *43*, 5134−5141.
(73) Evans, D. F. 400. The Determination of the Paramagnetic Susceptibility of Substances in Solution by Nuclear Magnetic Resonance. *J. Chem. Soc.* **1959**, 2003−2005.
(74) Schubert, E. M. Utilizing the Evans Method with a superconducting NMR spectrometer in the Undergraduate Laboratory. *J. Chem. Educ.* **1992**, *69*, 62.
(75) Piguet, C. Paramagnetic Susceptibility by NMR: The "Solvent Correction" Removed for Large Paramagnetic Molecules. *J. Chem. Educ.* **1997**, *74*, 815.
(76) Weiss, E. Die Kristallstruktur des Natriummethylats. *Z. Anorg. Allg. Chem.* **1964**, *332*, 197−203.
(77) Stechow, M. Über die Einwirkung von Alkali auf Äthyl-alkohol und die "Stickoxyd Reaktion" von Wilhelm Traube. *Ber. Dtsch. Chem. Ges. B* **1924**, *57*, 1611−1615.
(78) Lochmann, L.; Coupek, J.; Lim, D. Preparation of some Alkoxides of Alkali Metals. Collect. *Collect. Czech. Chem. Commun.* **1970**, *35*, 733−6.
(79) Boyle, T. J.; Alam, T. M.; Tafoya, C. J.; Mechenbier, E. R.; Ziller, J. W. Syntheses, Characterizations, and X-ray Structures of Alkali Metal Derivatives of Titanium(IV) Neopentoxides. *Inorg. Chem.* **1999**, *38*, 2422−2428.
(80) D'Alfonso, G.; Dragonetti, C.; Galli, S.; Lucenti, E.; Macchi, P.; Roberto, D.; Ugo, R. Surface Organometallic Chemistry — Carbonyl Complexes of Re(I) with Silanolates as Models of Silica Anchored Rhenium Carbonyl Species. *Can. J. Chem.* **2005**, *83*, 1017−1024.
(81) Hyde, J. F.; Johannson, O. K.; Daudt, W. H.; Fleming, R. F.; Laudenslager, H. B.; Roche, M. P. Sodium and Potassium Salts of Triorganosilanols. *J. Am. Chem. Soc.* **1953**, *75*, 5615−5618.

https://doi.org/10.1021/acs.organomet.1c00276
Organometallics 2021, 40, 1786−1800

(82) Marciniec, B.; Błażejewska-Chadyniak, P.; Kubicki, M. Synthesis, first Structures, and catalytic Activity of the monomeric Rhodium(I)-Siloxide Phosphine Complexes. *Can. J. Chem.* **2003**, *81*, 1292−1298.
(83) Thomson, R. K.; Scott, B. L.; Morris, D. E.; Kiplinger, J. L. Synthesis, Structure, Spectroscopy and Redox Energetics of a Series of Uranium(IV) Mixed-Ligand Metallocene Complexes. *C. R. Chim.* **2010**, *13*, 790−802.
(84) Panda, T. K.; Gamer, M. T.; Roesky, P. W. An Improved Synthesis of Sodium and Potassium Cyclopentadienide. *Organometallics* **2003**, *22*, 877−878.
(85) Darkwa, J.; Giolando, D. M.; Murphy, C. J.; Rauchfuss, T. B.; Müller, A. Bis(η^5-Methylcyclopentadienyl)Titanium Pentasulfide, Bis(-Methylcyclopentadienyl)-Divanadium Pentasulfide, and Bis(η^5-Methylcyclopentadienyl)Divanadium Tetrasulfide. *Inorganic Syntheses* **2007**, 51.
(86) *COSMO, v. 1.61*; Bruker AXS Inc.: Madison, WI, 2012.
(87) *APEX 3, V. 2017.3-0*; Bruker AXS Inc.: Madison, WI, 2017.
(88) *SAINT, v. 8.38A*; Bruker AXS Inc.: Madison, WI, 2017.
(89) Krause, L.; Herbst-Irmer, R.; Sheldrick, G. M.; Stalke, D. *J. Appl. Crystallogr.* **2015**, *48*, 3−10.
(90) Sheldrick, G. M. *Acta Crystallogr., Sect. A: Found. Adv.* **2015**, *71*, 3−8.
(91) Hübschle, C. B.; Sheldrick, G. M.; Dittrich, B. J. *J. Appl. Crystallogr.* **2011**, *44*, 1281−1284.
(92) Macrae, C. F.; Bruno, I. J.; Chisholm, J. A.; Edgington, P. R.; McCabe, P.; Pidcock, E.; Rodriguez-Monge, L.; Taylor, R.; van de Streek, J.; Wood, P. A. *J. Appl. Crystallogr.* **2008**, *41*, 466−470.
(93) Kratzert, D.; Holstein, J. J.; Krossing, I. DSR: enhanced Modelling and Refinement of disordered Structures with SHELXL. *J. Appl. Crystallogr.* **2015**, *48*, 933−938.

https://doi.org/10.1021/acs.organomet.1c00276
Organometallics 2021, 40, 1786−1800

Supporting Information

TUNING ORGANOCERIUM ELECTROCHEMICAL POTENTIALS BY EXTENDING TRIS(CYCLOPENTADIENYL) SCAFFOLDS WITH TERMINAL HALOGENIDO, SILOXY, and ALKOXY LIGANDS

Lars Hirneise,[†] Jan Langmann,[‡] Georg Zitzer,[§] Lukas Ude,[†] Cäcilia Maichle-Mössmer,[†] Wolfgang Scherer,[‡*] Bernd Speiser,[§*] and Reiner Anwander[†*]

[†]Institut für Anorganische Chemie, Eberhard Karls Universität Tübingen, Auf der Morgenstelle 18, 72076 Tübingen, Germany

[§]Institut für Organische Chemie, Eberhard Karls Universität Tübingen, Auf der Morgenstelle 18, 72076 Tübingen, Germany

[‡]Institut für Physik, Universität Augsburg, Universitätsstr. 1, 86159 Augsburg, Germany

*reiner.anwander@uni-tuebingen.de

Table of Contents

Magnetic Measurements (Evan's method)

Table S1. Data from magnetic measurements for compounds **6b** and **13b** (Evans' method)

Compound	X_{mass} [10^{-7} cm^3 kg^{-1}]	X_{mol} [10^{-4} cm^3 mol^{-1}]	X_{para} [10^{-4} cm^3 mol^{-1}]	μ_{eff} [μ_B]
6b	4.56	0.778	0.231	0.58
13b	1.19	1.93	1.38	0.24

Magnetic Measurements (SQUID)

Table S2. Content in ferromagnetic impurities as estimated from the remnant magnetization M_R divided by the magnetic moments of the common ferromagnetic metals iron (2.2 μB), cobalt (1.7 μB) and nickel (0.6 μB).[1]

Compound	M_R [10^{-5} μ_B/f.u.]	Fe [10^{-3} at.-%]	Co [10^{-3} at.-%]	Ni [10^{-3} at.-%]
2b	5.16	2.3	3.0	8.6
8b	0.68	0.3	0.4	1.1
11b	1.81	0.8	1.1	3.0
13b	1.49	0.7	0.9	2.5

(1) Lueken, H. *Magnetochemie*, 1st ed.; Teubner: Stuttgart, 1999.

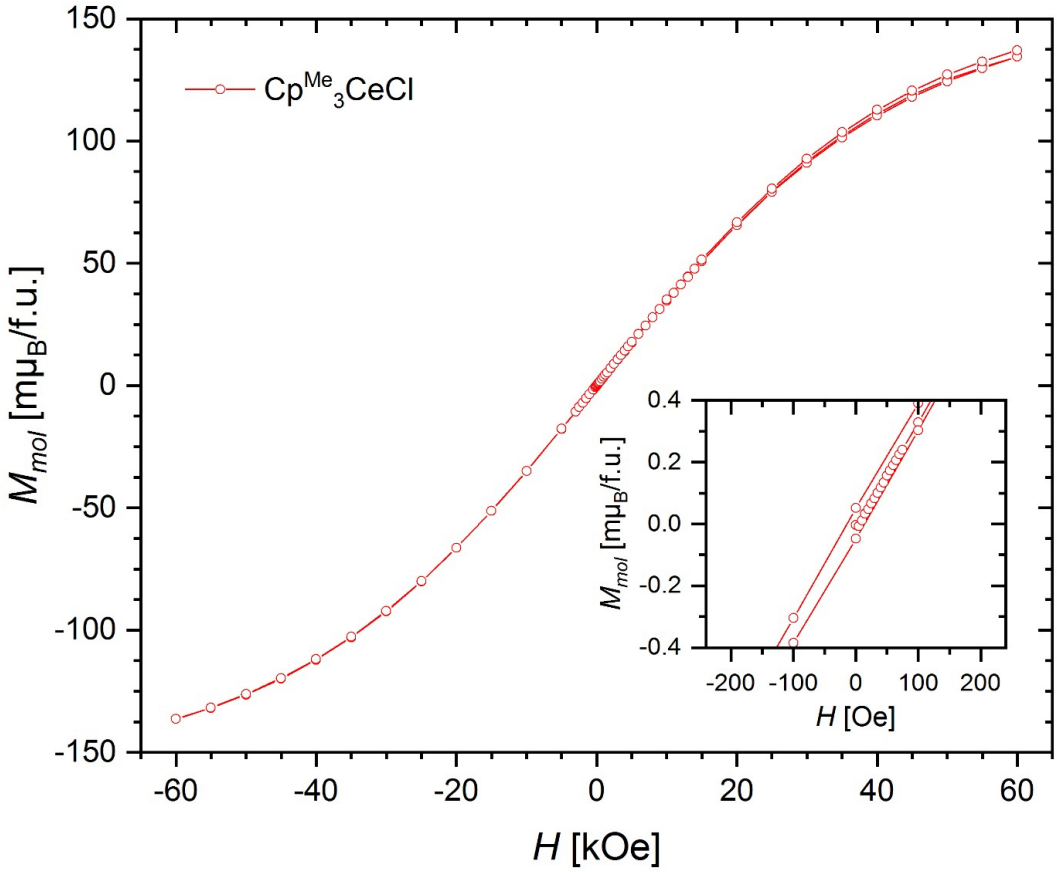

Figure S1. Field-dependent molar magnetization $M(H)$ for the complex Cp^{Me}_3CeCl **2b** (red circles and line) measured at a temperature T = 2 K. A strongly enlarged view of the portion of $M(H)$ close to the origin demonstrating a dismal hysteresis due to ferromagnetic impurities is given in the inset.

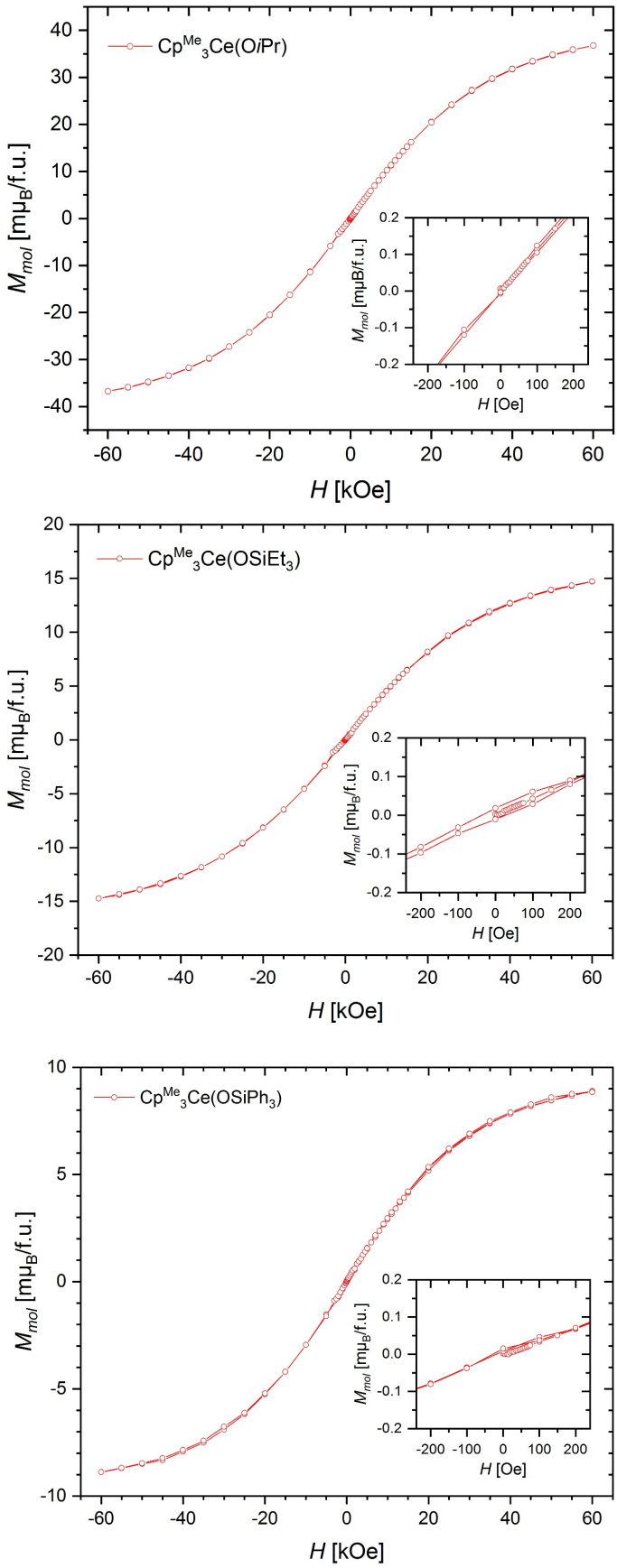

Figure S2. Field-dependent molar magnetization $M(H)$ for the complexes $Cp^{Me}_3Ce(OiPr)$ **8b** (top), $Cp^{Me}_3Ce(OSiEt_3)$ **11b** (middle) and $Cp^{Me}_3Ce(OSiPh_3)$ **13b** (bottom) (red circles and lines) measured at a temperature T = 2 K. A strongly enlarged view of the portions of $M(H)$ close to the origin demonstrating a dismal hysteresis due to ferromagnetic impurities is given in the insets.

NMR spectra

* → solvent, # → small impurities

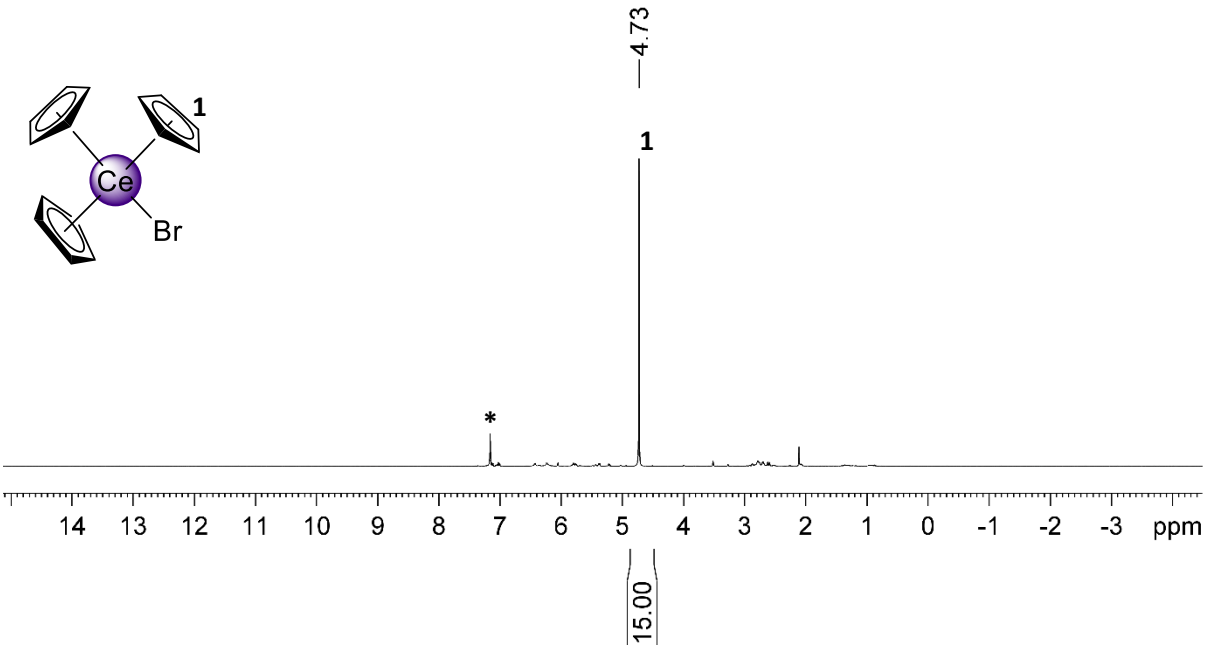

Figure S3. ^{1}H NMR spectrum (400.1 MHz, C_6D_6, 26 °C) of **3a**.

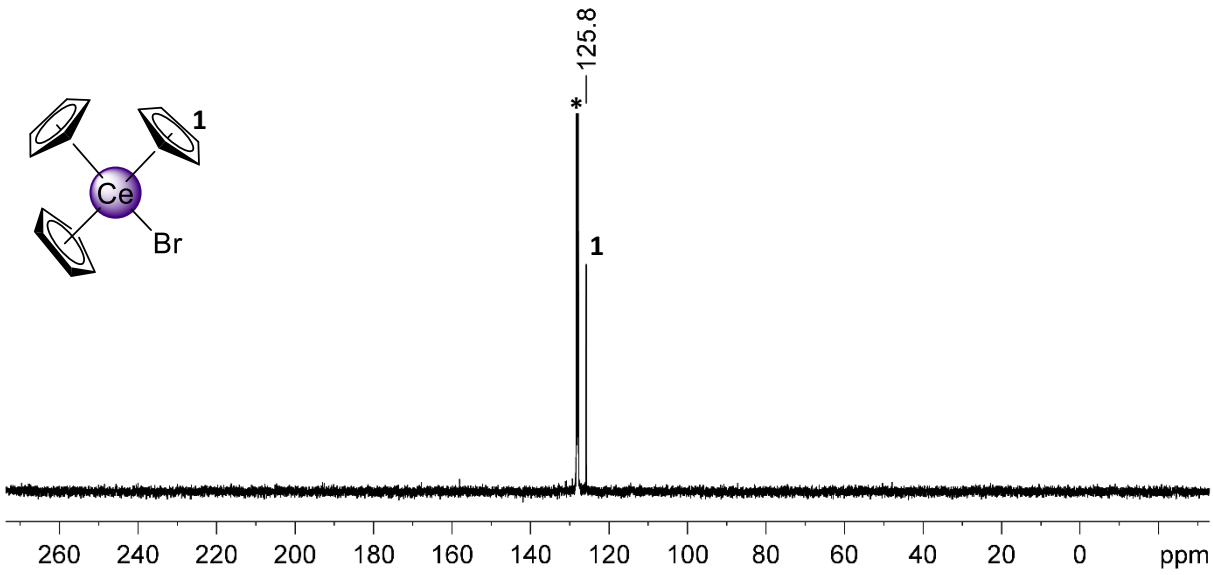

Figure S4. $^{13}C\{^{1}H\}$ NMR spectrum (100.6 MHz, C_6D_6, 26 °C) of **3a**.

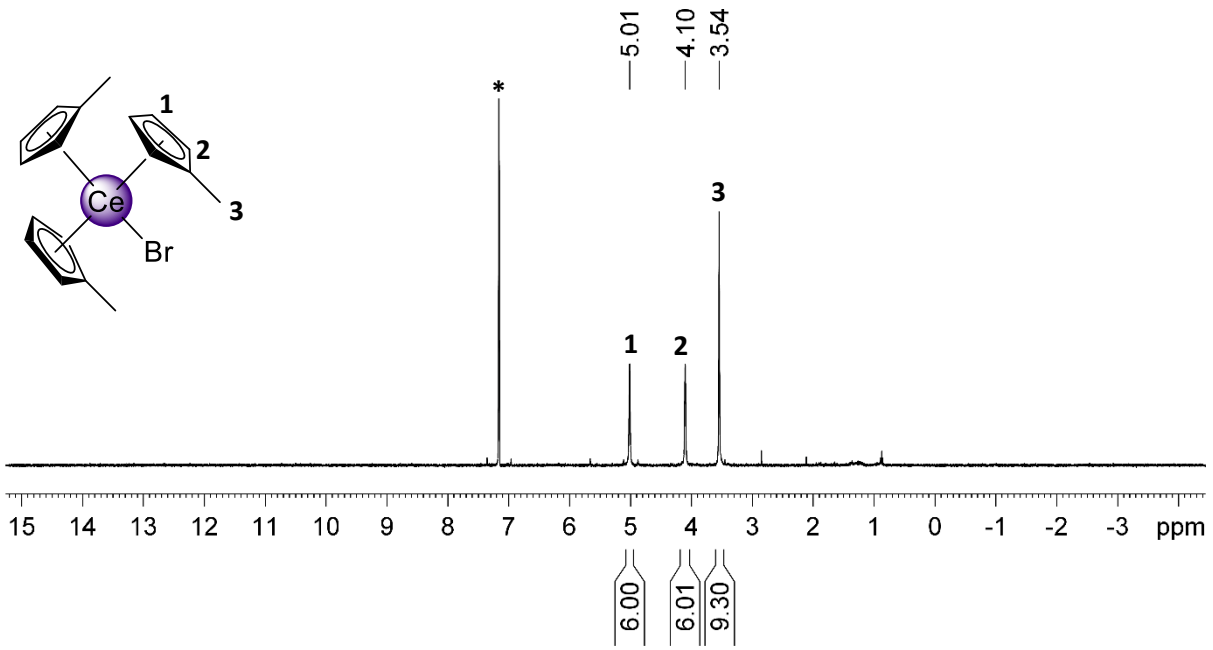

Figure S5. ^{1}H NMR spectrum (400.1 MHz, C_6D_6, 26 °C) of **3b**.

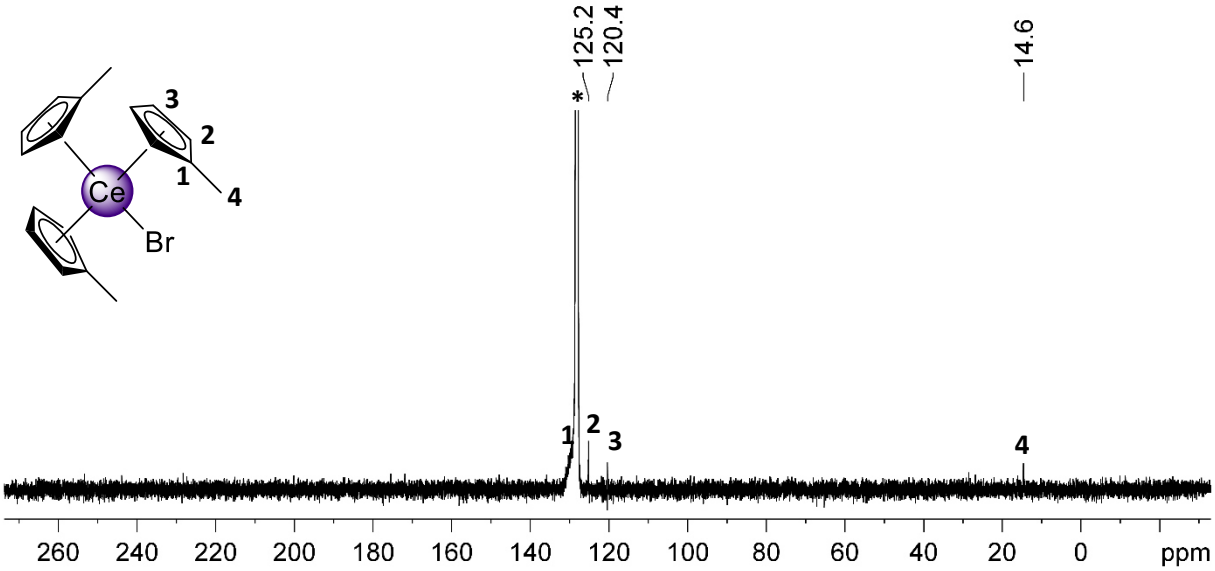

Figure S6. $^{13}C\{^{1}H\}$ NMR spectrum (100.6 MHz, C_6D_6, 26 °C) of **3b**.

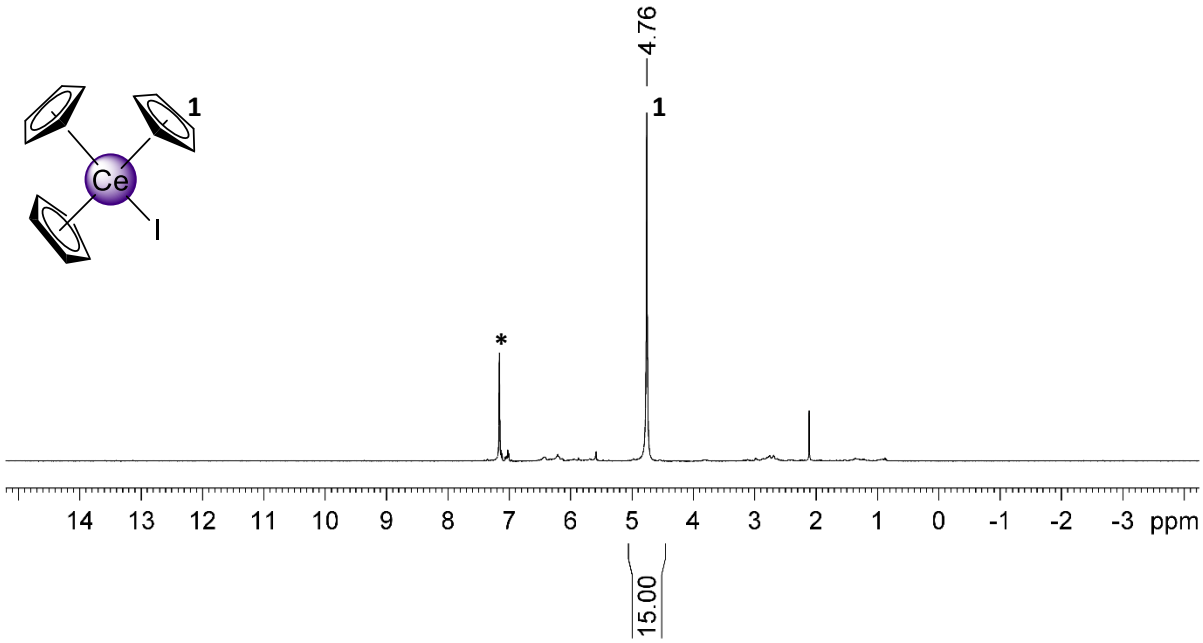

Figure S7. ^{1}H NMR spectrum (400.1 MHz, C_6D_6, 26 °C) of **4a**.

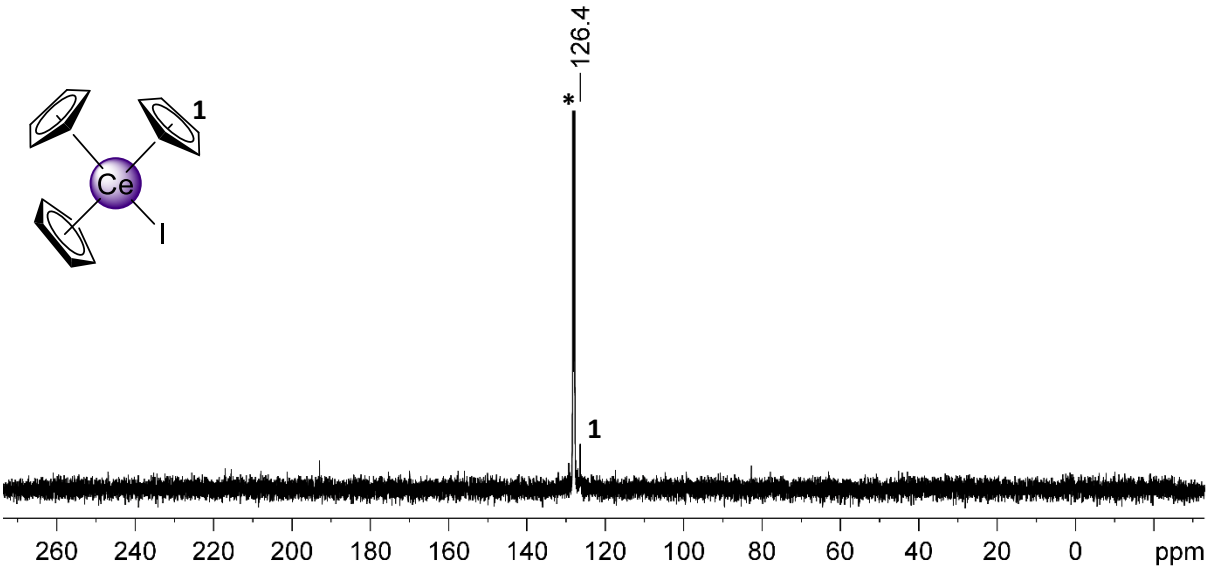

Figure S8. $^{13}C\{^{1}H\}$ NMR spectrum (100.6 MHz, C_6D_6, 26 °C) of **4a**.

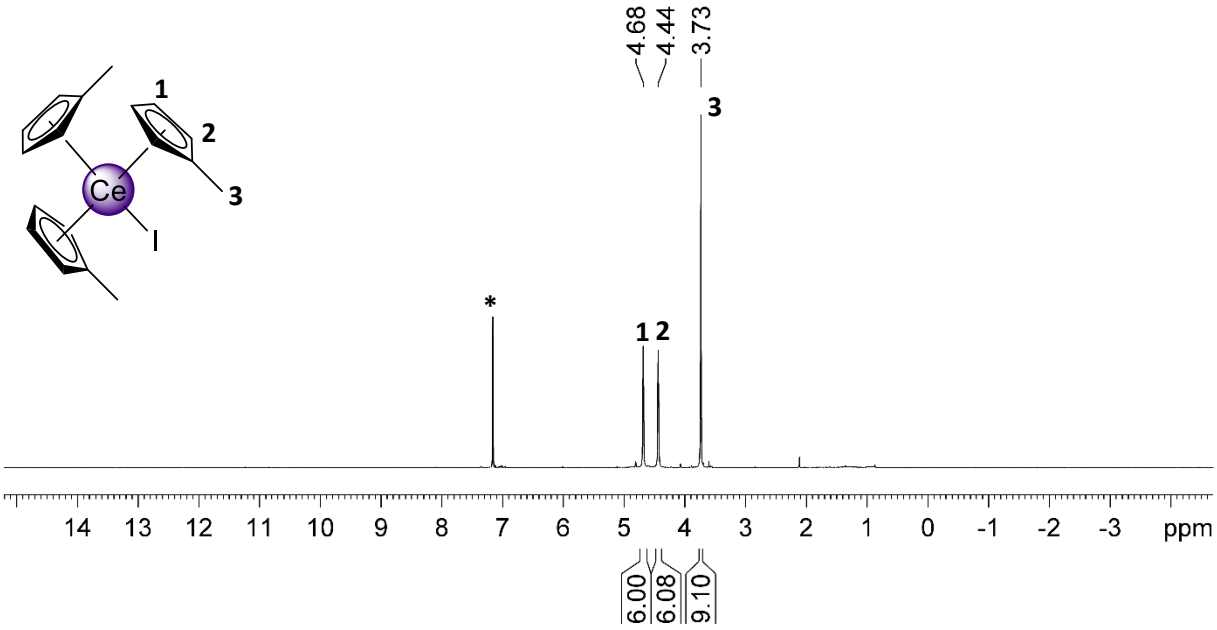

Figure S9. ^{1}H NMR spectrum (400.1 MHz, C_6D_6, 26 °C) of **4b**.

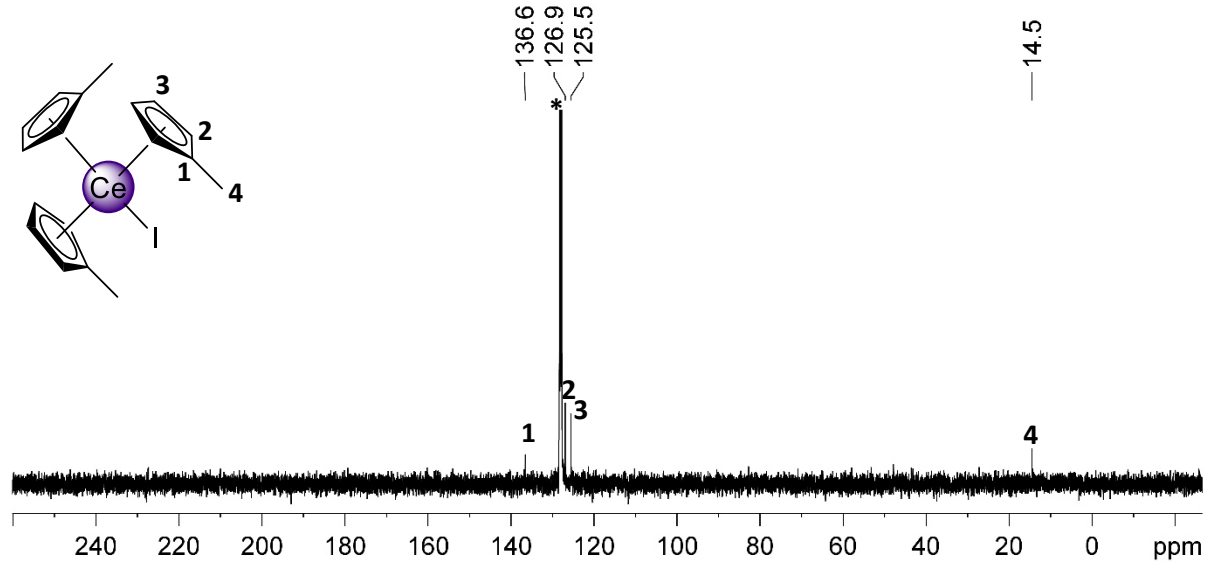

Figure S10. $^{13}C\{^{1}H\}$ NMR spectrum (100.6 MHz, C_6D_6, 26 °C) of **4b**.

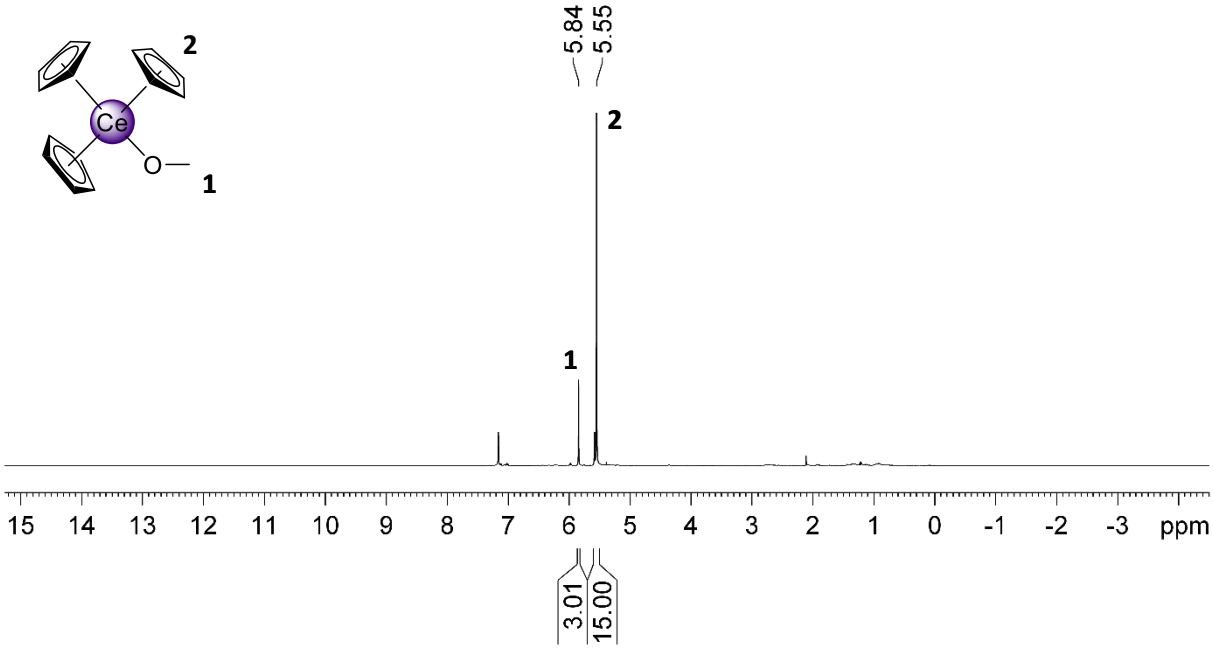

Figure S11. ^{1}H NMR spectrum (400.1 MHz, C_6D_6, 26 °C) of **5a**.

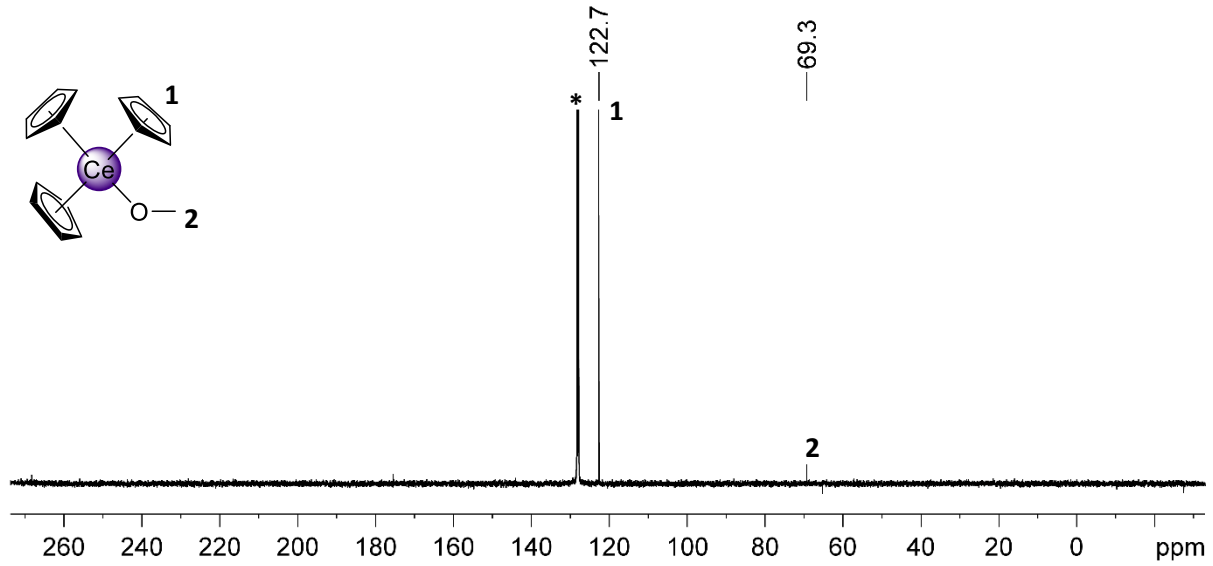

Figure S12. $^{13}C\{^{1}H\}$ NMR spectrum (100.6 MHz, C_6D_6, 26 °C) of **5a**.

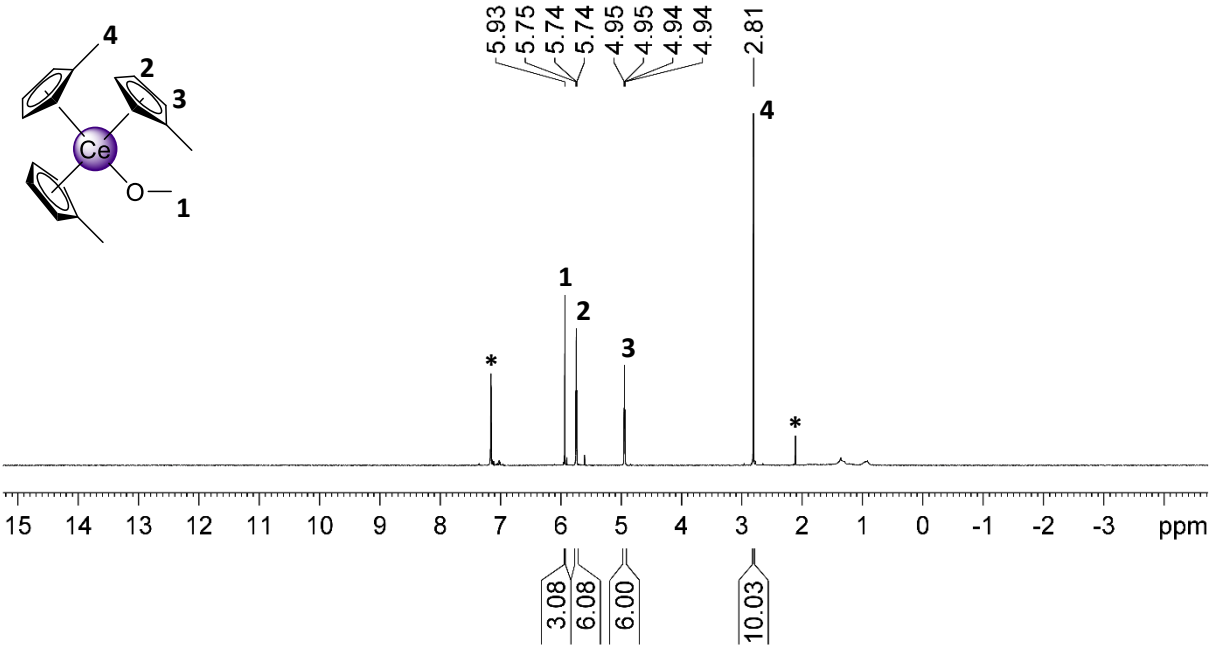

Figure S13. ^{1}H NMR spectrum (400.1 MHz, C_6D_6, 26 °C) of **5b**.

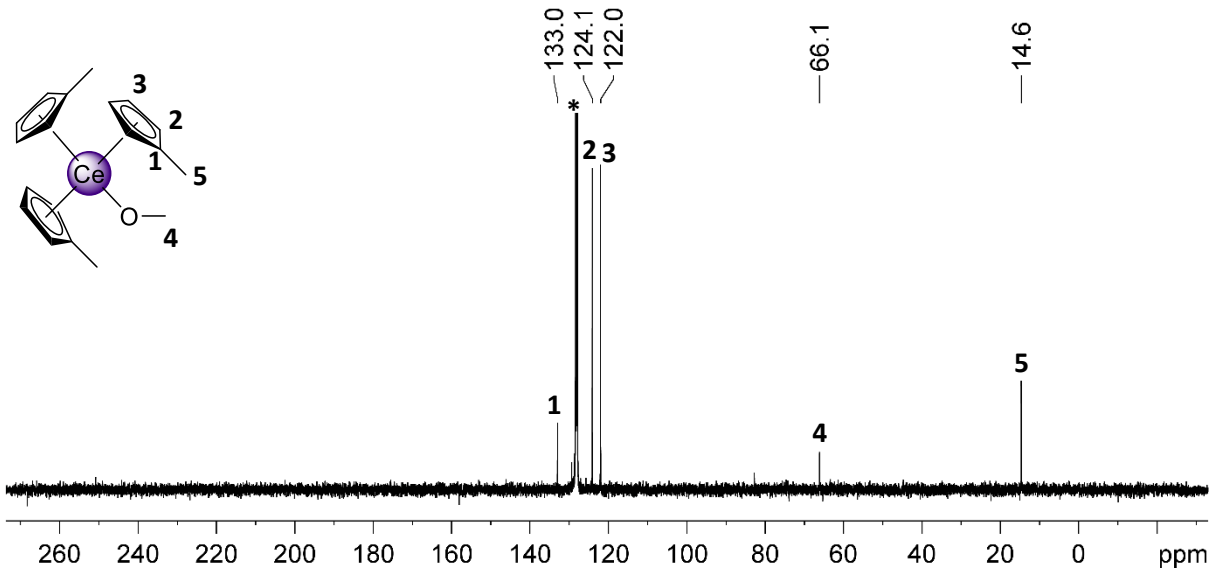

Figure S14. $^{13}C\{^{1}H\}$ NMR spectrum (100.6 MHz, C_6D_6, 26 °C) of **5b**.

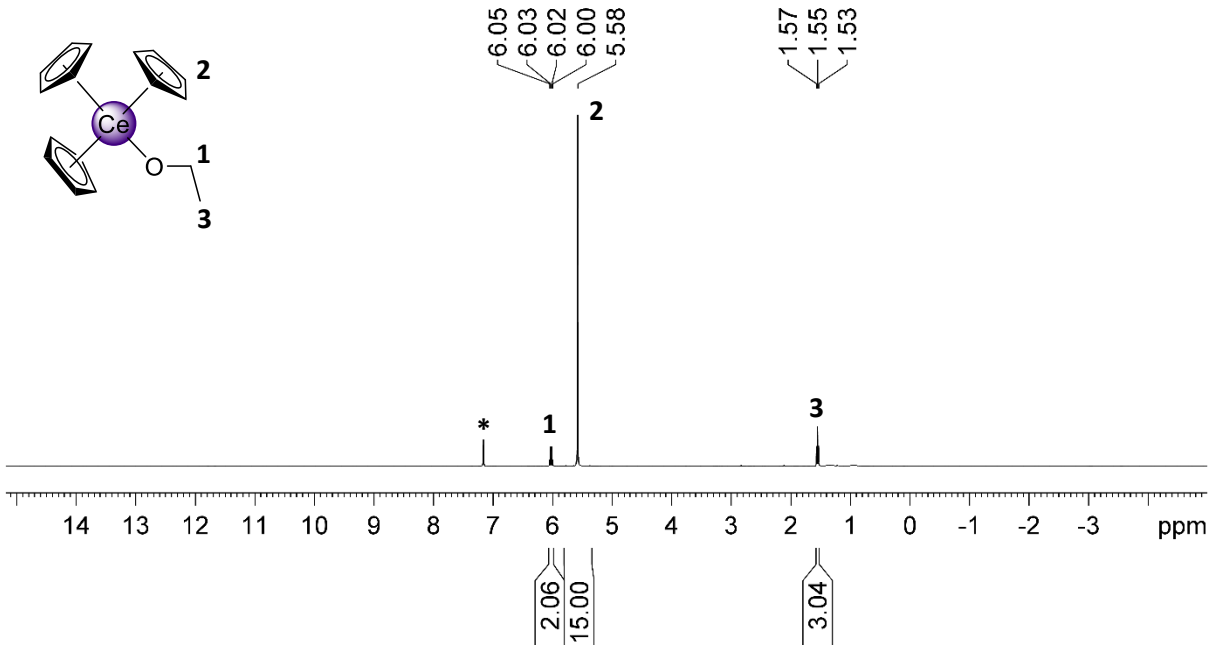

Figure S15. ^{1}H NMR spectrum (400.1 MHz, C_6D_6, 26 °C) of **6a**.

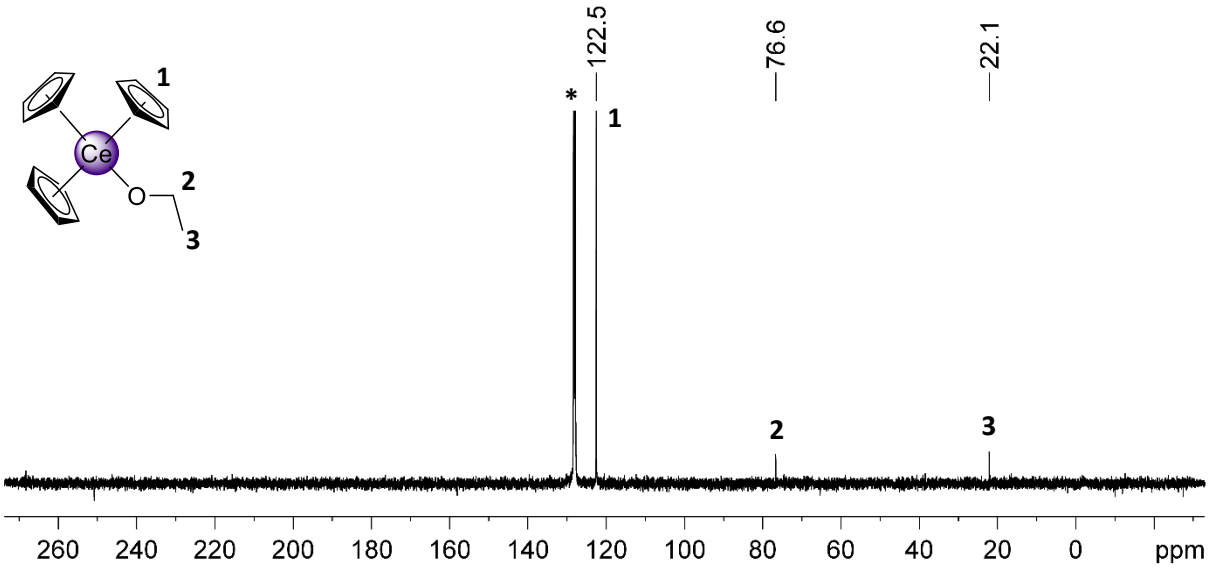

Figure S16. $^{13}C\{^{1}H\}$ NMR spectrum (100.6 MHz, C_6D_6, 26 °C) of **6a**.

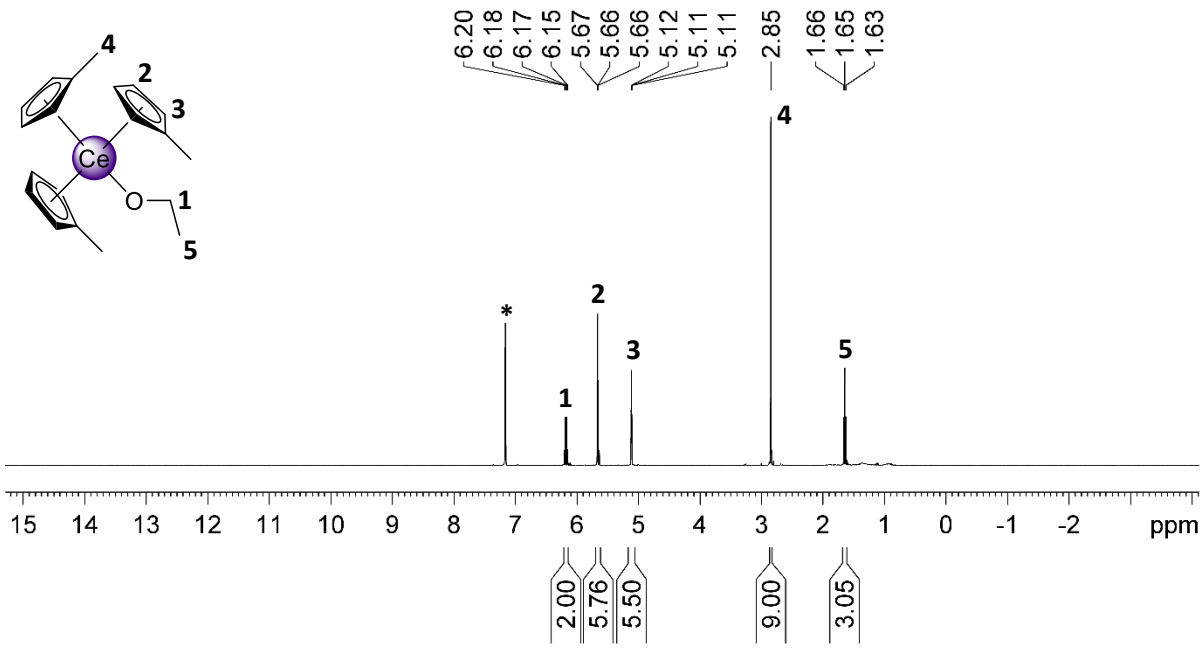

Figure S17. ^{1}H NMR spectrum (400.1 MHz, C_6D_6, 26 °C) of **6b**.

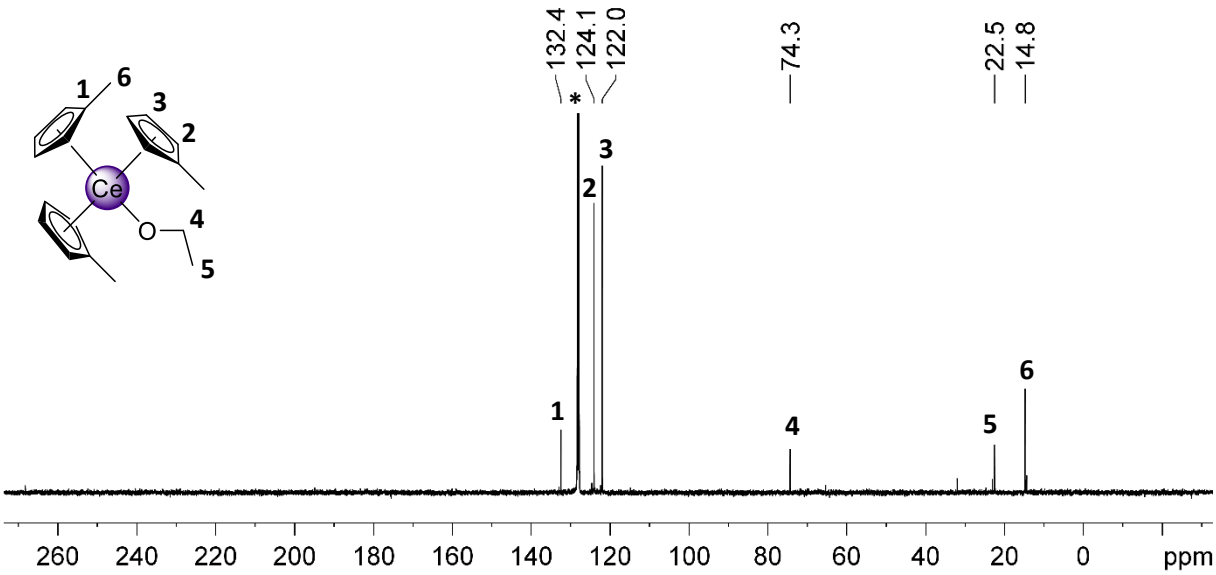

Figure S18. ^{13}C{^{1}H} NMR spectrum (100.6 MHz, C_6D_6, 26 °C) of **6b**.

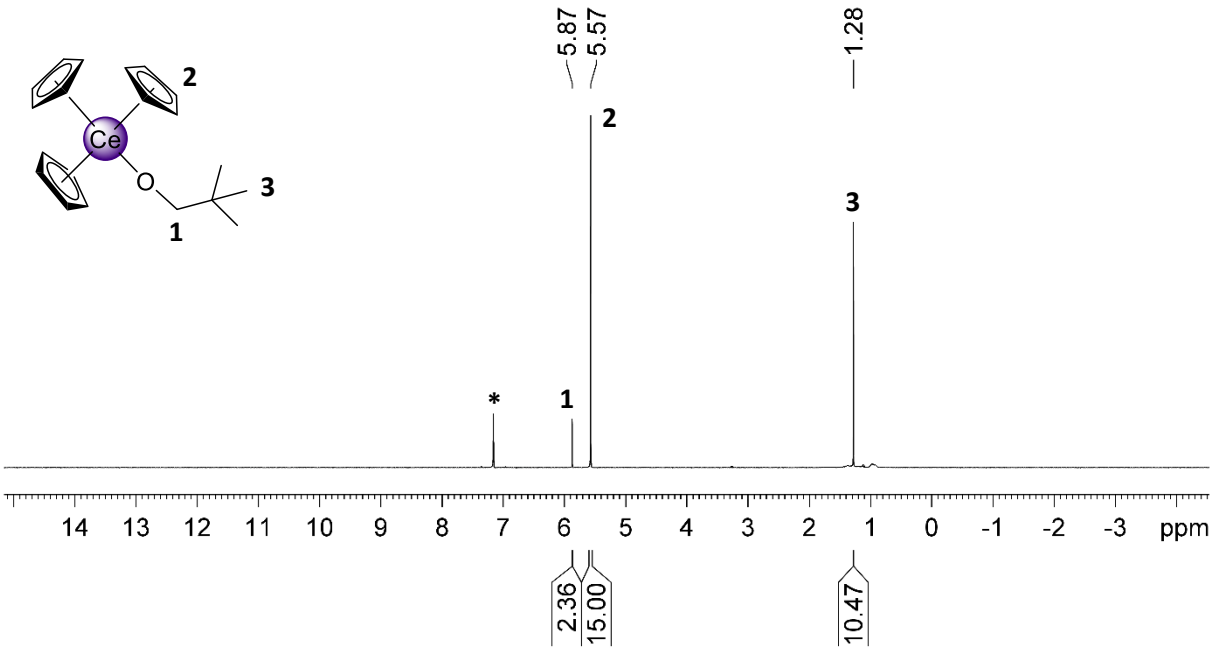

Figure S19. ^{1}H NMR spectrum (400.1 MHz, C_6D_6, 26 °C) of **7a**.

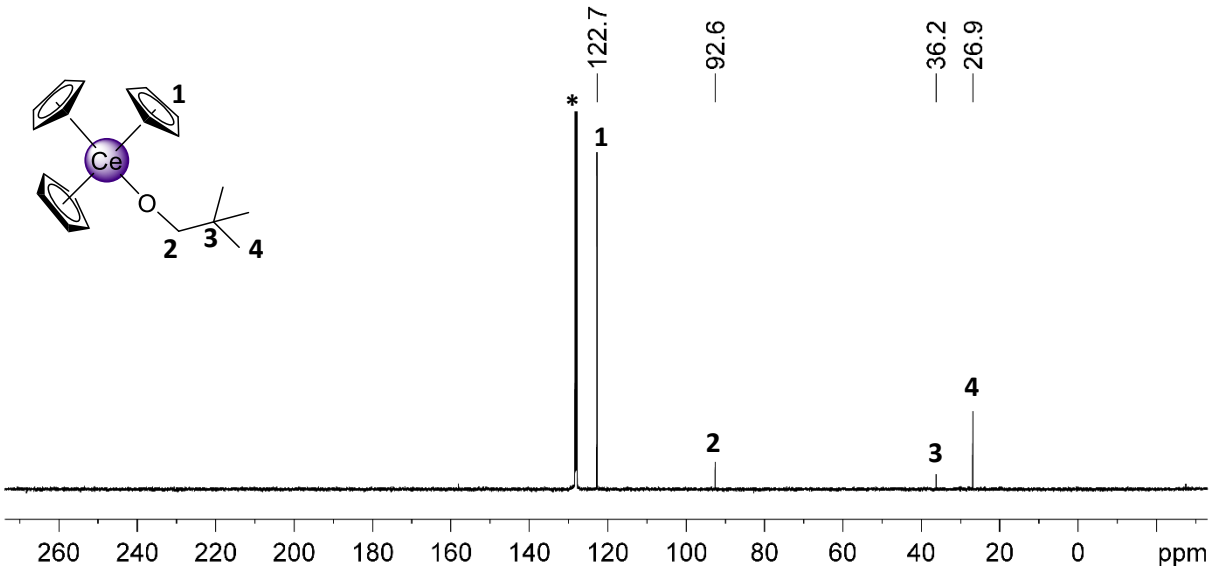

Figure S20. $^{13}C\{^{1}H\}$ NMR spectrum (100.6 MHz, C_6D_6, 26 °C) of **7a**.

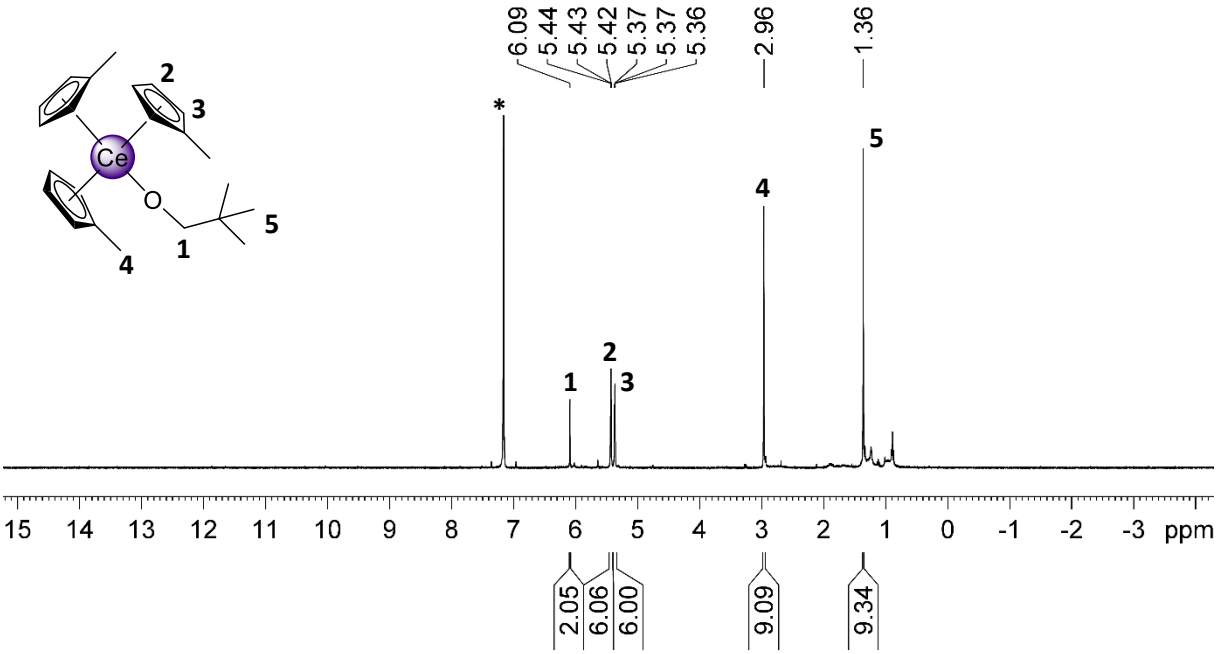

Figure S21. ^{1}H NMR spectrum (400.1 MHz, C_6D_6, 26 °C) of **7b**.

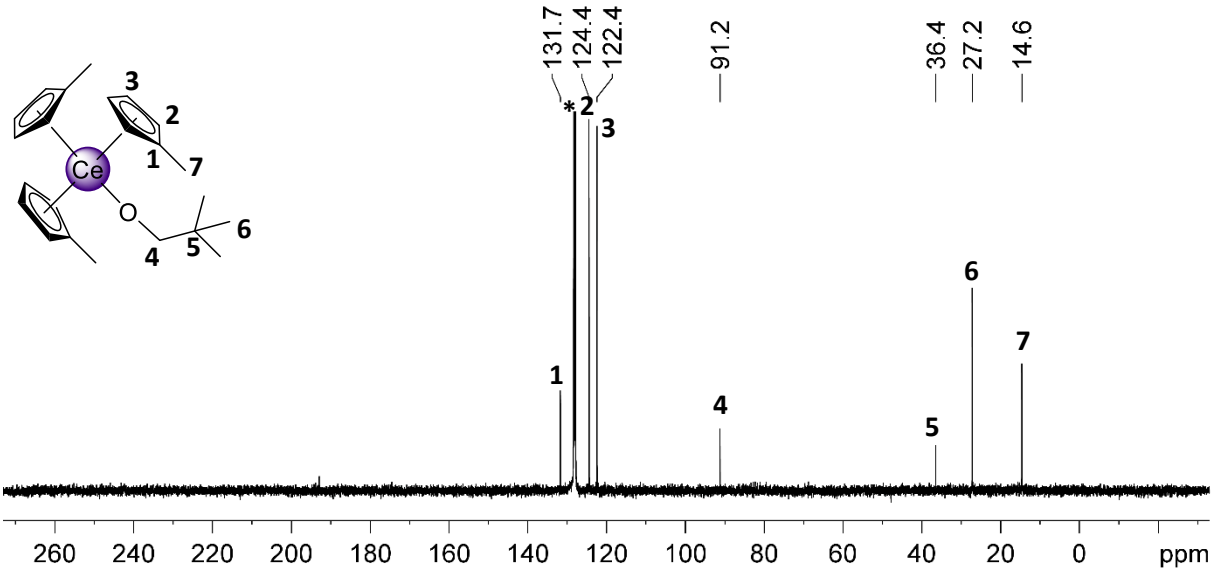

Figure S22. $^{13}C\{^{1}H\}$ NMR spectrum (100.6 MHz, C_6D_6, 26 °C) of **7b**.

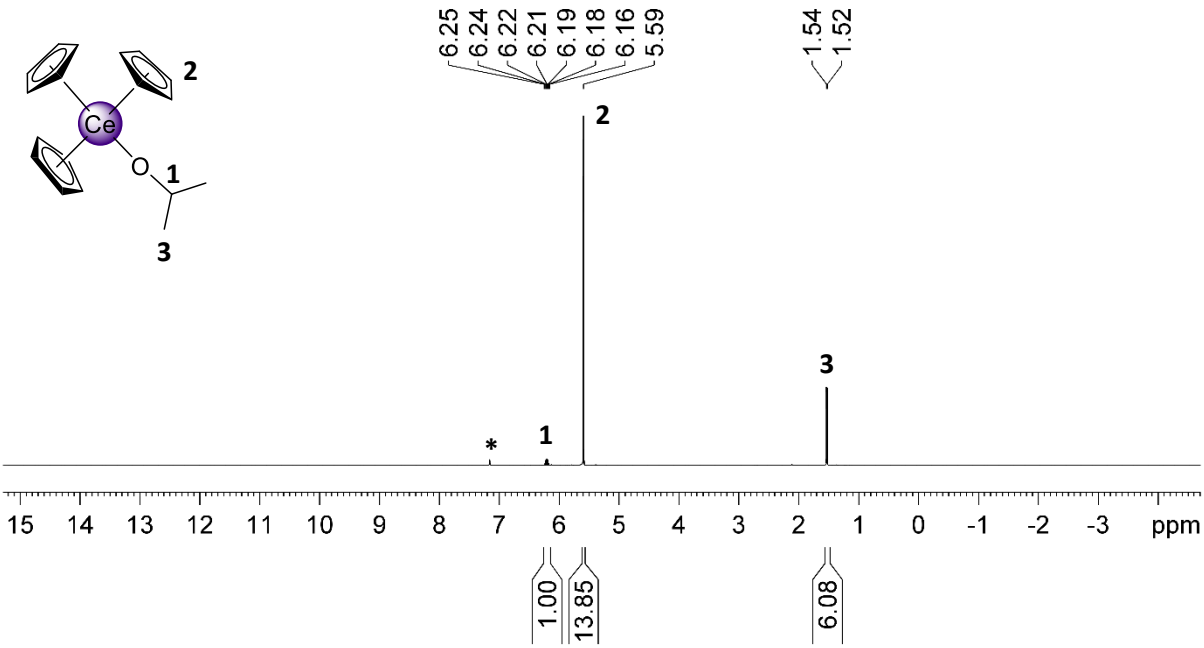

Figure S23. ^{1}H NMR spectrum (400.1 MHz, C_6D_6, 26 °C) of **8a**.

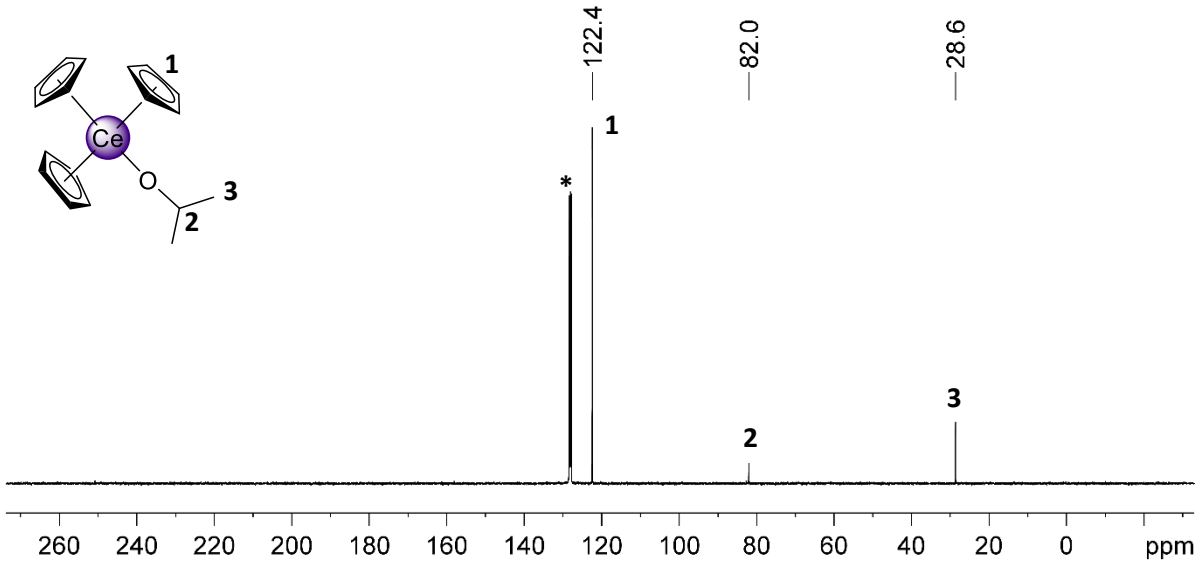

Figure S24. ^{13}C{^{1}H} NMR spectrum (100.6 MHz, C_6D_6, 26 °C) of **8a**.

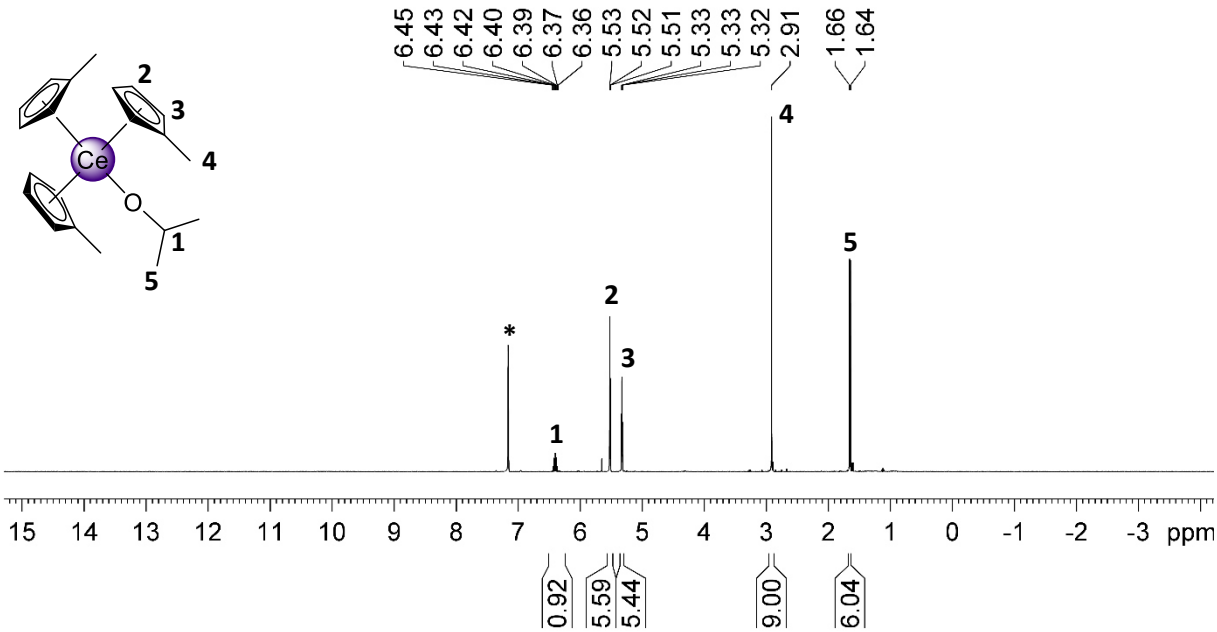

Figure S25. ^{1}H NMR spectrum (400.1 MHz, C_6D_6, 26 °C) of **8b**.

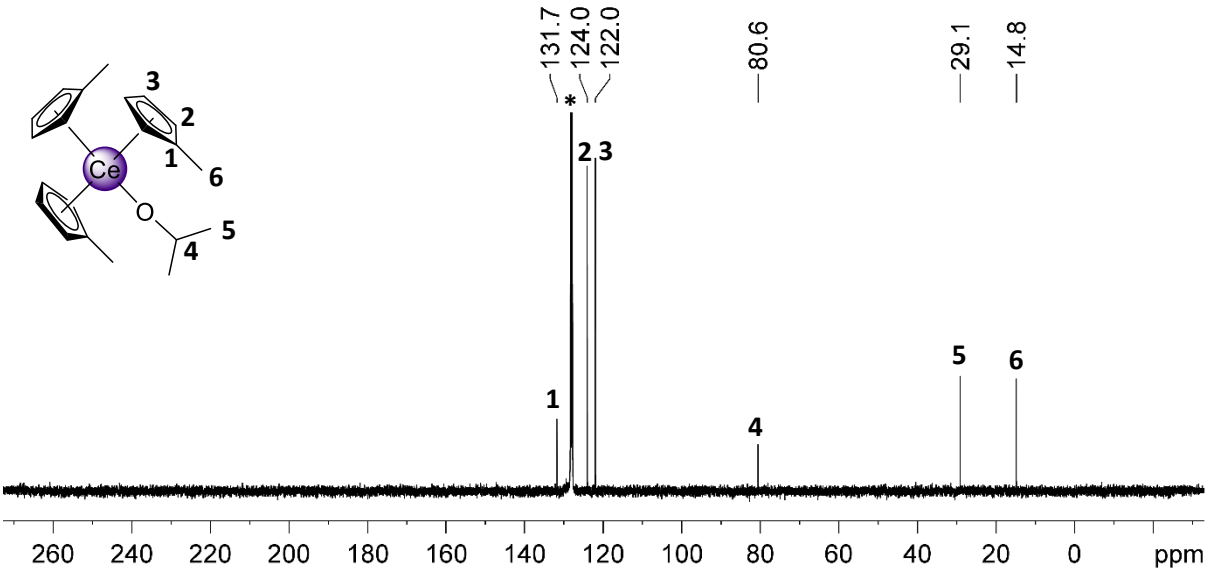

Figure S26. $^{13}C\{^{1}H\}$ NMR spectrum (100.6 MHz, C_6D_6, 26 °C) of **8b**.

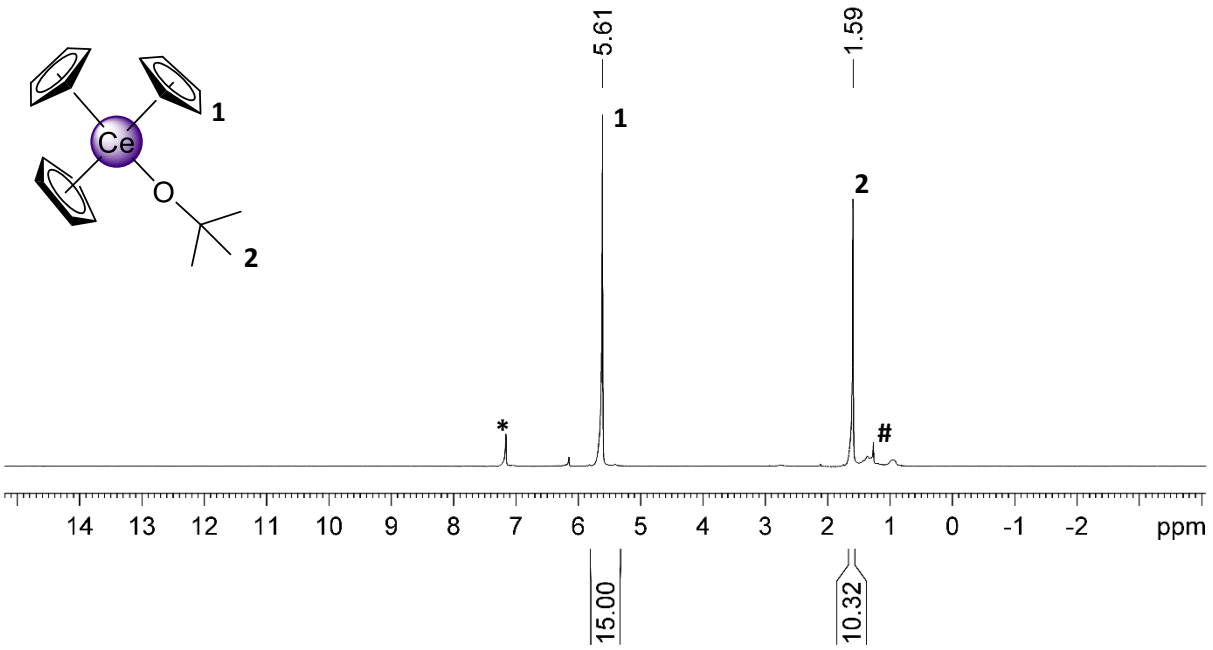

Figure S27. ^{1}H NMR spectrum (400.1 MHz, C_6D_6, 26 °C) of **9a**.

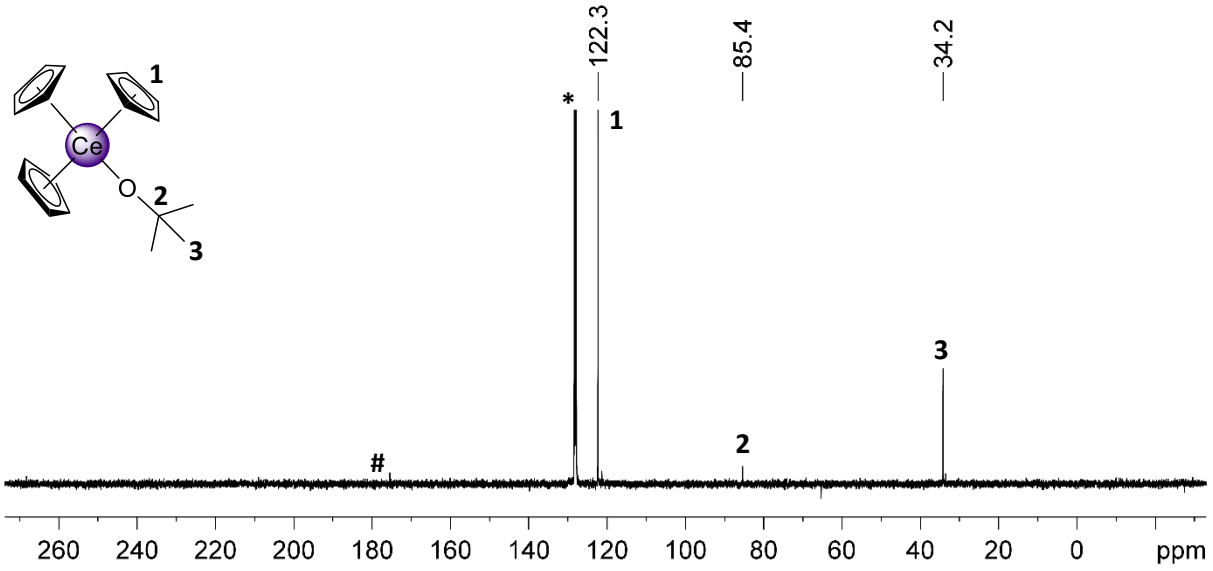

Figure S28. $^{13}C\{^{1}H\}$ NMR spectrum (100.6 MHz, C_6D_6, 26 °C) of **9a**.

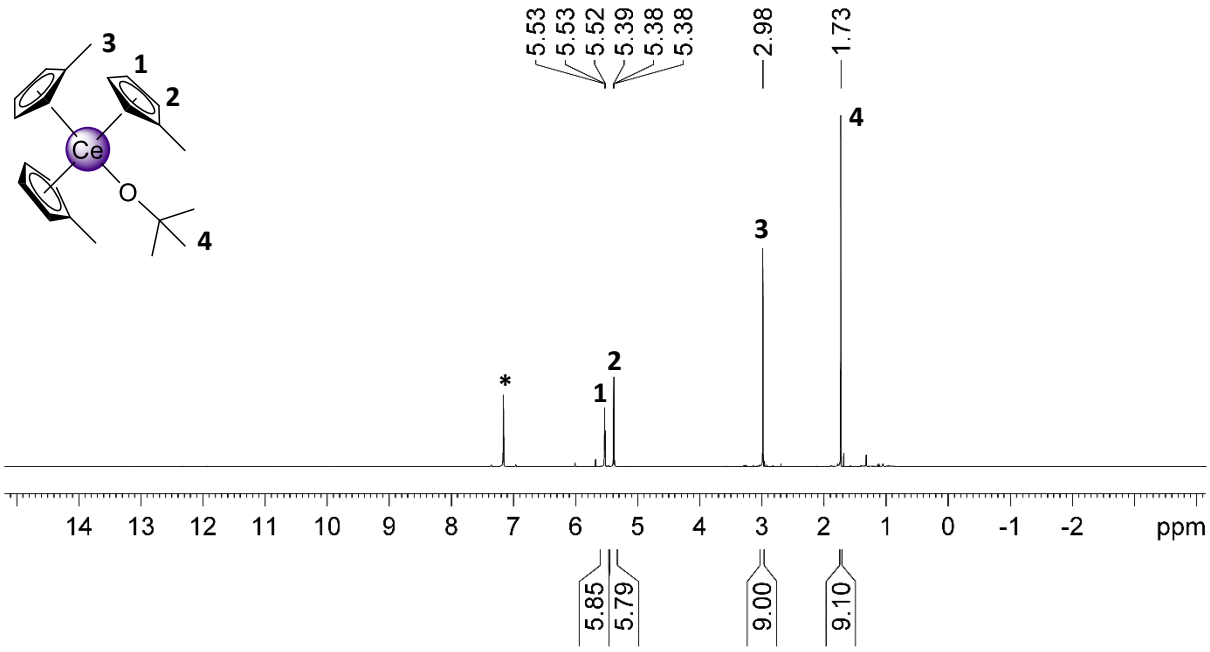

Figure S29. ^{1}H NMR spectrum (400.1 MHz, C_6D_6, 26 °C) of **9b**.

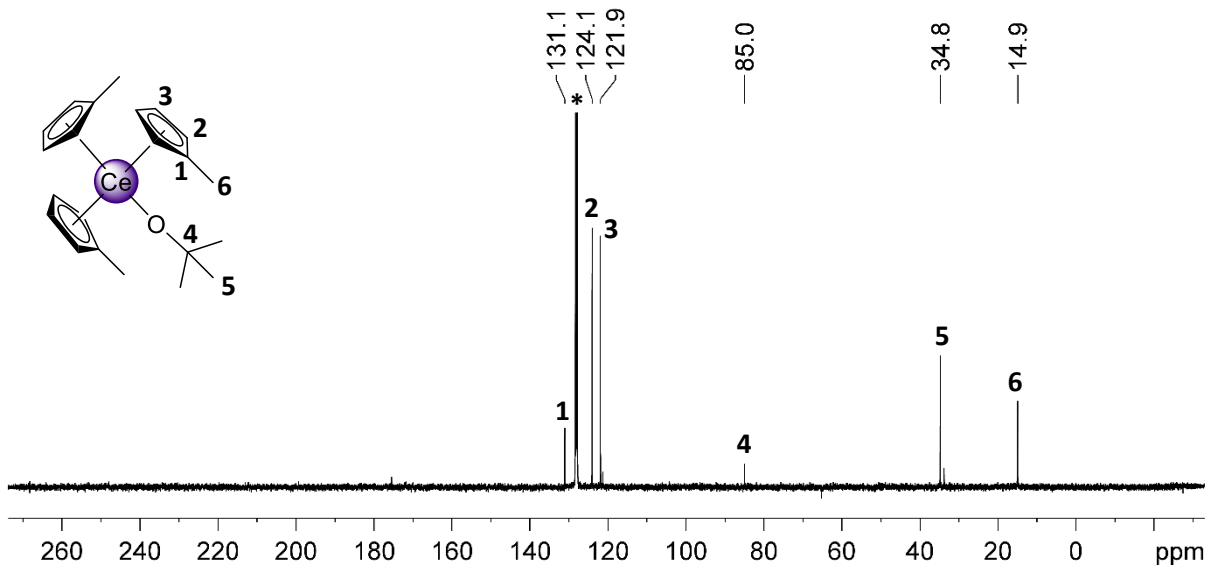

Figure S30. ^{13}C{^{1}H} NMR spectrum (100.6 MHz, C_6D_6, 26 °C) of **9b**.

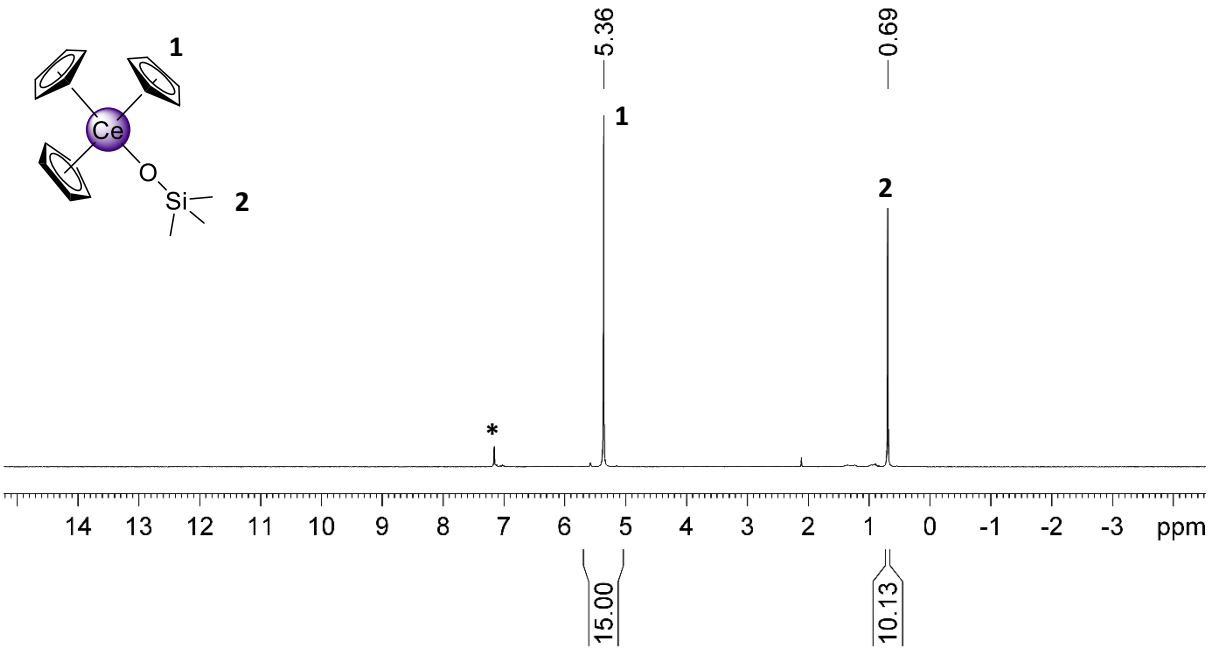

Figure S31. ^{1}H NMR spectrum (400.1 MHz, C_6D_6, 26 °C) of **10a**.

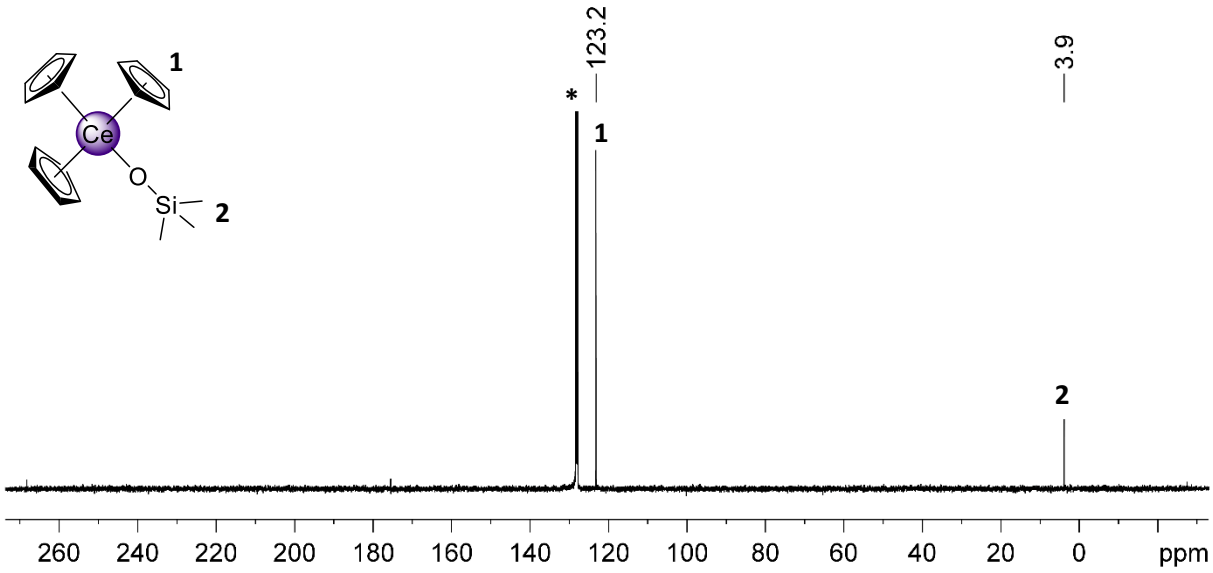

Figure S32. $^{13}C\{^{1}H\}$ NMR spectrum (100.6 MHz, C_6D_6, 26 °C) of **10a**.

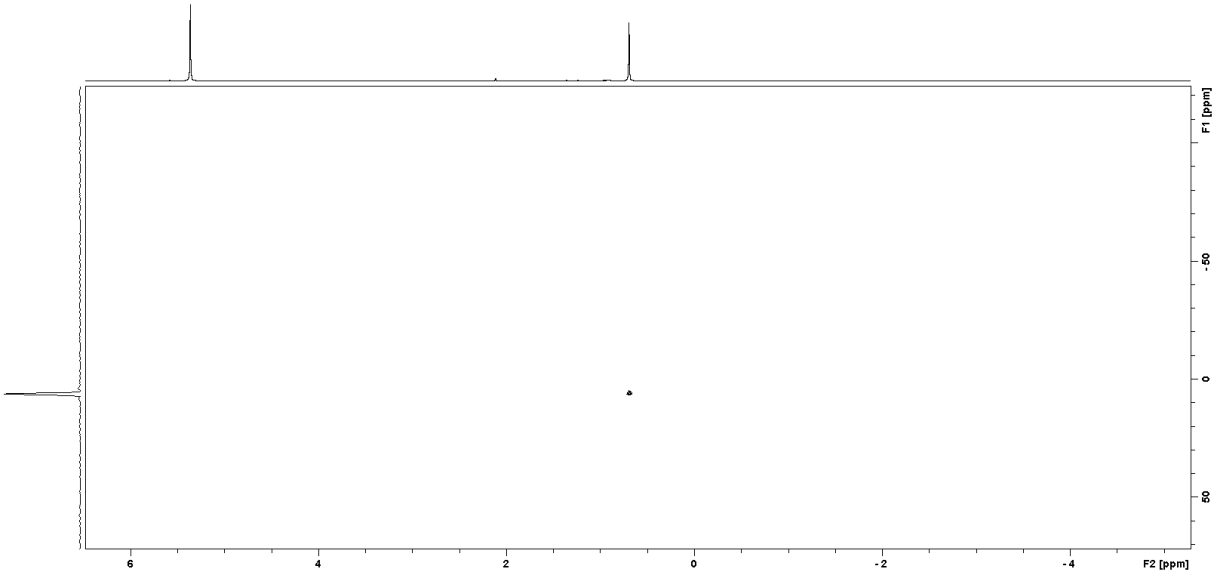

Figure S33. ^{1}H-^{29}Si HSQC NMR spectrum (79.5 MHz, C_6D_6, 26 °C) of **10a**.

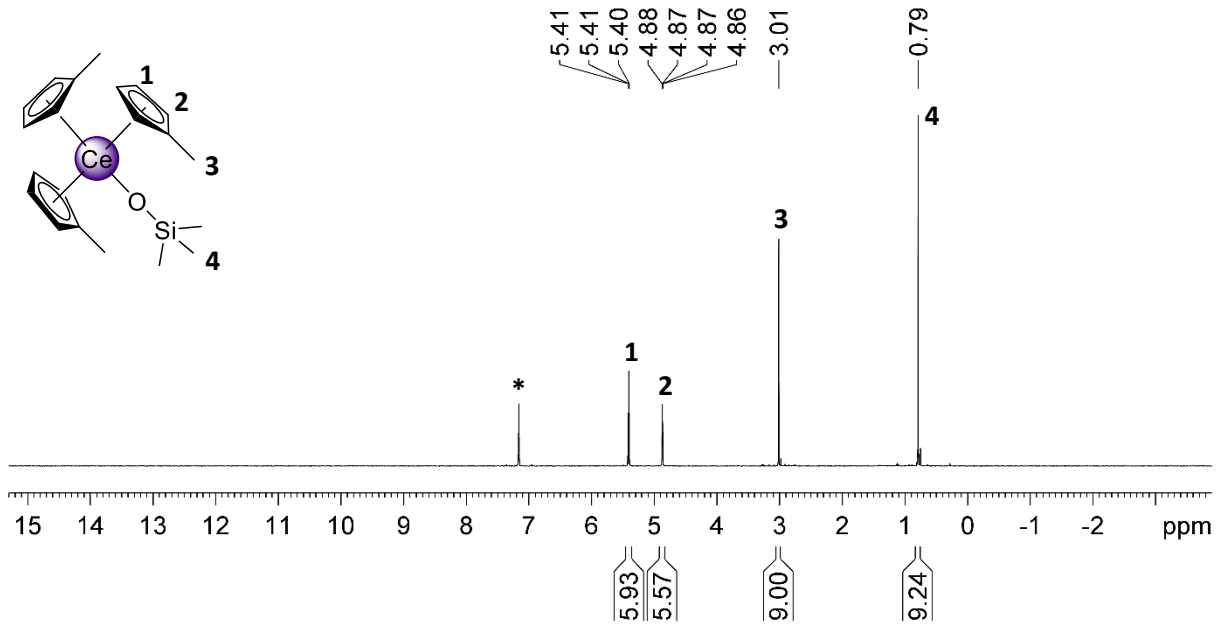

Figure S34. ^{1}H NMR spectrum (400.1 MHz, C_6D_6, 26 °C) of **10b**.

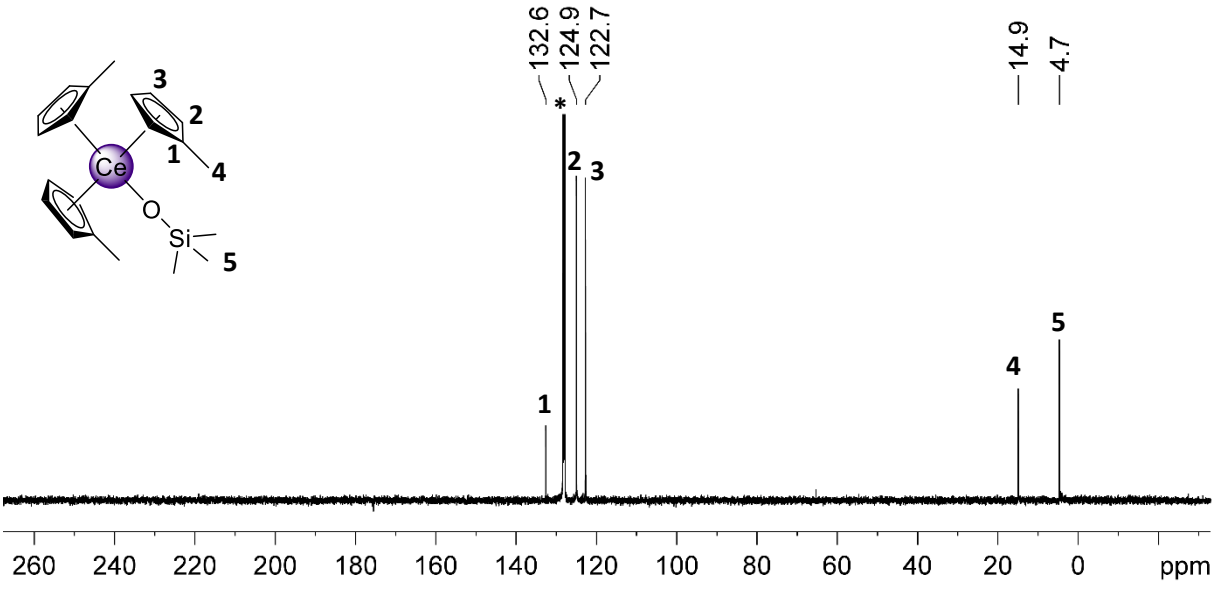

Figure S35. $^{13}C\{^{1}H\}$ NMR spectrum (100.6 MHz, C_6D_6, 26 °C) of **10b**.

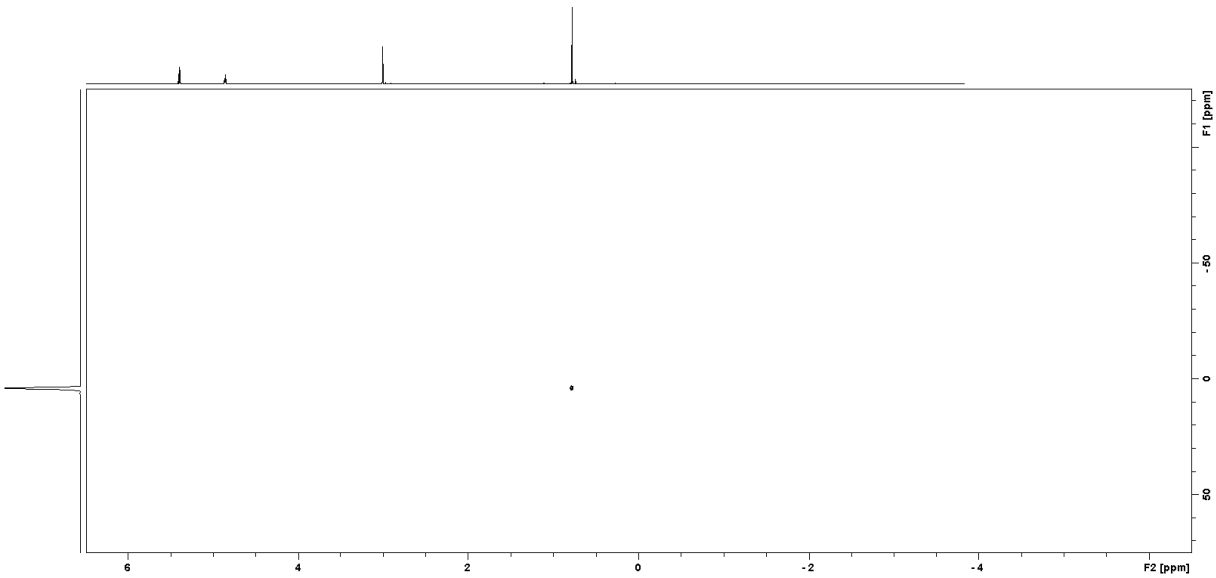

Figure S36. ^{1}H-^{29}Si HSQC NMR spectrum (79.5 MHz, C_6D_6, 26 °C) of **10b**.

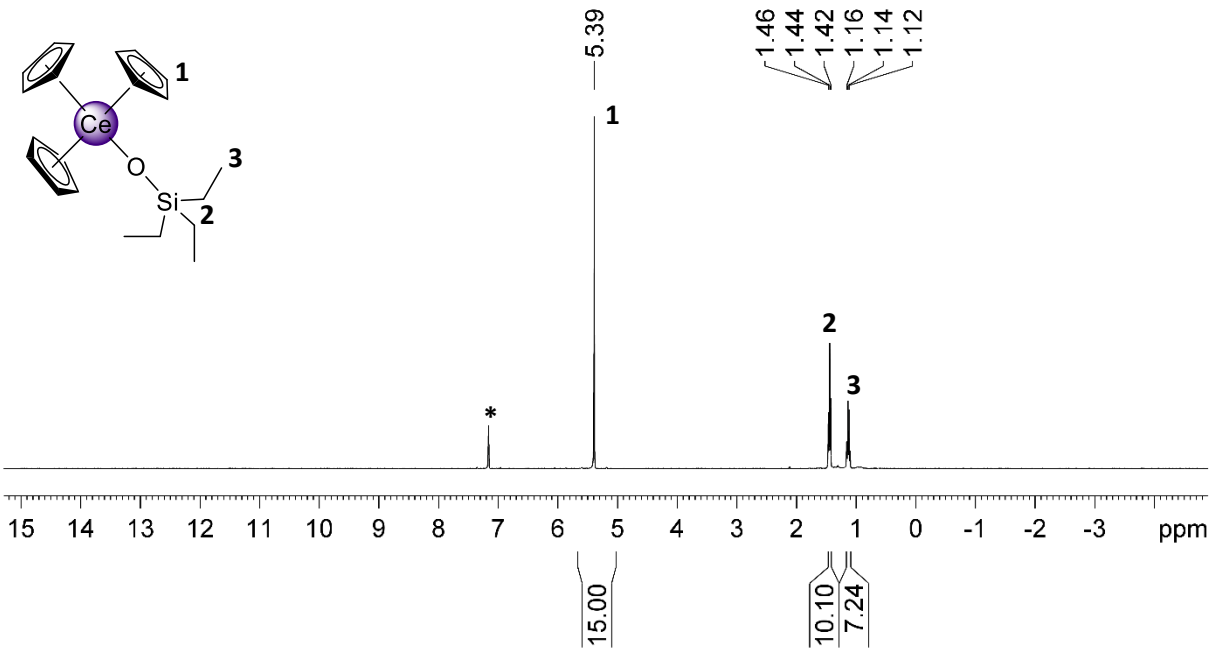

Figure S37. ^{1}H NMR spectrum (400.1 MHz, C_6D_6, 26 °C) of **11a**.

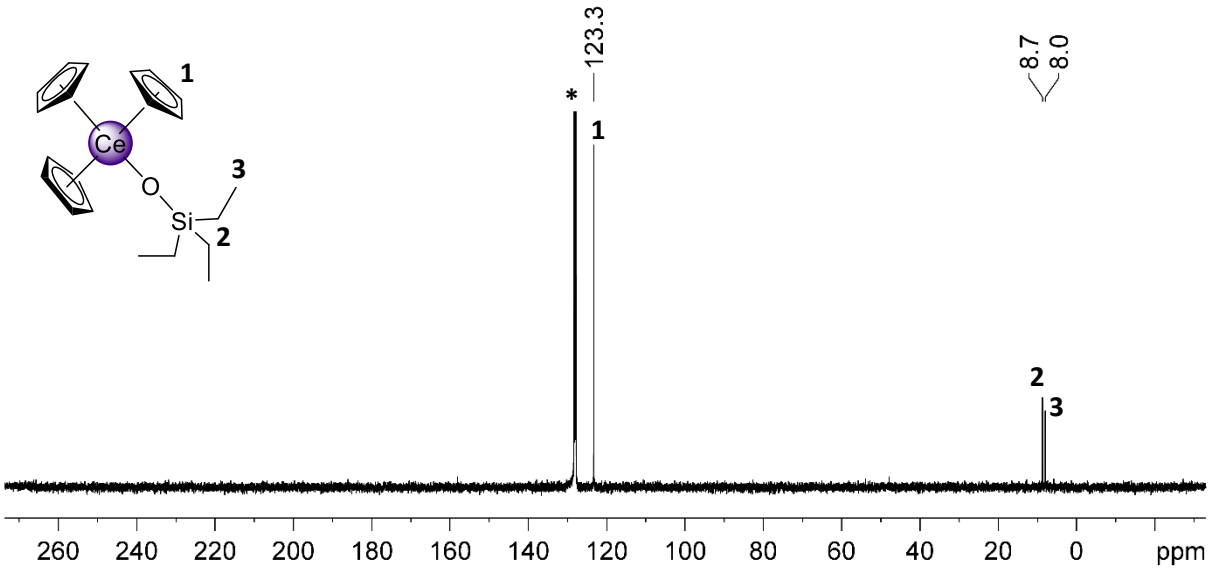

Figure S38. $^{13}C\{^{1}H\}$ NMR spectrum (100.6 MHz, C_6D_6, 26 °C) of **11a**.

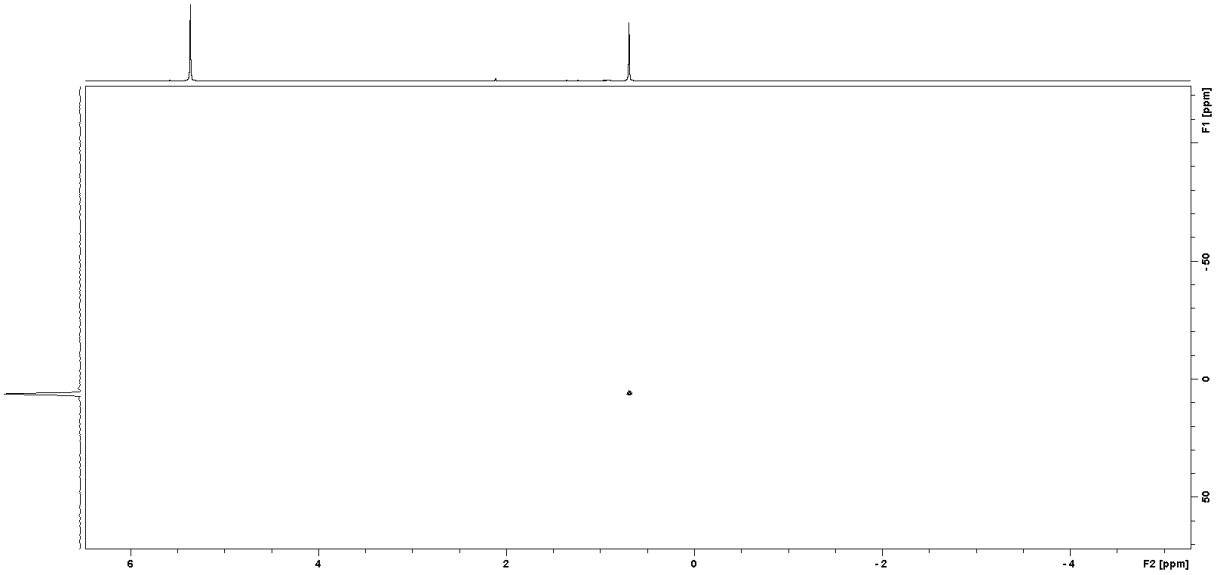

Figure S39. ^{1}H-^{29}Si HSQC NMR spectrum (79.5 MHz, C_6D_6, 26 °C) of **11a**.

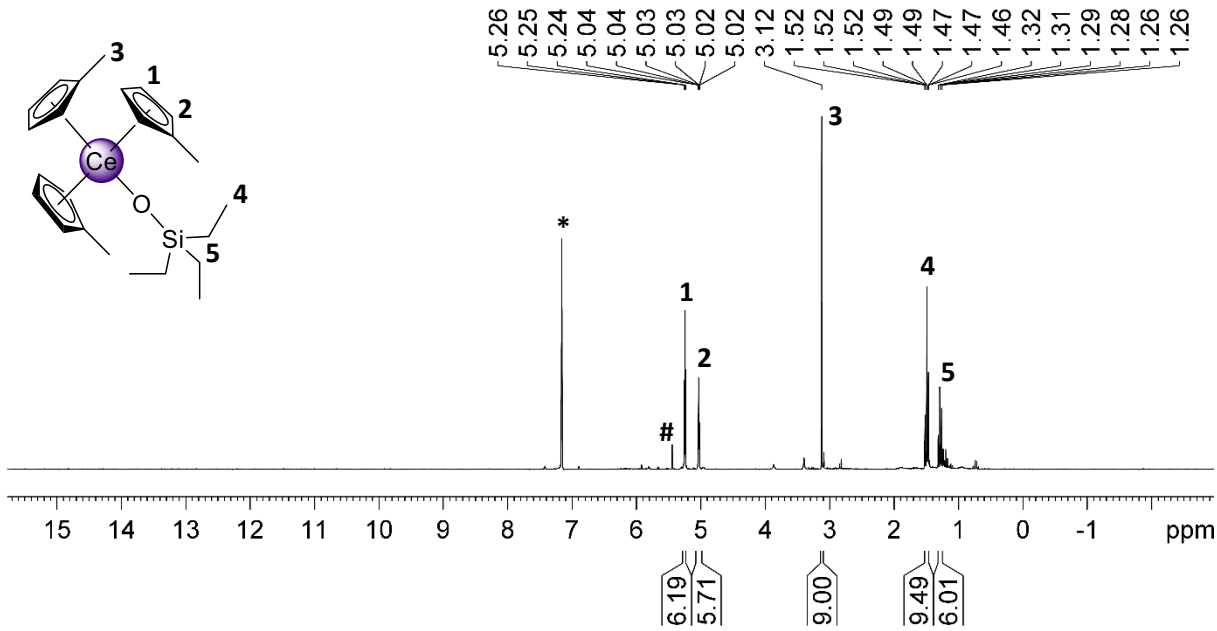

Figure S40. ^{1}H NMR spectrum (400.1 MHz, C_6D_6, 26 °C) of **11b**.

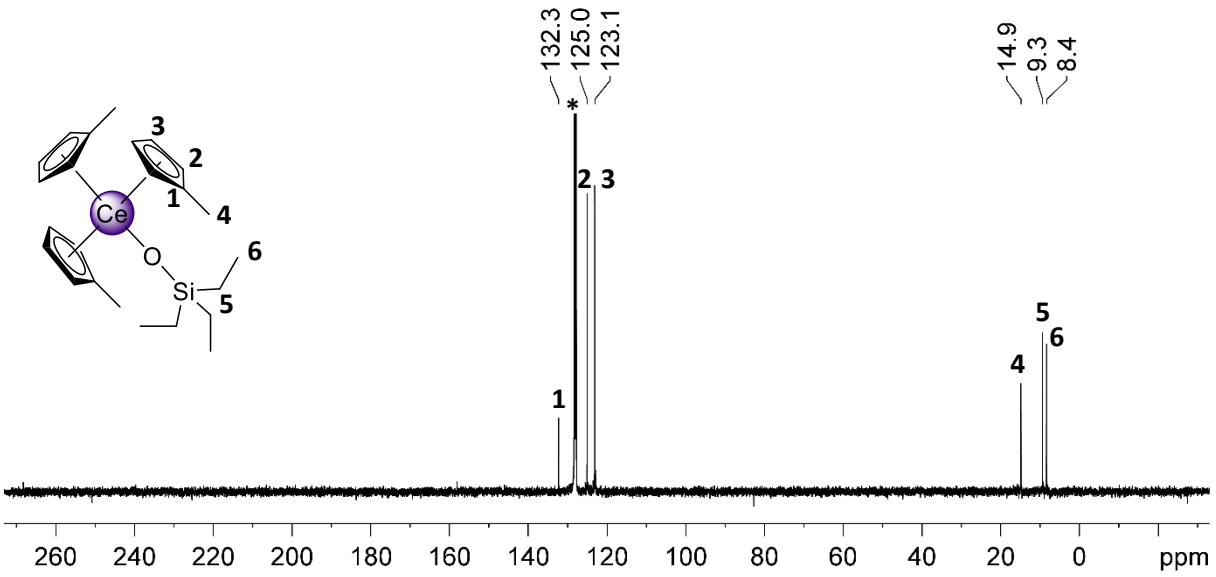

Figure S41. $^{13}C\{^{1}H\}$ NMR spectrum (100.6 MHz, C_6D_6, 26 °C) of **11b**.

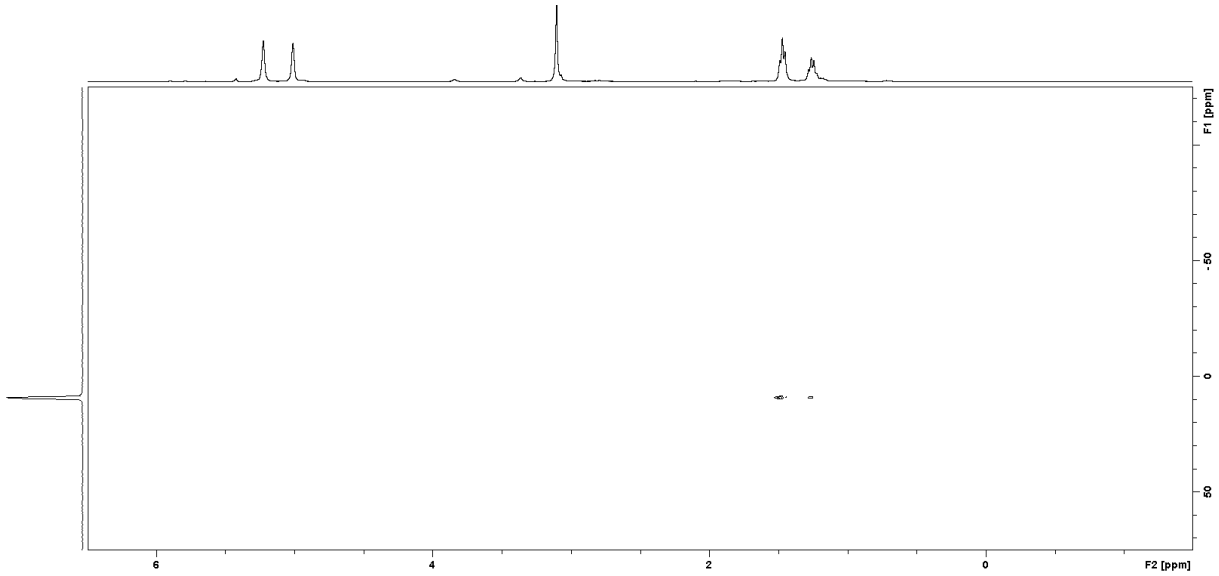

Figure S42. ^{1}H-^{29}Si HSQC NMR spectrum (79.5 MHz, C_6D_6, 26 °C) of **11b**.

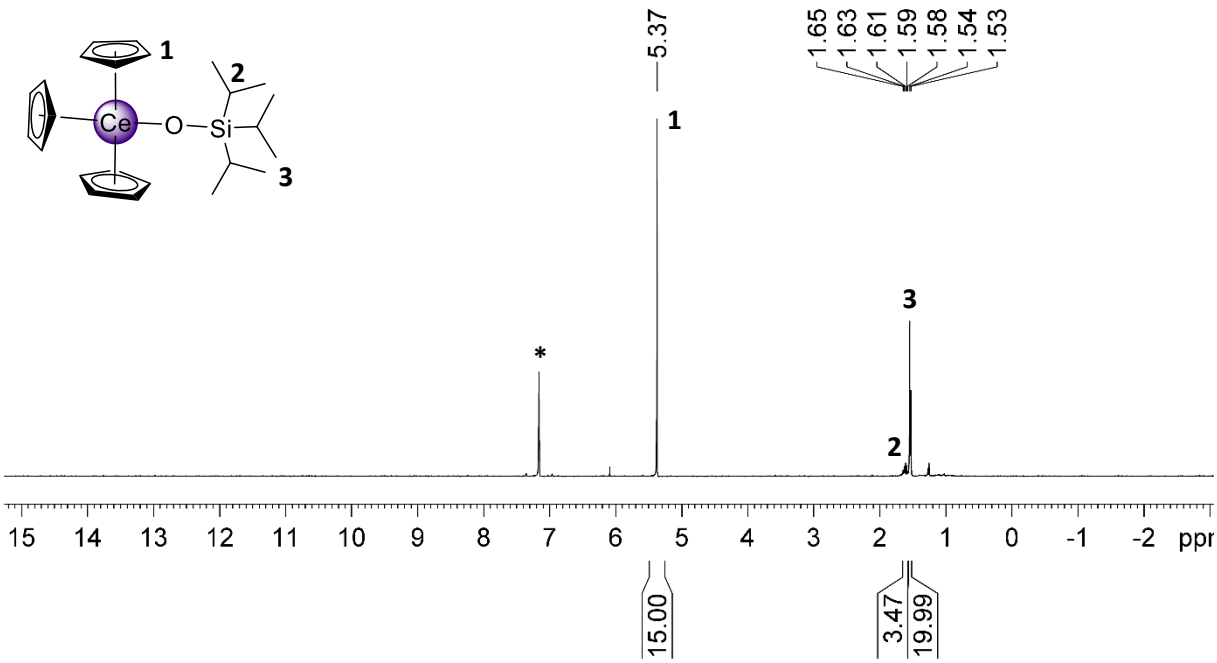

Figure S43. ^{1}H NMR spectrum (400.1 MHz, C_6D_6, 26 °C) of **12a**.

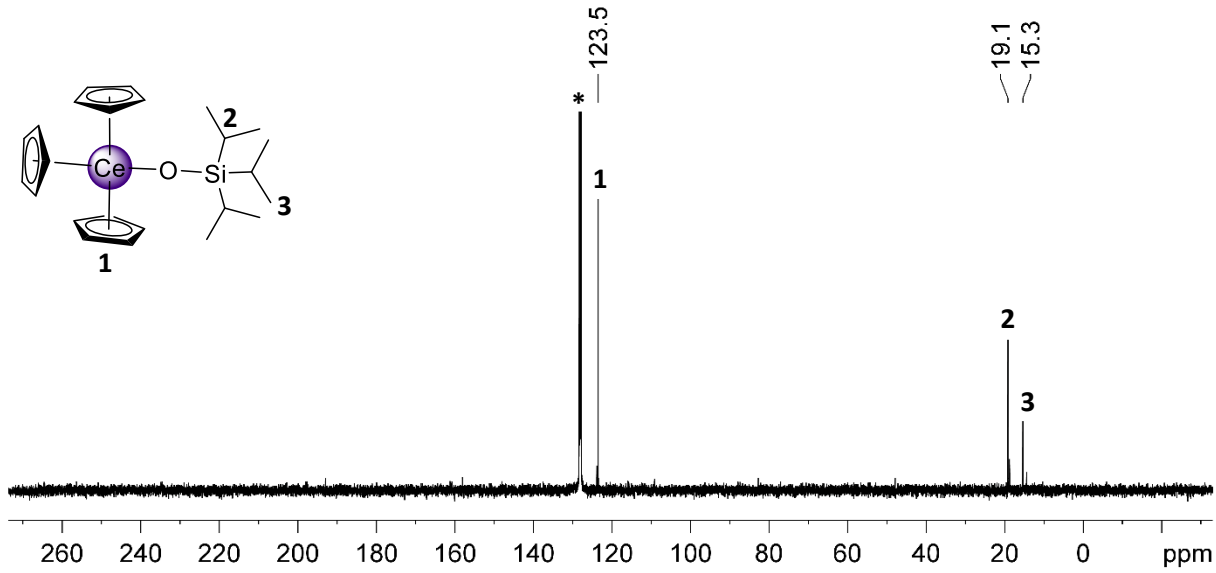

Figure S44. $^{13}C\{^{1}H\}$ NMR spectrum (100.6 MHz, C_6D_6, 26 °C) of **12a**.

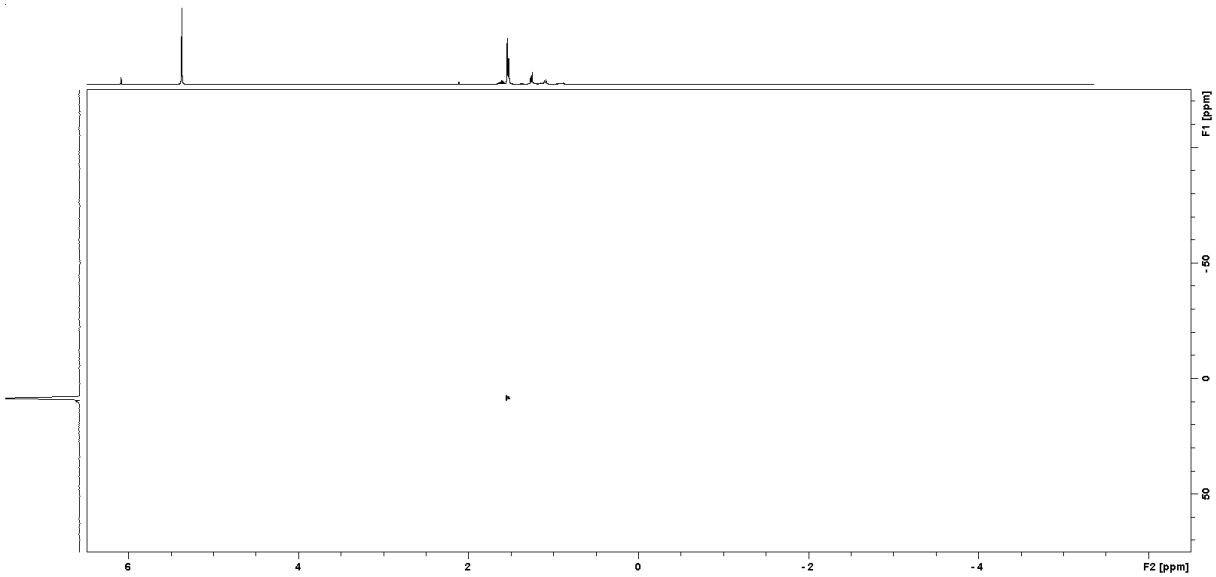

Figure S45. ^{1}H-^{29}Si HSQC NMR spectrum (79.5 MHz, C_6D_6, 26 °C) of **12a**.

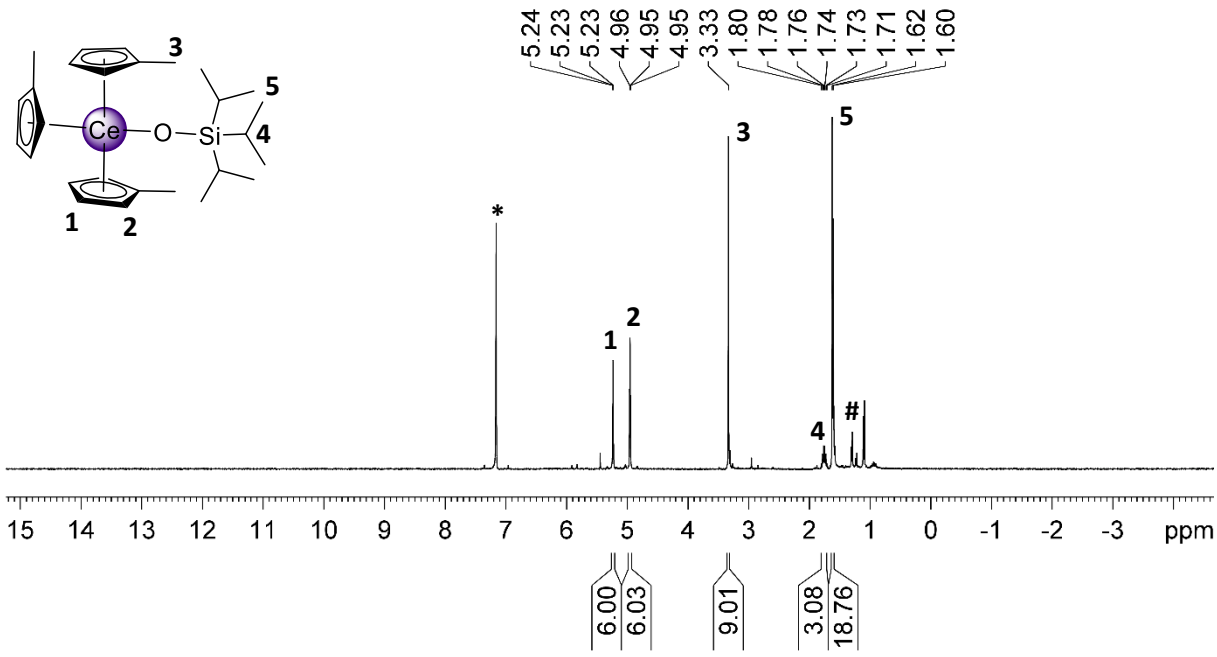

Figure S46. ^{1}H NMR spectrum (400.1 MHz, C_6D_6, 26 °C) of **12b**.

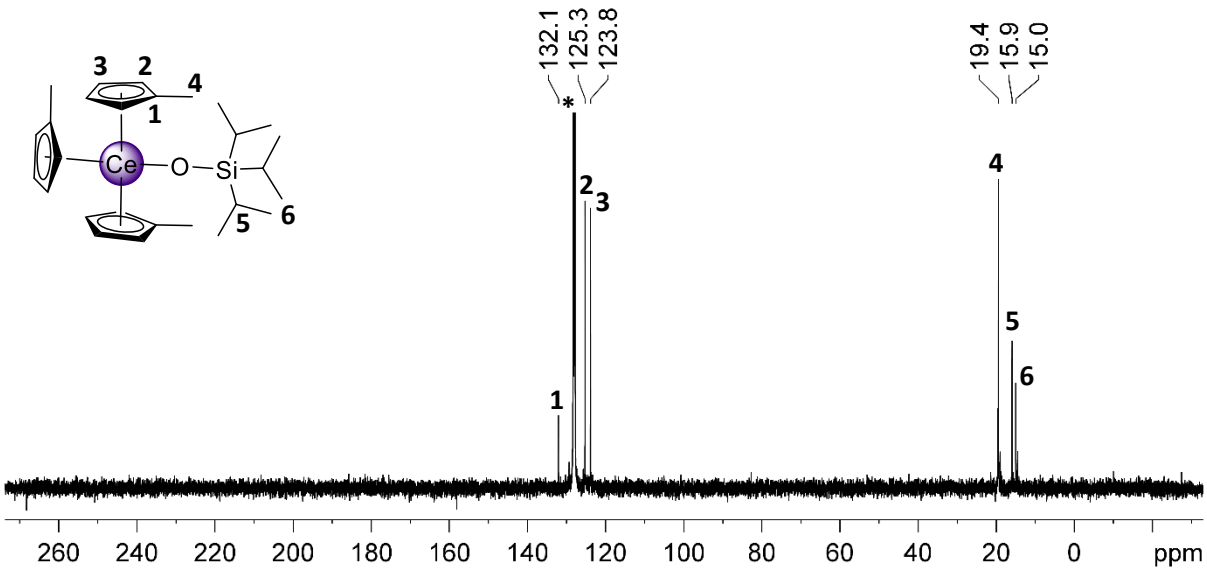

Figure S47. $^{13}C\{^{1}H\}$ NMR spectrum (100.6 MHz, C_6D_6, 26 °C) of **12b**.

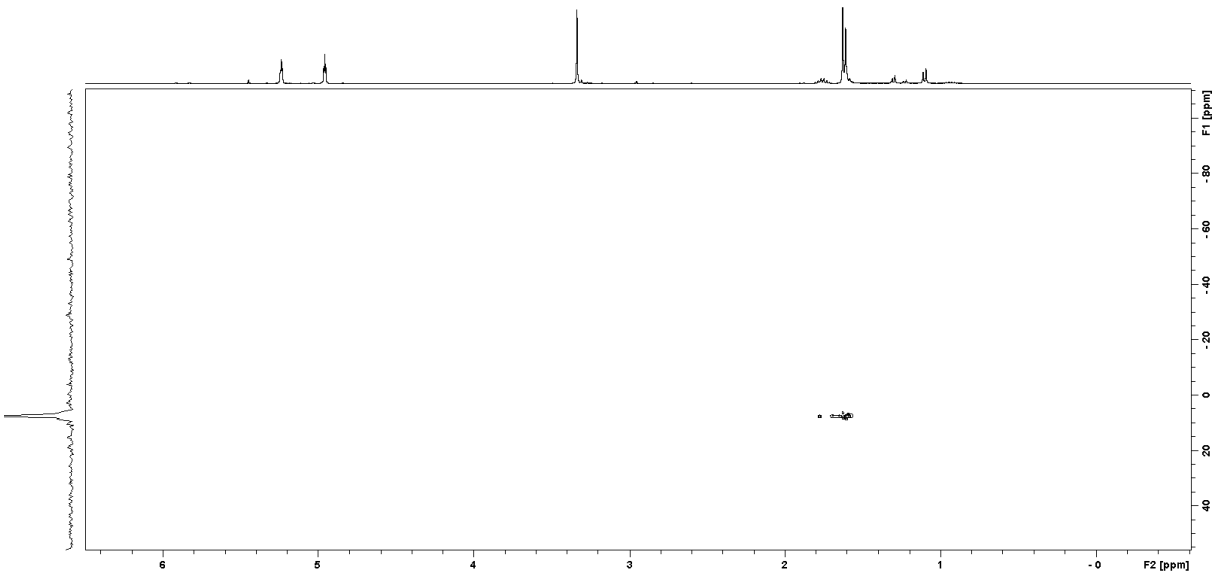

Figure S48. ^{1}H-^{29}Si HSQC NMR spectrum (79.5 MHz, C_6D_6, 26 °C) of **12b**.

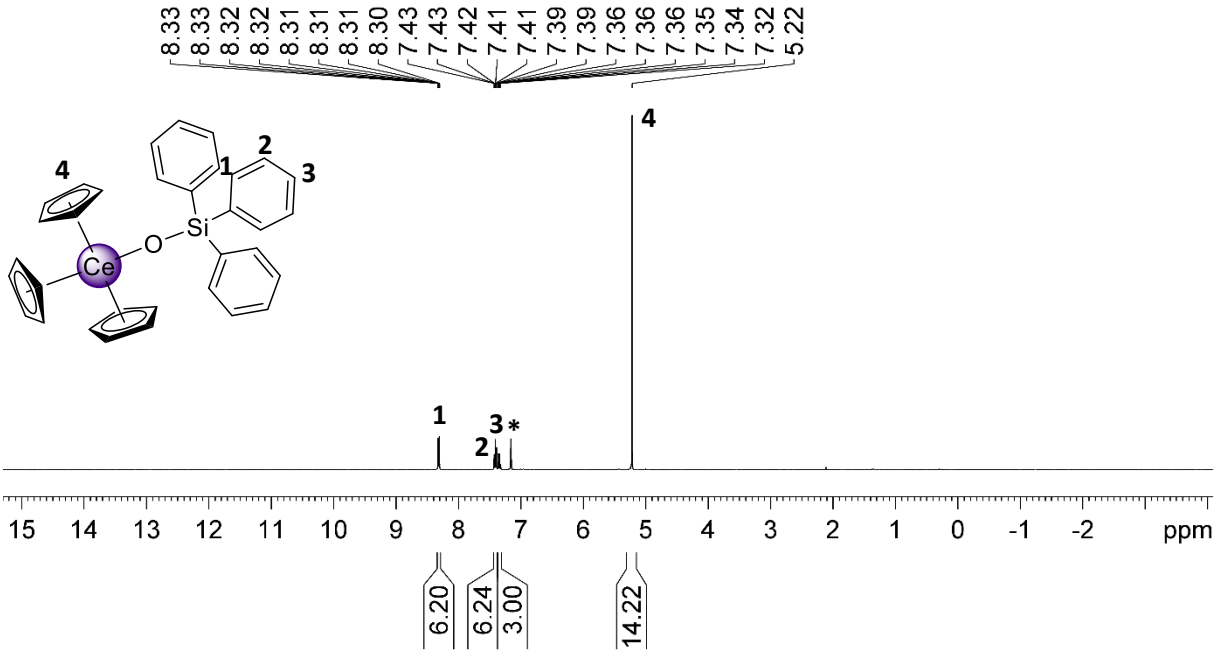

Figure S49. ^{1}H NMR spectrum (400.1 MHz, C_6D_6, 26 °C) of **13a**.

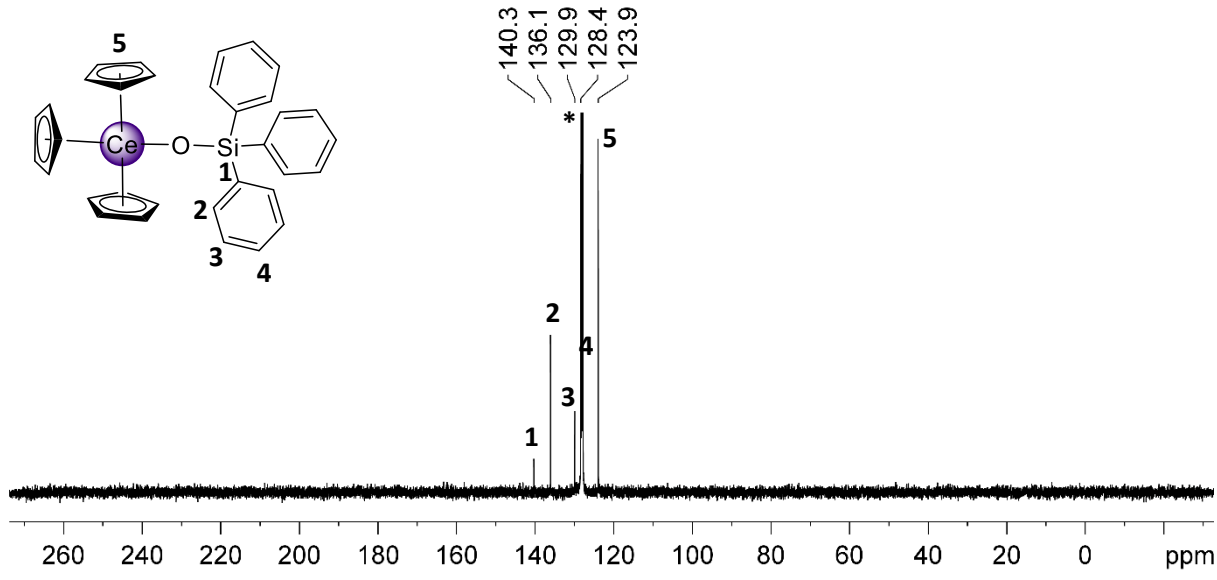

Figure S50. $^{13}C\{^{1}H\}$ NMR spectrum (100.6 MHz, C_6D_6, 26 °C) of **13a**.

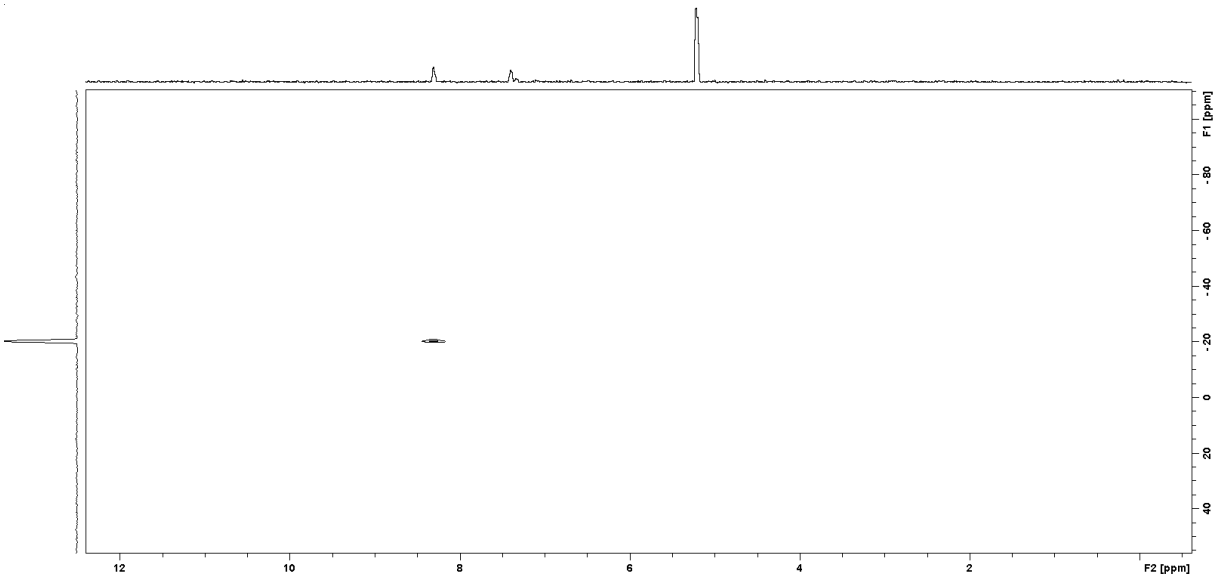

Figure S51. ^{1}H-^{29}Si HSQC NMR spectrum (79.5 MHz, C_6D_6, 26 °C) of **13a**.

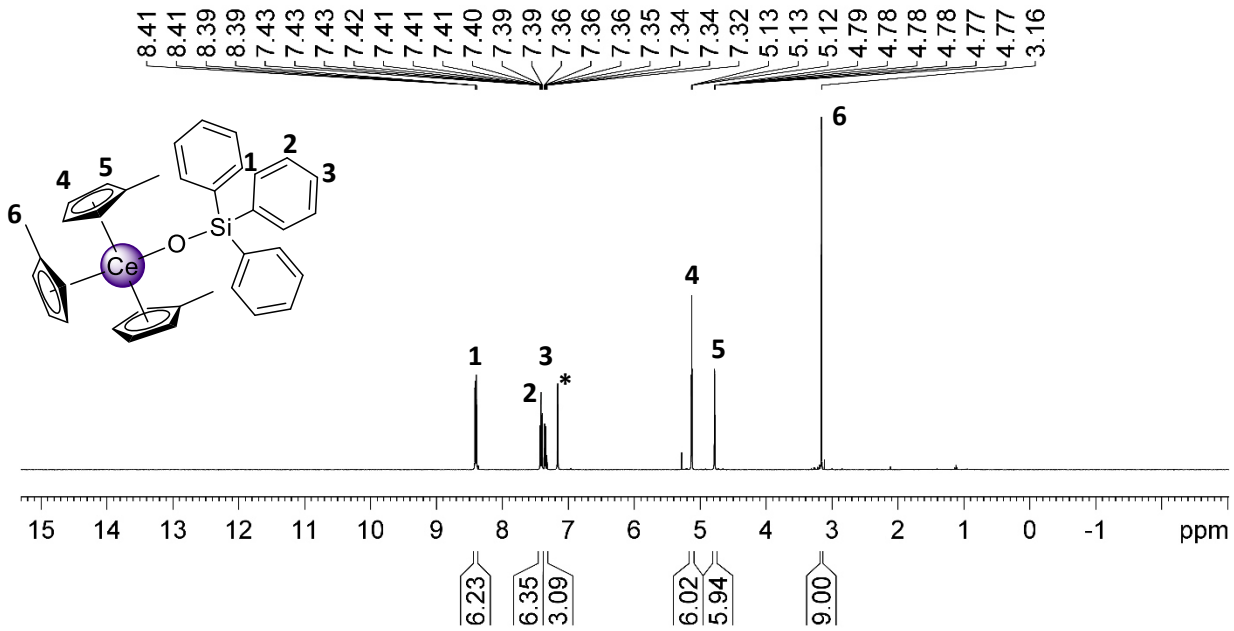

Figure S52a. ^{1}H NMR spectrum (400.1 MHz, C_6D_6, 26 °C) of **13b**.

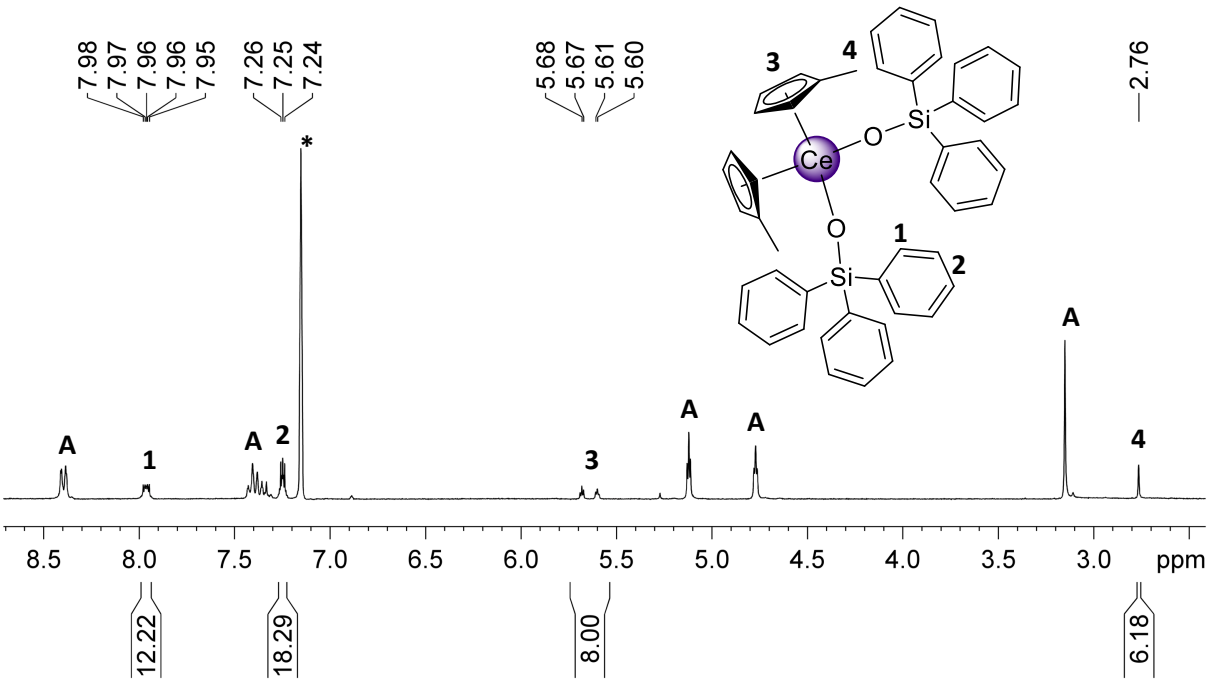

Figure S52b. ^{1}H NMR spectrum (400.1 MHz, C_6D_6, 26 °C) of **13b** (**A**) after several weeks at ambient temperature under argon atmosphere; Tetravalent decomposition product is assumed to be $Cp^{Me}{}_2Ce(OSiPh_3)_2$.

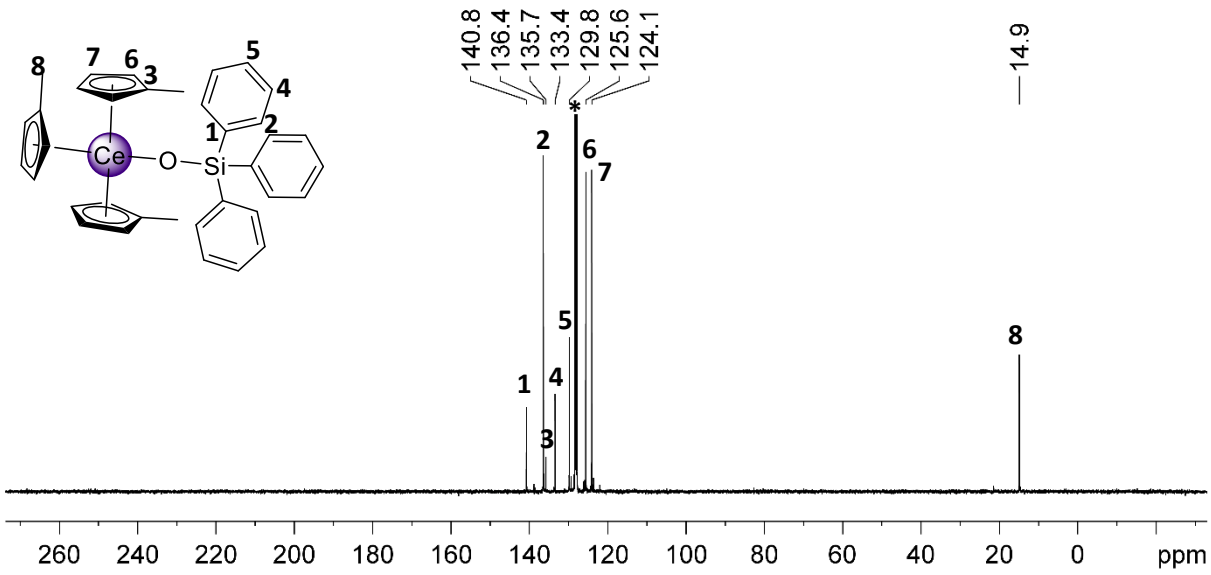

Figure S53. $^{13}C\{^{1}H\}$ NMR spectrum (100.6 MHz, C_6D_6, 26 °C) of **13b**.

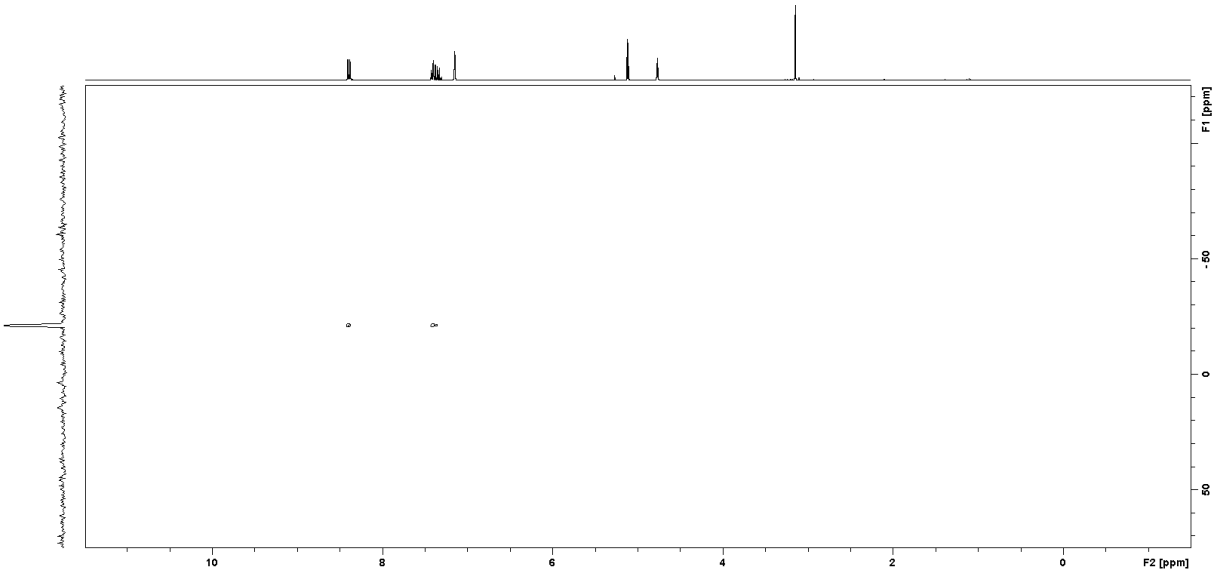

Figure S54. ^{1}H-^{29}Si HSQC NMR spectrum (79.5 MHz, C_6D_6, 26 °C) of **13b**.

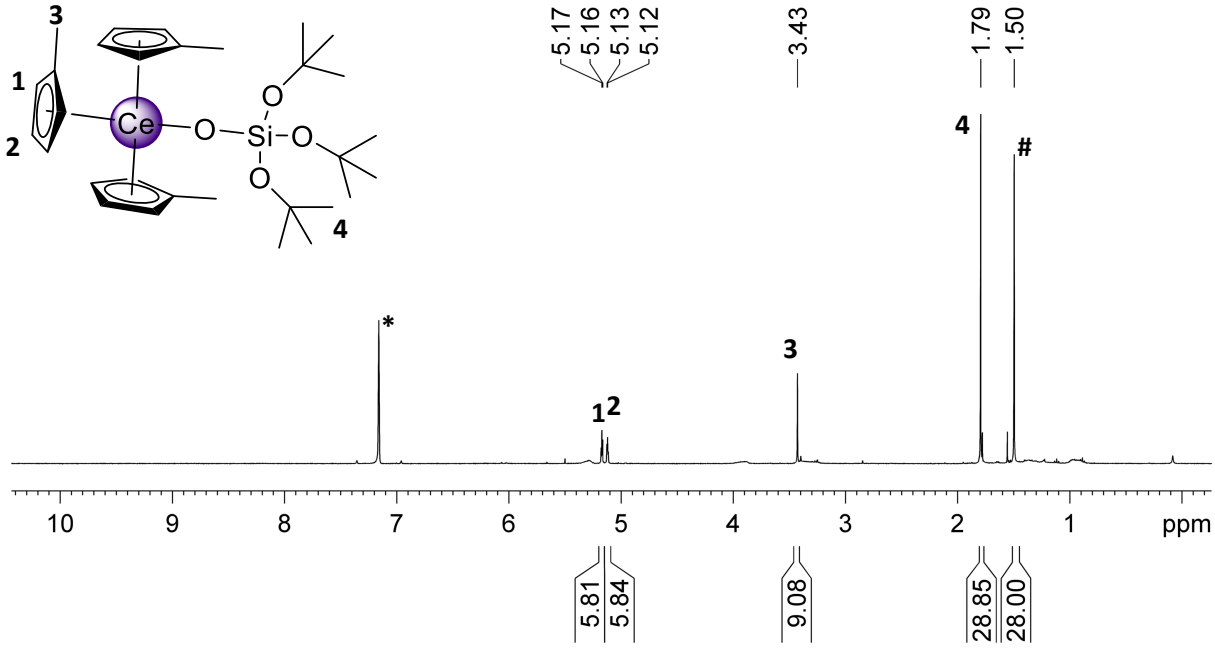

Figure S55. ^{1}H NMR spectrum (400.1 MHz, C_6D_6, 26 °C) of **14**.

Crystallographic Data

Table S3. Collection of crystallographic data of **3b**, **4b, 5a**, **6a**, **8a**, **8b**, **9b**, **10b**, **11a**, **11b**, **13a**, and **13b**

	3b	**4b**[a]	**5a**	**6a**	**8a**	**8b**
formula	$C_{18}H_{21}CeBr$	$C_{18}H_{21}CeI$	$C_{16}H_{18}CeO$	$C_{17}H_{20}CeO$	$C_{18}H_{22}CeO$	$C_{21}H_{28}CeO$
CCDC	2075865	2075873	2075871	2075875	2075867	2075869
M [g · mol^{-1}]	457.38	504.37	366.42	380.45	394.47	436.55
λ [Å]	0.71073	0.71073	0.71073	0.71073	0.71073	0.71073
cell	orthorhombic	monoclinic	ortho-rhombic	triclinic	orthorhombic	monoclinic
space group	Pnma	$P2_1/n$	Pbca	$P\bar{1}$	$P2_12_12_1$	$P2_1/c$
a [Å]	14.6292(14)	8.076(2)	8.3115(7)	8.1676(13)	8.3115(4)	14.909(3)
b [Å]	13.9720(13)	13.951(3)	13.5552(12)	8.1694(13)	8.8292(5)	8.1653(15)
c [Å]	7.9273(7)	15.147(3)	24.315(2)	13.241(2)	22.0449(12)	15.214(3)
α [°]	90	90	90	99.487(2)	90	90
β [°]	90	90.070(7)	90	99.533(2)	90	94.457(4)
γ [°]	90	90	90	117.644(2)	90	90
V [Å^3]	1620.3(3)	1706.5(7)	2739.4(4)	741.7(2)	1617.74(15)	1846.5(6)
Z	4	4	8	2	4	4
F(000)	888	960	1440	376	784	880
T [K]	100(2)	100(2)	100(2)	100(2)	100(2)	100(2)
ρ_{calcd} [g · mol^3]	1.875	1.963	1.777	1.703	1.620	1.570
μ [mm^{-1}]	5.263	4.465	3.308	3.058	2.807	2.468
R_1 (I>2σ(I))[b]	0.0219	0.0374	0.0233	0.0314	0.0171	0.0226
ωR_2 (all data)[c]	0.0548	0.0982	0.0591	0.0833	0.0402	0.0563
Goodness of fit[d]	1.058	1.046	1.062	1.206	1.050	1.102

Table S3 continued

	9b	10b	11a	11b	13a	13b	14
formula	$C_{22}H_{30}CeO$	$C_{21}H_{30}CeOSi$	$C_{21}H_{30}CeOSi$	$C_{24}H_{36}CeOSi$	$C_{33}H_{30}CeOSi$	$C_{36}H_{36}CeOSi$	$C_{30}H_{48}CeO_4Si$
CCDC	2075866	2075870	2075868	2075877	2075872	2075874	2075876
M [g · mol^{-1}]	450.58	466.66	466.66	508.74	610.78	652.86	640.89
λ [Å]	0.71073	0.71073	0.71073	0.71073	0.71073	0.71073	0.71073
cell	orthorhom-bic	monoclinic	monoclinic	orthorhom-bic	monoclinic	monoclinic	trigonal
space group	$Pna2_1$	$P\ 2_1/c$	$P2_1/c$	Pnma	$P2_1/n$	Cc	R3
a [Å]	19.4929(12)	16.1422(9)	13.247(4)	21.875(5)	10.6765(5)	15.3409(14)	39.719(6)
b [Å]	8.2376(5)	16.9608(10)	8.200(3)	12.932(3)	17.1329(8)	9.7484(9)	39.719(6)
c [Å]	12.2421(7)	16.2020(9)	19.059(6)	8.2534(18)	15.1392(7)	20.7801(19)	11.6419(17)
α [°]	90	90	90	90	90	90	90
β [°]	90	113.3020(10)	90.401(5)	90	106.4980(10)	108.5230(10)	90
γ [°]	90	90	90	90	90	90	120
V [Å^3]	1965.8(2)	4074.0(4)	2070.3(12)	2334.8(9)	2655.2(2)	2946.7(5)	15905(5)
Z	4	8	4	4	4	4	21
F(000)	912	1888	944	1040	1232	1328	6972
T [K]	100(2)	100(2)	100(2)	100(2)	100(2)	100(2)	100(2)
ρ_{calcd} [g · mol^3]	1.522	1.522	1.497	1.447	1.528	1.472	1.405
μ [mm^{-1}]	2.321	2.298	2.261	2.011	1.784	1.613	1.573
R_1 (I>2σ(I))[b]	0.0324	0.0340	0.0635	0.0483	0.0298	0.0257	0.0555
ωR_2 (all data)[c]	0.0739	0.0843	0.1506	0.1285	0.0654	0.0599	0.1442
Goodness of fit[d]	1.071	1.077	1.051	1.067	1.033	1.058	1.024

[a] For **4b**, two Cp^{Mc} rings and the iodido ligand could be modeled as a "two part" disorder. The third Cp^{Mc} ring seems to be η^3 coordinated. Taking the third Cp^{Mc} and Ce into account for the disorder, does not fix the problem. One individual shows η^3 and the other η^5 coordination and the R values became slightly larger. The η^3 coordination seems to be a consequence of the insufficient disorder model.

[b] $R1 = \Sigma(||F_0| - |F_c||) / \Sigma|F_0|$, $F_0 > 4\sigma(F_0)$. [c] $wR_2 = \{\Sigma[w(F_0^2 - F_c^2)^2 / \Sigma[w(F_0^2)^2]\}^{1/2}$. [d] $GOF = [\Sigma w(F_0^2 - F_c^2)^2 / (n_0 - n_p)]^{1/2}$.

Figures of solid-state structures

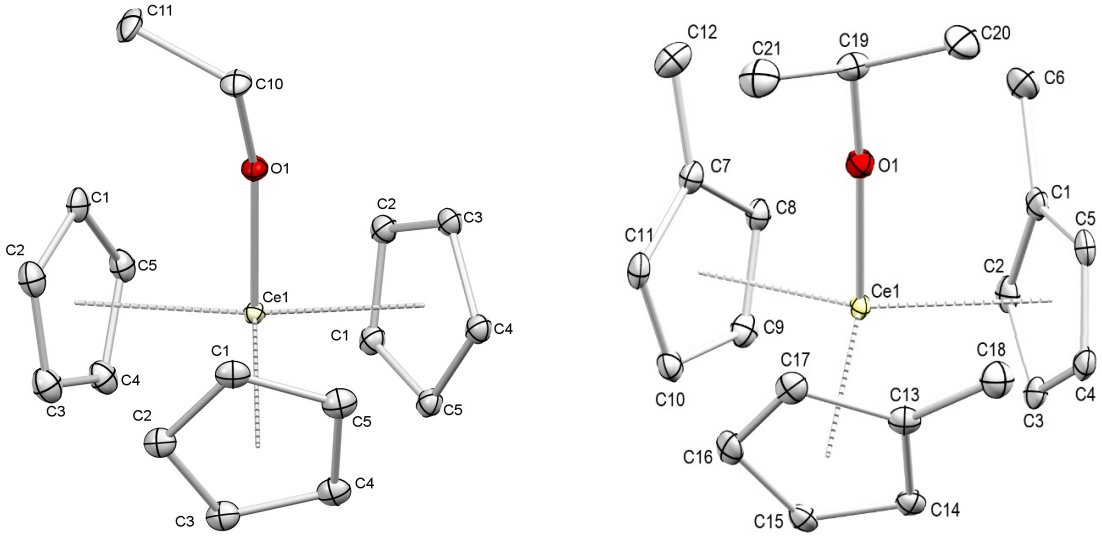

Figure S56. Crystal structures of $Cp_3Ce(OEt)$ (**6a**, left) and $Cp^{Me}_3Ce(O\textit{i}Pr)$ (**8b**, right). Hydrogen atoms are omitted for clarity. Atomic displacement ellipsoids are set at the 30% probability level. Selected interatomic distances and angles are listed in Table 2.

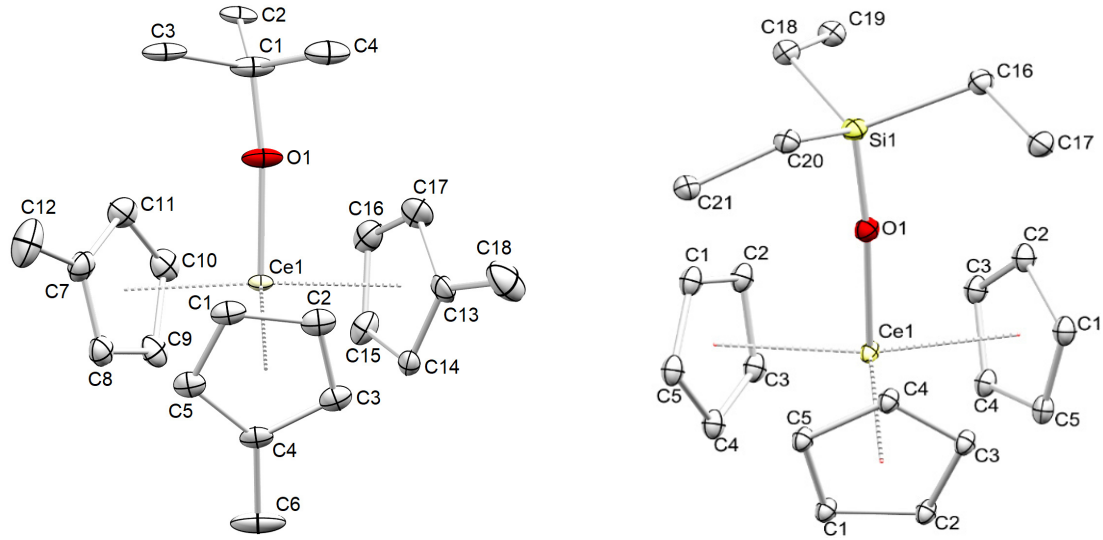

Figure S57. Crystal structures of $Cp^{Me}_3Ce(O\textit{t}Bu)$ (**9b**, left) and $Cp_3Ce(OSiEt_3)$ (**11a**, right). Hydrogen atoms are omitted for clarity. Atomic displacement ellipsoids are set at the 30% probability level. Selected interatomic distances and angles are listed in Table 2.

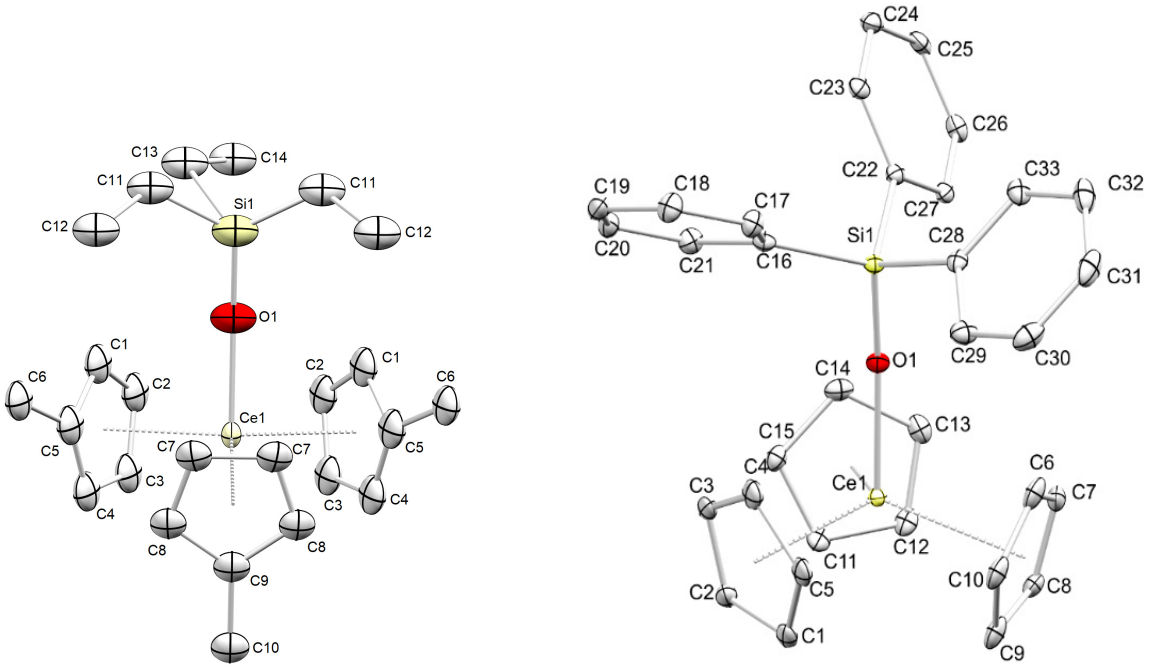

Figure S58. Crystal structures of $Cp^{Me}_3Ce(OSiEt_3)$ (**11b**, left) and $Cp_3Ce(OSiPh_3)$ (**13a**, right). Hydrogen atoms are omitted for clarity. Atomic displacement ellipsoids are set at the 30% probability level. Selected interatomic distances and angles are listed in Table 2.

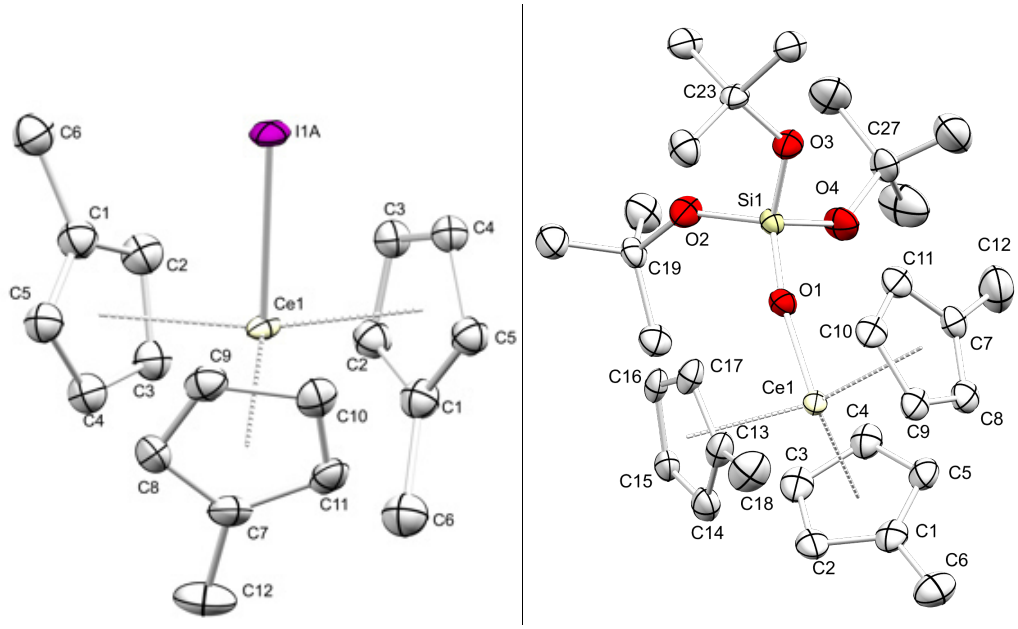

Figure S59. Crystal structures of and Cp^{Me}_3CeI (**4b**, left) and $Cp^{Me}_3Ce[OSi(OtBu)_3]$ (**14**, right). Hydrogen atoms are omitted for clarity. Atomic displacement ellipsoids are set at the 30% probability level. Selected interatomic distances and angles: **4b**: Ce−C(Cp) range 2.65(2) – 2.971(6) Å, Ce−C(Cp) avg: 2.761 Å, Ce−Cnt(avg) 2.536 Å, Ce−I 2.8507 Å, Cnt−Ce−Cnt 110.00 – 126.42° Cnt−Ce−I 96.99 – 103.37°; **14**: Ce−C(Cp) range 2.70(3) – 2.82(4) Å, Ce−C(Cp) avg: 2.764 Å, Ce−Cnt(avg) 2.497 Å, Ce−O1 2.126(7) Å, O1−Si 1.589(8) Å, Cnt−Ce−Cnt 115.85 – 117.10°, Ce−O−Si 170.7(4)°. Only one of three molecules of **14** in the unit cell are shown.

Cyclic Voltammetry Experiments

Table S4. Electrochemical data for the redox couple of complex **1a** vs Fc/Fc^+ in THF/ [nPr$_4$N][BARF]

Scan rate v	E_{pa} vs Fc/Fc^+ [V]	E_{pc} vs Fc/Fc^+ [V]	E^0 vs Fc/Fc^+ [V]	ΔE_p [V]	i_{pc}/i_{pa}
50 mV/s	-0.227	-0.300	-0.263	0.073	0.85
100 mV/s	-0.219	-0.309	-0.264	0.090	0.87
250 mV/s	-0.218	-0.311	-0.264	0.093	0.87
500 mV/s	-0.215	-0.312	-0.263	0.097	0.88
1000 mV/s	-0.213	-0.313	-0.263	0.100	0.89
2000 mV/s	-0.210	-0.318	-0.264	0.108	0.90

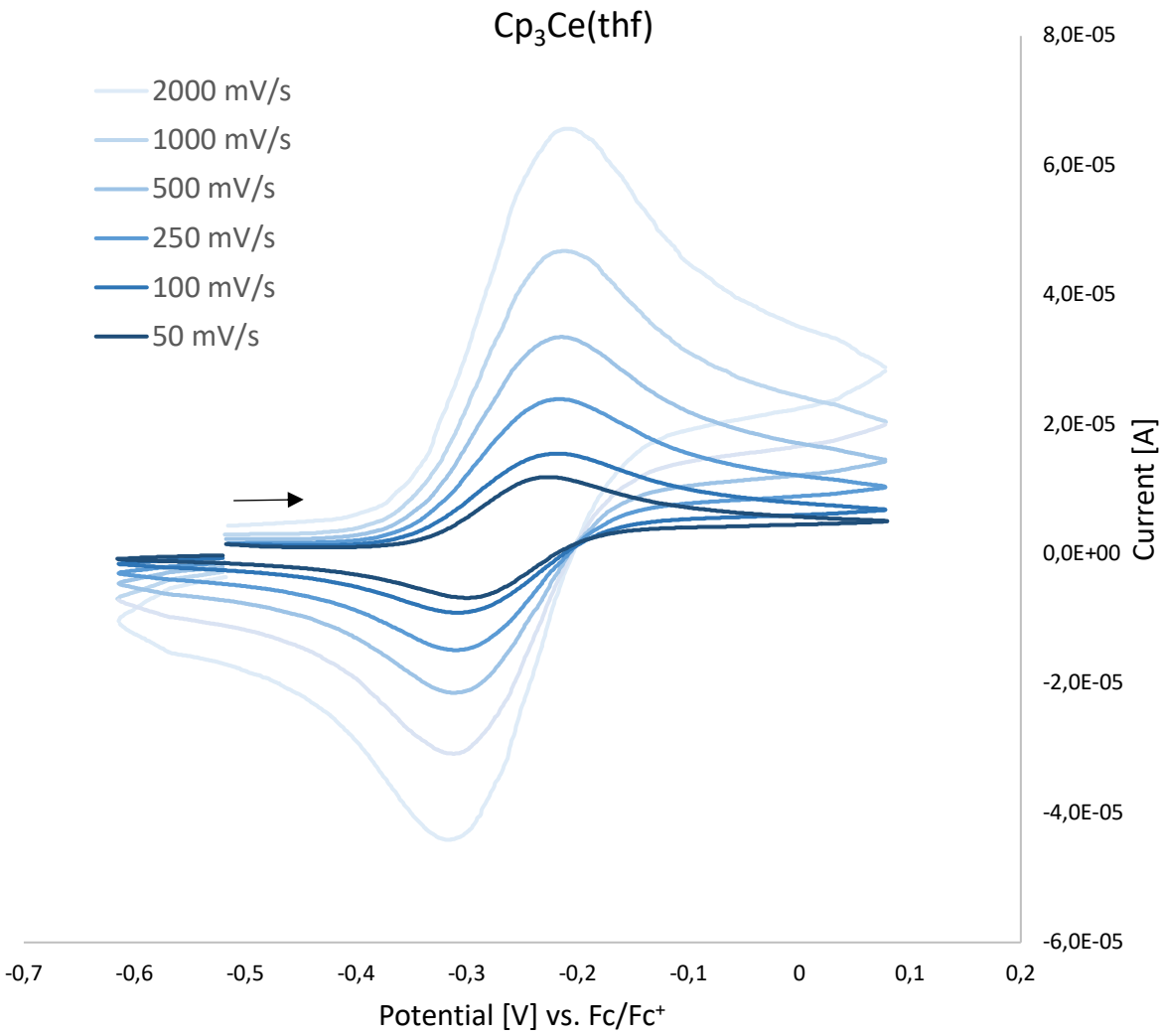

Figure S60. Cerium(III/IV) redox couple of **1a** vs Fc/Fc^+ in THF obtained at different scan rates; arrow indicates initial scan direction; c(analyte) 1mM, c(electrolyte) 0.1 M [nPr$_4$N][BARF].

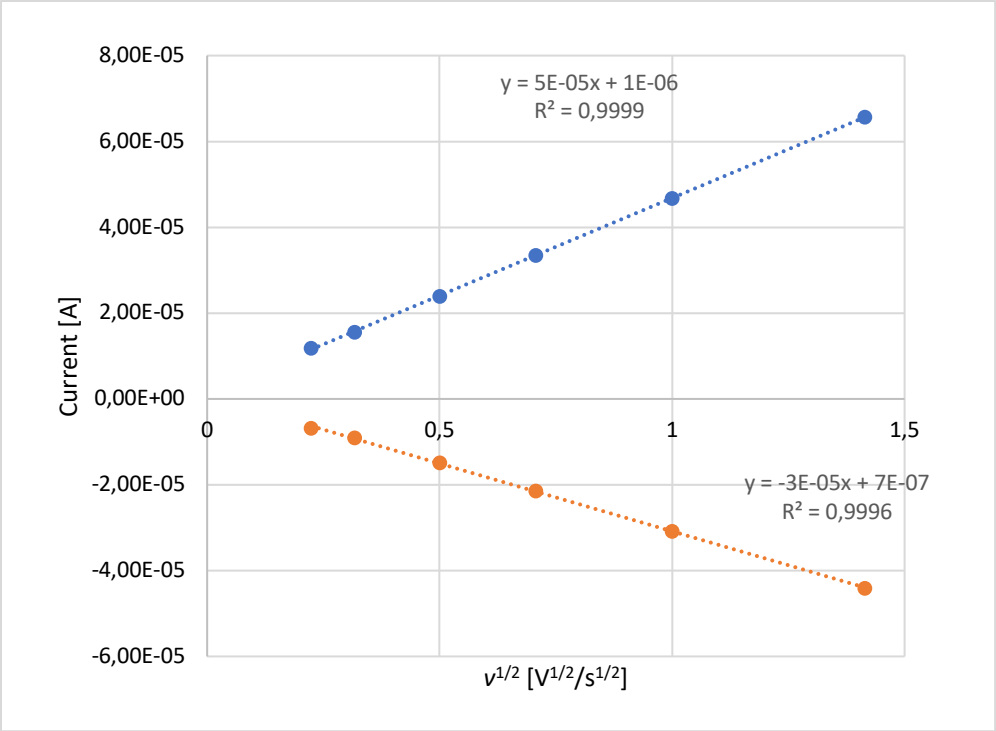

Figure S61. I_p versus $v^{1/2}$ plot of the anodic (blue) and cathodic (orange) peak currents in cyclic voltammograms of **1a**.

Table S5. Electrochemical data for the redox couple of complex **1b** vs Fc/Fc^+ in THF/ [nPr$_4$N][BARF]

Scan rate v	E_{pa} vs Fc/Fc^+ [V]	E_{pc} vs Fc/Fc^+ [V]	E^0 vs Fc/Fc^+ [V]	ΔE_p [V]	i_{pc}/i_{pa}
50 mV/s	-0.347	-0.408	-0.377	0.061	0.89
100 mV/s	-0.324	-0.395	-0.359	0.071	0.91
250 mV/s	-0.299	-0.374	-0.336	0.075	0.93
500 mV/s	-0.295	-0.374	-0.334	0.079	0.94
1000 mV/s	-0.288	-0.376	-0.332	0.088	0.95
2000 mV/s	-0.282	-0.378	-0.330	0.096	0.96

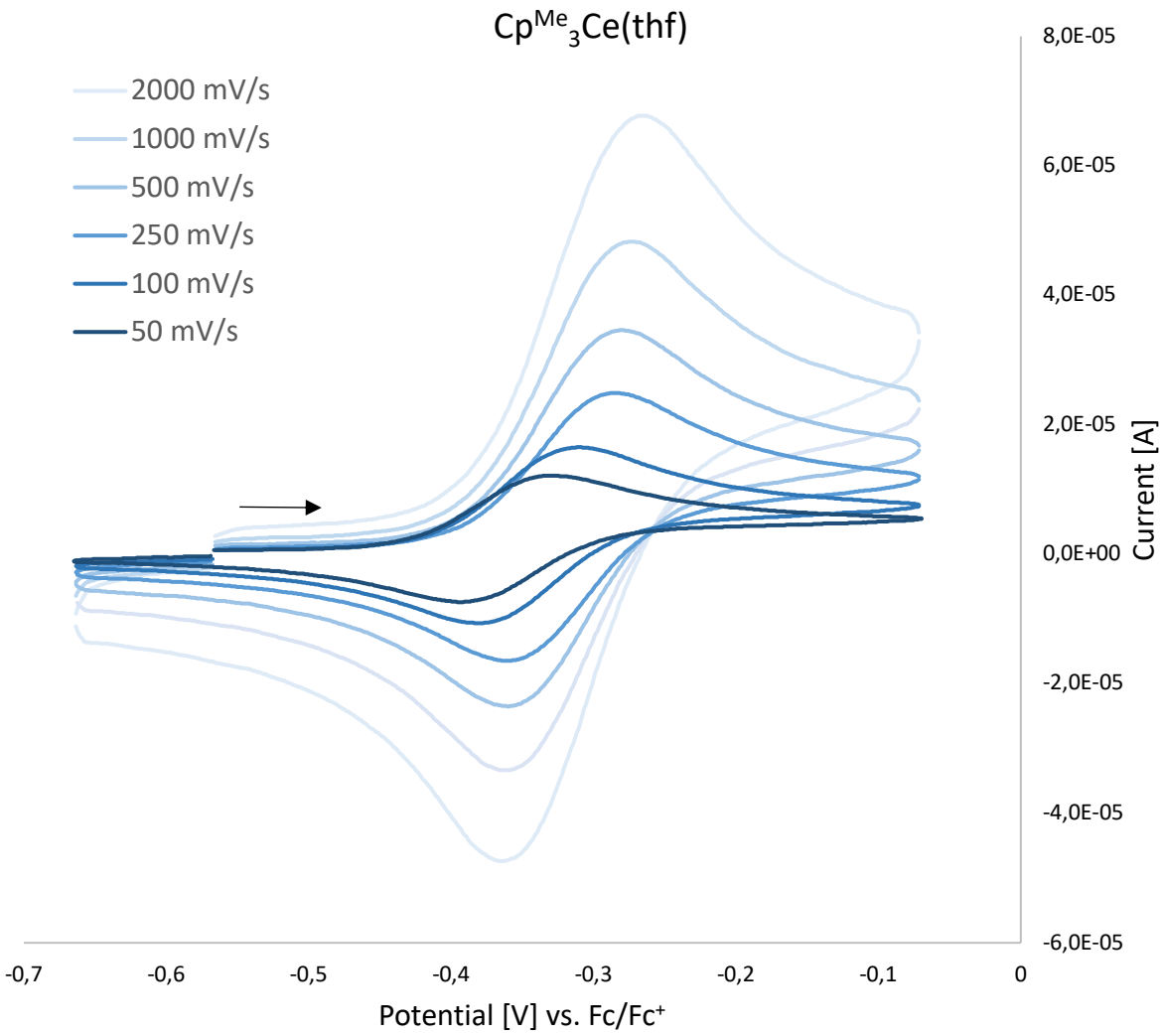

Figure S62. Cerium(III/IV) redox couple of **1b** vs Fc/Fc^+ in THF obtained at different scan rates; arrow indicates initial scan direction; *c*(analyte) 1mM, *c*(electrolyte) 0.1 M [nPr_4N][BARF].

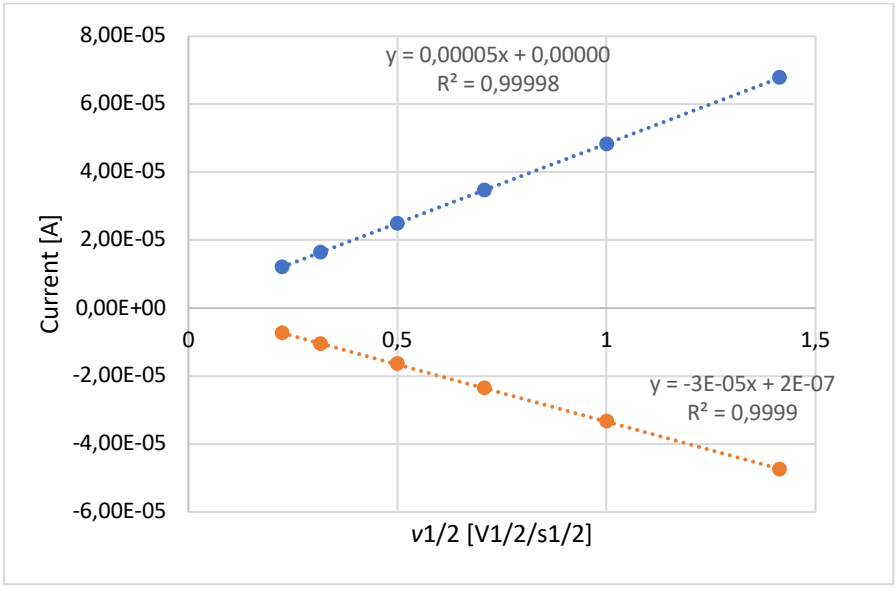

Figure S63. I_p versus $v^{1/2}$ plot of the anodic (blue) and cathodic (orange) peak currents in cyclic voltammograms of **1b**.

Table S6. Electrochemical data for the redox couple of complex **2a** vs Fc/Fc^+ in THF/ [nPr$_4$N][BARF]

Scan rate v	E_{pa} vs Fc/Fc^+ [V]	E_{pc} vs Fc/Fc^+ [V]	E^0 vs Fc/Fc^+ [V]	ΔE_p [V]	i_{pa}/i_{pc}
50 mV/s	-0.960	-0.730	-0.695	0.070	0.96
100 mV/s	-0.659	-0.739	-0.699	0.080	0.96
250 mV/s	-0.656	-0.740	-0.698	0.084	0.97
500 mV/s	-0.656	-0.745	-0.700	0.089	0.97
1000 mV/s	-0.653	-0.748	-0.700	0.095	0.97
2000 mV/s	-0.647	-0.757	-0.702	0.110	0.96

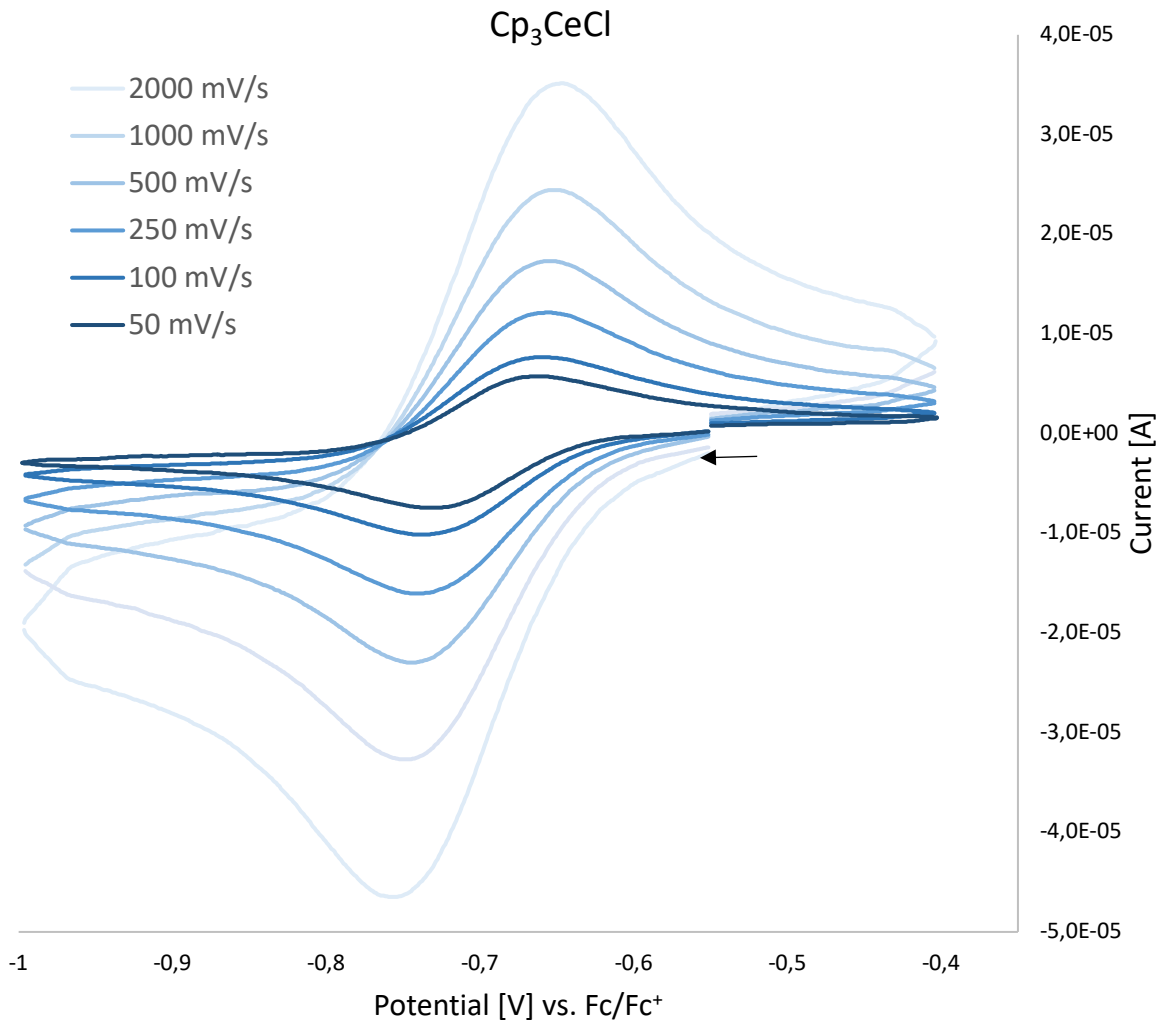

Figure S64. Cerium(III/IV) redox couple of **2a** vs Fc/Fc^+ in THF obtained at different scan rates; arrow indicates initial scan direction; c(analyte) 1mM, c(electrolyte) 0.1 M [nPr$_4$N][BARF].

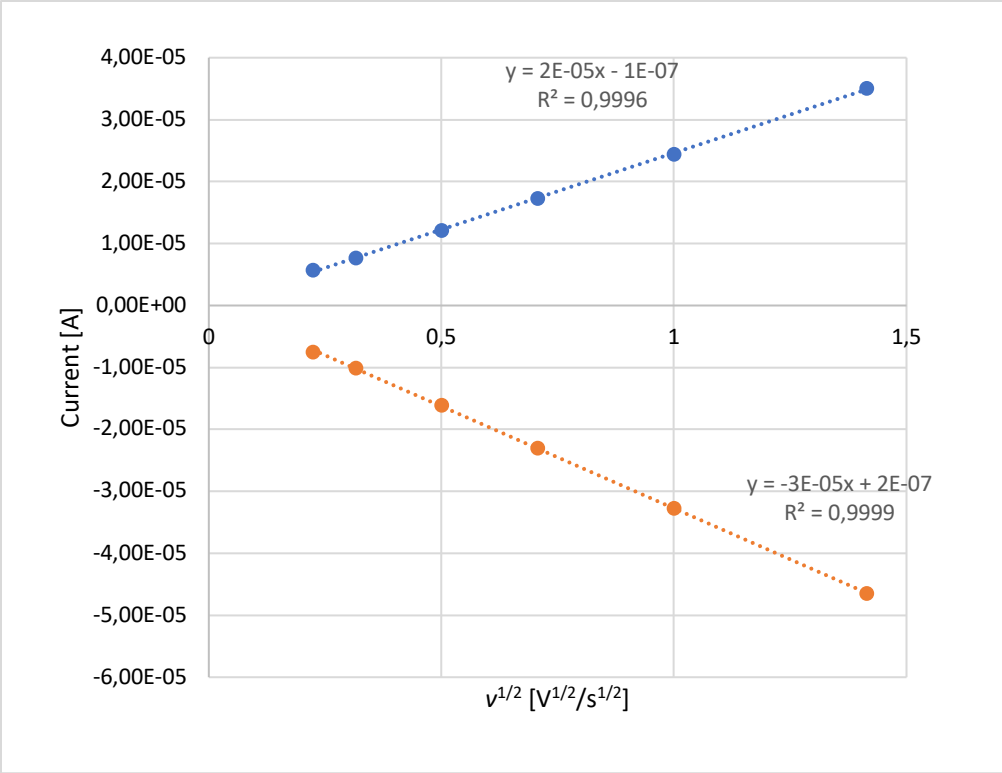

Figure S65. I_p versus $v^{1/2}$ plot of the anodic (blue) and cathodic (orange) peak currents in cyclic voltammograms of **2a**.

Table S7. Electrochemical data for the redox couple of complex **2b** vs Fc/Fc^+ in THF/ [*n*Pr_4N][BARF]

Scan rate *v*	E_{pa} vs Fc/Fc^+ [V]	E_{pc} vs Fc/Fc^+ [V]	E^0 vs Fc/Fc^+ [V]	ΔE_p [V]	i_{pa}/i_{pc}
50 mV/s	-0.764	-0.837	-0.801	0.073	1.00
100 mV/s	-0.760	-0.841	-0.801	0.081	1.00
250 mV/s	-0.754	-0.847	-0.801	0.093	1.00
500 mV/s	-0.750	-0.852	-0.801	0.102	1.00
1000 mV/s	-0.746	-0.857	-0.802	0.111	0.99
2000 mV/s	-0.742	-0.860	-0.801	0.118	1.00

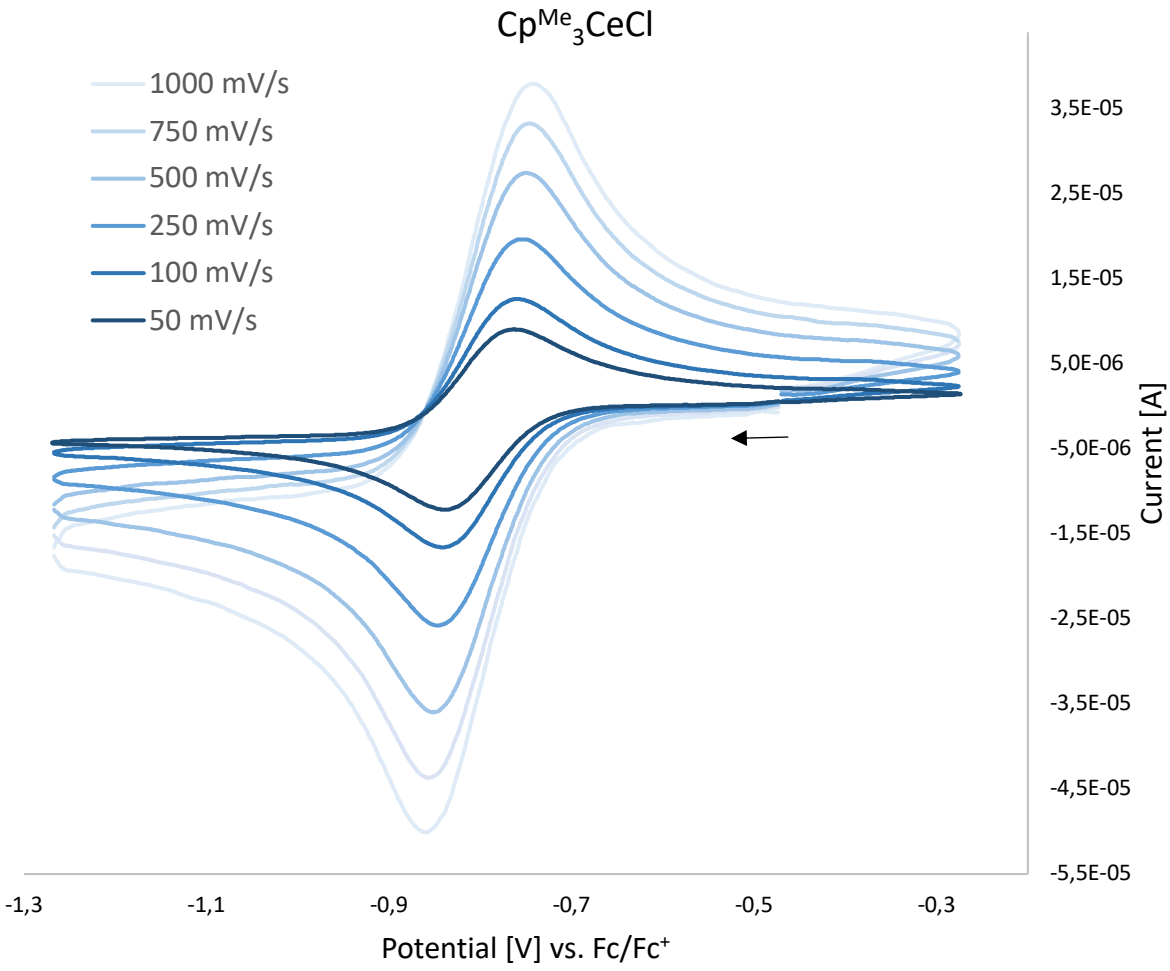

Figure S66. Cerium(III/IV) redox couple of **2b** vs Fc/Fc^+ in THF obtained at different scan rates; arrow indicates initial scan direction; *c*(analyte) 1mM, *c*(electrolyte) 0.1 M [nPr_4N][BARF].

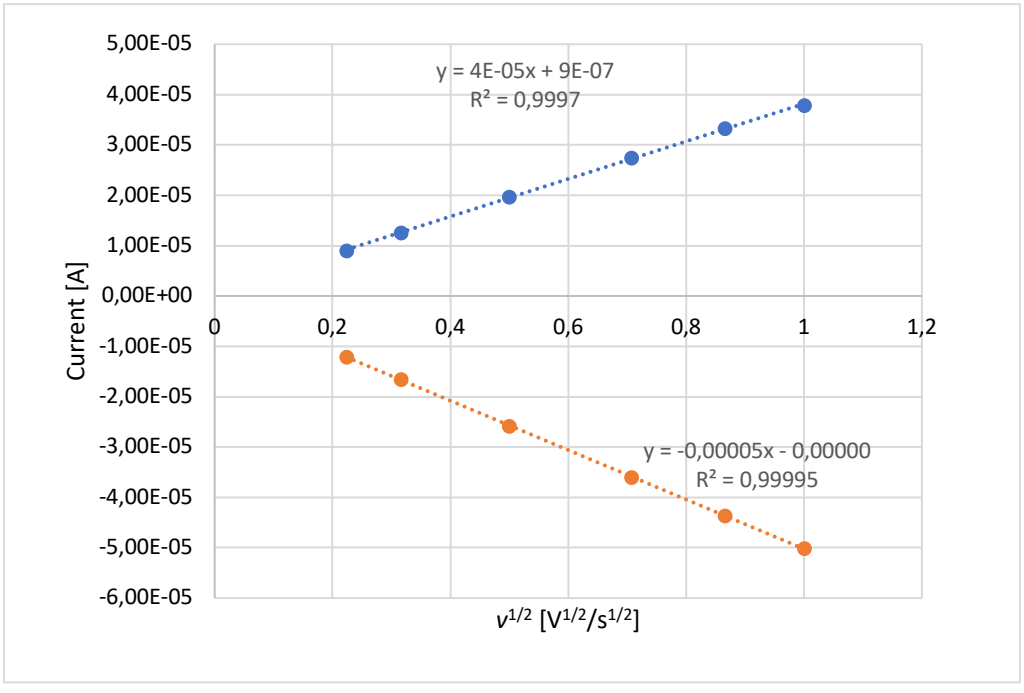

Figure S67. I_p versus $v^{1/2}$ plot of the anodic (blue) and cathodic (orange) peak currents in cyclic voltammograms of **2b**.

Table S8. Electrochemical data for the redox couple of complex **3a** vs Fc/Fc^+ in THF/ [nPr$_4$N][BARF]

Scan rate v	E_{pa} vs Fc/Fc^+ [V]	E_{pc} vs Fc/Fc^+ [V]	E^0 vs Fc/Fc^+ [V]	ΔE_p [V]	i_{pa}/i_{pc}
50 mV/s	-0.609	-0.694	-0.652	0.085	0.98
100 mV/s	-0.608	-0.699	-0.654	0.091	1.00
250 mV/s	-0.602	-0.703	-0.653	0.101	1.00
500 mV/s	-0.595	-0.713	-0.654	0.118	0.99
1000 mV/s	-0.586	-0.722	-0.654	0.136	0.99
2000 mV/s	-0.576	-0.738	-0.657	0.162	0.99

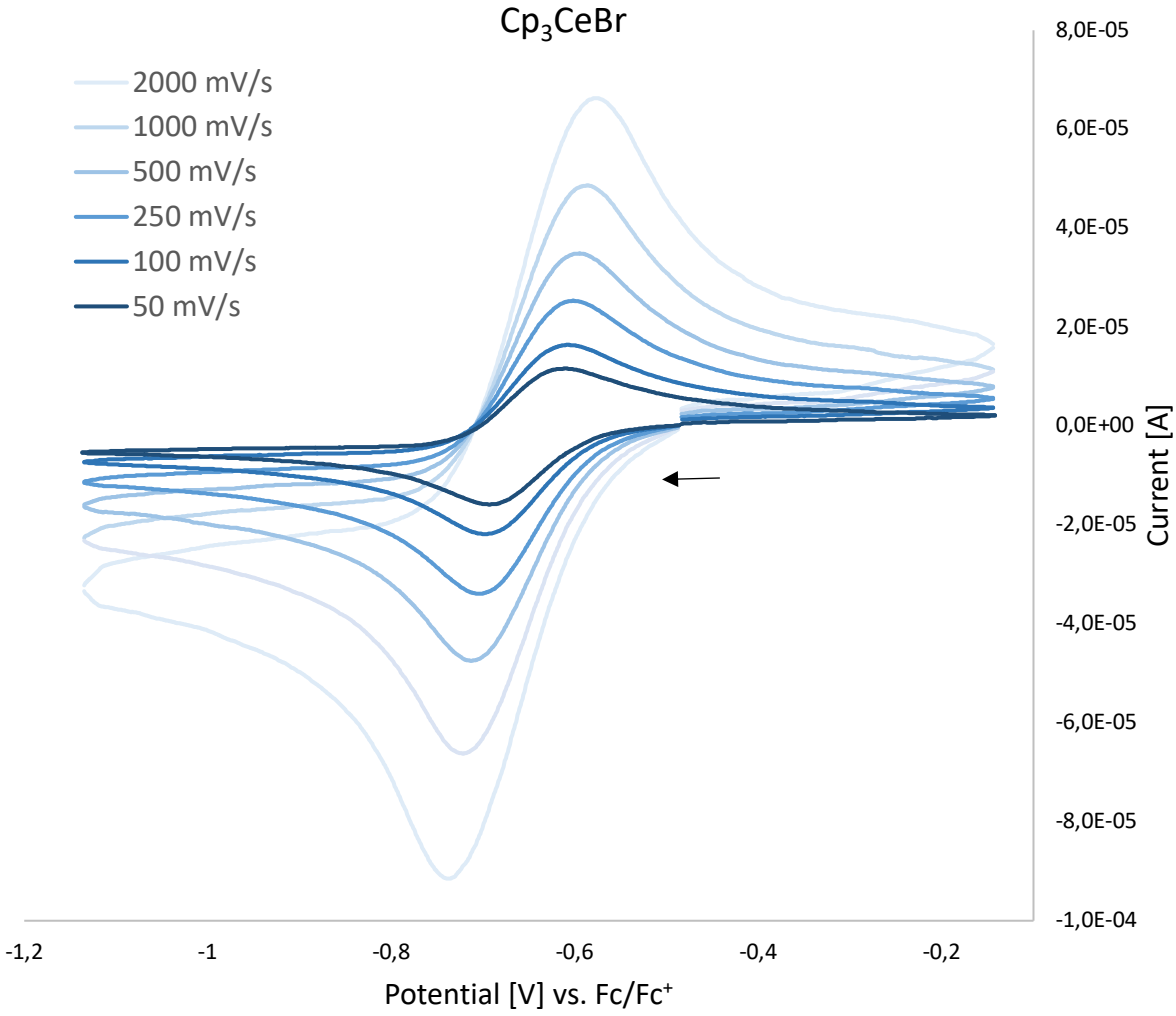

Figure S68. Cerium(III/IV) redox couple of **3a** vs Fc/Fc^+ in THF obtained at different scan rates; arrow indicates initial scan direction; c(analyte) 1mM, c(electrolyte) 0.1 M [nPr$_4$N][BARF].

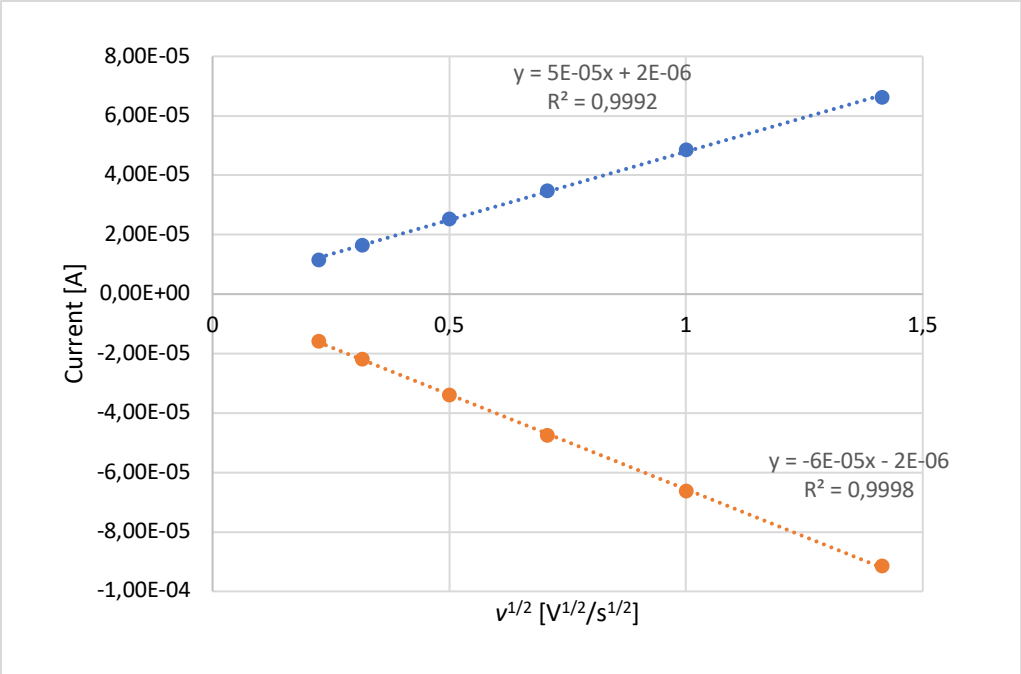

Figure S69. I_p versus $v^{1/2}$ plot of the anodic (blue) and cathodic (orange) peak currents in cyclic voltammograms of **3a**.

Table S9. Electrochemical data for the redox couple of complex **3b** vs Fc/Fc^+ in THF/ [*n*Pr$_4$N][BARF]

Scan rate *v*	E_{pa} vs Fc/Fc^+ [V]	E_{pc} vs Fc/Fc^+ [V]	E^0 vs Fc/Fc^+ [V]	ΔE_p [V]	i_{pa}/i_{pc}
50 mV/s	-0.713	-0.816	-0.764	0.103	0.98
100 mV/s	-0.707	-0.824	-0.765	0.117	0.98
250 mV/s	-0.693	-0.837	-0.765	0.144	0.98
500 mV/s	-0.679	-0.853	-0.766	0.174	0.98
1000 mV/s	-0.665	-0.874	-0.769	0.209	0.98
2000 mV/s	-0.648	-0.904	-0.776	0.256	0.99

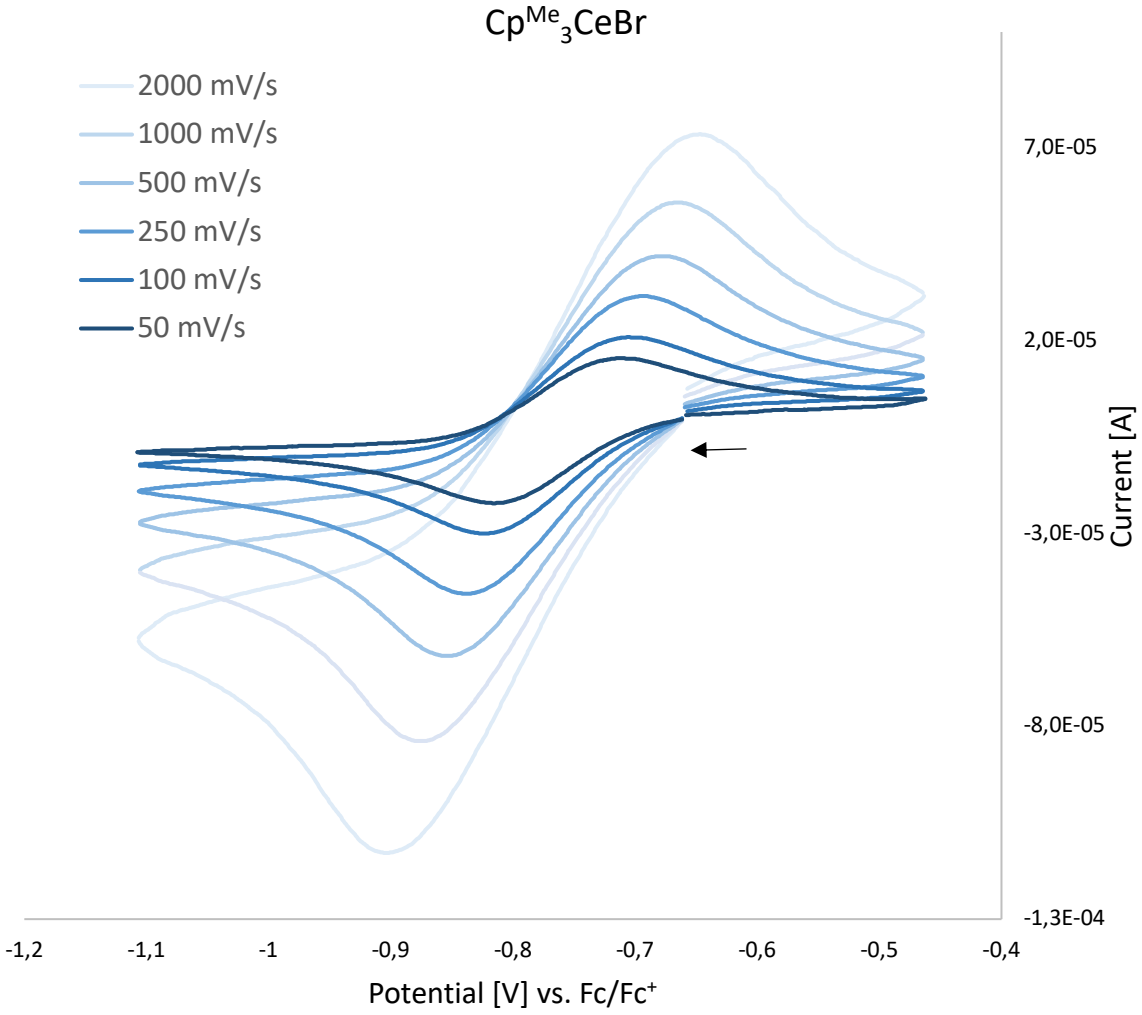

Figure S70. Cerium(III/IV) redox couple of **3b** vs Fc/Fc^+ in THF obtained at different scan rates; arrow indicates initial scan direction; *c*(analyte) 1mM, *c*(electrolyte) 0.1 M [nPr_4N][BARF].

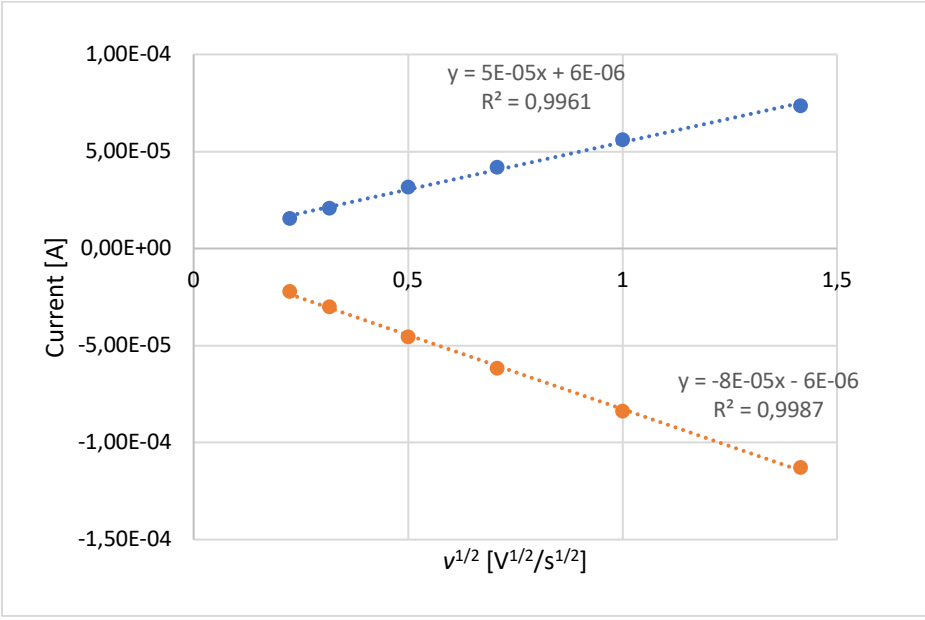

Figure S71. I_p versus $v^{1/2}$ plot of the anodic (blue) and cathodic (orange) peak currents in cyclic voltammograms of **3b**.

Table S10. Electrochemical data for the redox couple of complex **4a** vs Fc/Fc^+ in THF/ [nPr$_4$N][BARF]

Scan rate v	E_{pa} vs Fc/Fc^+ [V]	E_{pc} vs Fc/Fc^+ [V]	E^0 vs Fc/Fc^+ [V]	ΔE_p [V]	i_{pa}/i_{pc}
50 mV/s	-0.535	-0.631	-0.583	0.096	0.97
100 mV/s	-0.534	-0.627	-0.580	0.093	0.97
250 mV/s	-0.525	-0.630	-0.577	0.105	0.96
500 mV/s	-0.520	-0.637	-0.578	0.117	0.95
1000 mV/s	-0.514	-0.644	-0.579	0.130	0.95
2000 mV/s	-0.502	-0.656	-0.579	0.154	0.94

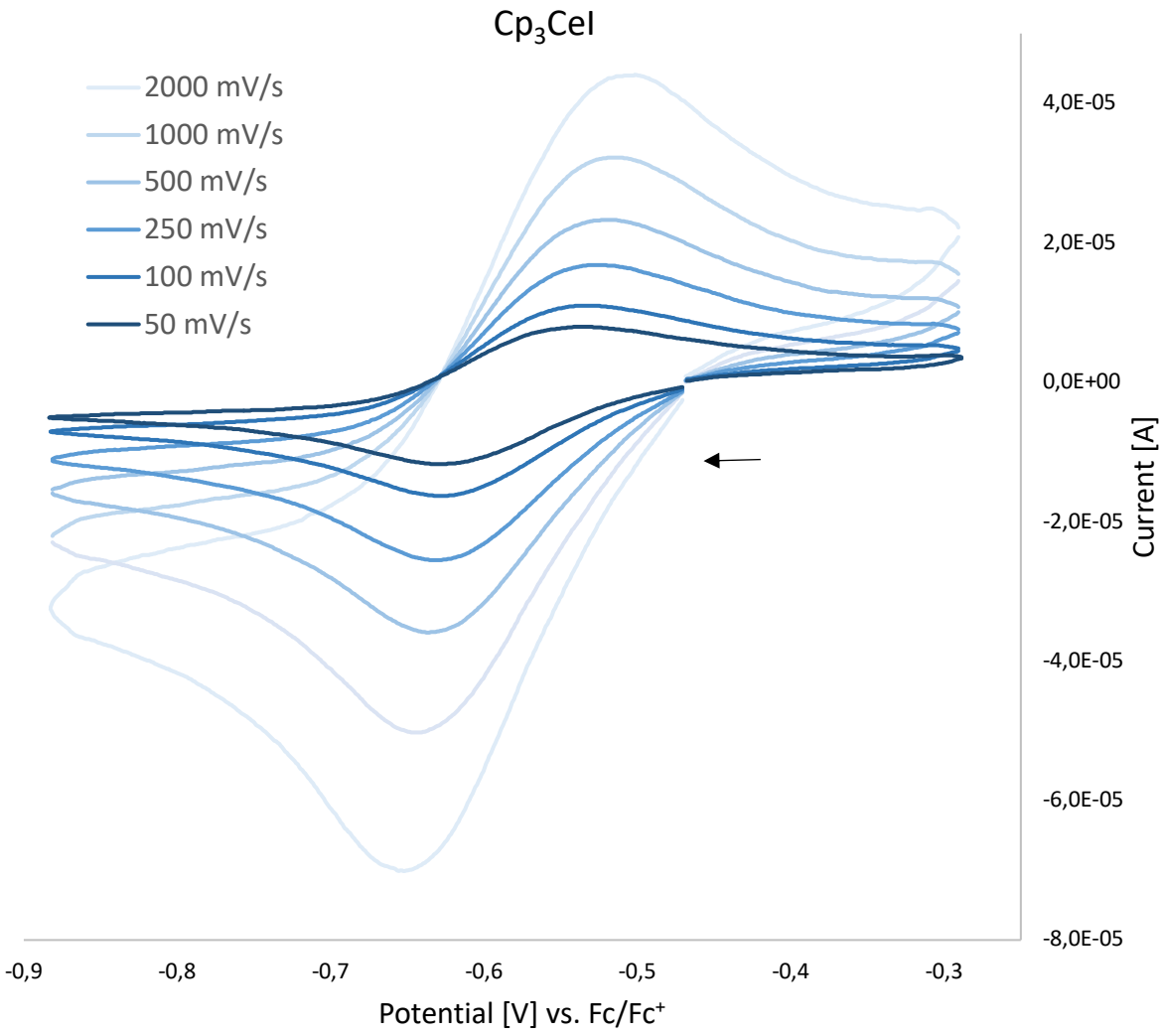

Figure S72. Cerium(III/IV) redox couple of **4a** vs Fc/Fc^+ in THF obtained at different scan rates; arrow indicates initial scan direction; c(analyte) 1mM, c(electrolyte) 0.1 M [nPr$_4$N][BARF].

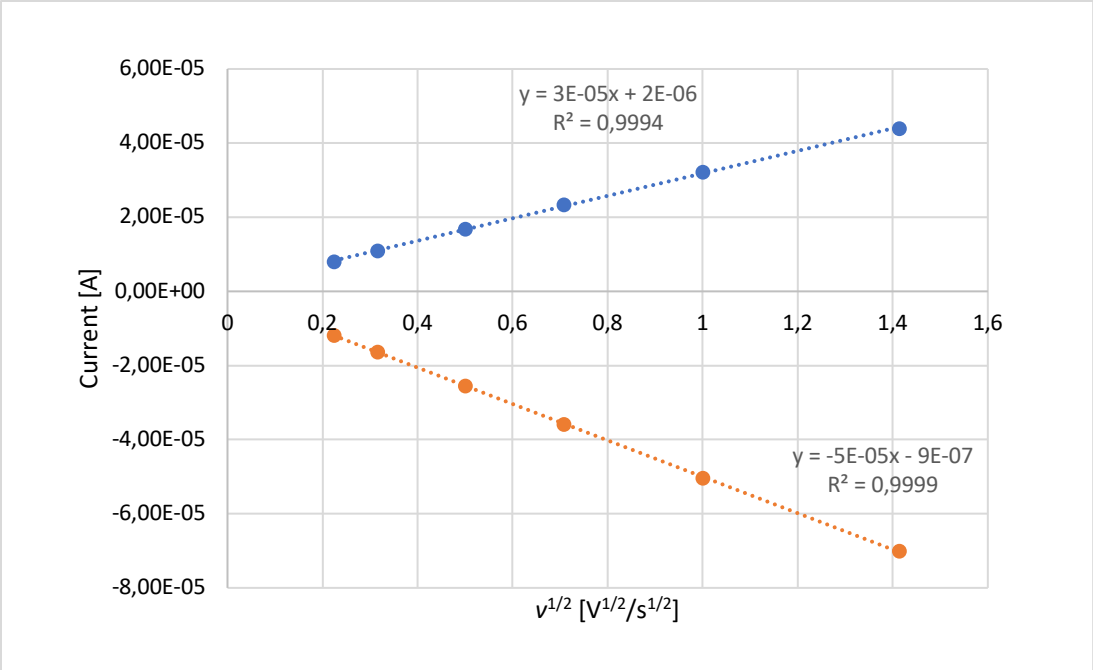

Figure S73. I_p versus $v^{1/2}$ plot of the anodic (blue) and cathodic (orange) peak currents in cyclic voltammograms of **4a**.

Table S11. Electrochemical data for the redox couple of complex **4b** vs Fc/Fc^+ in THF/ [nPr$_4$N][BARF]

Scan rate v	E_{pa} vs Fc/Fc^+ [V]	E_{pc} vs Fc/Fc^+ [V]	E^0 vs Fc/Fc^+ [V]	ΔE_p [V]	i_{pa}/i_{pc}
50 mV/s	-0.640	-0.724	-0.682	0.084	0.99
100 mV/s	-0.633	-0.723	-0.678	0.090	0.98
250 mV/s	-0.630	-0.725	-0.677	0.095	0.96
500 mV/s	-0.624	-0.728	-0.676	0.104	0.95
1000 mV/s	-0.616	-0.734	-0.675	0.118	0.94
2000 mV/s	-0.614	-0.744	-0.679	0.130	0.93

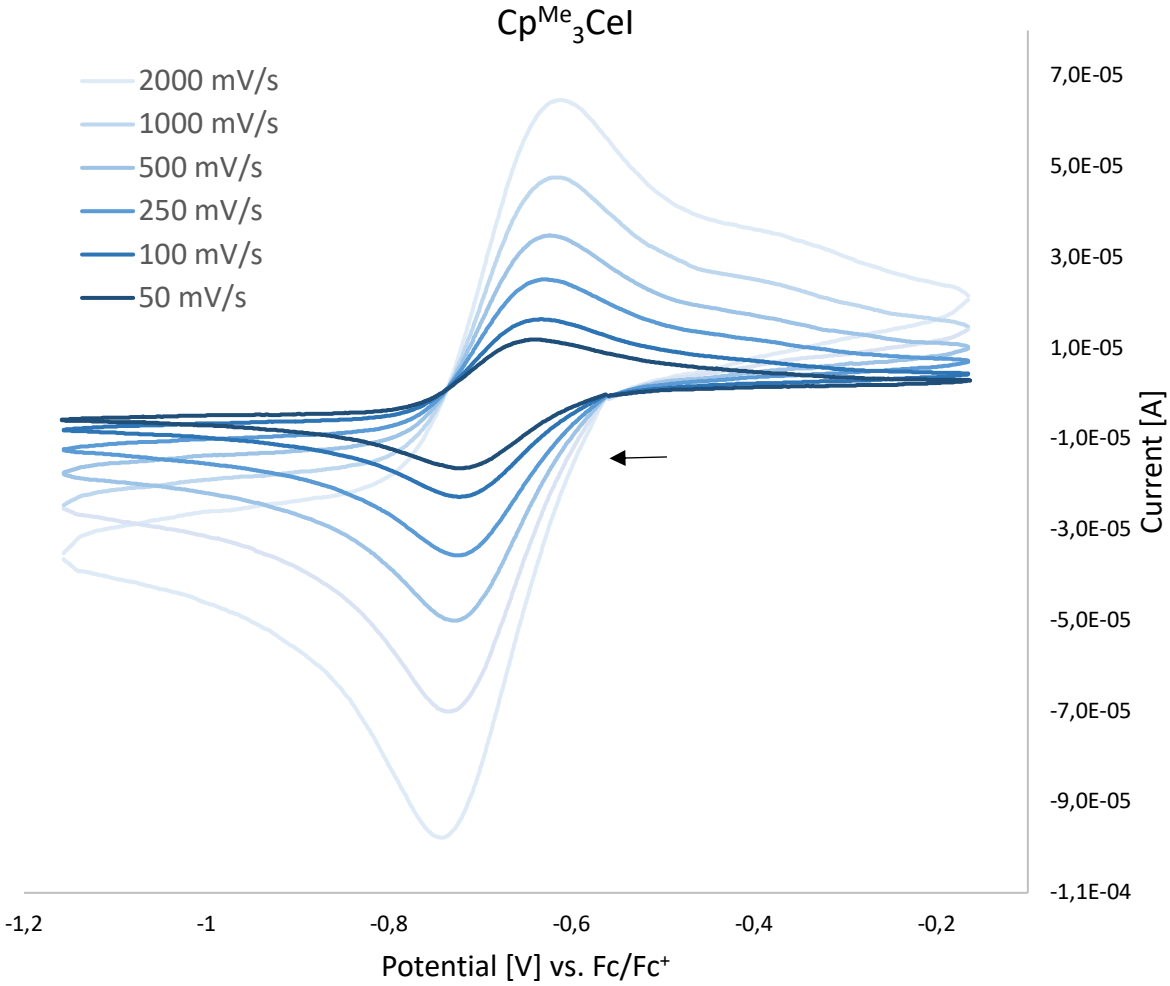

Figure S74. Cerium(III/IV) redox couple of **4b** vs Fc/Fc^+ in THF obtained at different scan rates; arrow indicates initial scan direction; *c*(analyte) 1mM, *c*(electrolyte) 0.1 M $[nPr_4N][BARF]$.

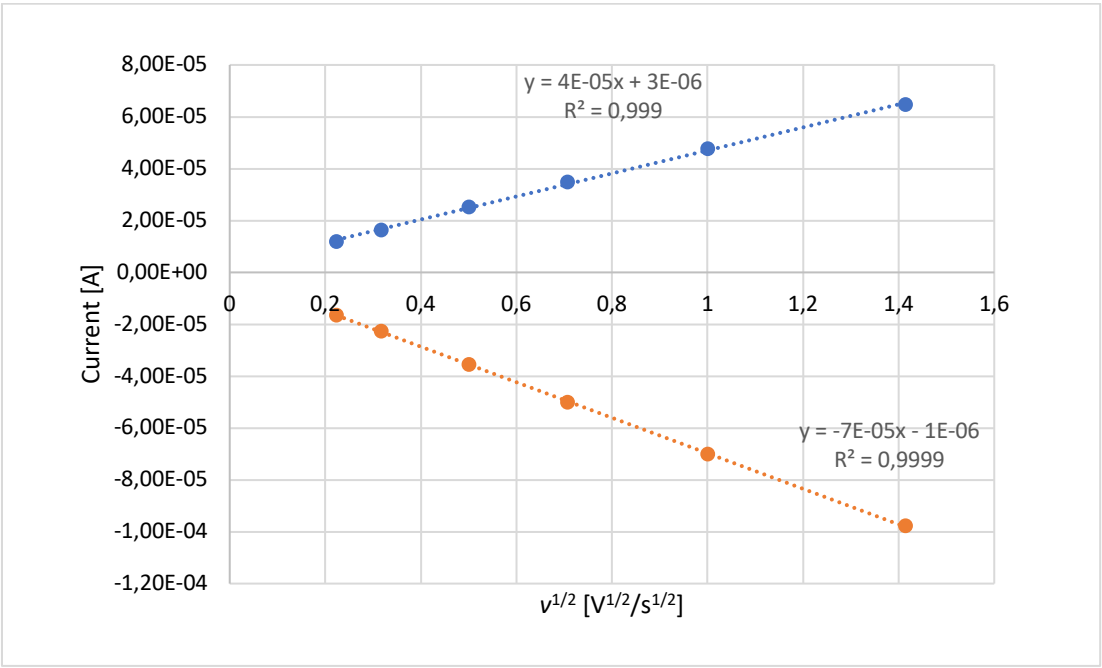

Figure S75. I_p versus $v^{1/2}$ plot of the anodic (blue) and cathodic (orange) peak currents in cyclic voltammograms of **4b**.

Table S12. Electrochemical data for the redox couple of complex **5a** vs Fc/Fc^+ in THF/ [nPr$_4$N][BARF]

Scan rate v	E_{pa} vs Fc/Fc^+ [V]	E_{pc} vs Fc/Fc^+ [V]	E^0 vs Fc/Fc^+ [V]	ΔE_p [V]	i_{pa}/i_{pc}
50 mV/s	–*	-1.345	–*	–*	–*
100 mV/s	–*	-1.148	–*	–*	–*
250 mV/s	-1.010	-1.155	-1.082	0.145	0.78
500 mV/s	-1.037	-1.161	-1.099	0.124	0.75
1000 mV/s	-1.037	-1.167	-1.102	0.130	0.75
2000 mV/s	-1.059	-1.171	-1.115	0.112	0.84

*could not be determined

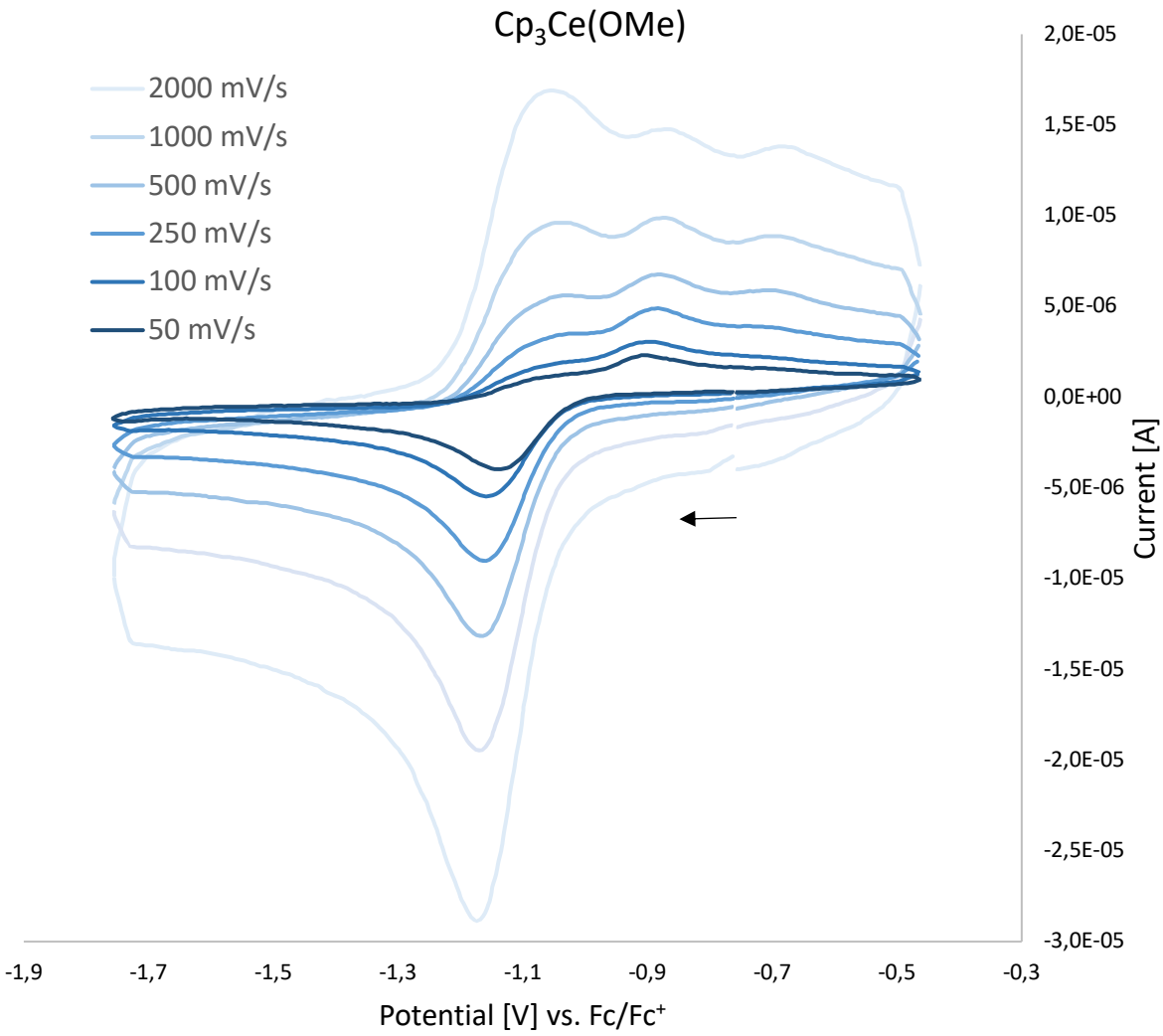

Figure S76. Cerium(III/IV) redox couple of **5a** vs Fc/Fc^+ in THF obtained at different scan rates; arrow indicates initial scan direction; c(analyte) 1mM, c(electrolyte) 0.1 M [nPr$_4$N][BARF].

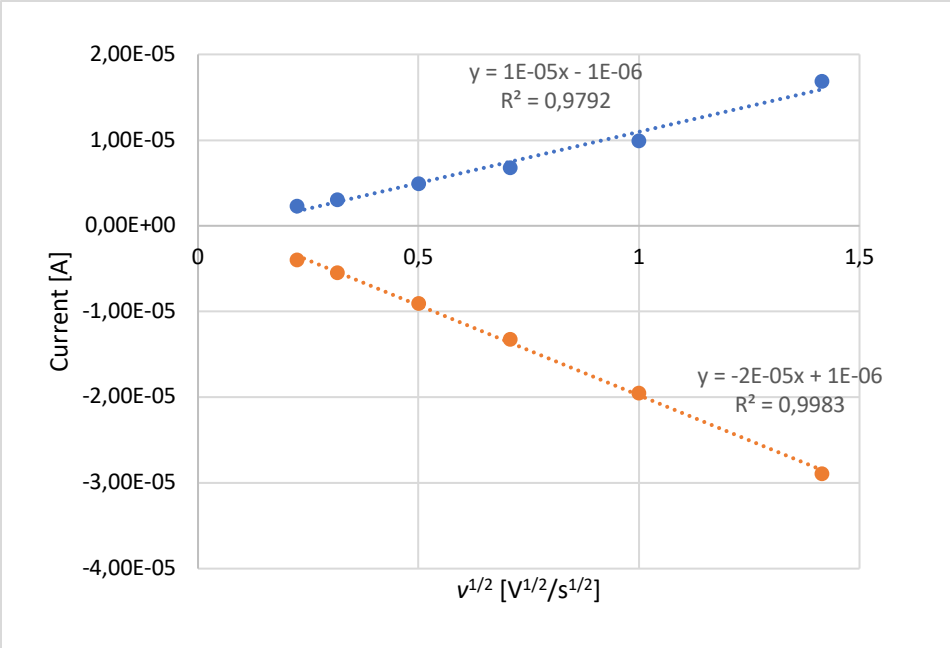

Figure S77. I_p versus $v^{1/2}$ plot of the anodic (blue) and cathodic (orange) peak currents in cyclic voltammograms of **5a**.

Table S13. Electrochemical data for the redox couple of complex **5b** vs Fc/Fc^+ in THF/ [*n*Pr$_4$N][BARF]

Scan rate *v*	E_{pa} vs Fc/Fc^+ [V]	E_{pc} vs Fc/Fc^+ [V]	E^0 vs Fc/Fc^+ [V]	ΔE_p [V]	i_{pa}/i_{pc}
50 mV/s	-1.075	-1.301	-1.188	0.226	0.61
100 mV/s	-0.985	-1.300	-1.142	0.315	0.70
250 mV/s	-1.019	-1.330	-1.174	0.311	0.80
500 mV/s	-0.996	-1.374	-1.185	0.378	0.91
1000 mV/s	-0.961	-1.452	-1.206	0.491	0.99
2000 mV/s	-0.927	-1.551	-1.239	0.624	1.00

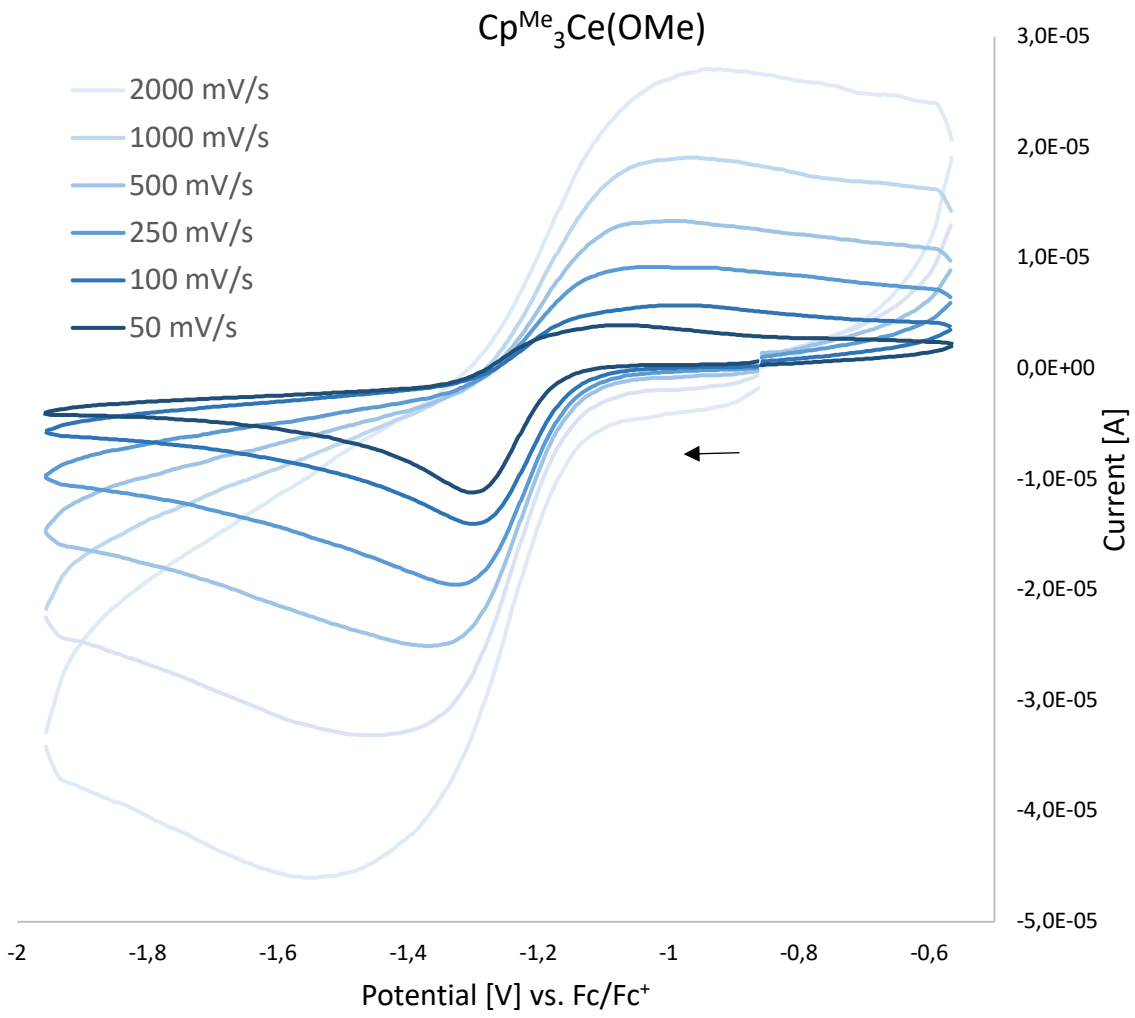

Figure S78. Cerium(III/IV) redox couple of **5b** vs Fc/Fc^+ in THF obtained at different scan rates; arrow indicates initial scan direction; *c*(analyte) 1mM, *c*(electrolyte) 0.1 M $[nPr_4N][BARF]$.

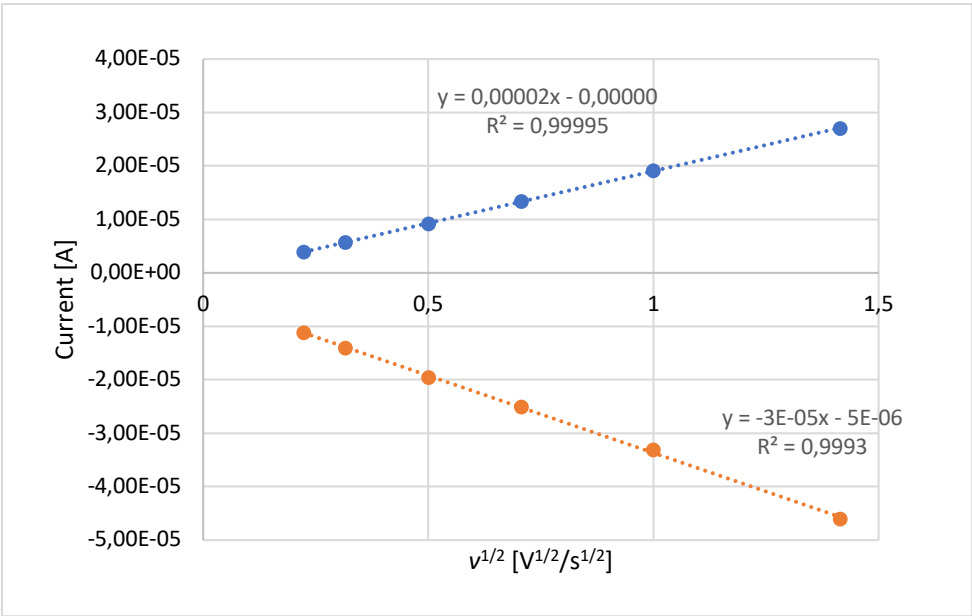

Figure S79. I_p versus $v^{1/2}$ plot of the anodic (blue) and cathodic (orange) peak currents in cyclic voltammograms of **5b**.

Table S14. Electrochemical data for the redox couple of complex **6a** vs Fc/Fc^+ in THF/ [nPr$_4$N][BARF]

Scan rate v	E_{pa} vs Fc/Fc^+ [V]	E_{pc} vs Fc/Fc^+ [V]	E^0 vs Fc/Fc^+ [V]	ΔE_p [V]	i_{pa}/i_{pc}
50 mV/s	-1.111	-1.196	-1.154	0.080	0.51
100 mV/s	-1.104	-1.210	-1.145	0.096	0.57
250 mV/s	-1.103	-1.221	-1.150	0.108	0.60
500 mV/s	-1.105	-1.231	-1.152	0.121	0.66
1000 mV/s	-1.096	-1.245	-1.155	0.143	0.72
2000 mV/s	-1.086	-1.265	-1.155	0.171	0.80

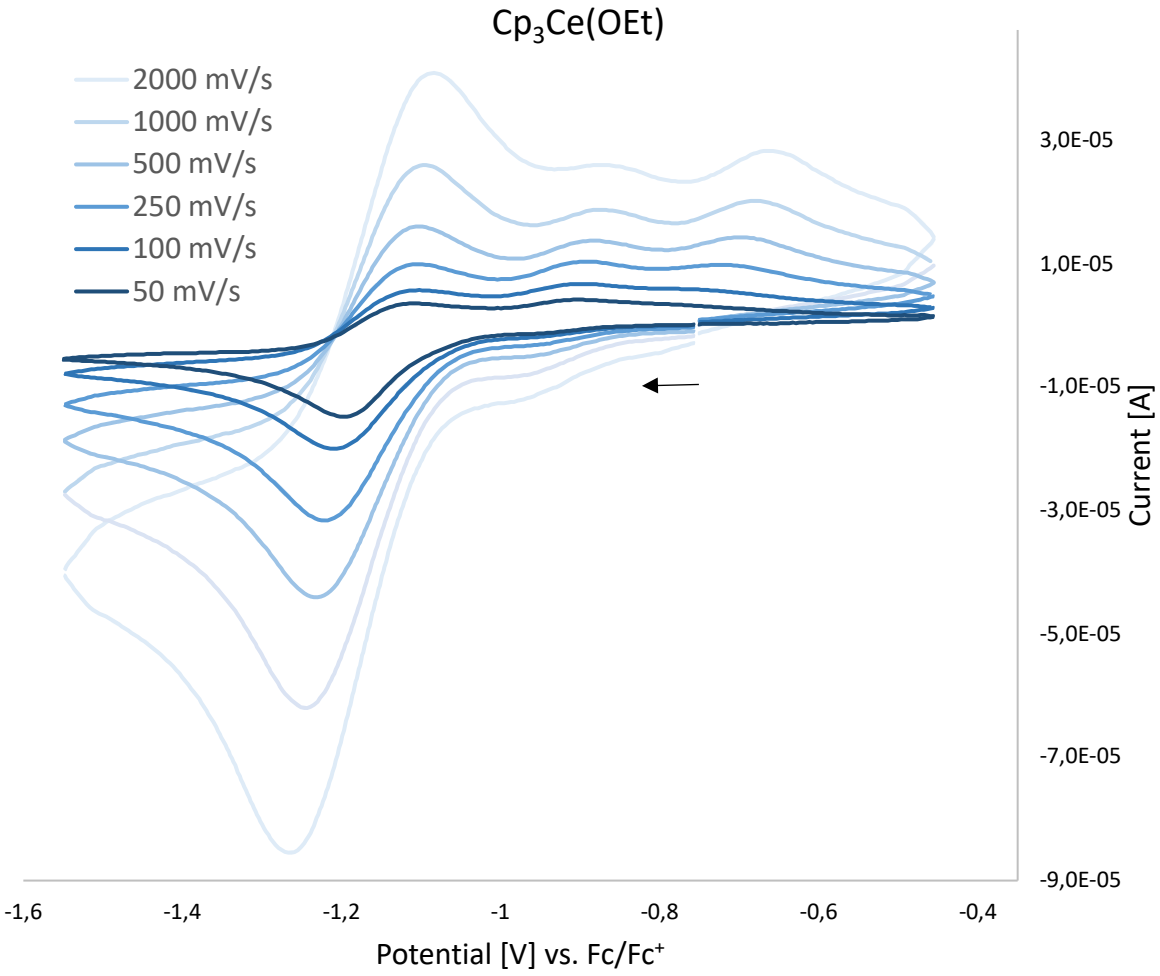

Figure S80. Cerium(III/IV) redox couple of **6a** vs Fc/Fc^+ in THF obtained at different scan rates; arrow indicates initial scan direction; c(analyte) 1mM, c(electrolyte) 0.1 M [nPr$_4$N][BARF].

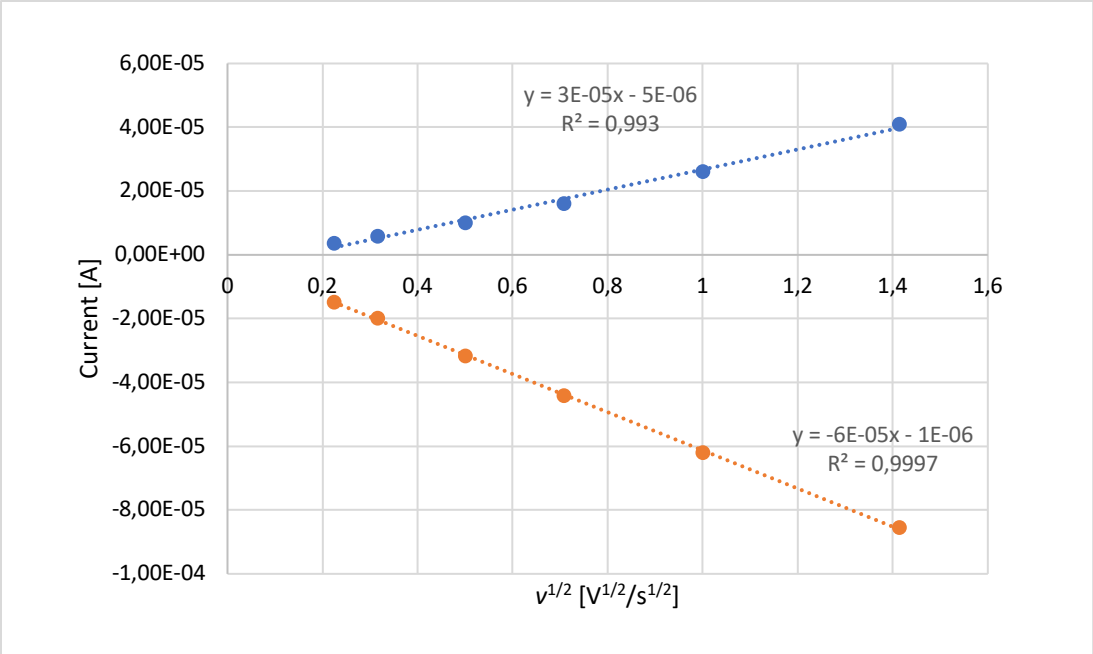

Figure S81. I_p versus $v^{1/2}$ plot of the anodic (blue) and cathodic (orange) peak currents in cyclic voltammograms of **6a**.

Table S15. Electrochemical data for the redox couple of complex **6b** vs Fc/Fc^+ in THF/ [nPr$_4$N][BARF]

Scan rate v	E_{pa} vs Fc/Fc^+ [V]	E_{pc} vs Fc/Fc^+ [V]	E^0 vs Fc/Fc^+ [V]	ΔE_p [V]	i_{pa}/i_{pc}
50 mV/s	-1.222	-1.295	-1.259	0.073	0.66
100 mV/s	-1.212	-1.293	-1.253	0.081	0.73
250 mV/s	-1.204	-1.296	-1.250	0.092	0.83
500 mV/s	-1.200	-1.302	-1.251	0.102	0.88
1000 mV/s	-1.194	-1.309	-1.252	0.115	0.92
2000 mV/s	-1.182	-1.320	-1.251	0.138	0.95

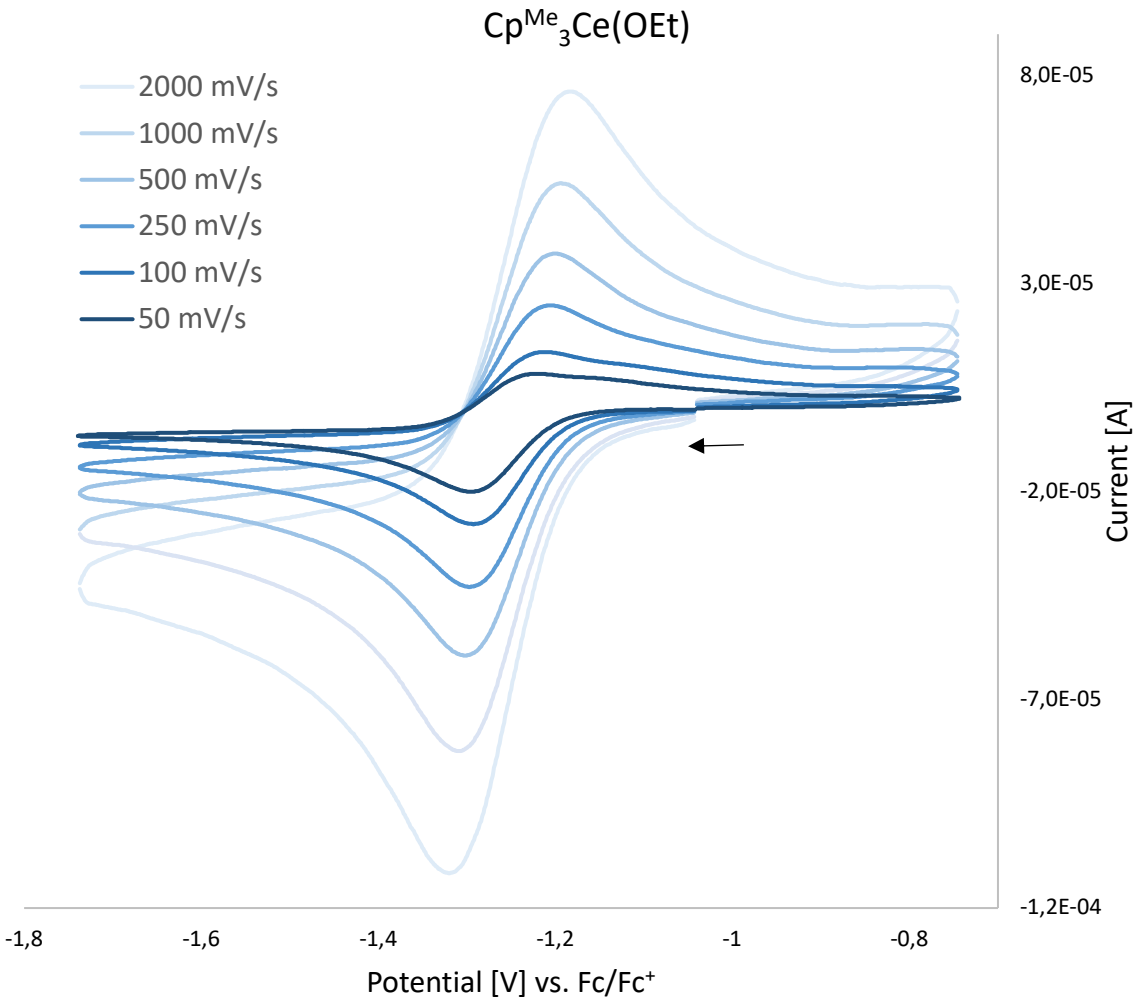

Figure S82. Cerium(III/IV) redox couple of **6b** vs Fc/Fc^+ in THF obtained at different scan rates; arrow indicates initial scan direction; *c*(analyte) 1mM, *c*(electrolyte) 0.1 M [nPr_4N][BARF].

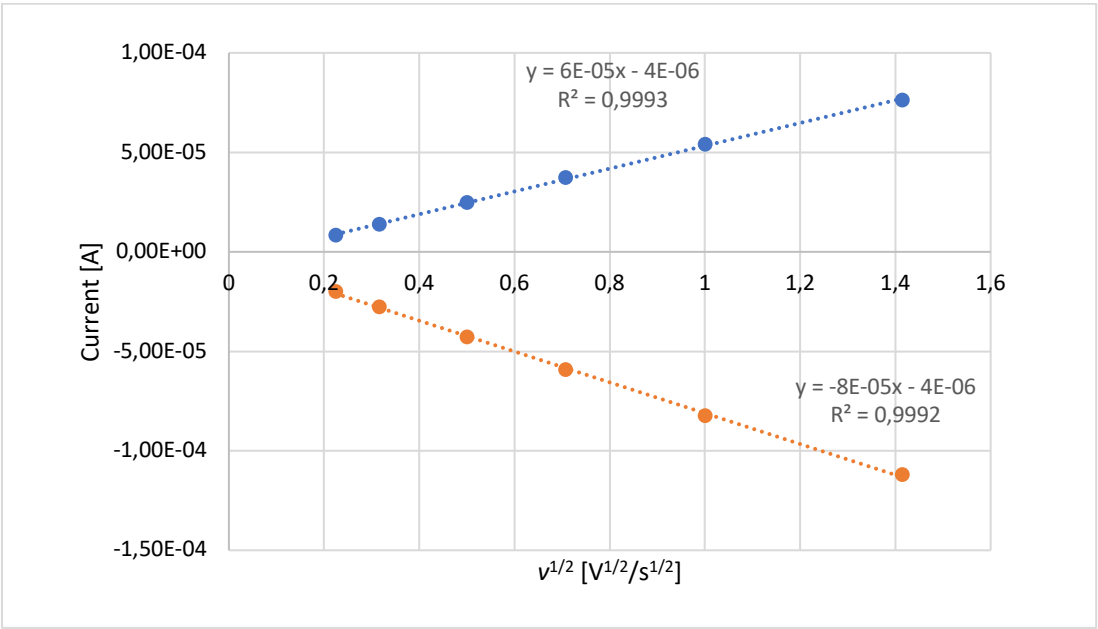

Figure S83. I_p versus $v^{1/2}$ plot of the anodic (blue) and cathodic (orange) peak currents in cyclic voltammograms of **6b**.

Table S16. Electrochemical data for the redox couple of complex **7a** vs Fc/Fc^+ in THF/ [nPr$_4$N][BARF]

Scan rate v	E_{pa} vs Fc/Fc^+ [V]	E_{pc} vs Fc/Fc^+ [V]	E^0 vs Fc/Fc^+ [V]	ΔE_p [V]	i_{pa}/i_{pc}
50 mV/s	-1.072	-1.182	-1.127	0.110	0.54
100 mV/s	-1.082	-1.190	-1.136	0.108	0.56
250 mV/s	-1.092	-1.197	-1.145	0.105	0.60
500 mV/s	-1.090	-1.203	-1.147	0.113	0.67
1000 mV/s	-1.093	-1.209	-1.151	0.116	0.77

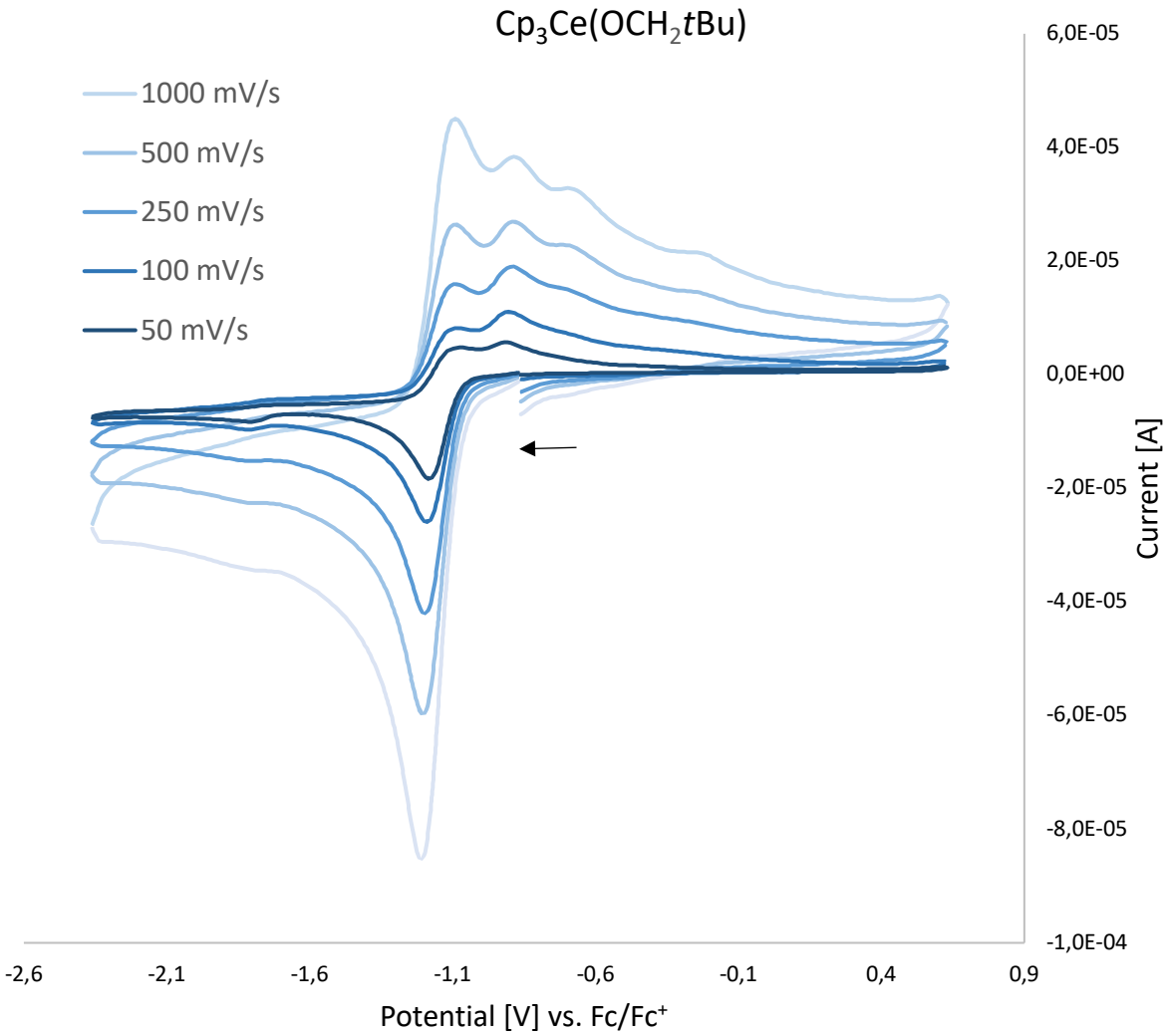

Figure S84. Cerium(III/IV) redox couple of **7a** vs Fc/Fc^+ in THF obtained at different scan rates; arrow indicates initial scan direction; c(analyte) 1mM, c(electrolyte) 0.1 M [nPr$_4$N][BARF].

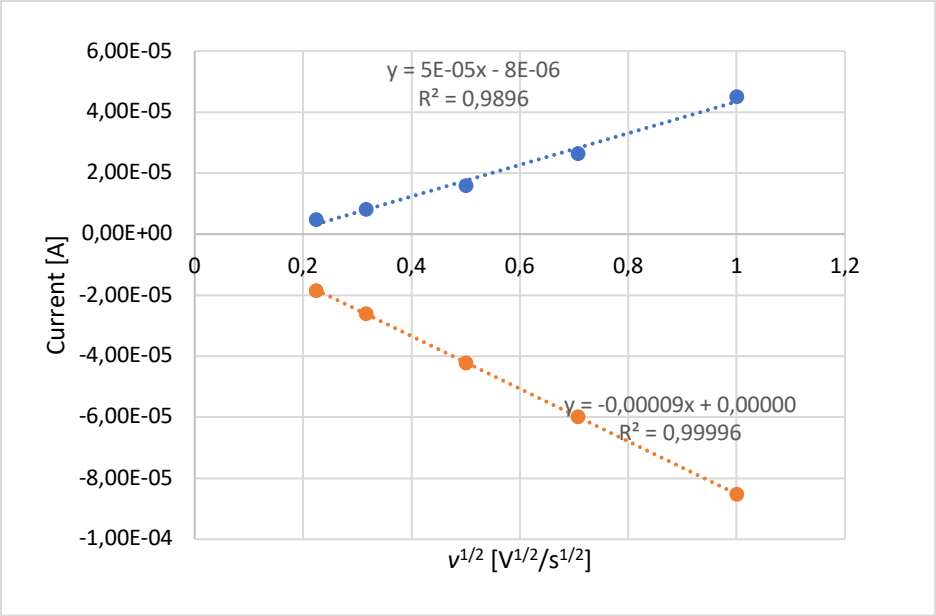

Figure S85. I_p versus $v^{1/2}$ plot of the anodic (blue) and cathodic (orange) peak currents in cyclic voltammograms of **7a**.

Table S17. Electrochemical data for the redox couple of complex **7b** vs Fc/Fc^+ in THF/ [nPr$_4$N][BARF]

Scan rate *v*	**E_{pa} vs Fc/Fc^+ [V]**	**E_{pc} vs Fc/Fc^+ [V]**	**E^0 vs Fc/Fc^+ [V]**	**ΔE_p [V]**	**i_{pa}/i_{pc}**
50 mV/s	-1.178	-1.252	-1.215	0.074	0.99
100 mV/s	-1.175	-1.259	-1.217	0.084	0.97
250 mV/s	-1.171	-1.263	-1.217	0.092	0.97
500 mV/s	-1.171	-1.267	-1.219	0.096	0.96
1000 mV/s	-1.169	-1.271	-1.220	0.102	0.96
2000 mV/s	-1.161	-1.283	-1.222	0.122	0.95

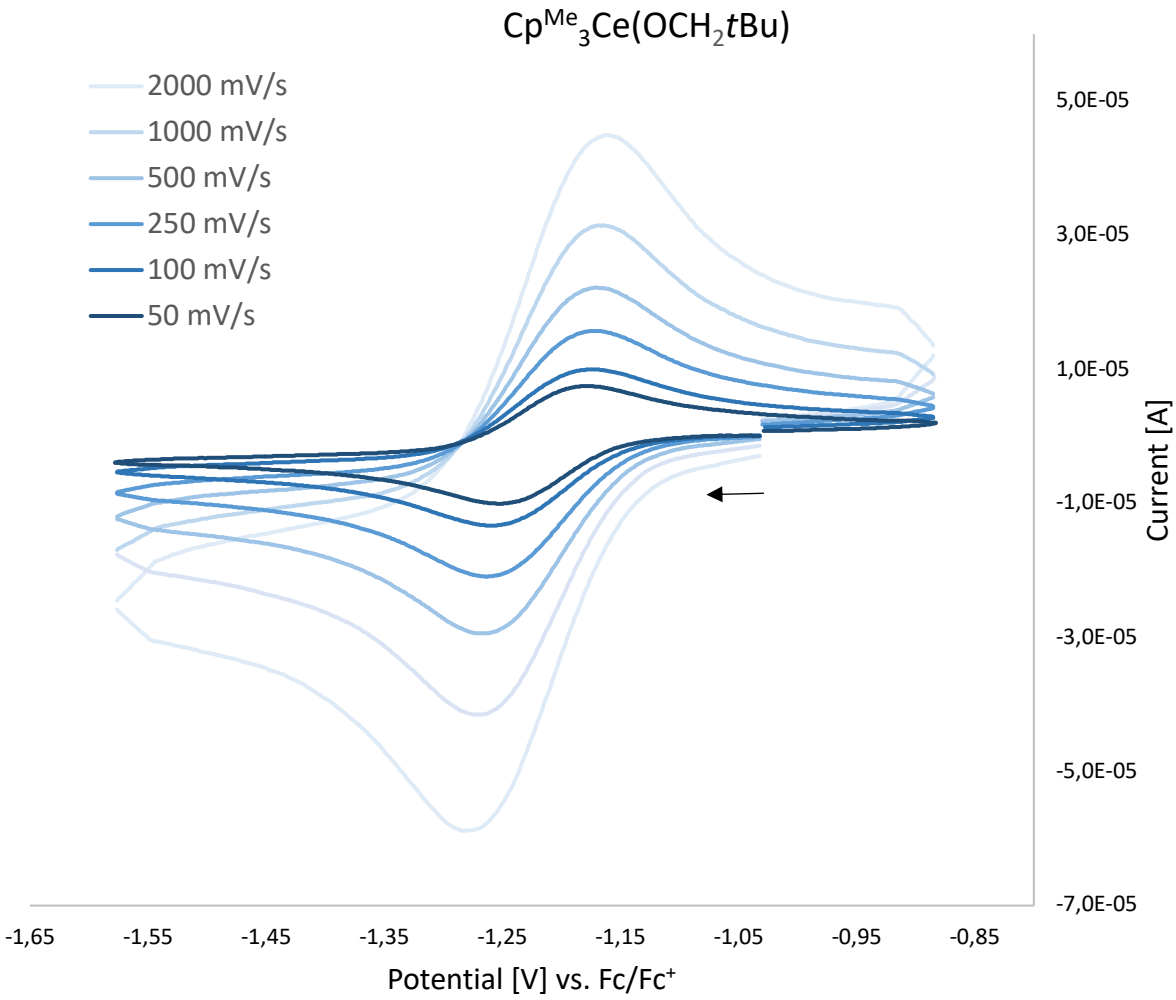

Figure S86. Cerium(III/IV) redox couple of **7b** vs Fc/Fc^+ in THF obtained at different scan rates; arrow indicates initial scan direction; *c*(analyte) 1mM, *c*(electrolyte) 0.1 M [nPr_4N][BARF].

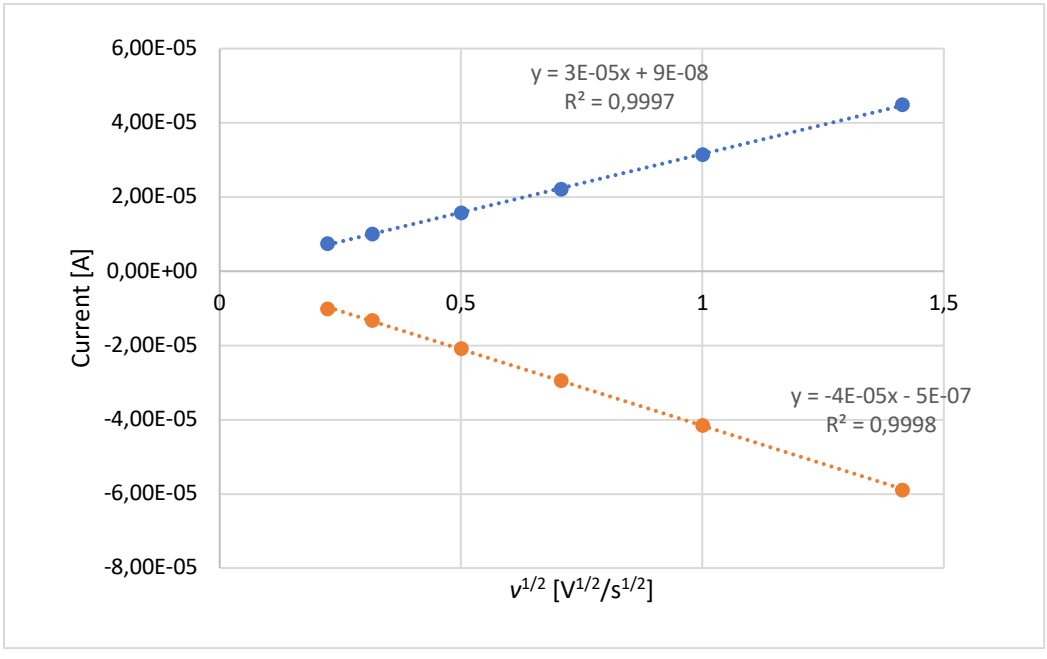

Figure S87. I_p versus $v^{1/2}$ plot of the anodic (blue) and cathodic (orange) peak currents in cyclic voltammograms of **7b**.

Table S18. Electrochemical data for the redox couple of complex **8a** vs Fc/Fc^+ in THF/ [nPr$_4$N][BARF]

Scan rate v	E_{pa} vs Fc/Fc^+ [V]	E_{pc} vs Fc/Fc^+ [V]	E^0 vs Fc/Fc^+ [V]	ΔE_p [V]	i_{pa}/i_{pc}
50 mV/s	–*	-1.228	–*	–*	–*
100 mV/s	-1.132	-1.221	-1.176	0.089	0.66
250 mV/s	-1.143	-1.210	-1.176	0.067	0.66
500 mV/s	-1.156	-1.210	-1.183	0.054	0.68
1000 mV/s	-1.145	-1.210	-1.177	0.065	0.81
2000 mV/s	-1.152	-1.210	-1.181	0.058	0.93

*could not be determined

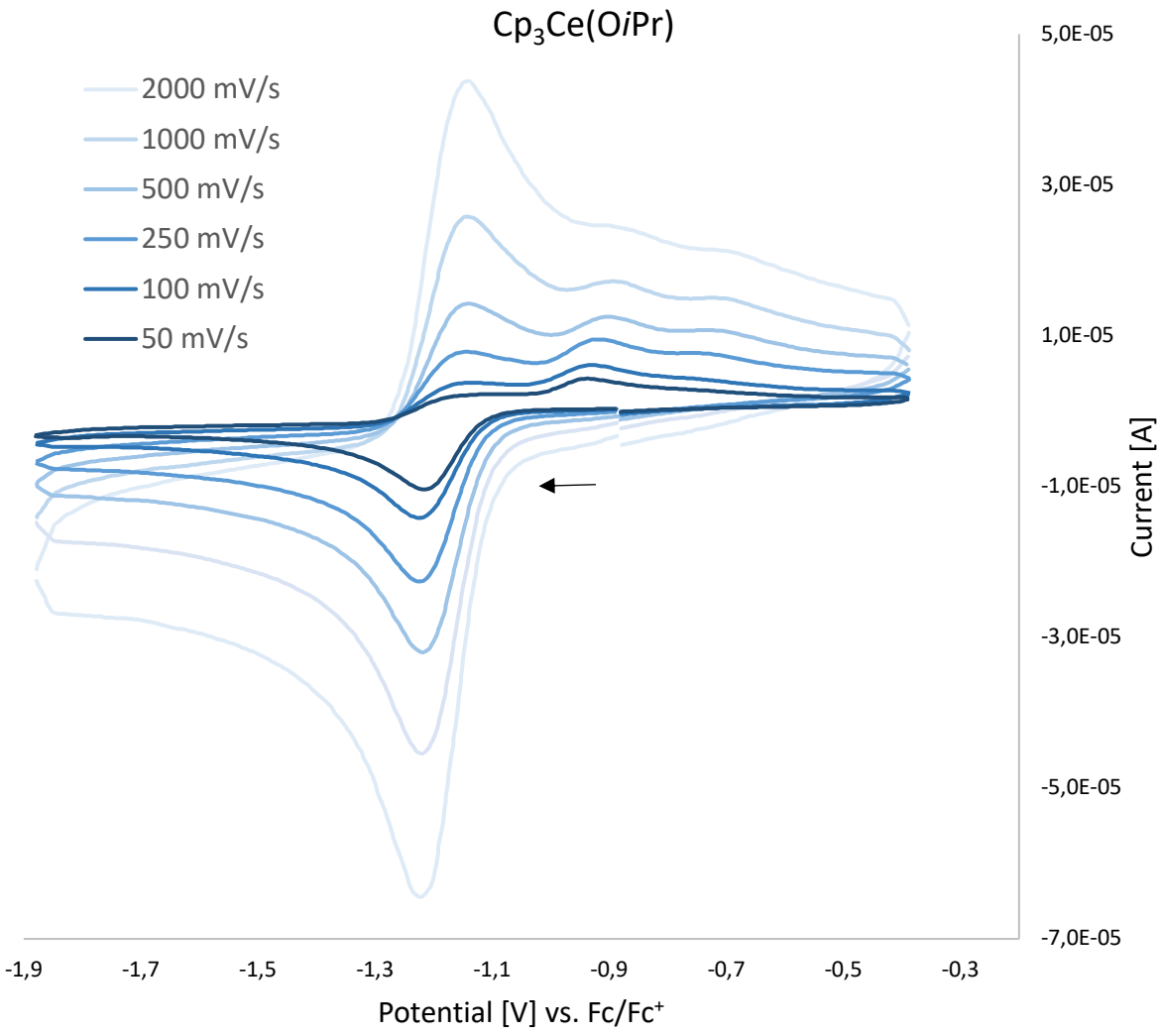

Figure S88. Cerium(III/IV) redox couple of **8a** vs Fc/Fc^+ in THF obtained at different scan rates; arrow indicates initial scan direction; c(analyte) 1mM, c(electrolyte) 0.1 M [nPr$_4$N][BARF].

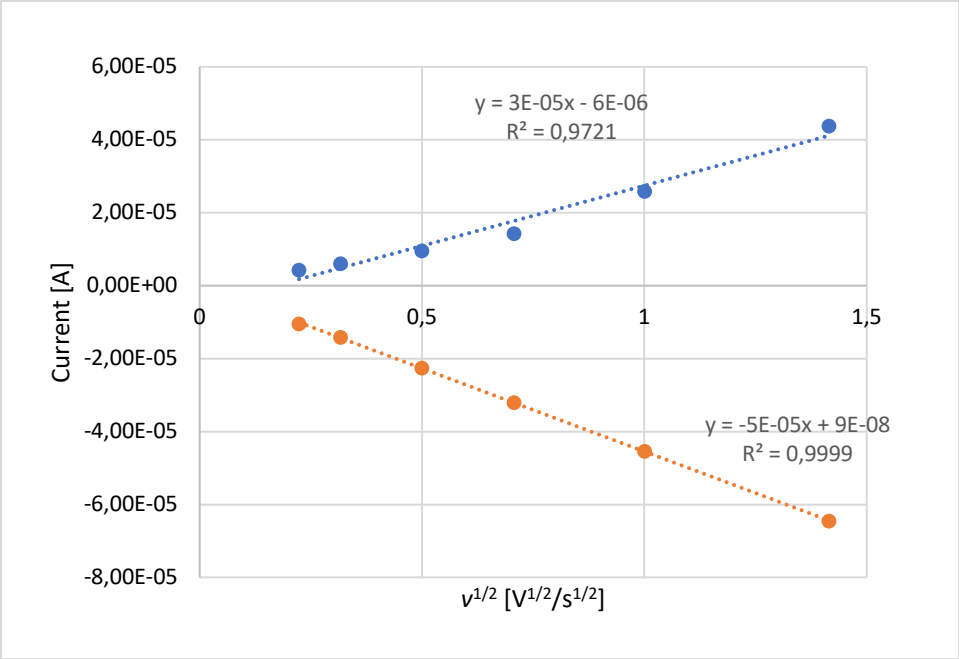

Figure S89. I_p versus $v^{1/2}$ plot of the anodic (blue) and cathodic (orange) peak currents in cyclic voltammograms of **8a**.

Table S19. Electrochemical data for the redox couple of complex **8a** vs Fc/Fc^+ in $THF/TBABF_4$

Scan rate *v*	E_{pa} vs Fc/Fc^+ [V]	E_{pc} vs Fc/Fc^+ [V]	E^0 vs Fc/Fc^+ [V]	ΔE_p [V]	i_{pa}/i_{pc}
50 mV/s	-1.035	-1.206	-1.121	0.171	0.55
100 mV/s	-1.023	-1.230	-1.127	0.207	0.59
250 mV/s	-1.003	-1.271	-1.137	0.268	0.68
500 mV/s	-0.975	-1.311	-1.143	0.336	0.79
1000 mV/s	-0.941	-1.364	-1.153	0.423	0.86
2000 mV/s	-0.889	-1.431	-1.160	0.542	0.91

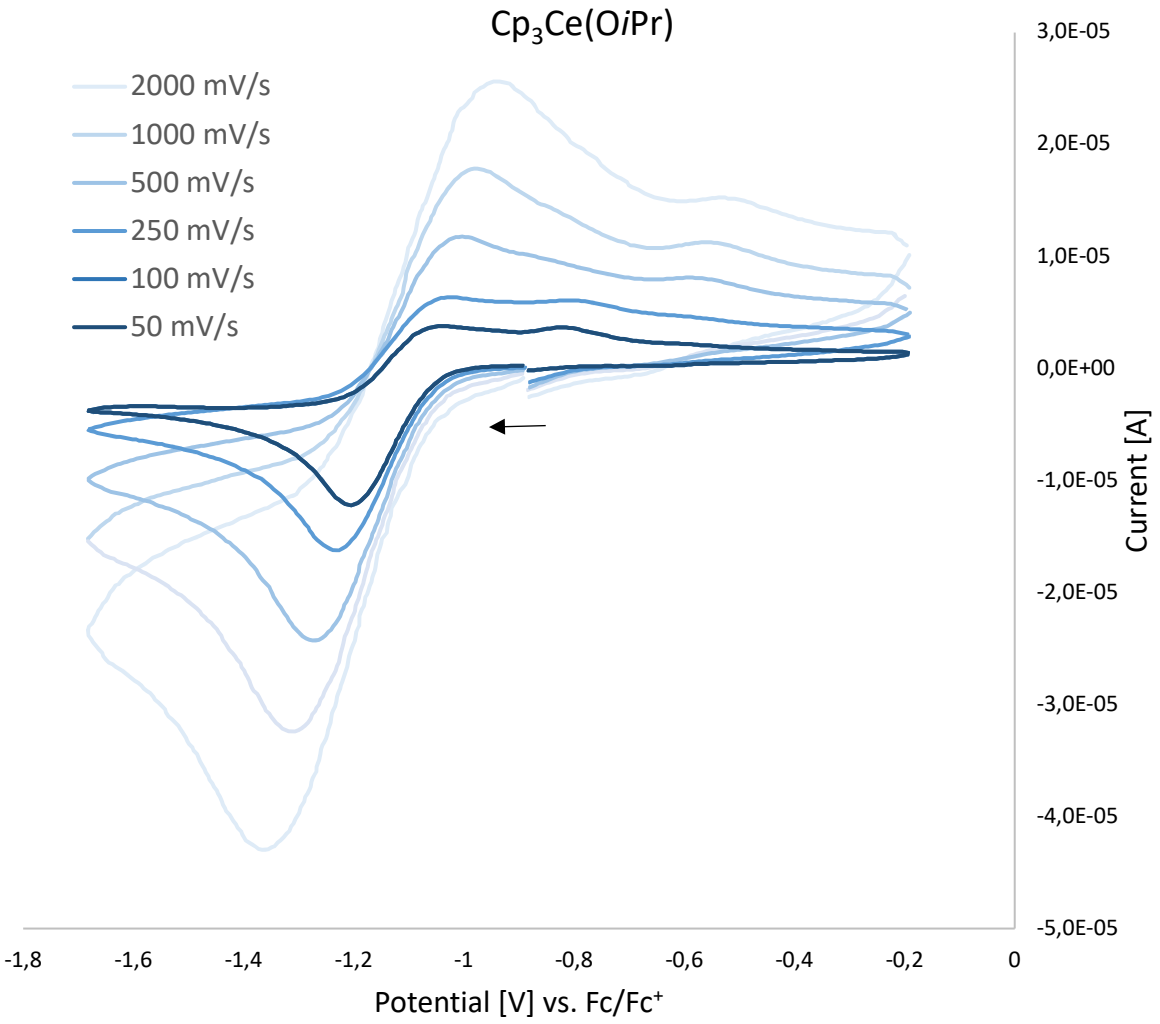

Figure S90. Cerium(III/IV) redox couple of **8a** vs Fc/Fc^+ in THF obtained at different scan rates; arrow indicates initial scan direction; *c*(analyte) 1mM, *c*(electrolyte) 0.25 M $TBABF_4$.

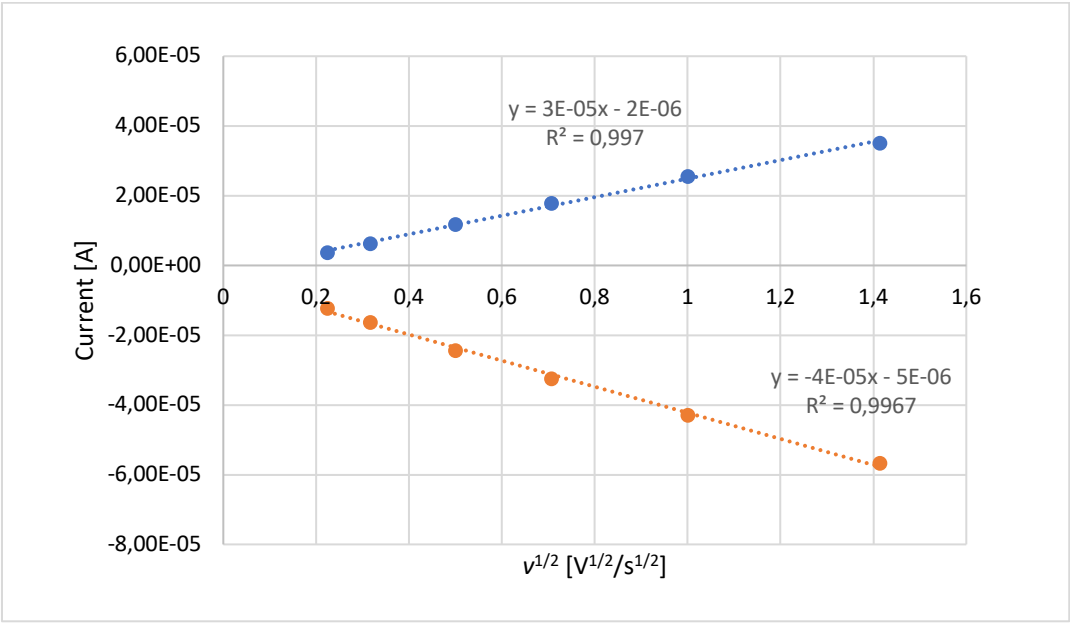

Figure S91. I_p versus $v^{1/2}$ plot of the anodic (blue) and cathodic (orange) peak currents in cyclic voltammograms of **8a**.

Table S20. Electrochemical data for the redox couple of complex **8b** vs Fc/Fc^+ in THF/ [nPr$_4$N][BARF]

Scan rate v	E_{pa} vs Fc/Fc^+ [V]	E_{pc} vs Fc/Fc^+ [V]	E^0 vs Fc/Fc^+ [V]	ΔE_p [V]	i_{pa}/i_{pc}
50 mV/s	-1.197	-1.283	-1.240	0.086	0.68
100 mV/s	-1.192	-1.284	-1.238	0.092	0.76
250 mV/s	-1.189	-1.290	-1.239	0.101	0.87
500 mV/s	-1.185	-1.301	-1.243	0.116	0.92
1000 mV/s	-1.177	-1.311	-1.244	0.134	0.97
2000 mV/s	-1.167	-1.327	-1.247	0.160	1.00

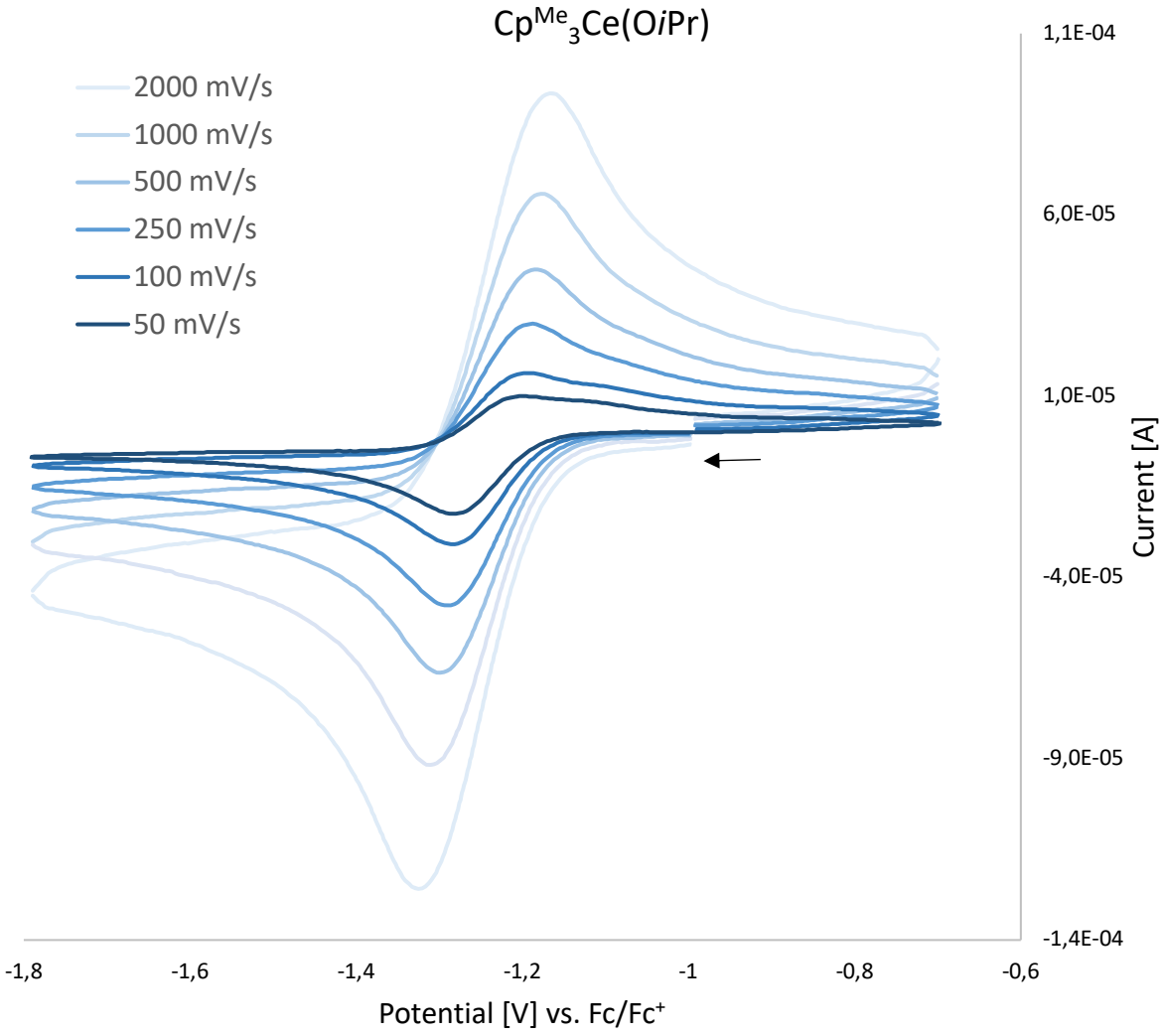

Figure S92. Cerium(III/IV) redox couple of **8b** vs Fc/Fc^+ in THF obtained at different scan rates; arrow indicates initial scan direction; c(analyte) 1mM, c(electrolyte) 0.1 M [nPr$_4$N][BARF].

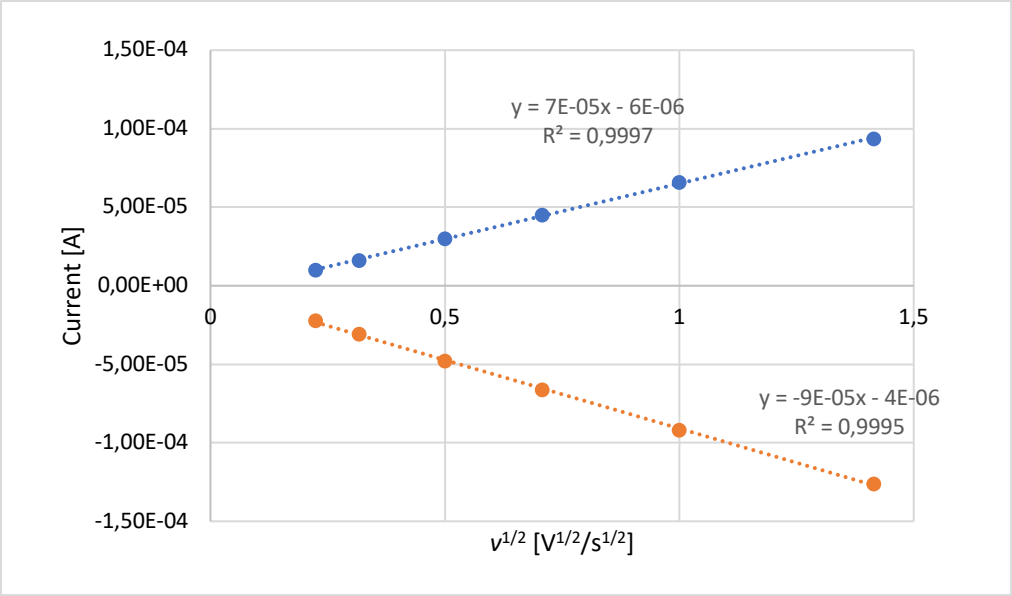

Figure S93. I_p versus $v^{1/2}$ plot of the anodic (blue) and cathodic (orange) peak currents in cyclic voltammograms of **8b**.

Table S21. Electrochemical data for the redox couple of complex **9a** vs Fc/Fc^+ in THF/ [nPr$_4$N][BARF]

Scan rate v	E_{pa} vs Fc/Fc^+ [V]	E_{pc} vs Fc/Fc^+ [V]	E^0 vs Fc/Fc^+ [V]	ΔE_p [V]	i_{pa}/i_{pc}
50 mV/s	–*	-1.200	– *	–*	–*
100 mV/s	-1.130	-1.204	-1.167	0.073	0.67
250 mV/s	-1.126	-1.209	-1.168	0.083	0.64
500 mV/s	-1.131	-1.215	-1.173	0.084	0.75
1000 mV/s	-1.124	-1.223	-1.174	0.099	0.87
2000 mV/s	-1.125	-1.231	-1.178	0.106	0.96

*could not be determined

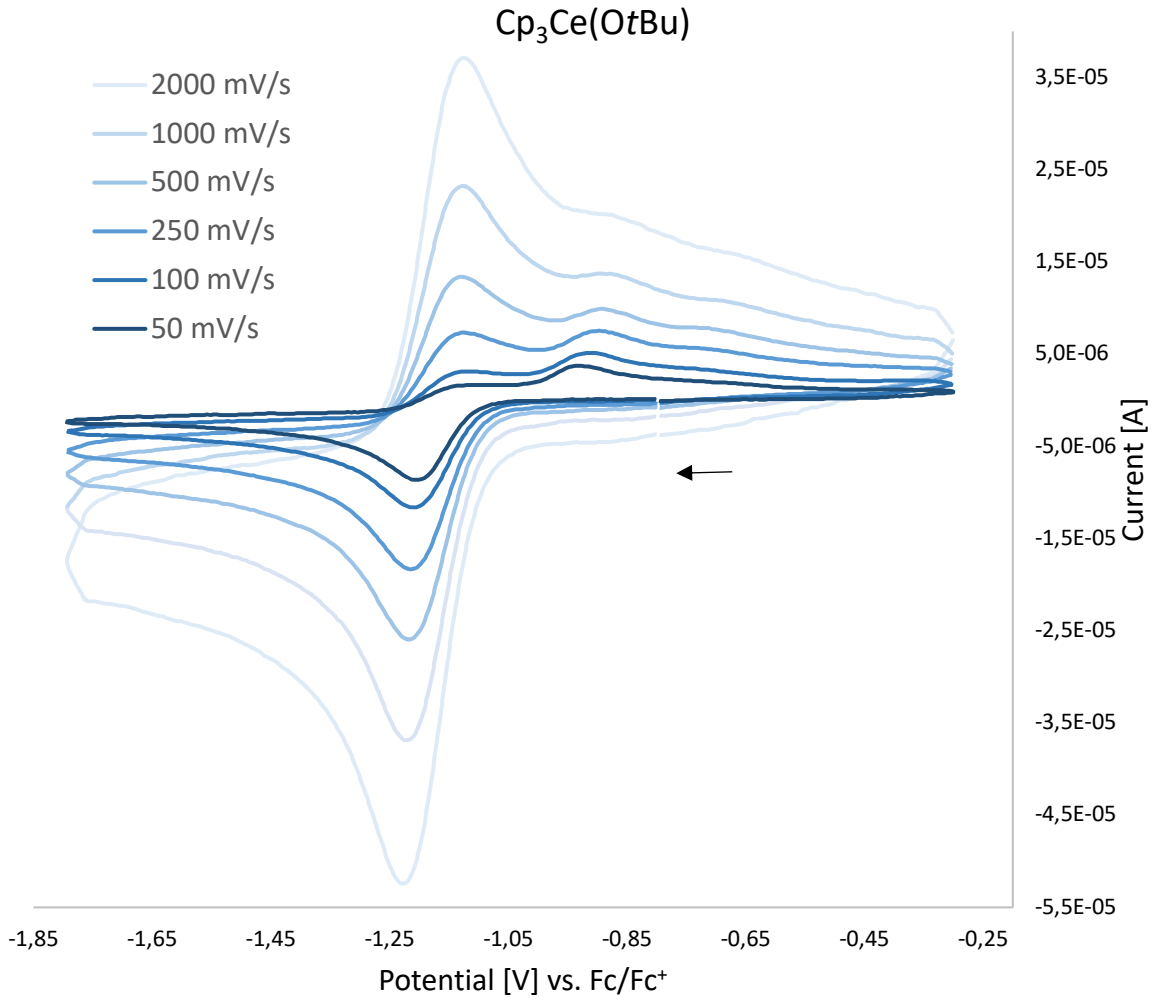

Figure S94. Cerium(III/IV) redox couple of **9a** vs Fc/Fc^+ in THF obtained at different scan rates; arrow indicates initial scan direction; *c*(analyte) 1mM, *c*(electrolyte) 0.1 M [nPr_4N][BARF].

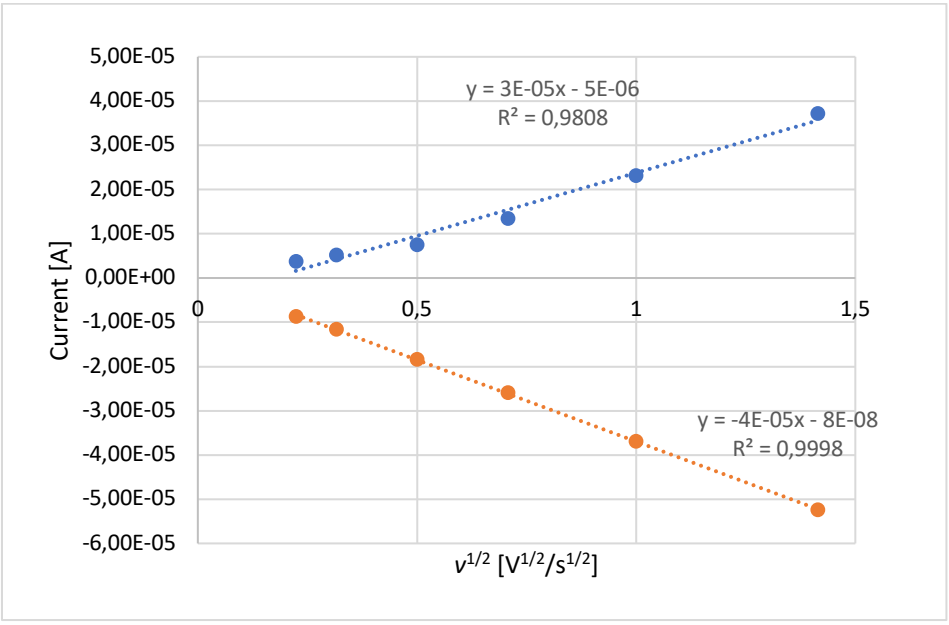

Figure S95. I_p versus $v^{1/2}$ plot of the anodic (blue) and cathodic (orange) peak currents in cyclic voltammograms of **9a**.

Table S22. Electrochemical data for the redox couple of complex **9b** vs Fc/Fc^+ in THF/ [nPr$_4$N][BARF]

Scan rate v	E_{pa} vs Fc/Fc^+ [V]	E_{pc} vs Fc/Fc^+ [V]	E^0 vs Fc/Fc^+ [V]	ΔE_p [V]	i_{pa}/i_{pc}
50 mV/s	-1.202	-1.275	-1.238	0.073	0.71
100 mV/s	-1.203	-1.286	-1.244	0.083	0.79
250 mV/s	-1.201	-1.295	-1.248	0.094	0.89
500 mV/s	-1.197	-1.304	-1.250	0.107	0.94
1000 mV/s	-1.191	-1.313	-1.252	0.122	0.98
2000 mV/s	-1.181	-1.323	-1.252	0.142	1.00

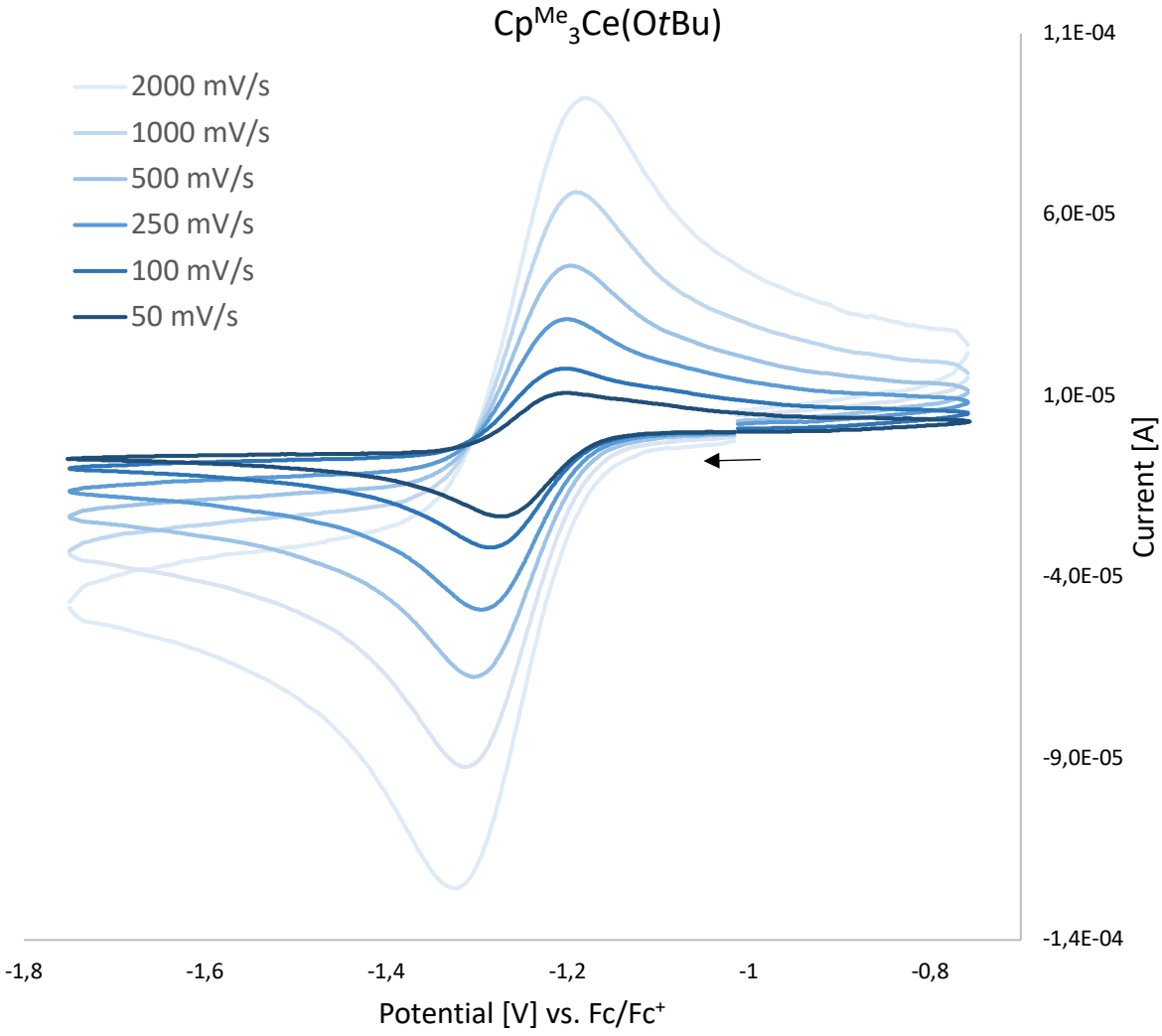

Figure S96. Cerium(III/IV) redox couple of **9b** vs Fc/Fc^+ in THF obtained at different scan rates; arrow indicates initial scan direction; c(analyte) 1mM, c(electrolyte) 0.1 M [nPr$_4$N][BARF].

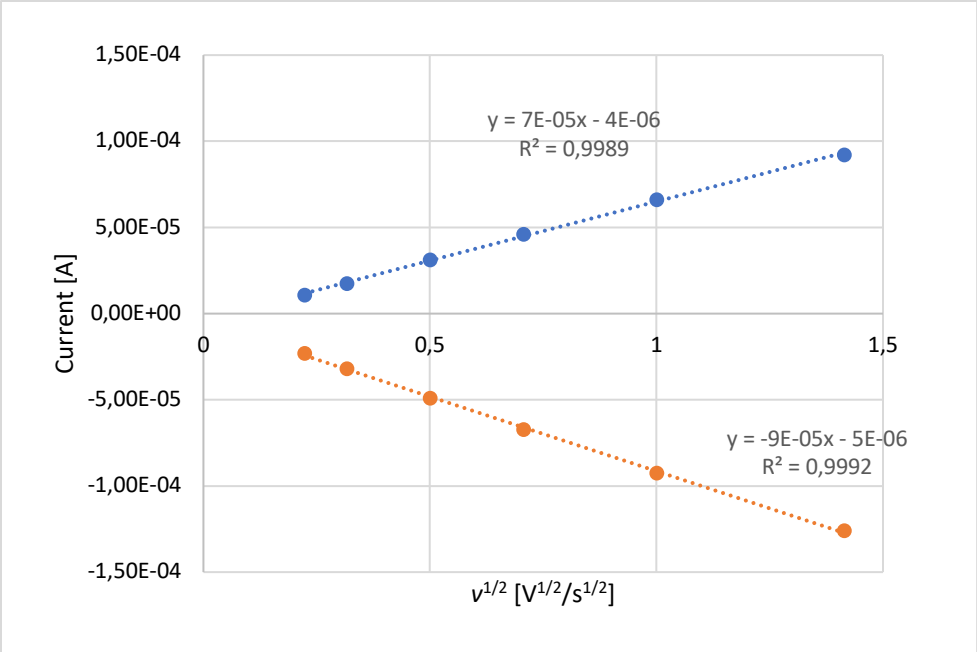

Figure S97. I_p versus $v^{1/2}$ plot of the anodic (blue) and cathodic (orange) peak currents in cyclic voltammograms of **9b**.

Table S23. Electrochemical data for the redox couple of complex **10a** vs Fc/Fc^+ in THF/ [*n*Pr$_4$N][BARF]

Scan rate *v*	E_{pa} vs Fc/Fc^+ [V]	E_{pc} vs Fc/Fc^+ [V]	E^0 vs Fc/Fc^+ [V]	ΔE_p [V]	i_{pa}/i_{pc}
50 mV/s	-0.984	-1.058	-1.021	0.074	0.96
100 mV/s	-0.979	-1.052	-1.016	0.073	0.97
250 mV/s	-0.971	-1.055	-1.013	0.084	0.97
500 mV/s	-0.963	-1.058	-1.011	0.095	0.95
1000 mV/s	-0.951	-1.063	-1.007	0.112	0.96
2000 mV/s	-0.941	-1.071	-1.006	0.130	0.97

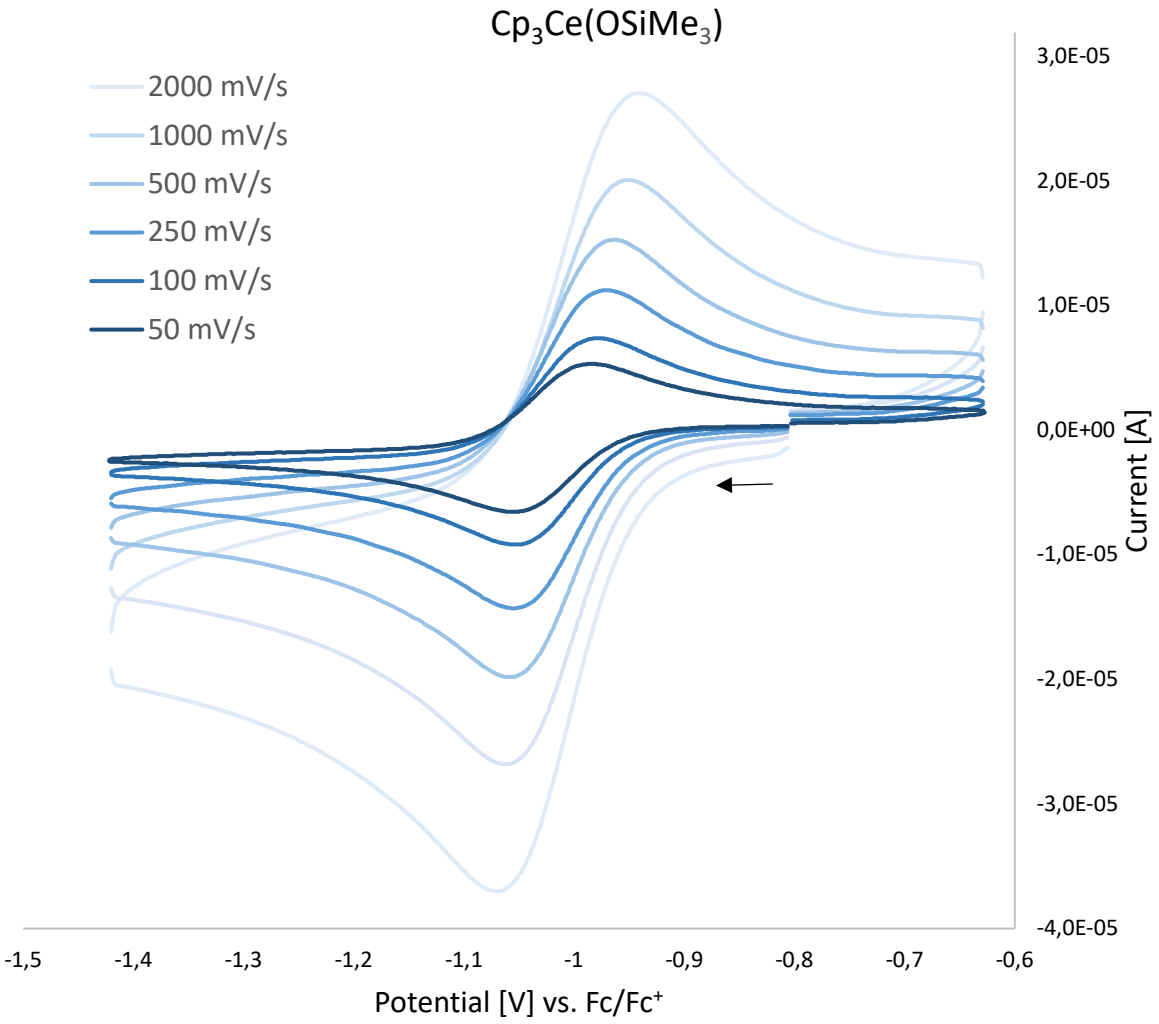

Figure S98. Cerium(III/IV) redox couple of **10a** vs Fc/Fc^+ in THF obtained at different scan rates; arrow indicates initial scan direction; *c*(analyte) 1mM, *c*(electrolyte) 0.1 M [nPr_4N][BARF].

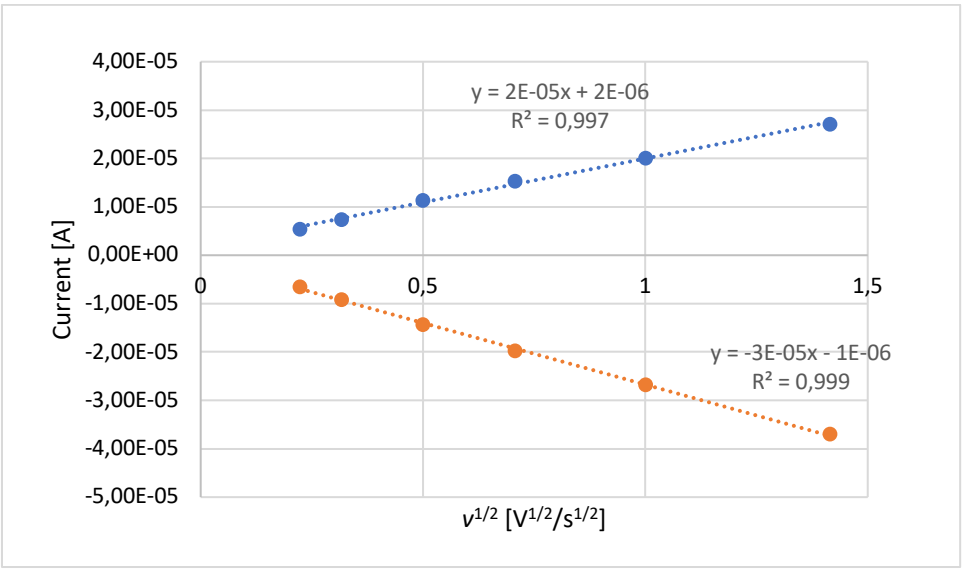

Figure S99. I_p versus $v^{1/2}$ plot of the anodic (blue) and cathodic (orange) peak currents in cyclic voltammograms of **10a**.

Table S24. Electrochemical data for the redox couple of complex **10b** vs Fc/Fc^+ in THF/ [nPr$_4$N][BARF]

Scan rate v	E_{pa} vs Fc/Fc^+ [V]	E_{pc} vs Fc/Fc^+ [V]	E^0 vs Fc/Fc^+ [V]	ΔE_p [V]	i_{pa}/i_{pc}
50 mV/s	-1.054	-1.124	-1.089	0.070	1.00
100 mV/s	-1.041	-1.119	-1.080	0.078	1.00
250 mV/s	-1.036	-1.125	-1.080	0.089	1.00
500 mV/s	-1.032	-1.127	-1.079	0.095	1.00
750 mV/s	-1.029	-1.131	-1.080	0.102	0.99
1000 mV/s	-1.024	-1.137	-1.080	0.113	1.00

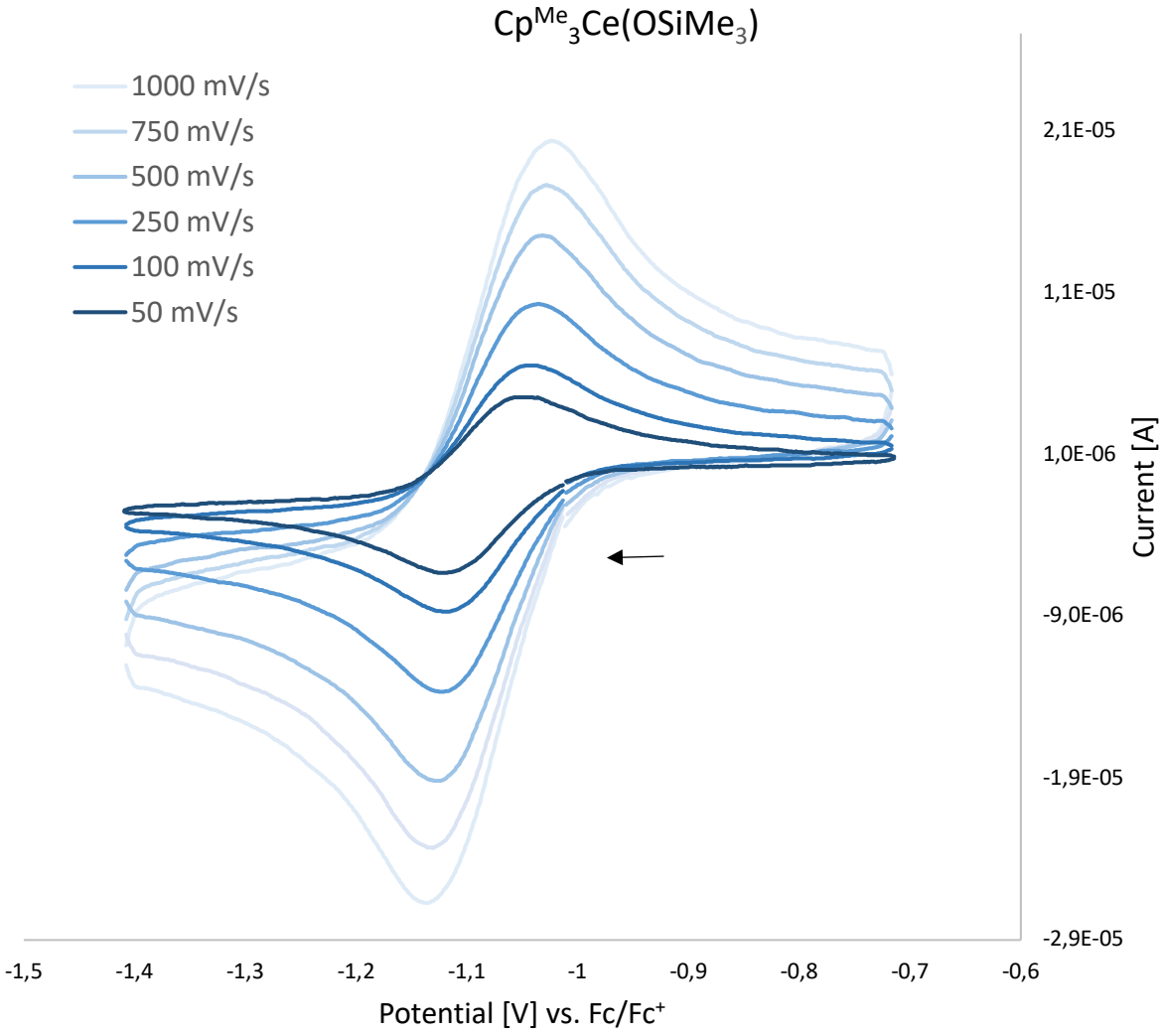

Figure S100. Cerium(III/IV) redox couple of **10b** vs Fc/Fc^+ in THF obtained at different scan rates; arrow indicates initial scan direction; c(analyte) 1mM, c(electrolyte) 0.1 M [nPr$_4$N][BARF].

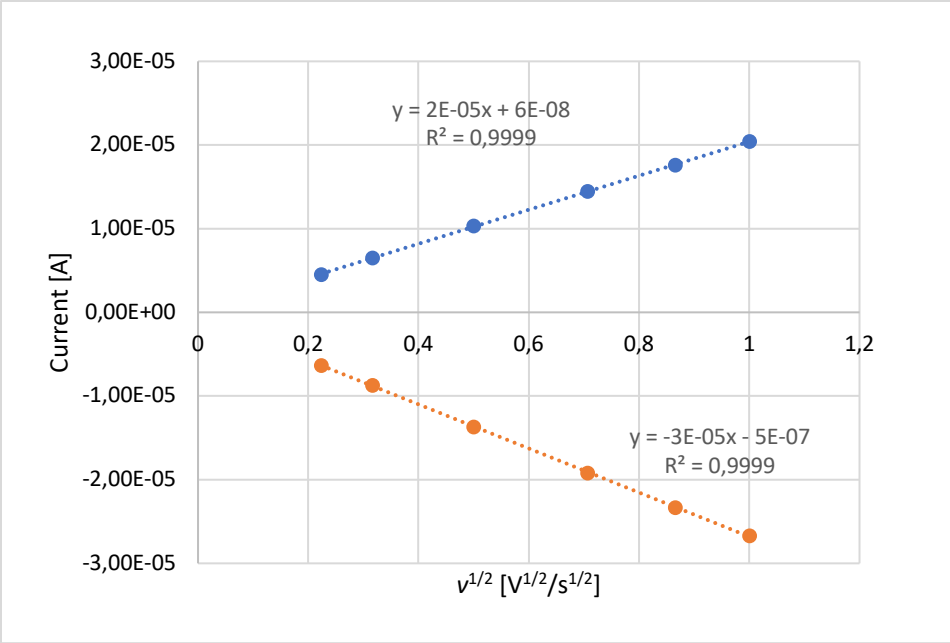

Figure S101. I_p versus $v^{1/2}$ plot of the anodic (blue) and cathodic (orange) peak currents in cyclic voltammograms of **10b**.

Table S25. Electrochemical data for the redox couple of complex **11a** vs Fc/Fc^+ in THF/ [nPr$_4$N][BARF]

Scan rate v	E_{pa} vs Fc/Fc^+ [V]	E_{pc} vs Fc/Fc^+ [V]	E^0 vs Fc/Fc^+ [V]	ΔE_p [V]	i_{pa}/i_{pc}
50 mV/s	-0.943	-1.003	-0.973	0.060	0.95
100 mV/s	-0.909	-0.989	-0.949	0.080	1.00
250 mV/s	-0.903	-0.995	-0.949	0.092	1.00
500 mV/s	-0.892	-1.000	-0.946	0.108	1.00
1000 mV/s	-0.881	-1.006	-0.944	0.125	0.99
2000 mV/s	-0.867	-1.015	-0.941	0.148	0.98

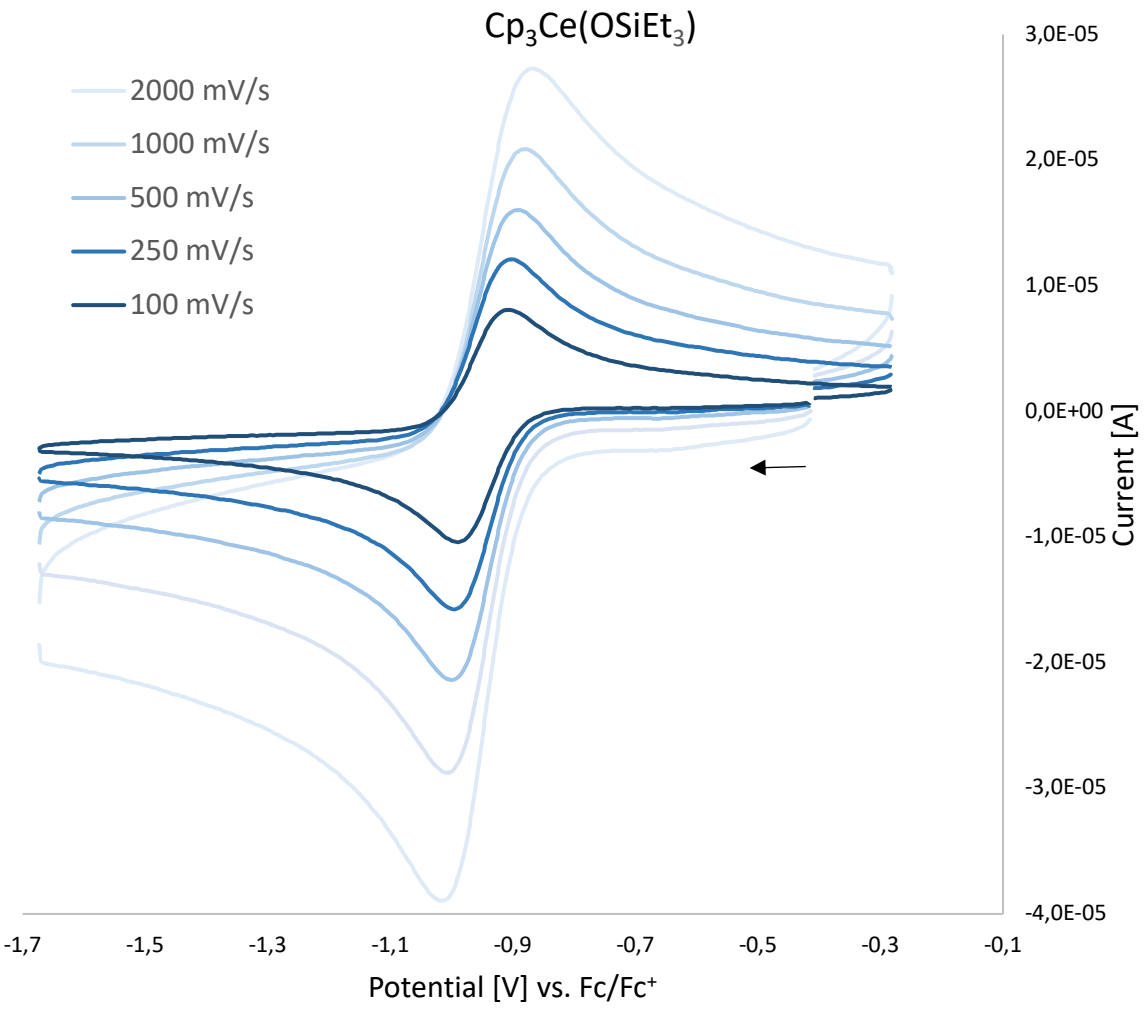

Figure S102. Cerium(III/IV) redox couple of **11a** vs Fc/Fc^+ in THF obtained at different scan rates; arrow indicates initial scan direction; *c*(analyte) 1mM, *c*(electrolyte) 0.1 M [nPr_4N][BARF].

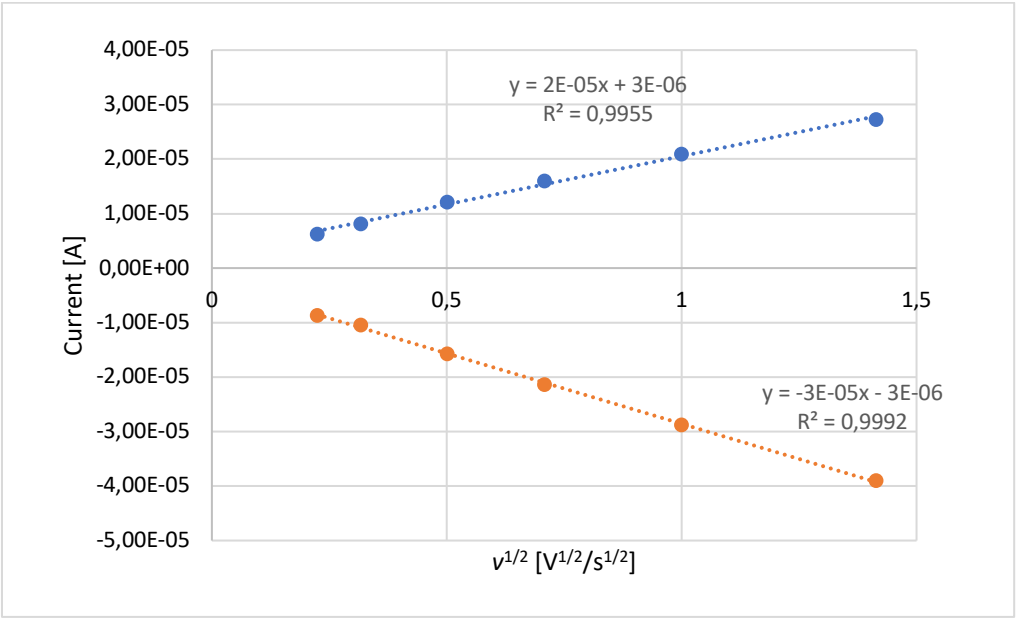

Figure S103. I_p versus $v^{1/2}$ plot of the anodic (blue) and cathodic (orange) peak currents in cyclic voltammograms of **11a**.

Table S26. Electrochemical data for the redox couple of complex **11b** vs Fc/Fc^+ in THF/ [nPr$_4$N][BARF]

Scan rate v	E_{pa} vs Fc/Fc^+ [V]	E_{pc} vs Fc/Fc^+ [V]	E^0 vs Fc/Fc^+ [V]	ΔE_p [V]	i_{pa}/i_{pc}
50 mV/s	-1.045	-1.115	-1.080	0.070	0.99
100 mV/s	-1.039	-1.115	-1.077	0.076	0.99
250 mV/s	-1.038	-1.118	-1.078	0.080	0.98
500 mV/s	-1.032	-1.118	-1.075	0.086	0.97
1000 mV/s	-1.027	-1.126	-1.076	0.099	0.96
2000 mV/s	-1.022	-1.130	-1.076	0.108	0.96

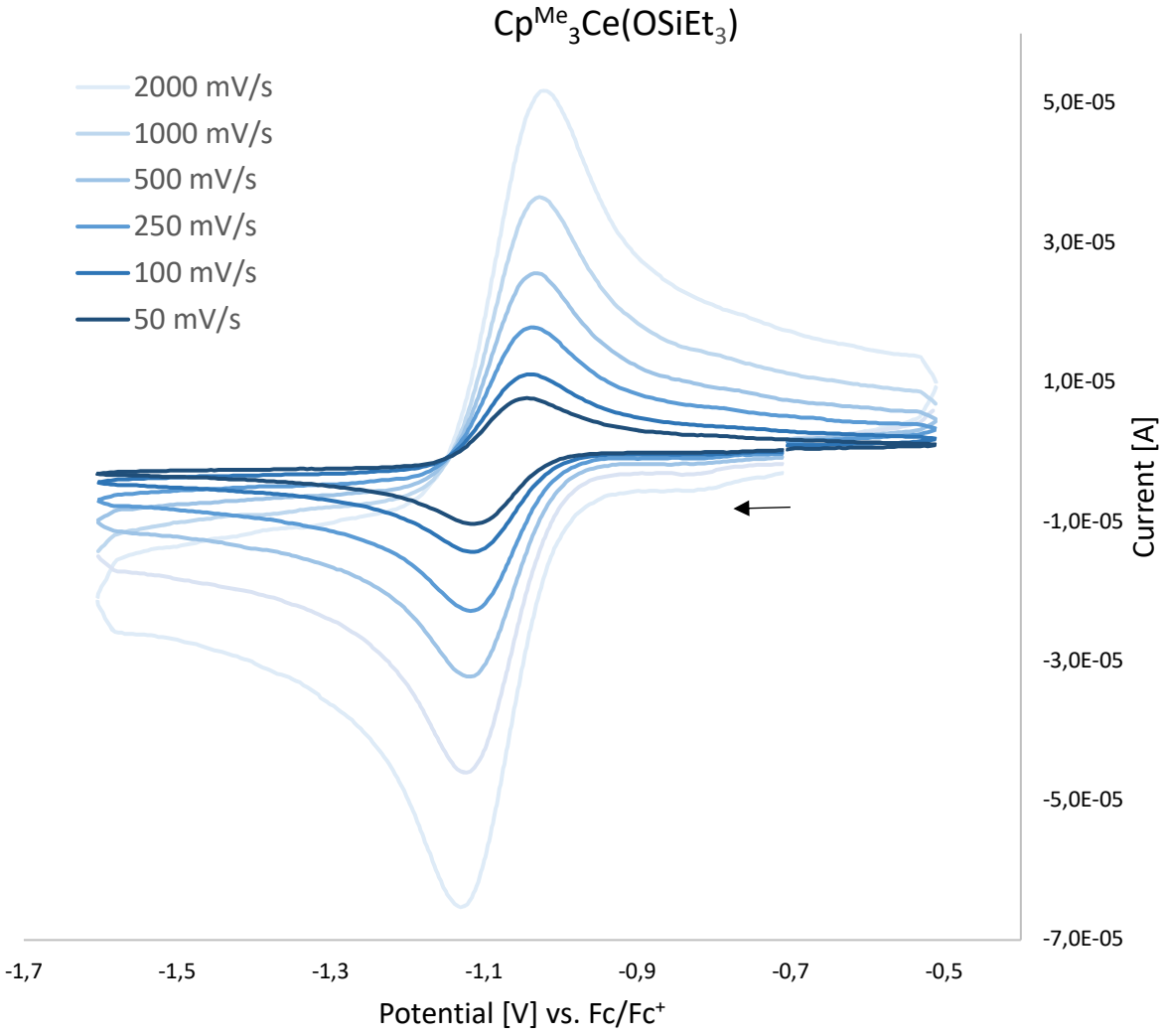

Figure S104. Cerium(III/IV) redox couple of **11b** vs Fc/Fc^+ in THF obtained at different scan rates; arrow indicates initial scan direction; c(analyte) 1mM, c(electrolyte) 0.1 M [nPr$_4$N][BARF].

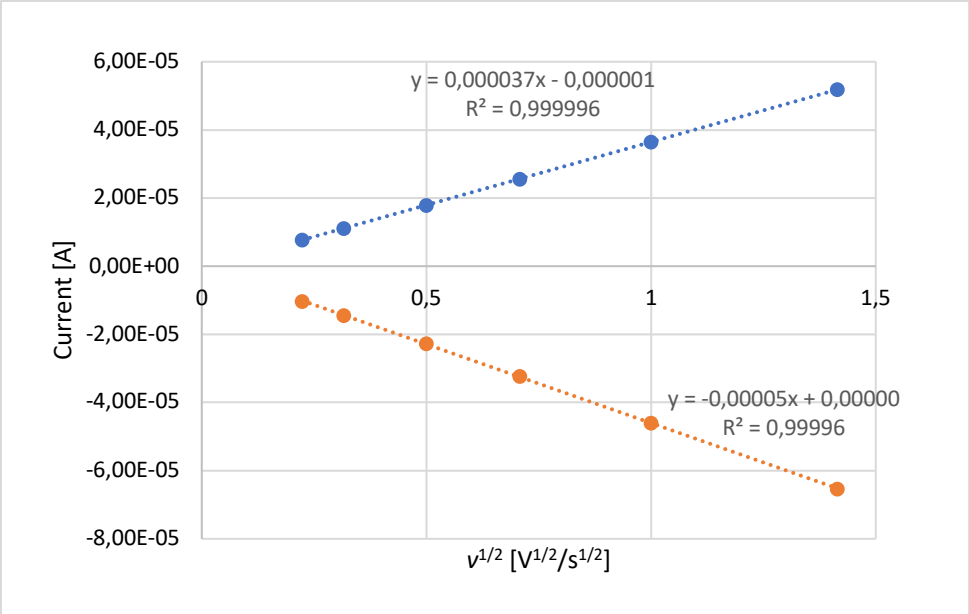

Figure S105. I_p versus $v^{1/2}$ plot of the anodic (blue) and cathodic (orange) peak currents in cyclic voltammograms of **11b**.

Table S27. Electrochemical data for the redox couple of complex **12a** vs Fc/Fc^+ in THF/ [nPr$_4$N][BARF]

Scan rate v	E_{pa} vs Fc/Fc^+ [V]	E_{pc} vs Fc/Fc^+ [V]	E^0 vs Fc/Fc^+ [V]	ΔE_p [V]	i_{pa}/i_{pc}
50 mV/s	-0.948	-1.013	-0.980	0.065	0.92
100 mV/s	-0.946	-1.021	-0.983	0.075	0.93
250 mV/s	-0.946	-1.024	-0.985	0.078	0.93
500 mV/s	-0.943	-1.023	-0.983	0.080	0.95
1000 mV/s	-0.938	-1.027	-0.982	0.089	0.95
2000 mV/s	-0.935	-1.032	-0.983	0.097	0.95

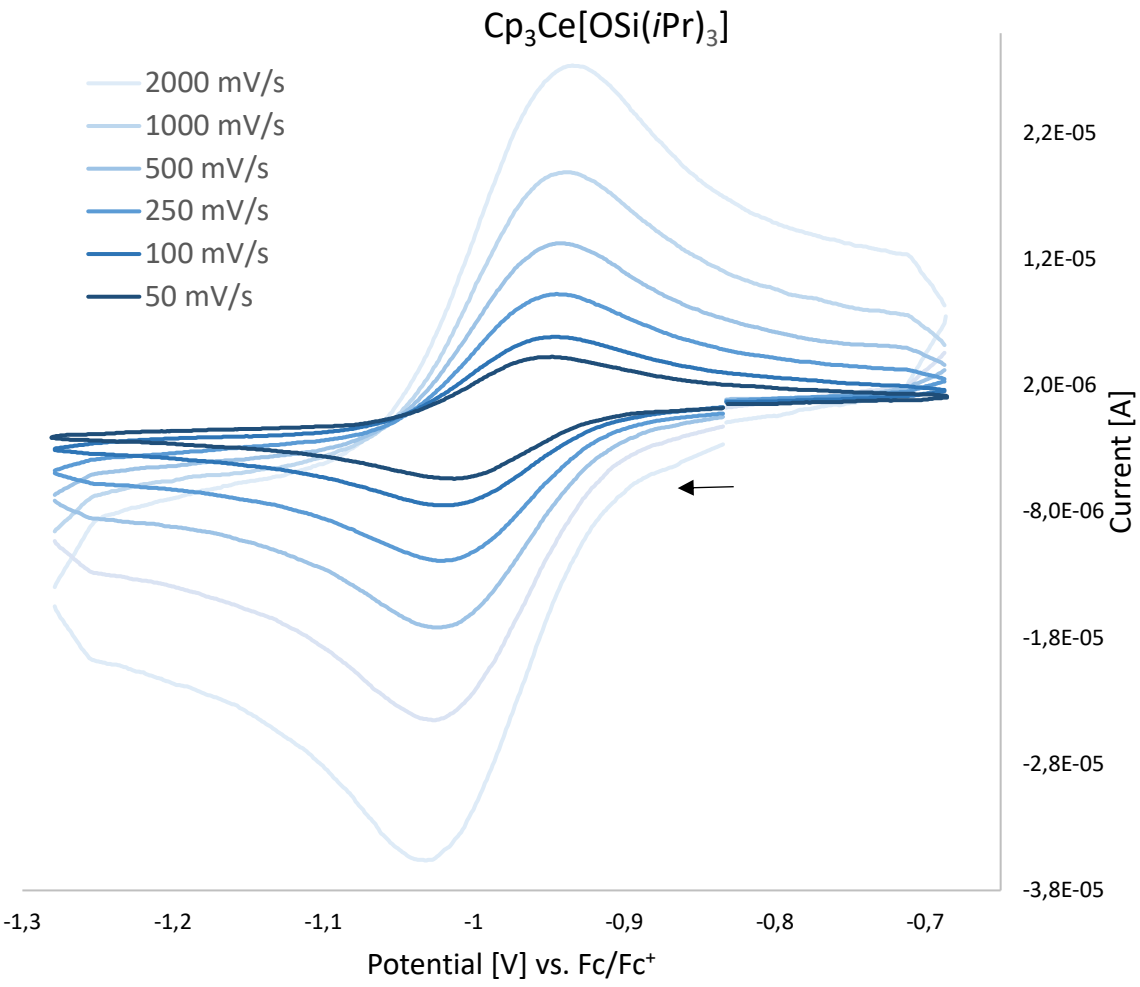

Figure S106. Cerium(III/IV) redox couple of **12a** vs Fc/Fc^+ in THF obtained at different scan rates; arrow indicates initial scan direction; *c*(analyte) 1mM, *c*(electrolyte) 0.1 M [nPr_4N][BARF].

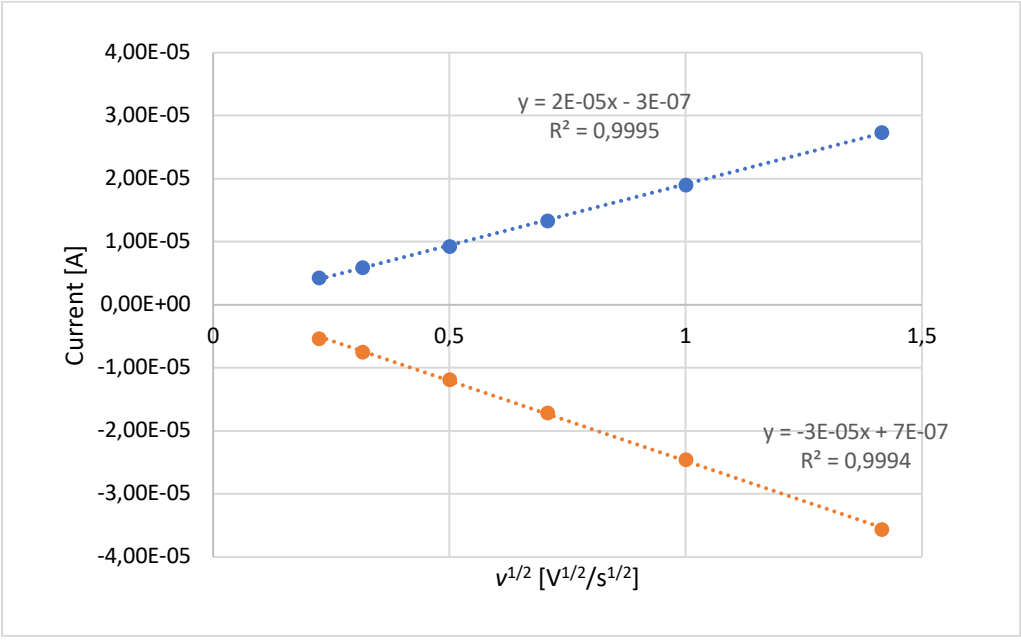

Figure S107. I_p versus $v^{1/2}$ plot of the anodic (blue) and cathodic (orange) peak currents in cyclic voltammograms of **12a**.

Table S28. Electrochemical data for the redox couple of complex **12b** vs Fc/Fc^+ in THF/ [nPr$_4$N][BARF].

Scan rate v	E_{pa} vs Fc/Fc^+ [V]	E_{pc} vs Fc/Fc^+ [V]	E^0 vs Fc/Fc^+ [V]	ΔE_p [V]	i_{pa}/i_{pc}
50 mV/s	-1.009	-1.070	-1.039	0.061	0.99
100 mV/s	-1.002	-1.068	-1.035	0.066	0.98
250 mV/s	-0.995	-1.069	-1.032	0.074	0.97
500 mV/s	-0.990	-1.071	-1.030	0.081	0.96
1000 mV/s	-0.987	-1.071	-1.029	0.084	0.98
2000 mV/s	-0.980	-1.077	-1.028	0.097	0.99

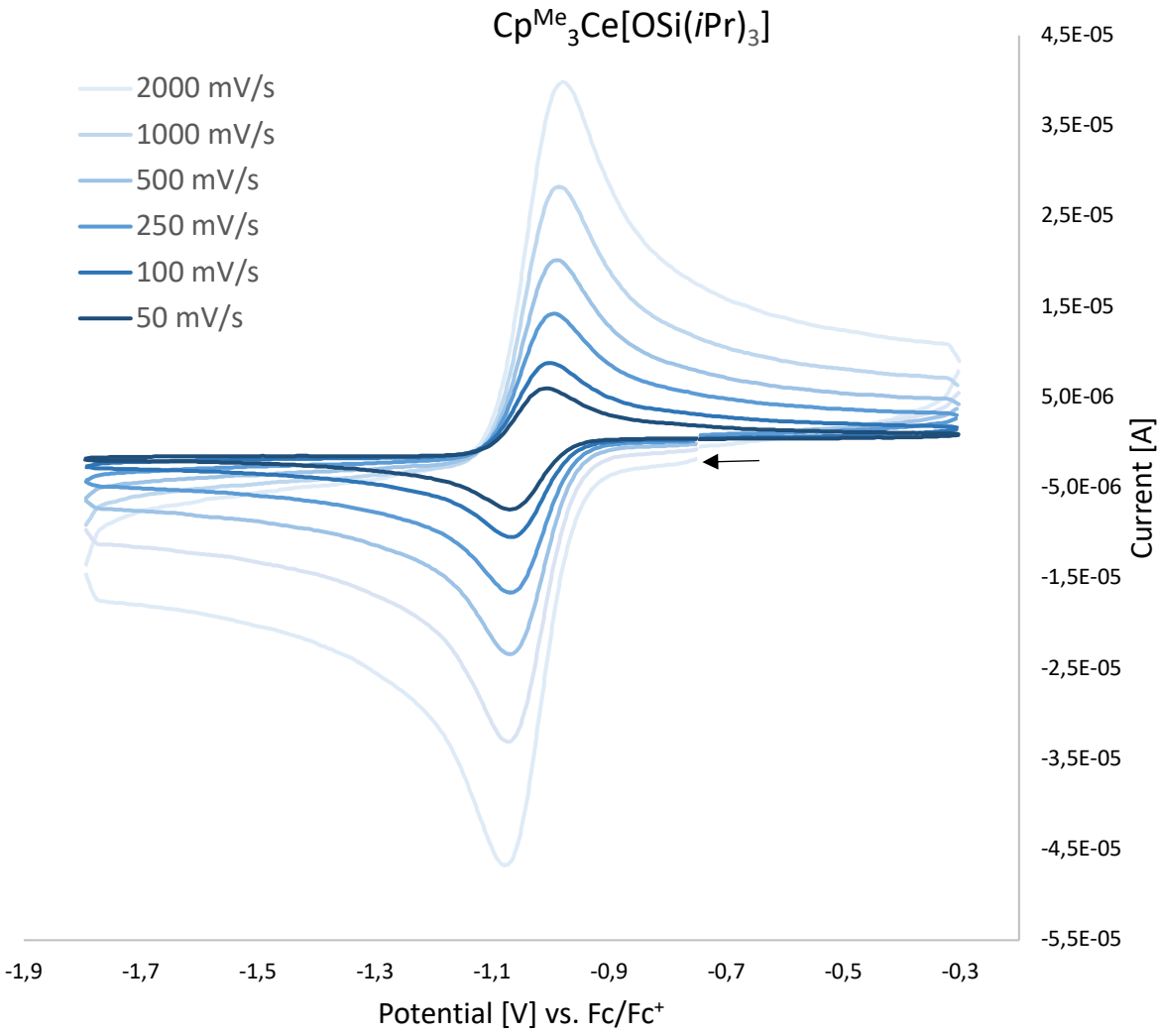

Figure S108. Cerium(III/IV) redox couple of **12b** vs Fc/Fc^+ in THF obtained at different scan rates; arrow indicates initial scan direction; c(analyte) 1mM, c(electrolyte) 0.1 M [nPr$_4$N][BARF].

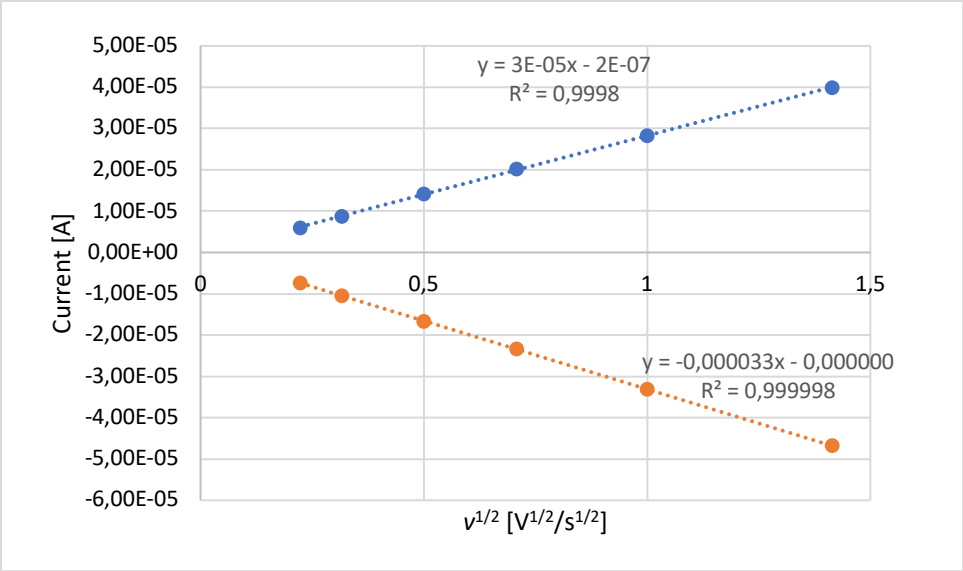

Figure S109. I_p versus $v^{1/2}$ plot of the anodic (blue) and cathodic (orange) peak currents in cyclic voltammograms of **12b**.

Table S29. Electrochemical data for the redox couple of complex **13a** vs Fc/Fc^+ in THF/ [*n*Pr_4N][BARF]

Scan rate *v*	E_{pa} vs Fc/Fc^+ [V]	E_{pc} vs Fc/Fc^+ [V]	E^0 vs Fc/Fc^+ [V]	ΔE_p [V]	i_{pa}/i_{pc}
50 mV/s	-0.903	-0.970	-0.936	0.067	1.00
100 mV/s	-0.900	-0.971	-0.935	0.071	1.00
250 mV/s	-0.899	-0.972	-0.935	0.073	0.99
500 mV/s	-0.899	-0.972	-0.935	0.073	1.00
1000 mV/s	-0.892	-0.976	-0.934	0.084	0.99
2000 mV/s	-0.890	-0.982	-0.936	0.092	0.97

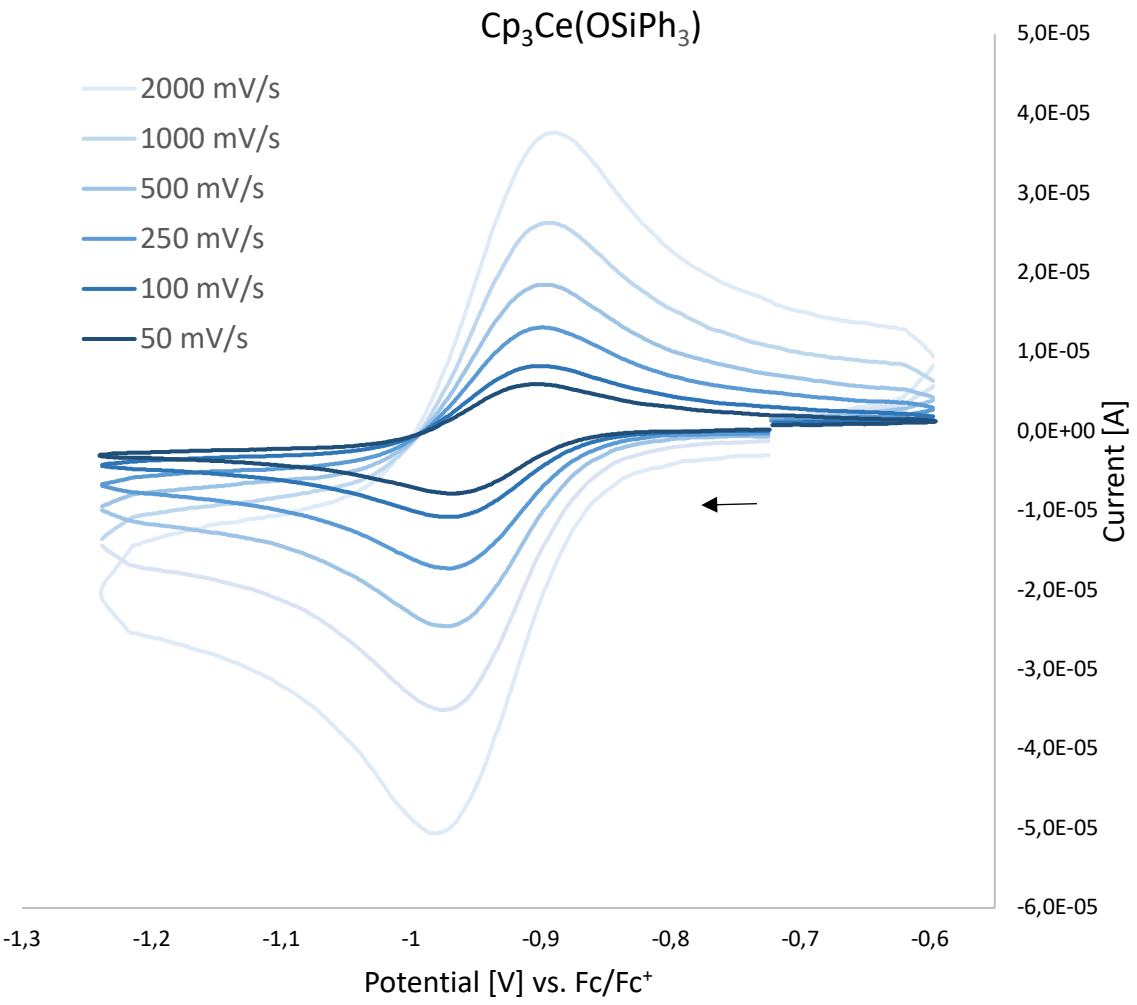

Figure S110. Cerium(III/IV) redox couple of **13a** vs Fc/Fc^+ in THF obtained at different scan rates; arrow indicates initial scan direction; *c*(analyte) 1mM, *c*(electrolyte) 0.1 M [nPr_4N][BARF].

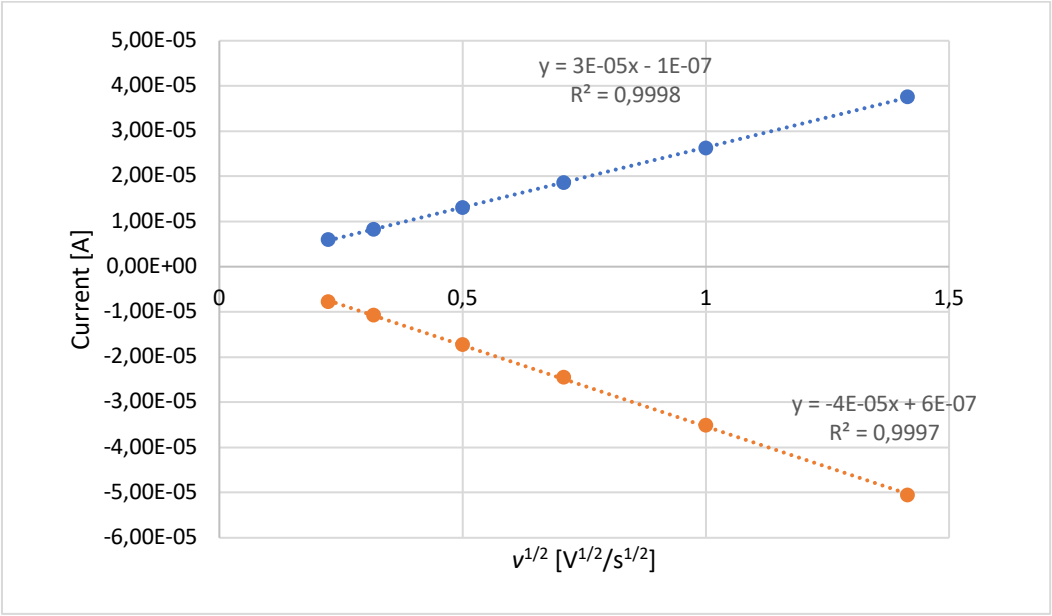

Figure S111. I_p versus $v^{1/2}$ plot of the anodic (blue) and cathodic (orange) peak currents in cyclic voltammograms of **13a**.

Table S30. Electrochemical data for the redox couple of complex **13b** vs Fc/Fc^+ in THF/ [nPr$_4$N][BARF]

Scan rate v	E_{pa} vs Fc/Fc^+ [V]	E_{pc} vs Fc/Fc^+ [V]	E^0 vs Fc/Fc^+ [V]	ΔE_p [V]	i_{pa}/i_{pc}
50 mV/s	-0.981	-1.044	-1.013	0.063	0.93
100 mV/s	-0.974	-1.047	-1.011	0.073	0.96
250 mV/s	-0.968	-1.052	-1.010	0.084	1.00
500 mV/s	-0.965	-1.062	-1.014	0.097	1.00
1000 mV/s	-0.960	-1.074	-1.017	0.114	1.00
2000 mV/s	-0.948	-1.082	-1.015	0.134	0.97

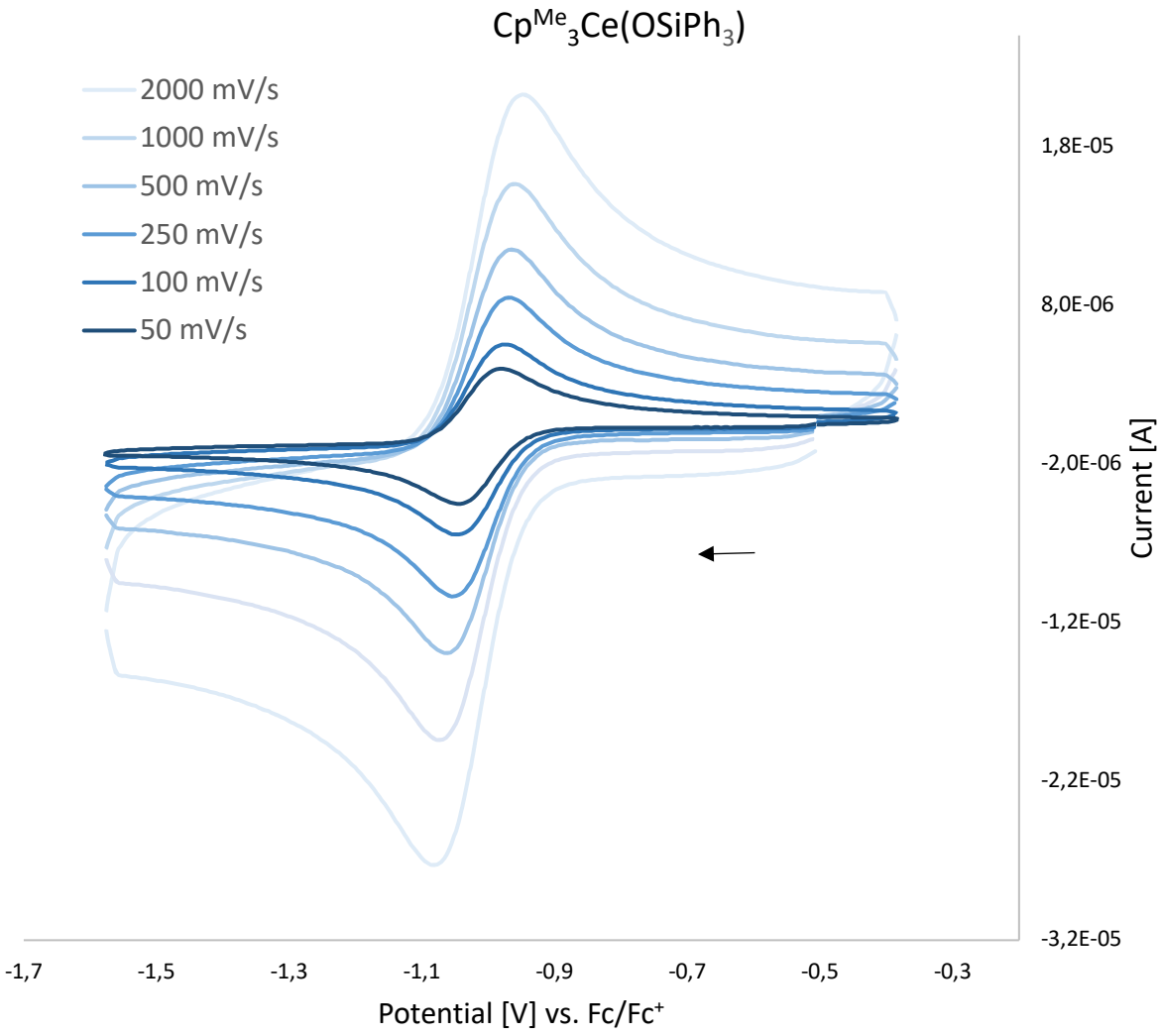

Figure S112. Cerium(III/IV) redox couple of **13b** vs Fc/Fc^+ in THF obtained at different scan rates; arrow indicates initial scan direction; c(analyte) 1mM, c(electrolyte) 0.1 M [nPr$_4$N][BARF].

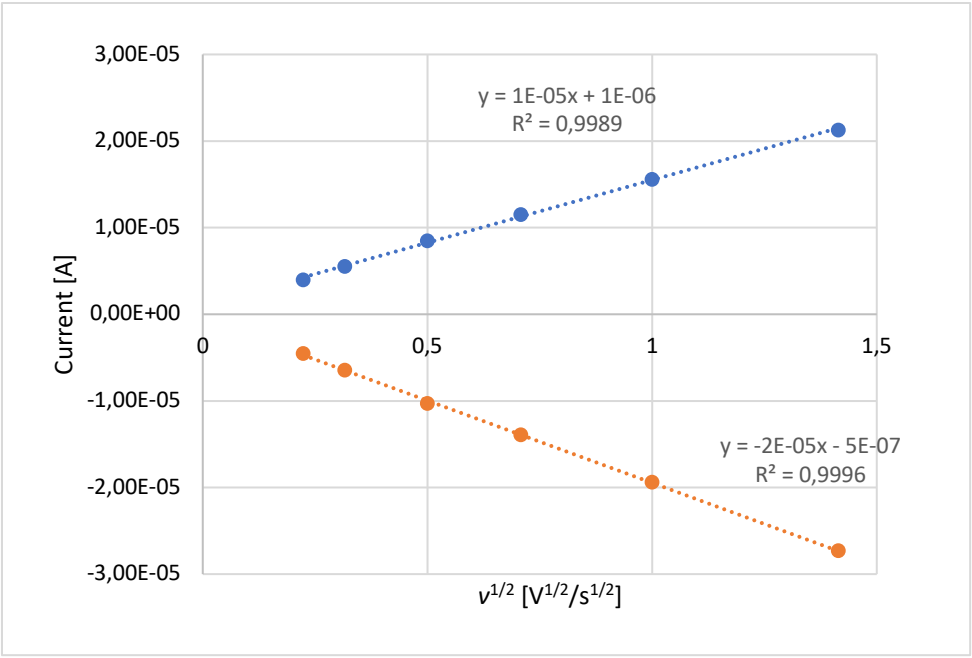

Figure S113. I_p versus $v^{1/2}$ plot of the anodic (blue) and cathodic (orange) peak currents in cyclic voltammograms of **13b**.

Calculation of diffusion coefficient and simulation of cyclic voltammograms

Experimental Conditions for Table S31, Figure S114 and Figure S115.

THF, silver perchlorate ($AgClO_4$), tetrabutylammonium hexafluorophosphate (NBu_4PF_6), and ferrocene were purchased from Alfa Aesar. THF was stored over KOH for one week, heated under reflux over sodium/benzophenone for 24 h, distilled, heated under reflux over potassium under argon for 48 h, and then subjected to a final distillation. NBu_4PF_6 was recrystallized three times from ethanol/water (3:1) and dried at 3 mbar and 100 °C for one week. The supporting electrolyte NBu_4PF_6 was used in 0.1 M concentration. The electrolyte solution was degassed by argon bubbling. For the electrochemical experiments, an Eco Chemie BV Autolab PG-STAT100 (Metrohm, Filderstadt, Germany) was used with control software GPES (v. 4.9). Cyclic voltammograms were recorded at 17 °C with a glassy carbon electrode. All experiments were carried out under argon with a gas-tight full-glass cell in a three-electrode arrangement.[2] *iR* drop was compensated by positive feedback through the GPES software. Cyclic voltammetric scan rates ranged from 0.05 to 2 V s^{-1}. All CV experiments were carried out for several concentrations. Background was recorded for various scan rates in the first part of an experiment session for later use. Then substrate was added in the form of several aliquots from a stock solution. *i-E*-curves were recorded at all scan rates after each addition. Finally, background currents were subtracted from these data. E^0 was determined vs. a Ag/Ag^+ (0.01 M in MeCN/0.1 M NBu_4PF_6) electrode with a Haber-Luggin dual reference electrode system.[3] The values were rescaled to the Fc/Fc^+ standard (E^0_{Fc/Fc^+} = 163 ± 1 mV). The diffusion coefficient was calculated with Randles-Sevcik-equation for n=1 and A=6.4 mm^2. The electroactive surface was determined from cyclic voltammetric peak currents or chronoamperometric currents for Fc in DCM / 0.1 NBu_4PF_6 at 17 °C assuming a diffusion coefficient D(Fc) = 2.06*10^{-5} cm^2/s.[4]

Table S31. Electrochemical data for the redox couple of complex **13b** vs Fc/Fc^+ in THF/Pt/[nBu$_4$N][PF_6]

$(Cp^{Me})_3Ce(IV)OSiPh_3$ 13b THF/Pt/[nBu$_4$N][PF_6] vs. Fc/Fc^+

		c [mmol/L]							c [mmol/L]				
v [V/s]	E_{Ox} [V]	0.10	0.20	0.29	0.38	0.38	v [V/s]	E_{Red} [V]	0.10	0.20	0.29	0.38	0.38
v = 0.05		-0.895	-0.895	-0.895	-0.896	-0.896	0.05		-0.964	-0.964	-0.964	-0.965	-0.962
0.1		-0.896	-0.893	-0.893	-0.892	-0.893	0.1		-0.965	-0.965	-0.967	-0.966	-0.963
0.2		-0.893	-0.895	-0.893	-0.891	-0.893	0.2		-0.965	-0.966	-0.967	-0.969	-0.965
0.5		-0.893	-0.893	-0.891	-0.889	-0.897	0.5		-0.965	-0.967	-0.969	-0.971	-0.962
1		-0.890	-0.886	-0.884	-0.885	-0.892	1		-0.968	-0.977	-0.975	-0.976	-0.962
2		-0.895	-0.888	-0.884	-0.879	-0.897	2		-0.973	-0.975	-0.979	-0.980	-0.962
v [V/s]	ΔE [V]	0.10	0.20	0.29	0.38	0.38	v [V/s]	I_{Red} / I_{ox}	0.10	0.20	0.29	0.38	0.38
0.05		0.069	0.069	0.069	0.069	0.066	0.05		0.91	0.93	0.94	0.93	0.92
0.1		0.069	0.072	0.074	0.074	0.070	0.1		0.95	0.96	0.96	0.96	0.95
0.2		0.072	0.072	0.074	0.078	0.072	0.2		0.97	0.97	0.97	0.96	0.97
0.5		0.072	0.074	0.078	0.082	0.065	0.5		0.97	0.97	0.96	0.94	0.97
1		0.078	0.091	0.091	0.091	0.069	1		0.99	0.96	0.96	0.94	0.96
2		0.078	0.087	0.095	0.102	0.065	2		0.96	0.94	0.93	0.93	0.94
v [V/s]	E^0 [V]	0.10	0.20	0.29	0.38	0.38	v [V/s]	i_{Norm}	0.10	0.20	0.29	0.38	0.38
0.05		-0.929	-0.929	-0.929	-0.930	-0.929	0.05		0.91	0.87	0.84	0.75	0.71
0.1		-0.930	-0.929	-0.930	-0.929	-0.928	0.1		0.88	0.85	0.82	0.75	0.69
0.2		-0.929	-0.930	-0.930	-0.930	-0.929	0.2		0.87	0.83	0.80	0.74	0.67
0.5		-0.929	-0.930	-0.930	-0.930	-0.929	0.5		0.86	0.83	0.80	0.73	0.65
1		-0.929	-0.931	-0.929	-0.930	-0.927	1		0.85	0.82	0.78	0.71	0.65
2		-0.934	-0.931	-0.931	-0.929	-0.929	2		0.82	0.78	0.75	0.68	0.67
Ø		-0.930		±		0.001							
DPV		-0.929											

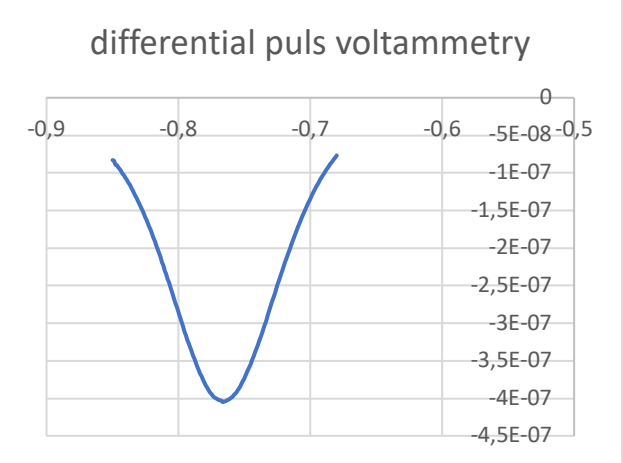

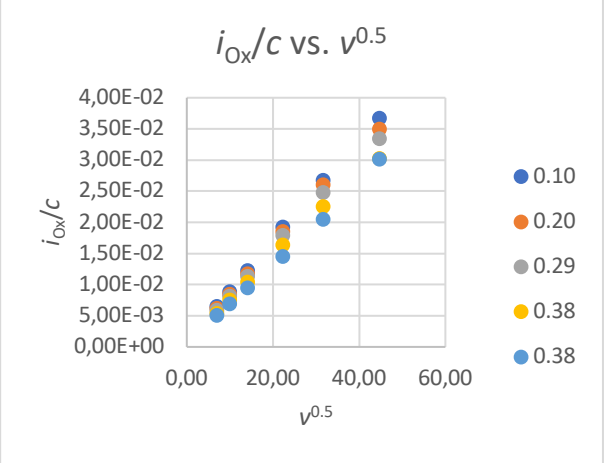

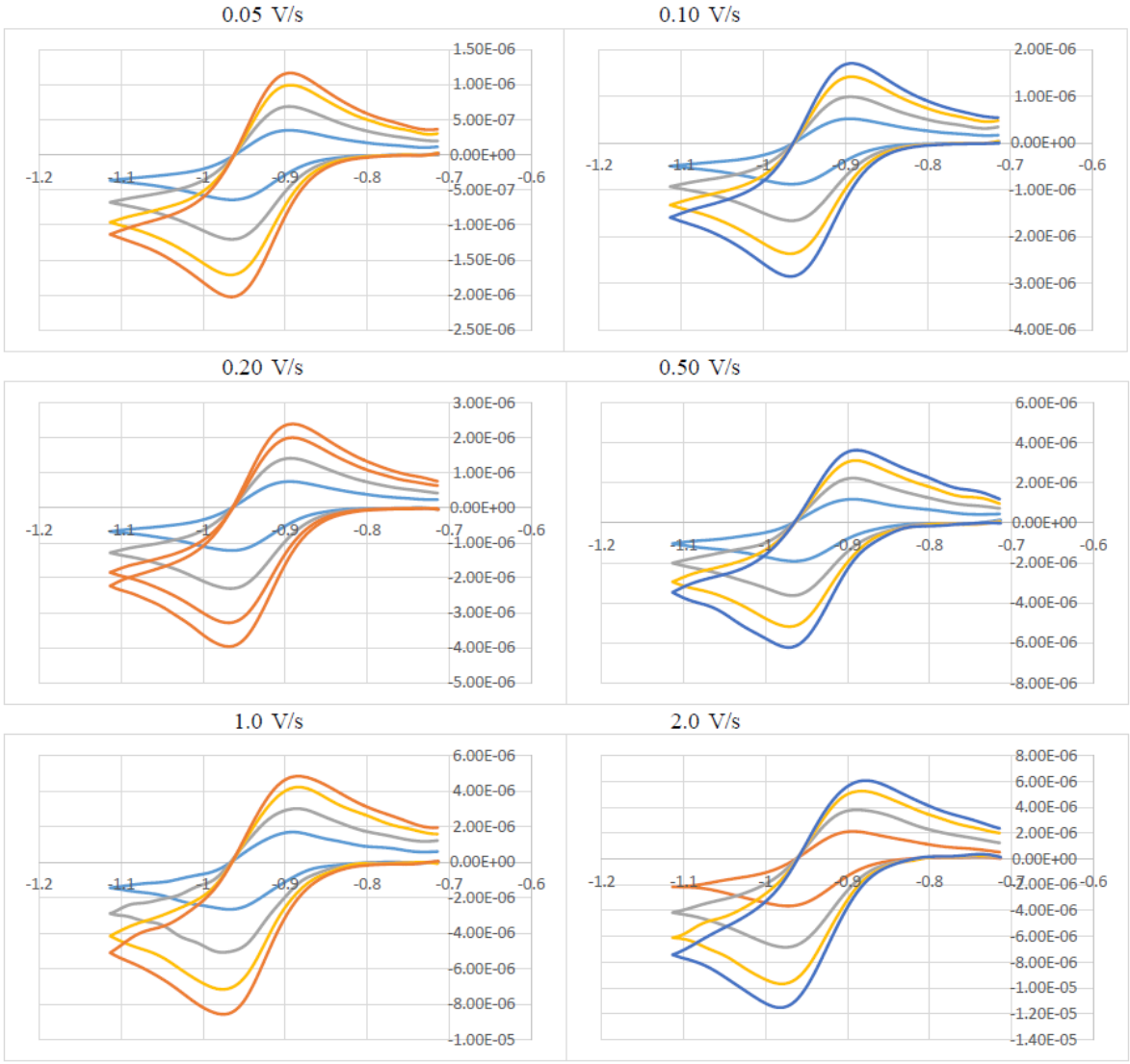

Figure S114. Electrochemical data for the redox couple of complex **13b** vs Fc/Fc^{+} in THF/Pt/[nBu$_4$N][PF$_6$].

Calculation of diffusion coefficient and simulation of cyclic voltammograms

Simulations were performed with DigiSim (v. 2.1) under the assumption of planar, semi-infinite diffusion and Butler-Volmer kinetics for the electron transfers with a step width of 1 mV. The pre-equilibrium functionality of the software was set to ``chemical reactions only''.

$(Cp^{Me})_3Ce(IV)OSiPh_3$ THF/Pt/[nBu$_4$N][PF$_6$]

A [mm^2]	6.4
k_s [cm/s]	0.03
α [eV]	0.5
D [10^{-6} cm^2/s]	2.75
E^0 [V]	-0.930

A	electrochemical surface area of electrode
k_s	rate constant electron transfer
α	electron transfer coefficient
D	diffusion coefficient

Concentration: 9.92E-05 mol/L

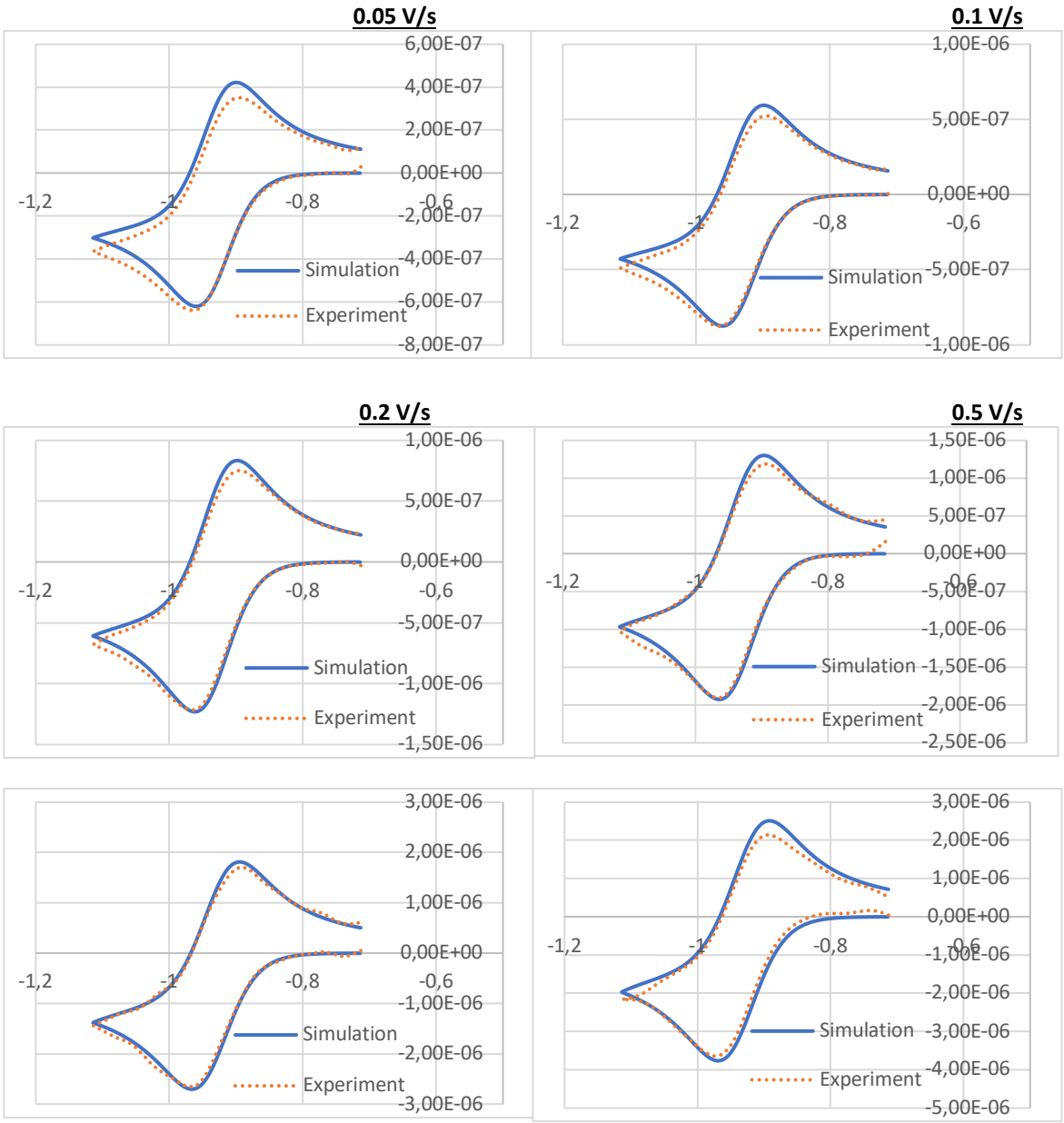

Figure S115. Calculation of diffusion coefficient and simulation of cyclic voltammograms of **13b** in THF, electrolyte [nBu$_4$N][PF$_6$].

IR Spectra

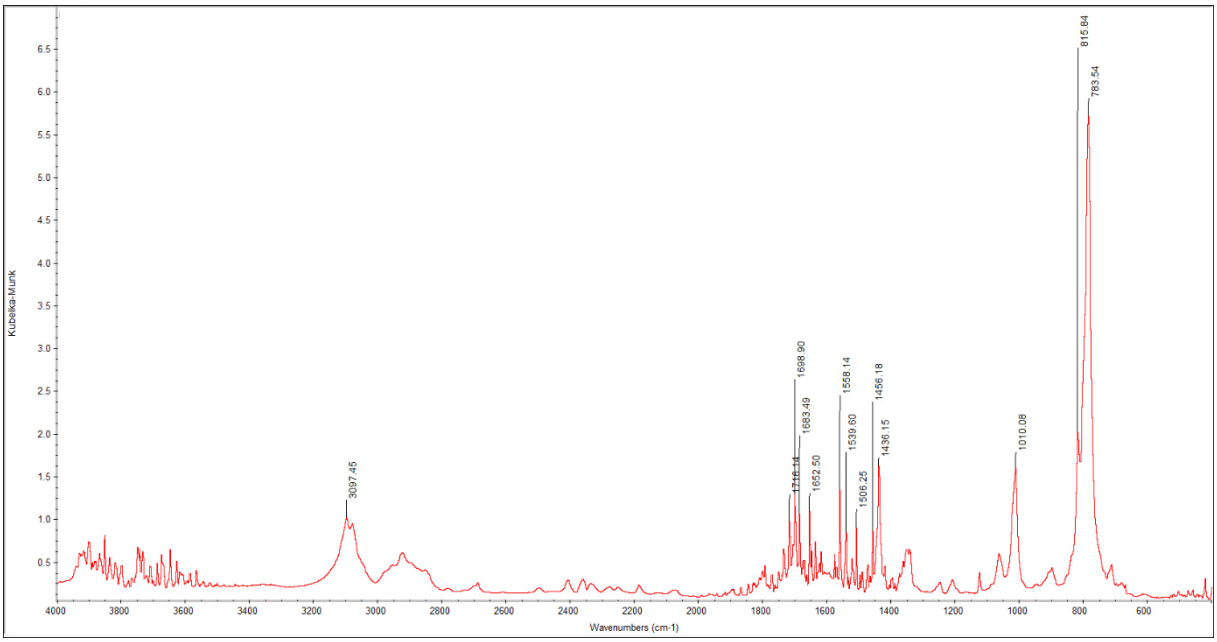

Figure S116. DRIFT spectrum of Cp_3CeBr (**3a**).

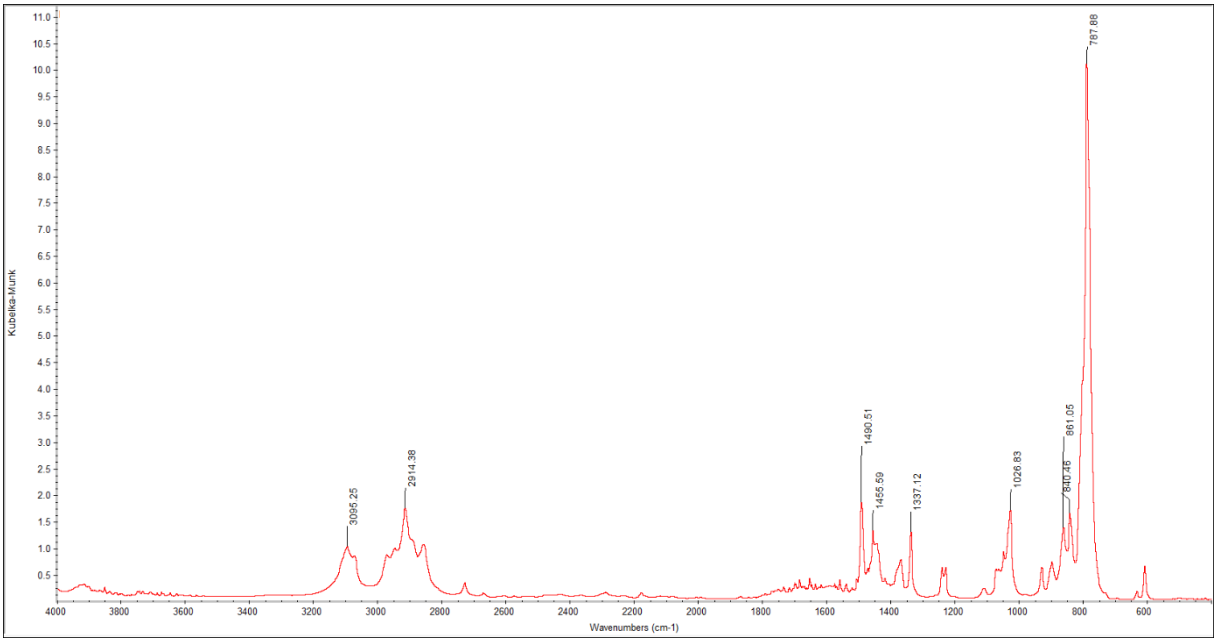

Figure S117. DRIFT spectrum of Cp^{Me}_3CeBr (**3b**).

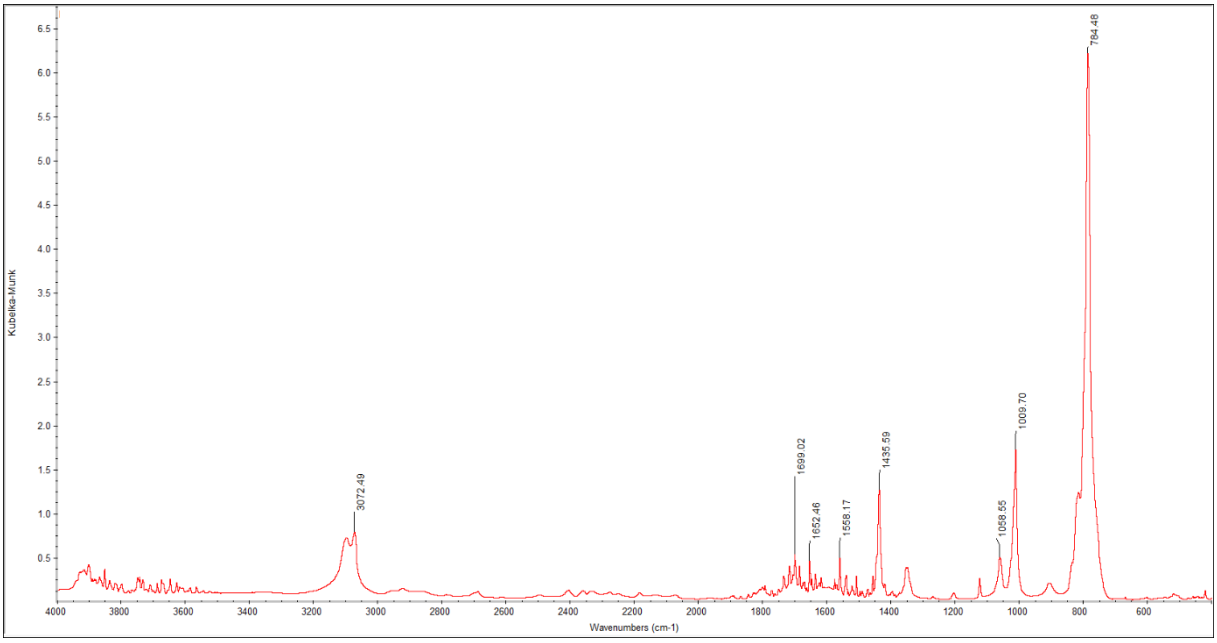

Figure S118. DRIFT spectrum of Cp_3CeI (**4a**).

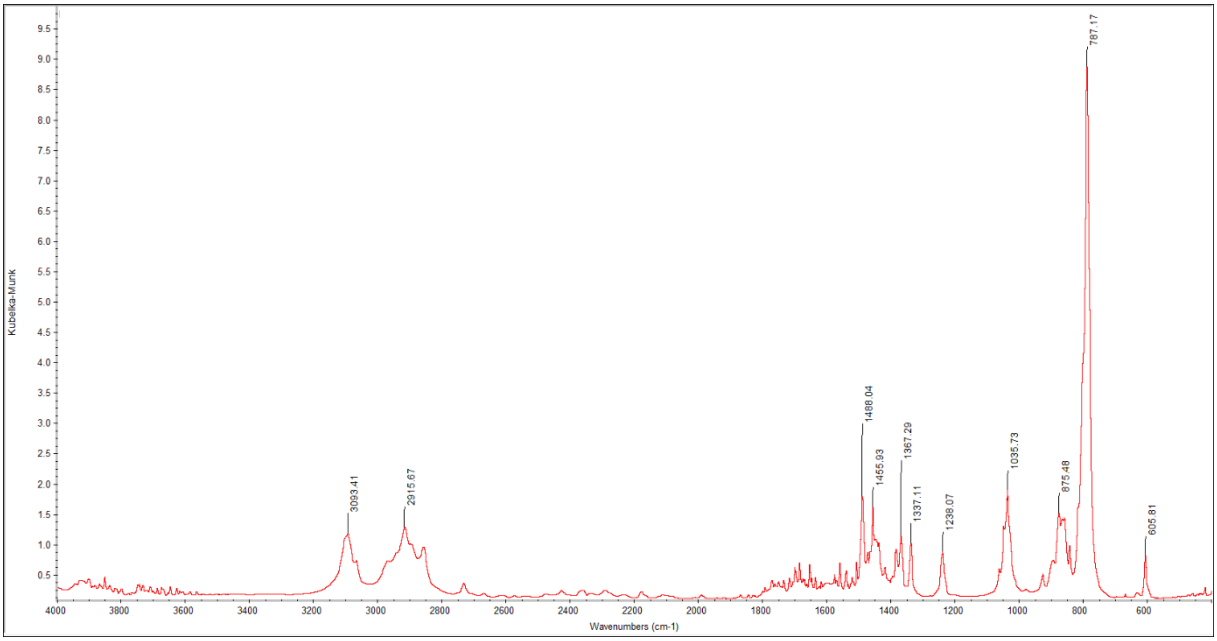

Figure S119. DRIFT spectrum of Cp^{Me}_3CeI (**4b**).

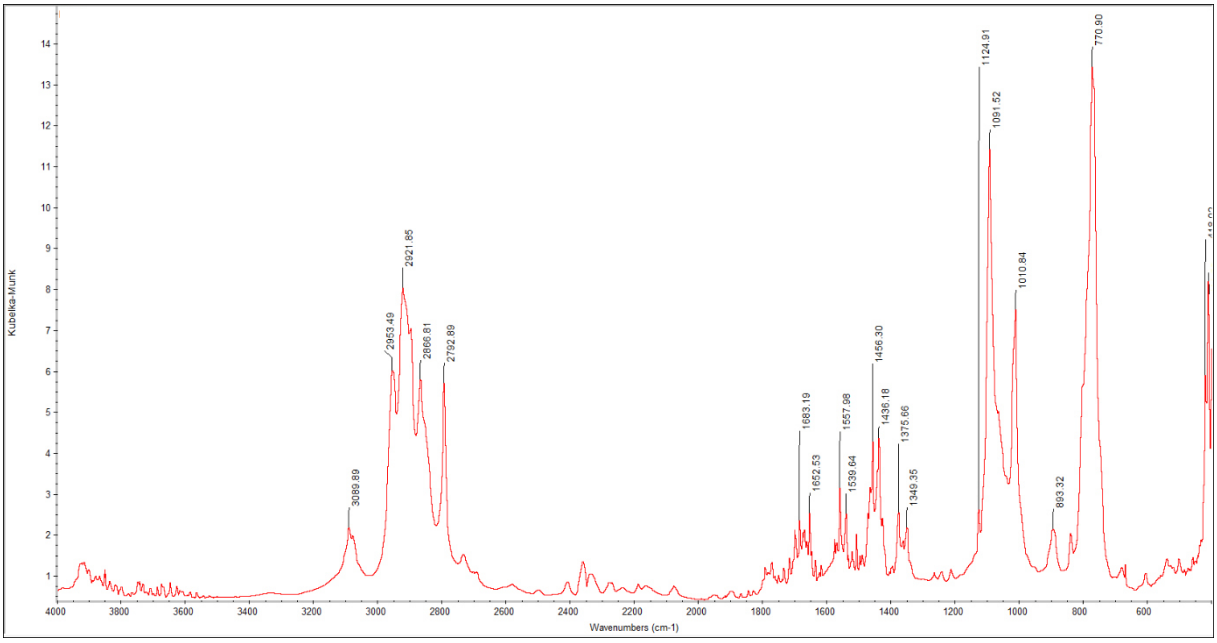

Figure S120. DRIFT spectrum of $Cp_3Ce(OMe)$ (**5a**).

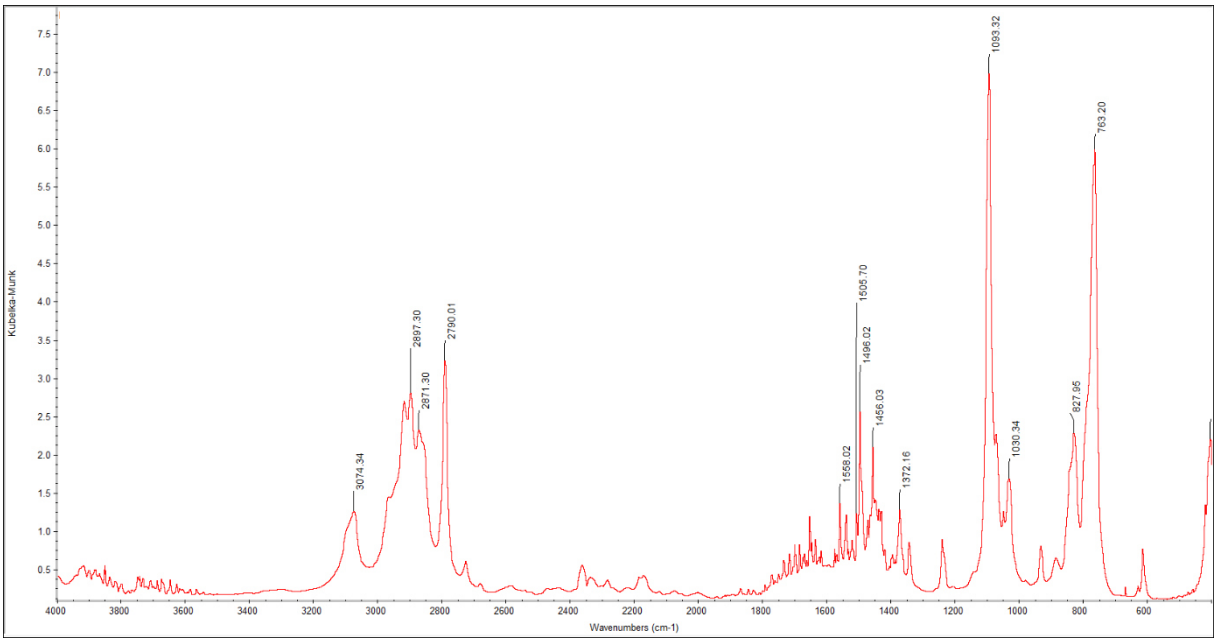

Figure S121. DRIFT spectrum of $Cp^{Me}_3Ce(OMe)$ (**5b**).

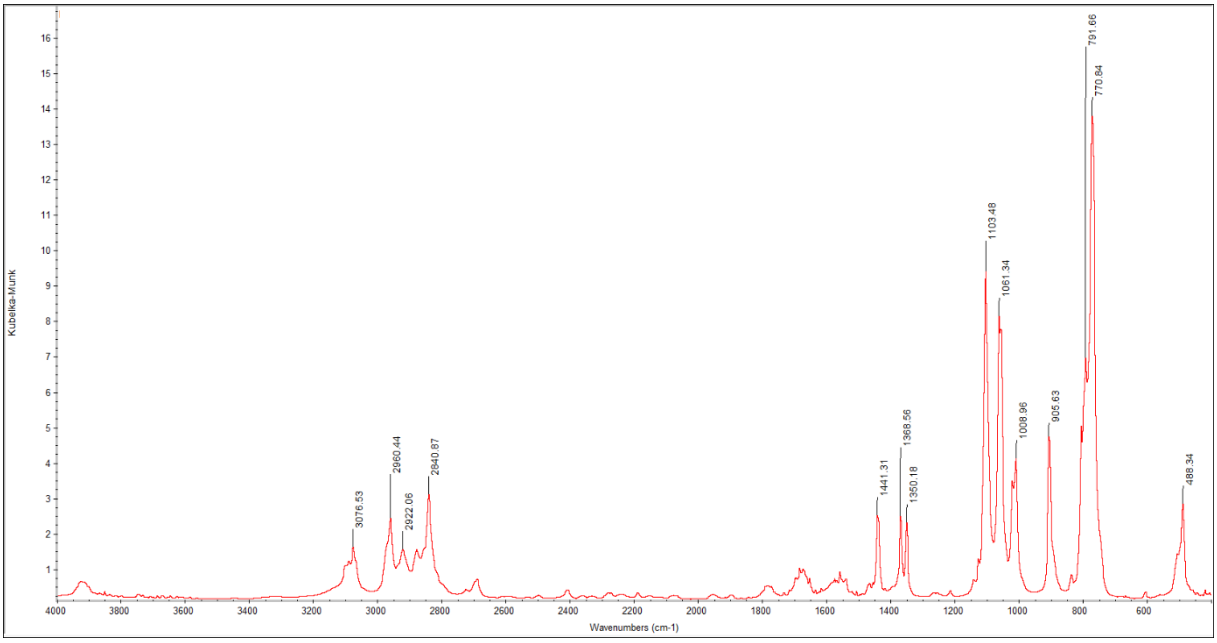

Figure S122. DRIFT spectrum of $Cp_3Ce(OEt)$ (**6a**).

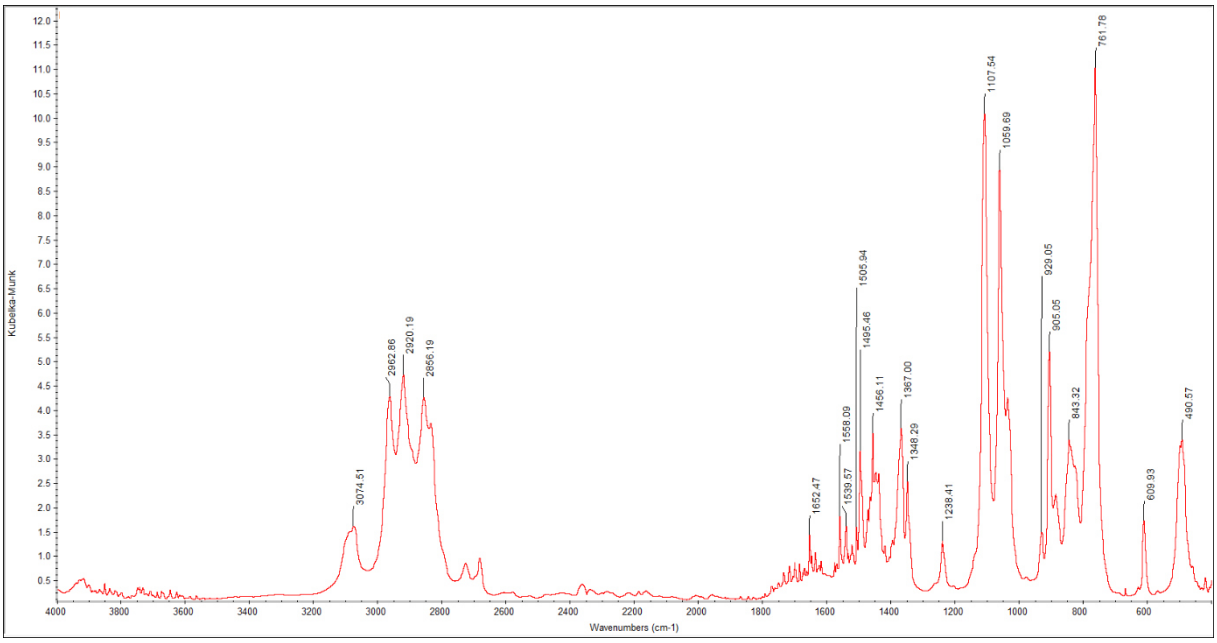

Figure S123. DRIFT spectrum of $Cp^{Me}_3Ce(OEt)$ (**6b**).

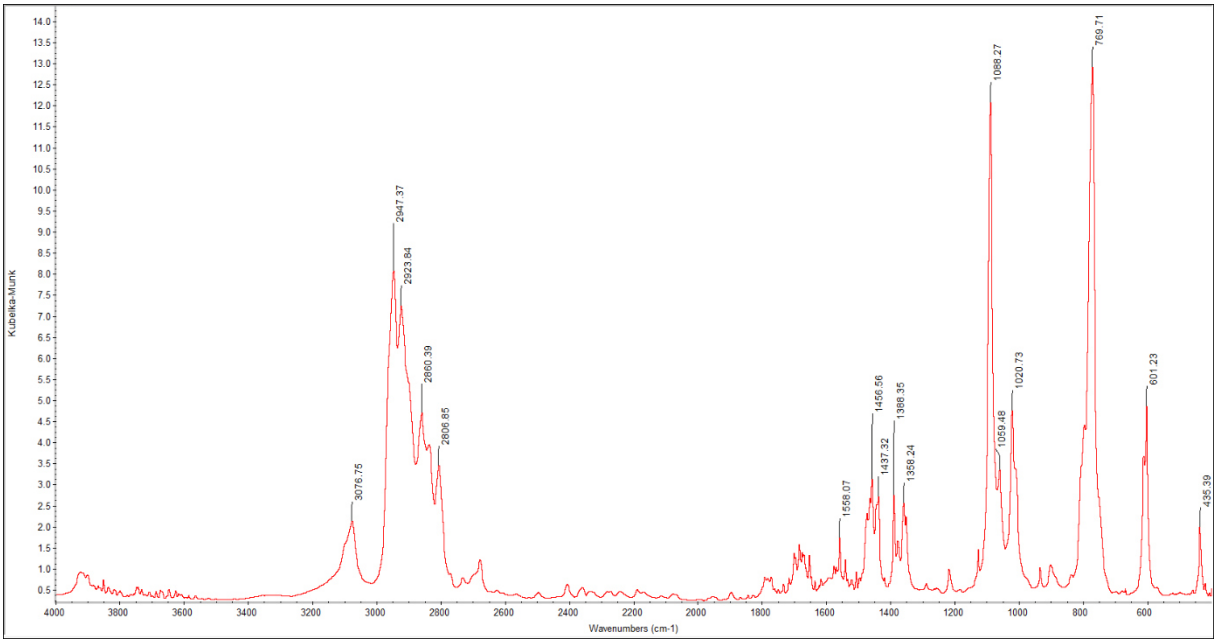

Figure S124. DRIFT spectrum of $Cp_3Ce(OCH_2tBu)$ (**7a**).

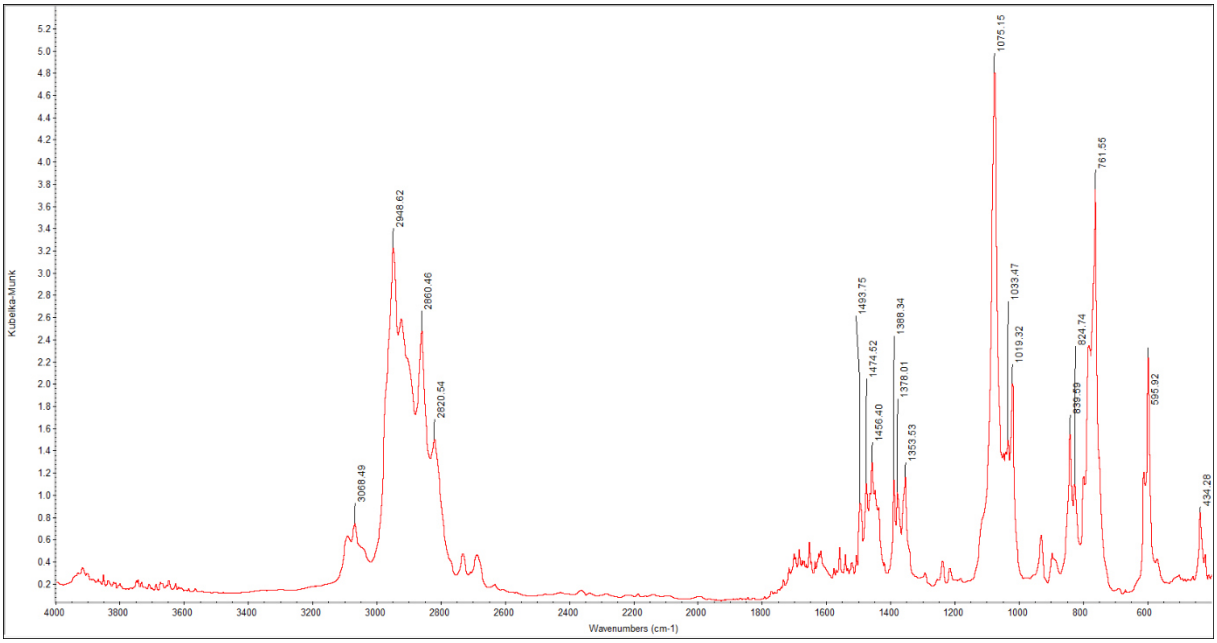

Figure S125. DRIFT spectrum of $Cp^{Me}{}_3Ce(OCH_2tBu)$ (**7b**).

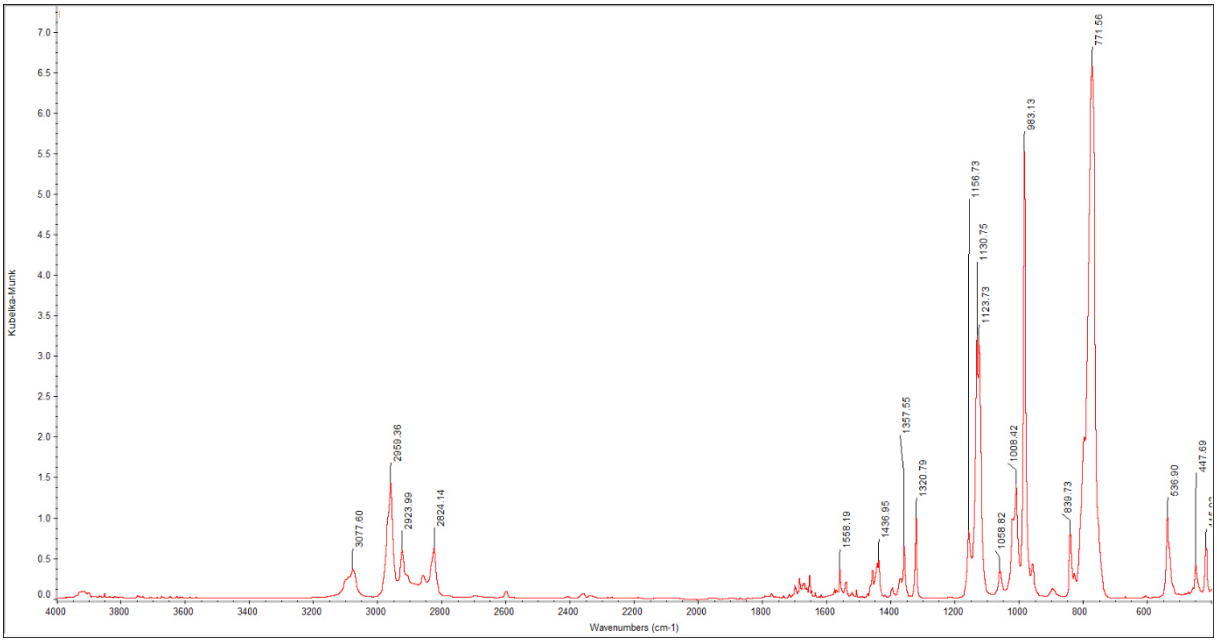

Figure S126. DRIFT spectrum of $Cp_3Ce(O\textit{i}Pr)$ (**8a**).

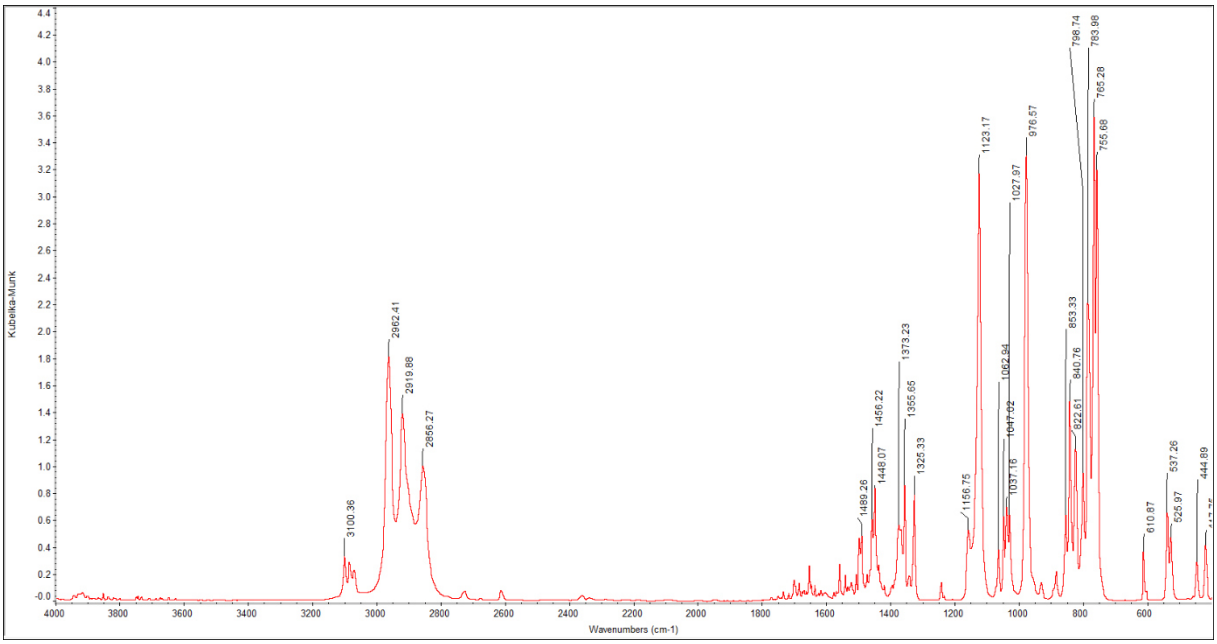

Figure S127. DRIFT spectrum of $Cp^{Me}{}_3Ce(O\textit{i}Pr)$ (**8b**).

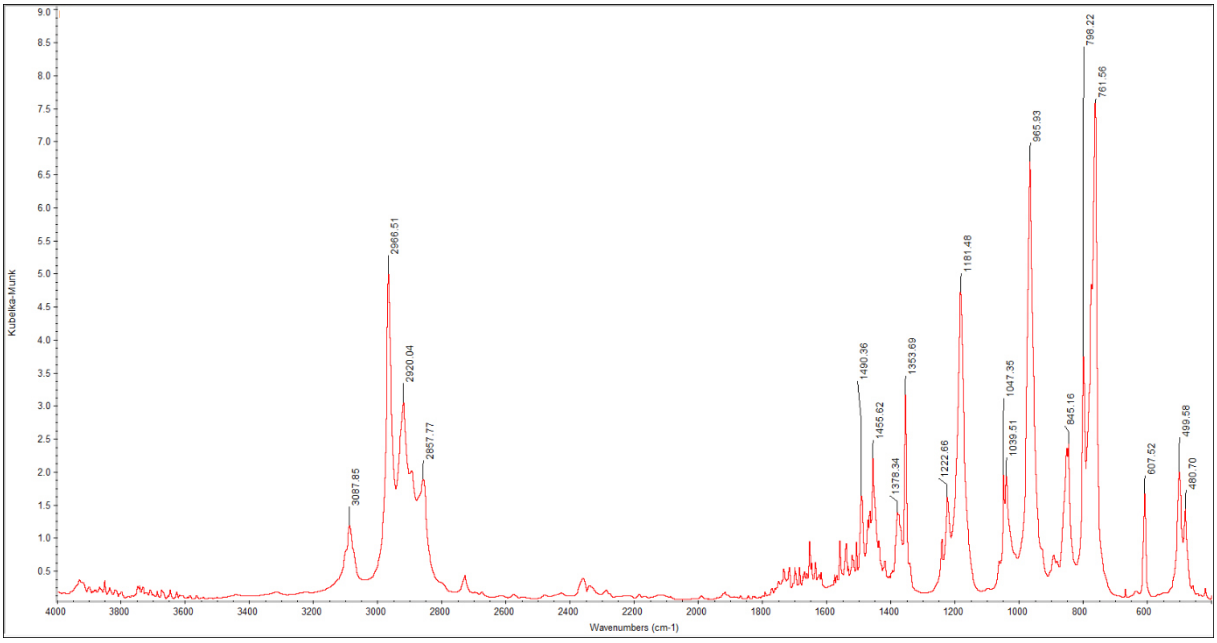

Figure S128. DRIFT spectrum of $Cp^{Me}_3Ce(O\textit{t}Bu)$ (**9b**).

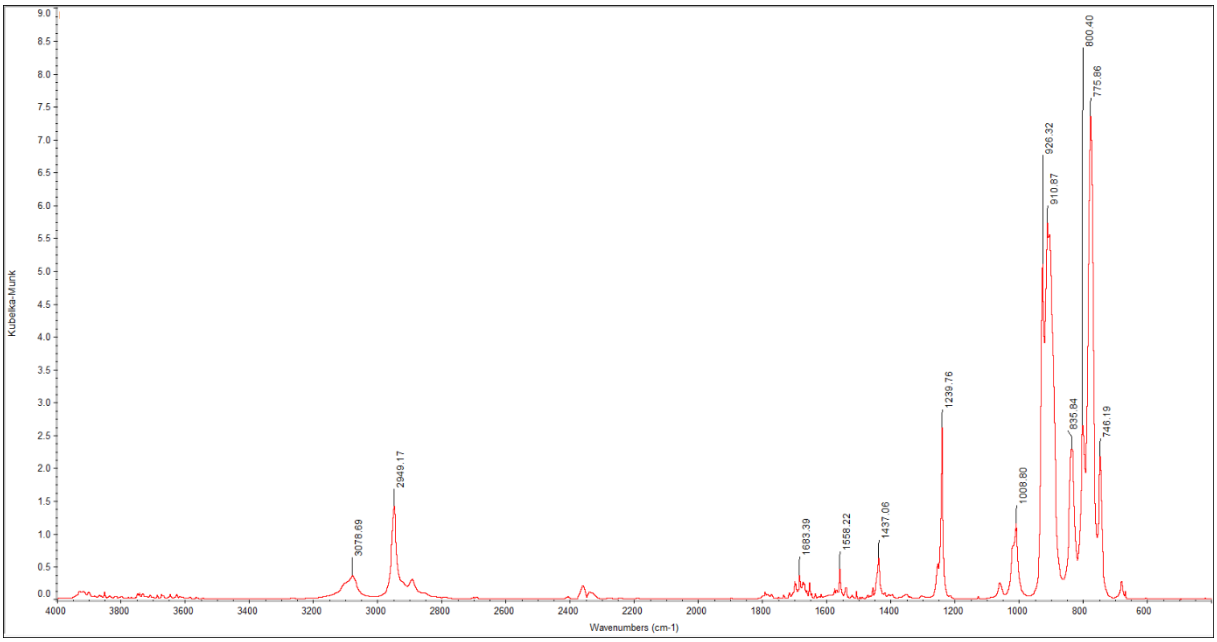

Figure S129. DRIFT spectrum of $Cp_3Ce(OSiMe_3)$ (**10a**).

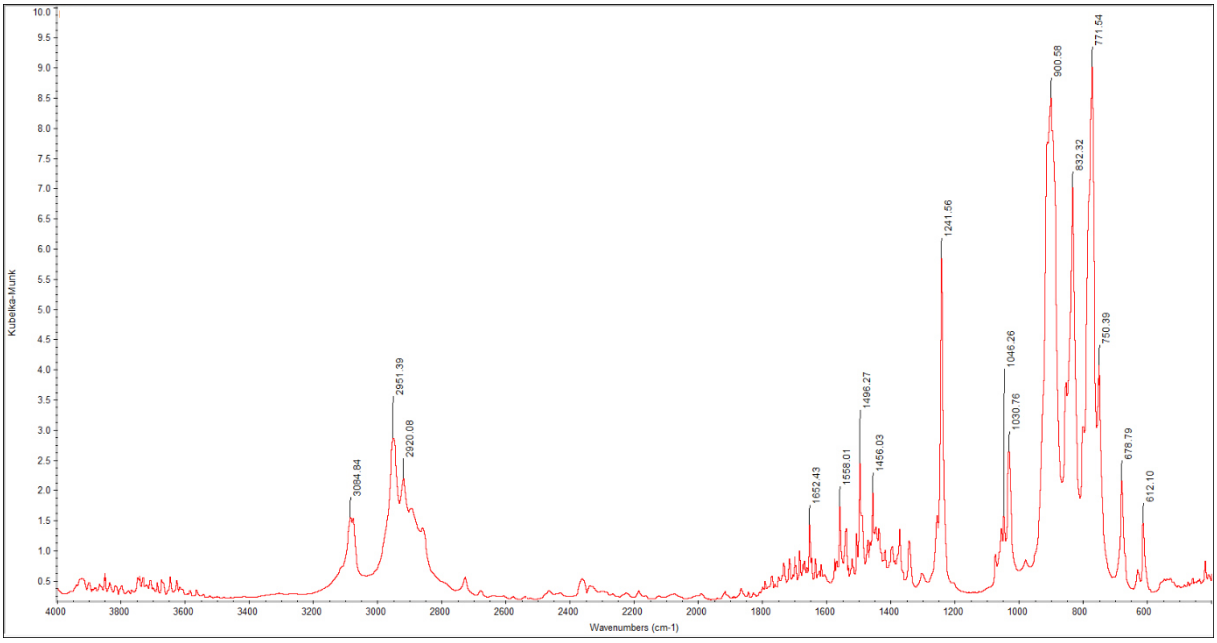

Figure S130. DRIFT spectrum of $Cp^{Me}_3Ce(OSiMe_3)$ (**10b**).

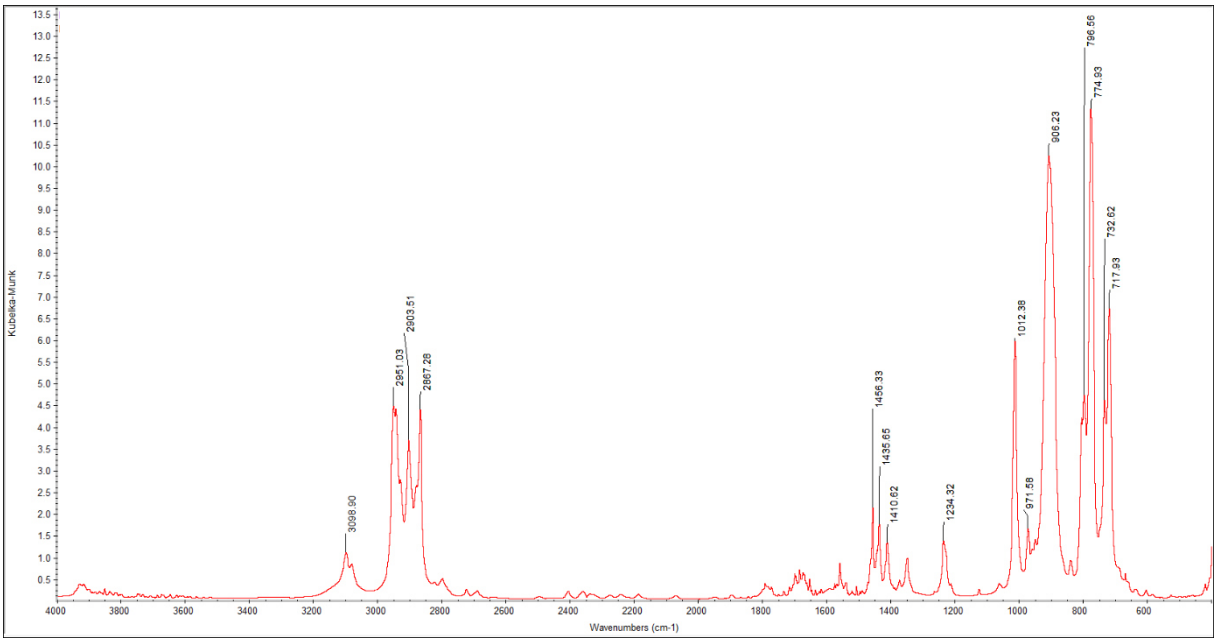

Figure S131. DRIFT spectrum of $Cp_3Ce(OSiEt_3)$ (**11a**).

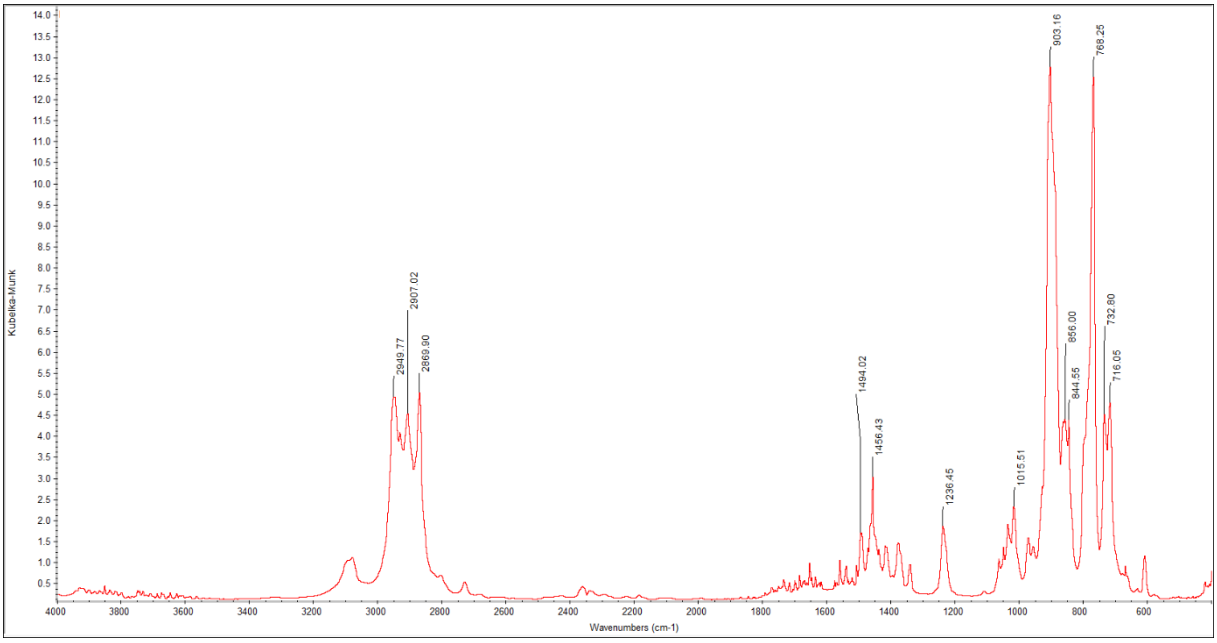

Figure S132. DRIFT spectrum of $Cp^{Me}_3Ce(OSiEt_3)$ (**11b**).

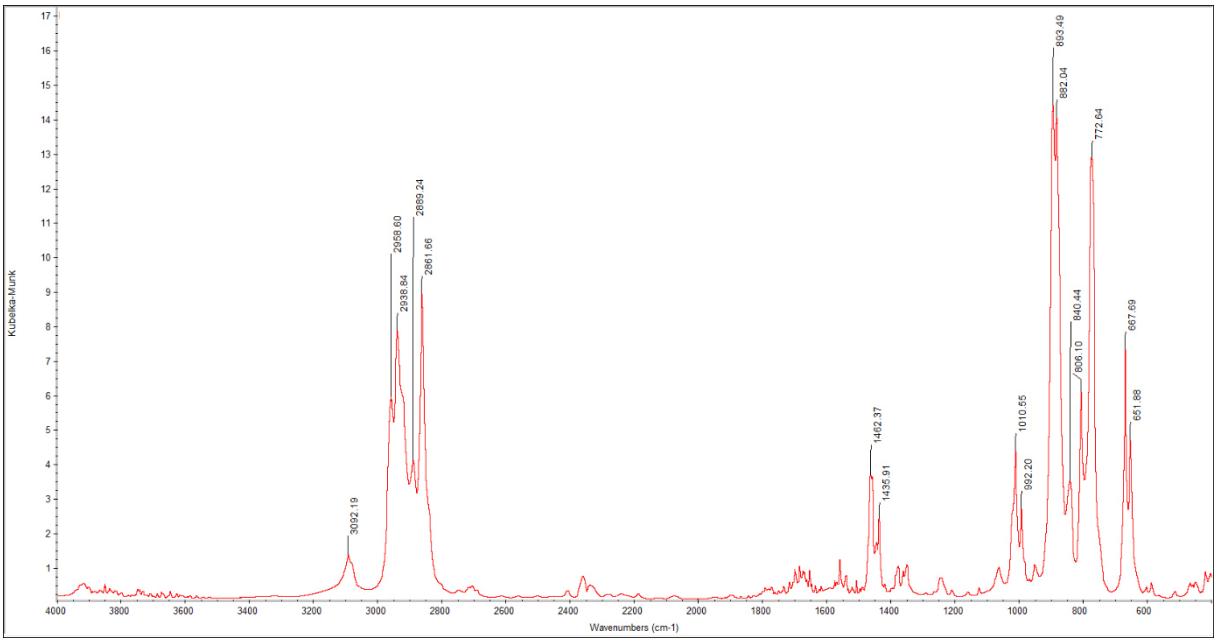

Figure S133. DRIFT spectrum of $Cp_3Ce[OSi(iPr)_3]$ (**12a**).

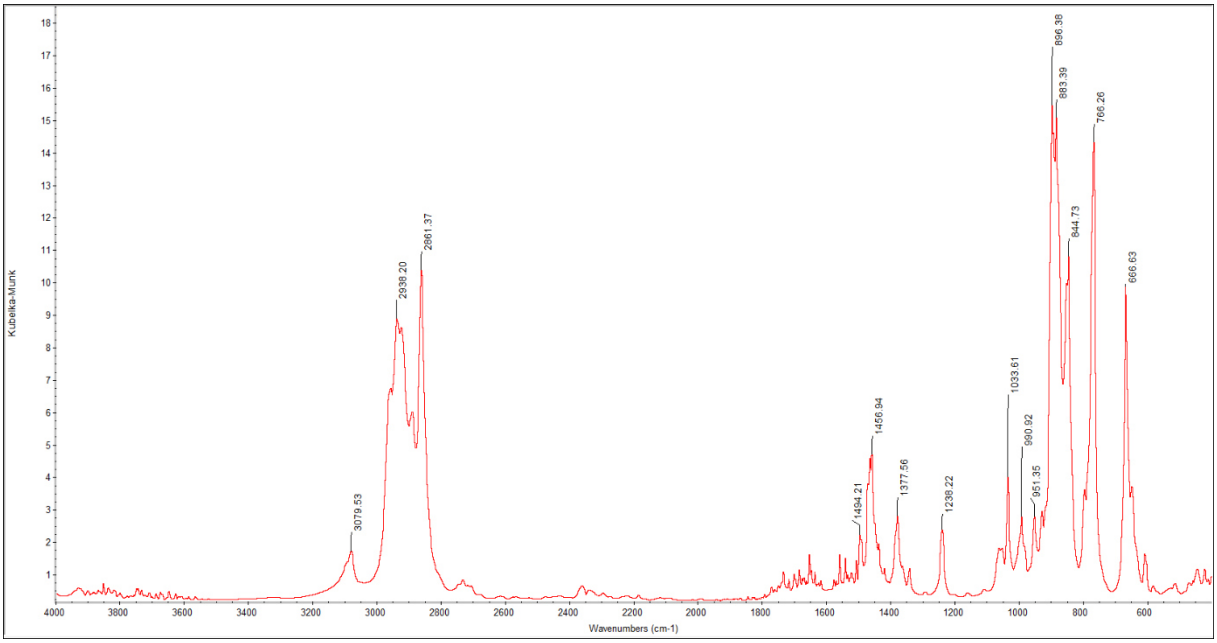

Figure S134. DRIFT spectrum of $Cp^{Me}_3Ce[OSi(iPr)_3]$ (**12b**).

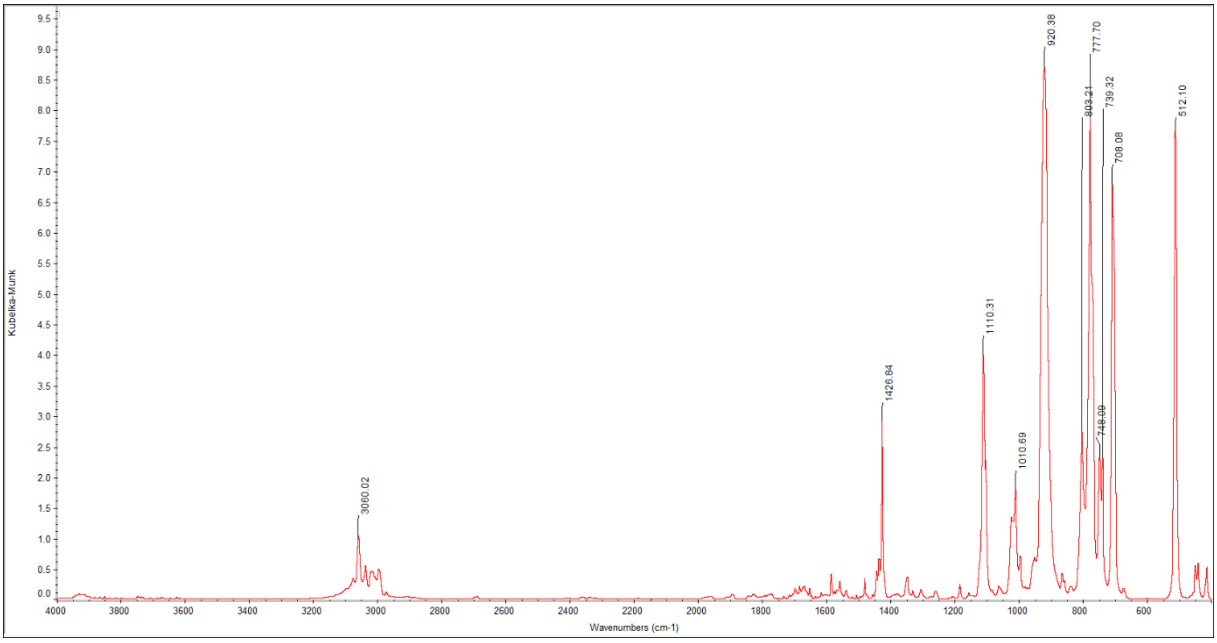

Figure S135. DRIFT spectrum of $Cp_3Ce(OSiPh_3)$ (**13a**).

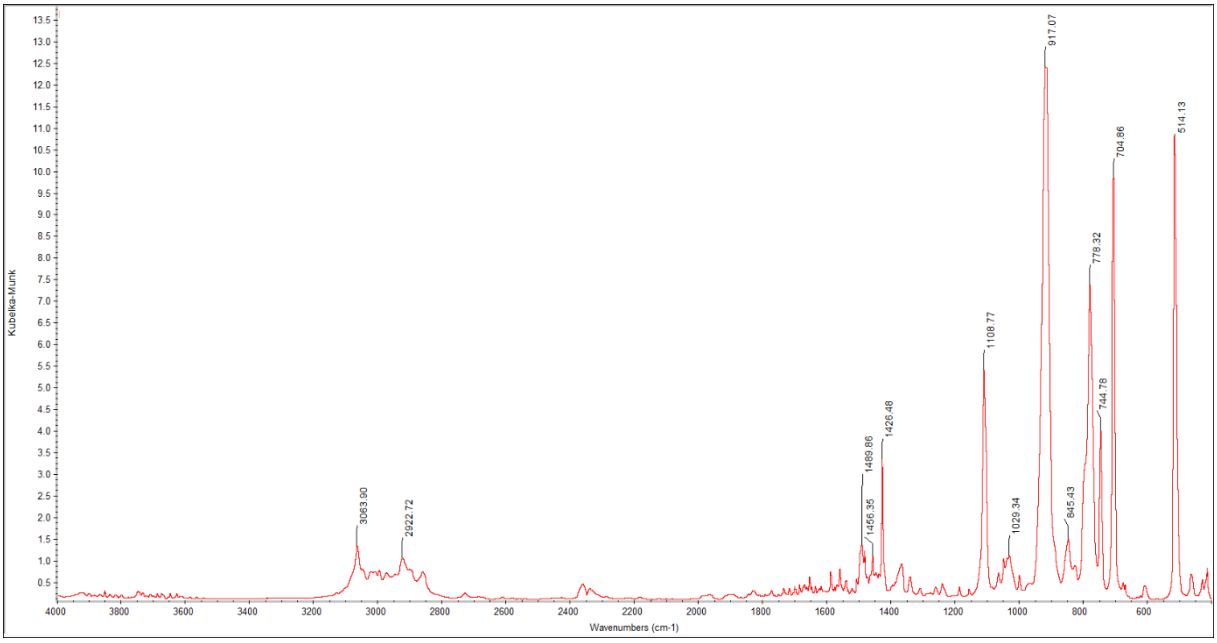

Figure S136. DRIFT spectrum of $Cp^{Me}_3Ce(OSiPh_3)$ (**13b**).

References

1. Lueken, H. *Magnetochemie*, 1st ed.; Teubner: Stuttgart, 1999.
2. Dümmling, S. ; Eichhorn, E.; Schneider, S.; Speiser, B.; Würde, M. *Curr. Sep.* **1986**, *15*, 53-56.
3. Gollas, B.; Krauß, B.; Speiser, B.; Stahl, H. *Curr. Sep.* **1994**, *13*, 42-44.
4. Schank, A.; Speiser, B.; Stickel, A. *J. Electroanal. Chem.* **2016**, *779*, 137-145.

F

Appendix

Appendix

Analytical data of compounds not included in the main results or manuscripts

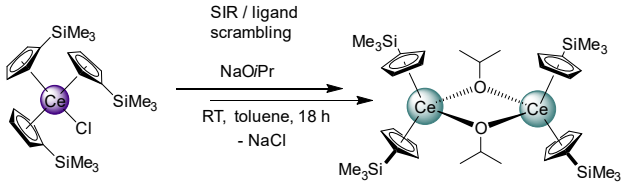

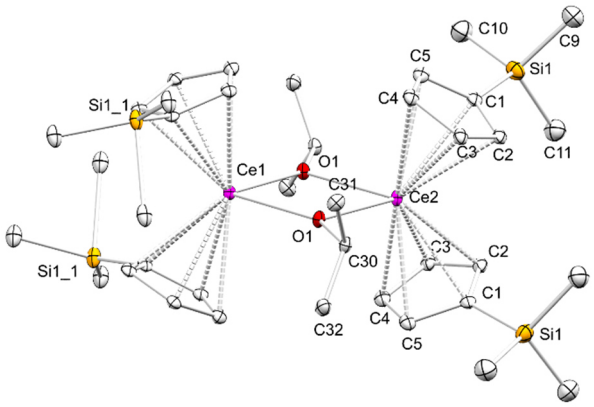

$[Cp'_2Ce(O\mathit{i}Pr)]_2$ LK72

$R_1[I > 2\sigma(I)]$ 6.07%, wR_2(all data) 17.01%

a = 9.2728(7) Å, α = 90°

b = 13.7498(10) Å, β = 101.167(2)°

c = 17.8961(13) Å, γ = 90°

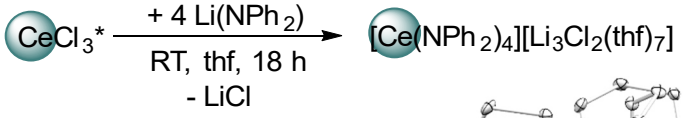

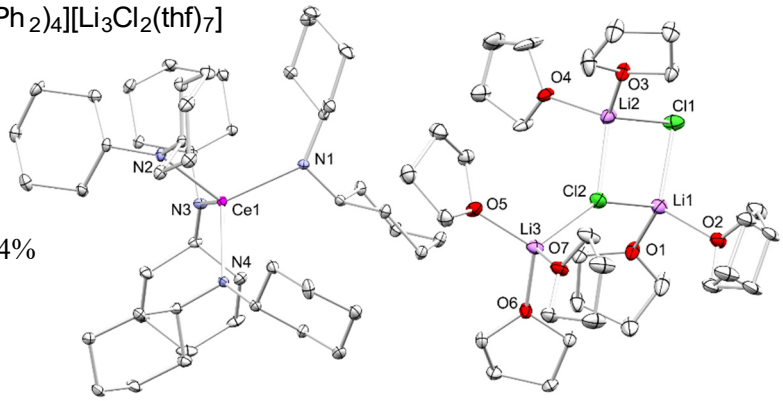

$[Ce(NPh_2)_4][Li_3Cl_2(thf)_7]$ LK172

$R_1[I > 2\sigma(I)]$ 3.65%, wR_2(all data) 8.54%

a = 14.7893(5) Å, α = 90°

b = 10.4857(3) Å, β = 95.4600(10)°

c = 27.4714(9) Å, γ = 90°

Structurally characterized complexes

On the following pages all compounds characterized by X-ray structure analysis are listed as *ChemDraw* sketches.

Cerium Fluorenyl Half-Sandwich Complexes

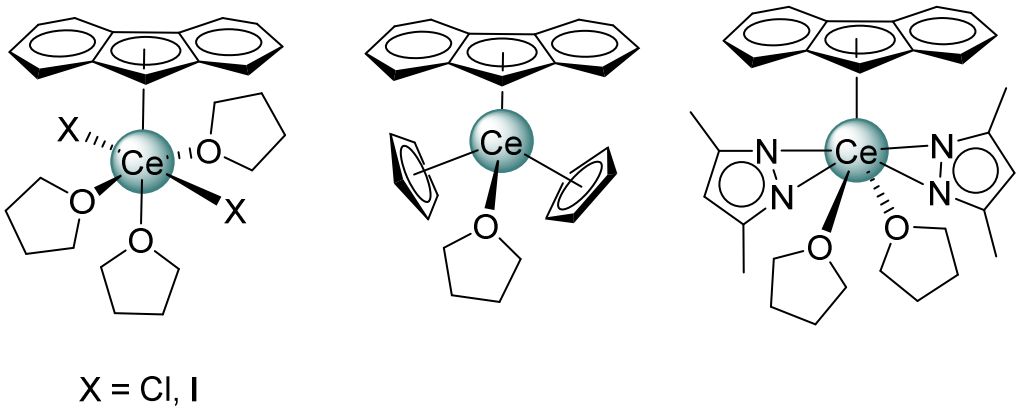

X = Cl, I

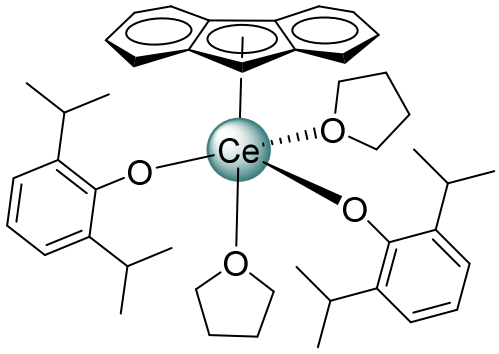

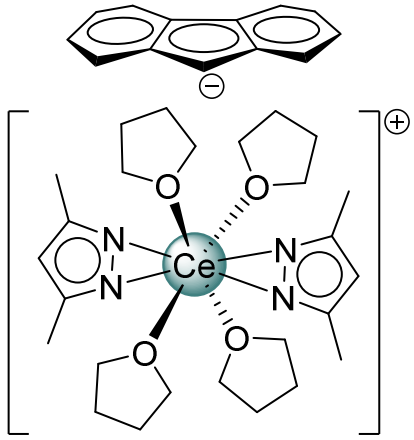

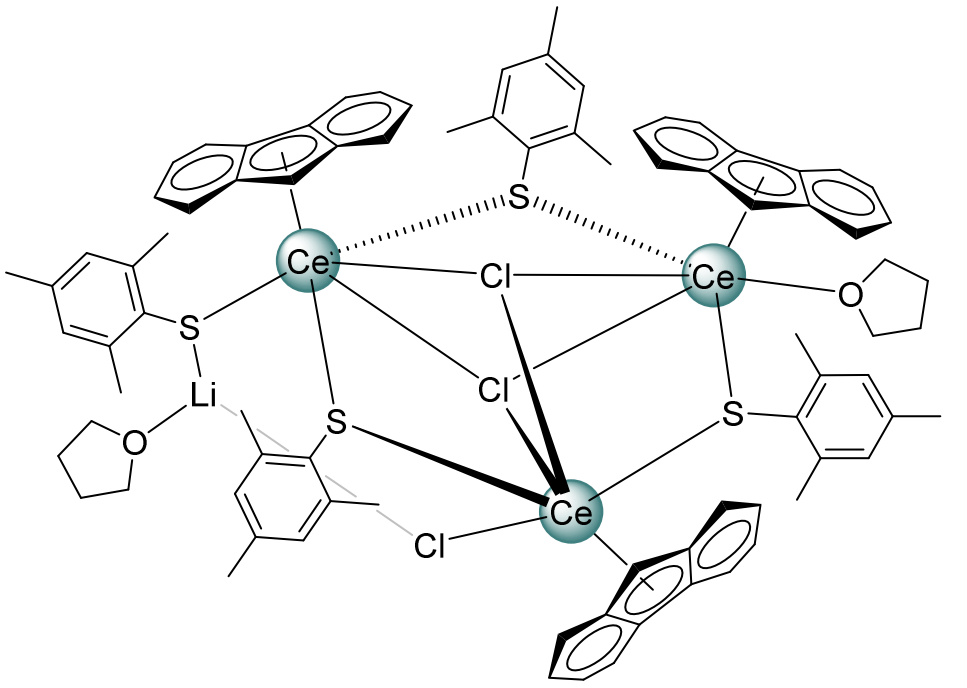

Cerium Fluorenyl Sandwich Complexes

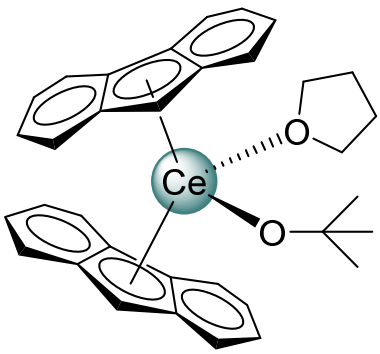

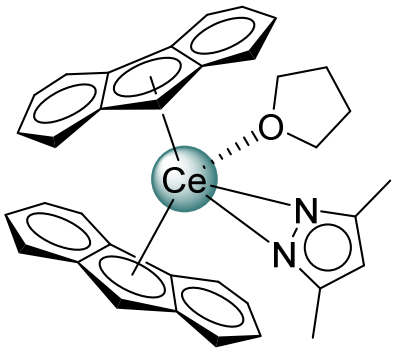

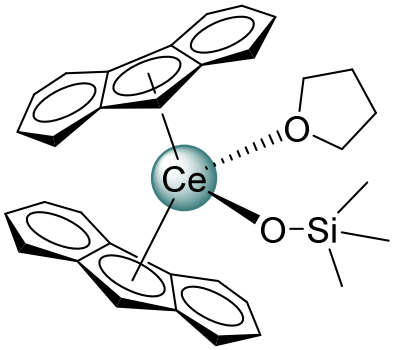

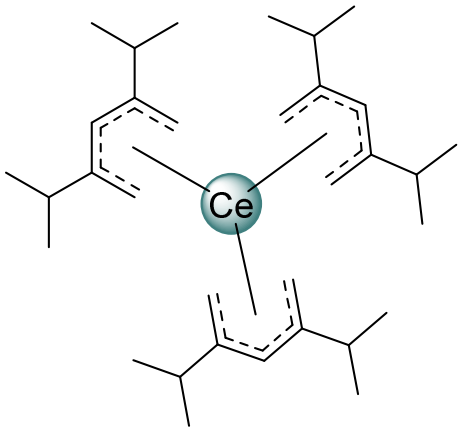

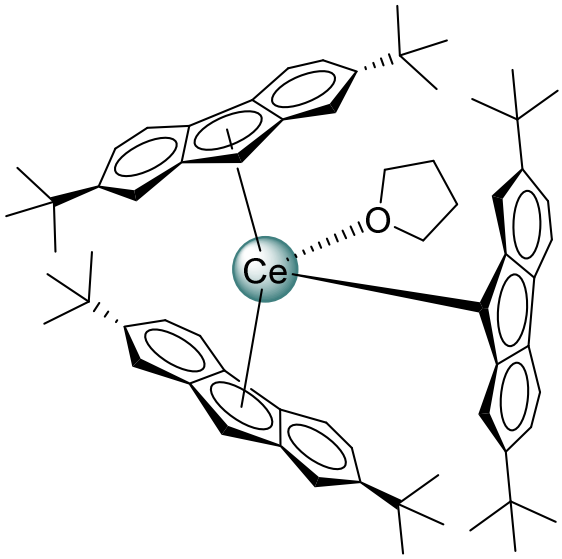

Pentamethylcyclopentadienyl-supported Cerocene complexes

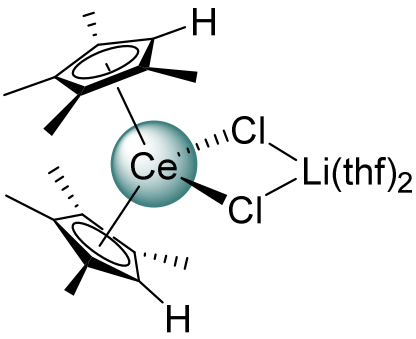

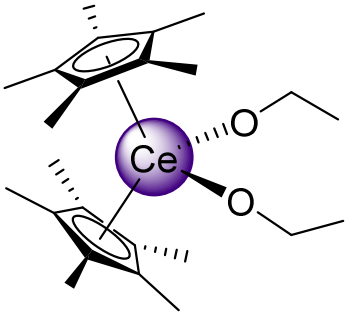

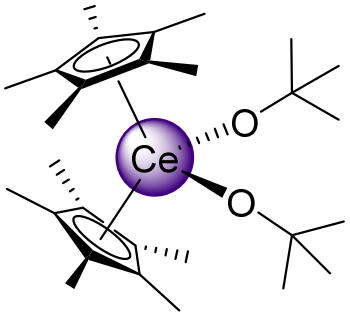

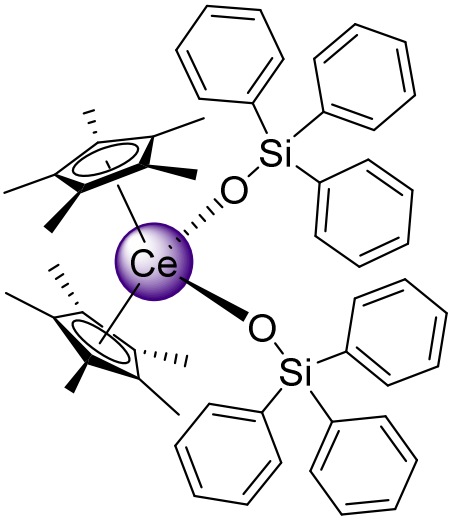

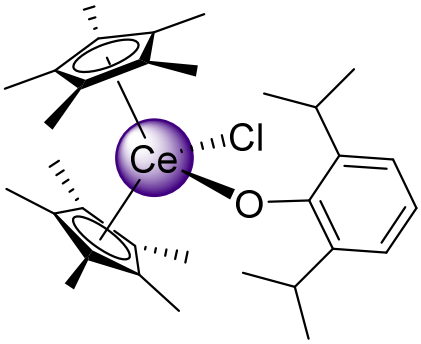

Cerium (Tris Cyclopentadienyl) Complexes

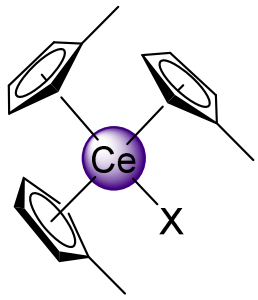

X = Br, I

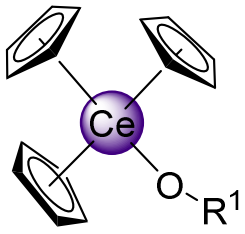

R^1 = Me, Et, *i*Pr

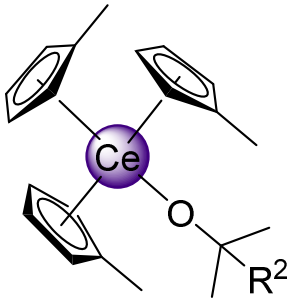

R^2 = H, Me

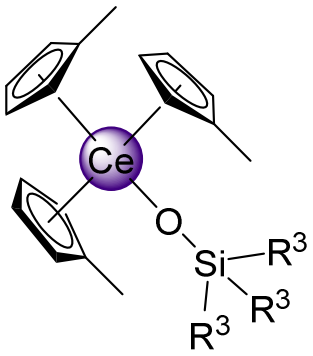

R^3 = Me, Et, Ph

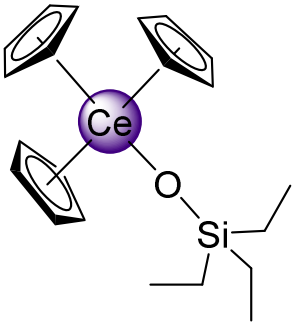

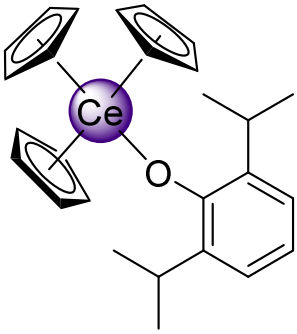

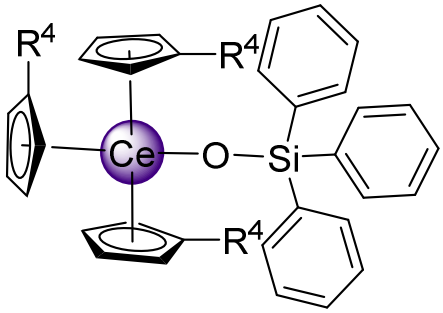

R^4 = H, Me

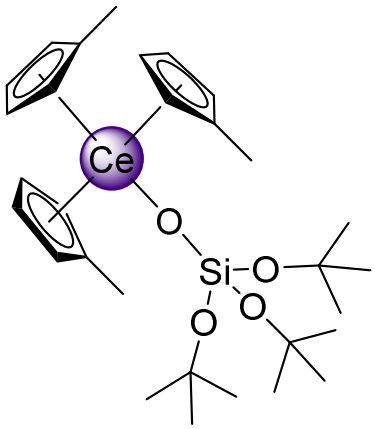

Other Solid-state Structures